

The background of the cover features a complex, abstract molecular structure. It consists of numerous interconnected nodes and lines, rendered in a palette of blue, green, yellow, and orange. The nodes vary in size and opacity, creating a sense of depth and complexity. The overall design is modern and scientific, typical of a research journal cover.

METABOLISM AND VASCULAR DISEASES

EDITED BY: Kangkang Zhi, Xiaojing Liu, Hanjun Wang and Dongze Zhang
PUBLISHED IN: *Frontiers in Physiology*



frontiers

Frontiers eBook Copyright Statement

The copyright in the text of individual articles in this eBook is the property of their respective authors or their respective institutions or funders. The copyright in graphics and images within each article may be subject to copyright of other parties. In both cases this is subject to a license granted to Frontiers.

The compilation of articles constituting this eBook is the property of Frontiers.

Each article within this eBook, and the eBook itself, are published under the most recent version of the Creative Commons CC-BY licence.

The version current at the date of publication of this eBook is CC-BY 4.0. If the CC-BY licence is updated, the licence granted by Frontiers is automatically updated to the new version.

When exercising any right under the CC-BY licence, Frontiers must be attributed as the original publisher of the article or eBook, as applicable.

Authors have the responsibility of ensuring that any graphics or other materials which are the property of others may be included in the CC-BY licence, but this should be checked before relying on the CC-BY licence to reproduce those materials. Any copyright notices relating to those materials must be complied with.

Copyright and source acknowledgement notices may not be removed and must be displayed in any copy, derivative work or partial copy which includes the elements in question.

All copyright, and all rights therein, are protected by national and international copyright laws. The above represents a summary only. For further information please read Frontiers' Conditions for Website Use and Copyright Statement, and the applicable CC-BY licence.

ISSN 1664-8714

ISBN 978-2-88976-153-1

DOI 10.3389/978-2-88976-153-1

About Frontiers

Frontiers is more than just an open-access publisher of scholarly articles: it is a pioneering approach to the world of academia, radically improving the way scholarly research is managed. The grand vision of Frontiers is a world where all people have an equal opportunity to seek, share and generate knowledge. Frontiers provides immediate and permanent online open access to all its publications, but this alone is not enough to realize our grand goals.

Frontiers Journal Series

The Frontiers Journal Series is a multi-tier and interdisciplinary set of open-access, online journals, promising a paradigm shift from the current review, selection and dissemination processes in academic publishing. All Frontiers journals are driven by researchers for researchers; therefore, they constitute a service to the scholarly community. At the same time, the Frontiers Journal Series operates on a revolutionary invention, the tiered publishing system, initially addressing specific communities of scholars, and gradually climbing up to broader public understanding, thus serving the interests of the lay society, too.

Dedication to Quality

Each Frontiers article is a landmark of the highest quality, thanks to genuinely collaborative interactions between authors and review editors, who include some of the world's best academicians. Research must be certified by peers before entering a stream of knowledge that may eventually reach the public - and shape society; therefore, Frontiers only applies the most rigorous and unbiased reviews.

Frontiers revolutionizes research publishing by freely delivering the most outstanding research, evaluated with no bias from both the academic and social point of view. By applying the most advanced information technologies, Frontiers is catapulting scholarly publishing into a new generation.

What are Frontiers Research Topics?

Frontiers Research Topics are very popular trademarks of the Frontiers Journals Series: they are collections of at least ten articles, all centered on a particular subject. With their unique mix of varied contributions from Original Research to Review Articles, Frontiers Research Topics unify the most influential researchers, the latest key findings and historical advances in a hot research area! Find out more on how to host your own Frontiers Research Topic or contribute to one as an author by contacting the Frontiers Editorial Office: frontiersin.org/about/contact

METABOLISM AND VASCULAR DISEASES

Topic Editors:

Kangkang Zhi, Shanghai Changzheng Hospital, China

Xiaojing Liu, Sichuan University, China

Hanjun Wang, University of Nebraska Medical Center, United States

Dongze Zhang, University of Nebraska Medical Center, United States

Citation: Zhi, K., Liu, X., Wang, H., Zhang, D., eds. (2022). Metabolism and Vascular Diseases. Lausanne: Frontiers Media SA. doi: 10.3389/978-2-88976-153-1

Table of Contents

- 04 Editorial: Metabolism and Vascular Diseases**
Kangkang Zhi, Dongze Zhang, Xiaojing Liu and Wang Han-Jun
- 06 How Perturbed Metabolites in Diabetes Mellitus Affect the Pathogenesis of Hypertension?**
Zhangchi Ning, Zhiqian Song, Chun Wang, Shitao Peng, Xiaoying Wan, Zhenli Liu and Aiping Lu
- 27 Association of Plasma Metabolic Biomarker Sphingosine-1-Phosphate With Cerebral Collateral Circulation in Acute Ischemic Stroke**
Fang Yu, Xianjing Feng, Xi Li, Zeyu Liu, Di Liao, Yunfang Luo, Minping Wei, Qin Huang, Lin Zhang and Jian Xia
- 39 Revealing the Angiopathy of Lacrimal Gland Lesion in Type 2 Diabetes**
Junfa Xue, Bin Zhang, Shengqian Dou, Qingjun Zhou, Min Ding, Mingming Zhou, Huifeng Wang, Yanling Dong, Dongfang Li and Lixin Xie
- 57 Thrombus-Targeting Polymeric Nanocarriers and Their Biomedical Applications in Thrombolytic Therapy**
Qixiao Guan and Hongjing Dou
- 65 QiShenYiQi Pills Attenuates Ischemia/Reperfusion-Induced Cardiac Microvascular Hyperpermeability Implicating Src/Caveolin-1 and RhoA/ROCK/MLC Signaling**
Chun-Shui Pan, Li Yan, Se-Qi Lin, Ke He, Yuan-Chen Cui, Yu-Ying Liu, Bai-He Hu, Xin Chang, Xin-Rong Zhao, Jing-Yu Fan and Jing-Yan Han
- 78 Prospective Study of Serum Uric Acid Levels and First Stroke Events in Chinese Adults With Hypertension**
Feng Hu, Longlong Hu, Rihua Yu, Fengyu Han, Wei Zhou, Tao Wang, Linjuan Zhu, Xiao Huang, Huihui Bao and Xiaoshu Cheng
- 92 Myricanol Inhibits Platelet Derived Growth Factor-BB-Induced Vascular Smooth Muscle Cells Proliferation and Migration in vitro and Intimal Hyperplasia in vivo by Targeting the Platelet-Derived Growth Factor Receptor- β and NF- κ B Signaling**
Siyan Fan, Cheng Wang, Kai Huang and Minglu Liang
- 102 The Integration of Metabolomic and Proteomic Analyses Revealed Alterations in Inflammatory-Related Protein Metabolites in Endothelial Progenitor Cells Subjected to Oscillatory Shear Stress**
Jie Yu, Jie Fu, Xiaoyun Zhang, Xiaodong Cui and Min Cheng
- 113 Mechanotransduction Regulates the Interplays Between Alveolar Epithelial and Vascular Endothelial Cells in Lung**
Chuyang Lin, Xiaolan Zheng, Sha Lin, Yue Zhang, Jinlin Wu and Yifei Li
- 129 Testosterone Contributes to Vascular Dysfunction in Young Mice Fed a High Fat Diet by Promoting Nuclear Factor E2-Related Factor 2 Downregulation and Oxidative Stress**
Rafael M. Costa, Rhéure Alves-Lopes, Juliano V. Alves, Carolina P. Servian, Fabíola L. Mestriner, Fernando S. Carneiro, Núbia de S. Lobato and Rita C. Tostes



Editorial: Metabolism and Vascular Diseases

Kangkang Zhi^{1*}, Dongze Zhang², Xiaojing Liu³ Wang Han-Jun⁴

¹Department of Vascular and Endovascular Surgery, Changzheng Hospital, Navy Medical University, Shanghai, China,

²Department of Emergency Medicine, University of Nebraska Medical Center, Omaha, NE, United States, ³Laboratory of Cardiovascular Diseases and Regenerative Medicine Research Center, West China Hospital, Sichuan University, Chengdu, China, ⁴Department of Anesthesiology, University of Nebraska Medical Center, Omaha, NE, United States

Keywords: metabolism, vascular diseases, editorial, basic research, clinical research

Editorial on the Research Topic

Metabolism and Vascular Diseases

Vascular disease is now the leading cause of death worldwide, with cardiovascular and cerebrovascular diseases being the main contributors (Andersson and Vasan, 2018; Doria and Forgacs, 2019). However, its pathological mechanism is not definite yet. Currently, various kinds of vascular diseases are supposed to be related to metabolic disturbance (Gao et al., 2020; Marini et al., 2020). Generally, specific vascular disease indicates a disorder in the whole circulatory system (Guľašová et al., 2020; Lorenzon Dos Santos et al., 2020). The systemic metabolic disturbance would result in various kinds of pathologic changes in the circulatory system and undermine vascular homeostasis, involve atherosclerosis, vascular remodeling, etc (Huo et al., 2018; Katakami, 2018; Neeland et al., 2019). Meanwhile, cellular metabolism makes a strong bond with the local vascular lesion, like atheromatosis, endothelium injury, etc (Tabas and Bornfeldt, 2020; Wu et al., 2021). However, the metabolic balance would also be affected by local vascular cells' physiological regulation, vascular development, and hemodynamics (Smith and Ainslie, 2017; Yang et al., 2020). The characterization of metabolic disturbance and related vascular diseases involves many events and complicated connections, which leave quite a lot of gaps in the field to be further studied. This Topic aimed to cover promising and novel research trends in metabolism and related vascular diseases. Several papers which include Basic or Clinical Medical Research and Review from excellent researchers in multiple fields have been collected to date.

As the dominating part of this Topic, papers of basic research that we primarily collected have revealed some interesting relationships between metabolic abnormalities and vascular diseases. The paper by Yu et al. attempted to illustrate the association between plasma metabolic profiles and cerebral collateral circulation in patients with acute ischemic stroke (AIS). They found that the sphingosine-1-phosphate (S1P) level in plasma showed significant positive correlation with good collateral circulation and which might be a potential diagnostic biomarker for predicting collateral circulation status in patients with AIS. The paper by Xue et al. focused on excavating the potential biomarkers in lacrimal diabetic angiopathy and its potential mechanism. Hub genes *App*, *F5*, *Fgg*, and *Gas6* related to the regulation of circulation and coagulation were identified. Meanwhile, certain small molecular compounds were considered that might reverse the altered differentially expressed genes. This study might empower the novel potential targets to treat lacrimal angiopathy and other diabetes-related diseases. The paper by Fan et al. found that myricanol could inhibit proliferation and migration of vascular smooth muscle cells (VSMCs) induced by platelet-derived growth factor-BB by suppressing the platelet-derived growth factor receptor- β and NF- κ B p65 translocation. Furthermore, myricanol was found suppressing the intimal hyperplasia in mice with carotid stenosis. The paper by da Costa et al. found the events that HFD-fed leading decreased *Nrf2*

OPEN ACCESS

Edited and reviewed by:

Gerald A. Meininger,
University of Missouri, United States

*Correspondence:

Kangkang Zhi
kangkang_zhi@163.com

Specialty section:

This article was submitted to
Vascular Physiology,
a section of the journal
Frontiers in Physiology

Received: 03 March 2022

Accepted: 18 March 2022

Published: 25 April 2022

Citation:

Zhi K, Zhang D, Liu X and Han-Jun W
(2022) Editorial: Metabolism and
Vascular Diseases.
Front. Physiol. 13:888676.
doi: 10.3389/fphys.2022.888676

nuclear accumulation, decreased mRNA expression and activity of Nrf2-regulated enzymes (catalase, heme oxygenase-1, peroxiredoxin and thioredoxin) were prevented in castrated mice. The study indicate that testosterone would downregulate Nrf2, leading to oxidative stress and vascular dysfunction in HFD-fed obese mice.

However, papers of clinical research presented in this Topic have significant discoveries as well. The paper by Hu et al. showed that there was no significant correlation between increased serum uric acid levels and the risk of first stroke in the Chinese adults with hypertension. Meanwhile, risk of the first stroke in patients with hyperuricemia less than 60 years old was significantly higher than control. The paper by Yu et al. was based on bioinformatic analysis of metabolomic and proteomic to reveal that the dysregulation of

glutamate and glycine metabolism, upregulated glycolysis and fatty acid synthesis in the endothelial progenitor cells that treated with the oscillatory shear stress.

Meanwhile, the Review paper by Ning et al. with creative perspective summarized the potential mechanism underlying metabolic perturbation that type 2 diabetes mellitus (DM) affect the hypertension (HTN), what may be involved in the metabolism of insulin and angiotensin II, sympathetic nervous system as well as the energy reprogramming.

AUTHOR CONTRIBUTIONS

This Editorial was prepared jointly by DZ, XL and WH-J.

REFERENCES

- Andersson, C., and Vasan, R. S. (2018). Epidemiology of Cardiovascular Disease in Young Individuals. *Nat. Rev. Cardiol.* 15 (4), 230–240. doi:10.1038/nrcardio.2017.154
- Doria, J. W., and Forgacs, P. B. (2019). Incidence, Implications, and Management of Seizures Following Ischemic and Hemorrhagic Stroke. *Curr. Neurol. Neurosci. Rep.* 19 (7), 37. doi:10.1007/s11910-019-0957-4
- Gao, M., Lv, J., Yu, C., Guo, Y., Bian, Z., Yang, R., et al. (2020). Metabolically Healthy Obesity, Transition to Unhealthy Metabolic Status, and Vascular Disease in Chinese Adults: A Cohort Study. *Plos Med.* 17 (10), e1003351. doi:10.1371/journal.pmed.1003351
- Gulašová, Z., Guerreiro, S. G., Link, R., Soares, R., and Tomečková, V. (2020). Tackling Endothelium Remodeling in Cardiovascular Disease. *J. Cel Biochem* 121 (2), 938–945. doi:10.1002/jcb.29379
- Huo, Y., Wu, X., Ding, J., Geng, Y., Qiao, W., Ge, A., et al. (2018). Vascular Remodeling, Oxidative Stress, and Disrupted PPAR γ Expression in Rats of Long-Term Hyperhomocysteinemia with Metabolic Disturbance. *PPAR Res.* 2018, 6738703. doi:10.1155/2018/6738703
- Katakami, N. (2018). Mechanism of Development of Atherosclerosis and Cardiovascular Disease in Diabetes Mellitus. *Jat* 25 (1), 27–39. doi:10.5551/jat.rv17014
- Lorenzon Dos Santos, J., Schaaf de Quadros, A., Weschenfelder, C., Bueno Garofalo, S., and Marcadenti, A. (2020). Oxidative Stress Biomarkers, Nut-Related Antioxidants, and Cardiovascular Disease. *Nutrients* 12 (3), 682. doi:10.3390/nu12030682
- Marini, S., Merino, J., Montgomery, B. E., Malik, R., Sudlow, C. L., Dichgans, M., et al. (2020). Mendelian Randomization Study of Obesity and Cerebrovascular Disease. *Ann. Neurol.* 87 (4), 516–524. doi:10.1002/ana.25686
- Neeland, I. J., Ross, R., Després, J.-P., Matsuzawa, Y., Yamashita, S., Shai, I., et al. (2019). Visceral and Ectopic Fat, Atherosclerosis, and Cardiometabolic Disease: a Position Statement. *Lancet Diabetes Endocrinol.* 7 (9), 715–725. doi:10.1016/s2213-8587(19)30084-1
- Smith, K. J., and Ainslie, P. N. (2017). Regulation of Cerebral Blood Flow and Metabolism during Exercise. *Exp. Physiol.* 102 (11), 1356–1371. doi:10.1113/ep086249
- Tabas, I., and Bornfeldt, K. E. (2020). Intracellular and Intercellular Aspects of Macrophage Immunometabolism in Atherosclerosis. *Circ. Res.* 126 (9), 1209–1227. doi:10.1161/circresaha.119.315939
- Wu, D., Harrison, D. L., Szasz, T., Yeh, C.-F., Shentu, T.-P., Meliton, A., et al. (2021). Single-cell Metabolic Imaging Reveals a SLC2A3-dependent Glycolytic Burst in Motile Endothelial Cells. *Nat. Metab.* 3 (5), 714–727. doi:10.1038/s42255-021-00390-y
- Yang, J., Ren, B., Yang, G., Wang, H., Chen, G., You, L., et al. (2020). The Enhancement of Glycolysis Regulates Pancreatic Cancer Metastasis. *Cell. Mol. Life Sci.* 77 (2), 305–321. doi:10.1007/s00018-019-03278-z

Conflict of Interest: The authors declare that the research was conducted in the absence of any commercial or financial relationships that could be construed as a potential conflict of interest.

Publisher's Note: All claims expressed in this article are solely those of the authors and do not necessarily represent those of their affiliated organizations, or those of the publisher, the editors and the reviewers. Any product that may be evaluated in this article, or claim that may be made by its manufacturer, is not guaranteed or endorsed by the publisher.

Copyright © 2022 Zhi, Zhang, Liu and Han-Jun. This is an open-access article distributed under the terms of the Creative Commons Attribution License (CC BY). The use, distribution or reproduction in other forums is permitted, provided the original author(s) and the copyright owner(s) are credited and that the original publication in this journal is cited, in accordance with accepted academic practice. No use, distribution or reproduction is permitted which does not comply with these terms.



How Perturbated Metabolites in Diabetes Mellitus Affect the Pathogenesis of Hypertension?

Zhangchi Ning^{1†}, Zhiqian Song^{1†}, Chun Wang¹, Shitao Peng¹, Xiaoying Wan¹, Zhenli Liu^{1*} and Aiping Lu^{2*}

¹Institute of Basic Theory for Chinese Medicine, China Academy of Chinese Medical Sciences, Beijing, China, ²School of Chinese Medicine, Hong Kong Baptist University, Hong Kong, China

OPEN ACCESS

Edited by:

Hanjun Wang,
University of Nebraska Medical
Center, United States

Reviewed by:

Shyam Sundar Nandi,
University of Nebraska Medical
Center, United States
Baojian Xue,
The University of Iowa, United States

*Correspondence:

Aiping Lu
lap64067611@126.com
Zhenli Liu
zhenli_liu@sina.com

[†]These authors have contributed
equally to this work

Specialty section:

This article was submitted to
Metabolic Physiology,
a section of the journal
Frontiers in Physiology

Received: 05 May 2021

Accepted: 26 July 2021

Published: 18 August 2021

Citation:

Ning Z, Song Z, Wang C, Peng S,
Wan X, Liu Z and Lu A (2021) How
Perturbated Metabolites in Diabetes
Mellitus Affect the Pathogenesis
of Hypertension?
Front. Physiol. 12:705588.
doi: 10.3389/fphys.2021.705588

The presence of hypertension (HTN) in type 2 diabetes mellitus (DM) is a common phenomenon in more than half of the diabetic patients. Since HTN constitutes a predictor of vascular complications and cardiovascular disease in type 2 DM patients, it is of significance to understand the molecular and cellular mechanisms of type 2 DM binding to HTN. This review attempts to understand the mechanism via the perspective of the metabolites. It reviewed the metabolic perturbations, the biological function of perturbated metabolites in two diseases, and the mechanism underlying metabolic perturbation that contributed to the connection of type 2 DM and HTN. DM-associated metabolic perturbations may be involved in the pathogenesis of HTN potentially in insulin, angiotensin II, sympathetic nervous system, and the energy reprogramming to address how perturbated metabolites in type 2 DM affect the pathogenesis of HTN. The recent integration of the metabolism field with microbiology and immunology may provide a wider perspective. Metabolism affects immune function and supports immune cell differentiation by the switch of energy. The diverse metabolites produced by bacteria modified the biological process in the inflammatory response of chronic metabolic diseases either. The rapidly evolving metabolomics has enabled to have a better understanding of the process of diseases, which is an important tool for providing some insight into the investigation of diseases mechanism. Metabolites served as direct modulators of biological processes were believed to assess the pathological mechanisms involved in diseases.

Keywords: diabetes mellitus, the pathogenesis of hypertension, perturbated metabolites, metabolic function, connected metabolic mechanism

INTRODUCTION

Diabetes mellitus (DM) is an endocrine metabolic disease with an increasing prevalence all over the world. According to data released by the International Diabetes Federation, the number of DM patients is predicted to rise to 552 million by the year 2030. Type 1 and type 2 are the two main types, with type 2 DM accounting for the majority (>85%) of total DM prevalence (Forouhi and Wareham, 2014). Hypertension (HTN) is a crucial risk factor for type 2 DM-associated vascular complications. Vascular process whereby type 2 DM and HTN predispose to cardiovascular diseases. When combined with DM, HTN has been shown to predict and promote increased

risk for cardiovascular diseases, which is the major cause of mortality in patients with type 2 DM (Petrie et al., 2018). Furthermore, up to 75% of diabetic cardiovascular diseases may be attributable to HTN (Sowers et al., 2001). There is a clinical impression that HTN occurs more frequently among diabetic patients than in the healthy population. It was proved to present in more than 50% of patients with type 2 DM. It is closely related to the occurrence and development of diabetic microvascular and macrovascular diseases. Indeed, DM and HTN were four times more likely to develop cardiovascular disease than non-diabetic controls with normal blood pressure. They also increased the incidence of other diabetes complications, such as kidney disease and retinopathy (Lastra et al., 2014). Hence, it is urgent to understand the molecular and cellular mechanisms of the combination of DM and HTN.

The rapidly evolving field of metabolomics is aiming at a comprehensive measurement of all endogenous metabolisms in biological systems (Acevedo-Calado et al., 2017). It represents both the upstream input from the environment and the downstream output of the genome (Wishart, 2016). Panels of multiple biomarkers reflecting their specificity and potentials for prediction have been developed (Savolainen et al., 2017a). In recent years, the value of metabolomics has been redefined from biomarker recognition tools as a technology for active drivers of biological processes (Johnson et al., 2016). The search for genes that are associated with metabolite levels, or whose products catalyze reactions, including disease-related metabolites and pathways, may explain the way these metabolic phenotypes are regulated (Zhang et al., 2018).

Moreover, metabolic research could also make it possible to understand the effects of specific microbes on specific metabolites better. Growing evidence accumulated that gut microbiota may not be overlooked in the pathogenesis of diseases. The gut microbiota affects the host by producing metabolites systematically. Small-molecule metabolites are one of the contributions of gut bacteria to host biology (Dodd et al., 2017). Metabolomics is a promising technology to contribute to the disease mechanism investigation since metabolites were served as direct modulators of biological processes and active entities in a biological process.

This review attempts to understand the mechanism of the combination of type 2 DM and HTN *via* the perspective of the metabolites. Firstly, it focuses on the metabolic perturbations of type 2 DM and HTN. After summarizing the biological function of perturbed metabolites, the paper associated the perturbed metabolites with the mechanisms in type 2 DM and HTN. Finally, the review reveals the effect of type 2 DM-associated metabolic perturbations on the pathogenesis of HTN.

METABOLIC PERTURBATIONS IN TYPE 2 DM AND HTN

Metabolites are substrates or products of metabolic pathways. The changes in the metabolome directly reflect the gene expression, physiological status, and environmental effects on

the biological system (Monteiro et al., 2013). Metabolic perturbations have been studied to diagnose and prediction of diseases by biomarkers. Over the past 15 years, advances in metabolomics techniques, together with improvements in bioinformatics and mathematical modeling approaches, have provided the scientific community with tools to describe DM and HTN metabolomics. Three general techniques have become the main tools for metabolomics data acquisition: liquid chromatography-mass spectrometry (LC-MS), gas chromatography-mass spectrometry (GC-MS), and nuclear magnetic resonance (NMR). Metabolites are typically separated using gas chromatography (GC) and liquid chromatography (LC) before MS, and compounds are identified by mass and fragmentation patterns. However, there is no need to separate metabolites in NMR spectroscopy instead of measuring all metabolites at once. The use of multiple technologies was proved to broaden the level of metabolite coverage greatly. Metabolomics raw data processing involves noise reduction, spectrum deconvolution, peak detection and integration, chromatogram alignment, compound identification, and quantification (Shulaev, 2006). It is of great significance to perform statistical analysis on the processed data, reduce the number of variables, and obtain irrelevant features in the data. It can be best achieved either through unsupervised significance algorithms, such as principal component analysis (PCA), or through supervised methods, including *t*-test, χ^2 -tests, ANOVA, orthogonal partial least square discriminant analysis (OPLS-DA), and partial least squares (PLS; Lazar et al., 2015). The numbers of metabolites and metabolic classes have garnered much attention as biomarkers in the field of DM and HTN investigations. Validated biomarkers become alter markers that can substitute for clinical endpoints to monitor disease progression. An overview of the observed metabolic changes of type 2 DM and HTN is shown in **Table 1**. The comparison and correlation of the perturbed metabolites in type 2 DM and HTN were performed. The perturbed metabolites in common, perturbed metabolites in type 2 DM, and the perturbed metabolites in HTN were listed individually.

The metabolites, including amino acids, energy-related metabolites, lipids and fatty acids, carnitines, and bile acids were associated with type 2 DM and HTN. According to **Table 1**, we calculated proportions of different kinds of perturbed metabolites in the whole panel of metabolic markers of DM, HTN, and both of the two diseases individually and showed the ratios of each metabolic marker classes in DM, HTN, and the common of two diseases in the pie chart of **Figure 1**.

Amino acids – Based on the review of the relevant literature, we listed the disturbances of amino acids in DM and HTN in **Table 1** and pictured the blue pie charts to represent the ratio of amino acids in the whole panel of metabolic markers in **Figure 1**. The level of branched-chain amino acids (BCAAs; valine, leucine, and isoleucine) and aromatic amino acids (AAAs; tyrosine, phenylalanine, and tryptophan) was increasing in DM adults (Walford et al., 2013). Although most research is conducted in European populations, an analysis in Chinese and Asian-Indian men showed that the associated decrease in glycine

TABLE 1 | Summary of metabolic perturbations of DM and HTN.

Type of metabolites	Metabolic perturbations of DM	Metabolic perturbations of HTN	Common metabolic perturbations of both DM and HTN	Multivariate statistical method	References
Amino acid	N6-acetyllysine; N-trimethyl- β -aminovalerate; 2-oxoarginine; homocitrulline; N-acetylcitrulline; N-delta-acetylornithine; N2, N5-diacetylornithine; isoleucine; leucine; threonine; tryptophan; tyrosine; γ -glutamyl-leucine; N,N-dimethylglycine; tau-methylhistidine; asparagine; n-alpha-acetyllysine; hydroxyproline; aspartate; proline; dimethylglycine; 2-aminoadipic acid; β -alanine; and histidine.	L-arginine; phenyl propionic acid; 3-hydroxyproline; β -aminoisobutyric acid; 4-hydroxy-proline; and N-acetylornithine	Arginine; valine; Alanine; tyrosine; glycine; lysine; glutamine; threonine; tryptophan; phenylalanine; citrulline; methionine; ornithine; serine; glutamate; and cystine	Bonferroni-corrected threshold, Pearson correlation coefficients, Wilcoxon signed-rank, independent-sample t -test, χ^2 -tests, PCA, OPLS-DA on Pareto scaled, Pearson correlation coefficients, Partial least-squares PLS-DA, Logistic regression models, PLS, McNemar's test, Fisher's exact test, Mann-Whitney U-test, orthogonal signal correction (OSC), and random forest analysis.	Lu et al., 2008; Wang et al., 2011; Ho et al., 2013; Würtz et al., 2013; Cooper-DeHoff et al., 2014; Pena et al., 2014; Friedrich et al., 2015; Palmer et al., 2015; Yokoi et al., 2015; Fall et al., 2016; Nikolic et al., 2016; Hernández-Alvarez et al., 2017; Kappel et al., 2017
Energy-related metabolites	6-oxopiperidine-2-carboxylate	D-methylglucopyranoside		PCA, PLS-DA, OSC, paired Student t -test, independent-sample t -test, Chi-squared tests, ANOVA, orthogonal projection to latent structure discriminant analysis (OPLS-DA), nonparametric Mann-Whitney, and nonparametric Kruskal-Wallis test.	Brindle et al., 2003; Akira et al., 2008; Lu et al., 2008; Fiehn et al., 2010; Liu et al., 2011; Guan et al., 2013; Ho et al., 2013; Li et al., 2013; Filla et al., 2014; Pena et al., 2014; Grapov et al., 2015; Rotroff et al., 2015; van Deventer et al., 2015; Wu et al., 2015; Allalou et al., 2016; LauraGonzalez-Calero et al., 2016; Nikolic et al., 2016; Wang et al., 2016; Yu et al., 2016; Kappel et al., 2017; Martin-Lorenzo et al., 2017
Lipids and fatty acids	SMs; PCs; palmitoleic acid; lysoPC/PC (O-16:1/0:0); monoacylglycerol (18:2), CerPE (38:2); SM (d18:2/18:1); SM (d18:2/18:1); nitric oxide-derived saccharic acid; arachidonic acid; linoleoylglycerophosphocholine; diacyl-phosphatidylcholines C32:1, C36:1, C38:3, C40:5; sphingomyelin C16:1; acyl-alkyl-phosphatidylcholines C34:3, C40:6, C42:5, C44:4, and C44:5; sphingomyelin C16:1; acyl-alkyl-phosphatidylcholines C34:3, C40:6, C42:5, C44:4, and C44:5; lysophosphatidylcholine C18:2; triacylglycerols; cholesterol esters; linoleic acid (18:2 n-6); palmitic acid (16:0); monounsaturated palmitoleic (16:1 n-7); oleic (18:1 n-9) acids; PE (C16:0/C22:6); PE (C18:0/C20:4); stearic acid; Linoleic acid; palmitic acid; eicosapentaenoic acid; and 3-carboxy-4-methyl-5-propyl-2-furanpropanoic oleic acid	13-OxoODE; 9-OxoODE; sphinganine 1-phosphate; sphinganine; thromboxane; PA (16:0/16:0); 9(S)-HPODE; LPA (0:0/18:0); 9,12,13-TriHOME; phyto sphingosine; 12(S)-HPETE; HETE; HDoHE; hexacosahexanoic acid; behenic acid; 1-stearoylglycerol; hexadecanoic acid; stearic acid; ceramide; acyl-alkyl-phosphatidylcholines C42:4; C44:3; diacyl-phosphatidylcholine C38:4; C38:3; monohexosylceramides; and phosphatidylinositols	PCs; diacylglycerols; lysoPCs; and linoleic acid	ANOVA, Benjamini-Hochberg procedure, PCA, PLS-DA, t -test, χ^2 -tests, and least absolute shrinkage and selection operator (LASSO) regression.	Kottronen et al., 2009; Mäkinen et al., 2012; Floegel et al., 2013; Dietrich et al., 2016; Fall et al., 2016; Yu et al., 2016; de Mello et al., 2017; Liu et al., 2017a,c, 2018; Bujak et al., 2018; Tian et al., 2018

(Continued)

Type of metabolites	Metabolic perturbations of DM	Metabolic perturbations of HTN	Common metabolic perturbations of both DM and HTN	Multivariate statistical method	References
Carnitine	Tiglylcarnitine; benzoylcarnitine; 3-methyladipoylcarnitine; octanoylcarnitine; cis-4-decenoylcarnitine; decanoylcarnitine; arachidonoylcarnitine (C20:4); 3-hydroxybutyrylcarnitine; acylcarnitine; 2-methylbutyrylcarnitine; palmitoylcarnitine; carnitine; butenoylcarnitine; and 3-hydroxybutyrylcarnitine	\	\	Pearson correlation coefficients, Wilcoxon signed-rank, independent-sample <i>t</i> -test, χ^2 -tests, principal component analysis (PCA), and orthogonal partial least square discriminant analysis (OPLS-DA)	Kappel et al., 2017
Bile acid	deoxycholic acid and cholate; deoxycholates	Hydroxyoxocholanoic acid	\	PCA, PLS-DA, OSC, paired Student <i>t</i> -test, independent-sample <i>t</i> -test, and Chi-squared tests	Ho et al., 2013; Fall et al., 2016; Bujak et al., 2018
Others	Pipecolate; urea; cortisol; trimethylamine N-oxide; allantoin; amines; carbonyls; cholate; cystathionine; indole propionate; uridine; trimethylamine; quinolate; urate; acetoacetate; methylamine; glyoxal hydroimidazolone; 3-deoxyglucosone hydroimidazolone; and alkylresorcinols C17 and C19	17 α -hydroxypregnenolone; 5,6-dihydroxyprostaglandin F1 α ; decanamide; dodecanamide; 1-hexadecanol; erythritol; α -1 acid glycoproteins; choline; sitosterol; adenine; uracil; glycerate; 3-ureidopropionate; 3-hydroxybutyrate; guanidinoacetate; hexadecanedioate; dicarboxylic acid; epiandrosterone sulfate; 5 α -androstan-3 β ; 17 β -diol disulgate; androsterone sulfate; 4-hydroxyhippuric; hippurate; N-methylnicotinate; and creatine	Formate; kynurenine; xanthine; pantothenate; creatinine; 5-hydroxy indole acetic acid; tocopherol; and betaine	ANOVA, Benjamini-Hochberg procedure, PCA, PLS-DA, <i>t</i> -test, χ^2 -tests, least absolute shrinkage and selection operator (LASSO) regression, and ANOVA	Akira et al., 2005; Holmes et al., 2008; Ferrannini et al., 2013; Guan et al., 2013; Ho et al., 2013; Menni et al., 2013; Zheng et al., 2013; Grapov et al., 2015; Rotroff et al., 2015; Yokoi et al., 2015; Fall et al., 2016; Wang et al., 2016; de Mello et al., 2017; Kappel et al., 2017; Murfitt et al., 2017; Savolainen et al., 2017b; Bujak et al., 2018; Tian et al., 2018

was consistent with the increase in valine and leucine levels with multiple presentations of the development of type 2 DM and insulin resistance (Huffman et al., 2011). However, their role in the few available pediatric studies was controversial, with lower levels of BCAA (Michaliszyn et al., 2012; Mihalik et al., 2012; Frohnert and Rewers, 2016). A case-cohort study showed that the increased plasma levels of BCAAs/AAAs were associated with higher type 2 diabetes risk (Ruiz-Canela et al., 2018). Glycine and glutamine are reduced in insulin resistance (Sekhar et al., 2011; Stančáková et al., 2012). The potential role of BCAAs and AAAs with incident HTN is increasingly recognized. High plasma concentrations of BCAAs and AAAs are proved to be associated with an increased risk of newly developed HTN (Teymoori et al., 2018; Flores-Guerrero et al., 2019). According to the clinical implications, BCAAs were associated with the incident of type 2 DM. They also seem on the pathway from DM to cardiovascular diseases for the attenuation of the association of BCAA and cardiovascular patients without type 2 DM. However, it is still too early to tell whether BCAAs are the marker of risk for DM or cardiovascular diseases in DM.

Energy-related metabolites – The gray pie charts represent the ratio of energy-related metabolites in the whole panel of metabolic markers in **Figure 1**. The energy metabolism abnormalities are commonly associated with DM and HTN. The two diseases are related to gluconeogenesis, glycolysis, pentose phosphate, and tricarboxylic acid (TCA) cycle (Iemitsu et al., 2003; Ho et al., 2013). Hexose sugars are primarily accounted for by disease-defining increasing glucose and positively associated with DM. And the elevations of fructose, mannose, sorbitol, lactate, and malate have been proved to be associated with DM (Fiehn et al., 2010; Hwang et al., 2010; Menni et al., 2013). α -ketoglutarate, fumarate, and succinate levels in urine are decreased in DM patients (Salek et al., 2007).

Lipids and fatty acids – The green pie charts represent the ratio of lipids and fatty acids in the whole panel of metabolic markers in **Figure 1**. Given the significance of obesity as one of the risk factors for type 2 DM and HTN, it is not surprising that both DM and HTN patients have increased fat-derived metabolites. Phosphatidylcholine (PC), lysophosphatidylcholine (LPC), phosphatidylethanolamine (PE), and diacylglycerol (DAG) increased the risk of DM (Floegel et al., 2013). Conversely, a

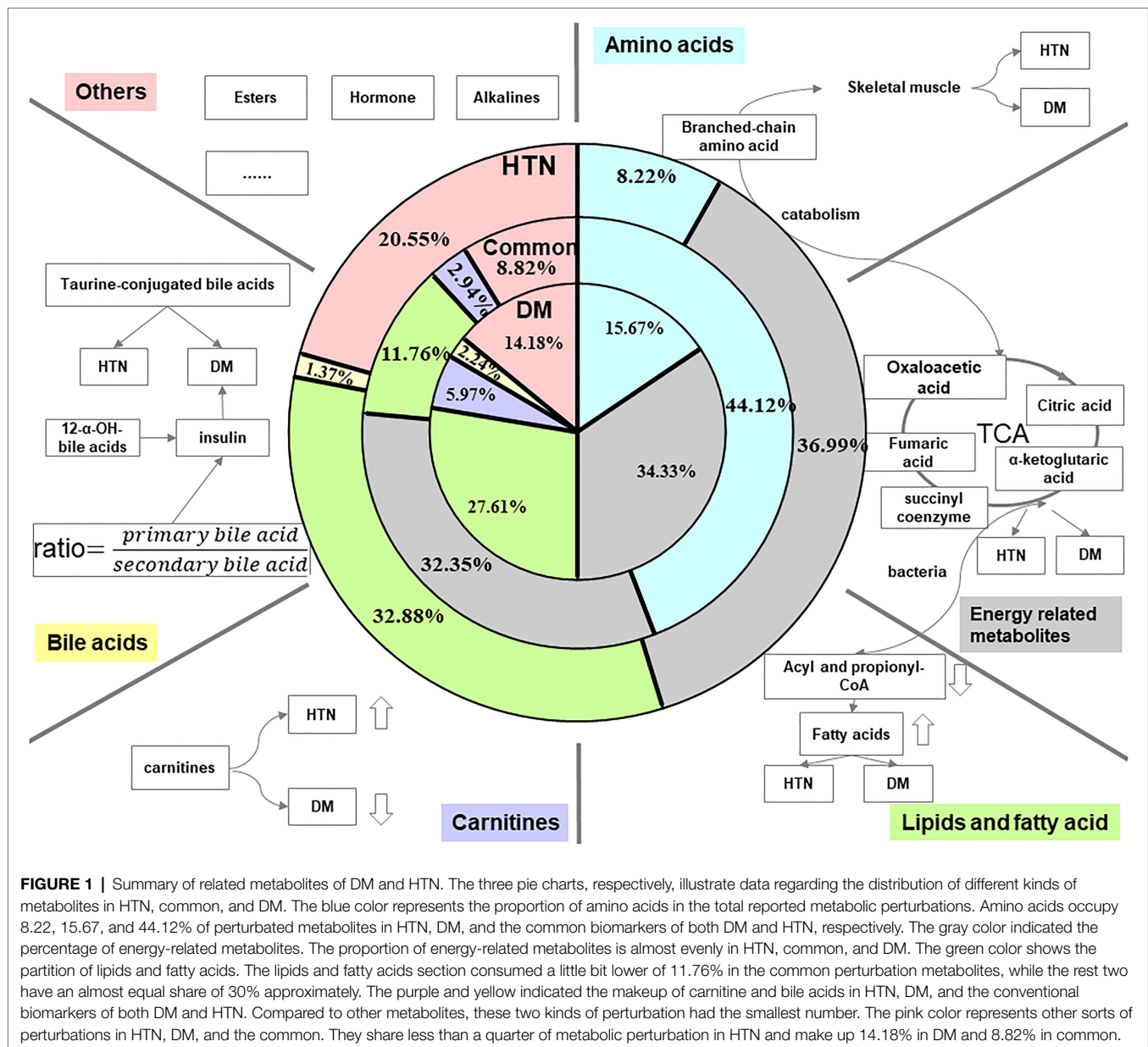


FIGURE 1 | Summary of related metabolites of DM and HTN. The three pie charts, respectively, illustrate data regarding the distribution of different kinds of metabolites in HTN, common, and DM. The blue color represents the proportion of amino acids in the total reported metabolic perturbations. Amino acids occupy 8.22, 15.67, and 44.12% of perturbed metabolites in HTN, DM, and the common biomarkers of both DM and HTN, respectively. The gray color indicated the percentage of energy-related metabolites. The proportion of energy-related metabolites is almost evenly in HTN, common, and DM. The green color shows the partition of lipids and fatty acids. The lipids and fatty acids section consumed a little bit lower of 11.76% in the common perturbation metabolites, while the rest two have an almost equal share of 30% approximately. The purple and yellow indicated the makeup of carnitine and bile acids in HTN, DM, and the conventional biomarkers of both DM and HTN. Compared to other metabolites, these two kinds of perturbation had the smallest number. The pink color represents other sorts of perturbations in HTN, DM, and the common. They share less than a quarter of metabolic perturbation in HTN and make up 14.18% in DM and 8.82% in common.

major class of sphingolipids, sphingomyelins (SM), and ceramide (Cer) was linked with a decreased risk of DM (Fall et al., 2016). Thromboxane, linoleic, phosphatidic acid (PA), lysophosphatidic acid (LPA), and phytosphingosine were increased, while sphinganine decreased in the HTN group (Tian et al., 2018). More and more evidence pointed to a mental disorder sphingolipid pathway trigger HTN. Hydroxyoctadecadienoic acids (HODEs) are related to HTN, the generation of which is increased where oxidative stress is increased. 9-HODE and 13-HODE are generated nonenzymatically in atherosclerosis. Increased HODE levels were proved to contribute to HTN and atherosclerosis progression (Vangaveti et al., 2010). Richard et al. highlight the discovery of 20-hydroxyeicosatetraenoic acid (20-HETE) in the regulation of renal function, vascular tone, and the development of HTN

(Roman and Fan, 2018). The increasing levels of 12-HETE and 12-hydroperoxyeicosatetraenoic acid (12-HPETE) in HTN patients suggested roles for these metabolites in HTN (González-Núñez et al., 2000). The perturbed lipids in DM and HTN are listed in **Table 1**.

Carnitines – The purple pie charts represent the ratio of carnitines in the whole panel of metabolic markers in **Figure 1**. Propionyl carnitine, α-methyl butyl carnitine, and isovaleryl carnitine were elevated in type 2 DM (Pena et al., 2014; Qiu et al., 2016). The decrease of short-chain acylcarnitines and long-chain acylcarnitines, including C14:1 and C14:2, was observed in HTN patients (Bai et al., 2018).

Bile acids (BAs) – The yellow pie charts represent the ratio of carnitines in the whole panel of metabolic markers in **Figure 1**. In healthy subjects, insulin resistance increased

by 12 α -hydroxylated BAs. The ratios of non-12 α -hydroxylated and 12 α -hydroxylated BAs are related to the main characteristics of insulin resistance (Hausler et al., 2013). Marlene et al. revealed that total taurine-conjugated BA concentration was higher in DM patients (Wewalka et al., 2014). A systematic evaluation of bile acid kinetics revealed that the contribution of specific types of bile acids varies in type 2 DM even though there was no difference in the size of the total BA pool. The level of deoxycholic acid was increased, and chenodeoxycholic acid was decreased (Brufau et al., 2010). Another study showed that lower cholic acid and higher plasma levels of deoxycholic acid occurred in diabetic patients compared to controls (Suhre et al., 2010).

Amino acids, energy-related metabolites, lipids, and fatty acids made up the biggest percentage of the total disturbed metabolites compared with BAs and other metabolites. They may play a significant role in the pathogenesis of HTN in DM. Hence, the biological function of these metabolites should be illustrated. It also can be found that the commonality of DM and HTN among metabolites is limited. To reveal how they are different or more interestingly amalgamated in both disease phenotypes, which leads to an intermediate or tertiary state that the patient's metabolic physiology, the biological mechanism should also be discussed.

THE BIOLOGICAL FUNCTION OF PERTURBATED METABOLITES IN TYPE 2 DM AND HTN

The metabolic biomarkers served as mechanistic discoveries. Metabolites modulate biological processes and phenotypes directly (Johnson et al., 2016). Direct modulation was associated with alterations in host metabolism, mainly through immune systems and hormone secretion (Li et al., 2018a). The metabolic potential of the gut microbiota is another contributing element in the development of DM and HTN (Kitai and Tang, 2017), with metabolites acting on distant target organs like the human host's endocrine organ. The representative biological functions of each class of metabolites are shown in **Figure 1**.

Amino acids – Studies of BCAAs, such as valine, leucine, and isoleucine supplementation in animals and humans, suggest that circulating amino acids may promote insulin resistance directly, possibly *via* disrupting insulin signaling in skeletal muscle. BCAA in combination with hyperinsulinemia exerts a large amount of secretory pressure on pancreatic accessory cells, resulting in dysfunction of accessory cells. BCAAs catabolism offered intermediates to the TCA cycle, which may boost energy production (O'Connell, 2013). Metabolism studies indicated that changes in TCA flux in diabetic patients (Guan et al., 2013; Li et al., 2013). The reduction of the tricarboxylic acid cycle was shown in DM and HTN (Brindle et al., 2003). Betaine is a tertiary amine dimethylglycine (DMG) produced by homocysteine remethylation to methionine. It is catalyzed by betaine-homocysteine methyltransferase (BHMT). DMG is catalyzed by DMG dehydrogenase (DMGDH) and sarcosine dehydrogenase in turn. Epidemiological data

indicated that plasma levels of betaine correlate with key components of the metabolic syndrome in the opposite direction (Konstantinova et al., 2008). High plasma glycine levels are also thought to be associated with increased insulin sensitivity (Menni et al., 2013).

Metabolites involved in energy metabolism – Energy metabolism includes energy release and energy restoration, which provides a source of energy for the daily activity of cells. Mitochondrial is of significance in maintaining cellular energy metabolic homeostasis (Alston et al., 2017). The disequilibrium of mitochondrial functions in type 2 DM leads to the deficits of downstream in several parts, including cardiac output, skeletal muscle contraction, β -cell insulin production, and hepatocyte metabolism (Pinti et al., 2019). HTN, one of the cardiovascular diseases, is closely related to myocardial energy metabolism (Polak-Iwaniuk et al., 2019). Recent research proved that the improved skeletal muscle energy metabolism correlates to the recovery of β cell function and benefits the glucose control of type 2 patients (Tang et al., 2019). Fatty acids are the main fuel for the heart, while glucose and lactate serve the remaining need (Calvani et al., 2000). It is reported that the changes in glucose and fatty acids utilization appear in the diabetic heart fuel selection (Stanley et al., 1997). A downshifting of ketone body production and the breakdown and the tricarboxylic acid cycle was observed in insulin resistance (Heinonen et al., 2015). HTN shifts substrate preference toward increased glucose utilization in cardiac muscle. Citrate, pyruvate, malate, and adenosine monophosphate were the common metabolic markers for DM and HTN. When perfusion is reduced, there is an increase in the rate of glycolysis and a switch from lactate uptake to lactate production. During reperfusion, fatty acid oxidation quickly recovers. Otherwise, carbohydrates, such as hexoses, fructose, and gluconic acid, and nucleotides, such as adenosine, were the marker for DM and HTN, which linked to endothelial dysfunction, insulin resistance (Khitan and Kim, 2013).

Lipids and fatty acids – DM significantly decreased levels of acetyl- and propionyl-CoA means that it prevents the degradation of fatty acids, amino acids and ketone bodies. In contrast, an increase in free fatty acids (FFAs) occurred in HTN (Aa et al., 2010). FFAs regulate glucose counter-regulation by mediating hepatic glucose production (Fanelli et al., 1993). Lipolysis also mediates the delayed glucose-antiregulation pathway of growth hormone and cortisol stimulation. Hyperinsulinemic hypoglycemia increases the production of non-esterified fatty acids, indicating the role of lipids as alternative energy sources (Voss et al., 2017). The prevailing theory of lipid-induced hepatic insulin resistance is that lipid species accumulate due to oxidative damage to fatty acids, leading to the redirection of long-chain acyl-coenzyme A (LC-CoAs) to endoplasmic reticulum (ER) localization and cytosolic lipid species, such as triglycerides, diacylglycerols, and ceramides (Muoio and Newgard, 2008). Type 2 diabetes can be the result of the loss of or deficiency of beneficial functions, such as short-chain fatty acid produced by carbohydrate fermentation in the intestinal ecosystem (Zhao et al., 2018). Meanwhile, FFAs influence HTN (Aa et al., 2010). 12-HETE, transformed from arachidonic acid,

acted as vasoconstrictors in the renal arteries, which cause the elevation of blood pressure (González-Núñez et al., 2000). The critical role of 20-HETE in the regulation of renal function and vascular tone makes it participate in the development of HTN and cardiovascular diseases.

Carnitines – According to the researches, 13 kinds of carnitines were the biomarkers of DM (Kappel et al., 2017). It transported long-chain fatty acids to the mitochondria and then to be oxidized to produce energy. In the cardiac muscle and skeletal, carnitine utilizes fatty acids as fuel. Insulin resistance is associated with oxidative defects in muscle fatty acids and played a crucial part in the development of type 2 DM (Mingrone, 2004). Studies also have shown that intravenous L-carnitine supplementation reduces insulin sensitivity in the distal muscles of diabetic patients (Gaetano et al., 1999). Finding from the study shows that carnitine lowers diastolic blood pressure in adults (Askarpour et al., 2019). L-carnitine and propionyl-L-carnitine can reduce the species of reactive oxygen species in HTN and increase the involvement of nitric oxide (NO) in endothelium-dependent relaxation (Bueno et al., 2005). The action of carnitine-dependent enzymes produces acetyl-CoA through the β -oxidation pathway, which modulates the intramitochondrial acetyl-CoA/CoA ratio affecting glucose oxidation (Calvani et al., 2000). An affected carbohydrate and lipid metabolism are verified in type 2 DM and HTN. The dysregulated fatty acid metabolism, along with tissue lipid accumulation, is associated with the development of HTN in type 2 DM. As the dominant role of carnitines in the balance of carbohydrate and fatty acid metabolism, it is likely to be a potential adjuvant in the treatment of type 2 DM.

BAs – BAs are steroid acids found in the bile of mammals predominantly. Primary BAs (cholic acid and chenodeoxycholic acid) are synthesized in the liver. Intestinal bacterial converts

primary BAs into secondary BAs (Russell, 2003). In humans, taurocholic acid and glycocholic acid and taurochenodeoxycholic acid and glycochenodeoxycholic acid are the main bile salts in bile, with approximately equal concentrations (Hofmann, 1999). The level of taurine-conjugated BAs is elevated in type 2 diabetes (Liu et al., 2013), and the ratio of 12- α OH BAs has been reported to relative to insulin resistance (Hausler et al., 2013). Acarbose increases the ratio of primary BAs and secondary BAs. Uncombined BAs have also been proved to be elevated in type 2 DM patients at the beginning of treatment (Gu et al., 2017). Taurine is higher in DM and HTN groups (Fujiwara et al., 2005; Yokoi et al., 2015). An enhancement of creatinine was occurred in HTN, while it decreases in type 2 DM (Grapov et al., 2015). The supplementation with cholic acid and activation of the G protein-coupled bile acid receptor can significantly reduce the blood pressure (Shi et al., 2021).

Gut microbiome-related metabolites – In recent years, the relationship between the complexity and diversity of the gut microbiota and host diseases has been demonstrated (Weiss and Hennet, 2017; Li et al., 2018b). The gut microbiota constantly communicates hypotheses were brain-gut-microbiome axis (Mahony et al., 2015), brain-gut-kidney axis (Yang et al., 2018), and gut-liver axis (Tripathi et al., 2018). It produces several metabolites and accumulated in the bloodstream (Nicholson et al., 2012). High levels of AAAs, such as AA-phenylalanine, tyrosine, and glycine, occurred (Neis et al., 2015). Antidiabetic medication Acarbose was proved to alter plasma and fecal BAs composition *via* the mediate gut microbiota. The relative abundances of Lactobacillus and Bifidobacterium in the gut microbiota increased, while Bacteroides reduced. Moderating the relative abundance of microbial genes is related to bile acid metabolism (Gu et al., 2017). Studies have shown that the negative correlation between the hippurate reflects the

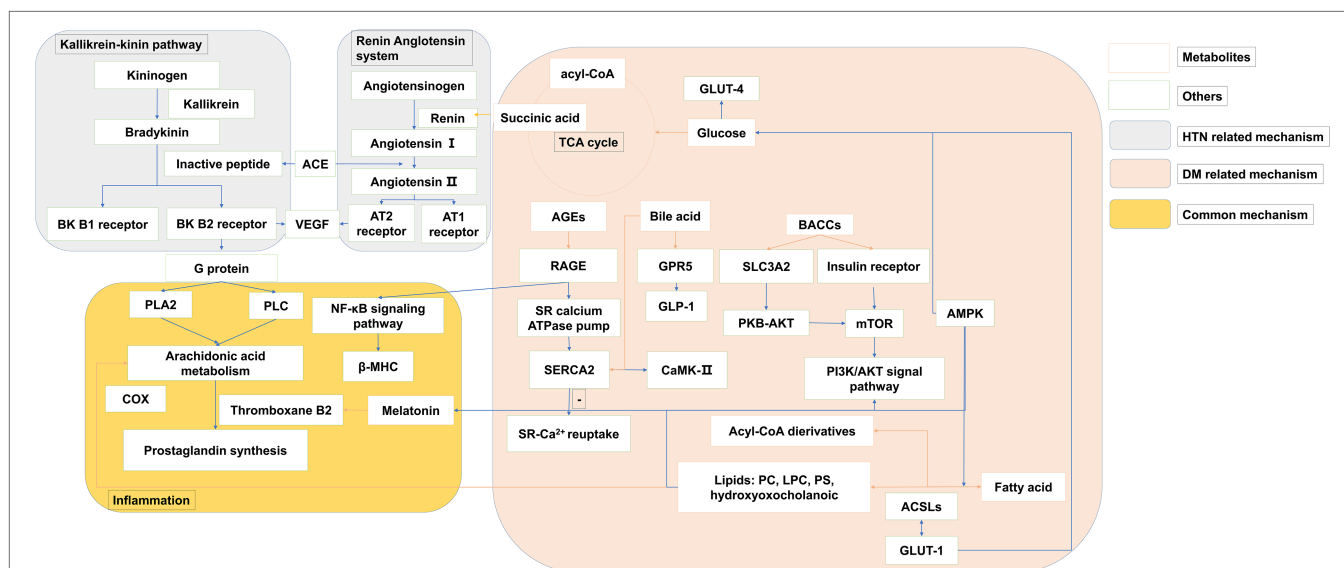


FIGURE 2 | The overview of metabolites related common mechanisms of type 2 DM and HTN. The pink panel summarized the metabolites mechanism related to type 2 DM. The gray panel consists of the kallikrein-kinin pathway and the renin-angiotensin system, which are the main progress of HTN. The yellow panel presented the common metabolic mechanism of both type 2 DM and HTN. Orange row arrows the association of metabolites and biomolecules.

physiological relationship with gut microbial (Holmes et al., 2008). Minocycline can cure resistant HTN patients because of its potent antihypertensive effect on the gut microbiota (Qi et al., 2015). Gut microbial composition research found that hypertensive rats having reduced taxa richness and altered microbial composition. The Firmicutes to Bacteroidetes ratio was higher in the hypertensive rats (Yang et al., 2015). Salt-sensitive rats showed higher blood pressure rather than salt-resistant rats, which was related to the elevated plasma levels of the short-chain fatty acids (SCFAs). It suggested gut microbiota-derived SCFAs produce the endocrine hormones. SCFAs, as a source of energy for colonocytes and bacterial communities, help maintain gut barrier function by inhibiting pathogenic microorganisms and reducing luminal pH. Host-signaling mechanisms, such as the G-protein-coupled receptors (GPR) 41 and olfactory receptor 78 (Olf78), can modulate blood pressure (Tang and Hazen, 2017). Trimethylamine-N-oxide (TMAO), amino acids, and creatine related to energy metabolism were proved to contribute to HTN (Mell et al., 2015). TMAO was proved to be a strong predictor of coronary artery disease risk. Mechanistically, gut microbes transformed trimethylamine-containing nutrients, such as carnitine, phosphatidylcholine, and choline to TMAO, which leads to atherogenesis and thrombosis. In mice, increasing TMAO level decreased reverse cholesterol transport and altered bile acid transport, composition and pool size (Koeth et al., 2013). Meanwhile, TMAO modulated stimulus-dependent calcium mobilization in platelets, enhancing platelet responsiveness (Zhu et al., 2016). Accompanying metabolism functional changes, gut dysbiosis has been implicated in the pathogenesis ranging from insulin resistance to atherosclerosis and thrombosis.

What is noteworthy is that the biggest percentage of the total disturbed metabolites share a common biological function: provide energy. Besides amino acids, energy-related metabolites, lipids, and fatty acids, carnitines play the regulation role of the fatty acids and glucose metabolism in physiological and pathological conditions. A decreased ratio can relieve the transfer of acetyl groups from acetyl-CoA to carnitine, forming acetylcarnitine, a reaction catalyzed by carnitine acetyltransferase. This activity of L-carnitine in the modulation of the intramitochondrial acetyl-CoA/CoA ratio affects glucose oxidation (Calvani et al., 2000). Other circulating substrates, such as ketones or BCAAs, may become an alternative source of energy.

THE CONNECTION OF MECHANISM UNDERLYING METABOLIC PERTURBATION BETWEEN TYPE 2 DM AND HTN

The development of metabolomics has facilitated the pathophysiology discovery of DM and HTN. The biomarker identified to reveal the mechanism of diseases *via* early changes highlights pathways and targets. Integration of the metabolism field with other disciplines, such as endocrinology and

immunology, hints the metabolic alterations and substrate utilization. Here, as shown in **Figure 2**, we associated the biological function of metabolites with the mechanism of DM and HTN. DM and HTN are frequent comorbid conditions that may share underlying metabolic pathways, including the sympathetic nervous and renin-angiotensin-aldosterone system, insulin resistance, and inflammation processes (Schutta, 2007; Cheung and Li, 2012).

Role of Metabolic Perturbations in HTN

A variety of disorders have been identified in HTN, including the renin-angiotensin system, the autonomic nervous system, and the immune system (as shown in the *gray* panel in **Figure 2**). Changes in the autonomic nervous system associated with increases in peripheral and neuroinflammation are associated with the pathogenesis of drug resistance to HTN. Recent evidence suggests that the increased peripheral and neuronal inflammation of HTN is due to the effect of autonomic nerves on bone marrow activity (Zubcevic et al., 2014). The SCFA olfactory Olf78 is also expressed in the kidneys, where it regulates blood pressure. Elevated FFAs may alter membrane fluidity by altering Na⁺-K⁺ ATPase pump, Na⁺, K⁺, and Ca²⁺ currents, membrane phospholipids structure, and intracellular Na⁺ and Ca²⁺ levels. This is the mechanism that increased the vascular muscle tension and consequently HTN (Ordway et al., 1991).

Emerging evidence suggested that gut microbiota plays a crucial part in the development of HTN. This effect was thought to be mainly due to the SCFAs (Holmes et al., 2008). The phylum *Bacteroidetes* and family *Veillonellaceae* were proved to be more abundant in salt-sensitive than in salt-resistant rats (Mell et al., 2015).

Role of Metabolic Perturbations in DM

As shown in the *pink* panel in **Figure 2**, the increased level of BCAAs was improved to make an influence in insulin sensitivity *via* the mammalian target of rapamycin complex (mTORC) and target ribosomal protein S6 kinase 1 (S6K1) in the downstream (O'Connell, 2013). The effector of mTOR, S6K1, is sensitive to both AA and insulin. Phosphatidylinositol 3-kinase (PI3K)/Akt signaling can downregulate autophagy by inhibiting the mTOR, and the changes in autophagy were associated with reduced PI3K/Akt signaling in insulin resistance (Bugger and Abel, 2014). The numbers of metabolites separating the DM groups were associated with mitochondria. The centrality of the mitochondrial function in catabolic and metabolic diseases of BCAA has been noted previously (Newgard, 2012). BCAA may damage mitochondrial oxidation of glucose and lipids, which can lead to mitochondrial stress and impaired insulin secretion and action. Impaired mitochondrial function in DM could decrease the capacity of the mitochondria to decompose BCAAs, resulting in elevated levels of BCAAs and BCKAs. The dysfunction of reduced mitochondrial biogenesis was rescued by augmentation of adenosine 5' monophosphate-activated protein kinase (AMPK) activity (Dugan et al., 2013). The studies showed that the peptide hormone is produced by adipose cells, such as

adiponectin/Acrp 30 and retinol-binding protein-4 (RBP4). They also produce resistin and proinflammatory cytokines, such as interleukin-6 (IL-6) and tumor necrosis factor- α (TNF- α). Several BA species have been recognized as modulators of energy metabolism by activation of nuclear receptors, such as G-protein-coupled BA receptor (TGR5) and farnesoid X receptor (FXR) (Thomas et al., 2008). The activation of FXR induces fibroblasts to grow in the intestine. Although the mechanisms are not yet fully understood, the release of glucagon-like peptide 1 (GLP-1) and peptide YY (PYY), as well as changes in BA metabolism and enhancing signaling *via* FXR, is thought to play a role. TGR5 is necessary to improve glucose metabolism, which may be related to DM (Tremaroli et al., 2015). SCFAs can stimulate GPR 41 and 43, and these are expressed in the renal vasculature. These effects include several processes such as inflammation and intestinal endocrine regulation (Samuel et al., 2008). However, the balance across these G-protein-coupled receptor activities is complex and likely to be dynamic (Pluznick, 2013). SCFAs can also trigger GPR41 and GPR43 to secrete GLP-1, which plays a substantial role in pancreatic function and insulin release. GPR41 induces intestinal endocrine hormone PYY expression in the epithelial L cells through increasing dietary energy gain (Samuel et al., 2008). Adipose cells also produce other peptide hormones, including retinol-binding protein RBP4 and adiponectin/Acrp 30). Fat-specific glucose transporter 4 (GLUT4) knockout mice showed elevated RBP4 levels (Yang et al., 2005). The expression of monocyte chemoattractant protein-1 (MCP1) and I κ B kinase catalyzes injury and infection of subunit- β (IKK β) recruitment sites in the adipocyte. It may be a mechanism for increased inflammatory signals during the development of DM (Arkan et al., 2005; Chen et al., 2005).

Recent studies show that individual bacteria concerned with insulin resistance have the same phenotype for recipient mice when transferred to normal, specific, and non-pathogenic mice (Pedersen et al., 2016; Liu et al., 2017b). Amino acids act on mTOR receptor regulating pathways and physiological processes, like insulin. Gut microbiota can regulate TGR5 signal-generating receptor agonists and FXR signal metabolism antagonists, such as tauro- β -muricholic acid (Sayin et al., 2013). TGR5 is required for improved metabolism of glucose (Tremaroli et al., 2015). Propionate SCFs stimulate GLP1 and PYY hormone release in the primary gut culture of mice through the FFA receptor 2 (FFAR2) dependent mechanism (Tolhurst et al., 2012). Gut microbiota induces PYY in an FFAR3-dependent manner (Psichas et al., 2015).

Role of Metabolic Perturbations in DM and HTN

As shown in **Figure 2** (yellow panel), both of the metabolic perturbation mechanisms of DM and HTN link to the inflammation. Subjects with DM had elevated plasma FFA levels, which played a detrimental role in the pathogenesis of HTN. FFAs lead to multiple mechanisms, including the activation of the renin-angiotensin system, impaired insulin signaling and NO production, oxidative stress, inflammation, and apoptosis in the endothelial cells, which make an influence in the DM and HTN

co-exist (Ghosh et al., 2017). Melatonin has a special place in the prevention and treatment of metabolic syndromes, such as DM and HTN (Cardinali et al., 2011). It has an anti-inflammatory property, partly for its role as a metabolic regulator. Melatonin's resistance to inflammation occurs in the correction of metabolic disorders, which prevent insulin resistance. Impaired serine phosphorylation of insulin receptor substrate 1 (IRS-1) and the subsequent upregulation of IRS-1 expression may be crucial (She et al., 2014). *Via* the activation of CREB-PGC-1 α pathway, melatonin could prevent insulin resistance and mitochondrial dysfunction (Teodoro et al., 2014). Both melatonin and melatonergic agonists counteract the blockade of this critical step in insulin signal (She et al., 2009; Quan et al., 2015). Regeneration and pancreatic β -cells lead to decreased blood glucose after melatonin treatment in the diabetic rats model (KanterEmail et al., 2006). Melatonin treatment improves insulin sensitivity and lipid metabolism in type 2 diabetic rats (R.C. Mazepa et al., 1999; Shieh et al., 2009). The inhibition effect of melatonin on platelet aggregation and thromboxane B2 was also proved.

TYPE 2 DM-ASSOCIATED METABOLIC PERTURBATIONS POTENTIALLY INVOLVED IN THE PATHOGENESIS OF HTN

Perturbated metabolites exert several physiological responses either directly through the activation of powerful humoral systems, indirectly stimulation localized target organs, or *via* postganglionic sympathetic nerves. The actions and interactions of insulin, angiotensin II, inflammation, vascular dysfunction, or central nervous systems lead to the pathogenesis and progression of HTN. Here, we pictured the overview of physiological processes in **Figure 3**.

Insulin Sensitivity in Cells and Tissue

Reduced sensitivity to insulin in tissue is a characteristic of multiple pathological conditions (Du et al., 2006). HTN in subjects with DM was significantly related to insulin resistance (Rewers et al., 2004). Acute hyperglycemia consistently impairs endothelial function in type 2 DM patients (Wallis et al., 2005). Reducing glucose levels may inhibit vascular changes leading to HTN (The DCCT Research Group, 1988; Purnell et al., 1998).

Insulin metabolism is often mediated by insulin signaling. PI3K/Akt pathway causes atherothrombosis *via* multiple mechanisms. On the one hand, it produces several beneficial molecules. On the other hand, it inhibits plasminogen activator inhibitor type 1 (PAI-1), E-selection, intercellular adhesion molecule (ICAM), and vascular cell adhesion molecule (VCAM). The increased expression level of VCAM1 and ICAM1 and inflammatory cytokines, like interleukin IL6, IL18, IL1 β , TNF α , and TGF- β , lead to myocyte inflammation in the DM and HTN (Rajesh et al., 2012). Glucotoxicity, lipotoxicity, and inflammation impair the PI3K-dependent insulin signaling pathway, which constructs the combination of DM and HTN (Muniyappa et al., 2008). PI3K-dependent insulin signaling

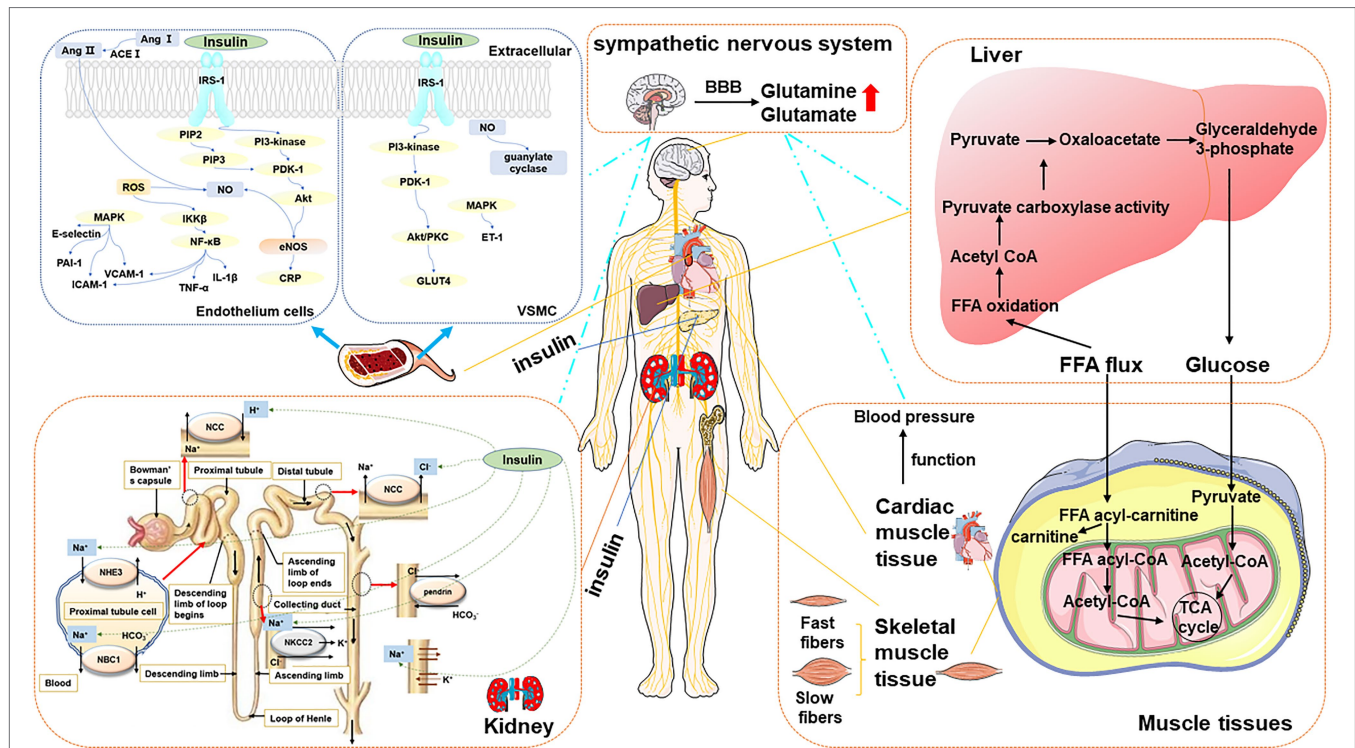


FIGURE 3 | The overview of type 2 DM-associated metabolic perturbations potentially involved in the pathogenesis of HTN. *Blood vessel* The left panel presented the mechanisms of HTN in DM in the endothelium cell. The mechanism started with IRS triggered activation of PI3K and the conversion from PIP₂ to PIP₃. It allowed PDK-1 to access, leading to Akt activation. Akt increased eNOS activity and stimulated the production of NO. Meanwhile, Ang II and ROS are another way to produce NO. MAPK-dependent insulin signaling pathways tend to promote pro-HTN insulin metabolite. It inhibits PAI-1, E-selectin, ICAM, and VCAM. *The right panel* presented the mechanism of HTN in DM in VSMC. The increased blood flow further facilitates glucose uptake by provoking insulin-responsive GLUT4 translocation in PI3K-dependent metabolic actions. MAPK-dependent insulin signaling pathways tend to promote ET-1. The production of NO is related to guanylate cyclase. *Kidney* The sodium-chloride cotransporter (NCC) has the function of reabsorbing sodium and chloride ions from the tubular fluid. Insulin promotes the resorption of chloride ions. Insulin stimulates the NHE3 on the apical membrane and upregulates the NBC1 on the basolateral membrane. In the thick ascending limb of Henle, insulin stimulates NaCl reabsorption by activating NKCC2 and Na-K-ATPase. The sodium and bicarbonate were reabsorbed. Insulin can also stimulate the Na-K-ATPase in the proximal tubule in the proximal tubule. *Liver and muscular tissue* FFA is the major oxidation fuel for muscular tissue, such as cardiac muscle tissue and skeletal muscle tissue, while glucose provides the remaining need. The transformation of cardiac function metabolites affects the function of the heart, which is closely related to blood pressure. The balance of FFA and glucose results in the transformation of two muscle types: slow-twitch myofibers and fast-twitch fibers. *Sympathetic nervous system* It controls peripheral organs, including the liver, skeletal muscle, pancreas, vascular and cardiovascular system resulting in glucose disorder, insulin resistance, insulin secretion impairment, and blood pressure increase, which are predicted to chronically contribute to the development of DM and HTN.

pathways regulate vasodilator and insulin metabolite in skeletal muscle and vascular endothelium. MAPK-dependent insulin signaling pathways tend to promote pro-HTN insulin metabolite. Insulin resistance, hyperglycemia, oxidative stress, and attenuate inflammation and renin-angiotensin process in endothelial smooth muscle and kidney issues are predicted to make a simultaneous beneficial influence in the co-existed DM and HTN.

In vein endothelial and endothelial cells – One of the important roles of insulin is to accelerate the production of the effective vasodilator factor NO by endothelial cells (Vincent et al., 2003; Muniyappa et al., 2007). The binding of insulin binding to its receptor (a receptor tyrosine kinase) causes phosphorylation of IRS-1, which can activate PI3K. The lipid products of PI3K [PI-3,4,5-triphosphate (PIP₃)] can stimulate the phosphorylation and activation of PDK1, which in turn phosphorylates and activates Akt. Akt increased the eNOS activity and stimulated the production of NO, which is calcium-independent

(Montagnani et al., 2001). NO inhibits the production of ROS, which leads to endothelial dysfunction and promotes the development of atherosclerosis (Muniyappa et al., 2008). ET-1, as a potent vasoconstrictor, is stimulated by insulin and plays a crucial role in endothelial dysfunction and contributes to the development of HTN, using the MAPK-dependent signaling pathway (Marasciulo et al., 2006). And the increased expression level of PAI-1, ICAM-1, VCAM-1, and E-selectin may contribute to accelerated atherosclerosis in insulin-resistant conditions (Bonetti et al., 2003). Insulin stimulates the expression of VCAM-1, PAI-1, and E-selectin in endothelial cells through the MAPK-dependent pathway (Montagnani et al., 2002; Mukai et al., 2007). The suppression of PI3K or Akt174 increased the insulin-induced PAI-1 and adhesion molecule expression.

When endothelial cells are exposed to high concentrations of glucose, insulin-stimulated Akt and eNOS activation is significantly reduced (Du et al., 2001; Wang et al., 2006).

Hyperglycemia is also believed to be associated with impaired glucose tolerance. It induces an increasing level of ROS production, post-translational O-GlcNacylation, PKC activity, and advanced glycation end products (AGEs), which is known to specifically inhibit the PI3K/Akt/eNOS pathway. Diabetes causes insulin resistance and endothelial dysfunction by increasing oxidative stress, and forming AGEs (Du et al., 2001; Muniyappa et al., 2007). Compared with the harmful effects of the PI3K/Akt/eNOS pathway, hyperglycemia can enhance the secretion of endothelial endothelin (ET-1), thereby changing the balance between NO and ET-1, which is beneficial to endothelial dysfunction (Muniyappa et al., 2008). *In vivo*, acute intravenous glucosamine causes metabolic insulin resistance and impairs insulin-mediated increase in femoral arterial blood flow and capillary replacement (Wallis et al., 2005).

Elevated circulating markers of inflammation characterize insulin resistance and endothelial dysfunction. The most widely studied proinflammatory cytokine related to insulin resistance is IKK β , TNF- α , and C-Jun N-terminal kinase (JNK) (Kim et al., 2005). IL-1 β receptor-associated kinase was activated by TNF- α , which stimulated serine phosphorylation of IRS-1/2 directly or indirectly. It compounds the decreasing activation of PI3K/Akt/eNOS in endothelial cells (Zhang et al., 2003; Anderson et al., 2004; Eringa et al., 2004; Gustafson et al., 2007). TNF- α can also increase ET-1 secretion in a MAPK-dependent fashion (Sury et al., 2006). Another cytokine, IL-6, was elevated and can inhibit increased eNOS activity and increased NO production stimulated by insulin in endothelial cells (Andreozzi et al., 2007). C-reactive protein (CRP), which served as a marker of inflammation, was proved to inhibit insulin-induced NO production in endothelial cells by inhibiting the PI3K/Akt/eNOS pathway (Schwartz et al., 2007; Xu et al., 2007).

In vascular smooth muscle and vascular smooth muscle cells (VSMC) – Endothelial NO diffuses into adjacent VSMC, where it stimulates guanosine cyclase. The elevated levels of cGMP can give rise to vasorelaxation. NO can also modulate vascular tone by reducing monocyte adhesion, increasing the production of proinflammatory cytokines, attenuating the expression of vascular cell adhesion molecules, limiting the recruitment of leukocytes, inhibiting VSMC, avoiding platelet aggregation, and opposing apoptosis (Herman and Moncada, 2005). The increased blood flows further facilitate the glucose uptake by provoking insulin-responsive GLUT4 in PI3K-dependent metabolic actions (Zeng and Quon, 1996; Vincent et al., 2004). In human cells, three IRS subtypes (IRS-1, -2, and -4) have been identified to have a distinct role based on cell type and metabolic status. The function of IRS-1 is related to the insulin secretion mechanism, which plays a vital role in skeletal muscle (Taguchi and White, 2008). Animal models showed retarded growth of IRS-1 knockout mice especially skeletal muscle (Withers et al., 1998). Glucosamine can impair insulin and stimulate the uptake of glucose in skeletal muscle and NO production. It can also increase the blood flow in femoral arterial and capillary recruitment (Wallis et al., 2005).

In the kidney – Reduced insulin sensitivity leads to compensatory hyperinsulinemia. Maintaining normal blood sugar, glucose is taken up by skeletal muscle and adipose cells.

Compensatory hyperinsulinemia with insulin resistance reinforced the salt absorption of the proximal tubule, which may lead to salt overload and HTN (Soleimani, 2015). The sodium-chloride cotransporter (NCC) has the function of reabsorbing sodium and chloride ions from the tubular fluid. Insulin promotes the resorption of chloride ions. The effect of insulin on IRS1-mediated adipocyte glucose uptake is severely attenuated, and the effect on IRS2-mediated proximal renal tubular salt reabsorption remains (Zheng et al., 2005). The kidney tubules are significant for maintaining vascular flow and blood pressure because of the sodium reabsorption regulation. Insulin was proved to promote salt reabsorption. Insulin stimulates the Na⁺/H⁺ exchanger type 3 (NHE3) on the apical membrane and upregulates the sodium-bicarbonate cotransporter (NBC1) on the basolateral membrane. The sodium and bicarbonate were reabsorbed. Insulin can also stimulate the Na-K-ATPase in the proximal tubule in the proximal tubule (Landsberg et al., 2013). In the thick ascending limb of Henle, insulin stimulates NaCl reabsorption by activating Na-K-2Cl cotransporters (NKCC2) and Na-K-ATPase (Horita et al., 2011). Insulin enhanced the epithelial sodium channel density in the distal nephron and the connecting tubule membrane (Landsberg et al., 2013). The accumulated reports showed that the stimulatory effect of insulin on with-no-lysine kinases (WNK), suggesting that sodium increases sodium reabsorption through sodium-chloride cotransporter in the distal nephron (Landsberg et al., 2013).

The Activation of Angiotensin II

DM-induced hyperglycemia can cause HTN by activating Angiotensin II (Ang II). Ang II is involved in the pathogenesis of insulin resistance through the induction of key signaling elements of the insulin AKT (also known as protein kinase B) pathway (Andreozzi et al., 2004). It also serves as an essential vasoconstrictor hormone in the renin-angiotensin system (RAS), where RAS is activated (Kobori et al., 2007). These findings suggested that the cross-action of insulin AKT and Ang II signaling pathways plays a significant role in the co-occurrence of DM and HTN. Ang II inhibits insulin metabolism signals and promotes insulin resistance by activating the mTOR/S6 kinase 1 (S6K1)-mediated IRS-1 serine phosphorylation (Pulakat et al., 2011). Ang II reduces glucose uptake by inhibiting IRS1 phosphorylation, inhibiting PI3-K function and reducing GLUT-4 to interfere with the insulin pathway (Manrique et al., 2009). Moreover, Ang II hinders the bioavailability of NO through NADPH oxidase activation and ROS generation, which impeding endothelium. And it can also enhance NF- κ B, which in turn promotes the production of TNF- α and IL-6 and adhesion molecule VCAM-1, regulating inflammation (Pueyo et al., 2000).

The Activation of the Sympathetic Nervous System

The activation of the sympathetic nervous system exerts a number of physiological responses either directly through stimulation of postganglionic sympathetic nerves localized in target organs or indirectly through the activation of powerful

humoral systems. The importance of sympathetic tone is readily acknowledged for blood pressure regulation and type 2 DM (Thorp and Schlaich, 2015). The sympathetic nervous system control over peripheral organs, including the liver, skeletal muscle, pancreas, and cardiovascular system, is perturbed, resulting in glucose disorder, insulin resistance, insulin secretion impairment, and blood pressure increase, which are predicted to chronically contribute to the development of DM and HTN. Otherwise, the RAS and inflammation activated by metabolites or insulin are demonstrated to increase the central sympathetic nervous system activity to elevate blood pressure.

Glutamate and glutamine, as common metabolic perturbations of both DM and HTN, are listed in **Table 1**. Previous research indicated that glutamate could penetrate the blood–brain barrier, excite the presympathetic neurons within the paraventricular nucleus, and increase the sympathetic outflow (Li et al., 2006). Glutamine abounds in the central nervous system, and its interstitial and cerebrospinal fluid concentration are at least one the order of magnitude higher than of any other amino acid. It is a major excitatory neurotransmitter in the vertebrate nervous system, and glutamatergic synaptic inputs innervate the presympathetic neurons located in the autonomic nucleus in the brain stem and hypothalamus. The effects of metabolites on brain regions involved in insulin and blood pressure regulation are a mechanism of DM that resulted in the pathogenesis of HTN.

The Energy Reprograming

It found that the commonality of DM and HTN among metabolites is limited. How they are different or more interestingly amalgamated in both disease phenotypes, which leads to an intermediate or tertiary state, should be explored. After summarizing the metabolic distribution in DM and HTN, amino acids, energy-related metabolites, lipids, and fatty acids were revealed to be made up the biggest percentage of the total disturbed metabolites and share a common biological function: provide energy. Here, we discussed the energy-provide metabolites transformation in the cardiac muscle and skeletal muscles.

Cardiac muscle – The transformation of cardiac function metabolites seems to disturb much more metabolites and affect the pathogenesis of HTN in type 2 DM. In the normal heart, carbohydrate and FFA oxidation mainly contribute to energy production. While type 2 DM dysregulated cardiac FFA oxidation and impaired glucose oxidation/uptake, other circulating substrates, such as ketones or BACCs, may become an alternative source of energy, which injured the heart and cause high blood pressure. Bedi et al. (2016) recently demonstrated that in the severely failing heart increased the utilization of ketone. Although the role of BCAA is less clear because of the diminishment of BCAA catabolism in heart failure, ketones and BCAAs can directly influence cardiac signaling processes. It may potentially exhibit additional beneficial effects on the heart. In the recent EMPA-REG OUTCOME trial, treatment with empagliflozin, it was observed the reduction of cardiovascular mortality and hospitalization for heart failure in patients with type 2 DM. The research that investigated the effect of empagliflozin on metabolism showed that it reduced the glucose and other sugars

in the serum and degraded FFAs, amino acids, and ketone with increased levels of acetyl- and propionyl carnitine.

Skeletal muscles – Similar to the heart muscle, skeletal muscles play key roles in the regulation of systemic energy homeostasis in metabolic responses to physical activity. Excess triglycerides, FFAs, and glucose, coupled with physical inactivity, perturb the metabolism in skeletal muscle. Skeletal muscle made an influence on energy homeostasis by changing the composition of slow and fast-twitch fiber types muscles, which differ in the composition of contractile proteins, oxidative capacity, and substrate preference for ATP production (Baskin et al., 2015). Fast-twitch fibers have a higher fatigability, higher strength of contraction, lower oxidative capacity, and a preference for glucose as a substrate for ATP production through anaerobic glycolysis. Slow-twitch myofibers have a high oxidative capacity and prefer fatty acids as substrate for ATP production, while fast-twitch fibers have a lower oxidative capacity and prefer glucose.

Muscle profoundly impacts systemic energy consumption. In the pathological state of DM, the energy reprogramming changes the metabolic function of the heart and then changes the cardiac output which affects blood pressure directly.

CONCLUSION AND PERSPECTIVES

Type 2 DM is known to be associated with HTN. The widespread of type 2 DM also poses many problems. The presence of type 2 DM increases the risk of HTN. When combined with DM, HTN has been shown to predict and promote increased risk for cardiovascular diseases, which is the leading cause of death in patients with DM. Metabolites reflect both the upstream input from the environment and the downstream output of the genome, making it possible to explore the interaction between genes and the environment. Focusing on the application of metabolomics seems to contribute to reveal the root cause of type 2 DM. Knowledge of the pathophysiological derangements involved in the occurrence of type 2 DM and HTN is critical for successful prevention and control solutions. In this review, metabolites perturbation and the underlying metabolic mechanism were summarized. Among the metabolites, amino acid, lipid metabolites, carnitines, bile acids, and other metabolites were elaborated. And the related metabolites resulted in insulin resistance, increased tissue inflammatory, ROS production, endothelial dysfunction, the distribution of the renin-angiotensin system, the activation of the sympathetic nervous system, and the energy reprogramming.

There were several limitations in the present review. First, the prior mechanism studies that are relevant to the thesis might be limited because of the scope of the HTN topic. The complex influence factors are involved in the endocrine system, nervous system, and immune system. Direct influences and feedback interaction conveyed by the bloodstream from one tissue to another exacerbate the complexity of the problem. The deep mechanism researches should continue to be followed up in the future. Second, the current review is focused on how perturbed metabolites in diabetes mellitus affect the pathogenesis of hypertension. A contextual focus on *vice-versa*

relations may need in-depth further exploration and contextual consideration.

With the development of informatics, integration of orthogonal biological approaches, and analytical technologies, it is of possibility to expand the application of metabolomics to understand the systemic function of metabolites. It seems to be promising to elaborate the mechanism in HTN in type 2 DM by regarding the metabolites as the beginning of the biological process and reveal the active role (Rinschen et al., 2019). With the review, the mechanism of HTN in type 2 DM may be investigated by gut microbial, inflammation, and energy metabolism processes.

Gut Microbial in HTN and Type 2 DM

Intestinal microbial populations contribute to energy collection, host metabolism, and disturbances in these population balances affect inflammation, glucose metabolic changes, and energy metabolomics. Furthermore, through diligent research efforts in gut microbial metabolites, the underlying mechanisms of type 2 DM and HTN are beginning to be elucidated. Microbial influenced metabolites were proved to link the microbiota and host blood pressure regulation (Shi et al., 2021). Microbial gene was proved to facilitate metabolites conversion by functional and genetic engineering studies. The microbial *porA* gene promotes phenylalanine change to phenylacetic acid, with the host generation fostering platelet responsiveness and thrombosis potential (Nemet et al., 2020). The *Casp1^{-/-}* microbiota reduced microbiota-derived anti-inflammatory SCFAs (Brandsma et al., 2019). The gut microbiota also proved to regulate blood glucose via modulating the enteric neurons (Matheis et al., 2020).

Inflammation in HTN With Type 2 DM

In this review, inflammation is proved to be a potential common mechanism of type 2 DM and HTN. It is widely acknowledged that inflammatory disorder is the main pathological process of many diseases (Hummasti and Hotamisligil, 2010). Indeed, subclinical chronic inflammation is a common feature in their natural course. The application and development of pro-resolution therapeutic strategies for treating inflammatory pathology could lead to the revolutionary management of human ailments. Fullerton and Gilroy (2016) highlighted strive to identify pathways that target diseases that involve inflammation. Age, as a risk factor of the inflammation, underlies type 2 DM and HTN (Yandrapalli et al., 2018). Elie Metchnikoff proposed that bacterial products activated phagocytes resulting in inflammation (Metchnikoff, 2003). Aging-associated microbiota was proved to promote inflammation

and reversing age-related microbiota variation for reducing inflammation and the accompanying morbidity in recent research (Thevaranjan et al., 2017). And the enhancement of autophagy and the normalization of mitochondrial function can alleviate aging-associated inflammation (Bharath et al., 2020). Novel insights into the cellular processes especially the metabolic reprogramming of immune cells driving inflammation are more or less established (Pålsson-McDermott and O'Neill, 2020). Adaptive immune memory, macrophage iron handling, epigenetic regulation of immunity, and Th2 immunity can directly affect immune function and ultimately systemic metabolism (Caslin and Hasty, 2019). The mechanism by which DM and HTN may synergistically induce macrophage metabolic dysfunction, especially during cardiac remodeling, is not fully understood (Mouton et al., 2020). It will provoke a re-think of chronic inflammation in HTN and type 2 DM therapeutically.

Energy Metabolism Switch of the Immune System in HTN With Type 2 DM

The idea that cellular metabolism affects immune function is currently being pursued. The physical activities and cellular functions related to energy were decreased owing to unmatched energy demand and supply. In return, the metabolic shift was accelerated and forming a vicious cycle. Reprogramming of energy metabolism causes a shift in energy metabolism from oxidative metabolism to glycolysis, which promotes the prevalence of aging-associated diseases, such as type 2 DM and HTN (Feng et al., 2016). These findings provide a reference for future research on the pathogenesis of type 2 DM and diabetic complications.

AUTHOR CONTRIBUTIONS

ZN and ZS wrote the paper. CW, SP, and XW revised the paper. ZL and AL designed the outline of the paper. All authors contributed to the article and approved the submitted version.

FUNDING

This work was supported by the National Natural Science Foundation Committee of China (Project Nos. 82003950 and 81873009) and the Central Research Institutes of Basic Research and Public Service Special Operations (Project Nos. YZ-202045 and YZ-1912).

REFERENCES

- Aa, J., Wang, G., Hao, H., Huang, Q., Lu, Y., Yan, B., et al. (2010). Differential regulations of blood pressure and perturbed metabolism by total ginsenosides and conventional antihypertensive agents in spontaneously hypertensive rats. *Acta Pharmacol. Sin.* 31, 930–937. doi: 10.1038/aps.2010.86
- Acevedo-Calado, M., James, E. A., Morran, M. P., Pietropaolo, S. L., Ouyang, Q., Arribas-Layton, D., et al. (2017). Identification of unique antigenic determinants in the amino terminus of IA-2 (ICA512) in childhood and adult autoimmune diabetes: new biomarker development. *Diabetes Care* 40, 561–568. doi: 10.2337/dc16-1527
- Akira, K., Imachi, M., and Hashimoto, T. (2005). Investigations into biochemical changes of genetic hypertensive rats using ¹H nuclear magnetic resonance-based metabolomics. *Hypertens. Res.* 28, 425–430. doi: 10.1291/hypres.28.425
- Akira, K., Masu, S., Imachi, M., Mitome, H., Hashimoto, M., and Hashimoto, T. (2008). ¹H NMR-based metabolomic analysis of urine from young spontaneously hypertensive rats. *J. Pharm. Biomed. Anal.* 46, 550–556. doi: 10.1016/j.jpba.2007.11.017

- Allalou, A., Nalla, A., Prentice, K. J., Liu, Y., Zhang, M., Dai, F. F., et al. (2016). A predictive metabolic signature for the transition from gestational diabetes mellitus to type 2 diabetes. *Diabetes* 65, 2529–2539. doi: 10.2337/db15-1720
- Alston, C. L., Rocha, M. C., Lax, N. Z., Turnbull, D. M., and Taylor, R. W. (2017). The genetics and pathology of mitochondrial disease. *J. Pathol.* 241, 236–250. doi: 10.1002/path.4809
- Anderson, H. D. I., Rahmutula, D., and Gardner, D. G. (2004). Tumor necrosis factor- α inhibits endothelial nitric-oxide synthase gene promoter activity in bovine aortic endothelial cells. *J. Biol. Chem.* 279, 963–969. doi: 10.1074/jbc.M309552200
- Andreozzi, F., Laratta, E., Procopio, C., Hribal, M. L., Sciacqua, A., Perticone, M., et al. (2007). Interleukin-6 impairs the insulin signaling pathway, promoting production of nitric oxide in human umbilical vein endothelial cells. *Mol. Cell. Biol.* 27, 2372–2383. doi: 10.1128/MCB.01340-06
- Andreozzi, F., Laratta, E., Sciacqua, A., Perticone, F., and Sesti, G. (2004). Angiotensin II impairs the insulin signaling pathway promoting production of nitric oxide by inducing phosphorylation of insulin receptor substrate-1 on Ser312 and Ser616 in human umbilical vein endothelial cells. *Circ. Res.* 94, 1211–1218. doi: 10.1161/01.RES.0000126501.34994.96
- Arkan, M. C., Hevener, A. L., Greten, F. R., Maeda, S., Li, Z.-W., Long, J. M., et al. (2005). IKK- β links inflammation to obesity-induced insulin resistance. *Nat. Med.* 11, 191–198. doi: 10.1038/nm1185
- Askarpour, M., Hadi, A., Bozorg, A. D. K., Sadeghi, O., Sheikhi, A., Kazemi, M., et al. (2019). Effect of L-carnitine supplementation on blood pressure: a systematic review and meta-analysis of randomized controlled trials. *J. Hum. Hypertens.* 33, 725–734. doi: 10.1038/s41371-019-0248-1
- Bai, Q., Peng, B., Wu, X., Cao, Y., Sun, X., Hong, M., et al. (2018). Metabolomic study for essential hypertension patients based on dried blood spot mass spectrometry approach. *IUBMB Life* 70, 777–785. doi: 10.1002/iub.1885
- Baskin, K. K., Winders, B. R., and Olson, E. N. (2015). Muscle as “mediator” of systemic metabolism. *Cell Metab.* 21, 237–248. doi: 10.1016/j.cmet.2014.12.021
- Bedi, L. C. Jr., Snyder, N. W., Brandimarto, J., Aziz, M., Mesaros, C., Worth, A. J., et al. (2016). Evidence for intramyocardial disruption of lipid metabolism and increased myocardial ketone utilization in advanced human heart failure. *Circulation* 133, 706–716. doi: 10.1161/CIRCULATIONAHA.115.017545
- Bharath, L. P., Agrawal, M., McCambridge, G., Nicholas, D. A., Hasturk, H., Liu, J., et al. (2020). Metformin enhances autophagy and normalizes mitochondrial function to alleviate aging-associated inflammation. *Cell Metab.* 32, 44–55. doi: 10.1016/j.cmet.2020.04.015
- Bonetti, P. O., Lerman, L., and Lerman, A. (2003). Endothelial dysfunction: a marker of atherosclerotic risk. *Arterioscler. Thromb. Vasc. Biol.* 23, 168–175. doi: 10.1161/01.ATV.0000051384.43104.FC
- Brandsma, E., Kloosterhuis, N. J., Koster, M., Dekker, D. C., and Gijbels, M. J. J., Velden, S. v. d., et al. (2019). A proinflammatory gut microbiota increases systemic inflammation and accelerates atherosclerosis. *Circ. Res.* 124, 94–100. doi: 10.1161/CIRCRESAHA.118.313234
- Brindle, J. T., Nicholson, J. K., Schofield, P. M., Grainger, D. J., and Holmes, E. (2003). Application of chemometrics to 1H NMR spectroscopic data to investigate a relationship between human serum metabolic profiles and hypertension. *Analyst* 128, 32–36. doi: 10.1039/b209155k
- Brufau, G., Bahr, M. J., Staels, B., Claudel, T., Ockenga, J., Böker, K. H., et al. (2010). Plasma bile acids are not associated with energy metabolism in humans. *Nutr. Metab. (Lond.)* 7:73. doi: 10.1186/1743-7075-7-73
- Bueno, R., de Sotomayor, M. A., Perez-Guerrero, C., Gomez-Amores, L., Vazquez, C. M., and Dolores Herrera, M. (2005). L-carnitine and propionyl-L-carnitine improve endothelial dysfunction in spontaneously hypertensive rats: different participation of NO and COX-products. *Life Sci.* 77, 2082–2097. doi: 10.1016/j.lfs.2005.01.035
- Bugger, H., and Abel, E. D. (2014). Molecular mechanisms of diabetic cardiomyopathy. *Diabetologia* 57, 660–671. doi: 10.1007/s00125-014-3171-6
- Bujak, R., Yumba-Mpanga, A., Struck-Lewicka, W., Kordalewska, M., Polonis, K., Patejko, M., et al. (2018). Untargeted metabolomics provides insight into mechanisms underlying resistant hypertension. *Curr. Med. Chem.* 25, 1–12. doi: 10.2174/0929867324666171006122656
- Calvani, M., Reda, E., and Arrighi-Martelli, E. (2000). Regulation by carnitine of myocardial fatty acid and carbohydrate metabolism under normal and pathological condition. *Basic Res. Cardiol.* 95, 75–83. doi: 10.1007/s003950050167
- Cardinali, D. P., Cano-Barquilla, P., Jiménez-Ortega, V., and Esquifino, A. (2011). Melatonin and the metabolic syndrome: physiopathologic and therapeutic implications. *Neuroendocrinology* 93, 133–142. doi: 10.1159/000324699
- Caslin, H. L., and Hasty, A. H. (2019). Extrinsic and intrinsic immunometabolism converge: perspectives on future research and therapeutic development for obesity. *Curr. Obes. Rep.* 8, 210–219. doi: 10.1007/s13679-019-00344-2
- Chen, A., Mumick, S., Zhang, C., Lamb, J., Dai, H., Weingarh, D., et al. (2005). Diet induction of monocyte chemoattractant protein-1 and its impact on obesity. *Obes. Res.* 13, 1311–1320. doi: 10.1038/oby.2005.159
- Cheung, B. M. Y., and Li, C. (2012). Diabetes and hypertension: is there a common metabolic pathway? *Curr. Atheroscler. Rep.* 14, 160–166. doi: 10.1007/s11883-012-0227-2
- Cooper-DeHoff, R. M., Hou, W., Weng, L., Baillie, R. A., Beitelshes, A. L., Gong, Y., et al. (2014). Is diabetes mellitus-linked amino acid signature associated with β -blocker-induced impaired fasting glucose. *Circ. Cardiovasc. Genet.* 7, 199–205. doi: 10.1161/CIRCGENETICS.113.000421
- de Mello, V. D., Paananen, J., Lindström, J., Lankinen, M. A., Shi, L., Kuusisto, J., et al. (2017). Indolepropionic acid and novel lipid metabolites are associated with a lower risk of type 2 diabetes in the Finnish diabetes prevention study. *Sci. Rep.* 7, 46337–46348. doi: 10.1038/srep46337
- Dietrich, S., Floegel, A., Weikert, C., Prehn, C., Adamski, J., Pischon, T., et al. (2016). Identification of serum metabolites associated with incident hypertension in the European prospective investigation into cancer and nutrition-Potsdam study. *Hypertension* 68, 471–477. doi: 10.1161/HYPERTENSIONAHA.116.07292
- Dodd, D., Spitzer, M. H., Treuren, W. V., Merrill, B. D., Hryckowian, A. J., Higginbottom, S. K., et al. (2017). A gut bacterial pathway metabolizes aromatic amino acids into nine circulating metabolites. *Nature* 551, 648–652. doi: 10.1038/nature24661
- Du, X., Edelstein, D., Dimmeler, S., Ju, Q., Sui, C., and Brownlee, M. (2001). Hyperglycemia inhibits endothelial nitric oxide synthase activity by posttranslational modification at the Akt site. *J. Clin. Invest.* 108, 1341–1348. doi: 10.1172/JCI11235
- Du, X., Edelstein, D., Obici, S., Higham, N., Zou, M., and Brownlee, M. (2006). Insulin resistance reduces arterial prostacyclin synthase and eNOS activities by increasing endothelial fatty acid oxidation. *J. Clin. Invest.* 116, 1071–1080. doi: 10.1172/JCI23354
- Dugan, L. L., You, Y.-H., Ali, S. S., Diamond-Stanic, M., Miyamoto, S., DeCleva, A.-E., et al. (2013). AMPK dysregulation promotes diabetes-related reduction of superoxide and mitochondrial function. *J. Clin. Invest.* 123, 4888–4899. doi: 10.1172/JCI66218
- Eringa, E. C., Stehouwer, C. D. A., van Amerongen, G. P. N., Ouweland, L., Westerhof, N., and Sipkema, P. (2004). Vasoconstrictor effects of insulin in skeletal muscle arterioles are mediated by ERK1/2 activation in endothelium. *Am. J. Physiol. Heart Circ. Physiol.* 287, H2043–H2048. doi: 10.1152/ajpheart.00067.2004
- Fall, T., Salihovic, S., Brandmaier, S., Nowak, C., Ganna, A., Gustafsson, S., et al. (2016). Non-target metabolomics combined with genetic analyses identifies bile acid synthesis and phospholipid metabolism as being associated with incident type 2 diabetes. *Diabetologia* 59, 2114–2124. doi: 10.1007/s00125-016-4041-1
- Fanelli, C., Calderone, S., Epifano, L., Vincenzo, A. D., Modarelli, F., Pampanelli, S., et al. (1993). Demonstration of a critical role for free fatty acids in mediating counterregulatory stimulation of gluconeogenesis and suppression of glucose utilization in humans. *J. Clin. Invest.* 92, 1617–1622. doi: 10.1172/JCI116746
- Feng, Z., Hanson, R. W., Berger, N. A., and Trubitsyn, A. (2016). Reprogramming of energy metabolism as a driver of aging. *Oncotarget* 7, 15410–15420. doi: 10.18632/oncotarget.7645
- Ferrannini, E., Natali, A., Camastra, S., Nannipieri, M., Mari, A., Adam, K.-P., et al. (2013). Early metabolic markers of the development of dysglycemia and type 2 diabetes and their physiological significance. *Diabetes* 62, 1730–1737. doi: 10.2337/db12-0707
- Fiehn, O., Garvey, W. T., Newman, J. W., Lok, K. H., Hoppel, C. L., and Adams, S. H. (2010). Plasma metabolomic profiles reflective of glucose homeostasis in non-diabetic and type 2 diabetic obese African-American women. *PLoS One* 5:e15234. doi: 10.1371/journal.pone.0015234
- Filla, L. A., Yuan, W., Feldman, E. L., Li, S., and Edwards, J. L. (2014). Global metabolomic and isobaric tagging capillary liquid chromatography-tandem

- mass spectrometry approaches for uncovering pathway dysfunction in diabetic mouse aorta. *J. Proteome Res.* 13, 6121–6134. doi: 10.1021/pr501030e
- Floegel, A., Stefan, N., Yu, Z., Mühlenbruch, K., Drogan, D., Joost, H.-G., et al. (2013). Identification of serum metabolites associated with risk of type 2 diabetes using a targeted metabolomic approach. *Diabetes* 62, 639–648. doi: 10.2337/db12-0495
- Flores-Guerrero, J. L., Groothof, D., Connelly, M. A., Otvos, J. D., Bakker, S. J. L., and Dullaart, R. P. F. (2019). Concentration of branched-chain amino acids is a strong risk marker for incident hypertension. *Hypertension* 74, 1428–1435. doi: 10.1161/HYPERTENSIONAHA.119.13735
- Forouhi, N. G., and Wareham, N. J. (2014). Epidemiology of diabetes. *Medicine* 42, 698–702. doi: 10.1016/j.mpmed.2014.09.007
- Friedrich, N., Budde, K., Suhre, K., Völker, U., John, U., Felix, S. B., et al. (2015). Sex differences in urine metabolites related with risk of diabetes using NMR spectroscopy: results of the study of health in pomerania. *Metabolomics* 11, 1405–1415. doi: 10.1007/s11306-015-0795-6
- Frohnert, B. I., and Rewers, M. J. (2016). Metabolomics in childhood diabetes. *Pediatr. Diabetes* 17, 3–14. doi: 10.1111/pedi.12323
- Fujiwara, M., Arifuku, K., Ando, I., and Nemoto, T. (2005). Pattern recognition analysis for classification of hypertensive model rats and diurnal variation using ¹H-NMR spectroscopy of urine. *Anal. Sci.* 21, 1259–1262. doi: 10.2116/analsci.21.1259
- Fullerton, J. N., and Gilroy, D. W. (2016). Resolution of inflammation: a new therapeutic frontier. *Nat. Rev. Drug Discov.* 15, 551–567. doi: 10.1038/nrd.2016.39
- Gaetano, A. D., Mingrone, G., Castagneto, M., and Calvani, M. (1999). Carnitine increases glucose disposal in humans. *J. Am. Coll. Nutr.* 18, 289–295. doi: 10.1080/07315724.1999.10718866
- Ghosh, A., Gao, L., Thakur, A., Parco, M. S., and Lai, C. W. K. (2017). Role of free fatty acids in endothelial dysfunction. *J. Biomed. Sci.* 24:50. doi: 10.1186/s12929-017-0357-5
- Gonzalez-Calero, L., Martin-Lorenzo, M., Martínez, P. J., Baldan-Martin, M., Ruiz-Hurtado, G., Segura, J., et al. (2016). Hypertensive patients exhibit an altered metabolism. A specific metabolite signature in urine is able to predict albuminuria progression. *Transl. Res.* 178, 25–37. doi: 10.1016/j.trsl.2016.07.003
- González-Núñez, D., Claria, J., Rivera, F., and Poch, E. (2000). Increased levels of 12(S)-HETE in patients with essential hypertension. *Hypertension* 37, 334–338. doi: 10.1161/01.hyp.37.2.334
- Grapov, D., Johannes, F., Hwang, J., Poudel, A., Jo, J., Periwal, V., et al. (2015). Diabetes associated metabolomic perturbations in NOD mice. *Metabolomics* 11, 425–437. doi: 10.1007/s11306-014-0706-2
- Gu, Y., Wang, X., Li, J., Zhang, Y., Zhong, H., Liu, R., et al. (2017). Analyses of gut microbiota and plasma bile acids enable stratification of patients for antidiabetic treatment. *Nat. Commun.* 8, 1785–1796. doi: 10.1038/s41467-017-01682-2
- Guan, M. M., Xie, L. Y., Diao, C. F., Wang, N., Hu, W. Y., Zheng, Y. Q., et al. (2013). Systemic perturbations of key metabolites in diabetic rats during the evolution of diabetes studied by urine metabolomics. *PLoS One* 8:e60409. doi: 10.1371/journal.pone.0060409
- Gustafson, B., Hammarstedt, A., Andersson, C. X., and Smith, U. (2007). Inflamed adipose tissue: a culprit underlying the metabolic syndrome and atherosclerosis. *Arterioscler. Thromb. Vasc. Biol.* 27, 2276–2283. doi: 10.1161/ATVBAHA.107.147835
- Hausler, R. A., Astiarraga, B., Camastra, S., Accili, D., and Ferrannini, E. (2013). Human insulin resistance is associated with increased plasma levels of 12 α -hydroxylated bile acids. *Diabetes* 62, 184–191. doi: 10.2337/db13-0639
- Heinonen, S., Buzkova, J., Muniandy, M., Kaksonen, R., Ollikainen, M., Ismail, K., et al. (2015). Impaired mitochondrial biogenesis in adipose tissue in acquired obesity. *Diabetes* 64, 3135–3145. doi: 10.2337/db14-1937
- Herman, A. G., and Moncada, S. (2005). Therapeutic potential of nitric oxide donors in the prevention and treatment of atherosclerosis. *Eur. Heart J.* 26, 1945–1955. doi: 10.1093/eurheartj/ehi333
- Hernández-Alvarez, M. I., Díaz-Ramos, A., Berdasco, M., Cobb, J., Planet, E., Cooper, D., et al. (2017). Early-onset and classical forms of type 2 diabetes show impaired expression of genes involved in muscle branched-chain amino acids metabolism. *Sci. Rep.* 7, 13850–13861. doi: 10.1038/s41598-017-14120-6
- Ho, J. E., Larson, M. G., Vasan, R. S., Ghorbani, A., Cheng, S., Rhee, E. P., et al. (2013). Metabolite profiles during oral glucose challenge. *Diabetes* 62, 2689–2698. doi: 10.2337/db12-0754
- Hofmann, A. F. (1999). The continuing importance of bile acids in liver and intestinal disease. *Arch. Intern. Med.* 159, 2647–2658. doi: 10.1001/archinte.159.22.2647
- Holmes, E., Loo, R. L., Stamler, J., Bictash, M., Yap, I. K. S., Chan, Q., et al. (2008). Human metabolic phenotype diversity and its association with diet and blood pressure. *Nature* 453, 396–400. doi: 10.1038/nature06882
- Horita, S., Seki, G., Yamada, H., Suzuki, M., Koike, K., and Fujita, T. (2011). Insulin resistance, obesity, hypertension, and renal sodium transport. *Int. J. Hypertens.* 2011, 391762–391769. doi: 10.4061/2011/391762
- Huffman, K. M., Slentz, C. A., Bateman, L. A., Thompson, D., Muehlbauer, M. J., Bain, J. R., et al. (2011). Exercise-induced changes in metabolic intermediates, hormones, and inflammatory markers associated with improvements in insulin sensitivity. *Diabetes Care* 34, 174–176. doi: 10.2337/dc10-0709
- Hummasti, S., and Hotamisligil, G. S. (2010). Endoplasmic reticulum stress and inflammation in obesity and diabetes. *Circ. Res.* 107, 579–591. doi: 10.1161/CIRCRESAHA.110.225698
- Hwang, G. S., Yang, J. Y., Ryu, D. H., and Kwon, T. H. (2010). Metabolic profiling of kidney and urine in rats with lithium-induced nephrogenic diabetes insipidus by (1)H-NMR-based metabolomics. *Am. J. Physiol. Ren. Physiol.* 298, F461–F470. doi: 10.1152/ajprenal.00389.2009
- Iemitsu, M., Miyauchi, T., Maeda, S., Sakai, S., Fujii, N., Miyazaki, H., et al. (2003). Cardiac hypertrophy by hypertension and exercise training exhibits different gene expression of enzymes in energy metabolism. *Hypertens. Res.* 26, 829–837. doi: 10.1291/hyres.26.829
- Johnson, C. H., Ivanisevic, J., and Siuzdak, G. (2016). Metabolomics: beyond biomarkers and towards mechanisms. *Nat. Rev. Mol. Cell Biol.* 17, 451–459. doi: 10.1038/nrm.2016.25
- KanterEmail, M., Uysal, H., Karaca, T., and Sagmanligil, H. O. (2006). Depression of glucose levels and partial restoration of pancreatic beta-cell damage by melatonin in streptozotocin-induced diabetic rats. *Arch. Toxicol.* 80, 362–369. doi: 10.1007/s00204-005-0055-z
- Kappel, B. A., Lehrke, M., Schütt, K., Artati, A., Adamski, J., Leberher, C., et al. (2017). Effect of empagliflozin on the metabolic signature of patients with type 2 diabetes mellitus and cardiovascular disease. *Circulation* 136, 969–972. doi: 10.1161/CIRCULATIONAHA.117.029166
- Khitan, Z., and Kim, D. H. (2013). Fructose: a key factor in the development of metabolic syndrome and hypertension. *J. Nutr. Metab.* 2013, 1–12. doi: 10.1155/2013/682673
- Kim, F., Tysseling, K. A., Rice, J., Pham, M., Haji, L., Gallis, B. M., et al. (2005). Free fatty acid impairment of nitric oxide production in endothelial cells is mediated by IKK β . *Arterioscler. Thromb. Vasc. Biol.* 25, 989–994. doi: 10.1161/01.ATV.0000160549.60980.a8
- Kitai, T., and Tang, W. H. W. (2017). The role and impact of gut microbiota in cardiovascular disease. *Rev. Esp. Cardiol.* 70, 799–800. doi: 10.1016/j.rec.2017.04.007
- Kobori, H., Nangaku, M., Navar, L. G., and Nishiyama, A. (2007). The intrarenal renin-angiotensin system: from physiology to the pathobiology of hypertension and kidney disease. *Pharmacol. Rev.* 59, 251–287. doi: 10.1124/pr.59.3.3
- Koeth, R. A., Wang, Z., Levison, B. S., Buffa, J. A., Org, E., Sheehy, B. T., et al. (2013). Intestinal microbiota metabolism of L-carnitine, a nutrient in red meat, promotes atherosclerosis. *Nat. Med.* 19, 576–585. doi: 10.1038/nm.3145
- Konstantinova, S. V., Tell, G. S., Vollset, S. E., Nygård, O., Bleie, Ø., and Ueland, P. M. (2008). Divergent associations of plasma choline and betaine with components of metabolic syndrome in middle age and elderly men and women. *J. Nutr.* 138, 914–920. doi: 10.1093/jn/138.5.914
- Kottronen, A., Velagapudi, V. R., Yetukrti, L., Makkonen, J., Taskinen, M. R., Orešić, M., et al. (2009). Serum saturated fatty acids containing triacylglycerols are better markers of insulin resistance than total serum triacylglycerol concentrations. *Diabetologia* 52, 684–690. doi: 10.1007/s00125-009-1282-2
- Landsberg, L., Aronne, L. J., Beilin, L. J., Burke, V., Igel, L. I., Lloyd-Jones, D., et al. (2013). Obesity-related hypertension: pathogenesis, cardiovascular risk, and treatment: a position paper of The Obesity Society and the American Society of Hypertension. *J. Clin. Hypertens.* 15, 14–33. doi: 10.1111/jch.12049
- Lastra, G., Syed, S., Kurukulasuriya, L. R., Manrique, C., and Sowers, J. R. (2014). Type 2 diabetes mellitus and hypertension: an update. *Endocrinol. Metab. Clin. N. Am.* 43, 103–122. doi: 10.1016/j.ecl.2013.09.005
- Lazar, A. G., Romanciuc, F., Socaci, M. A., and Socaci, C. (2015). Bioinformatics tools for metabolomic data processing and analysis using untargeted liquid

- chromatography couple with mass spectrometry. *Bull. UASVM Ani. Sci. Biotech.* 72, 103–115. doi: 10.15835/buasvmcn-asb:11536
- Li, Y. F., Jackson, K. L., Stern, J. E., Rabaler, B., and Patal, K. P. (2006). Interaction between glutamate and GABA systems in the integration of sympathetic outflow by the paraventricular nucleus of the hypothalamus. *Am. J. Physiol. Heart Circ. Physiol.* 291, H2847–H2856. doi: 10.1152/ajpheart.00625.2005
- Li, B., Selmi, C., Tang, R., Gershwin, M., and Ma, X. (2018a). The microbiome and autoimmunity: a paradigm from the gut-liver axis. *Cell. Mol. Immunol.* 15, 595–609. doi: 10.1038/cmi.2018.7
- Li, M., Wang, X., Aa, J., Qin, W., Zha, W., Ge, Y., et al. (2013). GC/TOFMS analysis of metabolites in serum and urine reveals metabolic perturbation of TCA cycle in db/db mice involved in diabetic nephropathy. *Am. J. Physiol. Ren. Physiol.* 304, F1317–F1324. doi: 10.1152/ajprenal.00536.2012
- Li, X. S., Wang, Z., Cajka, T., Buffa, J. A., Nemet, I., Hurd, A. G., et al. (2018b). Untargeted metabolomics identifies trimethyllysine, a TMAO-producing nutrient precursor, as a predictor of incident cardiovascular disease risk. *JCI Insight* 3, e99096–e99113. doi: 10.1172/jci.insight.99096
- Liu, Y., Chen, T., Qiu, Y., Cheng, Y., Cao, Y., Zhao, A., et al. (2011). An ultrasonication-assisted extraction and derivatization protocol for GC/TOFMS-based metabolite profiling. *Anal. Bioanal. Chem.* 400, 1405–1417. doi: 10.1007/s00216-011-4880-z
- Liu, A., Chu, Y., Wang, X., Yu, R., Jiang, H., Li, Y., et al. (2018). Serum metabolomics study based on LC-MS and antihypertensive effect of *Uncaria* on spontaneously hypertensive rats. *Evid. Based Complement. Alternat. Med.* 2018:9281946. doi: 10.1155/2018/9281946
- Liu, R., Hong, J., Xu, X., Feng, Q., Zhang, D., Gu, Y., et al. (2017b). Gut microbiome and serum metabolome alterations in obesity and after weight-loss intervention. *Nat. Med.* 23, 859–868. doi: 10.1038/nm.4358
- Liu, J., Semiz, S., van der Lee, S. J., van der Spek, A., Verhoeven, A., van Klinken, J. B., et al. (2017a). Metabolomics based markers predict type 2 diabetes in a 14-year follow-up study. *Metabolomics* 13:104. doi: 10.1007/s11306-017-1239-2
- Liu, X., Wang, Y., Gao, R., Xing, Y., Li, X., and Wang, Z. (2017c). Serum metabolomic response to exercise training in spontaneously hypertensive rats. *J. Am. Soc. Hypertens.* 11, 428–436. doi: 10.1016/j.jash.2017.05.003
- Liu, L., Wang, M., Yang, X., Bi, M., Na, L., Niu, Y., et al. (2013). Fasting serum lipid and dehydroepiandrosterone sulfate as important metabolites for detecting isolated postchallenge diabetes: serum metabolomics via ultra-high-performance LC-MS. *Clin. Chem.* 59, 1338–1348. doi: 10.1373/clinchem.2012.200527
- Lu, Y., Jiye, A., Wang, G., Hao, H., Huang, Q., Yan, B., et al. (2008). Gas chromatography/time-of-flight mass spectrometry based metabonomic approach to differentiating hypertension- and age-related metabolic variation in spontaneously hypertensive rats. *Rapid Commun. Mass Spectrom.* 22, 2882–2888. doi: 10.1002/rcm.3670
- Mahony, S. M. O., Clarke, G., Borre, Y. E., Dinan, T. G., and Cryan, J. F. (2015). Serotonin, tryptophan metabolism and the brain-gut-microbiome axis. *Behav. Brain Res.* 277, 32–48. doi: 10.1016/j.bbr.2014.07.027
- Mäkinen, V.-P., Tnkkynen, T., Soininen, P., Peltola, T., Kangas, A. J., Forsblom, C., et al. (2012). Metabolic diversity of progressive kidney disease in 325 patients with type 1 diabetes (the FinnDiane Study). *J. Proteome Res.* 11, 1782–1790. doi: 10.1021/pr201036j
- Manrique, C., Lastra, G., Gardner, M., and Sowers, J. R. (2009). The renin angiotensin aldosterone system in hypertension: roles of insulin resistance and oxidative stress. *Med. Clin. North Am.* 93, 569–582. doi: 10.1016/j.mcna.2009.02.014
- Marasciulo, F. L., Montagnani, M., and Potenza, M. A. (2006). Endothelin-1: the yin and yang on vascular function. *Curr. Med. Chem.* 13, 1655–1665. doi: 10.2174/09298670677441968
- Martin-Lorenzo, M., Martinez, P. J., Baldan-Martin, M., Ruiz-Hurtado, G., Prado, J. C., Segura, J., et al. (2017). Citric acid metabolism in resistant hypertension underlying mechanisms and metabolic prediction of treatment response. *Hypertension* 70, 1049–1056. doi: 10.1161/HYPERTENSIONAHA.117.09819
- Matheis, P. A. M. F., Schneeberger, M., Kerner, Z., Jové, V., and Mucida, D. (2020). Microbiota-modulated CART⁺ enteric neurons autonomously regulate blood glucose. *Science* 370, 314–321. doi: 10.1126/science.abd6176
- Mazepa, R. C., Cuevas, M. J., Collado, P. S., and González-Gallego, J. (1999). Melatonin increases muscle and liver glycogen content in nonexercised and exercised rats. *Life Sci.* 66, 153–160. doi: 10.1016/S0024-3205(99)00573-1
- Mell, B., Jala, V. R., Mathew, A. V., Byun, J., Waghulde, H., Zhang, Y., et al. (2015). Evidence for a link between gut microbiota and hypertension in the Dahl rat. *Physiol. Genomics* 47, 187–197. doi: 10.1152/physiolgenomics.00136.2014
- Menni, C., Fauman, E., Erte, I., Perry, J. R., Kastenmuller, G., Shin, S. Y., et al. (2013). Biomarkers for type 2 diabetes and impaired fasting glucose using a nontargeted metabolomics approach. *Diabetes* 62, 4270–4276. doi: 10.2337/db13-0570
- Metchnikoff, É. (2003). *The Prolongation of Life: Optimistic Studies*. London: Nabu Press.
- Michaliszyn, S. F., Sjaarda, L. A., Mihalik, S. J., Lee, S., Bacha, F., Chace, D. H., et al. (2012). Metabolomic profiling of amino acids and β -cell function relative to insulin sensitivity in youth. *J. Clin. Endocrinol. Metab.* 97, E2119–E2124. doi: 10.1210/jc.2012-2170
- Mihalik, S. J., Michaliszyn, S. F., Heras, J. D. L., Bacha, F., Lee, S., Chace, D. H., et al. (2012). Metabolomic profiling of fatty acid and amino acid metabolism in youth with obesity and type 2 diabetes: evidence for enhanced mitochondrial oxidation. *Diabetes Care* 35, 605–611. doi: 10.2337/DC11-1577
- Mingrone, G. (2004). Carnitine in type 2 diabetes. *Ann. N. Y. Acad. Sci.* 1033, 99–107. doi: 10.1196/annals.1320.009
- Montagnani, M., Chen, H., Barr, V. A., and Quon, M. J. (2001). Insulin-stimulated activation of eNOS is independent of Ca^{2+} but requires phosphorylation by Akt at Ser(1179). *J. Biol. Chem.* 276, 30392–30398. doi: 10.1074/jbc.M103702200
- Montagnani, M., Golovchenko, I., Kim, I., Koh, G. Y., Goalstone, M. L., Mundhekar, A. N., et al. (2002). Inhibition of phosphatidylinositol 3-kinase enhances mitogenic actions of insulin in endothelial cells. *J. Biol. Chem.* 277, 1794–1799. doi: 10.1074/jbc.M103728200
- Monteiro, M. S., Carvalho, M., Bastos, M. L., and Guedes de Pinho, P. (2013). Metabolomics analysis for biomarker discovery: advances and challenges. *Curr. Med. Chem.* 20, 257–271. doi: 10.2174/092986713804806621
- Mouton, A. J., Li, X., Hall, M. E., and Hall, J. E. (2020). Obesity, hypertension, and cardiac dysfunction: novel roles of immunometabolism in macrophage activation and inflammation. *Circ. Res.* 126, 789–806. doi: 10.1161/CIRCRESAHA.119.312321
- Mukai, Y., Wang, C.-Y., Rikitake, Y., and Liao, J. K. (2007). Phosphatidylinositol 3-kinase/protein kinase Akt negatively regulates plasminogen activator inhibitor type 1 expression in vascular endothelial cells. *Am. J. Physiol. Heart Circ. Physiol.* 292, H1937–H1942. doi: 10.1152/ajpheart.00868.2006
- Muniyappa, R., Iantorno, M., and Quon, M. J. (2008). An integrated view of insulin resistance and endothelial dysfunction. *Endocrinol. Metab. Clin. N. Am.* 37, 685–711. doi: 10.1016/j.ecl.2008.06.001
- Muniyappa, R., Montagnani, M., Koh, K. K., and Quon, M. J. (2007). Cardiovascular actions of insulin. *Endocr. Rev.* 28, 463–491. doi: 10.1210/er.2007-0006
- Muoio, D. M., and Newgard, C. B. (2008). Molecular and metabolic mechanisms of insulin resistance and β -cell failure in type 2 diabetes. *Nat. Rev. Mol. Cell Biol.* 9, 193–205. doi: 10.1038/nrm2327
- Murfitt, S. A., Zacccone, P., Wang, X., Acharjee, A., Sawyer, Y., Koulman, A., et al. (2017). A metabolomics and lipidomics study of mouse models of type 1 diabetes highlights divergent metabolism in purine and tryptophan metabolism prior to disease on-set. *J. Proteome Res.* 17, 946–960. doi: 10.1021/acs.jproteome.7b00489
- Neis, E. P. J. G., Dejong, C. H. C., and Rensen, S. S. (2015). The role of microbial amino acid metabolism in host metabolism. *Nutrients* 7, 2930–2946. doi: 10.3390/nu7042930
- Nemet, I., Saha, P. P., Gupta, N., Zhu, W., Romano, K. A., Skye, S. M., et al. (2020). A cardiovascular disease-linked gut microbial metabolite acts via adrenergic receptors. *Cell* 180, 862–877. doi: 10.1016/j.cell.2020.02.016
- Newgard, C. B. (2012). Interplay between lipids and branched-chain amino acids in development of insulin resistance. *Cell Metab.* 15, 606–614. doi: 10.1016/j.cmet.2012.01.024
- Nicholson, J. K., Holmes, E., Kinross, J., Burcelin, R., Gibson, G., and Pettersson, W. J. S. (2012). Host-gut microbiota metabolic interactions. *Science* 336, 1262–1267. doi: 10.1126/science.1223813
- Nikolic, S. B., Edwards, L. M., Karpievitch, Y. V., Wilson, R., Horne, J., Adams, M. J., et al. (2016). Serum metabolic profile predicts adverse central

- haemodynamics in patients with type 2 diabetes mellitus. *Acta Diabetol.* 53, 367–375. doi: 10.1007/s00592-015-0802-4
- O'Connell, T. M. (2013). The complex role of branched chain amino acids in diabetes and cancer. *Meta* 3, 931–945. doi: 10.3390/metabo3040931
- Ordway, R. W., Singer, J. J., and Walsh, J. V. Jr. (1991). Direct regulation of ion channels by fatty acids. *Trends Neurosci.* 14, 96–100. doi: 10.1016/0166-2236(91)90069-7
- Palmer, N. D., Stevens, R. D., Antinozzi, P. A., Anderson, A., Bergman, R. N., Wagenknecht, L. E., et al. (2015). Metabolomic profile associated with insulin resistance and conversion to diabetes in the insulin resistance atherosclerosis study. *J. Clin. Endocrinol. Metab.* 100, E463–E468. doi: 10.1210/jc.2014-2357
- Pålsson-McDermott, E. M., and O'Neill, L. A. J. (2020). Targeting immunometabolism as an anti-inflammatory strategy. *Cell Res.* 30, 300–314. doi: 10.1038/s41422-020-0291-z
- Pedersen, H. K., Gudmundsdottir, V., Nielsen, H. B., Hyötyläinen, T., Nielsen, T., Jensen, B. A. H., et al. (2016). Human gut microbes impact host serum metabolome and insulin sensitivity. *Nature* 535, 376–381. doi: 10.1038/nature18646
- Pena, M. J., Heerspink, H. J. L., Hellemons, M. E., Friedrich, T., Dallmann, G., Lajer, M., et al. (2014). Urine and plasma metabolites predict the development of diabetic nephropathy in individuals with type 2 diabetes mellitus. *Diabet. Med.* 31, 1138–1147. doi: 10.1111/dme.12447
- Petrie, J. R., Guzik, T. J., and Touyz, R. M. (2018). Diabetes, hypertension, and cardiovascular disease: clinical insights and vascular mechanisms. *Can. J. Cardiol.* 34, 575–584. doi: 10.1016/j.cjca.2017.12.005
- Pinti, M. V., Fink, G. K., Hathaway, Q. A., Durr, A. J., Kunovac, A., and Hollander, J. M. (2019). Mitochondrial dysfunction in type 2 diabetes mellitus: an organ-based analysis. *Am. J. Physiol. Endocrinol. Metab.* 316, E268–E285. doi: 10.1152/ajpendo.00314.2018
- Pluznick, J. L. (2013). Renal and cardiovascular sensory receptors and blood pressure regulation. *Am. J. Physiol. Ren. Physiol.* 305, F439–F444. doi: 10.1152/ajprenal.00252.2013
- Polak-Iwaniuk, A., Harasim-Symbor, E., Golaszewska, K., and Chabowski, A. (2019). How hypertension affects heart metabolism. *Front. Physiol.* 10:435. doi: 10.3389/fphys.2019.00435
- Psichas, A., Sleeth, M., Murphy, K., Brooks, L., Bewick, G., Hanyaloglu, A., et al. (2015). The short chain fatty acid propionate stimulates GLP-1 and PYY secretion via free fatty acid receptor 2 in rodents. *Int. J. Obes.* 39, 424–429. doi: 10.1038/ijo.2014.153
- Pueyo, M. E., Gonzalez, W., Nicoletti, A., Savoie, F., Arnal, J.-F., and Michel, J.-B. (2000). Angiotensin II stimulates endothelial vascular cell adhesion molecule-1 via nuclear factor-kappaB activation induced by intracellular oxidative stress. *Arterioscler. Thromb. Vasc. Biol.* 20, 645–651. doi: 10.1161/01.ATV.20.3.645
- Pulakat, L., DeMarco, V. G., Whaley-Connell, A., and Sowers, J. R. (2011). The impact of overnutrition on insulin metabolic signaling in the heart and the kidney. *Cardiorenal Med.* 1, 102–112. doi: 10.1159/000327140
- Purnell, J. Q., Hokanson, J. E., Marcovina, S. M., Steffes, M. W., Cleary, P. A., and Brunzell, J. D. (1998). Effect of excessive weight gain with intensive therapy of type 1 diabetes on lipid levels and blood pressure: results from the DCCT. Diabetes control and complications trial. *JAMA* 280, 140–146. doi: 10.1001/jama.280.2.140
- Qi, Y., Aranda, J. M., Rodriguez, V., Raizada, M. K., and Pepine, C. J. (2015). Impact of antibiotics on arterial blood pressure in a patient with resistant hypertension - A case report. *Int. J. Cardiol.* 201, 157–158. doi: 10.1016/j.ijcard.2015.07.078
- Qiu, G., Zheng, Y., Wang, H., Sun, J., Ma, H., Xiao, Y., et al. (2016). Plasma metabolomics identified novel metabolites associated with risk of type 2 diabetes in two prospective cohorts of Chinese adults. *Int. J. Epidemiol.* 45, 1507–1516. doi: 10.1093/ije/dyw221
- Quan, X., Wang, J., Liang, C., Zheng, H., and Zhang, L. (2015). Melatonin inhibits tunicamycin-induced endoplasmic reticulum stress and insulin resistance in skeletal muscle cells. *Biochem. Biophys. Res. Commun.* 463, 1102–1107. doi: 10.1016/j.bbrc.2015.06.065
- Rajesh, M., Bátkai, S., Kechrid, M., Mukhopadhyay, P., Lee, W.-S., Horváth, B., et al. (2012). Cannabinoid 1 receptor promotes cardiac dysfunction, oxidative stress, inflammation, and fibrosis in diabetic cardiomyopathy. *Diabetes* 61, 716–727. doi: 10.2337/db11-0477
- Rewers, M. F. S. M., Selby, J., Howard, G., Jinagouda, S., Fahmi, S., Zaccaro, D., et al. (2004). Insulin resistance and hypertension. *Hypertension* 43, 1324–1331. doi: 10.3109/10641969909061017
- Rinschen, M. M., Ivanisevic, J., Giera, M., and Siuzdak, G. (2019). Identification of bioactive metabolites using activity metabolomics. *Nat. Rev. Mol. Cell Biol.* 20, 353–367. doi: 10.1038/s41580-019-0108-4
- Roman, R. J., and Fan, F. (2018). 20-HETE hypertension and beyond. *Hypertension* 72, 12–18. doi: 10.1161/HYPERTENSIONAHA.118.10269
- Rotroff, D., Shahin, M., Gurley, S., Zhu, H., Motsinger-Reif, A., Meisner, M., et al. (2015). Pharmacometabolomic assessments of atenolol and hydrochlorothiazide treatment reveal novel drug response phenotypes. *CPT Pharmacometrics Syst. Pharmacol.* 4, 669–679. doi: 10.1002/psp4.12017
- Ruiz-Canela, M., Guasch-Ferré, M., Toledo, E., Clish, C. B., Razquin, C., Liang, L., et al. (2018). Plasma branched chain/aromatic amino acids, enriched Mediterranean diet and risk of type 2 diabetes: case-cohort study within the PREDIMED trial. *Diabetologia* 61, 1560–1571. doi: 10.1007/s00125-018-4611-5
- Russell, D. W. (2003). The enzymes, regulation, and genetics of bile acid synthesis. *Annu. Rev. Biochem.* 72, 137–174. doi: 10.1146/annurev.biochem.72.121801.161712
- Salek, R. M., Maguire, M. L., Bentley, E., Rubtsov, D. V., Hough, T., Cheeseman, M., et al. (2007). A metabolomic comparison of urinary changes in type 2 diabetes in mouse, rat, and human. *Physiol. Genomics* 29, 99–108. doi: 10.1152/physiolgenomics.00194.2006
- Samuel, B. S., Shaito, A., Motoike, T., Rey, F. E., Backhed, F., Manchester, J. K., et al. (2008). Effects of the gut microbiota on host adiposity are modulated by the short-chain fatty-acid binding G protein-coupled receptor, Gpr41. *Proc. Natl. Acad. Sci. U. S. A.* 105, 16767–16772. doi: 10.1073/pnas.0808567105
- Savolainen, O., Fagerberg, B., Vendelbo Lind, M., Sandberg, A. S., Ross, A. B., and Bergström, G. (2017a). Biomarkers for predicting type 2 diabetes development-can metabolomics improve on existing biomarkers? *PLoS One* 12:e0177738. doi: 10.1371/journal.pone.0177738
- Savolainen, O., Lind, M. V., Bergström, G., Fagerberg, B., Sandberg, A.-S., and Ross, A. (2017b). Biomarkers of food intake and nutrient status are associated with glucose tolerance status and development of type 2 diabetes in older Swedish women. *Am. J. Clin. Nutr.* 106, 1302–1310. doi: 10.3945/ajcn.117.152850
- Sayin, S. I., Wahlström, A., Felin, J., Jäntti, S., Marschall, H.-U., Bamberg, K., et al. (2013). Gut microbiota regulates bile acid metabolism by reducing the levels of tauro-beta-muricholic acid, a naturally occurring FXR antagonist. *Cell Metab.* 17, 225–235. doi: 10.1016/j.cmet.2013.01.003
- Schutta, M. H. (2007). Diabetes and hypertension: epidemiology of the relationship and pathophysiology of factors associated with these comorbid conditions. *Can. J. Cardiol.* 2, 124–130. doi: 10.1016/j.cjca.2017.12.005
- Schwartz, R., Osborne-Lawrence, S., Hahner, L., Gibson, L. L., Gormley, A. K., Vongpatanasin, W., et al. (2007). C-reactive protein downregulates endothelial NO synthase and attenuates reendothelialization *in vivo* in mice. *Circ. Res.* 100, 1452–1459. doi: 10.1161/01.RES.0000267745.03488.47
- Sekhar, R. V., McKay, S. V., Patel, S. G., Guthikonda, A. P., Reddy, V. T., Balasubramanyam, A., et al. (2011). Glutathione synthesis is diminished in patients with uncontrolled diabetes and restored by dietary supplementation with cysteine and glycine. *Diabetes Care* 34, 162–167. doi: 10.2337/dc10-1006
- She, M., Deng, X., Guo, Z., Laudon, M., Hu, Z., Liao, D., et al. (2009). NEU-P11, a novel melatonin agonist, inhibits weight gain and improves insulin sensitivity in high-fat/high-sucrose-fed rats. *Pharmacol. Res.* 59, 248–253. doi: 10.1016/j.phrs.2009.01.005
- She, M., Hou, H., Wang, Z., Zhang, C., Laudon, M., and Yin, W. (2014). Melatonin rescues 3T3-L1 adipocytes from FFA-induced insulin resistance by inhibiting phosphorylation of IRS-1 on Ser307. *Biochimie* 103, 126–130. doi: 10.1016/j.biochi.2014.05.001
- Shi, H., Zhang, B., Abo-Hamzy, T., Nelson, J. W., Ambati, C. S. R., Petrosino, J. F., et al. (2021). Restructuring the gut microbiota by intermittent fasting lowers blood pressure. *Circ. Res.* 128, 1240–1254. doi: 10.1161/CIRCRESAHA.120.318155
- Shieh, J. M., Wu, H. T., Cheng, K. C., and Cheng, J. T. (2009). Melatonin ameliorates high fat diet-induced diabetes and stimulates glycogen synthesis via a PKCzeta-Akt-GSK3beta pathway in hepatic cells. *J. Pineal Res.* 47, 339–344. doi: 10.1111/j.1600-079X.2009.00720.x
- Shulaev, V. (2006). Metabolomics technology and bioinformatics. *Brief. Bioinform.* 7, 128–139. doi: 10.1093/bib/bbl012
- Soleimani, M. (2015). Insulin resistance and hypertension: new insights. *Kidney Int.* 87, 497–499. doi: 10.1038/ki.2014.392

- Sowers, J. R., Epstein, M., and Frohlich, E. D. (2001). Diabetes, hypertension and cardiovascular disease. *Hypertension* 37, 1053–1059. doi: 10.1161/01.HYP.37.4.1053
- Stančáková, A., Civelek, M., Saleem, N. K., Soininen, P., Kangas, A. J., Cederberg, H., et al. (2012). Hyperglycemia and a common variant of GSKR are associated with the levels of eight amino acids in 9369 finnish men. *Diabetes* 61, 1895–1902. doi: 10.2337/db11-1378
- Stanley, W. C., Lopaschuk, G. D., and McCormack, J. G. (1997). Regulation of energy substrate metabolism in the diabetic heart. *Cardiovasc. Res.* 34, 25–33. doi: 10.1016/S0008-6363(97)00047-3
- Suhre, K., Meisinger, C., Doring, A., Altmaier, E., Belcredi, P., Gieger, C., et al. (2010). Metabolic footprint of diabetes: a multiplatform metabolomics study in an epidemiological setting. *PLoS One* 5:e13953. doi: 10.1371/journal.pone.0013953
- Sury, M. D., Frese-Schaper, M., Mühlemann, M. K., Schulthess, F. T., Blasiga, I. E., Täuber, M. G., et al. (2006). Evidence that N-acetylcysteine inhibits TNF- α -induced cerebrovascular endothelin-1 upregulation via inhibition of mitogen- and stress-activated protein kinase. *Free Radic. Biol. Med.* 41, 1372–1383. doi: 10.1016/j.freeradbiomed.2006.07.016
- Taguchi, A., and White, M. F. (2008). Insulin-like signaling, nutrient homeostasis, and life span. *Annu. Rev. Physiol.* 70, 191–212. doi: 10.1146/annurev.physiol.70.113006.100533
- Tang, W. H. W., and Hazen, S. L. (2017). The gut microbiome and its role in cardiovascular diseases. *Curr. Opin. Cardiol.* 135, 1008–1010. doi: 10.1097/HCO.0000000000000445
- Tang, W., Zhang, B., Wang, H., Li, M., Wang, H., Liu, F., et al. (2019). Improved skeletal muscle energy metabolism relates to the recovery of β cell function by intensive insulin therapy in drug naïve type 2 diabetes. *Diabetes Metab. Res. Rev.* 35:e3177. doi: 10.1002/dmrr.3177
- Teodoro, B. G., Baraldi, F. G., Sampaio, I. H., Bomfim, L. H. M., Queiroz, A. L., Passos, M. A., et al. (2014). Melatonin prevents mitochondrial dysfunction and insulin resistance in rat skeletal muscle. *J. Pineal Res.* 57, 155–167. doi: 10.1111/jpi.12157
- Teymoori, F., Asghari, G., Mirmiran, P., and Azizi, F. (2018). High dietary intake of aromatic amino acids increases risk of hypertension. *J. Am. Soc. Hypertens.* 12, 25–33. doi: 10.1016/j.jash.2017.11.004
- The DCCT Research Group (1988). Weight gain associated with intensive therapy in the diabetes control and complications trial. *Diabetes Care* 11, 567–573. doi: 10.2337/diacare.11.7.567
- Thevaranjan, N., Puchta, A., Schulz, C., Naidoo, A., Szamosi, J. C., Verschoor, C. P., et al. (2017). Age-associated microbial dysbiosis promotes intestinal permeability, systemic inflammation, and macrophage dysfunction. *Cell Host Microbe* 21, 455–466. doi: 10.1016/j.chom.2017.03.002
- Thomas, C., Pellicciari, R., Pruzanski, M., Auwerx, J., and Schoonjans, K. (2008). Targeting bile-acid signalling for metabolic diseases. *Nat. Rev. Drug Discov.* 7, 678–693. doi: 10.1038/nrd2619
- Thorpe, A. A., and Schlaich, M. P. (2015). Relevance of sympathetic nervous system activation in obesity and metabolic syndrome. *J. Diabetes Res.* 2015:341583. doi: 10.1155/2015/341583
- Tian, Y., Jiang, F., Li, Y., Jiang, H., Chu, Y., Zhu, L., et al. (2018). Evaluation of the anti-hypertensive effect of Tengfu Jiangya tablet by combination of UPLC-Q-exactive-MS-based metabolomics and iTRAQ-based proteomics technology. *Biomed. Pharmacother.* 100, 324–334. doi: 10.1016/j.biopha.2018.02.025
- Tolhurst, G., Heffron, H., Lam, Y. S., Parker, H. E., Habib, A. M., Diakogiannaki, E., et al. (2012). Short-chain fatty acids stimulate glucagon-like peptide-1 secretion via the G-protein-coupled receptor FFAR2. *Diabetes* 61, 364–371. doi: 10.2337/db11-1019
- Tremaroli, V., Karlsson, F., Werling, M., Ståhlman, M., Kovatcheva-Datchary, P., Olbers, T., et al. (2015). Roux-en-Y gastric bypass and vertical banded gastroplasty induce long-term changes on the human gut microbiome contributing to fat mass regulation. *Cell Metab.* 22, 228–238. doi: 10.1016/j.cmet.2015.07.009
- Tripathi, A., Debelius, J., Brenner, D. A., Karin, M., Loomba, R., Schnabl, B., et al. (2018). The gut-liver axis and the intersection with the microbiome. *Nat. Rev. Gastroenterol. Hepatol.* 15, 397–411. doi: 10.1038/s41575-018-0011-z
- van Deventer, C. A., Lindeque, Z., Rensburg, P. J. J., Malan, L., van der Westhuizen, F. H., and Louw, R. (2015). Use of metabolomics to elucidate the metabolic perturbation associated with hypertension in a black south African male cohort: the SABPA study. *J. Am. Soc. Hypertens.* 9, 104–114. doi: 10.1016/j.jash.2014.11.007
- Vangaveti, V., Baune, B. T., and Kennedy, R. L. (2010). Hydroxyoctadecadienoic acids: novel regulators of macrophage differentiation and atherogenesis. *Ther. Adv. Endocrinol. Metab.* 1, 51–60. doi: 10.1177/2042018810375656
- Vincent, M. A., Clerk, L. H., Lindner, J. R., Klibanov, A. L., Clark, M. G., Rattigan, S., et al. (2004). Microvascular recruitment is an early insulin effect that regulates skeletal muscle glucose uptake in vivo. *Diabetes* 53, 1418–1423. doi: 10.2337/diabetes.53.6.1418
- Vincent, M. A., Montagnani, M., and Quon, M. J. (2003). Molecular and physiologic actions of insulin related to production of nitric oxide in vascular endothelium. *Curr. Diab. Rep.* 3, 279–288. doi: 10.1007/s11892-003-0018-9
- Voss, T. S., Vendelbo, M. H., Kampmann, U., Pedersen, S. B., Nielsen, T. S., Johannsen, M., et al. (2017). Effects of insulin-induced hypoglycaemia on lipolysis rate, lipid oxidation and adipose tissue signalling in human volunteers: a randomised clinical study. *Diabetologia* 60, 143–152. doi: 10.1007/s00125-016-4126-x
- Walford, G. A., Davis, J., Warner, A. S., Ackerman, R. J., Billings, L. K., Chamarthi, B., et al. (2013). Branched chain and aromatic amino acids change acutely following two medical therapies for type 2 diabetes mellitus. *Metabolism* 62, 1–13. doi: 10.1016/j.metabol.2013.07.003
- Wallis, M. G., Smith, M. E., Kolka, C. M., Zhang, L., Richards, S. M., Rattigan, S., et al. (2005). Acute glucosamine-induced insulin resistance in muscle in vivo is associated with impaired capillary recruitment. *Diabetologia* 48, 2131–2139. doi: 10.1007/s00125-005-1887-z
- Wang, Y., Deng, G., and Davies, K. (2016). Metabolomics reveals differential changes in the energy generating pathways of the detrusor and urothelium caused by diabetes. *J. Urol.* 195, E414–E414. doi: 10.1016/j.juro.2016.02.1240
- Wang, T. J., Larson, M. G., Vasan, R. S., Cheng, S., Rhee, E. P., McCabe, E., et al. (2011). Metabolite profiles and the risk of developing diabetes. *Nat. Med.* 17, 448–453. doi: 10.1038/nm.2307
- Wang, X., Zhang, L., Youker, K., Zhang, M., Wang, J., LeMaire, S. A., et al. (2006). Free fatty acids inhibit insulin signaling-stimulated endothelial nitric oxide synthase activation through upregulating PTEN or inhibiting Akt kinase. *Diabetes* 55, 2301–2310. doi: 10.2337/db05-1574
- Weiss, G. A., and Hennot, T. (2017). Mechanisms and consequences of intestinal dysbiosis. *Cell. Mol. Life Sci.* 74, 2959–2977. doi: 10.1007/s00018-017-2509-x
- Wewalka, M., Patti, M.-E., Barbato, C., Houten, S. M., and Goldfine, A. B. (2014). Fasting serum taurine-conjugated bile acids are elevated in type 2 diabetes and do not change with intensification of insulin. *J. Clin. Endocrinol. Metab.* 99, 1442–1451. doi: 10.1210/jc.2013-3367
- Wishart, D. S. (2016). Emerging applications of metabolomics in drug discovery and precision medicine. *Nat. Rev. Drug Discov.* 15, 473–484. doi: 10.1038/nrd.2016.32
- Withers, D. J., Gutierrez, J. S., Towery, H., Burks, D. J., Previs, J.-M. R. S., Zhang, Y., et al. (1998). Disruption of IRS-2 causes type 2 diabetes in mice. *Nature* 391, 900–904. doi: 10.1038/361116
- Wu, T., Xie, G., Ni, Y., Liu, T., Yang, M., Wei, H., et al. (2015). Serum metabolite signatures of type 2 diabetes mellitus complications. *J. Proteome Res.* 14, 447–456. doi: 10.1186/s12967-019-2096-8
- Würtz, P., Soininen, P., Soininen, P., Rönnemaa, T., Lehtimäki, T., Kähönen, M., et al. (2013). Branched-chain and aromatic amino acids are predictors of insulin resistance in young adults. *Diabetes Care* 36, 648–655. doi: 10.2337/dc12-0895
- Xu, J., Morita, I., Ikeda, K., Miki, T., and Yamori, Y. (2007). C-reactive protein suppresses insulin signaling in endothelial cells: role of spleen tyrosine kinase. *Mol. Endocrinol.* 21, 564–573. doi: 10.1210/me.2006-0354
- Yandrapalli, S., Pal, S., Nabors, C., and Aronow, W. S. (2018). Drug treatment of hypertension in older patients with diabetes mellitus. *Expert. Opin. Pharmacother.* 19, 633–642. doi: 10.1080/14656566.2018.1456529
- Yang, Q., Graham, T. E., Mody, N., Preitner, F., Peroni, O. D., Zabolotny, J. M., et al. (2005). Serum retinol binding protein 4 contributes to insulin resistance in obesity and type 2 diabetes. *Nature* 436, 356–362. doi: 10.1038/nature03711
- Yang, T., Richards, E. M., Pepine, C. J., and Raizada, M. K. (2018). The gut microbiota and the brain-gut-kidney axis in hypertension and chronic kidney disease. *Nat. Rev. Nephrol.* 14, 442–456. doi: 10.1038/s41581-018-0018-2
- Yang, T., Santisteban, M. M., Rodriguez, V., Li, E., Ahmari, N., Carvajal, J. M., et al. (2015). Gut dysbiosis is linked to hypertension. *Hypertension* 65, 1331–1340. doi: 10.1161/HYPERTENSIONAHA.115.05315

- Yokoi, N., Beppu, M., Yoshida, E., Hoshikawa, R., Hidaka, S., Matsubara, T., et al. (2015). Identification of putative biomarkers for prediabetes by metabolome analysis of rat models of type 2 diabetes. *Metabolomics* 11, 1277–1286. doi: 10.1007/s11306-015-0784-9
- Yu, D., Moore, S. C., Matthews, C. E., Xiang, Y., Zhang, X., Gao, Y., et al. (2016). Plasma metabolomic profiles in association with type 2 diabetes risk and prevalence in Chinese adults. *Metabolomics* 12, 1–13. doi: 10.1007/s11306-015-0890-8
- Zeng, G., and Quon, M. J. (1996). Insulin-stimulated production of nitric oxide is inhibited by wortmannin. Direct measurement in vascular endothelial cells. *J. Clin. Invest.* 98, 894–898. doi: 10.1172/JCI118871
- Zhang, B., Hu, S., Baskin, E., Patt, A., Siddiqui, J. K., and Mathé, E. A. (2018). RaMP: a comprehensive relational database of metabolomics pathways for pathway enrichment analysis of genes and metabolites. *Meta* 8:16. doi: 10.3390/metabo8010016
- Zhang, L., Wheatley, C. M., Richards, S. M., Barrett, E. J., Clark, M. G., and Rattigan, S. (2003). TNF- α acutely inhibits vascular effects of physiological but not high insulin or contraction. *Am. J. Physiol. Endocrinol. Metab.* 285, E654–E660. doi: 10.1152/ajpendo.00119.2003
- Zhao, L., Zhang, F., Ding, X., Wu, G., Lam, Y. Y., Wang, X., et al. (2018). Gut bacteria selectively promoted by dietary fibers alleviate type 2 diabetes. *Science* 359, 1151–1156. doi: 10.1126/science.aao5774
- Zheng, Y., Yamada, H., Sakamoto, K., Horita, S., Kunimi, M., Endo, Y., et al. (2005). Roles of insulin receptor substrates in insulin-induced stimulation of renal proximal bicarbonate absorption. *J. Am. Soc. Nephrol.* 16, 2288–2295. doi: 10.1681/ASN.2005020193
- Zheng, Y., Yu, B., Alexander, D., Mosley, T. H., Heiss, G., Nettleton, J. A., et al. (2013). Metabolomics and incident hypertension among blacks: the atherosclerosis risk in communities study. *Hypertension* 62, 398–403. doi: 10.1161/HYPERTENSIONAHA.113.01166
- Zhu, W., Gregory, J. C., Org, E., Buffa, J. A., Gupta, N., Wang, Z., et al. (2016). Gut microbial metabolite TMAO enhances platelet hyperreactivity and thrombosis risk. *Cell* 165, 111–124. doi: 10.1016/j.cell.2016.02.011
- Zubcevic, J., Jun, J. Y., Kim, S., Perez, P. D., Afzal, A., Shan, Z., et al. (2014). Altered inflammatory response is associated with an impaired autonomic input to the bone marrow in the SHR. *Hypertension* 63, 542–550. doi: 10.1161/HYPERTENSIONAHA.113.02722

Conflict of Interest: The authors declare that the research was conducted in the absence of any commercial or financial relationships that could be construed as a potential conflict of interest.

Publisher's Note: All claims expressed in this article are solely those of the authors and do not necessarily represent those of their affiliated organizations, or those of the publisher, the editors and the reviewers. Any product that may be evaluated in this article, or claim that may be made by its manufacturer, is not guaranteed or endorsed by the publisher.

Copyright © 2021 Ning, Song, Wang, Peng, Wan, Liu and Lu. This is an open-access article distributed under the terms of the Creative Commons Attribution License (CC BY). The use, distribution or reproduction in other forums is permitted, provided the original author(s) and the copyright owner(s) are credited and that the original publication in this journal is cited, in accordance with accepted academic practice. No use, distribution or reproduction is permitted which does not comply with these terms.

GLOSSARY

DM	Diabetes mellitus
HTN	Hypertension
LC-MS	Liquid chromatography-mass spectrometry;
GC-MS	Gas chromatography-mass spectrometry
NMR	Nuclear magnetic resonance
GC	Gas chromatography
LC	Liquid chromatography
PCA	Principal component analysis
PLS	Partial least squares
OPLS-DA	Orthogonal partial least square discriminant analysis
OSC	Orthogonal signal correction
LASSO	Least absolute shrinkage and selection operator
BCAAs	Branched-chain amino acids
AAAs	Aromatic amino acids
TCA	Tricarboxylic acid
PC	Phosphatidylcholine
LPC	Lysophosphatidylcholine
PE	Phosphatidylethanolamine
DAG	Diacylglycerol
SM	Sphingomyelins
Cer	Ceramide
PA	Phosphatidic acid
LPA	Lysophosphatidic acid
HODEs	Hydroxyoctadecadienoic acids
HETE	Hydroxyeicosatetraenoic acid
HPETE	Hydroxyeicosatetraenoic acid
BAs	Bile acids
DMG	Dimethylglycine
BHMT	Methyltransferase
DMGDH	Methyltransferase dehydrogenase
FFAs	Free fatty acids
LC-CoAs	Long-chain acyl CoAs
ER	Endoplasmic reticulum
NO	Nitric oxide
SCFAs	Short-chain fatty acids
GPR	G-Protein-coupled receptors
Olf78	Olfactory receptor 78
TMAO	Trimethylamine-N-oxide
mTORC	The mammalian target of rapamycin complex
S6K1	S6 kinase 1
PI3K	Phosphatidylinositol 3-kinase
AMPK	Adenosine 5'-nucleotidophosphate-activated protein kinase
RBP4	Retinol-binding protein-4
IL-6	Interleukin-6
TNF- α	Tumor necrosis factor- α
FXR	Farnesoid X receptor
GLP-1	Glucagon-like peptide 1
PYY	Peptide YY
GPR41	G-Protein-coupled receptors 41
GPR43	G-Protein-coupled receptors 43
GLUT4	Glucose transporter-4
MCP1	Monocyte chemotactic protein-1
IKK β	I κ B Kinase catalytic subunit- β
FFAR2	Free fatty acid receptor 2
IRS-1	Insulin receptor substrate 1
PAI-1	Plasminogen activator inhibitor type 1
ICAM-1	Intercellular adhesion molecule 1
VCAM	Vascular cell adhesion molecule
PKC	Phosphoinositide-dependent protein kinase-1
ALSLs	Reactive oxygen species
RAGE	Protein kinase C
NF- κ B	Acyl-CoA synthetases
β -MHC	Receptors for advanced glycation end
PIP3	Nuclear factor kappa-B
	β -Myosin heavy chain
	PI-3,4,5-Triphosphate

AGEs	Advanced glycation end products
ET-1	Endothelin 1
JNK	C-Jun N-terminal kinase
CRP	C-Reactive protein
VSMC	Vascular smooth muscle and smooth muscle cells
NHE3	Na ⁺ /H ⁺ exchanger type 3
NBC1	Sodium-bicarbonate cotransporter
NKCC2	Na-K-2Cl Cotransporters
WNK	With-no-lysine kinases
RAS	Renin-angiotensin system
S6K1	S6 Kinase 1



Association of Plasma Metabolic Biomarker Sphingosine-1-Phosphate With Cerebral Collateral Circulation in Acute Ischemic Stroke

Fang Yu^{1†}, Xianjing Feng^{1†}, Xi Li¹, Zeyu Liu¹, Di Liao¹, Yunfang Luo¹, Minping Wei¹, Qin Huang¹, Lin Zhang¹ and Jian Xia^{1,2,3*}

¹ Department of Neurology, Xiangya Hospital, Central South University, Changsha, China, ² Clinical Research Center for Cerebrovascular Disease of Hunan Province, Central South University, Changsha, China, ³ National Clinical Research Center for Geriatric Disorders, Xiangya Hospital, Central South University, Changsha, China

OPEN ACCESS

Edited by:

Dongze Zhang,
University of Nebraska Medical
Center, United States

Reviewed by:

Sizhao Lu,
University of Colorado, United States
Wenfeng Hu,
University of Nebraska Medical
Center, United States

*Correspondence:

Jian Xia
xjian1216@csu.edu.cn

[†] These authors have contributed
equally to this work and share first
authorship

Specialty section:

This article was submitted to
Vascular Physiology,
a section of the journal
Frontiers in Physiology

Received: 04 June 2021

Accepted: 13 July 2021

Published: 19 August 2021

Citation:

Yu F, Feng X, Li X, Liu Z, Liao D, Luo Y,
Wei M, Huang Q, Zhang L and Xia J
(2021) Association of Plasma
Metabolic Biomarker
Sphingosine-1-Phosphate With
Cerebral Collateral Circulation in Acute
Ischemic Stroke.
Front. Physiol. 12:720672.
doi: 10.3389/fphys.2021.720672

Background: The contribution of metabolic profile to the cerebral collateral circulation in acute ischemic stroke (AIS) has not been fully outlined. In this study, we conducted a metabolomic study to assess the relationship between the metabolic biomarkers and the collateral status of AIS.

Methods: A two-stage study was conducted from September 2019 to June 2021 in our hospital. There were 96 subjects including 66 patients with AIS and 30 healthy controls in the discovery stage and 80 subjects including 53 patients with AIS and 27 healthy controls in the validation stage. Collateral circulation was assessed by the Tan score based on computed tomographic angiography (CTA). Liquid chromatography-tandem mass spectrometry was used to identify differential metabolic markers. Then, an ELISA was employed to detect the plasma levels of sphingosine-1-phosphate (S1P).

Results: There were 114 differential metabolites between patients with AIS and control groups and 37 differential metabolites between good collateral circulation (GCC) and poor collateral circulation (PCC) groups. The pathway enrichment analysis revealed that arginine biosynthesis was the only statistically significant pathway between AIS and control groups and sphingolipid metabolism was the only statistically significant pathway between GCC and PCC groups. The differential metabolites sphingosine-1-phosphate (SA1P) and S1P belong to the sphingolipid metabolism. In the discovery stage, when the GCC group was compared with the PCC group, the receiver operating characteristic (ROC) analysis showed that plasma SA1P relative levels demonstrated an area under the curve (AUC) of 0.719 (95% CI: 0.582–0.834), and S1P levels demonstrated an AUC of 0.701 (95% CI: 0.567–0.819). In addition, both plasma SA1P and S1P relative levels showed significant negative correlations with the 90-day modified Rankin Scale (mRS) score. In the validation sample, higher plasma S1P levels were independent predictors of GCC ($p = 0.014$), and plasma S1P levels demonstrated an AUC of 0.738 (95% CI: 0.599–0.849) to differentiate patients with GCC from patients with PCC. In addition, plasma S1P levels also showed significant negative correlations with the 90-day mRS score.

Conclusion: We first illustrated the association between plasma metabolic profiles and cerebral collateral circulation in patients with AIS. Plasma S1P levels might be a potential diagnostic biomarker for predicting collateral circulation status in patients with AIS.

Keywords: acute ischemic stroke, metabolomics, sphinganine-1-phosphate, sphingosine-1-phosphate, collateral circulation

INTRODUCTION

The cerebral collateral circulation status plays a vital role in protecting the brain against ischemia and reperfusion injury. Accumulating studies have shown that the well-developed collateral status independently predicted the favorable clinical outcomes in patients with acute ischemic stroke (AIS) in response to intravenous thrombolysis (IVT) or endovascular treatment (Bang et al., 2011; Menon et al., 2015).

Cerebral collateral circulation can be divided into primary (circle of Willis) and secondary collateral pathways (the ophthalmic artery and leptomeningeal vessels) (Liebeskind, 2003). Leptomeningeal collateral circulation is preexisting anastomoses that are crucial to the functional outcome of AIS, especially after mechanical thrombectomy (Lima et al., 2010). Clinically, available tools for the evaluation of collateral circulation are mostly based on imaging techniques like digital subtraction angiography, computed tomography perfusion, computed tomographic angiography (CTA), and some magnetic resonance-based methods. Although these imaging techniques play essential roles in differentiating collateral status, sometimes they are time-consuming, not cost-effective, and limited by some contraindications.

Collateral circulation varies greatly in patients, the reasons of which remain largely unknown. Several studies have shown that vascular risk factors like hypertension, metabolic syndrome, smoking, and aging were related to poor collaterals (Lima et al., 2010; Menon et al., 2013). However, the underlying molecular pathogenesis regulating the collateral circulation of the brain remains unclear. Biomarkers are crucial in the prediction and diagnosis of stroke and could also help improve our understanding of the etiology and pathophysiology of stroke, whereas only a few studies have explored the relationship between circulating biomarkers and collateral circulation status. Laura Mechtouff et al. found that high matrix metalloproteinase-9 (MMP-9) and low monocyte chemoattractant protein-1 (MCP-1) levels were associated with poor pretreatment collateral circulation in patients with stroke with large vessel occlusion (LVO) (Mechtouff et al., 2020). Another study demonstrated that higher plasma apelin-17 levels were positively associated with good collateral circulation (GCC) in patients with ischemic stroke (Jiang et al., 2019). Furthermore, plasma proteomic profiling of patients with AIS with LVO identified three collateral-related proteins, namely, IGF2, LYVE1, and THBS1 (Qin et al., 2019). However, none of these biomarkers entered reached clinical application.

Using an untargeted metabolomics based on liquid chromatography-tandem mass spectrometry (LC-MS) might

help decipher potential metabolites involved in the stroke onset and progression and uncover novel pathophysiological processes of ischemic stroke. Since metabolomics can uncover small metabolites which could penetrate the blood-brain barrier, it might be an emerging powerful tool for exploring novel biomarkers of ischemic stroke. Currently, several circulating metabolites and pathways have been found associated with stroke risk predictions and diagnosis. However, less is known about whether metabolomics also plays a role in the cerebral collateral circulation status. In this study, we conducted an untargeted metabolomics study using LC-MS (AB SCIEX TripleTOF 5600) to identify differential metabolites in patients with AIS with GCC and poor collateral circulation (PCC).

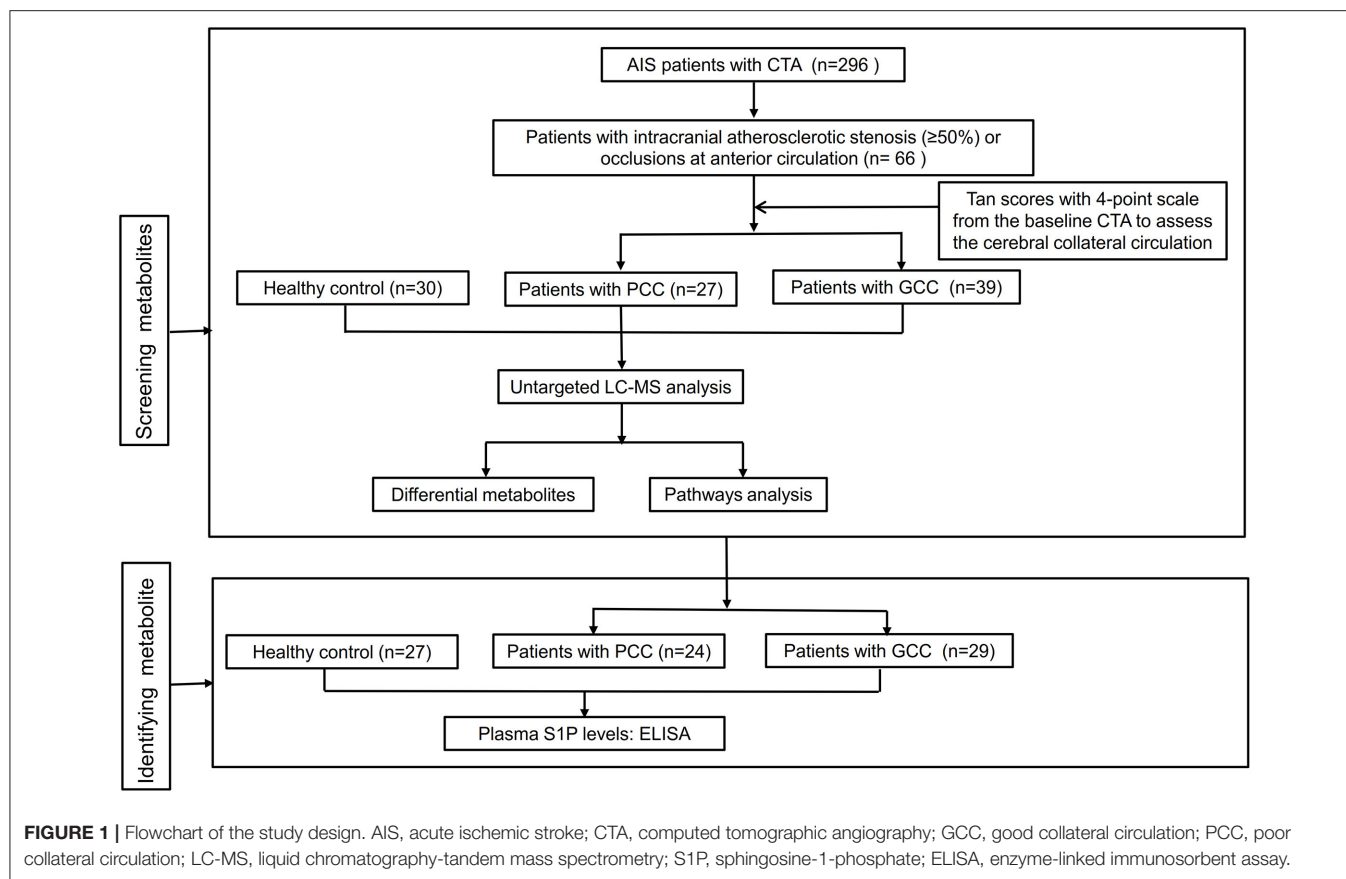
MATERIALS AND METHODS

Study Participants

A two-stage study was conducted from September 2019 to June 2021 in Xiangya Hospital, Central South University, and the flowchart of the study design is shown in **Figure 1**. A total of 119 patients with anterior circulation AIS (66 in the discovery stage and 53 in the verification stage) with intracranial atherosclerotic stenosis ($\geq 50\%$) or occlusions within 7 days after symptom onset were prospectively enrolled in this study. All patients underwent brain MRI and diffusion-weighted imaging (DWI) scans. Patients with histories of stroke, autoimmune disease, malignant tumors, severe infection, severe hepatic, and renal dysfunction were excluded. During the same period, we recruited 30 and 27 healthy control subjects from the physical examination center of Xiangya Hospital in the discovery and verification stages, respectively. This study was approved by the Ethics Committee of Xiangya Hospital of Central South University, and all patients provided written informed consent. EDTA-containing blood samples of all patients were collected after fasting overnight and then centrifuged at 3,000 rpm for 15 min at 4°C. These plasma samples were stored immediately at -80°C until analyses.

Image Acquisition and Imaging Analysis

All selected patients completed CTA examinations. We applied a previously reported Tan scoring system with a scale of 0–3 from the baseline CTA to assess the cerebral collateral circulation as follows: 0, absent collateral of the occluded vascular territory; 1, poor collateral filling ($>0\%$ but $\leq 50\%$ of the occluded vascular territory); 2, moderate collateral filling ($>50\%$ but $<100\%$ of the occluded vascular territory); and 3, good collateral filling (100% of the occluded vascular territory) (Wiegers et al., 2020). Based on the collateral circulation scores, patients with AIS were categorized into the following two groups: GCC group with the



Tan scores of 2–3 and PCC group with the Tan scores of 0–1. Two neurologists (FY and XJF) assessed the collateral status of patients with AIS together.

Clinical Examination

We collected the demographic and clinical data of all participants from the medical record. After overnight fasting, blood count, total cholesterol (TC), triglycerides (TG), high-density lipoprotein (HDL), low-density lipoprotein (LDL), and homocysteine (Hcy) were measured in the Department of the Clinical Laboratory in our hospital. Smoking and vascular risk factors (such as hypertension, diabetes mellitus, and dyslipidemia) were defined as described in previous studies (Yu et al., 2017, 2019). We also evaluated the National Institutes of Health Stroke Scale (NIHSS) at admission and the modified Rankin Scale (mRS) score at 90 days after stroke onset of all patients.

Sample Preparation

First, 100 μ l of plasma sample was placed in a 1.5-ml centrifuge tube, deproteinized with 400 μ l of acetonitrile and methanol mixture (1:1, v/v), vortexed for 30 s, sonicated for 10 min, and centrifuged at 12,000 rpm for 15 min at 4°C, and the supernatants of which were collected and transferred to another 1.5-ml centrifuge tube and dried with nitrogen. Then, the sample was dissolved with 100 μ l of acetonitrile and water (1:1, v/v), vortexed

for 30 s, sonicated for 5 min, and centrifuged at 12,000 rpm for 15 min at 4°C. Finally, the supernatant was transferred into autosampler vials.

Untargeted Metabolic Profiling

The AB SCIEX TripleTOF 5600 system (AB SCIEX, Foster City, CA, USA) was used for the LC-MS/MS analysis. The chromatographic separations were carried out using an ACQUITY UHPLC T3 column (100 \times 2.1 mm; 1.8 μ m). Mobile phase A consisted of 0.1% of aqueous formic acid and mobile phase B consisted of 0.1% of formic acid in acetonitrile. The injection volume was 2 μ l for positive and negative ESI modes. The gradient elution program was set as follows: 5% B (0–2 min), 5–70% B (2–5 min), 70–90% B (5–14 min), 90–100% B (14–16 min), 100% B (16–22 min), 100% to 5% B (22–22.1 min), and 5% B (22.1–25 min). The flow rate for the mobile phase was 0.3 ml/min. The eluent was sprayed into the TripleTOF 5600 electrospray tandem mass spectrometer and analyzed in the information-dependent acquisition (IDA) mode. The conditions set for the mass spectrometer were as follows: ion source gas1, 55 psi; ion source gas2, 55 psi; curtain gas, 35 psi; ion spray voltage floating, 5,500/–4,500 (+/–) V; declustering potential, 80 V; collision energy, 40 \pm 20 V; and temperature, 550°C. Dynamic background subtraction was used for screening the profile to fulfill the criteria of IDA and trace all probable minor metabolites.

TABLE 1 | General characteristics of control and patients with AIS in the discovery stage.

	Control (n = 30)	AIS patients (n = 66)			p	
		GCC (n = 39)	PCC (n = 27)	Total (n = 66)	AIS vs. Control	GCC vs. PCC
Age, years	60.53 ± 9.76	56.69 ± 11.82	58.89 ± 11.01	57.59 ± 11.46	0.226	0.448
Sex (male, N, %)	21 (70%)	24 (61.5%)	17 (63.0%)	41 (61.2%)	0.454	0.907
Hypertension (N, %)	12 (40%)	21 (53.8%)	20 (74.1%)	41 (62.1%)	0.043	0.096
Diabetes mellitus (N, %)	2 (6.7%)	9 (23.1%)	12 (44.4%)	21 (31.8%)	0.009	0.067
Hyperlipidemia (N, %)	17 (56.7 %)	20 (51.3%)	14 (51.9 %)	34 (51.5 %)	0.639	0.964
Smoking (N, %)	10 (33.3%)	16 (41.0%)	15 (55.6%)	31 (47.0%)	0.211	0.245
SBP, mmHg	129.97 ± 15.09	137.44 ± 17.57	149.70 ± 22.72	142.46 ± 20.59	0.001	0.016
DBP, mmHg	79.70 ± 10.74	80.92 ± 12.29	81.96 ± 13.37	81.35 ± 12.65	0.537	0.745
WBC, × 10 ⁹ /L	6.00 ± 1.23	7.25 ± 1.74	8.04 ± 3.14	7.57 ± 2.42	<0.001	0.237
TG, mmol/L	2.27 ± 1.58	1.63 ± 0.67	1.68 ± 0.81	1.64 ± 0.72	0.045	0.553
TC, mmol/L	4.79 ± 1.26	4.33 ± 1.24	4.06 ± 1.12	4.22 ± 1.19	0.035	0.368
HDL, mmol/L	1.20 ± 0.27	1.06 ± 0.24	0.98 ± 0.22	1.02 ± 0.23	0.001	0.150
LDL, mmol/L	2.99 ± 0.77	2.72 ± 0.921	2.57 ± 0.88	2.60 ± 0.90	0.089	0.509
Hcy, μmol/L	14.72 ± 9.44	13.70 ± 5.99	15.12 ± 9.51	14.28 ± 7.59	0.806	0.459
NIHSS score at admission	–	5.79 ± 3.91	9.63 ± 7.32	7.36 ± 5.83	–	0.018
mRS score on 90 days	–	1.69 ± 0.86	2.26 ± 1.13	2.76 ± 1.18	–	0.024

AIS, acute ischemic stroke; GCC, good collateral circulation; PCC, poor collateral circulation; SBP, systolic blood pressure; DBP, diastolic blood pressure; WBC, white blood cell; TC, total cholesterol; TG, triglycerides; HDL, high-density lipoprotein; LDL, low-density lipoprotein; Hcy, homocysteine; NIHSS, National Institutes of Health Stroke Scale; mRS, modified Rankin Scale.

Untargeted Metabolomics Data Processing

ProteoWizard software (<http://proteowizard.sourceforge.net>) was used to convert the acquired LC-MS raw data into mzML format files, after which the XCMSplus software (<https://sciex.com/products/software/xcms-plus-software>) was employed for data processing, including peak alignment, peak area extraction, and peak retention time correction (Smith et al., 2006). Metabolites were identified using HR-MS/MS library (AB Sciex, Forster City, CA, USA) and MetDNA (<http://metdna.zhulab.cn/>) (Shen et al., 2019). MetaboAnalyst software (<https://www.metaboanalyst.ca/>) was used for metabolite data analysis. Candidate metabolites were selected based on variable influence in projection (VIP) values >1 from the partial least-squares discriminant analysis (PLS-DA) model, fold change (FC) cutoff at >1.2 (or FC <0.83), and statistical significance ($p < 0.05$).

The Measurement of Sphingosine 1-Phosphate, MMP-9, and MCP-1

In the validation stage, the plasma levels of sphingosine 1-phosphate (S1P), MMP-9, and MCP-1 were determined by using the ELISA Kit (ELISA Kit for S1P, competitive method, Catalog No. CEG031Ge; ELISA Kit for MMP-9, double antibody sandwich method, Catalog No. SEA553Hu; ELISA Kit for MCP-1, double antibody sandwich method, Catalog No. SEA087Hu; USCN Business Co., Ltd., Wuhan, China USCN Business Co., Ltd., Wuhan, China) according to the instructions of the manufacturer.

Statistical Analysis

Statistical analyses for Student's *t*-test, Mann-Whitney *U*-test, the chi-square test, and the logistic regression analysis were performed using SPSS version 22.0 software (IBM SPSS, Chicago,

IL, USA). The Pearson's correlation analysis was calculated using GraphPad Prism version 8.0 software (La Jolla, CA, USA). Receiver operating characteristic (ROC) curves were calculated using MedCalc statistical software (MedCalc Inc., Mariakerke, Belgium).

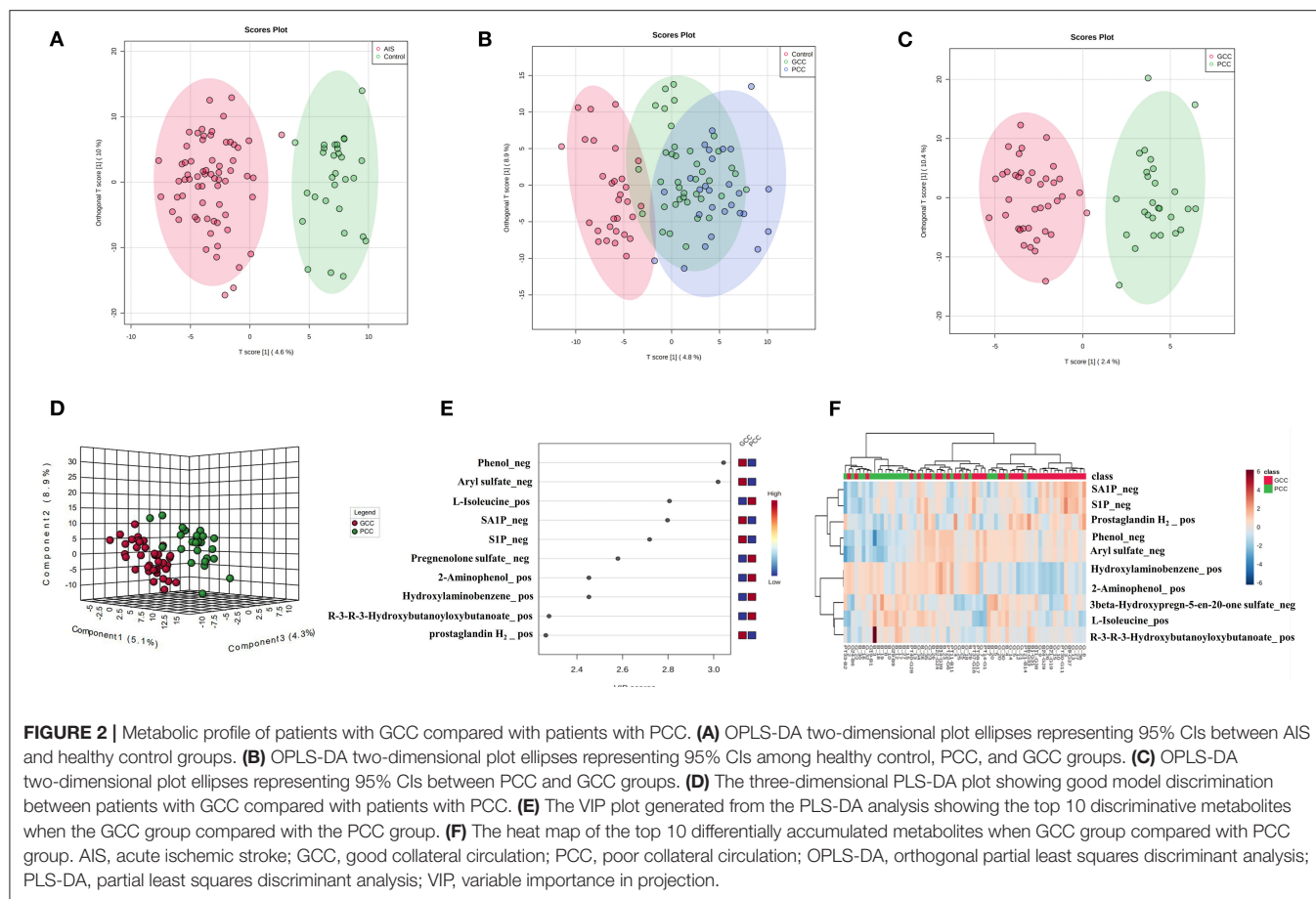
RESULTS

Characteristics of Participants in the Discovery Stage

In the discovery stage, 30 healthy control, 27 patients with AIS with PCC, and 39 patients with AIS with GCC were enrolled. There were 41 males and 25 females with an average age of 57.59 years in the AIS group and 21 men and 9 women with an average age of 60.53 years in the control group. There were higher frequencies of hypertension and diabetes mellitus, higher systolic blood pressure (SBP) and white blood cell (WBC), and lower levels of TC, TG, and HDL in the AIS group. In addition, the GCC groups had lower NIHSS scores and SBP at admission, and lower mRS scores at 90 days after stroke onset when compared with the PCC group. There were no significant differences between GCC and PCC groups regarding age, sex, and vascular risk factors. Meanwhile, diastolic blood pressure (DBP), WBC, TC, TG, LDL, HDL, and Hcy levels showed no significant difference between groups (Table 1).

Differential Metabolites in the Discovery Stage

Finally, there were 571 metabolites identified in our samples. A multivariate analysis was conducted using MetaboAnalyst software. PLS-DA or the orthogonal partial least squares



discriminant analysis (OPLS-DA) was used for the discriminant analysis. The OPLS-DA analysis showed good separations between control and AIS groups and GCC and PCC groups (Figures 2A,C). There was slight separation among the control, GCC, and PCC groups (Figure 2B). The PC1, PC2, and PC3 were able to account for 5.1, 8.9, and 4.3%, respectively, of the total variance by the PLS-DA analysis in the GCC group compared with the PCC group (Figure 2D).

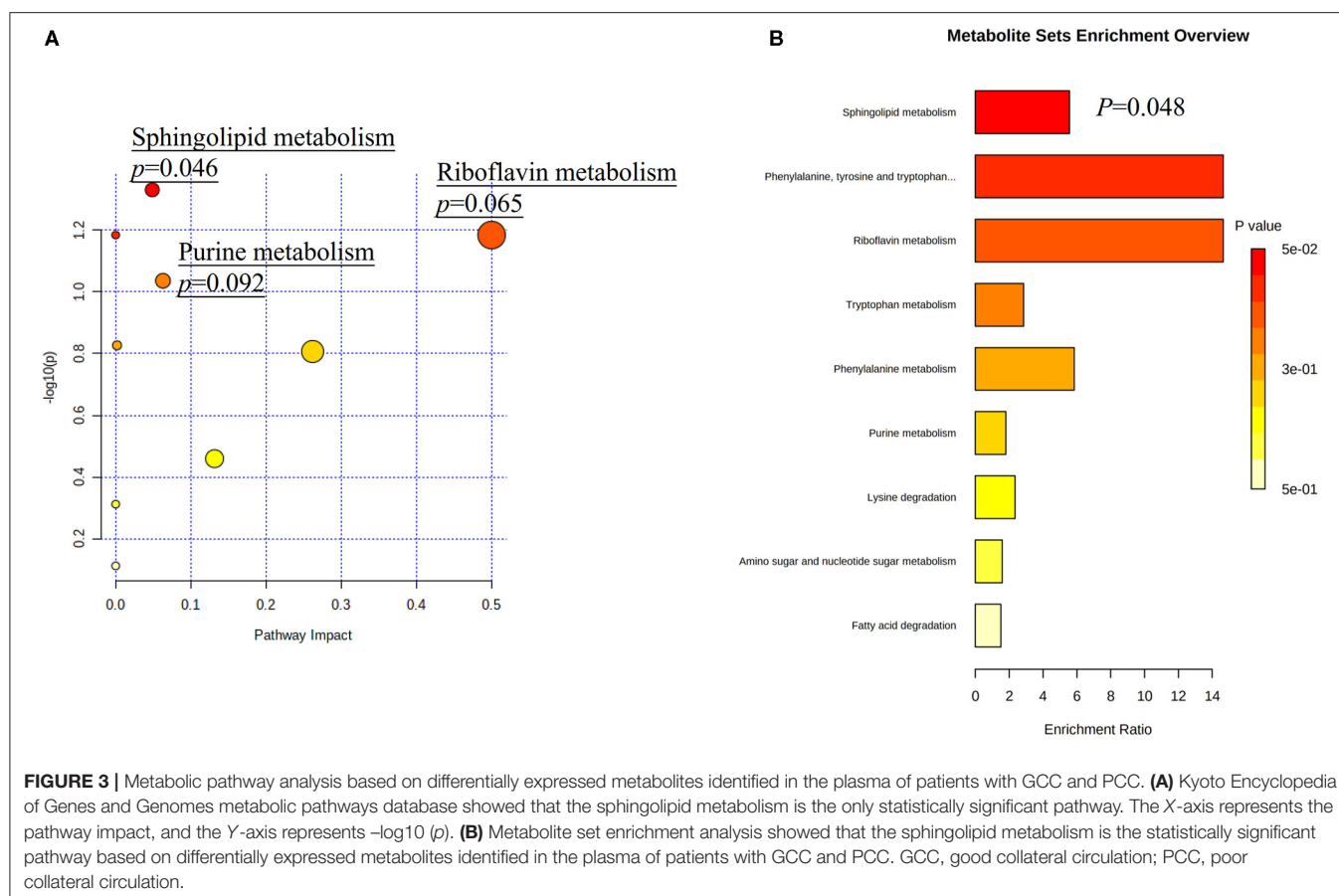
There were 114 metabolites that distinguished patients with AIS from controls [based on FC values ($FC > 1.2$ or $FC < 0.83$, AIS/control), $p < 0.05$, and $VIP > 1$, Supplementary Table 1], and the top 10 different metabolites between control and AIS groups were ranked according to the VIP scores (Supplementary Figure 1A). The heat map of the top 10 different plasma metabolites between patients with AIS and healthy controls is shown in Supplementary Figure 1B. Thirty-seven metabolites that distinguished patients with GCC from PCC were selected using MetaboAnalyst software (Supplementary Table 4). The top 10 metabolites that distinguished the characteristic metabolic profiles of GCC and PCC were also ranked according to VIP scores as shown in Figure 2E. Differences between the samples from patients with GCC and PCC were also confirmed by comparing heat maps with the top 10 metabolites ranked (Figure 2F).

Analyses of Metabolic Pathways

Among all detected metabolites, 114 variables were performed searching the pathway analysis between AIS and control groups (Supplementary Table 1), and 37 variables were performed searching the pathway analysis between GCC and PCC groups (Supplementary Table 4). The identified differential metabolites were analyzed using the metabolite set enrichment analysis and Kyoto Encyclopedia of Genes and Genomes metabolic pathway database using MetaboAnalyst software. We found that arginine biosynthesis was the only statistically significant pathway on the pathway enrichment analysis between AIS and control groups (Supplementary Figures 2A,B; Supplementary Tables 2, 3), and sphingolipid metabolism was the only statistically significant pathway on the pathway enrichment analysis between GCC and PCC groups (Figures 3A,B; Supplementary Tables 5, 6).

Identification of Potential Biomarkers

Among all detected metabolites, there were five metabolite molecules belonging to sphingolipids, including S1P_neg, S1P_pos, SA1P_neg, phytosphingosine_pos, and 3-dehydrosphinganine_pos. However, there was no significant difference in the relative plasma expression levels of these metabolites between the AIS and control groups (Supplementary Figures 3A–E).



The relative expression levels of plasma S1P_{neg} and SA1P_{neg} were statistically higher in the GCC group than PCC group and met the condition for screening based on FC values (FC >1.2 or FC <0.83, GCC/PCC), $p < 0.05$, and VIP >1 (Figures 4A,B; Supplementary Table 4). However, the differences in plasma S1P_{pos} levels, phytosphingosine_{pos} levels, and 3-dehydrosphinganine_{pos} levels between patients with GCC and patients with PCC have not filled the condition for screening (Supplementary Figures 4A–C). The ROC analysis showed a good separation of GCC and PCC groups with an area under the curve (AUC) of 0.701 (95% CI: 0.567–0.819) with 81.48% of specificity and 64.10% of sensitivity for S1P_{neg} (Figure 4A). SA1P_{neg} levels demonstrated an AUC of 0.719 (95% CI: 0.582–0.834) with 81.48% of specificity and 58.97% of sensitivity (Figure 4B).

Correlation Between the Potential Metabolites and Clinical Measures

Moreover, in the discovery stage, we did overall correlation between differential metabolites and clinical measures using the Pearson's correlation analysis in patients with AIS (Figures 5A–E; Supplementary Figures 5A,B). S1P_{neg} levels showed a negative significant correlation with the 90-day mRS score ($r = -0.354$; $p = 0.004$), without correlation with NIHSS scores ($r = -0.230$; $p = 0.06$) and SBP ($r = -0.047$;

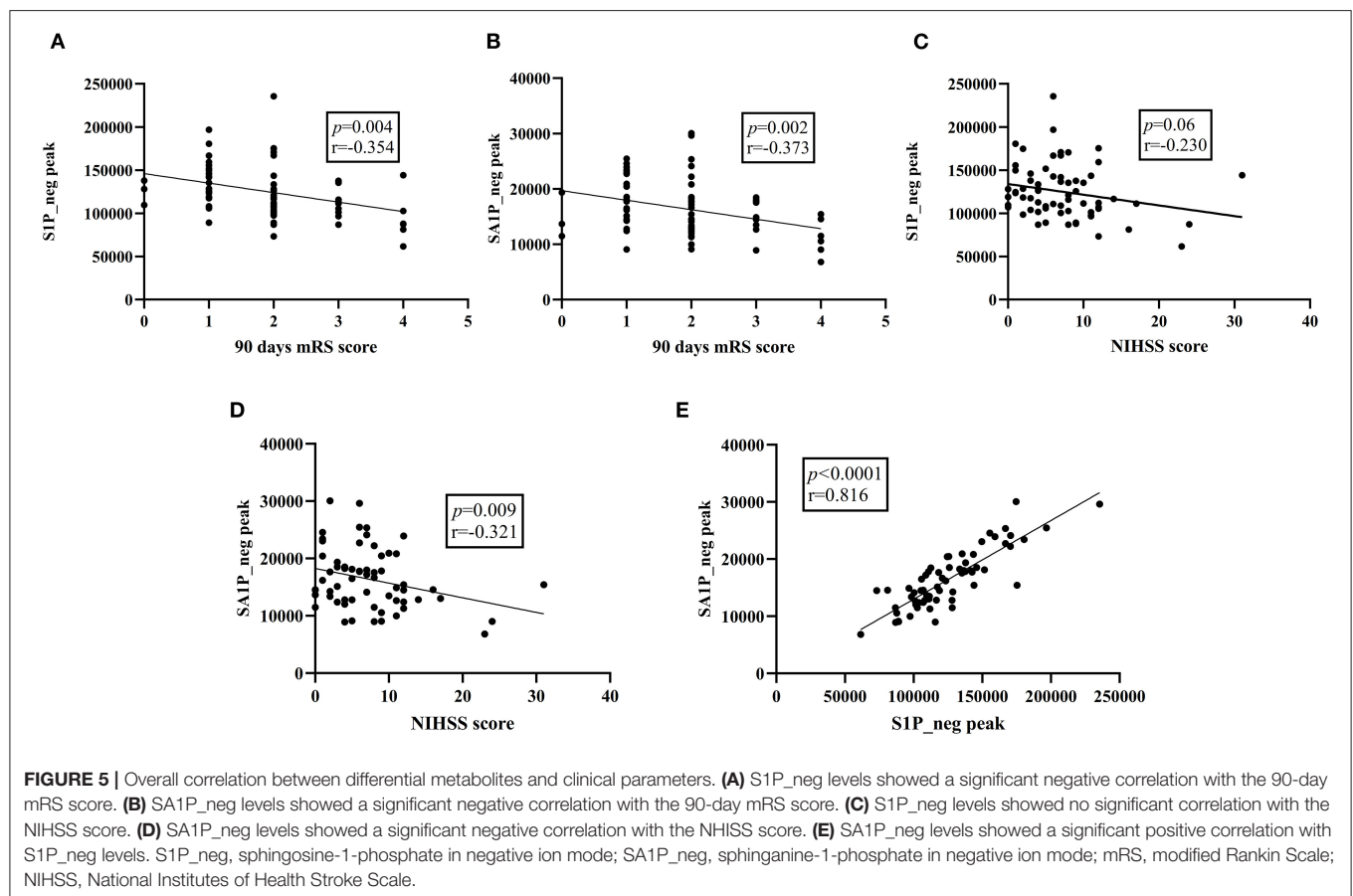
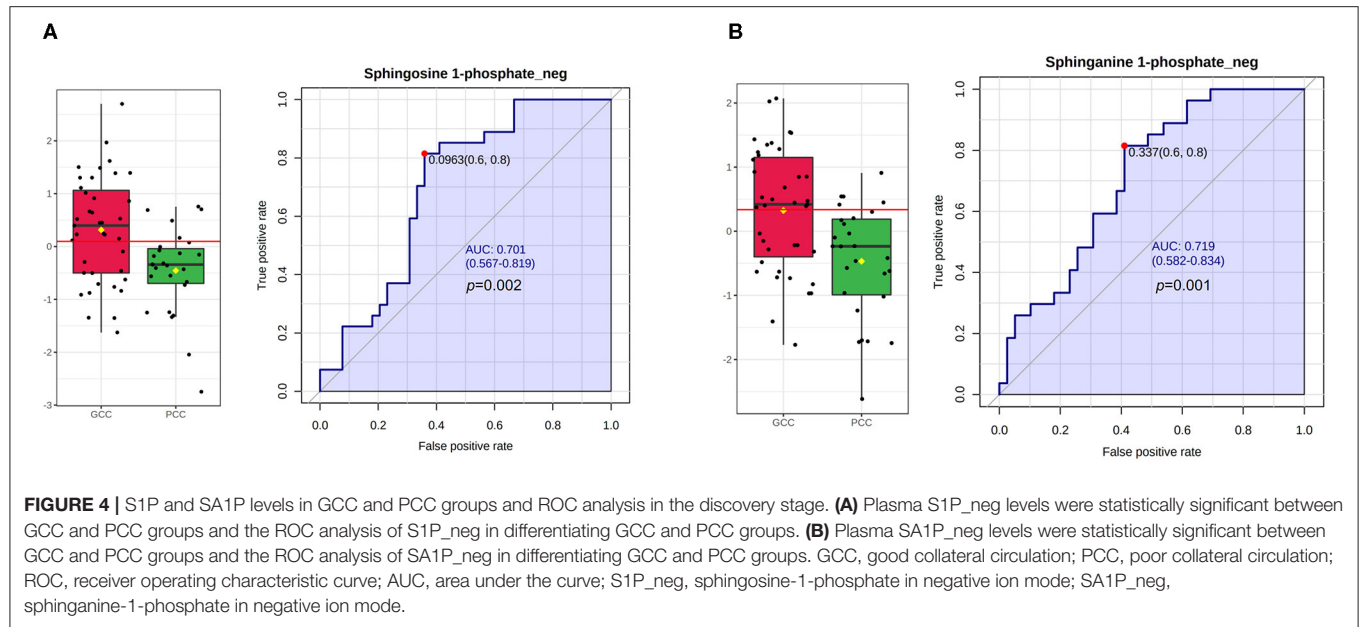
$p = 0.709$). Plasma SA1P_{neg} levels showed a negative significant correlation with the 90-day mRS score ($r = -0.373$; $p = 0.002$) and NIHSS scores ($r = -0.321$; $p = 0.009$). There was no correlation between SA1P_{neg} and SBP ($r = -0.161$; $p = 0.196$). SA1P_{neg} levels showed a positive significant correlation with S1P_{neg} levels ($r = 0.816$; $p < 0.001$).

Sphingosine-1-Phosphate Levels of the Validation Patients

In the validation stage, 27 healthy controls, 24 patients with PCC, and 29 patients with GCC were included. The baseline characteristics of these subjects are shown in Table 2. There were 37 males and 16 females with an average age of 62.49 years in the AIS group and 16 men and 11 women with an average age of 60.30 years in the control group (Table 2).

When the AIS group was compared with the control group, there were higher frequencies of hypertension and diabetes mellitus, higher levels of plasma S1P and SBP, and lower levels of TC, HDL, and LDL in the AIS group than in the control group (Table 2). S1P >244.49 ng/ml remained as the independent predictor of AIS compared with the control group after adjustment for hypertension, diabetes mellitus, and levels of SBP, TC, HDL, and LDL (Supplementary Table 7).

When compared with patients with PCC, patients with GCC had higher levels of S1P ($p = 0.001$, Figure 6A), and plasma



S1P levels demonstrated an AUC of 0.738 (95% CI: 0.599–0.849) to differentiate patients with GCC from PCC, with 86.20% of specificity and 50.00% of sensitivity (**Figure 6B**). High S1P levels

remained as an independent predictor of GCC (compared with the PCC group) after adjusting for SBP, DBP, MCP-1, TC, and LDL levels (**Table 3**). In addition, we also found a negative

TABLE 2 | General characteristics of control and patients with AIS in the validation stage.

	Control (n = 27)	AIS patients (n = 53)			p	
		GCC (n = 29)	PCC (n = 24)	Total (n = 53)	AIS vs. Control	GCC vs. PCC
Age, years	60.296 ± 8.30	62.07 ± 7.52	63.00 ± 11.40	62.49 ± 9.39	0.308	0.723
Sex (male, N, %)	16 (59.3%)	20 (68.97%)	17 (70.83%)	37 (68.9%)	0.345	0.883
Hypertension (N, %)	16 (40.7%)	24 (82.8%)	19 (79.2%)	43 (81.1%)	<0.001	0.739
Diabetes mellitus (N, %)	3 (11.1%)	10 (34.5%)	11 (45.8%)	21 (39.6%)	0.01	0.400
Hyperlipidemia (N, %)	16 (59.3%)	11 (45.8%)	19 (65.5%)	30 (56.6%)	0.820	0.150
Smoking (N, %)	10 (37.0%)	14 (48.3%)	12 (50.0%)	26 (49.1%)	0.307	0.901
S1P (ng/mL)	197.30 ± 105.21	320.75 ± 100.82	237.21 ± 72.44	282.91 ± 97.76	0.001	0.001
MMP-9 (ng/mL)	12.70 (6.63–16.19)	11.25 (6.19–27.17)	15.90 (8.65–33.70)	13.28 (7.49–27.90)	0.311	0.491
MCP-1 (ng/mL)	61.26 (49.10–68.10)	56.63 (46.47–73.44)	73.22 (53.09–126.35)	59.65 (49.00–83.24)	0.583	0.023
SBP, mmHg	132.82 ± 14.78	151.67 ± 21.76	151.67 ± 21.76	144.75 ± 20.81	0.004	0.026
DBP, mmHg	81.89 ± 11.69	81.17 ± 12.11	89.17 ± 11.65	84.79 ± 12.46	0.317	0.019
WBC, × 10 ⁹ /L	6.95 ± 1.99	7.25 ± 2.26	8.12 ± 2.86	7.65 ± 2.56	0.223	0.218
TG, mmol/L	1.98 ± 1.57	1.64 ± 0.68	1.68 ± 0.76	1.65 ± 0.72	0.318	0.511
TC, mmol/L	5.06 ± 1.31	4.05 ± 0.84	4.68 ± 1.05	4.35 ± 0.97	0.008	0.021
HDL, mmol/L	1.29 ± 0.33	0.97 ± 0.19	1.05 ± 0.20	1.01 ± 0.20	<0.001	0.133
LDL, mmol/L	3.18 ± 0.88	2.57 ± 0.59	3.00 ± 0.83	2.77 ± 0.73	0.020	0.039
Hcy, μmol/L	13.60 ± 3.08	16.64 ± 9.78	13.73 ± 4.31	15.34 ± 7.89	0.275	0.263
NIHSS score at admission	-	6.48 ± 4.89	8.21 ± 5.54	7.26 ± 5.21	-	0.234
mRS score at 90 days	-	1.83 ± 1.19	3.04 ± 1.33	2.38 ± 1.39	-	0.001

AIS, acute ischemic stroke; GCC, good collateral circulation; PCC, poor collateral circulation; S1P, sphingosine-1-phosphate; MMP-9, matrix metalloproteinase-9; MCP-1, monocyte chemoattractant protein-1; SBP, systolic blood pressure; DBP, diastolic blood pressure; WBC, white blood cell; TC, total cholesterol; TG, triglycerides; HDL, high-density lipoprotein; LDL, low-density lipoprotein; Hcy, homocysteine; NIHSS, National Institutes of Health Stroke Scale; mRS, modified Rankin Scale.

significant correlation between the S1P levels and mRS score at 90 days in the validation cohort (**Figure 6C**). Plasma S1P levels showed a negative significant correlation with TG ($r = -0.290$; $p = 0.039$), without correlation with NIHSS score ($r = -0.071$; $p = 0.612$) (**Supplementary Figures 6A,B**).

Since previous study found that circulating MMP-9 and MCP-1 levels were related to the opening of collateral circulation, we tested the expression of plasma MMP-9 and MCP-1 in this cohort and found no significant difference in plasma MMP-9 and MCP-1 levels between the AIS and control groups (**Supplementary Figures 7, 8**). When compared with patients with PCC, patients with GCC had lower MCP-1 levels (**Supplementary Figure 8**), but there was no statistical significance in the logistic regression analysis (**Table 3**).

DISCUSSION

In this study, we systematically analyzed the plasma metabolomic change among the AIS and control groups and patients with GCC and PCC. The metabolic profiles of plasma samples allowed the discrimination of patients with GCC and PCC. This study identified 37 metabolites that were expressed significantly differently between patients with GCC and PCC. Sphingolipid metabolism was the only significant disturbed pathway, including SA1P and S1P. In the discovery stage, compared with patients with PCC, patients with GCC had higher SA1P and S1P plasma relative levels. Besides, both SA1P and S1P had significant negative correlations with the 90-day mRS score. In the validation

sample, higher plasma S1P levels were independent predictors of GCC, and plasma S1P levels demonstrated an AUC of 0.738 (95% CI: 0.599–0.849) to differentiate patients with GCC from PCC. In addition, plasma S1P levels also showed significant negative correlations with the 90-day mRS score.

Over the past decades, increasing clinical studies have convincingly established that the status of the collateral circulation affected the prognosis of ischemic stroke (Ginsberg, 2018). Good pretreatment collaterals have been reported to be correlated with favorable functional outcomes after IVT and endovascular interventions therapy (Bang et al., 2011; Leng et al., 2016). The good leptomeningeal collateral status also independently predicted favorable functional outcomes at 6 months in patients with ischemic stroke who were not receiving IVT or endovascular interventions (Lima et al., 2010). Similarly, the *post-hoc* analysis of the Warfarin versus Aspirin for Symptomatic Intracranial Disease (WASID) trial showed that the collateral status had a strong association with subsequent territorial stroke (Liebeskind et al., 2011). In this study, we used the NIHSS score to assess the severity of the stroke and found that patients with PCC had more severe neurological deficits at admission than patients with GCC. In addition, we used the mRS score to assess 90-day functional outcomes and found that patients with PCC had poorer functional outcomes. These findings were consistent with earlier studies.

It is currently recognized that sphingolipid metabolism plays a vital role in regulating various cellular processes, which are important for health and disease (Hannun and

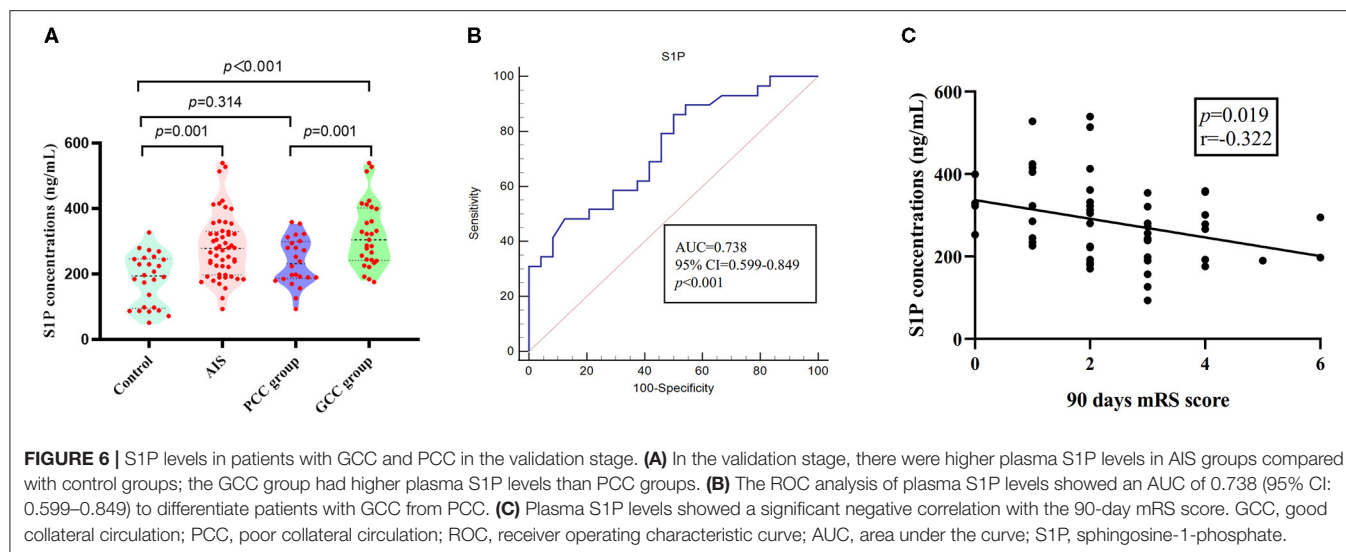


TABLE 3 | Logistic regression analysis of the association between S1P levels and cerebral collateral circulation (GCC vs. PCC).

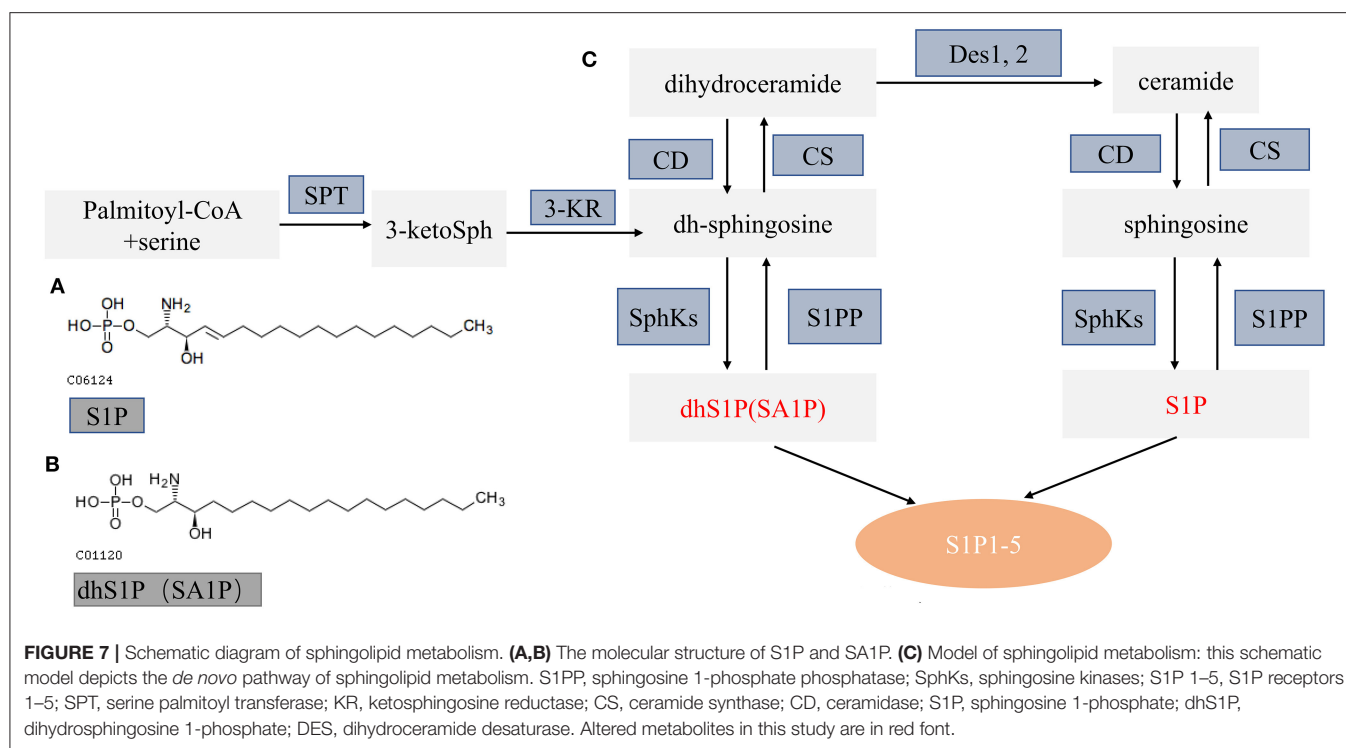
	P-value	OR (95% CI)
S1P (ng/mL)	0.014	1.013 (1.003–1.023)
MCP1 (ng/mL)	0.090	0.997 (0.950–1.004)
SBP, mmHg	0.962	0.999 (0.953–1.047)
DBP, mmHg	0.267	0.956 (0.883–1.035)
TC, mmol/L	0.737	0.562 (0.019–16.228)
LDL, mmol/L	0.962	1.115 (0.012–103.57)

GCC, good collateral circulation; PCC, poor collateral circulation; S1P, sphingosine-1-phosphate; MCP-1, monocyte chemoattractant protein-1; SBP, systolic blood pressure; DBP, diastolic blood pressure; TC, total cholesterol; LDL, low-density lipoprotein.

Obeid, 2018). *De novo* sphingolipid metabolism starts at the endoplasmic reticulum where condensation of serine and palmitoyl-CoA produce dihydroceramide and ceramide by several enzymatic reactions. Dihydroceramide and ceramide can be further hydrolyzed to dh-sphingosine and sphingosine and then phosphorylated to SA1P and S1P by sphingosine kinases (SphKs). Subsequently, SA1P and S1P were exported from cells to activate five specific G protein-coupled receptors (S1PR1–5) and function in diverse cell signaling pathways (**Figure 7**) (Callihan et al., 2012; Obinata and Hla, 2019).

To date, a mounting number of studies have demonstrated the moderating effects of the SphK-S1P-S1PR axis after stroke (Sun et al., 2016). For example, Nitzsche et al. found that endothelial S1PR1 could limit the expansion of the necrotic core in acute stroke by supporting local vasodilation (Nitzsche et al., 2021). S1P₂ also plays an essential role in cerebral ischemia. For example, S1P₂ could mediate M1 microglial polarization *via* the ERK1/2 and JNK pathway in the post-ischemic brain (Sapkota et al., 2019). Another study showed that the suppression of S1PR3 activity improved the neurological deficits by modulating microglial activation (Gaire et al., 2018). SphK2, mainly regulating the formation of S1P, is an important component of the sphingolipid pathway. Gene deletion studies

on SphK2 showed that SphK2 was an important protective molecule after cerebral ischemia *via* attenuating ischemic brain damages (Pfeilschifter et al., 2011). FTY720, an S1PR selective agonist, can also ameliorate brain injury through multiple mechanisms after ischemic stroke (Wang et al., 2020). Zhu et al. found that those patients with AIS who received a combination of fingolimod and alteplase had lower circulating lymphocytes and smaller ischemic volumes in a multicenter randomized trial (Zhu et al., 2015). As summarized above, the SphKs/S1P/S1PRs axis is involved in the regulation of many pathophysiological processes after cerebral ischemia. In this study, we found that patients with ischemic stroke had higher plasma S1P concentration compared with controls, similar to previous findings that circulating S1P levels were higher in patients with ischemic stroke than healthy controls (Testai et al., 2014; Lucaciu et al., 2020). Besides, we found that S1P had a significant negative correlation with the 90-day mRS score, indicating that higher S1P levels might predict favorable functional outcomes. Meanwhile, we also proved that patients with GCC had higher plasma S1P levels compared with patients with PCC and healthy controls, suggesting that higher S1P levels might promote collateral circulation. Previous studies have found that circulating MMP-9 and MCP-1 levels were closely related to the opening of collateral circulation after cerebral infarction (Mechtouff et al., 2020). In this study, we found that MMP-9 and MCP-1 were not associated with the collateral circulation status after cerebral infarction, which may be attributed to the difference in the sample size and research subjects. The S1P pathway is essential for vascular development and angiogenesis (Maceyka et al., 2012). Wang et al. found that reducing the expression of SphK1 resulted in suppression of the vascular endothelial growth factor (VEGF)–SphK1–S1P signal axis-related proteins and mRNAs, further inhibiting angiogenesis in the rheumatoid arthritis model (Wang et al., 2021). Abuhusain et al. suggested that S1P concentrations were higher in glioblastomas compared with the normal brain and critical to trigger angiogenesis in glioblastoma



cells (Abuhusain et al., 2013). Kiziltunç et al. found that high serum S1P levels were predictors of collateral circulation status of coronary in stable coronary artery disease (Kiziltunç et al., 2018). In the cerebral ischemia model, Nitzsche et al. found that S1P signaling played a key role in maintaining cerebral tissue perfusion and supporting vasoreactivity in the ischemic penumbra (Nitzsche et al., 2021). In a prospective and randomized clinical trial, Tian et al. found that fingolimod may preserve microvasculature function, sustain the perfusion of brain tissue, and promote retrograde reperfusion from collateral circulation (Tian et al., 2018). As summarized above, we hypothesized that the SphK1-S1P-S1PR signal axis might play a vital protective role in collateral circulation; however, the specific mechanism needs to be further explored.

SA1P, also known as dihydrosphingosine-1-phosphate (dhS1P), is produced by phosphorylation of dihydrosphingosine by sphingosine kinases (Figure 7) (Callihan et al., 2012; Magaye et al., 2019). SA1P has not been widely studied so far. Previous studies showed that SA1P treatment could protect the liver after ischemia/reperfusion *via* reducing hepatic necrosis and apoptosis and decreasing hepatic vascular permeability and expression of proinflammatory factors (Park et al., 2010a,b). Recently, studies demonstrated the reduced SA1P levels in the brains and plasma of rat models of Alzheimer's disease (Lin et al., 2017). In this study, we found that plasma SA1P levels were lower in patients with PCC compared with patients with GCC and had a negative correlation with the NIHSS score at admission and the 90-day mRS score, supporting that SA1P may be a biomarker for predicting collateral circulation, functional outcome, and disease severity.

This study had several limitations. First, since the number of cases was relatively small, the sample size needs to be expanded in future research. Second, the single-phase CTA used in this study was not the optimal approach to assess collateral circulation. Better methods of assessing collateral circulation, such as multiphase CTA or advanced perfusion software, might be more accurate. Third, due to the restricted research funding, we only validated S1P levels in another cohort, validation of other differential metabolites is needed.

CONCLUSION

Metabolic profiling on plasma samples from patients with GCC and PCC has identified 37 differential metabolites. Sphingolipid metabolism was the most affected pathway associated with brain collateral circulation. Plasma S1P levels may serve as a significant predictor of the status of collateral circulation. The results could provide new insights into the treatment of cerebral collateral circulation.

DATA AVAILABILITY STATEMENT

The original contributions generated for the study are included in the article/Supplementary Material, further inquiries can be directed to the corresponding author.

ETHICS STATEMENT

The studies involving human participants were reviewed and approved by the Ethics Committee of Xiangya Hospital of

Central South University. The patients/participants provided their written informed consent to participate in this study.

AUTHOR CONTRIBUTIONS

JX: concept and design. FY, XF, XL, ZL, DL, YL, MW, LZ, and QH: clinical data. XF and FY: metabolomic analysis and interpretations, statistical analyses, and draft manuscript. All authors reviewed and edited the draft manuscript and approved the final manuscript.

FUNDING

This study was supported by the Project Program of the National Clinical Research Center for Geriatric Disorders (Xiangya

Hospital, Grant No. 2020LNJJ16) and the Provincial Key Plan for Research and Development of Hunan (Grant No. 2020SK2067).

ACKNOWLEDGMENTS

We thank all the patients for their participation in this study. We thank Dr. Yuanlin Ying from the Department of Neurology, Xiangya Hospital, Central South University, for her help in language polishing.

SUPPLEMENTARY MATERIAL

The Supplementary Material for this article can be found online at: <https://www.frontiersin.org/articles/10.3389/fphys.2021.720672/full#supplementary-material>

REFERENCES

- Abuhusain, H. J., Matin, A., Qiao, Q., Shen, H., Kain, N., Day, B. W., et al. (2013). A metabolic shift favoring sphingosine 1-phosphate at the expense of ceramide controls glioblastoma angiogenesis. *J. Biol. Chem.* 288, 37355–37364. doi: 10.1074/jbc.M113.494740
- Bang, O. Y., Saver, J. L., Kim, S. J., Kim, G. M., Chung, C. S., Ovbiagele, B., et al. (2011). Collateral flow predicts response to endovascular therapy for acute ischemic stroke. *Stroke* 42, 693–699. doi: 10.1161/STROKEAHA.110.595256
- Callihan, P., Zitomer, N. C., Stoeling, M. V., Kennedy, P. C., Lynch, K. R., Riley, R. T., et al. (2012). Distinct generation, pharmacology, and distribution of sphingosine 1-phosphate and dihydrosphingosine 1-phosphate in human neural progenitor cells. *Neuropharmacology* 62, 988–996. doi: 10.1016/j.neuropharm.2011.10.005
- Gaire, B. P., Song, M. R., and Choi, J. W. (2018). Sphingosine 1-phosphate receptor subtype 3 (S1P3) contributes to brain injury after transient focal cerebral ischemia via modulating microglial activation and their M1 polarization. *J. Neuroinflammation* 15:284. doi: 10.1186/s12974-018-1323-1
- Ginsberg, M. D. (2018). The cerebral collateral circulation: relevance to pathophysiology and treatment of stroke. *Neuropharmacology* 134, 280–292. doi: 10.1016/j.neuropharm.2017.08.003
- Hannun, Y. A., and Obeid, L. M. (2018). Sphingolipids and their metabolism in physiology and disease. *Nat. Rev. Mol. Cell Biol.* 19, 175–191. doi: 10.1038/nrm.2017.107
- Jiang, W., Hu, W., Ye, L., Tian, Y., Zhao, R., Du, J., et al. (2019). Contribution of Apelin-17 to collateral circulation following cerebral ischemic stroke. *Transl. Stroke Res.* 10, 298–307. doi: 10.1007/s12975-018-0638-7
- Kiziltunç, E., Gök, M., Topçuoğlu, C., Kundi, H., Çetin, M., Turhan, T., et al. (2018). Serum sphingosine 1 phosphate levels in patients with and without coronary collateral circulation. *Acta Cardiologica Sinica* 34, 379–385. doi: 10.6515/ACS.201809_34(5).20180405A
- Leng, X., Lan, L., Liu, L., Leung, T. W., and Wong, K. S. (2016). Good collateral circulation predicts favorable outcomes in intravenous thrombolysis: a systematic review and meta-analysis. *Eur. J. Neurol.* 23, 1738–1749. doi: 10.1111/ene.13111
- Liebeskind, D. S. (2003). Collateral circulation. *Stroke* 34, 2279–2284. doi: 10.1161/01.STR.0000086465.41263.06
- Liebeskind, D. S., Cotsonis, G. A., Saver, J. L., Lynn, M. J., Turan, T. N., Cloft, H. J., et al. (2011). Collaterals dramatically alter stroke risk in intracranial atherosclerosis. *Ann. Neurol.* 69, 963–974. doi: 10.1002/ana.22354
- Lima, F. O., Furie, K. L., Silva, G. S., Lev, M. H., Camargo, E. C., Singhal, A. B., et al. (2010). The pattern of leptomeningeal collaterals on CT angiography is a strong predictor of long-term functional outcome in stroke patients with large vessel intracranial occlusion. *Stroke* 41, 2316–2322. doi: 10.1161/STROKEAHA.110.592303
- Lin, W., Zhang, J., Liu, Y., Wu, R., Yang, H., Hu, X., et al. (2017). Studies on diagnostic biomarkers and therapeutic mechanism of Alzheimer's disease through metabolomics and hippocampal proteomics. *Eur. J. Pharm. Sci.* 105, 119–126. doi: 10.1016/j.ejps.2017.05.003
- Lucaciu, A., Kuhn, H., Trautmann, S., Ferreirós, N., Steinmetz, H., Pfeilschifter, J., et al. (2020). A sphingosine 1-phosphate gradient is linked to the cerebral recruitment of T helper and regulatory T helper cells during acute ischemic stroke. *Int. J. Mol. Sci.* 21:6242. doi: 10.3390/ijms21176242
- Maceyka, M., Harikumar, K. B., Milstien, S., and Spiegel, S. (2012). Sphingosine-1-phosphate signaling and its role in disease. *Trends Cell Biol.* 22, 50–60. doi: 10.1016/j.tcb.2011.09.003
- Magaye, R. R., Savira, F., Hua, Y., Kelly, D. J., Reid, C., Flynn, B., et al. (2019). The role of dihydrosphingolipids in disease. *Cell. Mol. Life Sci.* 76, 1107–1134. doi: 10.1007/s00018-018-2984-8
- Mechatouff, L., Bochaton, T., Paccalet, A., Crola Da Silva, C., Buisson, M., Amaz, C., et al. (2020). Matrix metalloproteinase-9 and monocyte chemoattractant protein-1 are associated with collateral status in acute ischemic stroke with large vessel occlusion. *Stroke* 51, 2232–2235. doi: 10.1161/STROKEAHA.120.029395
- Menon, B. K., Qazi, E., Nambiar, V., Foster, L. D., Yeatts, S. D., Liebeskind, D., et al. (2015). Differential effect of baseline computed tomographic angiography collaterals on clinical outcome in patients enrolled in the interventional management of stroke III trial. *Stroke* 46, 1239–1244. doi: 10.1161/STROKEAHA.115.009009
- Menon, B. K., Smith, E. E., Coutts, S. B., Welsh, D. G., Faber, J. E., Goyal, M., et al. (2013). Leptomeningeal collaterals are associated with modifiable metabolic risk factors. *Ann. Neurol.* 74, 241–248. doi: 10.1002/ana.23906
- Nitzsche, A., Poittevin, M., Benarab, A., Bonnin, P., Faraco, G., Uchida, H., et al. (2021). Endothelial S1P(1) signaling counteracts infarct expansion in ischemic stroke. *Circ. Res.* 128, 363–382. doi: 10.1161/CIRCRESAHA.120.316711
- Obinata, H., and Hla, T. (2019). Sphingosine 1-phosphate and inflammation. *Int. Immunol.* 31, 617–625. doi: 10.1093/intimm/dxz037
- Park, S. W., Kim, M., Chen, S. W., Brown, K. M., D'Agati, V. D., and Lee, H. T. (2010a). Sphinganine-1-phosphate protects kidney and liver after hepatic ischemia and reperfusion in mice through S1P1 receptor activation. *Lab. Invest.* 90, 1209–1224. doi: 10.1038/labinvest.2010.102
- Park, S. W., Kim, M., Chen, S. W., D'Agati, V. D., and Lee, H. T. (2010b). Sphinganine-1-phosphate attenuates both hepatic and renal injury induced by hepatic ischemia and reperfusion in mice. *Shock (Augusta, Ga)* 33, 31–42. doi: 10.1097/SHK.0b013e3181c02c1f
- Pfeilschifter, W., Czech-Zechmeister, B., Sujak, M., Mirceska, A., Koch, A., Rami, A., et al. (2011). Activation of sphingosine kinase 2 is an endogenous protective mechanism in cerebral ischemia. *Biochem. Biophys. Res. Commun.* 413, 212–217. doi: 10.1016/j.bbrc.2011.08.070
- Qin, C., Zhao, X. L., Ma, X. T., Zhou, L. Q., Wu, L. J., Shang, K., et al. (2019). Proteomic profiling of plasma biomarkers in acute ischemic stroke due to large vessel occlusion. *J. Transl. Med.* 17:214. doi: 10.1186/s12967-019-1962-8
- Sapkota, A., Gaire, B. P., Kang, M. G., and Choi, J. W. (2019). S1P(2) contributes to microglial activation and M1 polarization following cerebral ischemia through ERK1/2 and JNK. *Sci. Rep.* 9:12106. doi: 10.1038/s41598-019-48609-z

- Shen, X., Wang, R., Xiong, X., Yin, Y., Cai, Y., Ma, Z., et al. (2019). Metabolic reaction network-based recursive metabolite annotation for untargeted metabolomics. *Nat. Commun.* 10:1516. doi: 10.1038/s41467-019-09550-x
- Smith, C. A., Want, E. J., O'Maille, G., Abagyan, R., and Siuzdak, G. (2006). XCMS: processing mass spectrometry data for metabolite profiling using nonlinear peak alignment, matching, and identification. *Anal. Chem.* 78, 779–787. doi: 10.1021/ac051437y
- Sun, N., Keep, R. F., Hua, Y., and Xi, G. (2016). Critical role of the sphingolipid pathway in stroke: a review of current utility and potential therapeutic targets. *Transl. Stroke Res.* 7, 420–438. doi: 10.1007/s12975-016-0477-3
- Testai, F. D., Kilgus, J. P., Berdyshev, E., Gorshkova, I., Natarajan, V., and Dawson, G. (2014). Multiple sphingolipid abnormalities following cerebral microendothelial hypoxia. *J. Neurochem.* 131, 530–540. doi: 10.1111/jnc.12836
- Tian, D. C., Shi, Z., Zhu, J., Yao, X., Yang, L., et al. (2018). Fingolimod enhances the efficacy of delayed alteplase administration in acute ischemic stroke by promoting anterograde reperfusion and retrograde collateral flow. *Ann. Neurol.* 84, 717–728. doi: 10.1002/ana.25352
- Wang, Y., Wu, H., Deng, R., Dai, X. J., Bu, Y. H., Sun, M. H., et al. (2021). Geniposide downregulates the VEGF/SphK1/S1P pathway and alleviates angiogenesis in rheumatoid arthritis *in vivo* and *in vitro*. *Phytother. Res.* doi: 10.1002/ptr.7130. [Epub ahead of print].
- Wang, Z., Kawabori, M., and Houkin, K. (2020). FTY720 (Fingolimod) Ameliorates Brain Injury through Multiple Mechanisms and is a Strong Candidate for Stroke Treatment. *Curr. Med. Chem.* 27, 2979–2993. doi: 10.2174/0929867326666190308133732
- Wiegers, E. J. A., Mulder, M., Jansen, I. G. H., Venema, E., Compagne, K. C. J., Berkhemer, O. A., et al. (2020). Clinical and imaging determinants of collateral status in patients with acute ischemic stroke in MR CLEAN trial and registry. *Stroke* 51, 1493–1502. doi: 10.1161/STROKEAHA.119.027483
- Yu, F., Lu, J., Li, Z., Zhou, X., Zeng, S., Zhan, Q., et al. (2017). Correlation of plasma vascular endothelial growth factor and endostatin levels with symptomatic intra- and extracranial atherosclerotic stenosis in a chinese han population. *J. Stroke Cerebrovasc. Dis.* 26, 1061–1070. doi: 10.1016/j.jstrokecerebrovasdis.2016.12.021
- Yu, F., Zhou, X., Li, Z., Feng, X., Liao, D., Liu, Z., et al. (2019). Diagnostic significance of plasma levels of novel adipokines in patients with symptomatic intra- and extracranial atherosclerotic stenosis. *Front. Neurol.* 10:1228. doi: 10.3389/fneur.2019.01228
- Zhu, Z., Fu, Y., Tian, D., Sun, N., Han, W., Chang, G., et al. (2015). Combination of the immune modulator fingolimod with alteplase in acute ischemic stroke: a pilot trial. *Circulation* 132, 1104–1112. doi: 10.1161/CIRCULATIONAHA.115.016371

Conflict of Interest: The authors declare that the research was conducted in the absence of any commercial or financial relationships that could be construed as a potential conflict of interest.

Publisher's Note: All claims expressed in this article are solely those of the authors and do not necessarily represent those of their affiliated organizations, or those of the publisher, the editors and the reviewers. Any product that may be evaluated in this article, or claim that may be made by its manufacturer, is not guaranteed or endorsed by the publisher.

Copyright © 2021 Yu, Feng, Li, Liu, Liao, Luo, Wei, Huang, Zhang and Xia. This is an open-access article distributed under the terms of the Creative Commons Attribution License (CC BY). The use, distribution or reproduction in other forums is permitted, provided the original author(s) and the copyright owner(s) are credited and that the original publication in this journal is cited, in accordance with accepted academic practice. No use, distribution or reproduction is permitted which does not comply with these terms.



Revealing the Angiopathy of Lacrimal Gland Lesion in Type 2 Diabetes

Junfa Xue^{1,2}, Bin Zhang², Shengqian Dou², Qingjun Zhou², Min Ding², Mingming Zhou³, Huifeng Wang^{2,4}, Yanling Dong³, Dongfang Li^{3,4*} and Lixin Xie^{3*}

¹ School of Medicine and Life Sciences, Shandong First Medical University, Jinan, China, ² State Key Laboratory Cultivation Base, Shandong Province Key Laboratory of Ophthalmology, Shandong Eye Institute, Shandong First Medical University & Shandong Academy of Medical Sciences, Qingdao, China, ³ Qingdao Eye Hospital of Shandong First Medical University, Qingdao, China, ⁴ Department of Medicine, Qingdao University, Qingdao, China

OPEN ACCESS

Edited by:

Dongze Zhang,
University of Nebraska Medical
Center, United States

Reviewed by:

Sizhao Lu,
University of Colorado, United States
Huocong Huang,
University of Texas Southwestern
Medical Center, United States

*Correspondence:

Dongfang Li
qdye_dfl@yeah.net
Lixin Xie
lixin_xie@hotmail.com

Specialty section:

This article was submitted to
Vascular Physiology,
a section of the journal
Frontiers in Physiology

Received: 26 June 2021

Accepted: 06 August 2021

Published: 31 August 2021

Citation:

Xue J, Zhang B, Dou S, Zhou Q, Ding M, Zhou M, Wang H, Dong Y, Li D and Xie L (2021) Revealing the Angiopathy of Lacrimal Gland Lesion in Type 2 Diabetes. *Front. Physiol.* 12:731234. doi: 10.3389/fphys.2021.731234

For a better understanding of diabetic angiopathy (DA), the potential biomarkers in lacrimal DA and its potential mechanism, we evaluated the morphological and hemodynamic alterations of lacrimal glands (LGs) in patients with type 2 diabetes and healthy counterparts by color Doppler flow imaging (CDFI). We further established a type 2 diabetic mice model and performed hematoxylin-eosin (HE) staining, immunofluorescence staining of CD31, RNA-sequencing analysis, and connectivity map (CMap) analysis. We found atrophy and ischemia in patients with type 2 diabetes and mice models. Furthermore, we identified 846 differentially expressed genes (DEGs) between type 2 diabetes mellitus (T2DM) and vehicle mice by RNA-seq. The gene ontology (GO) analysis indicated significant enrichment of immune system process, regulation of blood circulation, apoptotic, regulation of secretion, regulation of blood vessel diameter, and so on. The molecular complex detection (MCODE) showed 17 genes were involved in the most significant module, and 6/17 genes were involved in vascular disorders. CytoHubba revealed the top 10 hub genes of DEGs, and four hub genes (App, F5, Fgg, and Gas6) related to vascular regulation were identified repeatedly by MCODE and cytoHubba. GeneMANIA analysis demonstrated functions of the four hub genes above and their associated molecules were primarily related to the regulation of circulation and coagulation. CMap analysis found several small molecular compounds to reverse the altered DEGs, including disulfiram, bumetanide, genistein, and so on. Our outputs could empower the novel potential targets to treat lacrimal angiopathy, diabetes dry eye, and other diabetes-related diseases.

Keywords: diabetes, lacrimal gland, vasculature, DEGs, hub gene

INTRODUCTION

Type 2 diabetes mellitus (T2DM) and diabetic complications have been with high mortality and morbidity year by year and arouse great concern throughout the globe (Vujkovic et al., 2020). Dry eye (DE) syndrome, as one of the main diabetic complications on the ocular surface, is a common eye disease due to a reduction in the volume or quality of tears (Nakamachi et al., 2016) manifesting as increased tear evaporation, hyperosmolarity, and tear film instability, as well as vulnerability to infection, inflammation, sensory neuropathy, and damage of the ocular surface (Markoulli et al., 2018). Tear components are secreted mainly from the lacrimal gland (LG), which has a high risk

of lesion and secretion deficiency in patients affected by diabetes (Jiao et al., 2020; Qu et al., 2021). The possible reason for the lacrimal lesion in diabetes may be angiopathy for the dense vasculature distributions in LG and the critical role of angiopathy in the pathogenesis of diabetes, diabetic retinopathy, and diabetic nephropathy (Gao et al., 2019).

Previous studies have revealed the LG atrophied and morphology change in type 1 diabetes (Jiao et al., 2020; Qu et al., 2021). There is growing evidence that AGE, AGER, and immune-related molecules (like NF- κ B, interferons, and interleukin-27) are highly expressed in LGs of a diabetic animal model (Alves et al., 2005; Ciecko et al., 2019; Allred et al., 2021), which proves that these factors are involved in signaling and subsequent inflammatory alterations related to DE in diabetes. A study by our research groups has demonstrated that the mitochondrial bioenergetic deficit in diabetic LG may contribute to the early onset of DE, while mitochondria-targeted antioxidant has therapeutic potential for diabetic DE and keratopathy (Qu et al., 2021). However, type 2 diabetes accounts for 90–95% of all diabetes morbidity (Basterra-Gortari et al., 2019), the lacrimal lesion of which has not been fully elucidated. The microvascular complication of diabetes generated in retina, kidney, and nervous system (Knudsen et al., 2019) has not been clearly illustrated in the LG.

In the present study, we aim to investigate the morphology and blood flow status changes in LG of patients with type 2 diabetes by color Doppler flow imaging (CDFI) (Bilgili et al., 2005; Lecler et al., 2017). To better understand the potential biomarkers and mechanisms for diabetic lacrimal lesion, lacrimal angiopathy, diabetes, and other metabolic diseases, we established the type 2 diabetic mice model and

performed the RNA-sequencing. By using gene ontology (GO) analysis, protein-protein interaction (PPI) network, molecular complex detection (MCODE), cytoHubba, and geneMANIA, we aim to identify the hub biomarkers and their related mechanisms in diabetic lacrimal angiopathy. Furthermore, a connectivity map (CMap) analysis was performed to predict the potential therapeutic agents. The schematic diagram of the whole study is presented in **Figure 1**. Our output could empower the novel and more comprehensive diagnostic and therapeutic targets for type 2 diabetic lacrimal angiopathy, diabetic DE, and other chronic metabolic diseases.

MATERIALS AND METHODS

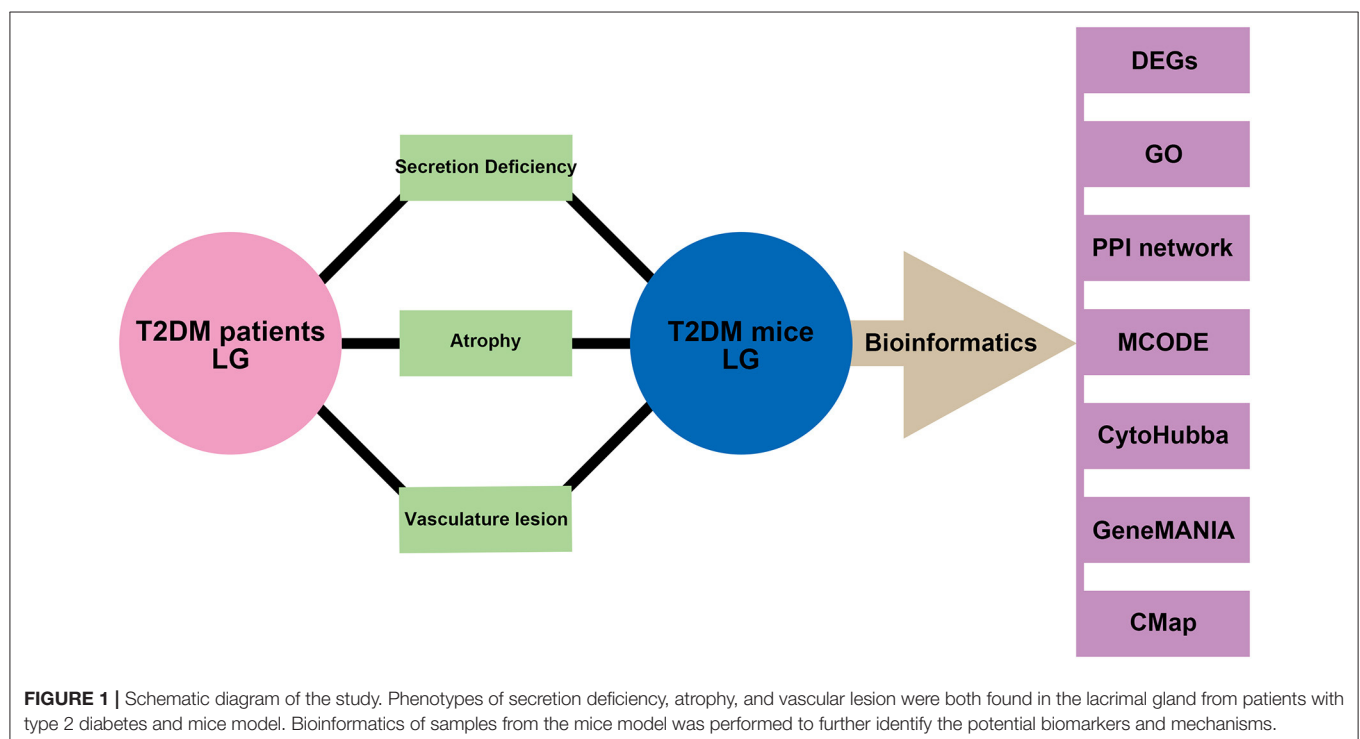
Ethical Approval

Clinical Research Section

The single-center prospective clinical controlled trial study was approved by the Ethics Committee of Qingdao Eye Hospital (No. 2019-27) and adhered to the Declaration of Helsinki's tenets. All subjects agreed to participate in this study and signed the informed consent. The clinical trial was registered on the Chinese Clinical Trial Registry (www.chictr.org.cn), and the registration number is ChiCTR2000032843.

Basic Research Section

All studies on animals were approved by the Experimental Animal Ethics Committee of Shandong first medical University and were performed in accordance with the Association for Research in Vision and Ophthalmology (ARVO) Statement for the Use of Animals in Ophthalmic and Vision Research.



Clinical General Information

Patients with type 2 diabetes were randomly selected from outpatients with a hemoglobin A1C value above 6.5% at Qingdao Eye Hospital. Thirty patients with diabetes for <10 years (average age, 59.00 ± 7.89 years), 30 patients with diabetes for more than 10 years (average age, 63.67 ± 9.00 years), and 30 controls with no history and signs of diabetes (average age, 60.97 ± 12.63 years) were enrolled and received examinations from June 2019 to June 2020. All of them had no history of ocular surgery or trauma, other systemic diseases, or utilization of drugs known to disturb blood flow. Female subjects were not in the menstrual period. All subjects lived in Shandong province for a long time (more than 10 years) and followed the diet habits of the Han nationality. All examinations were performed by a proficient operator (MZ).

Clinical Examination Methods

All subjects underwent a general ophthalmologic examination, including the Schirmer test and CDFI. The results of one randomly chosen eye of each subject were assessed. No complications or complaints of orbital tissue discomfort due to the measurements occurred. Researchers were blind to the history of diabetes of enrolled subjects before examinations.

All procedures of CDFI were performed in strict accordance with the standard process and previous research methods (Bilgili et al., 2005; Lecler et al., 2017). The CDFI was performed when patients were supine with eyelids closed. The lacrimal region (superolateral margin of the orbit) was scanned obliquely, with a scanning plane almost parallel to the anterior outline of the orbit, and using part of the ocular globe as an acoustic window. The lacrimal artery has proved to be an optimal landmark to identify the gland (Bilgili et al., 2005). As the LG was identified, the scanning plane was oriented to view its longest diameter. Color Doppler sonography was then performed by the same operator with an ultrasound scanner (Esaote MyLab Class C Advanced, Italy) equipped with a multifrequency linear-array transducer (6–18 MHz). Doppler parameters were adjusted for detection of low velocity or low volume flow or both. The pulse repetition frequency used was 1.3 kHz, the bandpass filter was set at 50 Hz, and high levels were adjusted for both color vs. echo priority and color persistence. To further increase the depiction of vessel continuity, the power Doppler mode was also used. To evaluate the lacrimal artery by pulsed Doppler sonography, we used a pulse repetition frequency of 1.3 kHz, a sample volume of 0.5 mm, and gain 55%. Peak systolic velocity (PSV) was measured. Resistance index (RI) and pulsatility index (PI) values were calculated to evaluate peripheral resistance inside the gland. To avoid the excessively high temperature caused by increased energy necessary for Doppler, the procedure was limited for the minimum amount of time required to effectively evaluate the patient. All the LGs were scanned in two dimensions (longitudinal section of the LG and cross-section of the LG), and the images were processed by ImageJ to calculate the pixels of the lacrimal area in the same size of graphs.

Animal Model

To establish the T2DM mice model (Xing et al., 2021), 4-week-old male C57BL/6 (B6) mice (purchased from the SPF

Biotechnology Co., Ltd., Beijing, China, and fed in the Laboratory animal Center of Shandong Eye Institute) were fed with a high-fat diet (HFD, Cat#D12451, Beijing Keao Xieli Feed Co., Ltd., China; 60 kcal% fat, HFD) for 6 weeks. The mice were then fasted and intraperitoneal injection of a low dose of streptozotocin (STZ) of 50 mg/kg (Sigma-Aldrich, St. Louis, MO) for 5 consecutive days, then kept on an HFD diet for the next 24 weeks. The control mice were fed with a normal diet and injected with citrate buffer only. Diabetic mice were defined as having instant blood glucose levels > 16.7 mmol/L. Experiments *in vivo* and *in vitro* were tabbed by one assistant and performed by another operator.

Histopathology and Immunofluorescence Staining

Paraffin sections of LGs were stained with hematoxylin and eosin. Immunohistochemistry of amyloid precursor protein (App; ab32136, Abcam) and fibrinogen gamma chain (Fgg; ab281924, Abcam) was performed following standard procedures. According to a previous study (Cao et al., 2011), the whole-mount immunofluorescence staining of LGs was collected and fixed in 4% paraformaldehyde in 0.1 M phosphate saline (Phosphate Buffered Saline, pH 7.2–7.4) for 45 min at room temperature. The samples were then washed in PBS, and permeabilized by acetone for 7 min. After being washed in PBS, the samples were blocked in PBS containing 0.3% Triton X-100, 10% donkey serum overnight, and then incubated in the same buffer with primary antibodies (CD31 antibody, 1:200, R&D systems, USA) for 2 nights. Secondary antibodies labeled with Alexa 594 (1:500; red fluorescence, Invitrogen) were used for 48 h after washing off the primary antibody with PBS. After washing each LG six times, the flattened samples were examined under a confocal microscope (Zeiss, Rosdorf, Germany). Images were processed using Image-pro Plus 6.0 (Media cybematics, USA) and Adobe Photoshop (Adobe Systems, Inc., San Jose, CA, USA) software. CD31 positive staining quantification: the area of the positive staining pixel and corresponding tissue pixel in each field was measured with the pixel area as the standard unit. And the percentage of positive area is given by, positive area (%) = positive pixel area/tissue pixel area \times 100.

RNA Extraction and PCR Analysis

The mRNA expression of CD31, F5, Gas6, Fgg, and App in normal and diabetic LG was detected. Total RNA was extracted from collected mouse LG using NucleoSpin RNA kits (Takara, Dalian, China). cDNAs were synthesized using PrimeScript RT

TABLE 1 | List of primers used for mRNA expression analyses.

Gene name	Forward primer, 5'-3'	Reverse primer, 5'-3'
GAPDH	CACTGAGCAAGAGAGGCCCTAT	GCAGCGAACTTTATTGATGGTATT
F5	ATACGCTGAAGTTGGGGACG	GGCATCATCCTTCCTCTCGG
Gas6	GGCTCAACTACACCCGAACA	GACAGTGACCGTGTGTTCTCT
Fgg	ACGAGACAAGCATTGCGTATT	AGAAGTGCTGCTTAGCTTTCAA
App	AAAGACAGACAGCACACCTAA	ACTGGTTCATGCGCTCGTA
CD31	CAGAGCGGATAATTGCCATTC	TTCACAGAGCACCCGAAGTACCA

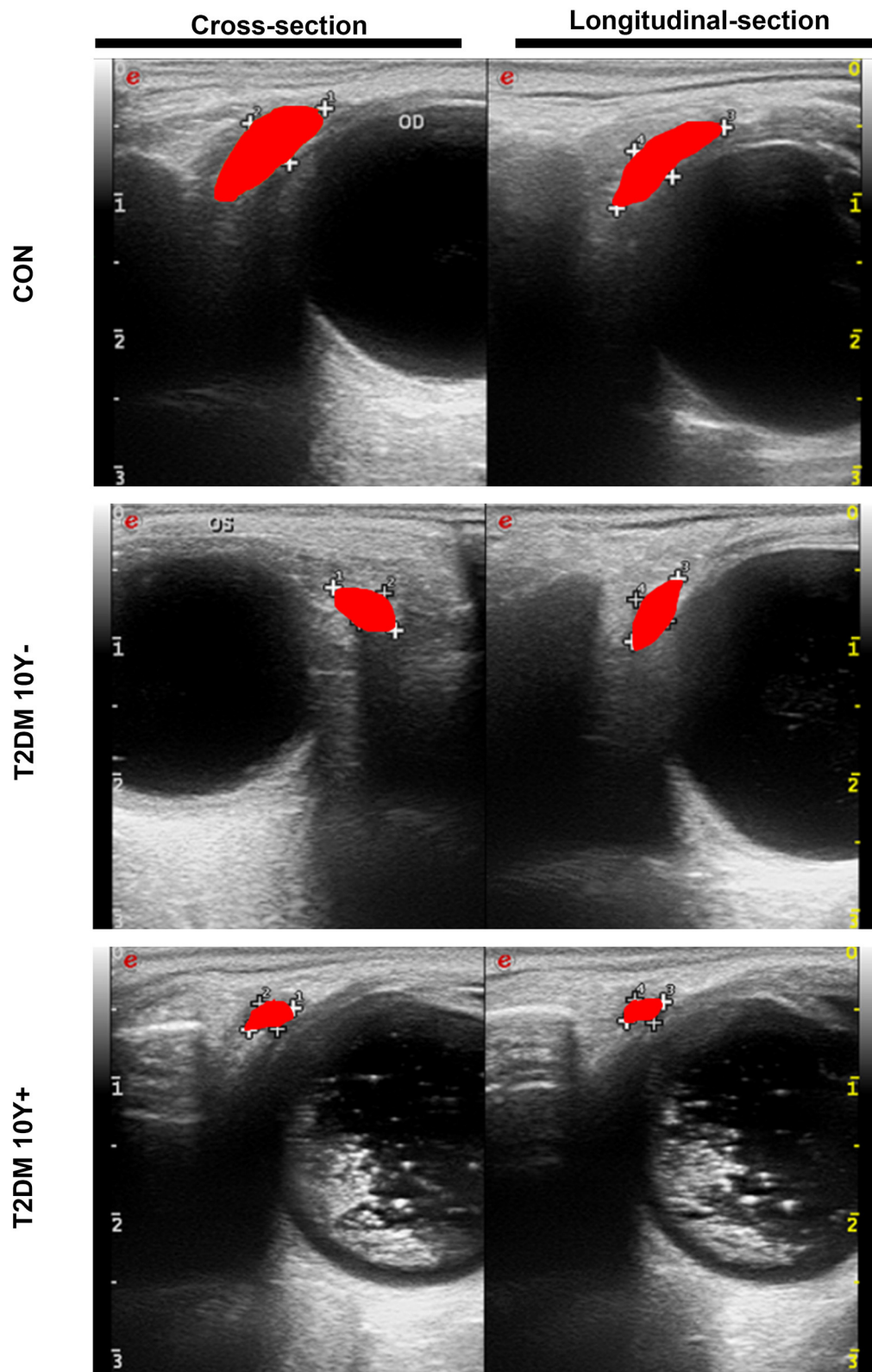


FIGURE 2 | Morphological changes of LGs in patients with type 2 diabetes and control by CDFI. LGs from patients with T2DM and controls were measured by CDFI in two dimensions including the cross-section and longitudinal-section to demonstrate the morphological changes. The red area indicates the position and size of the LG. T2DM 10Y-, diabetic duration <10 years; T2DM 10Y+, diabetic duration more than 10 years; LG, lacrimal gland.

Master Mix (Takara). Real time PCR [Quantitative Reverse Transcription (qRT)-PCR] was carried out using ChamQ Universal SYBR qPCR Master Mix (Vazyme Biotech Co., Ltd., Nanjing, China) and the 7500 Real-Time PCR System (Applied Biosystems, Foster City, CA). The thermocycling conditions used were 30 s at 95°C followed by 40 two-step cycles (10 s at 95°C and 30 s at 60°C). The sequences of the primers used in this assay are listed in **Table 1**. The quantification data were analyzed with Sequence Detection System software (Applied Biosystems), using b-actin expression as an internal control.

RNA-Sequencing and GO Analysis

The LG samples from type 2 diabetic mice or vehicles were collected with Trizol reagent. The mRNA was enriched by NEBNext® Poly(A) mRNA Magnetic Isolation Module (New England Biolabs), and the produced RNA was used for construction Library, *via* KAPA Stranded RNA-Seq Library Prep Kit (Illumina). The prepared RNA-seq libraries were qualified using Agilent 2100 Bioanalyzer and quantified by the qPCR absolute quantification method. The sequencing was then performed using Illumina NovaSeq 6000. After quality control, the fragments were 5', 3'-adaptor trimmed and filtered ≤ 16 bp reads with cutadapt software. The trimmed reads were aligned to a reference genome (source: genecode, version: GRCh38) with Hisat2 software. The transcript abundance for each sample was estimated with StringTie (v1.2.3), and the Fragments Per Kilobase of exon model per Million mapped fragments (FPKM) values for gene-level were calculated with R package Ballgown (v2.6.0). The differentially expressed genes (DEGs) analysis was also performed with Ballgown. Fold change (cutoff 1.5), *p*-value (cutoff 0.05), and FPKM (≥ 0.5 mean in one group) were used for filtering DEGs and transcripts. GO analyses of DEGs were performed *via* DAVID (6.8, <http://david.ncifcrf.gov>) (Gene Ontology, 2021). Gene count > 2 and *p* < 0.05 were set as the threshold.

PPI Network Creation and Hub Gene Identification

PPI network of DEGs was constructed by STRING (11.0b; <https://string-db.org/>) with a combined score > 0.9 as the cut-off point (Kwon et al., 2018). Hub genes were identified using cytoHubba (Su et al., 2021), a plug-in of Cytoscape software (Cytoscape, 3.8.2), and significant modules in the PPI network were identified by MCODE 2.0.0 (Azad et al., 2018), another plug-in of Cytoscape software. The parameters of DEGs clustering and scoring were set as follows: MCODE score ≥ 4 , degree cut-off = 2, node score cut-off = 0.2, max depth = 100, and k-score = 2.

GeneMANIA

GeneMANIA (3.5.2, <http://www.genemania.org>) finds the most connected genes to a set of known genes (Franz et al., 2018), using a very large set of functional association data. Association data include protein and genetic interactions, pathways, co-expression, co-localization, and protein domain similarity. We used it to the weight that indicates the predictive value of hub genes and seeks the interactive functional network.

CMap Analysis

The CMap (<https://portals.broadinstitute.org/cmap>) is an open resource that links disease, genes, and drugs by similar or opposite gene expression profiles (Yoo et al., 2019). CMap analysis is applied to predict potential small molecular compounds that can reverse altered expression of DEGs in cell lines. Mean < -0.4 and *p* < 0.05 were set as the screening criteria.

Enzyme-Linked Immunosorbent Assay

The LG samples of diabetic and vehicle mice were collected, crushed, and separated by centrifugation. App and Fgg levels were determined by mouse enzyme-linked immunosorbent assay (ELISA) kits (SEB020Mu, SEC477Mu, Cloud-clone, China) according to the protocol of the manufacturer.

TABLE 2 | Clinical characteristics of patients with type 2 diabetes and controls by color Doppler flow imaging (CDFI).

Groups	N (n = 30)	DM (10Y-, n = 30)	DM (10Y+, n = 30)	P-values		
				N vs. DM(10Y-)	N vs. DM(10Y+)	DM(10Y-) vs. DM(10Y+)
Gender						
Male	13	14	13	0.795	1.000	0.795
Female	17	16	17			
Age (years)	60.97 ± 12.63	59.00 ± 7.89	63.67 ± 9.00	0.45	0.28	0.07
DD (months)	0	4.47 ± 2.65	16.77 ± 6.92	<0.001	<0.001	<0.001
TS (mm)	9.17 ± 3.00	6.30 ± 4.22	6.33 ± 4.16	0.005	0.005	0.973
LG-L	1607.27 ± 456.39	1125.53 ± 383.15	1029.60 ± 294.01	<0.001	<0.001	0.34
LG-C	1297.77 ± 349.67	966.20 ± 404.34	853.73 ± 268.64	<0.001	<0.001	0.21
PSV(cm/s)	9.31 ± 3.13	8.17 ± 2.18	8.72 ± 2.82	0.11	0.41	0.44
PI	1.47 ± 0.42	1.72 ± 0.62	1.89 ± 0.58	0.081	0.003	0.215
RI	0.74 ± 0.10	0.76 ± 0.10	0.79 ± 0.09	0.44	0.02	0.11

Variables are presented as mean \pm SD. N, control group; DM10Y-, diabetic duration <10 years; DM10Y+, diabetic duration more than 10 years; OS, left eye; OD, right eye; DD, Duration of diabetes; TS, tear secretion; LG-L, longitudinal section of the lacrimal gland; LG-C, cross-section of the lacrimal gland; PSV, peak systolic velocity; RI, resistance index; PI, pulsatility index.

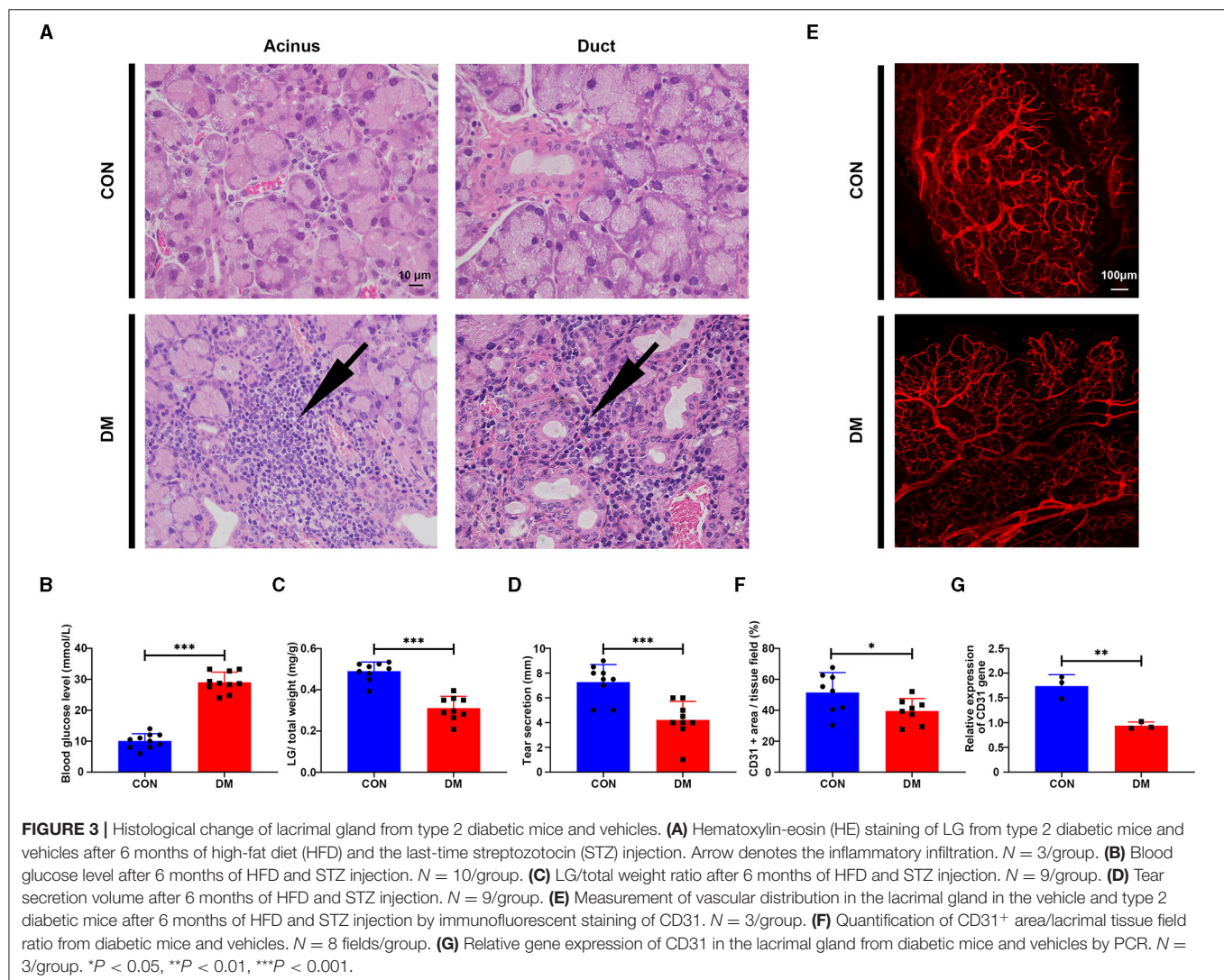
Statistical Analysis

Data were analyzed by SPSS version 22.0 (IBM Corp., Armonk, NY, USA) and presented as the mean \pm SD. Data normality was assessed by the Shapiro-Wilk test. Analysis of chi-squared test was performed to compare the gender and eye side of three groups of patients. Three groups of patients of age, duration of diabetes, tear secretion volume, longitudinal section of the LG, cross-section of the LG, PSV, RI, and PI were analyzed using one-way ANOVA and shown as mean \pm SD. Repeated-measurement analysis of the unpaired Student's *t*-test was performed to compare the numerical values including blood glucose level, LG/total weight ratio, mice tear secretion, CD31+area/tissue field, expression of App and Fgg proteins, and relative expression of F5, Gas6, Fgg, App, and CD31 genes in LG from diabetic mice and vehicle group. The statistical analyses of DEGs were done in R software. The *p*-values in CMap analysis were analyzed in the CMap (<https://portals.broadinstitute.org/cmap>). A least-significant difference (LDS) was used as *post-hoc* analysis with *P* < 0.05 considered as significant.

RESULTS

Comparison of LG Morphology and Hemodynamics Between Patients With Type 2 Diabetes and Healthy Controls

Lacrimal dysfunction is an important cause of morbidity in diabetic DE (Shih et al., 2017; Qu et al., 2021). To know the morphological and hemodynamic alterations of LG from patients with type 2 diabetes, the CDFI was performed for its advantage of not only demonstrating the shape of LGs but also providing real-time dynamic data of blood flow in LGs (Bilgili et al., 2005). As shown in **Figure 2**, **Table 2**, the tear secretion volume in the T2DM group decreased significantly, and the LG atrophied markedly in different dimensions in patients with diabetes as compared with healthy controls. However, the difference was not significant between patients with diabetes for <10 years and over 10 years. This suggested that, at the onset of type 2 diabetes, the LG had undergone an obvious pathological process that may continue to affect



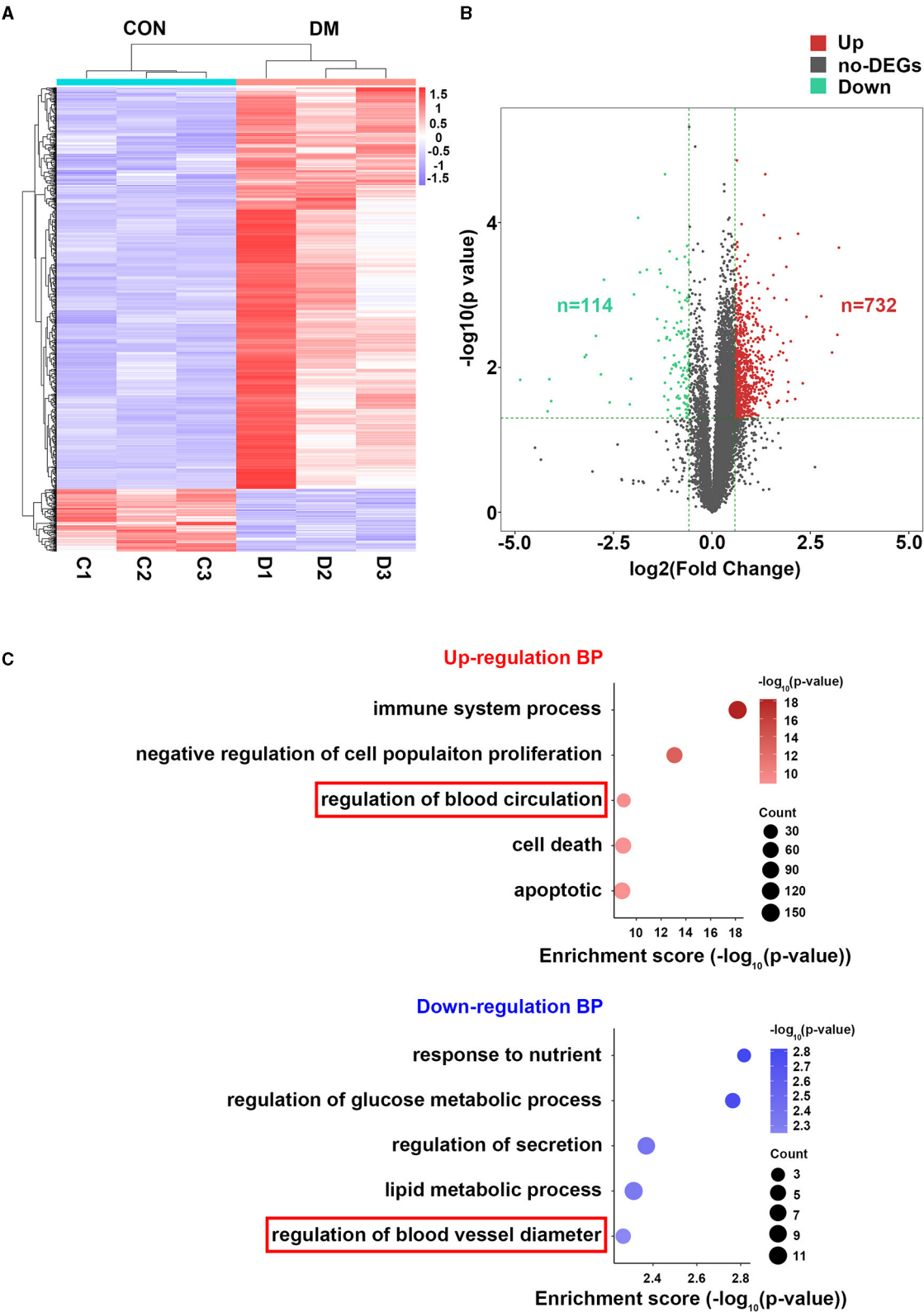


FIGURE 4 | Bioinformatics analysis of LGs from type 2 diabetic mice and vehicles after 24 weeks of HFD and STZ treatments. **(A)** Heatmap showing the differentially expressed genes (DEGs) between LGs from diabetic mice and vehicles. $N = 3/\text{group}$. **(B)** Volcano plot showing all the DEGs between LGs from diabetic mice and vehicles. There were 732 upregulated genes and 114 downregulated genes in the diabetic group. **(C)** The GO analysis of enrichment of upregulated BP and

(Continued)

FIGURE 4 | downregulated BP in the form of bubble plot where dot size represents the number of genes overlapping with each pathway and the adjusted *p*-value is depicted by the color of the dot. The red frame denoting vasculature-related BPs. HFD, high-fat diet; STZ, Streptozotocin; DEG, differentially expressed gene; GO, gene ontology; BP, biological process.

the growth and proliferation of the LG thereafter. Results of hemodynamics showed that no parameters displayed significant change compared with the control group within the early 10 years of diabetes. On the contrary, the RI and PI values increased significantly after 10 years of diabetes, indicating aggravated vascular resistance and the trend of insufficient blood supply or even ischemia in the LG after a long period of diabetic duration.

Histopathology and Vascular Distribution Alterations of LG in Type 2 Diabetic DE Mice Model

To feature the phenotypic and functional alterations of LG in type 2 diabetic DE, we established the type 2 diabetic mice model by a long-term HFD combined with STZ injection based on previous studies (Xing et al., 2021) and sacrificed them at the 24 weeks after the last time STZ injection. Hematoxylin-eosin (H&E), LG weighing, and phenol red thread tests were used to evaluate the histological change, LG size, and secretion function change in T2DM LG. The HE results showed that lacrimal acini atrophied and were transformed in diabetic mice, with severe inflammatory infiltrations gathered and aggravated around the acini and ducts (Figure 3A). The blood glucose level in T2DM mice was 29.06 ± 3.27 mmol/L compared with the level of 10 ± 2.36 mmol/L in the vehicle group (Figure 3B). The ratio of LG/total weight in the T2DM group was 0.31 ± 0.06 while it was 0.49 ± 0.04 in the vehicle group (Figure 3C). The results of phenol red thread tests showed tear secretion volume reduced to 4.22 ± 1.48 mm in T2DM mice, compared with the level of 7.28 ± 1.42 mm in the vehicle group (Figure 3D).

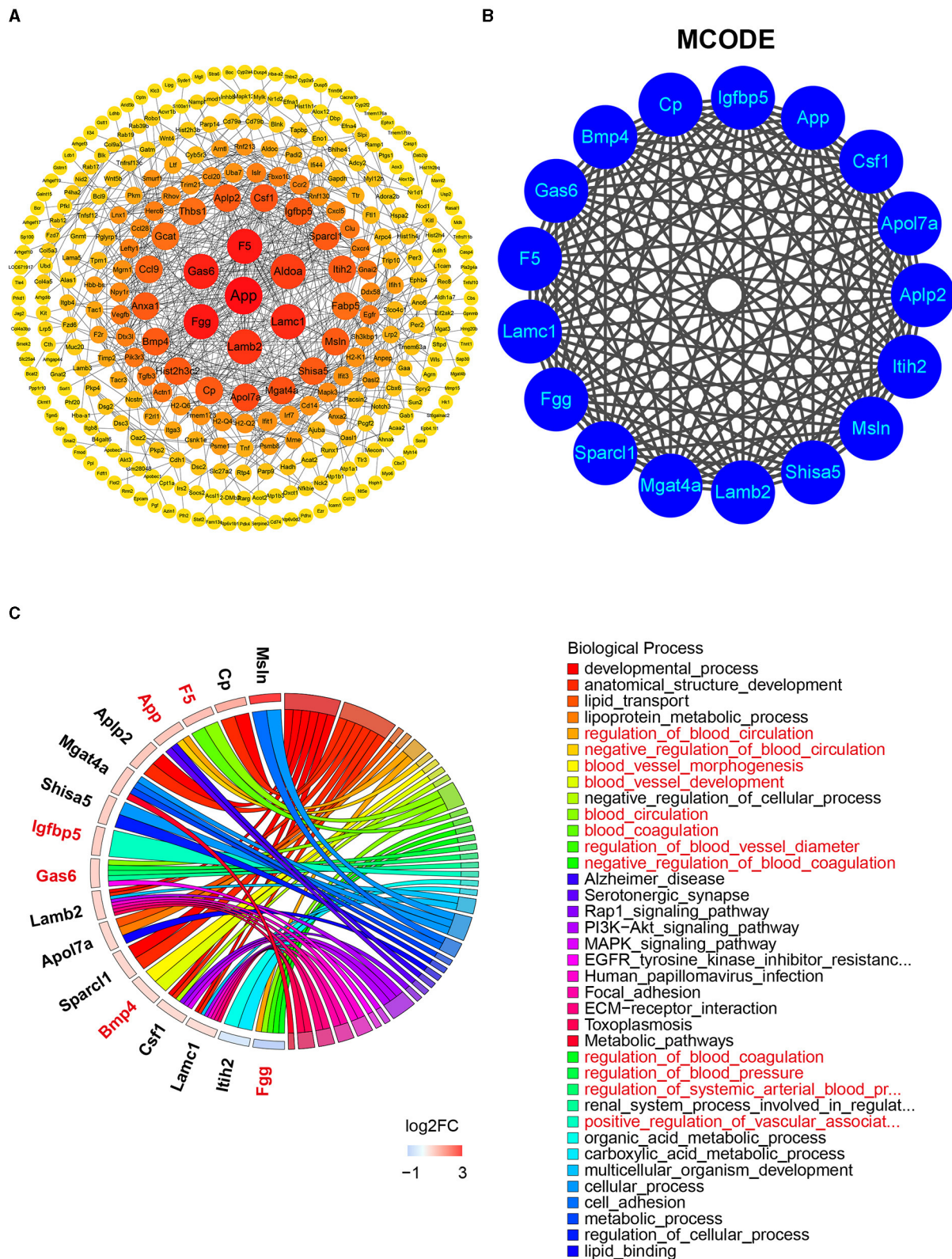
To test whether T2DM mice develop vasculature lesion in LG as diabetic patients, immunofluorescent staining and PCR analysis of CD31 (Angelini et al., 2018) were performed in mice LG samples. The results showed that the vessels (CD31⁺, red) in T2DM LGs were more sparsely distributed with less organized structures compared with the dense, aligned vasculature displayed by the healthy counterparts (Figures 3E,F). The gene expression level of CD31 was significantly downregulated with a level of 0.94 ± 0.07 in T2DM compared with 1.74 ± 0.23 in the vehicle group (Figure 3G). Taken together, these observations suggest that HFD+STZ treated mice model can successfully mimic the phenotype of patients with type 2 diabetes, exhibiting a reduction in tear secretion volume, lacrimal atrophy, and inflammatory infiltration. The sparsely distributed vasculature in T2DM mice may mimic the phenotypes of increased vascular resistance and the trend of insufficient blood supply in patients with T2DM.

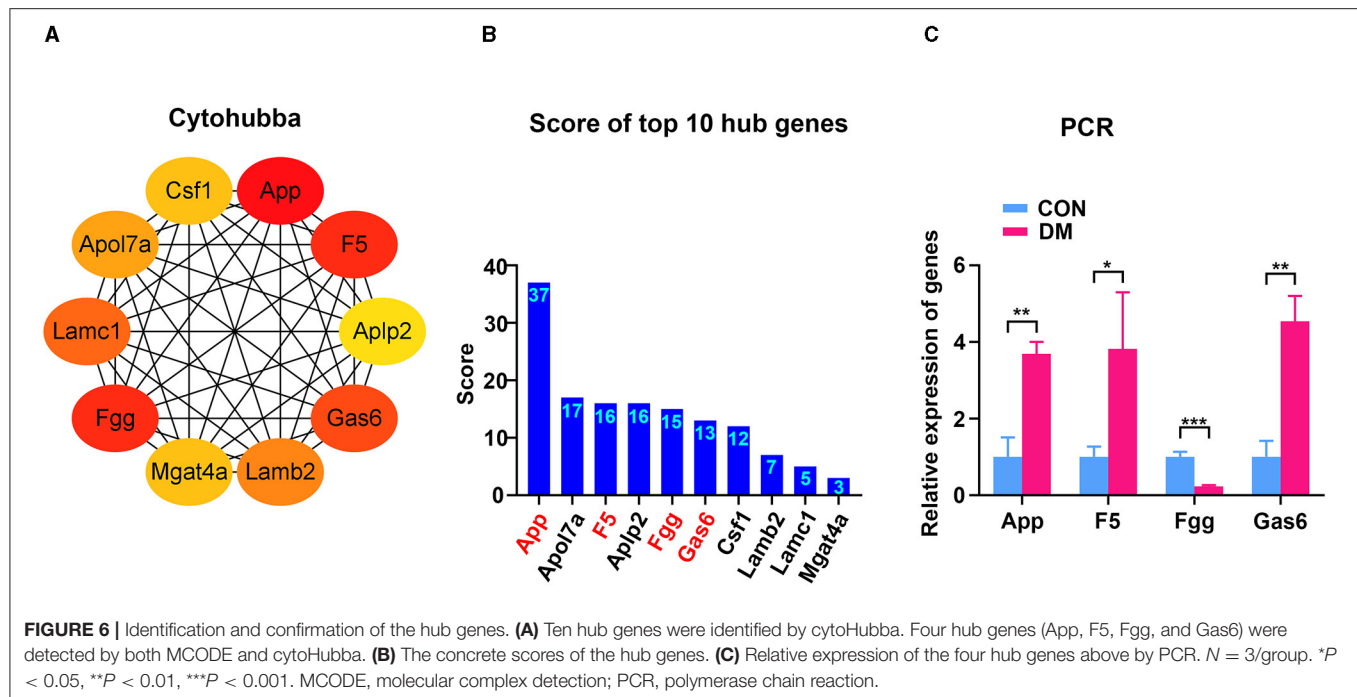
Identification of DEGs and GO Enrichment Analysis Related to Lacrimal Vasculopathy in T2DM

To understand the mechanisms by which T2DM lacrimal vasculopathy was stimulated, we performed RNA-sequencing to identify differentially expressed genes (DEGs) between control and T2DM LGs. A total of 846 DEGs between T2DM and vehicle subjects were found as shown in the heatmap (Figure 4A). Among them, 732 genes were upregulated and 114 genes were downregulated (Figure 4B). The GO analysis showed enrichment of upregulated biological process (BP) including apoptotic process, cell death, immune system process, negative regulation of cell population proliferation, regulation of blood circulation, and downregulated BP including regulation of blood vessel diameter, regulation of secretion, response to nutrient, regulation of glucose metabolic process, and lipid metabolic process (Figure 4C). These findings from RNA-seq confirm the original observations in patients with type 2 diabetes and mice model that LG atrophy, secretion deficiency, inflammatory infiltration, and vasculature dysregulation are involved in diabetic lacrimal lesions. It is worth noting that App participates in the regulation of blood circulation, and Fgg participates in the regulation of blood vessel diameter, which is related to our following analyses.

PPI Network and MCODE Analyses

To identify the most significant clusters of the DEGs, the PPI network of DEGs was constituted by STRING (confidence 0.9) and analyzed by Cytoscape. As shown in Figure 5A, the PPI network reflected the interaction between these potential targets. Seven targets highly related to the pathological process of diabetic LG lesion and dysfunction (DE), which were sorted according to the node degree, including App (degree = 42), F5 (Coagulation Factor V, degree = 25), Fgg (degree = 25), Gas6 (Growth Arrest Specific 6, degree = 24), Lamc1 (Laminin subunit gamma 1, degree = 22), Lamb2 (Laminin subunit beta 2, degree = 21), and Aldoa (Aldolase, Fructose-Bisphosphate A, degree = 20). The most significant module (score = 17) was recognized by MCODE (node score cutoff: 0.2, K-core: 2, degree cutoff: 2, maximum depth: 100), a plugin of Cytoscape (Figure 5B), with 17 genes (App, Csf1, Apol7a, Aplp2, Itih2, Msln, Shisa5, Lamb2, Mgat4a, Sparcl1, Fgg, Lamc1, F5, Gas6, Bmp4, Cp, and Igfbp5) involved. The BP related to these genes was present in Figure 5C. Among the 17 genes in the module, six genes (App, Gas6, F5, Fgg, Bmp4, and Igfbp5) were associated with vascular process/regulations, including regulation of blood circulation, blood vessel morphogenesis, blood vessel development, regulation of blood coagulation, and regulation of blood vessel diameter.





Identification of Hub Genes and Validation

To identify the hub gene in the DEGs, cytoHubba, another plug-in Cytoscape was applied. All the gene codes and edges were calculated. The top 10 genes were identified as hub genes (Figure 6A). The concrete scores of these hub genes were shown in Figure 6B. We have noticed that all the hub genes were included in the most significant module above, and four hub genes (App, F5, Fgg, and Gas6) related to vascular regulation were identified repeatedly. To verify the gene expression level of these four hub genes, PCR measurement was performed to confirm the expression (Figure 6C). Consistent with the results of RNA-seq, the gene expression of App, F5, and Gas6 were significantly upregulated in the T2DM group, while expression of Fgg was significantly downregulated. We chose the most significant upregulated gene (App) and downregulated gene (Fgg), which were related to vasculature lesion and examined their protein level by ELISA and immunochemistry. The results were consistent with our former observations. In T2DM LG, which expressed low amounts of Fgg (Figures 7B,D), App was expressed at high levels and mainly located at lacrimal ducts, vessels, and acini (Figures 7A,C).

GeneMANIA Analysis

To further investigate genes with shared properties and similar functions to the four hub genes identified above, and to display their interactive functional association network, GeneMANIA analysis was performed. The results revealed 20 kinds of molecules that most associated with the four hub genes. The functions of the hub genes and their associated molecules (such as Fgb, Fga, Pros1, Axl, F13b, Mertk, Gnao1, F2, and Tyro3) were primarily related to the regulation of coagulation and regulation of blood circulation (Figure 8A). To observe the expression of

all genes enriched in the circulation and coagulation-related BP, we extracted data from GO analysis. The results showed that 44 genes were upregulated and 8 genes were downregulated in the circulation-related process (Figure 8B), while 12 genes were upregulated and 2 genes were downregulated in the coagulation-related process (Figure 8C).

CMap Analysis

To search for potential small molecular compounds to reverse altered expression of DEGs, CMap analysis was performed. The most three significant small molecular compounds were Thapsigargin, Tanespimycin, and Lomustine (Table 3). Among the potential small molecular compounds, 5/20 (25%) compounds were related to the treatment of the diabetic vascular disorder, including Disulfiram, Bumetanide, Ambroxol, Chenodeoxycholic acid (CDCA), and genistein.

DISCUSSIONS

Although the morbidity of diabetes-related complications has reduced over the past decades, patients with diabetes still have a significantly increased risk for vascular complications as compared with individuals without diabetes (Low Wang et al., 2016; Ling et al., 2020). In this study, we explored whether vasculature dysfunction is involved in the lacrimal lesion to induce DE in type 2 diabetes by targeting vascular-related genes. Collectively, our study demonstrated that four critical genes and unbalanced circulation and coagulation signaling pathways were associated with lacrimal vasculature dysfunction in T2DM DE by bioinformatic methods.

Dry eye is one of the major complications of DM on the ocular surface, which is closely linked with lacrimal lesions

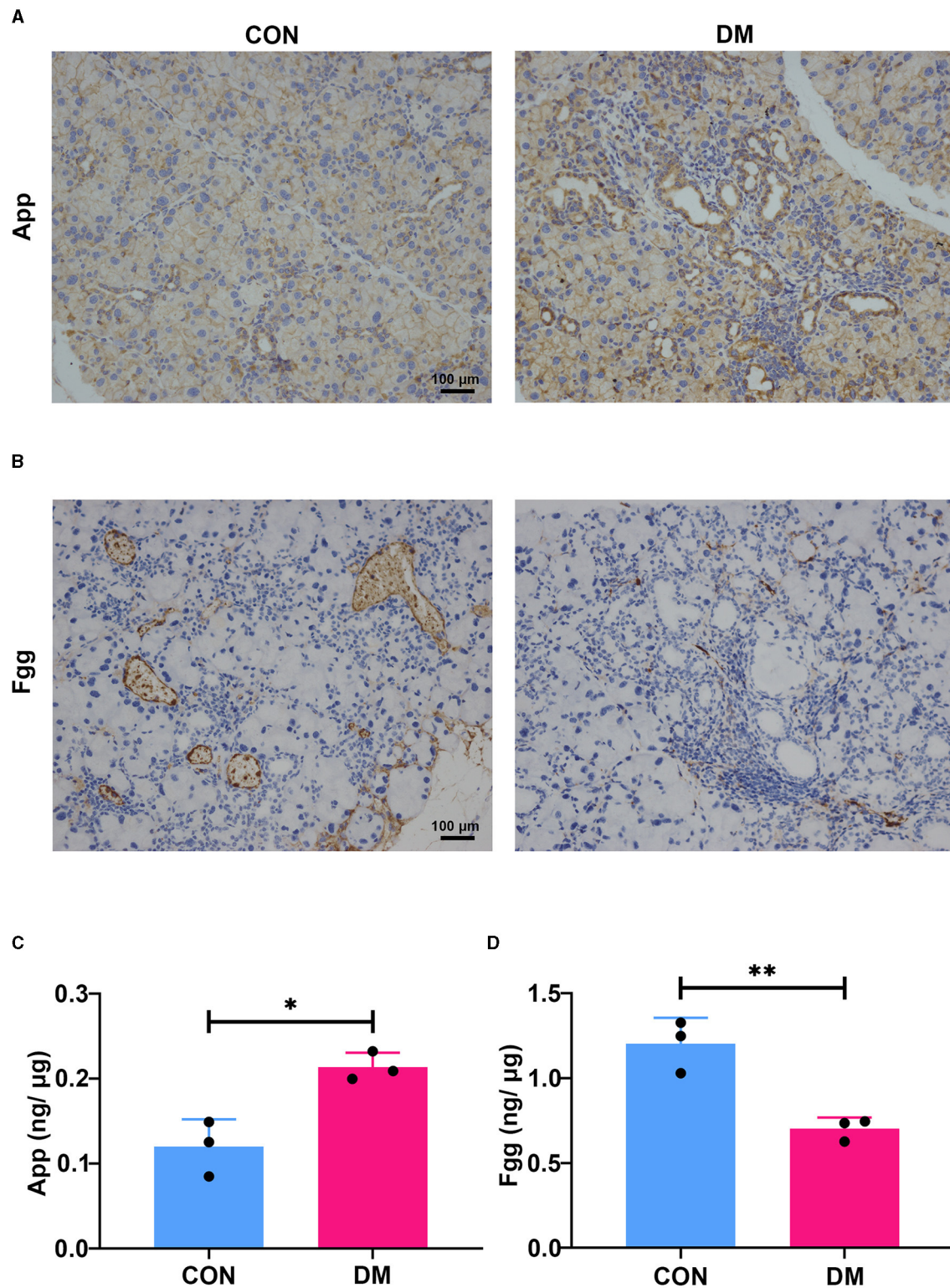


FIGURE 7 | Expression of App and Fgg in diabetic lacrimal glands. **(A)** The representative images of immunohistochemistry staining for App in T2DM and vehicle LGs at 6-month diabetic period. The App was mainly expressed at ducts, vessels, and acini. The diabetes group showed obvious expression aggravation. Scale bar: 100 μ m. **(B)** The representative images of immunohistochemistry staining for Fgg in T2DM and vehicle LGs at a 6-month diabetic period. Fgg was expressed in vessels and concentrated at a vascular endothelium. The diabetes group showed obvious expression reduction. Scale bar: 100 μ m. **(C)** The protein level of App in diabetic and age-matched vehicle LGs by ELISA ($N = 3$ /group). **(D)** The protein level of Fgg in diabetic and age-matched vehicle LGs by ELISA ($N = 3$ /group). **(A–D)**, data are representative of three independent experiments ($n = 3$ /group). C&D, Data were presented as the mean \pm SEM. * $P < 0.05$, ** $P < 0.01$. T2DM, type 2 diabetes; LG, lacrimal gland.

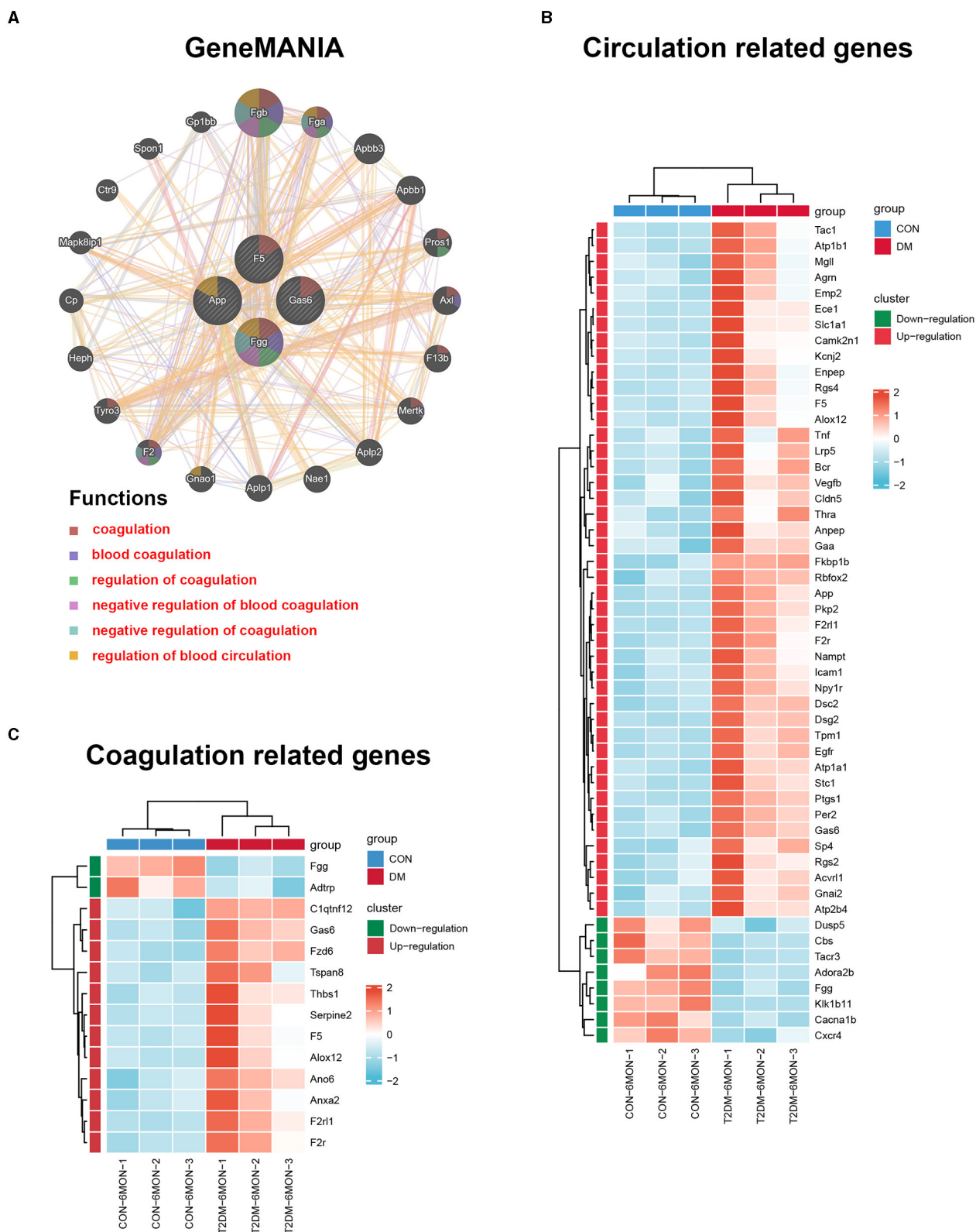
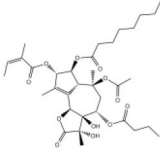
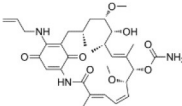
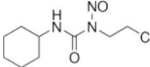
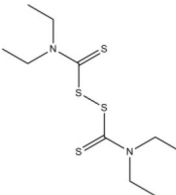
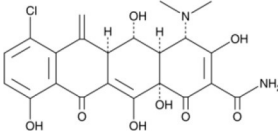
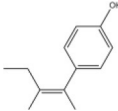
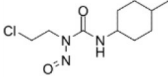
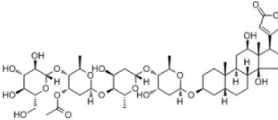
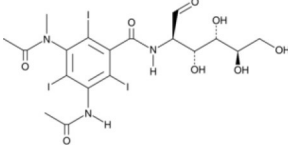
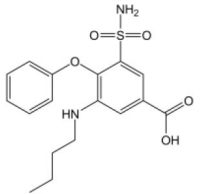
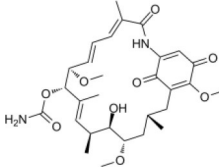
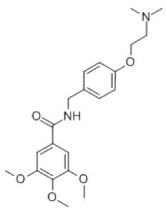
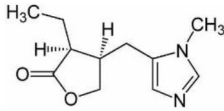
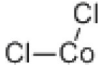


TABLE 3 | List of the 20 most significant small molecular compounds provided by connectivity map (CMap) analysis to reverse altered expression of differentially expressed genes (DEGs) in cell lines.

CMap name	Mean	Enrichment	P	Percent non-null	Structure
Thapsigargin	−0.841	−0.989	<0.00001	100	
Tanespimycin	−0.228	−0.382	<0.00001	59	
Lomustine	−0.672	−0.903	0.00016	100	
Disulfiram	−0.626	−0.838	0.0003	100	
Meclocycline	−0.558	−0.874	0.00054	100	
Diethylstilbestrol	−0.564	−0.728	0.00075	83	
Semustine	−0.639	−0.83	0.00157	100	
Lanatoside C	−0.48	−0.704	0.00157	83	
Metrizamide	−0.528	−0.815	0.00211	100	

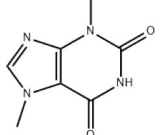
(Continued)

TABLE 3 | Continued

CMap name	Mean	Enrichment	P	Percent non-null	Structure
Bumetanide	−0.459	−0.809	0.00259	100	
Geldanamycin	−0.3	−0.454	0.00268	66	
Ambroxol	−0.642	−0.803	0.00292	100	
Trimethobenzamide	−0.312	−0.729	0.00308	60	
Chenodeoxycholic Acid	−0.564	−0.8	0.0031	100	
Pilocarpine	−0.547	−0.798	0.00332	100	
Genistein	−0.194	−0.421	0.00332	52	
Cobalt Chloride	−0.528	−0.857	0.00575	100	

(Continued)

TABLE 3 | Continued

CMap name	Mean	Enrichment	P	Percent non-null	Structure
Anisomycin	−0.56	−0.758	0.0071	75	
Estrone	−0.444	−0.752	0.00764	75	
Theobromine	−0.452	−0.724	0.0118	75	

(Shih et al., 2017; Jiao et al., 2020; Qu et al., 2021). Diabetic angiopathy (DA) is another common and severe complication of DM and is characterized by high morbidity, early-onset, and rapid progression (Packer, 2018). In diabetes, there is also impaired collateralization of vascular ischemic beds (Fadini et al., 2005), but phenotypes and mechanisms that involved lacrimal vasculature dysregulation in diabetes remain elusive. In this study, we evaluated the morphology and hemodynamics of LGs in patients with T2DM by CDFI. As a non-invasive imaging technique without radiations or high magnetic field exposure, CDFI can be used to measure the lacrimal morphology and hemodynamics (Lecler et al., 2017). We found that patients with diabetes exhibited prominently lacrimal atrophy in all dimensions along with RI and PI parameters elevation. RI and PI are vital parameters for characterizing the arterial waveform and vascular resistance (Halpern et al., 1998; Bude and Rubin, 1999; Grenier et al., 2001; Heine et al., 2005). Increased vascular resistance along with tissue atrophy in diabetes indicated the occurrence of the hypoxia-ischemic syndrome in the tissue endings (Liu et al., 2017; Nilsson et al., 2020), which is a common mechanism of diabetic vascular complications (Fadini et al., 2010; Mudaliar et al., 2021).

To further explore the mechanism of vascular complication in T2DM LG, we established the T2DM mice model by STZ+HDF treatments (a mice model progressively developed T2DM, which mimicked that seen in patients with diabetes, as opposed to genetic models that rapidly develop T2DM spontaneously) (Kleinert et al., 2018) and affirmed the appearance of diabetic DE phenotype. Consistent with patients with T2DM, we found lacrimal atrophy and vasculature lesion with sparse vascular distribution in T2DM mice as compared with the healthy counterparts. Even though we did not assess the vascular resistance parameters on the mice model, the sparse vasculature distribution may also represent a peripheral blood supply decrease and indicate an ischemia-like phenotype

(Yagihashi et al., 2011). Indeed, patients with DM and a prior ischemic vascular event are at an especially high risk of recurrent events (Mann et al., 2018; Verma et al., 2018; Rawshani et al., 2019). Depending on the severity, ischemia and ischemia/reperfusion injury (IRI) may lead to ischemic necrosis, which further leads to progressive injury, fibrosis, and atrophy irreversibly (Holderied et al., 2020). This partly explains why the vasculature changes in the LGs of diabetes are accompanied by tissue and acinus atrophy. However, the exact mechanism of lacrimal ischemia in type 2 diabetes remains elusive.

With further RNA-seq analysis, 846 DEGs were found between LGs from T2DM mice and vehicles. Functional enrichment analysis showed upregulation of immune system process, cell death, apoptosis process, blood circulation and downregulation of blood vessel diameter, secretion, response to nutrient, glucose metabolic process, and lipid metabolic process. All these terms were consistent with the phenotypes as seen in patients with T2DM and mice model, including inflammatory cell infiltration, tissue atrophy, abnormality of vascular distribution, high vascular resistance, tear secretion deficiency, high glucose levels, and so on. Most of these phenotypes were also seen in the mice model of T1DM (Jiao et al., 2020; Qu et al., 2021). To further explore the mechanism on lacrimal ischemia in T2DM, PPI network, MCODE, and cytoHubba analyses were applied as their function of finding the core module and hub genes among all the DEGs. We thus found four hub genes (App, F5, Fgg, and Gas6) that were closely related to vascular regulation and diabetes. Meakin Paul J reported that elevated App was linked with vascular disease development in obesity and diabetes (Meakin et al., 2020). Lodigiani C et al. revealed that there were connections between the F5 gene variant, diabetes and atherothrombosis and other vascular complications (Lodigiani et al., 2009). Activated protein C (APC) resistance is associated with the F5 Leiden mutation, and it is the most common risk factor for venous

thrombosis. Omarova F revealed that Fgg can increase plasma APC sensitivity and reduction of Fgg might decrease the basis for pharmacologic interventions to counteract APC resistance (Omarova et al., 2014). Lee CH reported that the plasma protein growth arrest-specific 6 (Gas6) is important to the inflammatory process and involved in the development of diabetic renal and vascular complications (Lee et al., 2012). Up to now, there is still no report on the correlation between the genes of App, F5, Fgg, and Gas6 with diabetic lacrimal lesions. The GeneMANIA further revealed that the functions of the four hub genes above and their associated molecules (such as Fgb, Fga, Prosl, Axl, F13b, Merlk, Gnaol, F2, and Tyro3) were primarily related to the regulation of circulation and coagulation. In addition, we found that 44 genes were upregulated in the circulation-related BP and 12 genes were upregulated in the coagulation-related BP. This is interesting for these two BPs are both connected with ischemia lesions (Dong et al., 2019; Wilbs et al., 2020). Activation of coagulation factors is a driving force of IRI in acute stroke (Stoll and Nieswandt, 2019). To counterpart this trend, angiogenesis and other pathways to promote blood circulation are required for tissue remodeling/repair following ischemia (Meng et al., 2018).

In the present study, we found several potential small molecular compounds to reverse the altered expression of the DEGs, which might improve lacrimal lesions and vasculature dysfunction in T2DM. It was reported that the therapy of an ophthalmic *in situ* gel formulation incorporating disulfiram (DIS) nanoparticles (Dis-NPs/ISG) might contribute to restore retinal dysfunction in diabetic retinopathy (DR), a diabetic vascular lesion (Deguchi et al., 2020). Bumetanide also has been demonstrated to play an important role in antidiabetic activity with low *in vitro* cell toxicity through antiinflammatory effects (Navas et al., 2020) and can reduce diabetic vascular dysfunction by suppression of angiogenesis (Topper et al., 1997; Guzel et al., 2020). Ambroxol can significantly inhibit proinflammatory cytokines, reduce lung inflammation, and accelerate recovery by reducing vascular permeability in acute lung injury (Su et al., 2004). However, whether ambroxol could improve diabetic vasculopathy remains unclear. CDCA was reported to promote eNOS phosphorylation and NO production that contributes to its vasorelaxant effect (Wang et al., 2017). Babu PV reported that genistein can improve diabetes-caused vascular inflammation by suppressing diabetes-induced adhesion of monocytes to endothelial cells and endothelial secretion of adhesion molecules (Babu et al., 2012). However, the other small molecular compounds have not been reported to have the function to reverse vasculature dysfunction or diabetes. The CMap data set uses cellular responses to mostly Food and Drug Administration (FDA) approved drugs to find relationships between small molecules, genes, and diseases (“connectivity mapping”), despite the need for further research of drugs

application (Kohonen et al., 2017). All these small molecular compounds could be explored as novel therapeutic targets to treat vasculature dysfunction, diabetes, and related metabolic diseases.

Overall, we may conclude that upregulation of App, F5, Gas6, and downregulation of Fgg may induce vasculature dysfunction in T2DM by modulating the regulation of circulation and coagulation pathways. Our results provide important novel information to further understand the effects of vasculature dysfunction in T2DM LG lesions and predict the potential therapeutic molecular compounds to reverse the gene expression in the disease. However, further work needs to address which of these possibilities targets and medications apply and whether they all act in unison.

DATA AVAILABILITY STATEMENT

The original contributions presented in the study are included in the article/**Supplementary Material**, further inquiries can be directed to the corresponding author/s. All RNA-seq data presented in this study are deposited in the Gene Expression Omnibus under the accession number GSE179231.

ETHICS STATEMENT

The studies involving human participants were reviewed and approved by Ethics Committee of Qingdao Eye Hospital. The patients/participants provided their written informed consent to participate in this study. The animal study was reviewed and approved by Experimental Animal Ethics Committee of Shandong first medical University.

AUTHOR CONTRIBUTIONS

JX, BZ, MD, MZ, and HW collected and analyzed the data. JX, BZ, and SD wrote the manuscript. DL, LX, JX, SD, BZ, QZ, and YD designed the research. All authors contributed to the article and approved the submitted version.

FUNDING

This study was supported by the Academic Promotion Program and Innovation Project of Shandong First Medical University (2009ZL001).

SUPPLEMENTARY MATERIAL

The Supplementary Material for this article can be found online at: <https://www.frontiersin.org/articles/10.3389/fphys.2021.731234/full#supplementary-material>

REFERENCES

- Allred, M. G., Chimenti, M. S., Ciecko, A. E., Chen, Y. G., and Lieberman, S. M. (2021). Characterization of Type I interferon-associated chemokines and cytokines in lacrimal glands of nonobese diabetic mice. *Int. J. Mol. Sci.* 22:3767. doi: 10.3390/ijms22073767
- Alves, M., Calegari, V. C., Cunha, D. A., Saad, M. J., Velloso, L. A., and Rocha, E. M. (2005). Increased expression of advanced glycation end-products and their

- receptor, and activation of nuclear factor kappa-B in lacrimal glands of diabetic rats. *Diabetologia* 48, 2675–2681. doi: 10.1007/s00125-005-0010-9
- Angelini, G., Flego, D., Vinci, R., Pedicino, D., Trotta, F., Ruggio, A., et al. (2018). Matrix metalloproteinase-9 might affect adaptive immunity in non-ST segment elevation acute coronary syndromes by increasing CD31 cleavage on CD4+ T-cells. *Eur. Heart J.* 39, 1089–1097. doi: 10.1093/eurheartj/ehx684
- Azad, A., Pavlopoulos, G. A., Ouzounis, C. A., Kyrpides, N. C., and Buluc, A. (2018). HipMCL: a high-performance parallel implementation of the Markov clustering algorithm for large-scale networks. *Nucleic Acids Res.* 46:e33. doi: 10.1093/nar/gkx1313
- Babu, P. V., Si, H., Fu, Z., Zhen, W., and Liu, D. (2012). Genistein prevents hyperglycemia-induced monocyte adhesion to human aortic endothelial cells through preservation of the cAMP signaling pathway and ameliorates vascular inflammation in obese diabetic mice. *J. Nutr.* 142, 724–730. doi: 10.3945/jn.111.152322
- Basterra-Gortari, F. J., Ruiz-Canela, M., Martinez-Gonzalez, M. A., Babio, N., Sorli, J. V., Fito, M., et al. (2019). Effects of a mediterranean eating plan on the need for glucose-lowering medications in participants with Type 2 diabetes: a subgroup analysis of the PREDIMED trial. *Diabetes Care* 42, 1390–1397. doi: 10.2337/dc18-2475
- Bilgili, Y., Taner, P., Unal, B., Simsir, I., Kara, S. A., Bayram, M., et al. (2005). Doppler sonography of the normal lacrimal gland. *J. Clin. Ultrasound* 33, 123–126. doi: 10.1002/jcu.20096
- Bude, R. O., and Rubin, J. M. (1999). Relationship between the resistive index and vascular compliance and resistance. *Radiology* 211, 411–417. doi: 10.1148/radiology.211.2.r99ma48411
- Cao, R., Lim, S., Ji, H., Zhang, Y., Yang, Y., Honek, J., et al. (2011). Mouse corneal lymphangiogenesis model. *Nat. Protoc.* 6, 817–826. doi: 10.1038/nprot.2011.359
- Ciecko, A. E., Foda, B., Barr, J. Y., Ramanathan, S., Atkinson, M. A., Serreze, D. V., et al. (2019). Interleukin-27 is essential for Type 1 diabetes development and sjogren syndrome-like inflammation. *Cell Rep.* 29, 3073–3086 e3075. doi: 10.1016/j.celrep.2019.11.010
- Deguchi, S., Ogata, F., Yamaguchi, M., Minami, M., Otake, H., Kanai, K., et al. (2020). *In situ* gel incorporating disulfiram nanoparticles rescues the retinal dysfunction via ATP collapse in otsuka long-evans tokushima fatty rats. *Cells* 9:2171. doi: 10.3390/cells9102171
- Dong, X., Gao, J., Zhang, C. Y., Hayworth, C., Frank, M., and Wang, Z. (2019). Neutrophil membrane-derived nanovesicles alleviate inflammation to protect mouse brain injury from ischemic stroke. *ACS Nano* 13, 1272–1283. doi: 10.1021/acsnano.8b06572
- Fadini, G. P., Albiero, M., Menegazzo, L., Boscaro, E., Pagnin, E., Iori, E., et al. (2010). The redox enzyme p66Shc contributes to diabetes and ischemia-induced delay in cutaneous wound healing. *Diabetes* 59, 2306–2314. doi: 10.2337/db09-1727
- Fadini, G. P., Miorin, M., Facco, M., Bonamico, S., Baesso, I., Grego, F., et al. (2005). Circulating endothelial progenitor cells are reduced in peripheral vascular complications of type 2 diabetes mellitus. *J. Am. Coll. Cardiol.* 45, 1449–1457. doi: 10.1016/j.jacc.2004.11.067
- Franz, M., Rodriguez, H., Lopes, C., Zuberi, K., Montojo, J., Bader, G. D., et al. (2018). GeneMANIA update 2018. *Nucleic Acids Res.* 46, W60–W64. doi: 10.1093/nar/gky311
- Gao, J. R., Qin, X. J., Fang, Z. H., Li, S., Han, L. P., Hui, J., et al. (2019). To explore the pathogenesis of vascular lesion of Type 2 diabetes mellitus based on the PI3K/Akt signaling pathway. *J. Diabetes Res.* 2019:4650906. doi: 10.1155/2019/4650906
- Gene Ontology, C. (2021). The gene ontology resource: enriching a GOld mine. *Nucleic Acids Res.* 49, D325–D334. doi: 10.1093/nar/gkaa1113
- Grenier, N., Basseau, F., Rey, M. C., and LaGoarde-Segot, L. (2001). Interpretation of doppler signals. *Eur. Radiol.* 11, 1295–1307. doi: 10.1007/s003300100913
- Guzel, S., Cai, C. L., Ahmad, T., Quan, M., Valencia, G. B., Aranda, J. V., et al. (2020). Bumetanide suppression of angiogenesis in a rat model of oxygen-induced retinopathy. *Int. J. Mol. Sci.* 21:987. doi: 10.3390/ijms21030987
- Halpern, E. J., Merton, D. A., and Forsberg, F. (1998). Effect of distal resistance on Doppler US flow patterns. *Radiology* 206, 761–766. doi: 10.1148/radiology.206.3.9494498
- Heine, G. H., Gerhart, M. K., Ulrich, C., Kohler, H., and Girndt, M. (2005). Renal Doppler resistance indices are associated with systemic atherosclerosis in kidney transplant recipients. *Kidney Int.* 68, 878–885. doi: 10.1111/j.1523-1755.2005.00470.x
- Holderied, A., Kraft, F., Marschner, J. A., Weidenbusch, M., and Anders, H. J. (2020). “Point of no return” in unilateral renal ischemia reperfusion injury in mice. *J. Biomed. Sci.* 27:34. doi: 10.1186/s12929-020-0623-9
- Jiao, X., Lu, D., Pei, X., Qi, D., Huang, S., Song, Z., et al. (2020). Type 1 diabetes mellitus impairs diurnal oscillations in murine extraorbital lacrimal glands. *Ocul. Surf.* 18, 438–452. doi: 10.1016/j.jtos.2020.04.013
- Kleinert, M., Clemmensen, C., Hofmann, S. M., Moore, M. C., Renner, S., Woods, S. C., et al. (2018). Animal models of obesity and diabetes mellitus. *Nat. Rev. Endocrinol.* 14, 140–162. doi: 10.1038/nrendo.2017.161
- Knudsen, J. G., Hamilton, A., Ramracheya, R., Tarasov, A. I., Brereton, M., Haythorne, E., et al. (2019). Dysregulation of glucagon secretion by hyperglycemia-induced sodium-dependent reduction of ATP production. *Cell Metab.* 29, 430–442 e434. doi: 10.1016/j.cmet.2018.10.003
- Kohonen, P., Parkkinen, J. A., Willighagen, E. L., Ceder, R., Wennerberg, K., Kaski, S., et al. (2017). A transcriptomics data-driven gene space accurately predicts liver cytopathology and drug-induced liver injury. *Nat. Commun.* 8:15932. doi: 10.1038/ncomms15932
- Kwon, D., Lee, D., Kim, J., Lee, J., Sim, M., and Kim, J. (2018). INTERSPIA: a web application for exploring the dynamics of protein-protein interactions among multiple species. *Nucleic Acids Res.* 46, W89–W94. doi: 10.1093/nar/gky378
- Lecler, A., Boucenna, M., Lafitte, F., Koskas, P., Nau, E., Jacomet, P. V., et al. (2017). Usefulness of colour Doppler flow imaging in the management of lacrimal gland lesions. *Eur. Radiol.* 27, 779–789. doi: 10.1007/s00330-016-4438-8
- Lee, C. H., Chu, N. F., Shieh, Y. S., and Hung, Y. J. (2012). The growth arrest-specific 6 (Gas6) gene polymorphism c.834+7G>A is associated with type 2 diabetes. *Diabetes Res. Clin. Pract.* 95, 201–206. doi: 10.1016/j.diabres.2011.09.013
- Ling, W., Huang, Y., Huang, Y. M., Fan, R. R., Sui, Y., and Zhao, H. L. (2020). Global trend of diabetes mortality attributed to vascular complications, 2000–2016. *Cardiovasc. Diabetol.* 19:182. doi: 10.1186/s12933-020-01159-5
- Liu, Z., Yan, S., Wang, J., Xu, Y., Wang, Y., Zhang, S., et al. (2017). Endothelial adenosine A2a receptor-mediated glycolysis is essential for pathological retinal angiogenesis. *Nat. Commun.* 8:584. doi: 10.1038/s41467-017-00551-2
- Lodigiani, C., Ferrazzi, P., Di Micco, P., Libre, L., Genovese, S., Quaglia, I., et al. (2009). Is there a relationship between factor V Leiden and type 2 diabetes? *J. Transl. Med.* 7:52. doi: 10.1186/1479-5876-7-52
- Low Wang, C. C., Hess, C. N., Hiatt, W. R., and Goldfine, A. B. (2016). Clinical update: cardiovascular disease in diabetes mellitus: atherosclerotic cardiovascular disease and heart failure in Type 2 diabetes mellitus - mechanisms, management, and clinical considerations. *Circulation* 133, 2459–2502. doi: 10.1161/CIRCULATIONAHA.116.022194
- Mann, J. F. E., Fonseca, V., Mosenzon, O., Raz, I., Goldman, B., Idorn, T., et al. (2018). Effects of liraglutide versus placebo on cardiovascular events in patients with Type 2 diabetes mellitus and chronic kidney disease. *Circulation* 138, 2908–2918. doi: 10.1161/CIRCULATIONAHA.118.036418
- Markoulli, M., Flanagan, J., Tummanapalli, S. S., Wu, J., and Willcox, M. (2018). The impact of diabetes on corneal nerve morphology and ocular surface integrity. *Ocul. Surf.* 16, 45–57. doi: 10.1016/j.jtos.2017.10.006
- Meakin, P. J., Coull, B. M., Tuharska, Z., McCaffery, C., Akoumianakis, I., Antoniadis, C., et al. (2020). Elevated circulating amyloid concentrations in obesity and diabetes promote vascular dysfunction. *J. Clin. Invest.* 130, 4104–4117. doi: 10.1172/JCI122237
- Meng, S., Gu, Q., Yang, X., Lv, J., Owusu, I., Matrone, G., et al. (2018). TBX20 regulates angiogenesis through the prokineticin 2-prokineticin receptor 1 pathway. *Circulation* 138, 913–928. doi: 10.1161/CIRCULATIONAHA.118.039399
- Mudaliar, S., Hupfeld, C., and Chao, D. L. (2021). SGLT2 inhibitor-induced low-grade ketonemia ameliorates retinal hypoxia in diabetic retinopathy—a novel hypothesis. *J. Clin. Endocrinol. Metab.* 106, 1235–1244. doi: 10.1210/clinem/dgab050
- Nakamachi, T., Ohtaki, H., Seki, T., Yofu, S., Kagami, N., Hashimoto, H., et al. (2016). PACAP suppresses dry eye signs by stimulating tear secretion. *Nat. Commun.* 7:12034. doi: 10.1038/ncomms12034

- Navas, A., Jannus, F., Fernandez, B., Cepeda, J., Medina O'Donnell, M., Diaz-Ruiz, L., et al. (2020). Designing single-molecule magnets as drugs with dual anti-inflammatory and anti-diabetic effects. *Int. J. Mol. Sci.* 21:3146. doi: 10.3390/ijms21093146
- Nilsson, J., Jernryd, V., Qin, G., Paskevicius, A., Metzsch, C., Sjöberg, T., et al. (2020). A nonrandomized open-label phase 2 trial of nonischemic heart preservation for human heart transplantation. *Nat. Commun.* 11:2976. doi: 10.1038/s41467-020-16782-9
- Omarova, F., Uitte de Willige, S., Simioni, P., Ariens, R. A., Bertina, R. M., Rosing, J., et al. (2014). Fibrinogen gamma' increases the sensitivity to activated protein C in normal and factor V Leiden plasma. *Blood* 124, 1531–1538. doi: 10.1182/blood-2014-02-554055
- Packer, M. (2018). Heart failure: the most important, preventable, and treatable cardiovascular complication of Type 2 diabetes. *Diabetes Care* 41, 11–13. doi: 10.2337/dci17-0052
- Qu, M., Wan, L., Dong, M., Wang, Y., Xie, L., and Zhou, Q. (2021). Hyperglycemia-induced severe mitochondrial bioenergetic deficit of lacrimal gland contributes to the early onset of dry eye in diabetic mice. *Free Radic. Biol. Med.* 166, 313–323. doi: 10.1016/j.freeradbiomed.2021.02.036
- Rawshani, A., Rawshani, A., Sattar, N., Franzen, S., McGuire, D. K., Eliasson, B., et al. (2019). Relative prognostic importance and optimal levels of risk factors for mortality and cardiovascular outcomes in Type 1 diabetes mellitus. *Circulation* 139, 1900–1912. doi: 10.1161/CIRCULATIONAHA.118.037454
- Shih, K. C., Lam, K. S., and Tong, L. (2017). A systematic review on the impact of diabetes mellitus on the ocular surface. *Nutr. Diabetes* 7:e251. doi: 10.1038/nutd.2017.4
- Stoll, G., and Nieswandt, B. (2019). Thrombo-inflammation in acute ischaemic stroke - implications for treatment. *Nat. Rev. Neurol.* 15, 473–481. doi: 10.1038/s41582-019-0221-1
- Su, W., Zhao, Y., Wei, Y., Zhang, X., Ji, J., and Yang, S. (2021). Exploring the pathogenesis of psoriasis complicated with atherosclerosis via microarray data analysis. *Front. Immunol.* 12:667690. doi: 10.3389/fimmu.2021.667690
- Su, X., Wang, L., Song, Y., and Bai, C. (2004). Inhibition of inflammatory responses by ambroxol, a mucolytic agent, in a murine model of acute lung injury induced by lipopolysaccharide. *Intensive Care Med.* 30, 133–140. doi: 10.1007/s00134-003-2001-y
- Topper, J. N., Wasserman, S. M., Anderson, K. R., Cai, J., Falb, D., Gimbrone, M. A., et al. (1997). Expression of the bumetanide-sensitive Na-K-Cl cotransporter BSC2 is differentially regulated by fluid mechanical and inflammatory cytokine stimuli in vascular endothelium. *J. Clin. Invest.* 99, 2941–2949. doi: 10.1172/JCI119489
- Verma, S., Poulter, N. R., Bhatt, D. L., Bain, S. C., Buse, J. B., Leiter, L. A., et al. (2018). Effects of liraglutide on cardiovascular outcomes in patients with Type 2 diabetes mellitus with or without history of myocardial infarction or stroke. *Circulation* 138, 2884–2894. doi: 10.1161/CIRCULATIONAHA.118.034516
- Vujkovic, M., Keaton, J. M., Lynch, J. A., Miller, D. R., Zhou, J., Tcheandjieu, C., et al. (2020). Discovery of 318 new risk loci for type 2 diabetes and related vascular outcomes among 1.4 million participants in a multi-ancestry meta-analysis. *Nat. Genet.* 52, 680–691. doi: 10.1038/s41588-020-0637-y
- Wang, Z., Lv, Q., Liu, H., Wu, Y., Bai, Y., Cheng, Y., et al. (2017). Caveolae depletion contributes to vasorelaxant effects of chenodeoxycholic acid. *Cell. Physiol. Biochem.* 42, 1013–1024. doi: 10.1159/000478683
- Wilbs, J., Kong, X. D., Middendorp, S. J., Prince, R., Cooke, A., Demarest, C. T., et al. (2020). Cyclic peptide FXII inhibitor provides safe anticoagulation in a thrombosis model and in artificial lungs. *Nat. Commun.* 11:3890.
- Xing, W., Tan, Y., Li, K., Tian, P., Tian, F., and Zhang, H. (2021). Upregulated hepatokine fetuin B aggravates myocardial ischemia/reperfusion injury through inhibiting insulin signaling in diabetic mice. *J. Mol. Cell. Cardiol.* 151, 163–172. doi: 10.1016/j.yjmcc.2020.03.002
- Yagihashi, S., Mizukami, H., and Sugimoto, K. (2011). Mechanism of diabetic neuropathy: where are we now and where to go? *J. Diabetes Investig.* 2, 18–32. doi: 10.1111/j.2040-1124.2010.00070.x
- Yoo, M., Shin, J., Kim, H., Kim, J., Kang, J., and Tan, A. C. (2019). Exploring the molecular mechanisms of Traditional Chinese Medicine components using gene expression signatures and connectivity map. *Comput. Methods Programs Biomed.* 174, 33–40. doi: 10.1016/j.cmpb.2018.04.002

Conflict of Interest: The authors declare that the research was conducted in the absence of any commercial or financial relationships that could be construed as a potential conflict of interest.

Publisher's Note: All claims expressed in this article are solely those of the authors and do not necessarily represent those of their affiliated organizations, or those of the publisher, the editors and the reviewers. Any product that may be evaluated in this article, or claim that may be made by its manufacturer, is not guaranteed or endorsed by the publisher.

Copyright © 2021 Xue, Zhang, Dou, Zhou, Ding, Zhou, Wang, Dong, Li and Xie. This is an open-access article distributed under the terms of the Creative Commons Attribution License (CC BY). The use, distribution or reproduction in other forums is permitted, provided the original author(s) and the copyright owner(s) are credited and that the original publication in this journal is cited, in accordance with accepted academic practice. No use, distribution or reproduction is permitted which does not comply with these terms.



Thrombus-Targeting Polymeric Nanocarriers and Their Biomedical Applications in Thrombolytic Therapy

Qixiao Guan and Hongjing Dou*

State Key Laboratory of Metal Matrix Composites, School of Materials Science and Engineering, Shanghai Jiao Tong University, Shanghai, China

OPEN ACCESS

Edited by:

Kangkang Zhi,
Shanghai Changzheng Hospital,
China

Reviewed by:

Huocong Huang,
University of Texas Southwestern
Medical Center, United States
Bing Xia,
Nanjing Forestry University, China
Thi Tuong Vy Phan,
Duy Tan University, Vietnam

*Correspondence:

Hongjing Dou
hjdou@sjtu.edu.cn

Specialty section:

This article was submitted to
Vascular Physiology,
a section of the journal
Frontiers in Physiology

Received: 23 August 2021

Accepted: 08 November 2021

Published: 30 November 2021

Citation:

Guan Q and Dou H (2021)
Thrombus-Targeting Polymeric
Nanocarriers and Their Biomedical
Applications in Thrombolytic Therapy.
Front. Physiol. 12:763085.
doi: 10.3389/fphys.2021.763085

Due to the high morbidity and mortality of cardiovascular diseases, there is an urgent need for research on antithrombotic strategies. In view of the short half-life, insufficient drug penetration, poor targeting capabilities, and hemorrhagic side-effects of traditional thrombus treatment methods, the combination of thrombolytic therapy and nanocarriers brought by the development of nanotechnology in recent years may provide effective solutions for these undesirable side-effects caused by insufficient targeting. Polymeric nanocarriers, based on macromolecules and various functional groups, can connect specific targeting molecules together through chemical modification to achieve the protection and targeted delivery of thrombolytic drugs. However, simple chemical molecular modifications may be easily affected by the physiological environment encountered in the circulatory system. Therefore, the modification of nanocarriers with cell membranes can provide camouflage to these platforms and help to extend their circulation time while also imparting them with the biological functions of cell membranes, thus providing them with precise targeting capabilities, among which the most important is the biological modification of platelet membranes. In addition, some nanoparticles with their own therapeutic functions have also been developed, such as polypyrrole, which can exhibit a photothermal effect to induce thrombolysis. Herein, combined with the mechanism of thrombosis and thrombolysis, we outline the recent advances achieved with thrombus-targeting nanocarriers with regard to thrombosis treatment. On this basis, the design considerations, advantages, and challenges of these thrombolytic therapies in clinical transformation are discussed.

Keywords: thrombosis, polymeric nanocarriers, targeted delivery, biomimetic technology, antithrombotic strategies

INTRODUCTION

At present, cardiovascular disease is still one of the most threatening diseases to human health and life in the world. Cardiovascular diseases have a high morbidity and mortality rate. According to statistics, approximately 179 million people die from cardiovascular diseases each year, accounting for about 31% of the world's death toll, and this number is anticipated to reach over 236 million by 2030 (Benjamin et al., 2020; Zenych et al., 2020). There are three

main types of cardiovascular diseases, including myocardial infarction, cerebral stroke, and deep vein thrombosis. These three cardiovascular diseases are primarily caused by thrombosis, which is a blood clot blockage of blood vessels (Fuster et al., 1992; Gao et al., 2021; Rodriguez and Harrington, 2021; Xue et al., 2021). Therefore, the prevention and treatment of thrombosis are an urgent issue, and it is also of great research significance.

Currently, the most important remedy for thrombosis and related cardiovascular diseases is prevention, but in cases involving long-term thrombosis, the main treatment options include balloon catheterization, surgical embolectomy, thrombolytic therapy, and other relevant surgeries (Powers et al., 2018). Taking into account the cost of surgical treatment and the damage it causes to the body, the application of thrombolytic drugs has increasingly become an important strategy. Thrombolytic agents include tissue plasminogen activators (tPA), recombinant tissue plasminogen activators (rtPA), urokinase (UK), streptokinase (SK), and other plasminogen activators (PAs; Marder, 2013; Cheng et al., 2018; Zamanlu et al., 2018; Ma et al., 2019; Hassanpour et al., 2020). The diverse antigenicity, half-life, lytic potential, fibrin specificity, and hemorrhagic risks associated with these agents lead to their differing effectiveness (Marshall, 2015). In addition, anticoagulants and antiplatelet drugs are often used to prevent clotting (Bala et al., 2018; Al Rawahi et al., 2019). These drugs often have only limited effectiveness when they are used alone, for example, their penetration into clots tends to be trivial and requires larger doses. Making matters worse, they may also cause hemorrhagic transformation leading to fatal intracerebral hemorrhage, as well as some other undesirable side-effects (Pfefferkorn and Rosenberg, 2003; Mao et al., 2017; Powers et al., 2018; Xu et al., 2021).

With the rapid development of nanotechnology and biotechnology (Jiang et al., 2020; Cornel et al., 2021), the combination of thrombolytic therapy and nanocarriers may provide a novel solution to key issues, such as the short half-life, low targeting ability, and unexpected bleeding complications of the existing therapeutic drugs (Zamanlu et al., 2018; Ma et al., 2019; Hassanpour et al., 2020). Polymeric nanocarriers based on macromolecules can provide the protection and targeted delivery of thrombolytic drugs through the unique physicochemical property brought by the nanoscale and the facile design of polymer chains. In addition, biologically inspired cell membrane modification strategies can transfer the specific functions and biological characteristics of cell membranes to the nanocarriers, thus improving the biocompatibility and precise targeting ability, and greatly enhancing the effect of thrombolytic therapy (Figure 1).

MECHANISM OF THROMBOSIS AND THROMBOLYSIS

Thrombosis is primarily triggered by collagen, tissue factor, thrombin, and other factors, which induce local platelet activation and fibronectin complex formation (Zenych et al., 2020). These

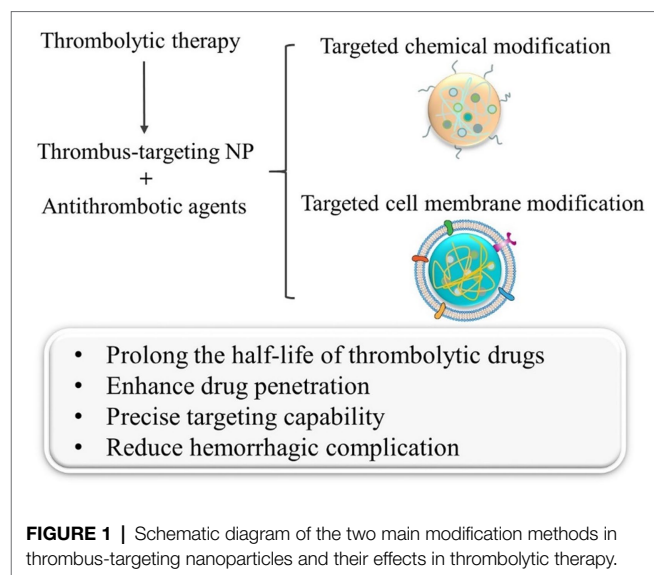


FIGURE 1 | Schematic diagram of the two main modification methods in thrombus-targeting nanoparticles and their effects in thrombolytic therapy.

key components jointly participate in the construction of the intravascular microenvironment that can lead to thrombosis and promote cancer. Fibrinogen is an important reaction substrate for thrombosis and is the key step involved in thrombosis (Undas and Ariens, 2011). When the endogenous coagulation system is abnormally activated, fibrinogen will form fibrin monomers under the action of thrombin, activated factor XIII, Ca^{2+} , and other coagulation factors, subsequently covalently binding with each other to form a fibrin polymer. This stable fibrin network finally captures red blood cells, platelets, $\alpha 2$ -antiplasmin, and other components to form a stable thrombus structure (Chernysh et al., 2011; Alkarithi et al., 2021).

A thrombus has a complex structure and composition, and notably, it bears numerous targetable receptors for nanocarriers that can themselves carry various ligands. By modifying the surfaces of nanocarriers with targeting moieties (such as antibodies, aptamers, peptides, and cell membrane proteins; Li et al., 2020), they can selectively target various biomarkers (P-selectin, Integrin GPIIb/IIIa, Factor XIII, and fibrin) at the thrombus site, thus achieving specific thrombus-targeting capabilities and enhancing the therapeutic effect due to the accumulation of thrombolytic drug at the surface of a clot (Karagkiozaki et al., 2015; Zenych et al., 2020). As far as the modification of the platelet membrane is concerned, the targeting mechanism may proceed *via* the upregulation of GP-Ib-V-IX glycoprotein complex and integrin GPIIb/IIIa residing on the surface of platelet membrane which in turn promotes the adhesion of fibrin and collagen, thus enabling the nanocarrier to target thrombi (Doshi et al., 2012; Chang et al., 2015).

In addition, the proportion of platelets is higher in the case of arterial thrombosis, while venous thrombosis contains more red blood cells and a denser fibrin network (Mackman, 2008; Martinelli et al., 2010). Consequently, existing strategies for thrombus treatment are primarily aimed at platelets and fibrin networks. For example, when the nanocarriers are targeted to reach the thrombus site, the plasminogen activator that

they release can activate the plasminogen near the thrombus to become plasmin (Altaf et al., 2021), and then dissolve the cross-linked bonds between fibrin, destroy its network structure, and thus dissolve the blood clot (Figure 2; Collen and Lijnen, 2005; Hassanpour et al., 2020).

TARGETED CHEMICAL MODIFICATION OF NANOCARRIERS AND APPLICATIONS

The development of antithrombotic therapy has been a high priority for many years (Zhao et al., 2020a). Owing to the rapid progression of nanotechnology, new antithrombotic nanotherapeutics have sprung up in recent years. The nanoscale characteristics of nanocarriers can introduce unique physical and chemical properties, and extend the circulation time of drugs in the bloodstream (Wang et al., 2018a; Zhang et al.,

2018). Moreover, the long-chain structure of polymer macromolecules also facilitates the modification of these platforms for targeting capability and enables researchers to design nanocarriers and impart them with specific functions in order to meet a given requirement (Guo et al., 2018; Wang et al., 2018b; Shakiba et al., 2021). Therefore, the design, modification, and application of polymeric nanocarriers for thrombolytic therapy have become a significant research focus in recent years (He et al., 2021).

The upregulation of integrin GPIIb/IIIa on the surfaces of activated platelets is considered to be an important sign of thrombosis (Bai et al., 2020). The ligand corresponding to this integrin is known to be cyclic arginine-glycine-aspartic acid (cRGD; Barre, 2007; Ye et al., 2020). Therefore, Huang et al. reported an activated-platelet-sensitive nanocarrier capable of inducing selective thrombolysis through targeted delivery and controlled release of tPA to blood clot (Huang et al., 2019). The nanothrombolytic system loaded with tPA was based on

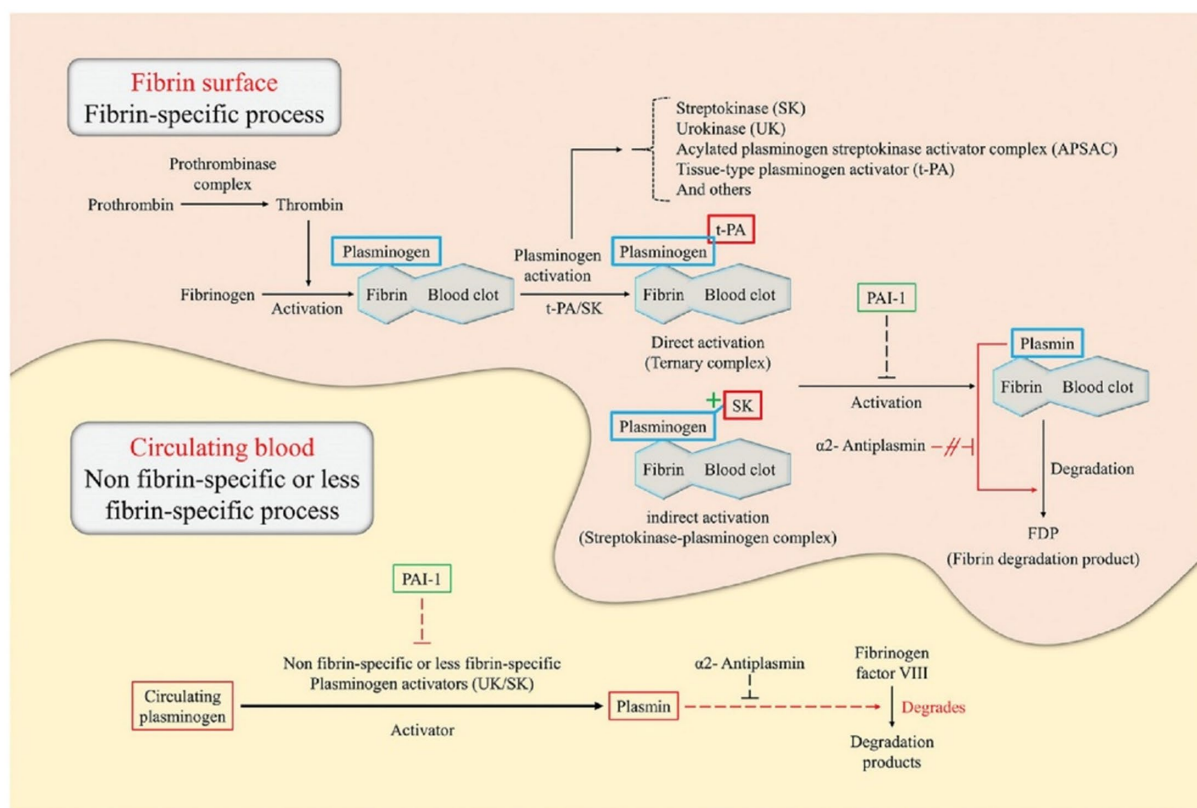


FIGURE 2 | Illustration of the principles of thrombolysis in a fibrin surface and circulating blood environment (Hassanpour et al., 2020). This figure describes the catalytic principle of the conversion of plasminogen to plasmin according to the binding method of the plasminogen activator [e.g., tissue-type plasminogen activator (tPA), urokinase (UK), and streptokinase (SK)]. Plasminogen specifically binds to the surface of the fibrin blood clot. In direct activation, tPA preferentially attaches to plasminogen, resulting in the formation of a ternary complex. On the other hand, in indirect activation, SK cannot directly bind to the plasminogen but induce conformational changes of the plasminogen to form a streptokinase-plasminogen complex. Subsequently, these complexes form plasmin through cleavage of the fibrin-associated plasminogen. Plasmin formed by direct/indirect activation breaks down fibrin into fibrin degradation products, which eventually dissolves blood clots. The thrombolytic process in circulating blood is triggered by non-fibrin-specific or less fibrin-specific plasminogen activators. Plasminogen activators, such as the UK and SK, induce plasmin production by cleavage of circulating plasminogen. Subsequently, plasmin degrades fibrinogen factor VIII instead of fibrinogen. Plasmin activator inhibitor-1 acts on plasminogen, blocking cleavage into plasmin, and causing blood clot formation. α 2-antiplasmin acts only on circulating blood and can inhibit thrombolysis by interfering with plasmin binding sites with fibrinogen factor VIII.

PEGylated liposome, which can provide better *in vivo* stability. The incorporation of cRGD on the surface of liposome is the source of activated platelet sensitivity, it has been reported that cRGD peptide has high specificity and affinity for integrin GPIIb/IIIa on activated platelets (Ye et al., 2020).

Several studies have demonstrated that cRGD-modified nanosystems can effectively induce the selective lysis of fibrin and blood clots, thus suggesting that they are promising candidates for targeted thrombolytic therapy (Li et al., 2019; Zhang et al., 2019; Zhong et al., 2020). However, it is worth noting that studies have shown that platelet activation primarily occurs during the early stage of thrombosis, and the influence of integrin GPIIb/IIIa on platelet aggregation and thrombosis also decreases with the progression from the early to the late stage of the thrombosis process (Yan et al., 2000; Zhou et al., 2011; Gambino et al., 2021). In other words, the treatment brought by cRGD-modified GPIIb/IIIa-targeting nanocarriers primarily targets the early stages of thrombosis. So in practical applications, attention should thus be paid to the specific development stage of thrombosis and suit the right medicine to the case. In addition to the above systems, an organic semiconducting nanoparticle has also been chemically modified with cRGD peptides for use as a photoacoustic (PA) contrast agent for selectively reducing of early thrombosis (Cui et al., 2017), and the addition of the PA signal enhancing molecules can achieve specific imaging and lysis of blood clots (Wang et al., 2021).

Injection of rtPA is the standard drug treatment for thrombolysis (Hassanpour et al., 2020). However, due to the short half-life of rtPA, it only exhibits limited therapeutic efficiency even at high doses, and it brings a higher risk of bleeding, resulting in a 6% intracranial hemorrhage rate and a 50% chance of subsequent mortality (Yaghi et al., 2014). Therefore, polysaccharide-poly(isobutylcyanoacrylate) nanoparticles functionalized with fucoidan and loaded with rtPA were designed to accumulate on the surface of a thrombus (Juenet et al., 2018). Low-molecular weight fucoidan has a nanomolar affinity for P-selectin, which is expressed by activated platelets in thrombus (Bachelet et al., 2009; Zenych et al., 2021). Positively charged aminated dextran was incorporated into the polysaccharide shell to promote electrostatic interactions (Mukwaya et al., 2019), thereby mimicking the natural fibrin binding sites. The experimental results emphasized the relevance of targeting P-selectin for the treatment of thrombosis with rtPA for the first time, which is of great significance for the subsequent development of nanoparticles with P-selectin as the target of thrombosis treatment. But in the actual treatment process, it is best to use it in combination with other targets, because P-selectin can also be used as a target in tumor treatment (Farokhzad, 2015).

By taking into account of the biological characteristics of thrombosis, including the upregulation of H_2O_2 and the abundance of fibrin (Dayal et al., 2013; Andreadou et al., 2021), Zhao et al. (2020b) have developed a H_2O_2 -responsive nanocarrier for the thrombus-targeting delivery of the antithrombotic agent tirofiban (Zhao et al., 2020b). This nanocarrier was composed of a dextran nanocore and a red blood cell (RBC) membrane

shell, and tirofiban was conjugated to dextran through a H_2O_2 -cleavable phenylboronic ester linkage. In contrast with the previous study on the nanosystem modified by fusion protein CREKA and H_2O_2 -scavenging boronate group (Kang et al., 2017), the coating of the RBC membrane can enhance the circulation ability *in vivo*, and the functionalized peptide CREKA on RBC membrane can provide the desired thrombus-specific targeting capability. The ingenuity of the structural design in this study is that it can not only use the H_2O_2 to cleave the phenylboronic ester linkage to release thrombolytic drugs, but also effectively scavenges H_2O_2 and protects cells against H_2O_2 -induced cytotoxicity. It is noteworthy that the platelet membrane may be more suitable for thrombus-targeting than the RBC membrane due to its unique thrombus-homing property, but tirofiban is likely to compromise the receptor on platelet membrane and thus may weaken the targeting capability (Chang et al., 2015). This work can also consider strengthening the research on the use of erythrocyte membrane to overcome barriers in biological microenvironments (Castro et al., 2021).

In addition, some nanoparticles with their own therapeutic functions have also been developed to utilize the photothermal effect as a means to achieve thrombolysis (Burnouf et al., 2019; Huang et al., 2020; Yuan et al., 2021). In order to avoid side-effects, such as hemorrhagic risk, that are generally associated with thrombolytic drugs, near-infrared light-mediated photothermal thrombolysis has been developed as a new treatment for thrombus (Ghosh and Pal, 2007; Singh et al., 2016). Following the initial work by Singh et al. (2016) and Chuang et al. (Mi et al., 2017; Satapathy et al., 2018), a new thrombolytic therapy utilizing photothermal decomposition of fibrin clots was explored by using dual-targeting glycol chitosan/heparin-modified polypyrrole nanoparticles to enhance targeted delivery and thrombolytic effect (Lu et al., 2021). Among them, glycol chitosan showed specific self-adaptive targeting capabilities in the acidic microenvironment of pathologically inflamed tissues at the thrombus (Lee et al., 2014), and heparin had potential biological affinity toward P-selectin that is highly expressed at the thrombus (Ludwig et al., 2004; Schwarz et al., 2020) and finally achieved high-efficiency thrombolysis by leveraging the photothermal effect exhibited by polypyrrole. In contrast with traditional thrombolytic therapy, this novel approach used external near-infrared light to cooperate with the nanoparticles delivered into the body to achieve thrombotic therapy and has promising prospects in the field of thrombolytic therapy.

TARGETED NATURAL CELL MEMBRANE MODIFICATION OF NANOCARRIERS AND APPLICATIONS

Although great progress has been made with chemically modified polymeric nanocarriers with regard to targeted thrombolytic therapy, simple chemical molecular modification may be easily affected by the physiological environment that is encountered during the blood circulation process, thus resulting in inactivation of targeting molecules, agglomeration and adhesion of nanocarriers,

and other issues. To address these issues, biologically inspired polymeric nanocarriers which were modified by cell membrane have been developed. This modification strategy serves to camouflage the nanocarriers and provides an extended circulation time, while also imparting the nanocarriers with the biological functions of natural cell membranes, so as to achieve more precise targeting capabilities (Xuan et al., 2019; Guan et al., 2021).

Inspired by the innate roles of platelets in hemostasis and pathological thrombus (Falati et al., 2002; Lippi et al., 2011), platelet membrane-camouflaged polymeric nanoparticles (nanoplatelets) have been developed to enable the targeted delivery of thrombolytic drug to local thrombus sites (Hu et al., 2015). In a recent study, Xu et al. (2020) bound a platelet membrane to the surface of poly(lactic-co-glycolic acid; PLGA) polymeric inner cores, and rtPA was then chemically conjugated to the activated sulfhydryl groups residing on the external surface of the platelet membrane to form PNP-PA (Xu et al., 2020). It was found that PNP-PA possesses the major membrane adhesion-associated proteins, which can be used to achieve targeted thrombolysis. In addition, researchers also determined the two most effective receptors on activated platelets for PNP-PA recruitment, namely, GPIIb/IIIa and P-selectin mentioned above. Furthermore, the analysis of *in vivo* coagulation indicators in different thrombosis models suggested that the nanoplatelets exhibit a low risk of bleeding complications. Therefore, this nanoplatelet strategy offers an integrated solution to address the drawbacks of clinically used thrombolytic drugs and has great potential to refine the current state of thrombosis treatment.

Using a conceptually similar strategy, Wang et al. (2020) developed platelet membrane-coated PLGA cores loading lumbrokinase as nanoplatelets (PNPs/LBK) to achieve effective thrombolysis with reduced hemorrhagic risk (Wang et al., 2020). Through platelet membrane coating, the circulation time of PNPs is as long as that of RBC membrane-coated nanoparticles. After the PNPs were anchored into the thrombus site through heteromultivalent ligand-mediated binding to active platelet integrin GPIIb/IIIa and P-selectin, the thrombolytic payload was released due to vesicle destabilization triggered by clot-relevant enzyme phospholipase-A2 (Pawlowski et al., 2017). Importantly, hemorrhagic tests reveal that the administration of free LBK leads to a significant prolongation of tail bleeding time, while administration of PNPs/LBK has little effect on the bleeding time. In addition, it is also a good choice to increase the function of responsive drug release on nanoplatelets, such as the use of hydrogen peroxide-responsive platelet membrane-coated nanoparticles for thrombus therapy (Zhao et al., 2021). These studies indicated that the nanoplatelets provide a promising thrombotherapeutic agent, which can effectively target the thrombus site, prolong the internal circulation time, and greatly reduce the hemorrhagic side-effects.

For traditional plasminogen activators, in addition to the hemorrhagic side-effects, there is also the risk of damaging the blood-brain barrier (BBB) and causing neurotoxic effects during ischemic stroke treatment (Su et al., 2008; Niego et al., 2012). In order to obtain the synergistic therapeutic effects provided by thrombolytics and neuroprotectants, a more complex dual-modified nanoplatelet (tP-NP-rtPA/ZL006e) has been developed,

which was composed of a neuroprotectant-loaded dextran derivative core and a platelet membrane shell that was conjugated with thrombin-cleavable Tat-peptide-coupled rtPA (Xu et al., 2019). This dual-modified nanoplatelet can be used to sequentially deliver rtPA and the neuroprotectant (ZL006e) in a site-specific manner. After reaching the thrombus site through platelet membrane targeting, the release of rtPA was triggered by the upregulated thrombin, and the Tat peptide exposed *in situ* enhanced the penetration of nanoplatelet across the BBB into the ischemic brain for the site-specific delivery of ZL006e. *In vitro* and *in vivo* evaluation showed that tP-NP-rtPA/ZL006e could significantly improve the anti-ischemic stroke efficacy in rat models, enhance the neuroprotective effect. It would be better if this study could be combined with reducing hemorrhagic function.

In the future, the above-mentioned modification method of nanoplatelets can be used for reference, by pre-processing platelet cells to over-express certain proteins on the platelet membrane, and then transfer the platelet membrane to the surface of polymeric nanoparticle to obtain more functionalized nanosystems.

CONCLUSION

With the further study of thrombosis mechanisms and the continuous development of bio-nanotechnology, strategies for thrombus treatment have been constantly improved. Polymeric nanocarrier-based delivery systems have been developed to address a series of challenges that are still encountered in thrombolytic drug therapy, and the application of novel biomimetic cell membrane-modified nanocarriers in thrombolytic therapy has also become the focus of current research.

Many factors should be considered with regard to the design of nanocarrier-based drug delivery systems, such as the collocation and encapsulation between thrombolytic drugs and polymeric nanocarriers, the specific targeting function and responsive release function of the nanosystem, as well as the biocompatibility and biosafety. Utilizing the modifiability of polymer nanoparticles, a variety of targeting molecules (cRGD and heparin, etc.) can be modified simultaneously on polymer nanoparticles, while targeting integrin, P-selectin, and fibrin to improve the targeting accuracy of thrombolytic drugs. Moreover, the drug utilization and therapeutic effect can be improved by various responsive drug release modifications, such as shear-stress response modification on the surface of polymer nanoparticles. In addition, some corresponding imaging diagnosis and other functions can also be considered.

Unlike most tumors, thrombus sites are located in the bloodstream, so the thrombolytic agent can more easily reach the pathological target *via* the circulatory system without crossing layers of barriers. Consequently, it is more necessary for the antithrombotic nanosystems to have stronger targeting and adhesion characteristics, be able to target and bind into the thrombus site in the bloodstream, and achieve deep penetration.

In addition, there are still many areas that can be improved in order to advance nanocarrier-based thrombus treatment technology from the laboratory to clinical practice. Since thrombosis occurs at different locations and at varying development levels

among different patients, it is possible to explore the utilization of fluorescent imaging, photoacoustic imaging and other diagnostic methods to determine the thrombosis development stage, and carry out corresponding personalized treatment, realize the integration of diagnosis, and treatment in the same nanosystem. If a platelet membrane-modified nanocarrier system is used, the patient's own platelets can be used as the membrane source to achieve individualized treatment. Moreover, leveraging the facile design of biomimetic polymer nanosystems to strengthen the synergetic treatment of multiple therapies will help to combine the advantages of various thrombolytic strategies, enhance their active targeting capabilities, and reduce the undesirable side-effects, such as hemorrhagic risk and neurotoxicity of thrombolytic therapy.

In conclusion, although extensive research has been conducted in recent decades, the translation of thrombolytic therapy from the experimental research stage to clinical applications still faces many challenges. With the continuous optimization of nanomaterials and the rapid advancement of nanotechnology, more innovative and efficient biomimetic polymeric nanocarrier-based systems can be anticipated, which will provide versatile platforms and opportunities for significant advances in antithrombotic therapy.

REFERENCES

- Al Rawahi, B., Almegren, M., and Carrier, M. (2019). The efficacy and safety of anticoagulation in cerebral vein thrombosis: A systematic review and meta-analysis. *Thromb. Res.* 180:28. doi: 10.1016/j.thromres.2019.05.020
- Alkharithi, G., Duval, C., Shi, Y., Macrae, F. L., and Ariens, R. A. S. (2021). Thrombus structural composition in cardiovascular disease. *Arterioscler. Thromb. Vasc. Biol.* 41, 2370–2383. doi: 10.1161/atvbaha.120.315754
- Altai, F., Wu, S., and Kasim, V. (2021). Role of Fibrinolytic enzymes in anti-thrombosis therapy. *Front. Mol. Biosci.* 8:476. doi: 10.3389/fmolb.2021.680397
- Andreadou, I., Daiber, A., Baxter, G. F., Brizzi, M. F., Lisa, F. D., Kaludercic, N., et al. (2021). Influence of cardiometabolic comorbidities on myocardial function, infarction, and cardioprotection: role of cardiac redox signaling. *Free Radic. Biol. Med.* 166, 33–52. doi: 10.1016/j.freeradbiomed.2021.02.012
- Bachelet, L., Bertholon, I., Lavigne, D., Vassy, R., Jandrot-Perrus, M., Chaubet, E., et al. (2009). Affinity of low molecular weight fucoidan for P-selectin triggers its binding to activated human platelets. *Biochim. Biophys. Acta Gen. Subj.* 1790, 141–146. doi: 10.1016/j.bbagen.2008.10.008
- Bai, S., Liao, J., Zhang, B., Zhao, M., You, B., Li, P., et al. (2020). Multimodal and multifunctional nanoparticles with platelet targeting ability and phase transition efficiency for the molecular imaging and thrombolysis of coronary microthrombi. *Biomater. Sci.* 8, 5047–5060. doi: 10.1039/d0bm00818d
- Bala, M. M., Paszek, E. B., Lesniak, W., Wloch-Kopec, D., Jasinska, K., and Undas, A. (2018). Antiplatelet and anticoagulant agents for primary prevention of thrombosis in individuals with antiphospholipid antibodies. *Cochrane Database Syst. Rev.* 7:CD012534. doi: 10.1002/14651858.CD012534.pub2
- Barre, D. E. (2007). Arginyl-glycyl-aspartyl (RGD) epitope of human apolipoprotein (a) inhibits platelet aggregation by antagonizing the IIb subunit of the fibrinogen (GPIIb/IIIa) receptor. *Thromb. Res.* 119, 601–607. doi: 10.1016/j.thromres.2006.04.013
- Benjamin, E. J., Muntner, P., Alonso, A., Bittencourt, M. S., Callaway, C. W., and Virani, S. S. (2020). Heart disease and stroke Statistics-2019 update: A report From the American Heart Association. *Circulation* 141:E33. doi: 10.1161/cir.0000000000000746
- Burnouf, T., Chen, C.-H., Tan, S.-J., Tseng, C.-L., Lu, K.-Y., Chang, L.-H., et al. (2019). A bioinspired hyperthermic macrophage-based polypyrrole-polyethylenimine (Ppy-PEI) nanocomplex carrier to prevent and disrupt thrombotic fibrin clots. *Acta Biomater.* 96, 468–479. doi: 10.1016/j.actbio.2019.06.053

AUTHOR CONTRIBUTIONS

QG reviewed the literatures and wrote the manuscript. HD revised and finalized the manuscript. All authors contributed to the article and approved the submitted version.

FUNDING

This work was supported by the National Natural Science Foundation of China (No. 21871180), the Tracking Program for Professor of Special Appointment (Eastern Scholar) at Shanghai Institutions of Higher Learning (No. SHDP201802), the Science and Technology Commission of Shanghai Municipality (Nos. 18520710300 and 18JC1413500), and the Open Project of Translational Medicine of SJTU (No. TMSK-2021-108).

ACKNOWLEDGMENTS

The authors would like to thank the members of the research group for their helpful discussions.

- Castro, F., Martins, C., Silveira, M. J., Moura, R. P., Pereira, C. L., and Sarmiento, B. (2021). Advances on erythrocyte-mimicking nanovehicles to overcome barriers in biological microenvironments. *Adv. Drug Deliv. Rev.* 170, 312–339. doi: 10.1016/j.addr.2020.09.001
- Chang, S.-T., Chung, C.-M., Chu, C.-M., Yang, T.-Y., Pan, K.-L., Hsu, J.-T., et al. (2015). Platelet glycoprotein IIb/IIIa inhibitor Tirofiban ameliorates cardiac reperfusion injury. *Int. Heart J.* 56, 335–340. doi: 10.1536/ihj.14-322
- Cheng, J.-W., Zhang, X.-J., Cheng, L.-S., Li, G.-Y., Zhang, L.-J., Ji, K.-X., et al. (2018). Low-dose tissue plasminogen activator in acute ischemic stroke: A systematic review and meta-analysis. *J. Stroke Cerebrovasc. Dis.* 27, 381–390. doi: 10.1016/j.jstrokecerebrovasdis.2017.09.014
- Chernysh, I. N., Nagaswami, C., and Weisel, J. W. (2011). Visualization and identification of the structures formed during early stages of fibrin polymerization. *Blood* 117, 4609–4614. doi: 10.1182/blood-2010-07-297671
- Collen, D., and Lijnen, H. R. (2005). Thrombolytic agents. *Thromb. Haemost.* 93, 627–630. doi: 10.1160/th04-11-0724
- Cornel, E. J., Jiang, J., Chen, S., and Du, J. (2021). Principles and characteristics of polymerization-induced self-assembly with various polymerization techniques. *CCS Chem.* 3, 2104–2125. doi: 10.31635/ccschem.020.202000470
- Cui, C., Yang, Z., Hu, X., Wu, J., Shou, K., Ma, H., et al. (2017). Organic semiconducting nanoparticles as efficient Photoacoustic agents for lightening early thrombus and monitoring thrombolysis in living mice. *ACS Nano* 11, 3298–3310. doi: 10.1021/acsnano.7b00594
- Dayal, S., Wilson, K. M., Motto, D. G., Miller, F. J. Jr., Chauhan, A. K., and Lentz, S. R. (2013). Hydrogen peroxide promotes aging-related platelet Hyperactivation and thrombosis. *Circulation* 127, 1308–1316. doi: 10.1161/circulationaha.112.000966
- Doshi, N., Orje, J. N., Molins, B., Smith, J. W., Mitragotri, S., and Ruggeri, Z. M. (2012). Platelet mimetic particles for targeting thrombi in flowing blood. *Adv. Mater.* 24, 3864–3869. doi: 10.1002/adma.201200607
- Falati, S., Gross, P., Merrill-Skoloff, G., Furie, B. C., and Furie, B. (2002). Real-time in vivo imaging of platelets, tissue factor and fibrin during arterial thrombus formation in the mouse. *Nat. Med.* 8, 1175–1180. doi: 10.1038/nm782
- Farokhzad, O. C. (2015). Nanotechnology Platelet mimicry. *Nature* 526, 47–48. doi: 10.1038/nature15218
- Fuster, V., Badimon, L., Badimon, J. J., and Chesebro, J. H. (1992). The pathogenesis of coronary artery disease and the acute coronary syndromes. *New Eng. J. Med.* 326, 242–250. doi: 10.1056/nejm199201233260406
- Gambino, G., Gambino, T., Connah, L., La Cava, F., Evrard, H., and Angelovski, G. (2021). RGD-peptide functionalization affects the In vivo diffusion of a

- responsive Trimeric MRI contrast agent through interactions with Integrins. *J. Med. Chem.* 64, 7565–7574. doi: 10.1021/acs.jmedchem.1c00264
- Gao, Y., Liu, Y., Yang, X., Zhang, T., Hou, Y., Wang, P., et al. (2021). Pseudoginsenoside-F11 ameliorates thromboembolic stroke injury in rats by reducing thromboinflammation. *Neurochem. Int.* 149:105108. doi: 10.1016/j.neuint.2021.105108
- Ghosh, S. K., and Pal, T. (2007). Interparticle coupling effect on the surface plasmon resonance of gold nanoparticles: From theory to applications. *Chem. Rev.* 107, 4797–4862. doi: 10.1021/cr0680282
- Guan, Q., Guo, H., and Dou, H. (2021). Nanocarriers modified by cell membrane and their applications in tumor immunotherapy. *Prog. Chem.* 33, 150–167. doi: 10.7536/pc201019
- Guo, H.-Z., Song, S., Dai, T.-T., Li, S.-L., and Dou, H.-J. (2018). Trypsin-responsive near-infrared fluorescent/magnetic resonance dual-imaging composite Nanospheres based on self-assembly. *Acta Polym. Sin.* 8, 1127–1140. doi: 10.11777/j.issn1000-3304.2018.18079
- Hassanpour, S., Kim, H.-J., Saadati, A., Tebon, P., Xue, C., van den Dolder, F. W., et al. (2020). Thrombolytic agents: Nanocarriers in controlled release. *Small* 16:2001647. doi: 10.1002/smll.202001647
- He, W., Zhang, Z., and Sha, X. (2021). Nanoparticles-mediated emerging approaches for effective treatment of ischemic stroke. *Biomaterials* 277:121111. doi: 10.1016/j.biomaterials.2021.121111
- Hu, C.-M. J., Ronnie, H. F., Wang, K.-C., Luk, B. T., Thamphiwatana, S., Dehaini, D., et al. (2015). Nanoparticle biointerfacing by platelet membrane cloaking. *Nature* 526, 118–121. doi: 10.1038/nature15373
- Huang, W., Gao, M., and Dou, H. (2020). Polypyrrole and its Nanocomposites applied in Photothermal therapy. *Prog. Chem.* 32, 371–380. doi: 10.7536/pc190906
- Huang, Y., Yu, L., Ren, J., Gu, B., Longstaff, C., Hughes, A. D., et al. (2019). An activated-platelet-sensitive nanocarrier enables targeted delivery of tissue plasminogen activator for effective thrombolytic therapy. *J. Control. Release* 300, 1–12. doi: 10.1016/j.jconrel.2019.02.033
- Jiang, J., Zhu, Y., and Du, J. (2020). Challenges and perspective on ring-opening polymerization-induced self-assembly. *Acta Chim. Sin.* 78, 719–724. doi: 10.6023/a20050162
- Juenet, M., Aid-Launais, R., Li, B., Berger, A., Aerts, J., Ollivier, V., et al. (2018). Thrombolytic therapy based on fucoidan-functionalized polymer nanoparticles targeting P-selectin. *Biomaterials* 156, 204–216. doi: 10.1016/j.biomaterials.2017.11.047
- Kang, C., Gwon, S., Song, C., Kang, P. M., Park, S.-C., Jeon, J., et al. (2017). Fibrin-targeted and H₂O₂-responsive nanoparticles as a Theranostics for Thrombosed vessels. *ACS Nano* 11, 6194–6203. doi: 10.1021/acsnano.7b02308
- Karakiozaki, V., Logothetidis, S., and Pappa, A.-M. (2015). Nanomedicine for atherosclerosis: molecular imaging and treatment. *J. Biomed. Nanotechnol.* 11, 191–210. doi: 10.1166/jbn.2015.1943
- Lee, S. J., Min, H. S., Ku, S. H., Son, S., Kwon, I. C., Kim, S. H., et al. (2014). Tumor-targeting glycol chitosan nanoparticles as a platform delivery carrier in cancer diagnosis and therapy. *Nanomedicine* 9, 1697–1713. doi: 10.2217/nmm.14.99
- Li, B., Chen, R., Zhang, Y., Zhao, L., Liang, H., Yan, Y., et al. (2019). RGD modified protein-polymer conjugates for pH-triggered targeted thrombolysis. *ACS Appl. Bio Mater.* 2, 437–446. doi: 10.1021/acsbm.8b00644
- Li, M., Li, J., Chen, J., Liu, Y., Cheng, X., Yang, F., et al. (2020). Platelet membrane biomimetic magnetic Nanocarriers for targeted delivery and in situ generation of nitric oxide in early ischemic stroke. *ACS Nano* 14, 2024–2035. doi: 10.1021/acsnano.9b08587
- Lippi, G., Franchini, M., and Targher, G. (2011). Arterial thrombus formation in cardiovascular disease. *Nat. Rev. Cardiol.* 8, 502–512. doi: 10.1038/nrcardio.2011.91
- Lu, T.-Y., Chiang, C.-Y., Fan, Y.-J., Jheng, P.-R., Quinones, E. D., Liu, K.-T., et al. (2021). Dual-targeting glycol chitosan/heparin-decorated Polypyrrole nanoparticle for augmented Photothermal thrombolytic therapy. *ACS Appl. Mater. Interfaces* 13, 10287–10300. doi: 10.1021/acsbm.0c20940
- Ludwig, R. J., Boehme, B., Podda, M., Henschler, R., Jager, E., Tandi, C., et al. (2004). Endothelial P-selectin as a target of heparin action in experimental melanoma lung metastasis. *Cancer Res.* 64, 2743–2750. doi: 10.1158/0008-5472.can-03-1054
- Ma, Y.-H., Liu, C.-H., Liang, Y., Chen, J.-P., and Wu, T. (2019). Targeted delivery of plasminogen activators for thrombolytic therapy: An integrative evaluation. *Molecules* 24, 1–15. doi: 10.3390/molecules24183407
- Mackman, N. (2008). Triggers, targets and treatments for thrombosis. *Nature* 451, 914–918. doi: 10.1038/nature06797
- Mao, L., Li, P., Zhu, W., Cai, W., Liu, Z., Wang, Y., et al. (2017). Regulatory T cells ameliorate tissue plasminogen activator-induced brain haemorrhage after stroke. *Brain* 140, 1914–1931. doi: 10.1093/brain/awx111
- Marder, V. J. (2013). Thrombolytic Therapy. *Cons. Hemo. Thrombosis*. 28, 526–537. doi: 10.1016/b978-1-4557-2296-9.00028-2
- Marshall, R. S. (2015). Progress in intravenous thrombolytic therapy for acute stroke. *JAMA Neurol.* 72, 928–934. doi: 10.1001/jamaneurol.2015.0835
- Martinelli, I., Bucciarelli, P., and Mannucci, P. M. (2010). Thrombotic risk factors: basic pathophysiology. *Crit. Care Med.* 38, S3–S9. doi: 10.1097/CCM.0b013e3181c9cbd9
- Mi, F.-L., Burnouf, T., Lu, S.-Y., Lu, Y.-J., Lu, K.-Y., Ho, Y.-C., et al. (2017). Self-targeting, immune transparent plasma protein coated Nanocomplex for noninvasive Photothermal anticancer therapy. *Adv. Healthc. Mater.* 6, 1–10. doi: 10.1002/adhm.201700181
- Mukwaya, V., Wang, C., and Dou, H. (2019). Saccharide-based nanocarriers for targeted therapeutic and diagnostic applications. *Polym. Int.* 68, 306–319. doi: 10.1002/pi.5702
- Niego, B. E., Freeman, R., Puschmann, T. B., Turnley, A. M., and Medcalf, R. L. (2012). T-PA-specific modulation of a human blood-brain barrier model involves plasmin-mediated activation of the rho kinase pathway in astrocytes. *Blood* 119, 4752–4761. doi: 10.1182/blood-2011-07-369512
- Pawlowski, C. L., Li, W., Sun, M., Ravichandran, K., Hickman, D., Kos, C., et al. (2017). Platelet microparticle-inspired clot-responsive nanomedicine for targeted fibrinolysis. *Biomaterials* 128, 94–108. doi: 10.1016/j.biomaterials.2017.03.012
- Pfefferkorn, T., and Rosenberg, G. A. (2003). Closure of the blood-brain barrier by matrix metalloproteinase inhibition reduces rtPA-mediated mortality in cerebral ischemia with delayed reperfusion. *Stroke* 34, 2025–2030. doi: 10.1161/01.str.0000083051.93319.28
- Powers, W. J., Rabinstein, A. A., Ackerson, T., Adeoye, O. M., Bambakidis, N. C., and Tirschwell, D. L. (2018). 2018 guidelines for the early Management of Patients With Acute Ischemic Stroke: A guideline for healthcare professionals From the American Heart Association/American Stroke Association. *Stroke* 49, E233–E234. doi: 10.1161/str.0000000000000172
- Rodriguez, F., and Harrington, R. A. (2021). Management of Antithrombotic Therapy after acute coronary syndromes. *New Engl. J. Med.* 384, 452–460. doi: 10.1056/NEJMr1607714
- Satapathy, M. K., Nyambat, B., Chiang, C.-W., Chen, C.-H., Wong, P.-C., Ho, P.-H., et al. (2018). A gelatin hydrogel-containing Nano-organic PEI-Ppy with a Photothermal responsive effect for tissue engineering applications. *Molecules* 23, 1–17. doi: 10.3390/molecules23061256
- Schwarz, S., Gockel, L. M., Naggi, A., Barash, U., Gobec, M., Bendas, G., et al. (2020). Glycosaminoglycans as tools to decipher the platelet tumor cell interaction: A focus on P-Selectin. *Molecules* 25, 1–16. doi: 10.3390/molecules25051039
- Shakiba, S., Astete, C. E., Cueto, R., Rodrigues, D. F., Sabliov, C. M., and Louie, S. M. (2021). Asymmetric flow field-flow fractionation (AF4) with fluorescence and multi-detector analysis for direct, real-time, size-resolved measurements of drug release from polymeric nanoparticles. *J. Control. Release* 338, 410–421. doi: 10.1016/j.jconrel.2021.08.041
- Singh, N., Varma, A., Verma, A., Maurya, B. N., and Dash, D. (2016). Relief from vascular occlusion using photothermal ablation of thrombus with a multimodal perspective. *Nano Res.* 9, 2327–2337. doi: 10.1007/s12274-016-1119-5
- Su, E. J., Fredriksson, L., Geyer, M., Folestad, E., Cale, J., Andrae, J., et al. (2008). Activation of PDGF-CC by tissue plasminogen activator impairs blood-brain barrier integrity during ischemic stroke. *Nat. Med.* 14, 731–737. doi: 10.1038/nm1787
- Undas, A., and Ariens, R. A. S. (2011). Fibrin clot structure and function A role in the pathophysiology of arterial and venous thromboembolic diseases. *Arterioscler. Thromb. Vasc. Biol.* 31, E88–E99. doi: 10.1161/atvbaha.111.230631
- Wang, H., Dai, T.-T., Lu, B.-L., Li, S.-L., Lu, Q., Mukwaya, V., et al. (2018a). Hybrid dextran-gadolinium Nano-suitcases as high-relaxivity MRI contrast agents. *Chin. J. Polym. Sci.* 36, 391–398. doi: 10.1007/s10118-018-2083-1
- Wang, J., Hu, X., and Xiang, D. (2018b). Nanoparticle drug delivery systems: an excellent carrier for tumor peptide vaccines. *Drug Deliv.* 25, 1319–1327. doi: 10.1080/10717544.2018.1477857

- Wang, S., Wang, R., Meng, N., Guo, H., Wu, S., Wang, X., et al. (2020). Platelet membrane-functionalized nanoparticles with improved targeting ability and lower hemorrhagic risk for thrombolysis therapy. *J. Control. Release* 328, 78–86. doi: 10.1016/j.jconrel.2020.08.030
- Wang, Y., Xu, X., Zhao, X., and Yin, Z. (2021). Functionalized polymeric hybrid micelles as an efficient nanotheranostic agent for thrombus imaging and thrombolysis. *Acta Biomater.* 122, 278–290. doi: 10.1016/j.actbio.2020.10.015
- Xu, J., Wang, X., Yin, H., Cao, X., Hu, Q., Lv, W., et al. (2019). Sequentially site-specific delivery of Thrombolytics and Neuroprotectant for enhanced treatment of ischemic stroke. *ACS Nano* 13, 8577–8588. doi: 10.1021/acsnano.9b01798
- Xu, J., Zhang, Y., and Nie, G. (2021). Intelligent antithrombotic nanomedicines: Progress, opportunities, and challenges. *Viewpoints* 2:20200145. doi: 10.1002/viw.20200145
- Xu, J., Zhang, Y., Xu, J., Liu, G., Di, C., Zhao, X., et al. (2020). Engineered Nanoplatelets for targeted delivery of plasminogen activators to reverse thrombus in multiple mouse thrombosis models. *Adv. Mater.* 32:1905145. doi: 10.1002/adma.201905145
- Xuan, M., Shao, J., and Li, J. (2019). Cell membrane-covered nanoparticles as biomaterials. *Natl. Sci. Rev.* 6, 551–561. doi: 10.1093/nsr/nwz037
- Xue, J., Ma, D., Jiang, J., and Liu, Y. (2021). Diagnostic and prognostic value of immune/inflammation biomarkers for venous thromboembolism: is it reliable for clinical practice. *J. Inflamm. Res.* 14, 5059–5077. doi: 10.2147/jir.s327014
- Yaghi, S., Eisenberger, A., and Willey, J. Z. (2014). Symptomatic Intracerebral hemorrhage in acute ischemic stroke After thrombolysis With intravenous recombinant tissue plasminogen activator A review of natural history and treatment. *JAMA Neurol.* 71, 1181–1185. doi: 10.1001/jamaneurol.2014.1210
- Yan, B., Hu, D. D., Knowles, S. K., and Smith, J. W. (2000). Probing chemical and conformational differences in the resting and active conformers of platelet integrin $\alpha(\text{IIb})\beta(3)$. *J. Biol. Chem.* 275, 7249–7260. doi: 10.1074/jbc.275.10.7249
- Ye, S., Liu, Y., Lu, Y., Ji, Y., Mei, L., Yang, M., et al. (2020). Cyclic RGD functionalized liposomes targeted to activated platelets for thrombosis dual-mode magnetic resonance imaging. *J. Mat. Chem.* 8, 447–453. doi: 10.1039/c9tb01834d
- Yuan, J., Li, L., Yang, Q., Ran, H., Wang, J., Hu, K., et al. (2021). Targeted treatment of ischemic stroke by bioactive nanoparticle-derived reactive oxygen species responsive and inflammation-resolving Nanotherapies. *ACS Nano* 15, 16076–16094. doi: 10.1021/acsnano.1c04753
- Zamanlu, M., Farhodi, M., Eskandani, M., Mahmoudi, J., Barar, J., Rafi, M., et al. (2018). Recent advances in targeted delivery of tissue plasminogen activator for enhanced thrombolysis in ischaemic stroke. *J. Drug Target.* 26, 95–109. doi: 10.1080/1061186x.2017.1365874
- Zenych, A., Fournier, L., and Chauvierre, C. (2020). Nanomedicine progress in thrombolytic therapy. *Biomaterials* 258, 120297–120225. doi: 10.1016/j.biomaterials.2020.120297
- Zenych, A., Jacqmarcq, C., Aid, R., Fournier, L., Ramirez, L. M. F., Chaubet, F., et al. (2021). Fucoidan-functionalized polysaccharide submicroparticles loaded with alteplase for efficient targeted thrombolytic therapy. *Biomaterials* 277:121102. doi: 10.1016/j.biomaterials.2021.121102
- Zhang, Y., Li, N., Suh, H., and Irvine, D. J. (2018). Nanoparticle anchoring targets immune agonists to tumors enabling anti-cancer immunity without systemic toxicity. *Nat. Commun.* 9, 6–15. doi: 10.1038/s41467-017-02251-3
- Zhang, F., Liu, Y., Lei, J., Wang, S., Ji, X., Liu, H., et al. (2019). Metal-organic-framework-derived carbon nanostructures for site-specific dual-modality Photothermal/photodynamic thrombus therapy. *Adv. Sci.* 6, 1–8. doi: 10.1002/advs.201901378
- Zhao, Y., Xie, R., Yodsanit, N., Ye, M., Wang, Y., and Gong, S. (2020a). Biomimetic fibrin-targeted and H₂O₂-responsive nanocarriers for thrombus therapy. *Nano Today* 35, 1–12. doi: 10.1016/j.nantod.2020.100986
- Zhao, Y., Xie, R., Yodsanit, N., Ye, M., Wang, Y., Wang, B., et al. (2021). Hydrogen peroxide-responsive platelet membrane-coated nanoparticles for thrombus therapy. *Biomater. Sci.* 9, 2696–2708. doi: 10.1039/d0bm02125c
- Zhao, Z., Yang, F., Zhang, X., Sun, J., He, Z., and Luo, C. (2020b). Emerging nanotherapeutics for antithrombotic treatment. *Biomaterials* 255:120200. doi: 10.1016/j.biomaterials.2020.120200
- Zhong, Y., Gong, W. J., Gao, X. H., Li, Y. N., Liu, K., Hu, Y. G., et al. (2020). Synthesis and evaluation of a novel nanoparticle carrying urokinase used in targeted thrombolysis. *J. Biomed. Mater. Res. Part A* 108, 193–200. doi: 10.1002/jbm.a.36803
- Zhou, Y., Chakraborty, S., and Liu, S. (2011). Radiolabeled cyclic RGD peptides as radiotracers for imaging tumors and thrombosis by SPECT. *Theranostics* 1, 58–82. doi: 10.7150/thno.v01p0058

Conflict of Interest: The authors declare that the research was conducted in the absence of any commercial or financial relationships that could be construed as a potential conflict of interest.

Publisher's Note: All claims expressed in this article are solely those of the authors and do not necessarily represent those of their affiliated organizations, or those of the publisher, the editors and the reviewers. Any product that may be evaluated in this article, or claim that may be made by its manufacturer, is not guaranteed or endorsed by the publisher.

Copyright © 2021 Guan and Dou. This is an open-access article distributed under the terms of the Creative Commons Attribution License (CC BY). The use, distribution or reproduction in other forums is permitted, provided the original author(s) and the copyright owner(s) are credited and that the original publication in this journal is cited, in accordance with accepted academic practice. No use, distribution or reproduction is permitted which does not comply with these terms.



QiShenYiQi Pills Attenuates Ischemia/Reperfusion-Induced Cardiac Microvascular Hyperpermeability Implicating Src/Caveolin-1 and RhoA/ROCK/MLC Signaling

Chun-Shui Pan^{1,2,3,4}, Li Yan^{1,2,3,4}, Se-Qi Lin⁵, Ke He^{1,2,3,4}, Yuan-Chen Cui^{1,2,3,4}, Yu-Ying Liu^{1,2,3,4}, Bai-He Hu^{1,2,3,4}, Xin Chang^{1,2,3,4}, Xin-Rong Zhao^{1,2,3,4}, Jing-Yu Fan^{1,2,4} and Jing-Yan Han^{1,2,3,4,6*}

OPEN ACCESS

Edited by:

Dongze Zhang,
University of Nebraska Medical
Center, United States

Reviewed by:

Liang Xiao,
Zhejiang University, China
Junping Zhang,
First Teaching Hospital of Tianjin
University of Traditional Chinese
Medicine, China

*Correspondence:

Jing-Yan Han
hanjingyan@bjmu.edu.cn

Specialty section:

This article was submitted to
Vascular Physiology,
a section of the journal
Frontiers in Physiology

Received: 05 August 2021

Accepted: 18 November 2021

Published: 17 December 2021

Citation:

Pan C-S, Yan L, Lin S-Q, He K, Cui Y-C, Liu Y-Y, Hu B-H, Chang X, Zhao X-R, Fan J-Y and Han J-Y (2021) QiShenYiQi Pills Attenuates Ischemia/Reperfusion-Induced Cardiac Microvascular Hyperpermeability Implicating Src/Caveolin-1 and RhoA/ROCK/MLC Signaling. *Front. Physiol.* 12:753761. doi: 10.3389/fphys.2021.753761

¹ Tasy Microcirculation Research Center, Peking University Health Science Center, Beijing, China, ² Key Laboratory of Microcirculation, State Administration of Traditional Chinese Medicine of the People's Republic of China, Beijing, China, ³ Key Laboratory of Stasis and Phlegm, State Administration of Traditional Chinese Medicine of the People's Republic of China, Beijing, China, ⁴ Department of Integration of Chinese and Western Medicine, School of Basic Medical Sciences, Peking University, Beijing, China, ⁵ Key Laboratory of Modern Preparation of Traditional Chinese Medicine, Ministry of Education, Jiangxi University of Traditional Chinese Medicine, Nanchang, China, ⁶ State Key Laboratory of Core Technology in Innovative Chinese Medicine, Tianjin, China

Aims: Coronary microvascular hyperpermeability is an important contributor to ischemia or reperfusion (I/R) injury. However, the effective strategy for this insult remains limited. This study aimed to explore the protective effect of the compound Chinese medicine QiShenYiQi Pills (QSYQ) against coronary microvascular hyperpermeability after cardiac I/R with focusing on the underlying mechanism.

Methods and Results: Male Sprague-Dawley rats under anesthesia were subjected to occlusion of left coronary anterior descending artery followed by reperfusion. QSYQ was administrated 90 min before ischemia initiation. Human cardiac microvascular endothelial cells (HCMECs) underwent hypoxia or reoxygenation (H/R) challenge with QSYQ administrated 1 h prior to hypoxia. QSYQ exhibited effects on attenuating microvascular damage and albumin leakage after I/R injury, showing a role in maintaining endothelial junctions, caveolae, and collagen in basement membrane (BM) of microvessels. Study using HCMECs disclosed that QSYQ protected endothelial barrier from impairment by H/R, attenuating the decline of respiratory chain complex I and ATP synthase, activation of Src/caveolin-1 and increase of RhoA/ROCK/p-MLC, MMP-9, and CTSS. PP2, a Src inhibitor, partially imitated the effect of QSYQ.

Conclusions: The QSYQ was able to prevent I/R-induced cardiac microvascular hyperpermeability via a mechanism involving Src/caveolin-1 and RhoA/ROCK/MLC signaling.

Keywords: QSYQ, cardiac microvascular hyperpermeability, endothelial damage, cell-cell junctions, cytoskeleton

NEW AND NOTEWORTHY

- QSYQ prevents I/R-induced cardiac microvascular hyperpermeability *in vivo* and *in vitro*.
- QSYQ interfered with Src/caveolin-1 and RhoA/ROCK signaling pathways in HCMECs exposed to H/R.

INTRODUCTION

Timely and complete reperfusion after acute myocardial infarction is the most effective way of limiting infarct size and subsequent ventricular remodeling, which, however, provokes irreversible injury to the myocardium and the coronary circulation (Heusch, 2004; Yellon and Hausenloy, 2007; Heusch et al., 2014) leading to ischemia and reperfusion (I/R) injury with microvascular hyperpermeability as an initiator (Heusch and Gersh, 2017). Thus, development of strategies to protect the microvasculature from impairment by I/R is required (Yang et al., 2016; Shen et al., 2018).

The microvascular endothelium constitutes a physical barrier that regulates the exchange of molecules between blood and tissues (Pries and Kuebler, 2006). The transport of macromolecules across the microvascular endothelium is adjusted by caveolae within endothelial cells (transcellular pathway) and the junctions between adjacent endothelial cells (paracellular pathway) (Weis, 2008) including tight and adherent junctions (TJs and AJs) (Wallez and Huber, 2008). Src/caveolin-1 signaling is known to mediate the transcellular traffic, whereas RhoA/ROCK pathway is involved in modulation of intercellular junctions by imposing effect on the expression of respiratory chain complex to restore the impaired energy metabolism (Pries and Kuebler, 2006; Yan et al., 2021) and depolymerized F-actin cytoskeleton after I/R (Yan et al., 2018). NDUFA12 encodes one of the accessory subunits of complex I (Ostergaard et al., 2011) and is required for the formation of the extramembrane arm of human mitochondrial complex I (Rak and Rustin, 2014). YME1L1, an ATP-dependent metalloprotease, plays an important role in regulating mitochondrial morphology and function and maintaining complex I respiration activity (Stiburek et al., 2012; El-Hattab et al., 2018). ATP5D is known as the delta subunit of mitochondrial ATP synthase and could be regulated by RhoA/ROCK pathway. Besides, vascular BM contributes to microvascular barrier significantly, which consists of laminins, collagen IV isoforms, nidogens, and heparan sulfate proteoglycans (Katt et al., 2018). The collagen degradation is mostly mediated by matrix metalloproteinases (MMPs) including MMP-2 and MMP-9. Cathepsin S (CTSS) released from lysosome also has elastolytic and collagenolytic activities (Brown et al., 2020). Obviously, to safeguard the microvascular barrier, a measure with potential to target most, if not all, the signaling involved is needed.

QiShenYiQi Pills (QSYQ) is a traditional Chinese medicine composing of *Astragalus membranaceus* (Huangqi), *Salvia miltiorrhiza* (Danshen), and *Panax notoginseng* (Sanqi), which was approved for treating coronary heart disease and angina by the Chinese State Food and Drug Administration. The metabolite profiling and pharmacokinetics of herbal compounds

following oral administration of QSYQ in rats have been reported (Zhang et al., 2012). Our laboratory revealed that QSYQ and its major effective ingredients, such as R1, Rb1, Rg1, DLA, and astragaloside IV, could alleviate infarct area, myocyte apoptosis, and cardiac dysfunction after I/R injury in rats (Lin et al., 2013; Tu et al., 2013; He et al., 2014; Yang et al., 2015; Cui et al., 2017; Li et al., 2018). It was also reported to cause a marked increase in myocardial capillary density and activation of endothelial growth factor in infarct heart (Zhang et al., 2010). However, the effect of QSYQ on cardiac microvascular hyperpermeability after I/R injury is still not clear. In this study, we explored whether QSYQ could reduce I/R-induced hyperpermeability of cardiac microvessels with focusing on the underlying mechanism.

MATERIALS AND METHODS

Animals

Male Sprague-Dawley (SD) rats weighing 230–270 g were obtained from the Animal Center of Peking University (certificate number SCXK (Jing) 2006-0008). The rats were raised at a temperature of $22 \pm 2^{\circ}\text{C}$ and relative humidity $40 \pm 5\%$ under a 12-h light/dark cycle with access to standard diet and water *ad libitum*. The rats were fasted for 12 h before experiment while allowing to reach water freely. The investigations complied with the Guide of Peking University Animal Research Committee. All experimental procedures were approved by Peking University Biomedical Ethics Committee Experimental Animal Ethics Branch (LA2016314). Animals were randomly assigned to different groups.

Drug

The QSYQ (batch number: 20120914) was obtained from Tasly Pharmaceutical Co. Ltd. (Tianjin, China), which was manufactured in accordance with the guidelines of Good Manufacturing Practice and Good Laboratory Practice.

Cardiac I/R Model and Experiment Protocols

Animals were anesthetized with urethane (1.25 g/kg, i.m) and placed backside down, assisted with an animal breathing apparatus (ALC-V8; Shanghai Alcott Biotech Co., Shanghai, China) through a tracheal cannula inserted *via* mouth, which was set at the breathing ratio 1:1, the frequency 75 times/min, and tidal volume 12 ml/kg. The heart was exposed by thoracotomy, and the left anterior descending coronary artery was ligated with a 5/0 silk. The suture silk was released after 30 min, allowing reperfusion for 90 min. The animals in normal saline (NS) + Sham and QSYQ + Sham groups underwent the same procedure except for ligation of suture silk. Ninety min before ischemia, the animals in QSYQ pretreatment group were administrated through gavage with QSYQ in saline at a dose of 0.6 g/kg. The animals in NS + Sham group and NS + I/R group received equal volume of saline in the same way.

Cell Culture and H/R Model

The primary human cardiac microvascular endothelial cells (HCMEC, ScienCell™ Research Laboratories, Carlsbad,

California, USA) were cultured in a 5% CO₂ incubator at 37°C with a culture medium containing 10% heat-inactivated fetal bovine serum (FBS, Gibco Laboratories, Grand Island, New York, USA), extracellular matrix (EMC, HyClone Laboratories, Logan, Utah, USA), and 100 units/mL penicillin or streptomycin (Gibco Laboratories, Grand Island, New York, USA). To establish hypoxia and reoxygenation (H/R) model, the cells were subjected to hypoxia (5% CO₂ and 1% O₂) by culturing in a microaerophilic system (Thermo Scientific, Waltham, MA) for 2 h with low glucose DMEM medium without FBS and then placed in the normoxic incubator for 3 h for reoxygenation with the normal culture medium. The control group cells were kept in the normal incubator. QSYQ (0.1 mg/ml) or PP2 (a Src inhibitor, 10 μM) was administrated 1 h ahead of H/R.

Vascular Corrosion Casts of Rat Heart

After 90-min reperfusion, the right atrium was cut, blood was flushed out with 60 ml of PBS (pH 7.4, room temperature) containing heparin (0.2 ml, 1,000 USP u/ml), and 30 ml of low-viscosity resin (xinxingbairui, China) was infused into left ventricle (LV). Fifteen min later, resin-filled heart was removed and immersed in water for 30 min to complete resin polymerization. Heart was cut with razor blades and immersed alternatively in 20% NaOH and distilled water to get rid of tissue. This procedure was undertaken about 1 week for complete removal of tissue. The coronary vascular casts were rinsed thoroughly in distilled water and air-dried and carefully mounted on an aluminum stub using double-stick carbon tape. Samples were then coated with gold in argon gas at 25 mA for 2 min in a sputter coater and examined in a field emission scanning electron microscope (SEM) (JSM-5600LV, JEOL, Tokyo, Japan).

Ultrastructure Examination

Rat heart was perfused for 40 min with 4% paraformaldehyde and 2% glutaraldehyde (Ted Pella, Redding, CA, USA) in 0.1 mol/L phosphate buffer at a speed of 3 ml/min and then removed. Myocardial tissue was collected from the surrounding region of infarct in LV and cut into blocks <1 mm³. The tissue blocks were fixed overnight at 4°C with 3% glutaraldehyde, washed 3 times with 0.1 mol/L phosphate-buffered solution (PBS), and then postfixed with 1% osmium tetroxide for 2 h. The ultrathin sections were prepared as routine and observed and photographed with a transmission electron microscope (JEM 1400 plus, JEOL, Tokyo, Japan).

Fluorescein Isothiocyanate Albumin Leakage From Coronary Venules

The animals were intravenously injected with FITC-bovine serum albumin (BSA) (SIGMA, USA) at 50 mg/kg after reperfusion. After 10 min of baseline observation, fluorescence intensity of FITC-BSA was recorded (excitation, 455 nm; emission, 530 nm) using a silicon-intensified target camera (C-2400-08; Hamamatsu, Shizuoka, Japan) and a DVD videocassette recorder (DVR-R25; Malata, Xiamen, China). The fluorescent intensity within the venules (I_v) and in the perivenular interstitium (I_p) was measured with Image-Pro Plus 5.0 software (Bethesda, MD). Albumin leakage was evaluated by I_p/I_v.

Cardiovascular Collagen Stain

To determine the collagen in vascular BM, the heart tissues were immersion-fixed in 4% paraformaldehyde, embedded in paraffin, and processed for 5-μm slices. Deparaffinized and rehydrated slices were stained with Sirius Red, examined using a light microscope (Olympus, Tokyo, Japan), and photographed with a digital camera.

Immunofluorescence Staining and Confocal Microscopy

Heart paraffin sections were permeabilized with 0.3% TritonX-100, blocked with goat serum, and incubated with primary antibodies diluted in PBS overnight at 4°C. The primary antibodies applied were as follows: mouse anti-claudin-5 (1:100, Invitrogen, Camarillo, CA, USA), rabbit anti-vWF (1:100, Millipore, Temecula, CA, USA), and rabbit anticollagen-IV (1:50, Invitrogen, Camarillo, CA, USA). After rinsing with PBS, heart sections were then incubated with Dylight 488-labeled goat antirabbit IgG (KPL, Gaithersburg, MD, USA) and Dylight 549-labeled goat antimouse IgG (KPL, Gaithersburg, MD, USA) for 2 h at room temperature.

The 4% paraformaldehyde-fixed HCMECs were permeabilized with 0.3% TritonX-100 and stained with rhodamine phalloidin (Invitrogen, Carlsbad, USA) for F-actin at 37°C for 2 h. Hoechst 33342 (Molecular Probes) was applied to stain all the nuclei. The results were examined by a laser scanning confocal microscope (TCS SP5, Mannheim, Germany).

Cell Viability Assay

Cell viability was assessed by a Cell Counting Kit-8 (CCK-8; Dojindo Molecular Technologies, Gaithersburg, MD, USA) according to the manufacturer's instructions. Briefly, after treatment of cells, the CCK-8 solution was added to the culture medium and incubated at 37°C for 1 h. The absorbance of each well was measured at 450 nm using microplate reader (Multiskan MK3, Thermo, USA). Cell viability was quantified using average absorbance × 100%.

ELISA for Content of ATP and AMP and the Activity of YME1L1, MMP2, MMP9, and CTSS

Human cardiac microvascular endothelial cells were harvested and mixed with 100 μL RIPA lysis buffer. The whole protein of cells was extracted with a protein extraction kit (Applygen, Beijing, China). In brief, the mixture was homogenized, incubated on ice for 30 min, and centrifuged at 20,000 g, 4°C, for 10 min. The resultant supernatant was taken as whole protein. The content of ATP and AMP and the activities of MMP2, MMP9, CTSS, and YME1L1 were assessed by respective ELISA kit (Huanya Biomedicine Technology, Beijing, Andygene, Beijing, China) and detected by microplate reader (Multiskan MK3, Thermo, USA), according to the manufacturer's instruction.

Activities of Mitochondrial Respiratory Chain Complex I and ATP Synthase

Human cardiac microvascular endothelial cells were harvested and then pipetted up and down to disperse the cells. The activity of mitochondrial respiratory chain complex I and ATP synthase was measured using respective ELISA kit (Abcam, Cambridge, United Kingdom). Briefly, samples were homogenized, pelleted and adjusted to 5.5 mg/ml, subjected to detergent extraction and centrifugation for 20 min at 16,000 g (for complex I), or 20,000 rpm (for ATP synthase), and followed by loading supernatant on plate and incubation for 3 h. Following washing for 3 times, optical density was measured after addition of assay solution. The activity was expressed as the change in absorbance at 340 nm (in optical density units/min).

Endothelial Cell Monolayer Permeability Assay

The endothelial monolayer permeability to FITC-conjugated dextran (FITC-dextran; Sigma-Aldrich Chemicals, St. Louis, MO, USA) was assessed by using transwell permeable membranes (24-well cell culture inserts) with 0.4- μ m pore size (Costar, Corning, NY, USA). HCMECs (2×10^5) were seeded on gelatin-coated transwell filters and allowed to grow for 2 days in high glucose DMEM medium with FBS. The concentration of FITC-dextran transferred to the lower chamber in different conditions was determined with excitation and emission wavelengths of 492 and 520 nm, respectively, using the microplate reader (Multiskan MK3, Thermo, USA).

Western Blot

The whole protein was extracted as described above. The concentration of total protein of each sample was determined two times with a BCA protein assay kit (Applygen Technologies, Beijing, China), according to the manufacturer's instruction, taking the average as the concentration. The protein was separated on 8 or 10% SDS-PAGE and transferred to polyvinylidene difluoride membrane. The membrane was incubated overnight at 4°C with antibodies, respectively, against p-Src/Src (1:1000, CST, Vermont, USA), p-caveolin-1/caveolin-1 (1:1000, CST, Vermont, USA), claudin-5 (1:1000, Invitrogen, California, USA), occludin (1:1000, Invitrogen, California, USA), VE-cadherin (1:1000, Abcam, Cambridge, UK), ZO-1 (1:1000, Invitrogen, California, USA), ATP5D (1:200, Santa Cruz, California, USA), p-MLC/MLC (1:1000, CST, Vermont, USA), ROCK (1:1000, Abcam, Cambridge, UK), RhoA (1:1000, Abcam, Cambridge, UK), YME1L1 (1:1000, Abcam, Cambridge, UK), NDUFA12 (1:1000, Abcam, Cambridge, UK), MMP-2 (1:1000, Abcam, Cambridge, UK), MMP-9 (1:1000, Abcam, Cambridge, UK), CTSS (1:1000, Abcam, Cambridge, UK), and GAPDH (1:1000, CST, Vermont, USA). GAPDH was used as a loading control. Enhanced chemiluminescence detection kit (Applygen Technologies, Beijing, China) was applied for revealing the bands. Band intensities were quantified by densitometry and presented as mean area density using Quantity One Image Analyzer software (Bio-Rad; Richmond, CA, USA).

Statistical Analysis

All parameters were expressed as mean \pm SE. Statistical analysis was performed using one-way ANOVA followed by Newman-Keuls test or using two-way ANOVA followed by Bonferroni for multiple comparisons. Data were analyzed using GraphPad Prism 7 software (GraphPad software Inc., USA). A $p < 0.05$ was considered to be statistically significant.

RESULTS

QSYQ Protected Vascular Architecture From Disorder in Rat Heart and Ameliorated Albumin Leakage From Coronary Venules

Illustrated in **Figure 1** are the representative SEM images of corrosion casting vasculatures in hearts from different groups. Capillaries in NS + Sham group (**Figure 1A,a1**) and QSYQ + Sham group (**Figure 1A,a2**) exhibited a rather regular orientation with uniform diameter. In contrast, capillaries in NS+I/R heart manifested distorted and narrowed vessel segments (**Figure 1A,a3**), which most likely resulted from the pressure imposed by interstice edema and accounts for the elevated resistance and slowed blood flow and indicates microcirculation disturbance. QSYQ pretreatment ameliorated vasculature disorders induced by I/R (**Figure 1A,a4**).

The observation of albumin leakage from coronary venules and ultrastructure of microvessels confirmed the results from corrosion casting and SEM. **Figure 1B** presented the representative images of FITC-labeled albumin leakage from coronary venules in different groups with statistic result depicting in **Figure 1C**. Compared with NS + Sham and QSYQ + Sham groups (**Figure 1B,b1,b2**), I/R evoked an obvious FITC-labeled albumin leakage from coronary venules (**Figure 1B,b3**), which was significantly prevented by pretreatment with QSYQ (**Figure 1B,b4**). Vascular permeability is regulated by endothelial cells, in which intercellular junctions are the major determinants. As expected, electron microscopy revealed an obvious intercellular gap in vascular endothelial cells in NS+I/R group (**Figure 2A,a3**) as compared to NS + Sham and QSYQ + Sham groups (**Figure 2A,a1,a2**), suggesting involvement of endothelial cell junctions in microvascular hyperpermeability after I/R, which was alleviated by pretreatment with QSYQ (**Figure 2A,a4**).

QSYQ Protected HCMECs From Damage and Ameliorated FITC-Dextran Moving Across HCMECs Monolayer After H/R

To assay the role of QSYQ in H/R-deteriorated viability of endothelial cells, HCMECs were examined in different conditions using the CCK-8 assay. There was no statistics difference between NS + Sham and QSYQ + Sham groups (1.18 ± 0.11 vs. 1.11 ± 0.06). Compared with NS + Sham, H/R evoked an obvious decrease in cell viability, which was significantly prevented by pretreatment with QSYQ in concentrations ranging from 0.05 to 1 mg/ml, with lower concentrations appearing more effective.

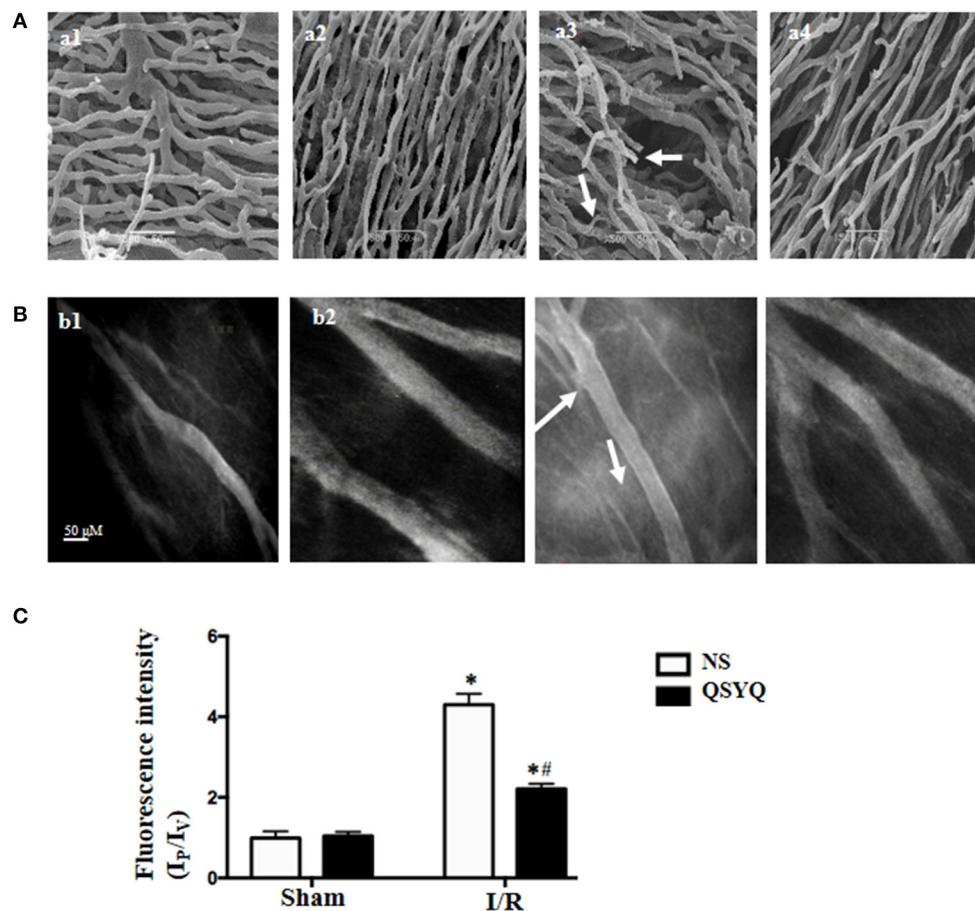


FIGURE 1 | Effect of pretreatment with QSYQ on the vascular corrosion casts and coronary venular albumin leakage of rat heart. **(A)** The representative scanning electron micrographs of myocardial vascular corrosion casts in different groups. Arrows: distorted and narrowed vessel segments. a1: NS + Sham group; a2: QSYQ + Sham group; a3: NS+I/R group; a4: QSYQ+I/R group. Bar = 50 μ m. **(B)** Representative images of FITC-albumin leakage from coronary venules in different groups. b1: NS + Sham group; b2: QSYQ + Sham group; b3: NS+I/R group; b4: QSYQ+I/R group. Bar = 50 μ m. **(C)** Statistical results of albumin leakage expressed as ratio of fluorescence intensity in the Ip to that Iv. Results are presented as mean \pm SEM ($n = 6$). * $p < 0.05$ vs. NS + Sham group, # $p < 0.05$ vs. NS + I/R group. Statistical analysis was performed using two-way ANOVA followed by Bonferroni for multiple comparisons.

The dose of 0.1 mg/ml QSYQ was applied in all subsequent *in vitro* experiments (**Figure 2B**).

The permeability of HCMECs monolayer for FITC-dextran was assessed in various conditions by culturing the cells in a 24-well transwell chamber. Compared with NS + Sham and QSYQ + Sham groups, a significant increase of FITC-dextran was observed in the lower chamber in H/R group, suggesting an increased permeability of the HCMECs monolayer (**Figure 2C**). Apparently, pretreatment with 0.1 mg/ml of QSYQ showed a reduced fluorescence intensity of liquid in the lower chamber as compared to H/R, suggesting the ameliorating effect of QSYQ on the endothelial barrier.

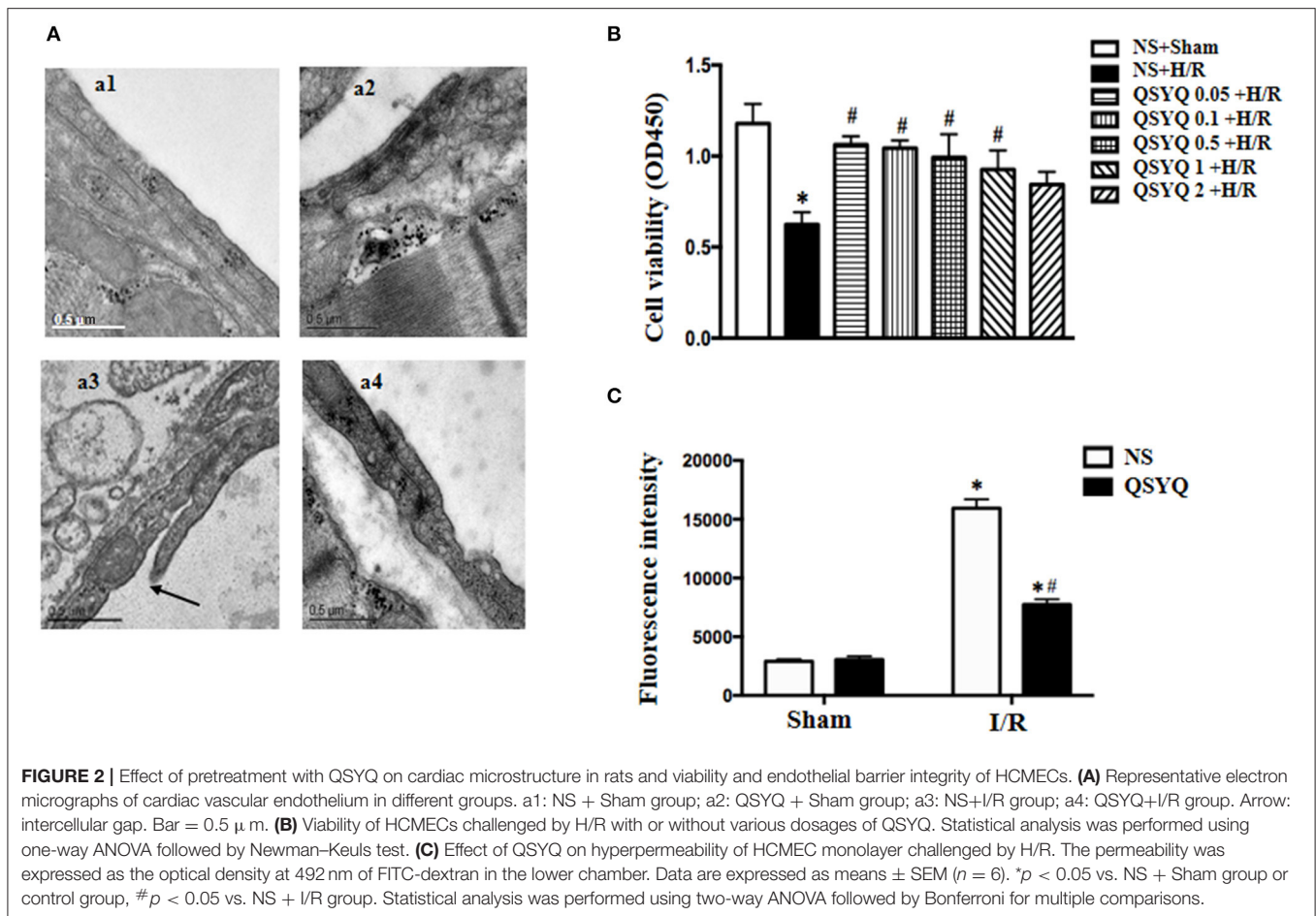
QSYQ Blocked the Phosphorylation of Src and Caveolin-1 in HCMECs Induced by H/R

Src has been known as an upstream signaling pathway to regulate endothelial permeability *via* modulation of caveolin activity. To investigate the role of Src in the protective effect of

QSYQ on microvascular endothelium barrier after I/R injury, we examined the expression and activation of Src and caveolin-1 in HCMECs by western blot. As shown in **Figures 3A,B**, H/R increased the phosphorylated Src obviously while had no effect on Src expression. On the other hand, H/R increased both the expression and phosphorylation of caveolin-1. The change in phosphorylation of Src and caveolin-1 and the expression of caveolin-1 in response to H/R were all alleviated by pretreatment with QSYQ significantly. This result suggests an involvement of Src/caveolin-1 signaling in QSYQ protective effect on endothelial hyperpermeability after H/R.

QSYQ Alleviated Degradation of Junction Proteins in I/R-Induced Rat Heart and HCMECs Induced by H/R

In view of the critical role of intercellular junctions in maintaining vascular integrity, the expression and distribution of vascular endothelial TJ protein claudin-5 were first examined



by confocal microscopy, with representative images of different groups displaying in **Figure 3C**. Apparently, claudin-5 localized between endothelial cells as continuous lines in Sham groups (**Figure 3C,c1–c2**). Reperfusion for 90 min disrupted the continuously distributed claudin-5, resulting in an intermittent and weakened staining, indicating degradation of claudin-5 in response to I/R (**Figure 3C,c3**). Interestingly, this degradation was reversed remarkably by QSYQ pretreatment (**Figure 3C,c4**).

The role of QSYQ in protection of endothelial junction proteins was further verified by *in vitro* study using HCMECs H/R model. Western blot showed that, as compared to NS + Sham and QSYQ + Sham groups, H/R exposure provoked a decrease in the expressions of TJ proteins claudin-5, occludin and zona occludens-1 protein (ZO-1) and the AJ protein VE-cadherin (**Figures 3D,E**), suggesting a damaged endothelial cell barrier induced by H/R. Pretreatment with QSYQ protected the changes in junction proteins after H/R significantly. This result suggests an implication of modulating junction proteins in QSYQ protective effect on endothelial hyperpermeability after H/R.

QSYQ Attenuated Actin Cytoskeleton Abnormality and ATP/AMP Ratio Decrease of HCMECs After H/R

Actin is known to play a crucial role in maintaining endothelium barrier integrity. We thus assessed the actin cytoskeleton of HCMECs by rhodamine-phalloidine staining in different conditions (**Figure 4A**). As compared to NS + Sham and QSYQ + Sham cells (a1, a2), H/R led to a dramatic change in F-actin structure and distribution in HCMECs, with most of the actin stress fibers localizing as bundles in the periphery of the cells, whereas those in the cytoplasm becoming disintegrated (a3). Obviously, the H/R-elicited change in actin stress fibers was significantly attenuated by pretreatment with QSYQ (a4).

The ATP is required for F-actin polymerization, and disarrangement of F-actin after H/R implied a depletion of ATP. We tested this deduction in HCMECs by ELISA. The result in **Figure 4B** shows that as compared to NS + Sham and QSYQ + Sham groups, ATP level in NS+H/R group significantly decreased, whereas AMP level increased, suggesting an impairment of energy metabolism after H/R. Interestingly,

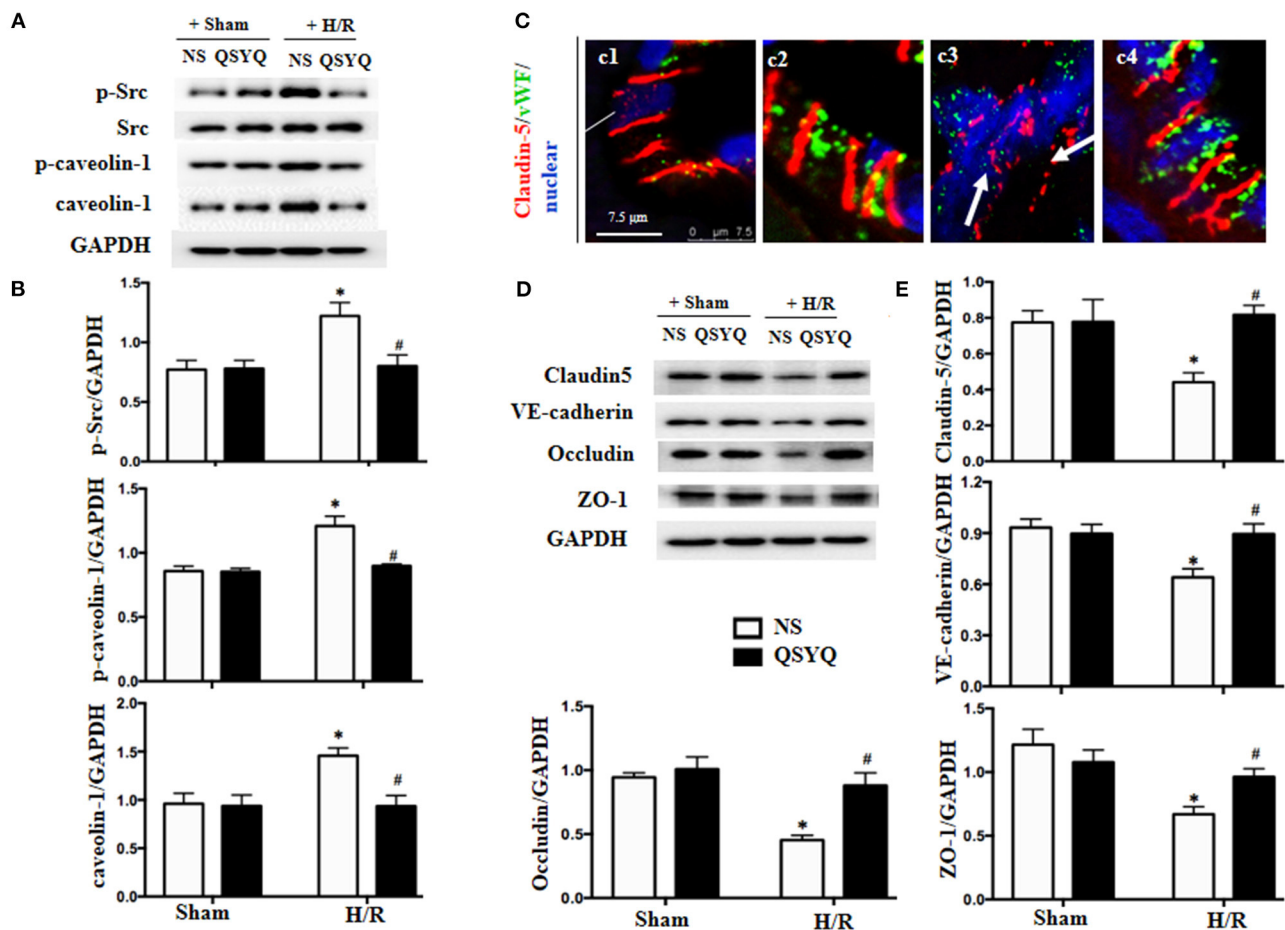


FIGURE 3 | Effect of QSYQ pretreatment on intercellular junction proteins and Src/caveolin-1 in HCMECs after H/R. **(A)** Representative western blot bands of Src, p-Src, caveolin-1, and p-caveolin-1 in various groups of HCMECs. GAPDH was used as a loading control. **(B)** Relative densitometric values of p-Src, caveolin-1, and p-caveolin-1 corrected for GAPDH. Data are expressed as means \pm SEM ($n = 6$). * $p < 0.05$ vs. NS + control group, # $p < 0.05$ vs. NS + H/R group. Statistical analysis was performed using two-way ANOVA followed by Bonferroni for multiple comparisons. **(C)** Representative immunofluorescence confocal images of claudin-5 in rat heart vessels. Arrows: discontinuous distribution of claudin-5. c1: NS + Sham group; c2: QSYQ + Sham group; c3: NS+H/R group; c4: QSYQ+H/R group. Claudin-5 (red) localized between the endothelial cells with marker vWF (green). Bar = 7.5 μ m. **(D,E)** Representative western blot bands **(D)** and relative densitometric values **(E)** of claudin-5, ZO-1, occludin, and VE-cadherin in HCMECs in different groups. GAPDH was used as a loading control. Data are expressed as means \pm SEM ($n = 6$). * $p < 0.05$ vs. NS + control group, # $p < 0.05$ vs. NS + H/R group. Statistical analysis was performed using two-way ANOVA followed by Bonferroni for multiple comparisons.

alteration in ATP and AMP levels caused by H/R was prevented by pretreatment with QSYQ.

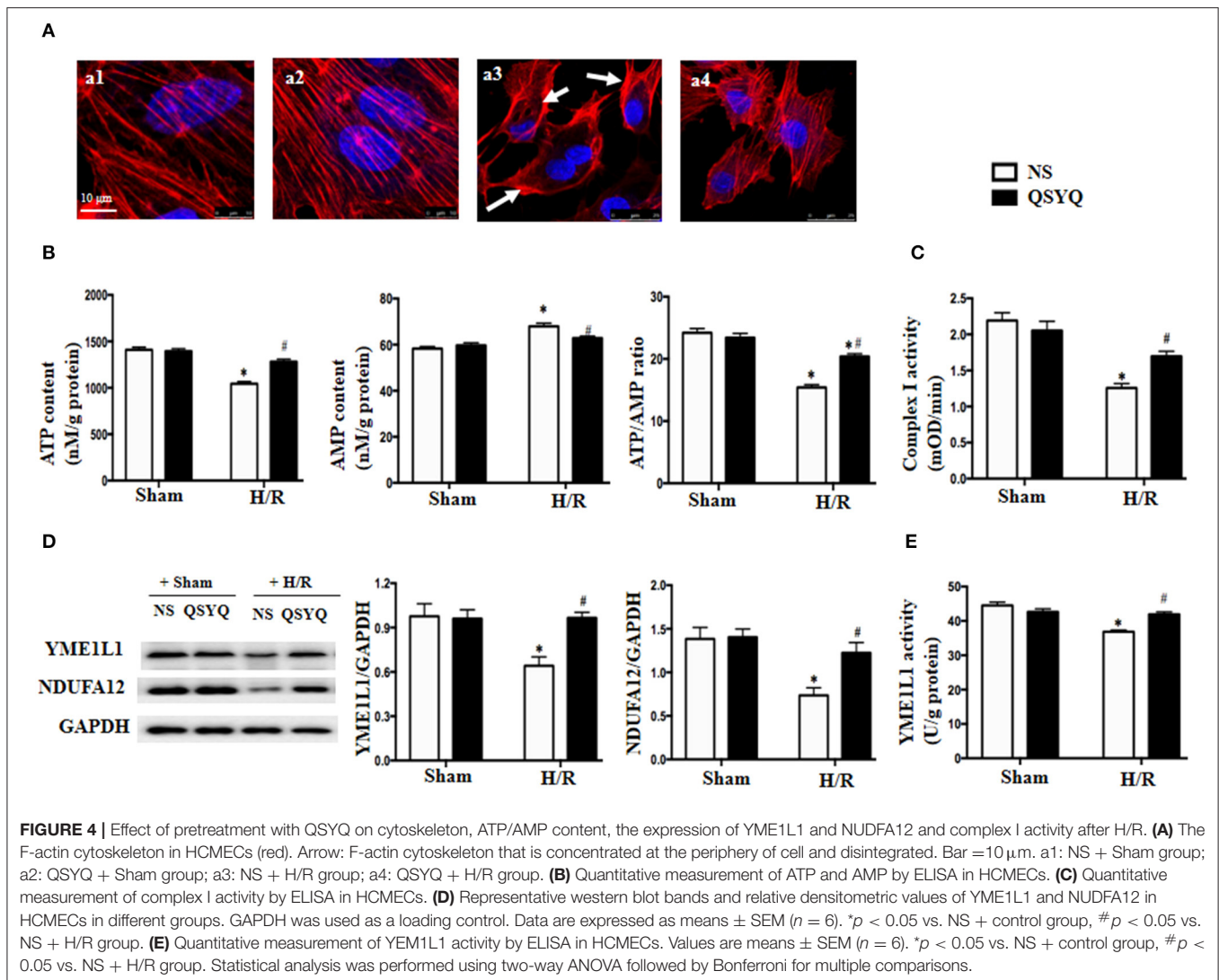
QSYQ Protected the Activity of Complex I and ATP Synthase From Decline During H/R

The majority of ATP in cells is generated by electron transport chain complexes in mitochondria. To assay the role of QSYQ on ATP production, we detected the activity of complex I and ATP synthase in HCMECs. The results showed that the activities of complex I and ATP synthase were remarkably reduced in NS+H/R group as compared to NS + Sham and QSYQ + Sham

groups, which were ameliorated by pretreatment with QSYQ (Figures 4C, 5A).

We next detected changes in NDUFA12 and YME1L1, two proteins that are important for the activity of mitochondrial complex I, in HCMECs under H/R by using western blot. The result showed that H/R challenge elicited a significant decline in the expression of both NDUFA12 and YME1L1 (Figure 4D) and also the activity of YME1L1 (Figure 4E), which were ameliorated by pretreatment with QSYQ (Figures 4D,E). This result suggests an implication of NDUFA12 and YME1L1 in the protective effect of QSYQ on the activity of complex I.

The ATP5D is the delta subunit of mitochondrial ATP synthase. Result of western blot revealed that compared with NS + Sham and QSYQ + Sham groups,



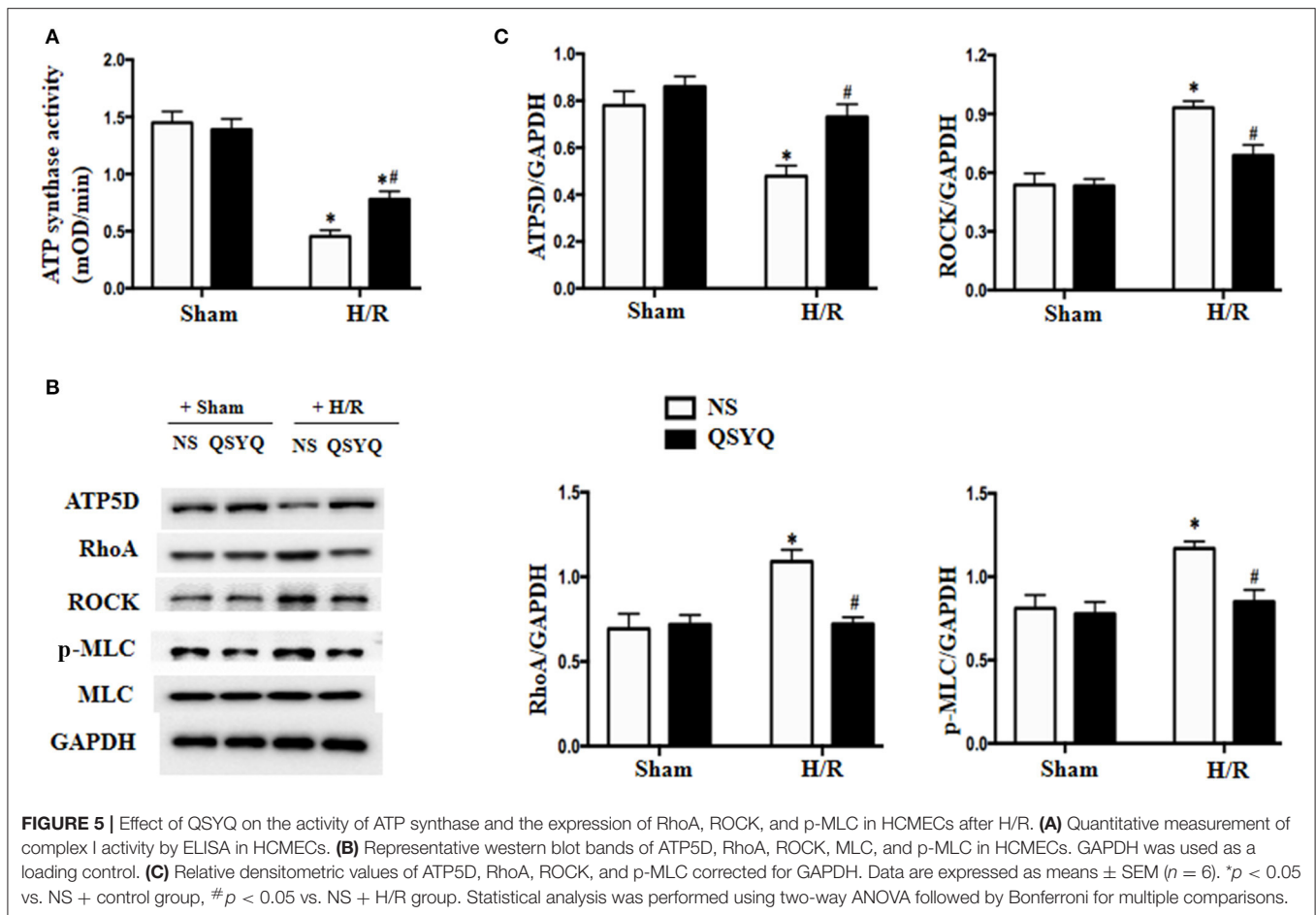
ATP5D level was remarkably reduced in NS+H/R group, which was reversed by pretreatment with QSYQ (Figures 5B,C).

RhoA/ROCK Signaling Pathway Is Involved in the Protected Effect of QSYQ on HCMECs During H/R

The RhoA/ROCK has been known to play an important role in endothelial barrier dysfunction, whereas MLC is one of the targets of ROCK. We thus tested the likely involvement of RhoA/ROCK in the mechanism of QSYQ effect. Western blot in Figures 5B,C showed that H/R significantly elevated the expressions of RhoA and ROCK and promoted myosin light chain (MLC) phosphorylation in HCMECs. QSYQ lessened RhoA/ROCK/p-MLC increase induced by H/R, highlighting an involvement of the RhoA/ROCK/MLC signaling in the beneficial role of QSYQ observed.

QSYQ Decreased the Expressions and Activities of MMP-2, MMP-9, and CTSS in HCMECs and Maintained the Vascular BM Integrity

Basement membrane is an essential part of vascular endothelium barrier, which contains collagen as a major component. We thus assessed the status of collagen deposition in microvascular wall to explore the role of QSYQ in maintaining BM integrity. Displayed in Figure 6A are the Sirius Red-stained cardiac microvessels from different groups, which shows that the area of collagen deposition in BM decreased significantly after I/R (a3) compared with Sham groups (a1, a2). In contrast, treatments with QSYQ enhanced the collagen deposition in the vascular walls after I/R (a4). This result was confirmed by immunofluorescence staining of collagen IV in cardiac vascular wall as shown in Figure 6B, wherein a discontinuous distribution of collagen IV was observed in NS+I/R group (b3), which is in striking contrast to Sham groups (b1, b2), indicating degradation of collagen-IV in response to I/R.



Interestingly, this degradation was restored by pretreatment with QSYQ (b4).

The collagen degradation is mostly mediated by MMPs including MMP-2 and MMP-9, and also by CTSS, an enzyme released from lysosomes having elastolytic and collagenolytic activities. We next examined the expression and activities of MMP-2, MMP-9, and CTSS in HCMECs from various groups by western blot and ELISA, respectively. The results showed that H/R led to an increase in expressions (**Figures 6C,D**) and activities (**Figure 6E**) of MMP-2, MMP-9, and CTSS, which was in consonance with collagen degradation found in cardiac vascular wall after I/R. Intriguingly, the alterations of MMP-2, MMP-9, and CTSS were relieved by pretreatment with QSYQ (**Figures 6C–E**).

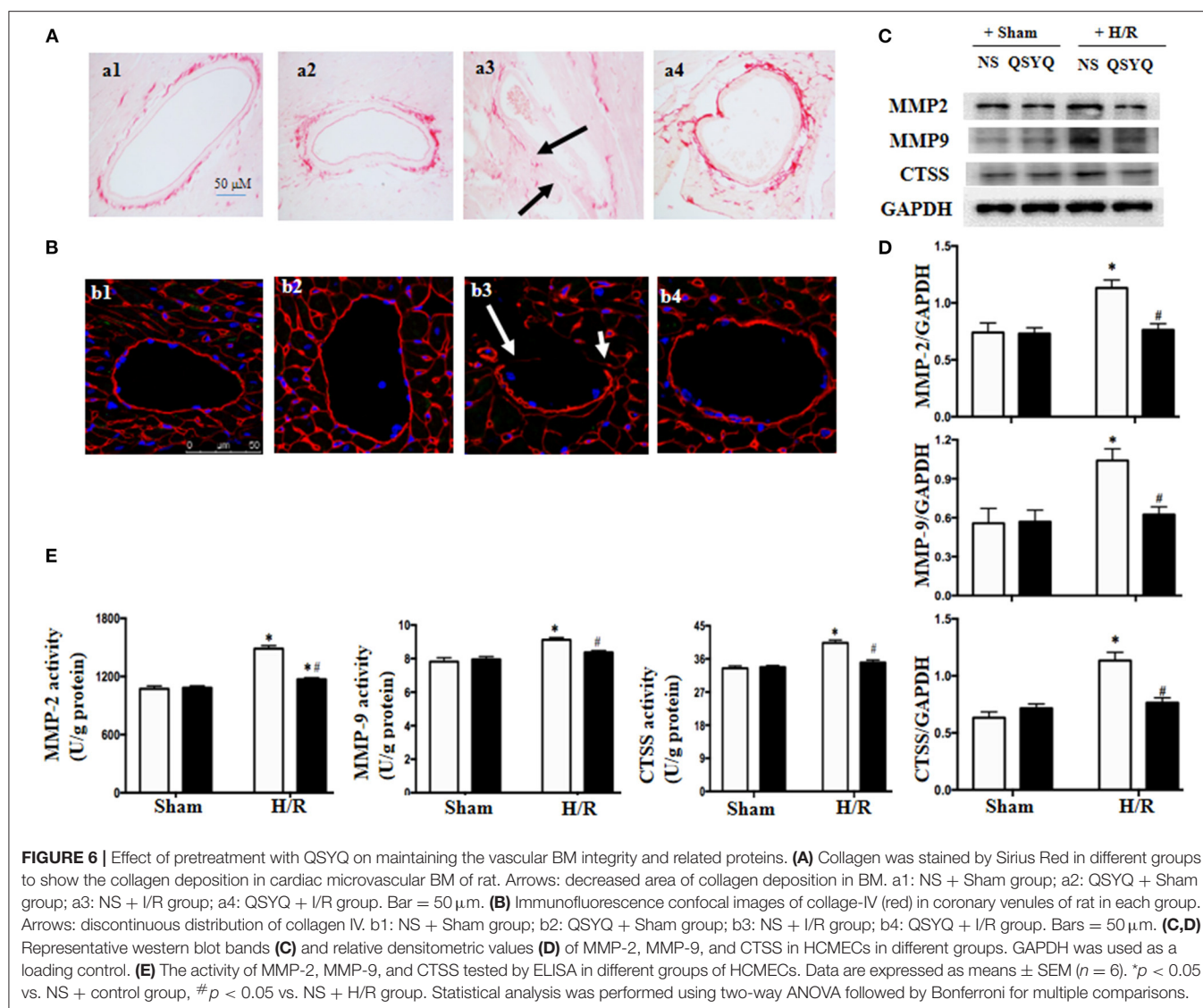
PP2, Inhibitor of Src, Had an Effect Similar to QSYQ on HCMECs Exposed to H/R

Caveolae-mediated transendothelial traffic contributes to endothelium permeability, which is regulated by Src. To explore whether Src/caveolae pathway is implicated in the mechanism whereby QSYQ takes effect, we treated HCMECs with PP2, a Src inhibitor, 1 h before H/R. The results showed that PP2 restored the level of p-caveolin-1 as QSYQ did (**Figures 7A,B**), demonstrating the role of Src in the mechanism for QSYQ

mediating vascular permeability *via* transendothelial pathway. Furthermore, akin to QSYQ, PP2 restored the expression of claudin-5 and inhibited the activity of CTSS and MMP-9 (**Figure 7C**), the two enzymes known to exhibit activity to hydrolyze both BM proteins and junction proteins. Finally, PP2 protected H/R-caused hyperpermeability of HCMEC monolayer to FITC-dextran (**Figure 7D**), similar to QSYQ, suggesting involvement of Src/caveolae signal pathway in the effect of QSYQ on ameliorating microvascular hyperpermeability.

DISCUSSION

This study showed that reperfusion following coronary occlusion impaired rat cardiac microvessels manifesting abnormal vascular morphology, increased albumin leakage from venules, concurrent with a disconnection of the junctions between adjacent endothelial cells in cardiac capillaries, a disarranged collagen deposition and a downregulated expression of collagen IV in vascular wall *in vivo*, all these alterations were ameliorated by pretreatment with QSYQ. Study using H/R-challenged HCMECs revealed the mechanism for QSYQ to protect cardiac microvascular barrier involving regulation of paracellular pathway and transcellular pathway and integrity of vascular



BM, a process implicating RhoA/ROCK/MLC and Src/caveolae signaling and restoration of energy metabolism.

Coronary microvascular dysfunction occurs in up to half of patients submitted to apparently successful primary percutaneous transluminal coronary intervention. Microvascular hyperpermeability after I/R results in no-reflow and myocardium tissue edema which limits tissue reoxygenation and provokes cardiac myocyte apoptosis (Kottke and Walters, 2016), aggravating ischemia-induced myocardium injury. Thus, development of approach to deal with I/R-elicited cardiac microvascular hyperpermeability has gained increasing attention. However, the so far proposed approaches prove to be either controversial (Zhao et al., 2006; Selker et al., 2012) in efficiency or inadequate (Erlinge et al., 2014; Montalescot et al., 2014; Korayem et al., 2017). In this work, we found that QSYQ ameliorated cardiac microvascular morphology and endothelial hyperpermeability induced by I/R, indicating QSYQ as a promising option for such a purpose.

Microvascular barrier is determined by TJs and AJs between adjacent endothelial cells, the number and function of caveolae in endothelial cell, and the integrity of BM under beneath the endothelial cell layer, which are regulated by a variety of signaling pathways. Besides, the actin filaments in the vascular endothelial cells contribute to keeping microvascular barrier integrity as well, which offer a support from inside for the intercellular junctions *via* ZO-1 (Alluri et al., 2016). Actin polymerization is an energy-dependent process, which may be reversed by depletion of ATP. This work found that I/R or H/R induced a decrease in junction proteins, an increase in the activity and level of caveolin-1, a disintegrated BM, a disrupted actin and a malregulated energy metabolism, including disfunction of mitochondrial respiratory chain. Pretreatment with QSYQ ameliorated all the insults, demonstrating its multitargeting edge over the currently available measure in containing I/R-caused cardiac microvascular hyperpermeability.

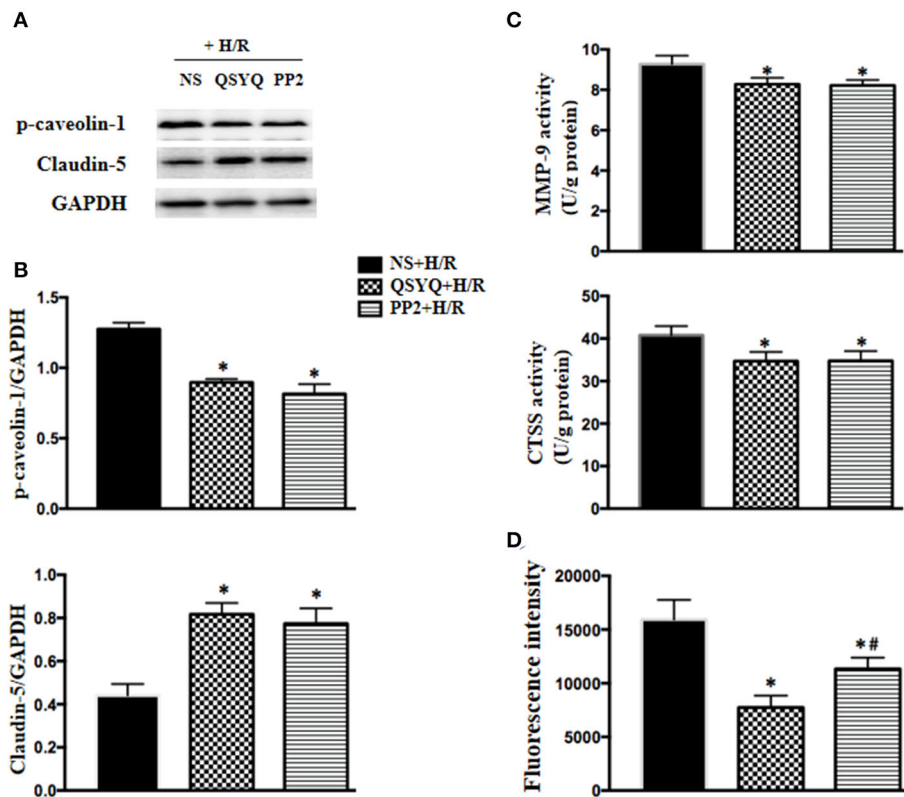


FIGURE 7 | Effect of PP2 on the expression of claudin-5 and p-caveolin-1, the activity of MMP-9 and CTSS, and hyperpermeability of HCMECs monolayer exposed to H/R. **(A)** Representative western blot bands **(A)** and relative densitometric values **(B)** of p-caveolin-1 and claudin-5 in HCMECs in different groups. GAPDH was used as a loading control. **(C)** Quantitative measurement of MMP-9 and CTSS activity by ELISA in HCMECs. **(D)** Effect of QSYQ on hyperpermeability of HCMEC monolayer induced by H/R. The permeability was expressed as the optical density of FITC-dextran at 492 nm in the lower chamber. Data are expressed as means \pm SEM ($n = 6$). * $p < 0.05$ vs. NS + Sham group or control group, # $p < 0.05$ vs. NS + I/R group. Statistical analysis was performed using one-way ANOVA followed by Newman-Keuls test.

Src family protein tyrosine kinases have been implicated in upstream signaling pathways that lead to endothelial hyperpermeability through both intercellular and transendothelial pathways (Mehta and Malik, 2006). This work showed an increase in activity of Src in HCMECs exposed to H/R, and PP2, the inhibitor of Src, ameliorated the H/R-induced increase in p-caveolin-1, MMP-9, and CTSS and decrease in claudin-5, similar to QSYQ did, suggesting Src/caveolin as one of the signaling that mediates QSYQ effect. As a compound Chinese medicine, QSYQ contains numerous bioactive ingredients, some of which have been reported to exert effect by targeting Src/caveolin-1 signaling. For example, salvianolic acid B was reported to ameliorate lipopolysaccharide-induced albumin leakage from rat mesenteric venules by binding to Src (Pan et al., 2015), Astragaloside IV was shown to enhance taxol chemosensitivity of breast cancer by targeting caveolin-1 (Zheng et al., 2019). Are there any other ingredients in QSYQ that interfere in Src/caveolin-1 signaling remain to be identified? Noticeably, PP2 was less effective than QSYQ in protection of H/R-elicited hyperpermeability of HCMEC monolayer, implying existence of another signaling (s) that participates in mediation of QSYQ effect. Further work is required to identify the target

(s) of QSYQ by specially mutating or blocking some potential targets downstream of QSYQ.

This study showed that H/R activated RhoA/ROCK/p-MLC signal in HCMECs which was attenuated by QSYQ, indicating an involvement of RhoA/ROCK/p-MLC in the mechanism for QSYQ to work. This result is in line with the reports regarding the effect of some QSYQ ingredients, such as ginsenoside Rb1 and R1, which were shown able to inhibit RhoA/ROCK meanwhile elevate ATP5D expression and ATP level (He et al., 2014; Cui et al., 2017), protecting I/R-induced energy metabolism disorder. Thus, in this case, among the ingredients of QSYQ, at least ginsenoside Rb1 and R1 contribute to the regulation of the disordered energy metabolism after I/R or H/R by targeting RhoA/ROCK signaling. In addition, the result of this study unraveled that H/R resulted in a decrease in NDUFA12 and YME1L1 alike, the two proteins essential for respiratory chain complex I with the former being one of the subunits of the complex while the later an ATP-dependent metalloprotease that regulates the function of the complex. The reduction in the two proteins partially accounts for the reduced activity of complex I in response to H/R challenge. QSYQ pretreatment restrained the decrease in these two proteins after H/R as

well. Dihydroxyphenyl lactic acid, an ingredient of QSYQ, has been reported having potential to restore respiratory chain complex I activity by preserving NDUFA10 *via* activation of Sirt1 (Yang et al., 2015), which certainly played a role as well in this case in attenuation of complex I dysfunction observed. On the other hand, the ingredient (s) in QSYQ responsible for protection of NDUFA12 and YME1L1 from decrease after H/R is so far unknown and needs to be identified by further research. Nevertheless, this result demonstrated once again the pleiotropic effects of QSYQ on I/R-caused cardiac vascular hyperpermeability.

In conclusion, this study showed that the cardiac microvascular hyperpermeability after I/R took place by a mechanism implicating multiple signaling, and QSYQ presented as an option to deal with this insult with advantage of targeting at least Src/caveolin-1 and RhoA/ROCK/MLC signaling.

DATA AVAILABILITY STATEMENT

The original contributions presented in the study are included in the article/**Supplementary Material**, further inquiries can be directed to the corresponding author/s.

REFERENCES

- Alluri, H., Grimsley, M., Anasooya Shaji, C., Varghese, K. P., Zhang, S. L., Peddaboina, C., et al. (2016). Attenuation of blood-brain barrier breakdown and hyperpermeability by calpain inhibition. *J. Biol. Chem.* 291, 26958–26969. doi: 10.1074/jbc.M116.735365
- Brown, R., Nath, S., Lora, A., Samaha, G., Elgamal, Z., Kaiser, R., et al. (2020). Cathepsin S: investigating an old player in lung disease pathogenesis, comorbidities, and potential therapeutics. *Respir. Res.* 21:111. doi: 10.1186/s12931-020-01381-5
- Cui, Y. C., Pan, C. S., Yan, L., Li, L., Hu, B. H., Chang, X., et al. (2017). Ginsenoside Rb1 protects against ischemia/reperfusion-induced myocardial injury via energy metabolism regulation mediated by RhoA signaling pathway. *Sci. Rep.* 7:44579. doi: 10.1038/srep44579
- El-Hattab, A. W., Suleiman, J., Almannai, M., and Scaglia, F. (2018). Mitochondrial dynamics: Biological roles, molecular machinery, and related diseases. *Mol. Genet. Metab.* 125, 315–321. doi: 10.1016/j.ymgme.2018.10.003
- Erlinge, D., Gotberg, M., Lang, I., Holzer, M., Noc, M., Clemmensen, P., et al. (2014). Rapid endovascular catheter core cooling combined with cold saline as an adjunct to percutaneous coronary intervention for the treatment of acute myocardial infarction. The CHILL-MI trial: a randomized controlled study of the use of central venous catheter core cooling combined with cold saline as an adjunct to percutaneous coronary intervention for the treatment of acute myocardial infarction. *J. Am. Coll. Cardiol.* 63, 1857–65. doi: 10.1016/j.jacc.2013.12.027
- He, K., Yan, L., Pan, C. S., Liu, Y. Y., Cui, Y. C., Hu, B. H., et al. (2014). ROCK-dependent ATP5D modulation contributes to the protection of notoginsenoside NR1 against ischemia-reperfusion-induced myocardial injury. *Am. J. Physiol. Heart Circ. Physiol.* 307, H1764–76. doi: 10.1152/ajpheart.00259.2014
- Heusch, G. (2004). Postconditioning: old wine in a new bottle? *J. Am. Coll. Cardiol.* 44, 1111–2. doi: 10.1016/j.jacc.2004.06.013
- Heusch, G. and Gersh, B. J. (2017). The pathophysiology of acute myocardial infarction and strategies of protection beyond reperfusion: a continual challenge. *Eur. Heart J.* 38, 774–784. doi: 10.1093/eurheartj/ehw224
- Heusch, G., Libby, P., Gersh, B., Yellon, D., Bohm, M., Lopaschuk, G., et al. (2014). Cardiovascular remodelling in coronary artery disease and heart failure. *Lancet* 383, 1933–1943. doi: 10.1016/S0140-6736(14)60107-0

AUTHOR CONTRIBUTIONS

C-SP performed the *in vitro* experiments, analyzed the data, and wrote the manuscript. Y-YL provided scientific guidance and oversight. LY and S-QL contributed to the animal experiments. KH and Y-CC contributed to confocal imaging. B-HH, XC, and X-RZ participated in the preparation of sample for a transmission electron microscope analysis. J-YF and J-YH revised the article. J-YH supervised the research and provided key research directions. All authors read and agreed with the final article.

FUNDING

This work was supported by the National Natural Science Foundation of China [81273637] for J-YH.

SUPPLEMENTARY MATERIAL

The Supplementary Material for this article can be found online at: <https://www.frontiersin.org/articles/10.3389/fphys.2021.753761/full#supplementary-material>

- Katt, M. E., Linville, R. M., Mayo, L. N., Xu, Z. S., and Searson, P. C. (2018). Functional brain-specific microvessels from iPSC-derived human brain microvascular endothelial cells: the role of matrix composition on monolayer formation. *Fluids Barriers CNS* 15:7. doi: 10.1186/s12987-018-0092-7
- Korayem, A. H., Mujica, P. E., Aramoto, H., Durán, R. G., Nepali, P. R., Kim, D. D., et al. (2017). Endothelial cAMP deactivates ischemia-reperfusion-induced microvascular hyperpermeability via Rap1-mediated mechanisms. *Am. J. Physiol. Heart Circ. Physiol.* 313, H179–H189. doi: 10.1152/ajpheart.00002.2017
- Kottke, M. A., and Walters, T. J. (2016). Where's the leak in vascular barriers? A review. *Shock* 46, 20–36. doi: 10.1097/SHK.0000000000000666
- Li, L., Pan, C. S., Yan, L., Cui, Y. C., Liu, Y. Y., Mu, H. N., et al. (2018). Ginsenoside Rg1 ameliorates rat myocardial ischemia-reperfusion injury by modulating energy metabolism pathways. *Front. Physiol.* 9:78. doi: 10.3389/fphys.2018.00078
- Lin, S. Q., Wei, X. H., Huang, P., Liu, Y. Y., Zhao, N., Li, Q., et al. (2013). QiShenYiQi Pills(R). prevent cardiac ischemia-reperfusion injury via energy modulation. *Int. J. Cardiol.* 168, 967–974. doi: 10.1016/j.ijcard.2012.10.042
- Mehta, D., and Malik, A. B. (2006). Signaling mechanisms regulating endothelial permeability. *Physiol. Rev.* 86, 279–367. doi: 10.1152/physrev.00012.2005
- Montalescot, G., van 't Hof, A. W., Lapostolle, F., Silvain, J., Lassen, J. F., Bolognese, L., et al. (2014). Prehospital ticagrelor in ST-segment elevation myocardial infarction. *N. Engl. J. Med.* 371, 1016–1027. doi: 10.1056/NEJMoa1407024
- Ostergaard, E., Rodenburg, R. J., van den Brand, M., Thomsen, L. L., Duno, M., Batbayli, M., et al. (2011). Respiratory chain complex I deficiency due to NDUFA12 mutations as a new cause of Leigh syndrome. *J. Med. Genet.* 48, 737–740. doi: 10.1136/jmg.2011.088856
- Pan, C. S., Liu, Y. H., Liu, Y. Y., Zhang, Y., He, K., Yang, X. Y., et al. (2015). Salvianolic acid B ameliorates lipopolysaccharide-induced albumin leakage from rat mesenteric venules through Src-regulated transcellular pathway and paracellular pathway. *PLoS ONE* 10:e0126640. doi: 10.1371/journal.pone.0126640
- Pries, A. R., and Kuebler, W. M. (2006). Normal endothelium. *Handb. Exper. Pharmacol.* 176, 1–40. doi: 10.1007/3-540-32967-6_1
- Rak, M., and Rustin, P. (2014). Supernumerary subunits NDUFA3, NDUFA5 and NDUFA12 are required for the formation of the extramembrane arm of human mitochondrial complex I. *FEBS Lett.* 588, 1832–8. doi: 10.1016/j.febslet.2014.03.046

- Selker, H. P., Beshansky, J. R., Sheehan, P. R., Massaro, J. M., Griffith, J. L., D'Agostino, R. B., et al. (2012). Out-of-hospital administration of intravenous glucose-insulin-potassium in patients with suspected acute coronary syndromes: the IMMEDIATE randomized controlled trial. *JAMA* 307, 1925–33. doi: 10.1001/jama.2012.426
- Shen, W. C., Chou, Y. H., Huang, H. P., Sheen, J. F., Hung, S. C., and Chen, H. F. (2018). Induced pluripotent stem cell-derived endothelial progenitor cells attenuate ischemic acute kidney injury and cardiac dysfunction. *Stem Cell Res. Ther.* 9:344. doi: 10.1186/s13287-018-1092-x
- Stiburek, L., Cesnekova, J., Kostkova, O., Fornuskova, D., Vinsova, K., Wenchich, L., et al. (2012). YME1L controls the accumulation of respiratory chain subunits and is required for apoptotic resistance, cristae morphogenesis, and cell proliferation. *Mol. Biol. Cell* 23, 1010–1023. doi: 10.1091/mbc.e11-08-0674
- Tu, L., Pan, C. S., Wei, X. H., Yan, L., Liu, Y. Y., Fan, J. Y., et al. (2013). Astragaloside IV protects heart from ischemia and reperfusion injury via energy regulation mechanisms. *Microcirculation* 20, 736–747. doi: 10.1111/micc.12074
- Wallez, Y., and Huber, P. (2008). Endothelial adherens and tight junctions in vascular homeostasis, inflammation and angiogenesis. *Biochim. Biophys. Acta* 1778, 794–809. doi: 10.1016/j.bbame.2007.09.003
- Weis, S. M. (2008). Vascular permeability in cardiovascular disease and cancer. *Curr. Opin. Hematol.* 15, 243–249. doi: 10.1097/MOH.0b013e3282f97d86
- Yan, L., Pan, C. S., Liu, Y. Y., Cui, Y. C., Hu, B. H., Chang, X., et al. (2021). The composite of 3, 4-dihydroxyl-phenyl lactic acid and notoginsenoside R1 attenuates myocardial ischemia and reperfusion injury through regulating mitochondrial respiratory chain. *Front. Physiol.* 12:538962. doi: 10.3389/fphys.2021.538962
- Yan, L. L., Zhang, W. Y., Wei, X. H., Yan, L., Pan, C. S., Yu, Y., et al. (2018). gualou xiebai decoction, a traditional chinese medicine, prevents cardiac reperfusion injury of hyperlipidemia rat via energy modulation. *Front. Physiol.* 9:296. doi: 10.3389/fphys.2018.00296
- Yang, Q., He, G. W., Underwood, M. J., and Yu, C. M. (2016). Cellular and molecular mechanisms of endothelial ischemia/reperfusion injury: perspectives and implications for postischemic myocardial protection. *Am. J. Transl. Res.* 8, 765–777.
- Yang, X. Y., He, K., Pan, C. S., Li, Q., Liu, Y. Y., Yan, L., et al. (2015). 3, 4-dihydroxyl-phenyl lactic acid restores NADH dehydrogenase 1 α subunit 10 to ameliorate cardiac reperfusion injury. *Sci. Rep.* 5:10739. doi: 10.1038/srep10739
- Yellon, D. M., and Hausenloy, D. J. (2007). Myocardial reperfusion injury. *N. Engl. J. Med.* 357, 1121–1135. doi: 10.1056/NEJMra071667
- Zhang, L., Wang, Y., Yu, L., Liu, L., Qu, H., Gao, X., et al. (2010). QI-SHEN-YI-QI accelerates angiogenesis after myocardial infarction in rats. *Int. J. Cardiol.* 143, 105–109. doi: 10.1016/j.ijcard.2008.11.210
- Zhang, Y., Shi, P., Yao, H., Shao, Q., Fan, X. (2012). Metabolite profiling and pharmacokinetics of herbal compounds following oral administration of a cardiovascular multi-herb medicine (Qishen yiqi pills). in rats. *Curr. Drug Metab.* 13, 510–523. doi: 10.2174/1389200211209050510
- Zhao, J. L., Yang, Y. J., You, S. J., Jing, Z. C., Wu, Y. J., Cheng, J. L., et al. (2006). Pretreatment with fosinopril or valsartan reduces myocardial no-reflow after acute myocardial infarction and reperfusion. *Coron. Artery Dis.* 17, 463–469. doi: 10.1097/00019501-200608000-00010
- Zheng, Y., Dai, Y., Liu, W., Wang, N., Cai, Y., Wang, S., et al. (2019). Astragaloside IV enhances taxol chemosensitivity of breast cancer via caveolin-1-targeting oxidant damage. *J. Cell. Physiol.* 234, 4277–4290. doi: 10.1002/jcp.27196

Conflict of Interest: The authors declare that the research was conducted in the absence of any commercial or financial relationships that could be construed as a potential conflict of interest.

Publisher's Note: All claims expressed in this article are solely those of the authors and do not necessarily represent those of their affiliated organizations, or those of the publisher, the editors and the reviewers. Any product that may be evaluated in this article, or claim that may be made by its manufacturer, is not guaranteed or endorsed by the publisher.

Copyright © 2021 Pan, Yan, Lin, He, Cui, Liu, Hu, Chang, Zhao, Fan and Han. This is an open-access article distributed under the terms of the Creative Commons Attribution License (CC BY). The use, distribution or reproduction in other forums is permitted, provided the original author(s) and the copyright owner(s) are credited and that the original publication in this journal is cited, in accordance with accepted academic practice. No use, distribution or reproduction is permitted which does not comply with these terms.



Prospective Study of Serum Uric Acid Levels and First Stroke Events in Chinese Adults With Hypertension

Feng Hu^{1,2†}, Longlong Hu^{1,2†}, Rihua Yu³, Fengyu Han^{1,2}, Wei Zhou^{2,4}, Tao Wang^{2,4}, Linjuan Zhu^{2,4}, Xiao Huang^{1,2}, Huihui Bao^{1,2,4*} and Xiaoshu Cheng^{1,2,4*}

¹ Department of Cardiovascular Medicine, The Second Affiliated Hospital of Nanchang University, Nanchang, China, ² Jiangxi Provincial Cardiovascular Disease Clinical Medical Research Center, Nanchang, China, ³ Department of General Practice Medicine, Xucun Town Health Center, Wuyuan, China, ⁴ Center for Prevention and Treatment of Cardiovascular Diseases, The Second Affiliated Hospital of Nanchang University, Nanchang, China

OPEN ACCESS

Edited by:

Kangkang Zhi,
Shanghai Changzheng Hospital,
China

Reviewed by:

Sebastjan Bevc,
Maribor University Medical Centre,
Slovenia
Mi Zhang,
Huazhong University of Science
and Technology, China
Denise C. Cornelius,
University of Mississippi Medical
Center, United States

*Correspondence:

Huihui Bao
huihui_bao77@126.com
Xiaoshu Cheng
xiaoshumenfan126@163.com

[†] These authors have contributed
equally to this work

Specialty section:

This article was submitted to
Metabolic Physiology,
a section of the journal
Frontiers in Physiology

Received: 02 November 2021

Accepted: 29 November 2021

Published: 23 December 2021

Citation:

Hu F, Hu L, Yu R, Han F, Zhou W,
Wang T, Zhu L, Huang X, Bao H and
Cheng X (2021) Prospective Study of
Serum Uric Acid Levels and First
Stroke Events in Chinese Adults With
Hypertension.
Front. Physiol. 12:807420.
doi: 10.3389/fphys.2021.807420

Objectives: We investigated the association between serum uric acid (SUA) levels and the risk of the first stroke in Chinese adults with hypertension.

Methods: A total of 11, 841 hypertensive patients were selected from the Chinese Hypertension Registry for analysis. The relationship between SUA levels and first stroke was determined using multivariable Cox proportional hazards regression, smoothing curve fitting, and Kaplan–Meier survival curve analysis.

Results: During a median follow-up of 614 days, 99 cases of the first stroke were occurred. Cox proportional hazards models indicated that SUA levels were not significantly associated with the first stroke event [adjusted-hazard ratio (HR) per SD increase: 0.98, 95% CI 0.76–1.26, $P = 0.889$]. In comparison to the group without hyperuricemia (HUA), there were no significantly higher risks of first stroke events (adjusted-HR: 1.22, 95% CI 0.79–1.90, $P = 0.373$) in the population with HUA. However, in the population less than 60 years old, subjects with HUA had a significantly higher risk of the first stroke than the population without HUA (adjusted-HR: 4.89, 95% CI 1.36–17.63, $P = 0.015$). In subjects older than 60 years, we did not find a significant relationship between HUA and first stroke (adjusted-HR: 0.97, 95% CI 0.60–1.56, $P = 0.886$). Survival analysis further confirmed this discrepancy (log-rank $P = 0.013$ or 0.899 for non-aging or aging group).

Conclusion: No significant evidence in the present study indicated that increased SUA levels were associated with the risk of first stroke in the Chinese adults with hypertension. Age played an interactive role in the relationship between HUA and the first stroke event.

Keywords: serum uric acid, first stroke, Chinese adults, hypertension, aging

INTRODUCTION

Serum uric acid (SUA) is a final enzymatic product of purine metabolism, and several gradual changes have led to the higher SUA levels in humans than in other mammals. This may hint at an evolutionary advantage owing to its antioxidant properties by acting as a scavenger of hydroxyl radicals and chelation of transition metals (Sautin and Johnson, 2008; Sinha et al., 2009). During

the past three decades, the role of hyperuricemia (HUA) on stroke incidence across populations has been controversial (Maloberti et al., 2020). Most prospective studies have assessed the association of HUA with stroke incidence in the general population (Chien et al., 2005; Bos et al., 2006; Gerber et al., 2006; Hozawa et al., 2006; Tu et al., 2019; Li J. et al., 2020), patients with hypertension (Shi et al., 2017; Zhang et al., 2020), atrial fibrillation (Chao et al., 2014), and non-insulin-dependent diabetes mellitus (DM) (Lehto et al., 1998). Most reported a positive association between HUA and stroke risk (Lehto et al., 1998; Chien et al., 2005; Bos et al., 2006; Chao et al., 2014; Tu et al., 2019; Li J. et al., 2020; Zhang et al., 2020), some reported an insignificant relationship (Gerber et al., 2006; Hozawa et al., 2006; Shi et al., 2017). Two meta-analytical reviews of prospective observational studies suggest that HUA may modestly increase the risks of both stroke incidence and mortality (Kim et al., 2009; Li et al., 2014).

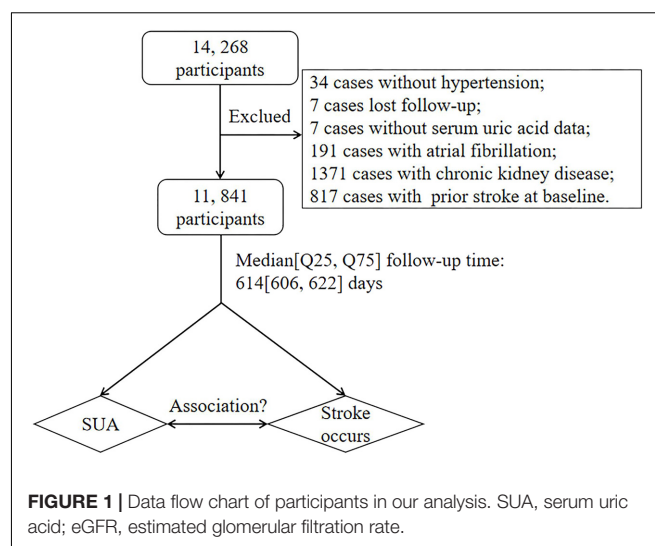
Furthermore, some previous studies indicated that the influence of SUA on stroke was due to the secondary association of SUA with other established etiological risk factors, such as hypertension, arterial stiffness, obesity, and hyperinsulinemia (Lehto et al., 1998; Hozawa et al., 2006; Ishizaka et al., 2007; Liang et al., 2009; Shi et al., 2017; Chaudhary et al., 2020). Multiple lines of evidence from epidemiological (Perlstein et al., 2006; Gaffo et al., 2013), animal (Kang et al., 2005; Corry et al., 2008) studies, and clinical trials (Feig et al., 2008) suggested that SUA might increase blood pressure (BP). Some studies indicated that hypertension might mediate the effect of HUA on stroke (Hozawa et al., 2006; Shi et al., 2017; Chaudhary et al., 2020).

China bears a huge burden of hypertension and stroke (Wang et al., 2018). Accumulating evidence suggests that hypertension plays a definitive role in the development of atherosclerosis and is the primary cause of stroke (Buonacera et al., 2019). Considering the controversial role of HUA as an independent risk factor for stroke events in the Chinese hypertensive patients (Chien et al., 2005; Bos et al., 2006; Shi et al., 2017; Zhang et al., 2020), we investigated the relationship between HUA and the risk of first stroke incidence in the Chinese adults with hypertension.

MATERIALS AND METHODS

Study Design and Participants

Data analyzed in this study were the baseline of the ongoing China H-type Hypertension Registry Study (registration number: ChiCTR1800017274). The data collection approaches and the established standards of inclusion or exclusion have been described previously (Li M. et al., 2020). Briefly, the study is a real-world, multicenter, observational study, conducted in March 2018 at Wuyuan, Jiangxi province of China. The enrolled population was hypertensive patients aged 18 years and older. The exclusion criteria included psychological or nervous system impairment resulting in an inability to demonstrate informed consent, unable to be a long-term follow-up according to the study protocol or plans to relocate in the near future. The study was conducted in accordance with the Declaration of Helsinki, and the protocol was approved by the Ethics Committee of



the Institute of Biomedicine, Anhui Medical University (no. CH1059). All participants provided written informed consent.

In total, 14,268 participants completed the baseline investigation between March 2018 and August 2018. We followed these participants between August 31, 2018 and March 31, 2020. The median follow-up duration was 614 (606, 622) days. After excluding 34 individuals without hypertension at baseline, 7 cases were lost to follow-up, 7 cases were without SUA data, 191 cases were with atrial fibrillation, 1,371 cases were with estimated glomerular filtration rate (eGFR) ≤ 60 ml/min/1.73 m², and 817 cases were with prior stroke at baseline, finally 11,841 participants were included in our analysis (Figure 1).

Clinical Data Collection at Baseline

Demographic characteristics (age and sex), lifestyle factors (smoking and drinking status), medical history [hypertension, DM, dyslipidemia, atrial fibrillation, cerebral stroke (ischemic stroke, intracerebral hemorrhage, or unspecified stroke), coronary heart disease (CHD) and chronic kidney disease (CKD)], and medication usage were gathered by professional researchers through questionnaire survey. A person who smoked at least one cigarette a day was classified as a smoker. A person who drank > 20 g of ethanol a day was considered a drinker. Atrial fibrillation was diagnosed based on a medical history and through resting supine standard 12-lead surface ECG.

Anthropometric measurements for each patient, such as weight, height, waistline, hipline, systolic blood pressure (SBP), diastolic blood pressure (DBP), and heart rate (HR), were obtained by researchers. Due to the health-screening protocols, single-point measurements of anthropometric indicators were obtained. Waistline and hipline were measured using an inelastic measuring tape with 0.1 cm resolution. BP was measured, with the participant in a sitting position using the Omron HBP-1,300 Professional Portable Blood Pressure Monitor (Kyoto, Japan) on the right arm, which was supported at the heart level. After a 5-min rest period, BP was measured four times, and SBP and DBP were calculated as the average of the last three readings. Body

TABLE 1 | Baseline characteristics of the study population.

Characteristics	Total subjects	Quartiles of serum uric acid levels (μ /L)				P-value
		Q1 [38.00, 325.80]	Q2 [326.00, 393.30]	Q3 [394.00, 472.00]	Q4 [473.00, 1056.00]	
Number of subjects (n)	11,841	2,960	2,936	2,967	2,978	
Age (years)	62.95 \pm 9.14	62.74 \pm 8.74	63.67 \pm 8.85	63.22 \pm 9.18	62.19 \pm 9.71	<0.001
Male, n (%)	5,408 (45.67%)	572 (19.32%)	1,109 (37.77%)	1,629 (54.90%)	2,098 (70.45%)	<0.001
SBP (mmHg)	148.52 \pm 17.37	150.44 \pm 16.91	149.37 \pm 17.31	148.12 \pm 17.55	146.18 \pm 17.41	<0.001
DBP (mmHg)	89.45 \pm 10.51	88.90 \pm 10.22	88.75 \pm 10.21	89.65 \pm 10.67	90.48 \pm 10.84	<0.001
MAP (mmHg)	109.14 \pm 11.07	109.42 \pm 10.84	108.96 \pm 10.90	109.14 \pm 11.27	109.05 \pm 11.25	0.440
HR (times/min)	76.56 \pm 13.84	77.57 \pm 14.48	76.41 \pm 13.41	75.97 \pm 13.24	76.28 \pm 14.15	<0.001
BMI (kg/m^2)	23.71 \pm 3.54	23.00 \pm 3.46	23.43 \pm 3.52	23.87 \pm 3.60	24.51 \pm 3.54	<0.001
BMI group (kg/m^2)						<0.001
Control (<24)	6,521 (55.10%)	1,906 (64.41%)	1,731 (59.04%)	1,547 (52.16%)	1,337 (44.90%)	
Overweight (≥ 24 , <28)	4,041 (34.14%)	850 (28.73%)	935 (31.89%)	1,069 (36.04%)	1,187 (39.86%)	
General obesity (≥ 28)	1,273 (10.76%)	203 (6.86%)	266 (9.07%)	350 (11.80%)	454 (15.25%)	
WHR	0.91 \pm 0.17	0.90 \pm 0.07	0.91 \pm 0.31	0.92 \pm 0.07	0.93 \pm 0.07	<0.001
Central obesity, n (%)	8,422 (71.13%)	2,065 (69.76%)	2,045 (69.65%)	2,082 (70.17%)	2,230 (74.88%)	<0.001
Smoking status, n (%)						
Never	7,035 (59.42%)	2,299 (77.67%)	1,891 (64.45%)	1,537 (51.80%)	1,308 (43.92%)	<0.001
Former	1,754 (14.82%)	222 (7.50%)	369 (12.58%)	517 (17.43%)	646 (21.69%)	
Current	3,050 (25.76%)	439 (14.83%)	674 (22.97%)	913 (30.77%)	1,024 (34.39%)	
Drinking status, n (%)						
Never	7,611 (64.29%)	2,298 (77.64%)	2,026 (69.05%)	1,761 (59.35%)	1,526 (51.24%)	<0.001
Former	1,481 (12.51%)	343 (11.59%)	356 (12.13%)	400 (13.48%)	382 (12.83%)	
Current	2,747 (23.20%)	319 (10.78%)	552 (18.81%)	806 (27.17%)	1,070 (35.93%)	
Hcy ($\mu\text{mol}/\text{L}$)	14.47 (12.25–17.95)	13.11 (11.41–16.00)	14.01 (11.99–16.95)	14.86 (12.58–18.34)	16.02 (13.42–20.30)	<0.001
FBG (mmol/L)	6.17 \pm 1.61	6.13 \pm 1.75	6.18 \pm 1.76	6.15 \pm 1.46	6.23 \pm 1.43	0.132
TC (mmol/L)	5.19 \pm 1.09	5.10 \pm 1.03	5.17 \pm 1.08	5.19 \pm 1.11	5.29 \pm 1.13	<0.001
TG (mmol/L)	1.47 (1.04–2.17)	1.32 (0.98–1.85)	1.42 (1.00–2.04)	1.52 (1.06–2.22)	1.74 (1.17–2.62)	<0.001
HDL-C (mmol/L)	1.58 \pm 0.43	1.64 \pm 0.43	1.60 \pm 0.42	1.55 \pm 0.42	1.53 \pm 0.43	<0.001
LDL-C (mmol/L)	3.00 \pm 0.80	2.93 \pm 0.75	2.99 \pm 0.81	3.02 \pm 0.81	3.09 \pm 0.82	<0.001
SUA ($\mu\text{mol}/\text{L}$)	406.26 \pm 113.31	275.18 \pm 39.35	359.72 \pm 19.25	430.54 \pm 22.70	558.23 \pm 75.72	<0.001
HUA, n (%)	6,184 (52.23%)	0 (0.00%)	820 (27.93%)	2,386 (80.42%)	2,978 (100.00%)	<0.001
BUN (mmol/L)	5.23 \pm 1.45	5.02 \pm 1.41	5.20 \pm 1.41	5.28 \pm 1.44	5.43 \pm 1.50	<0.001
Serum creatinine (mmol/L)	64.38 \pm 16.94	52.97 \pm 13.61	60.86 \pm 14.16	67.46 \pm 14.91	76.12 \pm 15.78	<0.001
eGFR ($\text{ml}/\text{min}/1.73\text{ m}^2$)	93.21 \pm 14.36	99.76 \pm 13.11	94.71 \pm 13.00	91.57 \pm 13.71	86.84 \pm 14.40	<0.001
Human serum albumin (g/L)	46.82 \pm 4.00	46.53 \pm 4.08	46.76 \pm 3.99	46.85 \pm 3.94	47.14 \pm 3.98	<0.001
Total bilirubin (mmol/L)	13.40 (10.40–17.50)	12.60 (9.88–16.20)	13.20 (10.20–17.40)	13.70 (10.60–17.80)	14.20 (10.90–18.60)	<0.001
Direct bilirubin (mmol/L)	5.20 (4.10–6.50)	4.90 (4.00–6.20)	5.10 (4.10–6.50)	5.20 (4.20–6.50)	5.40 (4.30–6.90)	<0.001
AST (U/L)	24.00 (20.00–30.00)	22.50 (19.00–27.00)	24.00 (20.00–29.00)	25.00 (21.00–31.00)	26.00 (22.00–33.00)	<0.001
ALT (U/L)	17.00 (13.00–24.00)	14.00 (11.00–20.00)	16.00 (12.00–23.00)	18.00 (13.00–25.00)	20.00 (14.00–28.00)	<0.001
CHD, n (%)	538 (4.54%)	113 (3.82%)	122 (4.16%)	151 (5.09%)	152 (5.10%)	0.032
DM, n (%)	2,064 (17.43%)	462 (15.61%)	485 (16.52%)	544 (18.34%)	573 (19.24%)	<0.001
Dyslipidemia, n (%)	4,402 (37.18%)	877 (29.63%)	1,001 (34.09%)	1,139 (38.39%)	1,385 (46.51%)	<0.001
Antihypertensive agents, n (%)	7,366 (62.22%)	1,760 (59.46%)	1,823 (62.13%)	1,871 (63.06%)	1,912 (64.20%)	0.001
Hypoglycemic agents, n (%)	554 (4.68%)	150 (5.07%)	149 (5.07%)	129 (4.35%)	126 (4.23%)	0.250
Lipid-lowering agents, n (%)	285 (2.41%)	81 (2.74%)	63 (2.15%)	74 (2.49%)	67 (2.25%)	0.452
Antiplatelet agents, n (%)	265 (2.24%)	57 (1.93%)	63 (2.15%)	79 (2.66%)	66 (2.22%)	0.274

SBP, systolic blood pressure; DBP, diastolic blood pressure; MAP, mean arterial pressure; HR, heart rate; BMI, body mass index; WHR, waist hip rate; Hcy, homocysteine; FBG, fasting blood glucose; TC, total cholesterol; TG, total triglyceride; HDL-C, high-density lipoprotein cholesterol; LDL-C, low-density lipoprotein cholesterol; SUA, serum uric acid; HUA, hyperuricemia; BUN, blood urea nitrogen; eGFR, estimated glomerular filtration rate; AST, aspartate aminotransferase; ALT, alanine aminotransferase; CHD, coronary heart disease; DM, diabetes mellitus.

mass index (BMI) was calculated as the body weight in kilograms divided by the square of the height in meters (kg/m^2). Waist hip rate (WHR) was calculated as the waistline in centimeters

divided by the hipline in centimeters. In our study, subjects were divided into three categories according to BMI levels (<24 kg/m^2 , control group; 24–28 kg/m^2 , overweight; and ≥ 28 kg/m^2 ,

TABLE 2 | Occurrence of follow-up events of the study population.

Characteristics	Total subjects	Quartiles of serum uric acid levels (μ mol/L)				P-value
		Q1 [38.00, 325.80]	Q2 [326.00, 393.30]	Q3 [394.00, 472.00]	Q4 [473.00, 1056.00]	
Incident stroke, n (%)	99 (0.84%)	22 (0.74%)	23 (0.78%)	29 (0.98%)	25 (0.84%)	0.772
Stroke subtypes, n (%)						0.859
Ischemic stroke	51 (0.43%)	10 (0.34%)	14 (0.48%)	12 (0.40%)	15 (0.50%)	
Hemorrhagic stroke	15 (0.13%)	3 (0.10%)	3 (0.10%)	6 (0.20%)	3 (0.10%)	
Unspecified stroke	33 (0.28%)	9 (0.30%)	6 (0.20%)	11 (0.37%)	7 (0.24%)	
Causes of death, n (%)						0.310
Stroke	34 (0.29%)	9 (0.30%)	8 (0.27%)	10 (0.34%)	7 (0.24%)	
Heart disease	29 (0.24%)	5 (0.17%)	2 (0.07%)	12 (0.40%)	10 (0.34%)	
Cancer	40 (0.34%)	13 (0.44%)	9 (0.31%)	9 (0.30%)	9 (0.30%)	
Respiratory diseases	4 (0.03%)	0 (0.00%)	1 (0.03%)	1 (0.03%)	2 (0.07%)	
Others	17 (0.14%)	2 (0.07%)	2 (0.07%)	6 (0.20%)	7 (0.24%)	

general obesity) (Liu et al., 2019). Central obesity was defined as WHR ≥ 0.9 for males and ≥ 0.85 for women (Liu et al., 2019).

Laboratory Assay

Blood samples were collected utilizing venipuncture after an overnight fast of at least 12 h. The levels of plasma total homocysteine (Hcy), fasting blood glucose (FBG), total cholesterol (TC), total triglyceride (TG), high-density lipoprotein cholesterol (HDL-C), low-density lipoprotein cholesterol (LDL-C), SUA, blood urea nitrogen (BUN), and serum creatinine, total and direct bilirubin, aspartate aminotransferase (AST), and alanine aminotransferase (ALT) were measured using automatic clinical analyzers (Beckman Coulter, Brea, CA, United States). In our analysis, diagnosis of DM was defined as fasting glucose > 7.0 mmol/l and/or self-reported diabetes (Jia et al., 2019). Dyslipidemia was defined as having one or more of the following features: elevated TG (≥ 2.3 mmol/L), elevated TC (≥ 6.2 mmol/L), elevated LDL-C (≥ 4.1 mmol/L), reduced HDL-C (< 1.0 mmol/L), or on appropriate lipid-lowering medication (Joint Committee for Developing Chinese guidelines on Prevention and Treatment of Dyslipidemia in Adults, 2007). HUA was defined as an SUA > 420 μ mol/L in men and > 360 μ mol/L in women among the Chinese population (Tu et al., 2019; Chen et al., 2020). The eGFR was calculated by the equation of CKD Epidemiology Collaboration (CKD-EPI) (Levey et al., 2009).

Primary Outcome and Definitions

CT or MRI was conducted to confirm first stroke events, which was defined as a sudden or rapid onset of a focal neurological deficit lasting more than 24 h or until death. According to the International Classification of Diseases, 10th edition (ICD-10), strokes were coded as I61 (hemorrhagic stroke), I63 (ischemic stroke), or I64 (unspecified stroke), and the patients were blinded to the baseline information collected by trained staff. If the patients experienced an in-hospital stroke event, facility and physician records were referred to for stroke diagnosis. In the event that a stroke occurred outside a hospital, the medical records of the patient, along with the accounts provided by

the family members, were used, allowing the experts to reach a consensus regarding the diagnosis of a stroke following a comprehensive consideration, such as the history, recent condition, and symptoms before and after the event. Causes of death included stroke, heart disease, cancer, and respiratory diseases. All the death mortalities were ascertained from the Local Healthcare Security Administration, Centers for Disease Control and Prevention, and hospitals.

Statistical Analysis

Continuous variables are presented as the means \pm SD or the median (quartiles), as appropriate, and are compared using the Student's *t*-test, one-way analysis, or the Mann-Whitney *U*-test, depending on whether the quantitative data were consistent with a normal distribution. Categorical variables were presented as count (percentage), differences between groups were measured by chi-square test.

Secondly, to address the linearity or not between continuous SUA levels and the risk of the first stroke, a Cox proportional hazards ratio (HR) model with cubic spline functions and smooth curve fitting (restricted cubic spline method) was performed (**Supplementary Figure 1**). We used three different Cox proportional hazards models to examine the association between SUA levels and the risk of first stroke. The crude model was not adjusted for any confounder. The model I was adjusted for age, sex, SBP, DBP, and HR. The model II was a confounder model. The confounder model screened covariates, such as age, sex, SBP, DBP, HR, BMI, WHR, smoking and drinking status, homocysteine, TC, TG, HDL-C, LDL-C, AST, ALT, eGFR, total and direct bilirubin, DM, antihypertensive agents, lipid-lowering agents, and antiplatelet agents except for the independent variable itself. We selected these confounders on the basis of their associations with the outcomes of interest or a change in effect estimate of more than 10% when added to this model. **Supplementary Table 1** shows the association of each confounder with stroke occurs. Linear trend tests were realized by entering a median value of each category of SUA levels as a continuous variable.

TABLE 3 | Hazard ratios of serum uric acid level categories for first stroke events.

Variables	Event, n (%)	Crude model		Model I		Model II	
		HR (95%CI)	P-value	HR (95%CI)	P-value	HR (95%CI)	P-value
Total stroke							
Per SD $\mu\text{mol/L}$ increase	99 (0.84%)	1.10 (0.91, 1.34)	0.308	1.05 (0.84, 1.30)	0.669	0.98 (0.76, 1.26)	0.889 ^a
HUA							
No	40 (0.71%)	Ref		Ref		Ref	
Yes	59 (0.95%)	1.35 (0.90, 2.02)	0.142	1.31 (0.87, 1.97)	0.195	1.22 (0.79, 1.90)	0.373 ^b
Quartiles of SUA							
Q1 [38.00, 325.80]	22 (0.74%)	Ref		Ref		Ref	
Q2 [326.00, 393.30]	23 (0.78%)	1.05 (0.59, 1.90)	0.860	0.93 (0.51, 1.69)	0.815	0.85 (0.46, 1.56)	0.602 ^c
Q3 [394.00, 472.00]	29 (0.98%)	1.32 (0.76, 2.30)	0.331	1.08 (0.60, 1.94)	0.786	0.92 (0.50, 1.70)	0.786 ^c
Q4 [473.00, 1056.00]	25 (0.84%)	1.13 (0.64, 2.01)	0.676	0.93 (0.50, 1.72)	0.815	0.72 (0.36, 1.44)	0.354 ^c
P for trend		0.576		0.896		0.391	
Ischemic stroke							
Per SD $\mu\text{mol/L}$ increase	51 (0.43%)	1.18 (0.91, 1.52)	0.225	1.18 (0.88, 1.58)	0.265	0.97 (0.69, 1.37)	0.871 ^d
HUA							
No	18 (0.32%)	Ref		Ref		Ref	
Yes	33 (0.53%)	1.68 (0.95, 2.99)	0.077	1.67 (0.94, 2.98)	0.083	1.28 (0.69, 2.39)	0.440 ^e
Quartiles of SUA							
Q1 [38.00, 325.80]	10 (0.34%)	Ref		Ref		Ref	
Q2 [326.00, 393.30]	14 (0.48%)	1.41 (0.63, 3.19)	0.404	1.28 (0.56, 2.90)	0.563	1.01 (0.44, 2.34)	0.975 ^f
Q3 [394.00, 472.00]	12 (0.40%)	1.20 (0.52, 2.78)	0.674	1.06 (0.44, 2.53)	0.894	0.73 (0.29, 1.80)	0.493 ^f
Q4 [473.00, 1056.00]	15 (0.50%)	1.49 (0.67, 3.33)	0.327	1.39 (0.59, 3.26)	0.454	0.77 (0.30, 1.99)	0.585 ^f
P for trend		0.417		0.535		0.498	
Hemorrhagic stroke							
Per SD $\mu\text{mol/L}$ increase	15 (0.13%)	0.99 (0.59, 1.64)	0.962	0.68 (0.38, 1.22)	0.197	0.73 (0.36, 1.48)	0.387 ^g
HUA							
No	6 (0.11%)	Ref		Ref		Ref	
Yes	9 (0.15%)	1.37 (0.49, 3.86)	0.548	1.06 (0.37, 3.06)	0.911	1.48 (0.45, 4.85)	0.516 ^h
Quartiles of SUA							
Q1 [38.00, 325.80]	3 (0.10%)	Ref		Ref		Ref	
Q2 [326.00, 393.30]	3 (0.10%)	1.01 (0.20, 5.00)	0.992	0.75 (0.14, 3.92)	0.735	0.79 (0.14, 4.49)	0.788 ⁱ
Q3 [394.00, 472.00]	6 (0.20%)	2.00 (0.50, 7.99)	0.328	1.09 (0.24, 4.93)	0.911	1.26 (0.25, 6.38)	0.782 ⁱ
Q4 [473.00, 1056.00]	3 (0.10%)	0.99 (0.20, 4.93)	0.994	0.40 (0.07, 2.33)	0.310	0.53 (0.08, 3.73)	0.527 ⁱ
P for trend		0.962		0.197		0.397	

HUA, hyperuricemia; Ref, reference; HR, hazard ratio; CI, confidence interval; SD, standard deviation.

Model I adjusted for age, sex, SBP, DBP, and HR.

Model II: ^aAdjusted for age, sex, SBP, DBP, HR, BMI, WHR, smoking and drinking status, Hcy, TG, HDL-C, LDL-C, eGFR, total bilirubin, AST, ALT, DM, and antiplatelet agents.

^bAdjusted for age, sex, SBP, DBP, HR, BMI, WHR, smoking and drinking status, Hcy, TG, eGFR, ALT, and antiplatelet agents. ^cAdjusted for age, sex, SBP, DBP, HR, BMI, WHR, smoking and drinking status, Hcy, TG, HDL-C, LDL-C, eGFR, total bilirubin, AST, ALT, and antiplatelet agents. ^dAdjusted for age, sex, SBP, DBP, BMI, WHR, smoking and drinking status, Hcy, TG, LDL-C, eGFR, AST, ALT, DM, antihypertensive agents, and lipid-lowering agents. ^eAdjusted for age, sex, SBP, BMI, drinking status, Hcy, TG, LDL-C, eGFR, and ALT. ^fAdjusted for age, sex, SBP, BMI, smoking and drinking status, Hcy, TG, HDL-C, LDL-C, eGFR, AST, ALT, DM, antihypertensive agents, and lipid-lowering agents. ^gAdjusted for age, sex, SBP, DBP, HR, BMI, WHR, smoking and drinking status, Hcy, TG, HDL-C, LDL-C, eGFR, total bilirubin, AST, ALT, DM, antihypertensive agents, and antiplatelet agents. ^hAdjusted for age, sex, SBP, DBP, HR, WHR, smoking and drinking status, Hcy, TG, HDL-C, LDL-C, eGFR, AST, and antiplatelet agents. ⁱAdjusted for age, sex, SBP, DBP, HR, BMI, WHR, smoking and drinking status, Hcy, TG, HDL-C, LDL-C, eGFR, total bilirubin, AST, ALT, DM, antihypertensive agents, lipid-lowering agents, and antiplatelet agents.

Furthermore, the effects of HUA on first stroke events were evaluated with the use of Kaplan-Meier curves (log-rank test). Finally, subgroup analysis was executed by stratified and interaction test to investigate the robustness between SUA levels and the risk of the first stroke. In consideration of that, there was a threshold effect of age on SUA levels, the generalized additive model and smooth curve fitting (penalized spline method) were used to visually show the relationship between age and SUA levels. If non-linearity was detected, we first use a recursive

algorithm to calculate the inflection points and then construct a two-segment binary logistic regression model on both sides of the inflection points.

All statistical analyses were performed using the statistical package R (The R Foundation, version 3.4.3)¹ and the Empower² (R; X&Y Solutions, Inc., Boston, MA, United States).

¹<http://www.R-project.org>

²www.empowerstats.com

All *P*-values are two-tailed, and $P < 0.05$ was considered statistically significant.

RESULTS

Patient Characteristics at Baseline

The present study included 11,841 Chinese adult hypertensive individuals (age: 62.95 ± 9.14 years, range 27–93 years; men, 45.67%), and the prevalence of HUA was 52.23%. The clinical characteristics of the study participants grouped by SUA quartiles are presented in **Table 1**. Compared with patients with SUA concentrations $\leq 325.80 \mu\text{mol/L}$, there was a higher proportion of men, overweight, general obesity, central obesity, smoking and drinking habits, CHD, DM, dyslipidemia and antihypertensive agent usage, elevated values of DBP, BMI, WHR, Hcy, TC, TG, LDL-C, BUN, serum creatinine, AST, ALT, total and direct bilirubin, and lower values of SBP, HDL-C, and eGFR in patients of the third and highest SUA quartiles (all *P*-values < 0.05 , **Table 1**). The clinical characteristics of participants grouped by age or sex are also assessed in **Supplementary Table 2**. Subjects aged less than 60 years had a higher prevalence of overweight and general obesity, central obesity, HUA, DM, and dyslipidemia, a lower prevalence of smoking habits, CHD, antihypertensive and antiplatelet agent usage, and a lower level of eGFR than the aging group (all *P*-values < 0.05 , **Supplementary Table 2**).

Cumulative Incidence of Incident Stroke

Of the study population, a total of 99 (0.84%) first stroke events (51 ischemic events, 15 hemorrhagic events, and 33 unspecified stroke events) occurred during a median 614-day follow-up period (**Table 2**). The average time was 612.14 ± 32.12 days from the baseline to the first stroke. There were no significant differences in stroke events groups by SUA quartiles ($P > 0.05$; **Table 2**). There was no difference in the causes of death between the groups (**Table 2**).

Association Between Serum Uric Acid Levels and First Stroke Events

There were no significant differences in the SUA levels and proportion of HUA between non-stroke patients and patients with first stroke ($P > 0.05$; **Supplementary Table 3**). Cox proportional hazards models indicated that SUA levels were not associated with the risk of first stroke events (adjusted-HR per SD increase: 0.98, 95% CI 0.76–1.26, $P = 0.889$, **Table 3**), ischemic stroke events (adjusted-HR per SD increase: 0.97, 95% CI 0.69–1.37, $P = 0.871$) or hemorrhagic stroke events (adjusted-HR per SD increase: 0.73, 95% CI 0.36–1.48, $P = 0.387$). In comparison to the group without HUA, there was also no significantly higher risk of total first stroke events (adjusted-HR: 1.22, 95% CI 0.79–1.90, $P = 0.373$, **Table 3**), ischemic stroke events (adjusted-HR: 1.28, 95% CI 0.69–2.39, $P = 0.440$), or hemorrhagic stroke events (adjusted-HR: 1.48, 95% CI 0.45–4.85, $P = 0.516$) in the population with HUA. Furthermore, compared with patients with SUA concentrations $\leq 325.80 \mu\text{mol/L}$, there

was no significantly higher risk of total first stroke events for patients in the third and highest SUA quartiles (adjusted-HR: 0.92, 95% CI 0.50–1.70, $P = 0.786$; adjusted-HR: 0.72, 95% CI 0.36–1.44, $P = 0.354$, respectively; P for trend = 0.391, **Table 3**), ischemic stroke events (adjusted-HR: 0.73, 95% CI 0.29–1.80, $P = 0.493$; adjusted-HR: 0.77, 95% CI 0.30–1.99, $P = 0.585$, respectively; P for trend = 0.498) or hemorrhagic stroke events (adjusted-HR: 1.26, 95% CI 0.25–6.38, $P = 0.782$; adjusted-HR: 0.53, 95% CI 0.08–3.73, $P = 0.527$, respectively; P for trend = 0.397).

Restricted cubic spline indicated that SUA levels were not associated with the risk of first stroke events (*P*-value of log-likelihood ratio test = 0.138, **Supplementary Figure 1**). Survival analysis further confirmed this irrelevant association of HUA with first stroke events (Kaplan–Meier, log-rank $P = 0.369$; **Figure 2A**).

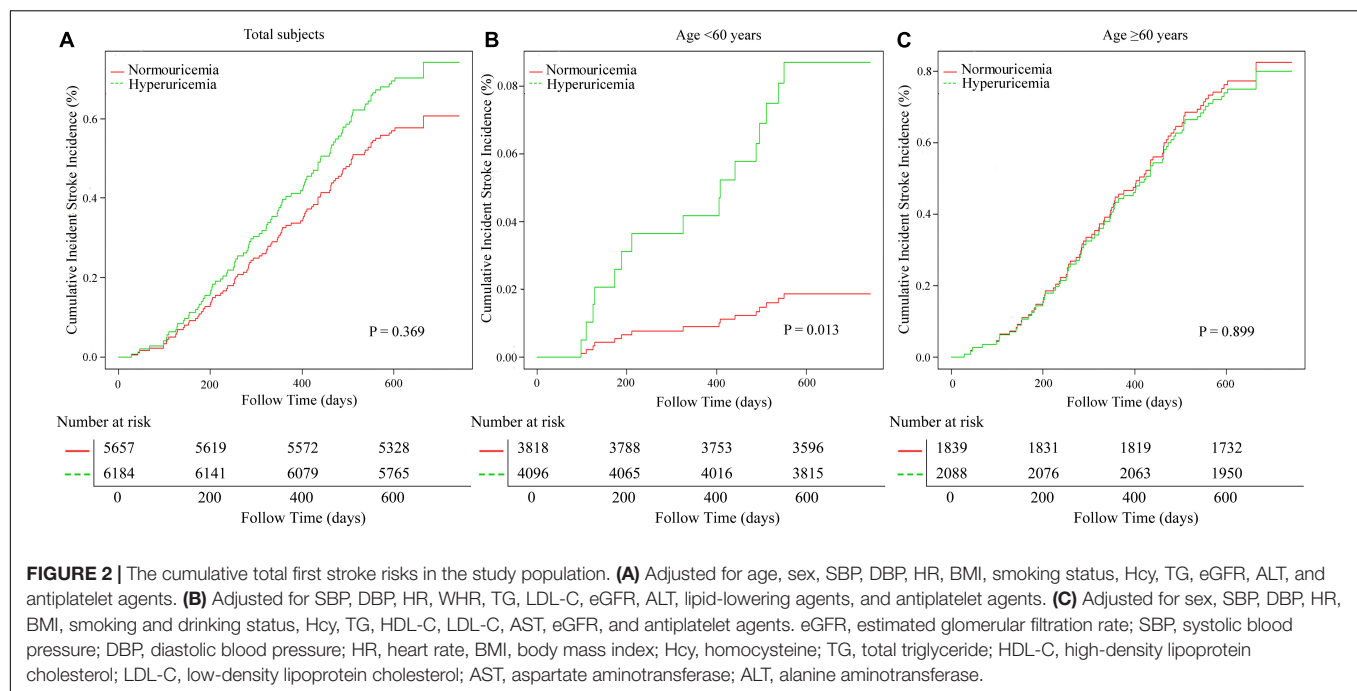
Subgroup Analyses by Potential Effect Modifiers

To explore whether this irrelevant association between SUA levels and first stroke events was still stable in different subgroups, we conducted stratified and interaction analyses.

We used the generalized additive model and penalized spline method to assess that whether there was a non-linear relationship between age and SUA levels (**Supplementary Figure 4**). In the adjusted smoothing curve, the relationship between age and SUA levels was not linear. With the increase of age, the SUA levels decreased first and then leveled off. Visual inspection shows that the inflection point is around 57 years old. We further fitted the association between age and SUA levels using the two-piecewise binary logistic regression model. The inflection point of age was 57 (**Supplementary Table 4**). Effect size [β (95% CI)] of age on SUA levels was -2.97 (-3.59 , -2.35) on the left side and -1.67 (-1.99 , -1.35) on the right of the inflection point. These results suggested that there was a threshold effect of age on SUA levels.

In consequence, we chose the age of 60 for stratification and sub-analysis. We found that this association between SUA levels and first stroke events was modified by aging (**Table 4**). In a group with ages of less than 60 years, subjects with HUA had a significantly higher risk of first stroke events compared to the population without HUA (adjusted-HR: 4.89, 95% CI 1.36–17.63, $P = 0.015$). However, this positive association was disappeared in aging population (adjusted-HR: 0.97, 95% CI 0.60–1.56, $P = 0.886$; *P*-value for interaction = 0.043). Survival analysis further confirmed this discrepancy (Kaplan–Meier, log-rank $P = 0.013$ for the non-aging group, $P = 0.899$ for aging group, respectively; **Figures 2B,C**).

However, subgroup analyses showed that there were not significant interactions in any of the subgroups, such as sex (men vs. women, **Table 5** and **Supplementary Figure 2**), mean arterial pressure tertiles (**Table 6** and **Supplementary Figure 3**), SBP tertiles (**Supplementary Table 5**), DBP tertiles (**Supplementary Table 6**), antihypertensive drugs usage (**Table 7**), body mass index tertiles (**Supplementary Table 7**), and central obesity (**Supplementary Table 8**).



DISCUSSION

We found that increased SUA levels were not significantly associated with the first stroke event in Chinese adults with hypertension. However, age played an interactive role in the relationship between HUA and the first stroke event. In the population, less than 60 years old subjects with HUA had a significantly higher risk of the first stroke than the population without HUA. In subjects older than 60 years, we did not find a significant relationship between HUA and first stroke.

Uric acid is an end enzymatic product of purine metabolism in humans, which can scavenge hydroxyl radicals or hydrogen peroxide and prevent lipid peroxidation (Becker, 1993; Sautin and Johnson, 2008; Sinha et al., 2009). The adaptive advantages of uric acid elevation as a result of a mutation in the uricase gene are at least partially attributable to uric acid antioxidant properties. It has been also suggested that the loss of the uricase gene and subsequent uric acid elevation may have occurred to compensate for reduced plasma antioxidant activity after the loss of ascorbate synthesis (Ames et al., 1981). Higher SUA levels have been related to better reaction ability to control BP at lower salt intake (Watanabe et al., 2002). Demonstration of lower uric acid levels in several neurodegenerative diseases, such as multiple sclerosis, Parkinson's disease, and Alzheimer's disease, has fueled the hypothesis that uric acid may be neuroprotective (Toncev et al., 2002; Irizarry et al., 2009; Kuo et al., 2010). Experimental evidence suggests that uric acid may serve as an immunity stimulator. Studies in mice showed that uric acid is released from injured somatic cells and functions as an innate immunity enhancer by stimulating the maturation of dendritic cells and antigen-presenting cells to endogenous antigens (Shi et al., 2003). Monosodium uric acid crystals activate the inflammasome

participating in innate immunity and initiation of inflammation (Martinon et al., 2006).

Most epidemiological studies but not all of them suggested the existence of an association between elevated SUA levels and cardiovascular diseases (CVDs), such as stroke (Lehto et al., 1998; Chien et al., 2005; Bos et al., 2006; Gerber et al., 2006; Hozawa et al., 2006; Kim et al., 2009; Chao et al., 2014; Li et al., 2014; Shi et al., 2017; Tu et al., 2019; Li J. et al., 2020; Zhang et al., 2020), CHD, arterial hypertension, and an increased risk for mortality due to CVDs in general population and subjects with confirmed CHD (Ndrepepa, 2018b; Khalil et al., 2020; Tatsumi et al., 2020). In the Saku study, HUA was found to be independently associated with the development of hypertension independent of alcohol drinking status (Ndrepepa, 2018b). Experimental and clinical studies have evidenced several mechanisms through which elevated UA level exerts deleterious effects on cardiovascular health including increased oxidative stress, reduced availability of nitric oxide and endothelial dysfunction, promotion of local and systemic inflammation, vasoconstriction and proliferation of vascular smooth muscle cells, insulin resistance, and metabolic dysregulation (Tatsumi et al., 2020).

Furthermore, some previous studies indicated that the influence of SUA on stroke was due to the secondary association of SUA with other established etiological risk factors, including hypertension, arterial stiffness, obesity, and hyperinsulinemia (Lehto et al., 1998; Hozawa et al., 2006; Ishizaka et al., 2007; Liang et al., 2009; Shi et al., 2017; Chaudhary et al., 2020). Multiple lines of evidence from epidemiological (Perlstein et al., 2006; Gaffo et al., 2013), animal (Kang et al., 2005; Corry et al., 2008) studies, and clinical trials (Feig et al., 2008) suggested that SUA might increase BP. The mechanism where elevated SUA levels induced hypertension remained elusive,

TABLE 4 | Hazard ratios of serum uric acid level categories for total first stroke events by age in different models.

Variables	Event, n (%)	Crude model		Model I		Model II		P-value for interaction
		HR (95%CI)	P-value	HR (95%CI)	P-value	HR (95%CI)	P-value	
Age < 60 years								
SUA								
Per SD $\mu\text{mol/L}$ increase	16 (0.41%)	1.19 (0.77, 1.84)	0.443	1.06 (0.63, 1.77)	0.837	1.75 (0.95, 3.20)	0.072 ^a	
HUA								
No	5 (0.27%)	Ref		Ref		Ref		
Yes	11 (0.53%)	1.94 (0.67, 5.60)	0.219	1.84 (0.61, 5.56)	0.280	4.89 (1.36, 17.63)	0.015 ^b	
Quartiles of SUA								
Q1 [93.00, 325.80]	3 (0.30%)	Ref		Ref		Ref		
Q2 [326.00, 393.30]	5 (0.56%)	1.89 (0.45, 7.91)	0.386	1.40 (0.31, 6.24)	0.658	1.84 (0.33, 10.22)	0.486 ^c	
Q3 [394.00, 472.00]	4 (0.42%)	1.42 (0.32, 6.36)	0.647	0.89 (0.18, 4.57)	0.893	1.55 (0.25, 9.62)	0.639 ^c	
Q4 [473.00, 1056.00]	4 (0.38%)	1.27 (0.28, 5.67)	0.757	0.79 (0.14, 4.29)	0.783	2.47 (0.33, 18.65)	0.382 ^c	
P for trend		0.931		0.619		0.442		
Age \geq 60 years								
SUA								
Per SD $\mu\text{mol/L}$ increase	83 (1.05%)	1.10 (0.89, 1.37)	0.387	1.02 (0.81, 1.29)	0.868	0.86 (0.65, 1.13)	0.284 ^d	0.042 ^g
HUA								
No	35 (0.92%)	Ref		Ref		Ref		0.043 ^h
Yes	48 (1.17%)	1.28 (0.83, 1.99)	0.267	1.24 (0.80, 1.92)	0.341	0.97 (0.60, 1.56)	0.886 ^e	
Quartiles of SUA								
Q1 [38.00, 325.00]	19 (0.98%)	Ref		Ref		Ref		0.482 ⁱ
Q2 [326.00, 393.00]	18 (0.88%)	0.90 (0.47, 1.73)	0.761	0.85 (0.44, 1.63)	0.620	0.70 (0.36, 1.36)	0.287 ^f	
Q3 [394.00, 472.00]	25 (1.24%)	1.28 (0.70, 2.32)	0.427	1.11 (0.59, 2.08)	0.747	0.78 (0.40, 1.51)	0.454 ^f	
Q4 [473.00, 879.00]	21 (1.10%)	1.13 (0.60, 2.10)	0.706	0.92 (0.47, 1.79)	0.808	0.55 (0.26, 1.17)	0.120 ^f	
P for trend		0.515		0.967		0.163		

SUA, serum uric acid; HUA, hyperuricemia; Ref, reference; HR, hazard ratio; CI, confidence interval; SD, standard deviation.

Model I adjusted for sex, SBP, DBP, and HR.

Model II: ^aAdjusted for sex, SBP, DBP, HR, BMI, WHR, Hcy, TG, LDL-C, eGFR, total bilirubin, AST, ALT, lipid-lowering agents and antiplatelet agents. ^bAdjusted for SBP, DBP, HR, WHR, TG, LDL-C, eGFR, ALT, lipid-lowering agents, and antiplatelet agents. ^cAdjusted for sex, SBP, DBP, BMI, WHR, smoking and drinking status, Hcy, TG, HDL-C, LDL-C, eGFR, total bilirubin, AST, ALT, DM, antihypertensive agents, lipid-lowering agents, and antiplatelet agents. ^dAdjusted for sex, SBP, DBP, HR, BMI, smoking and drinking status, Hcy, TG, HDL-C, LDL-C, and eGFR. ^eAdjusted for sex, SBP, DBP, HR, BMI, smoking and drinking status, Hcy, TG, HDL-C, LDL-C, AST, eGFR and antiplatelet agents. ^fAdjusted for sex, SBP, DBP, HR, BMI, WHR, smoking and drinking status, Hcy, TG, HDL-C, LDL-C, eGFR, and AST. ^gAdjusted for sex, SBP, DBP, HR, BMI, WHR, smoking and drinking status, Hcy, TG, HDL-C, LDL-C, eGFR, total bilirubin, ALT, DM, antiplatelet agents and the interaction terms for following variables: sex, SBP, DBP, HR, BMI, WHR, smoking and drinking status, Hcy, TG, HDL-C, LDL-C, eGFR, total bilirubin, ALT, DM, antiplatelet agents. ^hAdjusted for sex, SBP, DBP, HR, BMI, WHR, smoking status, Hcy, TG, eGFR, ALT, antiplatelet agents and the interaction terms for following variables: SBP, DBP, HR, Hcy, TG, eGFR, ALT, and antiplatelet agents. ⁱAdjusted for sex, SBP, DBP, HR, BMI, WHR, smoking and drinking status, Hcy, TG, HDL-C, LDL-C, eGFR, total bilirubin, ALT, AST, antiplatelet agents and the interaction terms for following variables: age, SBP, DBP, HR, BMI, WHR, smoking and drinking status, Hcy, TG, HDL-C, LDL-C, eGFR, total bilirubin, ALT, AST, antiplatelet agents.

involving crystal pathway, activation of the intrarenal renin-angiotensin system, reducing endothelial nitric oxide synthase phosphorylation, the elevation of aldose reductase, mitochondrial dysfunction, and superoxide generation (Lanaspa et al., 2020). Some studies indicated that hypertension might mediate the effect of HUA on stroke risk (Hozawa et al., 2006; Shi et al., 2017; Chaudhary et al., 2020). In the Atherosclerosis Risk in Communities (ARIC) study, over 13,000 participants were followed for incident stroke over 12.6 years, HUA was no longer independently associated with ischemic stroke after adjustment for diuretic-treated hypertension (Hozawa et al., 2006). In the REGARDS study, apparent treatment-resistant hypertension and separately count of antihypertensive medication classes significantly reduced the effect of HUA on ischemic stroke (Chaudhary et al., 2020). The evidence available also suggests an

association between elevated UA and traditional cardiovascular risk factors, metabolic syndrome, insulin resistance, obesity, non-alcoholic fatty liver disease, and CKD (Tatsumi et al., 2020). Thus, some scholars hypothesized that uric acid may be pathogenic and participate in the pathophysiology of CVDs by serving as a bridging mechanism mediating or potentiating the deleterious effects of cardiovascular risk factors on vascular tissue and myocardium (Ndrepepa, 2018a; Tatsumi et al., 2020).

The role of HUA as an independent risk factor for stroke in Chinese hypertensive patients was still controversial (Chien et al., 2005; Bos et al., 2006; Shi et al., 2017; Zhang et al., 2020). Baseline or time-dependent elevated SUA had a significant risk for stroke only in hypertension and metabolic syndrome subgroup across populations with relatively low CHD but high stroke risk in Taiwan (Chien et al., 2005). The Rotterdam study

TABLE 5 | Hazard ratios of serum uric acid level categories for total first stroke events by sex in different models.

Variables	Event, n (%)	Crude model		Model I		Model II		P-value for interaction
		HR (95%CI)	P-value	HR (95%CI)	P-value	HR (95%CI)	P-value	
Males								
SUA								
Per SD $\mu\text{mol/L}$ increase	56 (1.04%)	1.02 (0.78, 1.33)	0.905	1.05 (0.80, 1.39)	0.718	1.00 (0.72, 1.39)	0.987 ^a	
HUA								
No	22 (0.97%)	Ref		Ref		Ref		
Yes	34 (1.08%)	1.11 (0.65, 1.91)	0.699	1.14 (0.66, 1.95)	0.646	1.06 (0.58, 1.91)	0.856 ^b	
Quartiles of SUA								
Q1 [38.00, 325.00]	8 (1.40%)	Ref		Ref		Ref		
Q2 [326.00, 393.00]	9 (0.81%)	0.58 (0.22, 1.50)	0.260	0.56 (0.21, 1.46)	0.233	0.50 (0.19, 1.31)	0.159 ^c	
Q3 [394.00, 472.00]	19 (1.17%)	0.83 (0.36, 1.91)	0.665	0.80 (0.35, 1.85)	0.605	0.67 (0.28, 1.58)	0.356 ^c	
Q4 [473.00, 1056.00]	20 (0.95%)	0.68 (0.30, 1.55)	0.357	0.71 (0.31, 1.62)	0.411	0.54 (0.22, 1.35)	0.187 ^c	
P for trend		0.576		0.494		0.753		
Females								
SUA								
Per SD $\mu\text{mol/L}$ increase	43 (0.67%)	1.03 (0.73, 1.45)	0.864	1.02 (0.72, 1.45)	0.892	0.98 (0.66, 1.47)	0.922 ^d	1.000 ^g
HUA								
No	18 (0.53%)	Ref		Ref		Ref		0.274 ^h
Yes	25 (0.82%)	1.56 (0.85, 2.86)	0.154	1.54 (0.84, 2.85)	0.165	1.70 (0.87, 3.30)	0.118 ^e	
Quartiles of SUA								
Q1 [108.00, 325.80]	14 (0.59%)	Ref		Ref		Ref		0.539 ⁱ
Q2 [326.00, 393.00]	14 (0.77%)	1.31 (0.62, 2.75)	0.477	1.27 (0.60, 2.69)	0.529	1.30 (0.60, 2.82)	0.513 ^f	
Q3 [394.00, 472.00]	10 (0.75%)	1.28 (0.57, 2.88)	0.556	1.28 (0.56, 2.91)	0.557	1.21 (0.50, 2.94)	0.675 ^f	
Q4 [473.00, 879.00]	5 (0.57%)	0.97 (0.35, 2.70)	0.952	0.94 (0.34, 2.65)	0.914	0.84 (0.27, 2.66)	0.771 ^f	
P for trend		0.906		0.936		0.864		

SUA, serum uric acid; HUA, hyperuricemia; Ref, reference; HR, hazard ratio; CI, confidence interval; SD, standard deviation.

Model I adjusted for age, SBP, DBP, and HR.

Model II: ^aAdjusted for age, SBP, DBP, HR, BMI, WHR, smoking and drinking status, Hcy, TG, HDL-C, LDL-C, eGFR, total bilirubin, AST, ALT, and antiplatelet agents.

^bAdjusted for age, SBP, DBP, HR, BMI, WHR, smoking and drinking status, Hcy, TG, HDL-C, LDL-C, eGFR, and ALT. ^cAdjusted for age, SBP, DBP, BMI, WHR, Hcy, HDL-C, LDL-C, and eGFR. ^dAdjusted for age, SBP, DBP, HR, BMI, WHR, smoking and drinking status, Hcy, TG, HDL-C, LDL-C, eGFR, total bilirubin, AST, ALT, DM, antihypertensive agents, lipid-lowering agents, and antiplatelet agents. ^eAdjusted for age, SBP, DBP, HR, BMI, Hcy, LDL-C, ALT, eGFR, and antiplatelet agents. ^fAdjusted for age, SBP, DBP, HR, BMI, WHR, smoking and drinking status, Hcy, TG, HDL-C, LDL-C, eGFR, total bilirubin, AST, ALT, DM, and antiplatelet agents. ^gAdjusted for age, SBP, DBP, HR, BMI, WHR, smoking and drinking status, Hcy, TG, HDL-C, LDL-C, eGFR, total bilirubin, ALT, DM, antiplatelet agents and the interaction terms for following variables: age, SBP, DBP, HR, BMI, WHR, smoking and drinking status, Hcy, TG, HDL-C, LDL-C, eGFR, total bilirubin, ALT, DM, antiplatelet agents. ^hAdjusted for age, SBP, DBP, HR, BMI, smoking status, Hcy, TG, eGFR, ALT, antiplatelet agents and the interaction terms for following variables: age, SBP, DBP, HR, BMI, smoking status, Hcy, TG, eGFR, ALT, and antiplatelet agents. ⁱAdjusted for age, SBP, DBP, HR, BMI, WHR, smoking and drinking status, Hcy, TG, HDL-C, LDL-C, eGFR, total bilirubin, ALT, AST, antiplatelet agents and the interaction terms for following variables: age, SBP, DBP, HR, BMI, WHR, smoking and drinking status, Hcy, TG, HDL-C, LDL-C, eGFR, total bilirubin, ALT, AST, antiplatelet agents.

indicated that elevated SUA was a strong risk factor for stroke and this positive relationship was stronger in the population without hypertension than in those with hypertension (Bos et al., 2006). Increased SUA levels were positively associated with ischemic stroke and HUA has a good predictive value for ischemic stroke among hypertensive participants in the Chinese community (Zhang et al., 2020). Although elevated SUA was not significantly associated with the risk of the first stroke, there was a statistically significant decreased risk of hemorrhagic stroke for the second quartile of SUA levels compared to the first quartile in a Chinese population of hypertensive patients (Shi et al., 2017). Considering the rate differences of HUA in different sex and population attributable fractions across hypertensive patients, some previous studies suggested that women had a high risk of SUA on stroke events (Chien et al., 2005; Li J. et al., 2020).

However, no studies have been reported that age could modify the association between increased SUA levels and stroke events. To our knowledge, this was the first discovery that age played an interactive role between HUA with the first stroke event. In our analysis, subjects aged less than 60 years old had a higher prevalence of general or central obesity and dyslipidemia than the aging group (**Supplementary Table 2**), which might explain the interactive role of aging between HUA with the first stroke event. Therefore, targeted stroke prevention should include healthy lifestyle improvement and treatment of metabolic syndrome in an individualized and comprehensive way, especially younger Chinese adults with hypertension (Pandian et al., 2018).

Furthermore, current evidence showed that SUA levels increased rapidly after acute ischemic stroke (AIS). Nevertheless, the relationship between SUA levels and AIS outcome remained

TABLE 6 | Hazard ratios of serum uric acid level categories for total first stroke events by mean arterial pressure tertiles in different models.

Variables	Event, n (%)	Crude model		Model I		Model II		P-value for interaction
		HR (95%CI)	P-value	HR (95%CI)	P-value	HR (95%CI)	P-value	
MAP T1 [66.00, 104.65]								
SUA								
Per SD μmol/L increase	26 (0.66%)	1.36 (0.96, 1.93)	0.084	1.27 (0.87, 1.85)	0.219	1.16 (0.75, 1.79)	0.508 ^a	
HUA								
No	9 (0.48%)	Ref		Ref		Ref		
Yes	17 (0.83%)	1.75 (0.78, 3.92)	0.178	1.66 (0.74, 3.75)	0.220	1.42 (0.59, 3.43)	0.440 ^b	
Quartiles of SUA								
Q1 [118.00, 325.00]	5 (0.52%)	Ref		Ref		Ref		
Q2 [326.00, 393.30]	5 (0.51%)	0.99 (0.28, 3.42)	0.983	0.89 (0.25, 3.13)	0.860	0.82 (0.23, 2.94)	0.764 ^c	
Q3 [394.00, 472.00]	6 (0.62%)	1.20 (0.36, 3.93)	0.769	0.97 (0.29, 3.30)	0.963	0.83 (0.24, 2.94)	0.776 ^c	
Q4 [473.00, 1029.00]	10 (0.98%)	1.91 (0.65, 5.59)	0.241	1.50 (0.48, 4.66)	0.486	1.12 (0.31, 3.98)	0.864 ^c	
P for trend		0.172		0.373		0.762		
MAP T2 [104.55, 113.22]								
SUA								
Per SD μmol/L increase	27 (0.68%)	0.91 (0.62, 1.35)	0.637	0.87 (0.55, 1.35)	0.527	0.75 (0.45, 1.25)	0.263 ^d	
HUA								
No	12 (0.64%)	Ref		Ref		Ref		
Yes	15 (0.72%)	1.12 (0.52, 2.39)	0.774	1.13 (0.52, 2.44)	0.755	1.07 (0.46, 2.52)	0.871 ^e	
Quartiles of SUA								
Q1 [38.00, 325.80]	8 (0.82%)	Ref		Ref		Ref		
Q2 [326.00, 393.00]	6 (0.61%)	0.74 (0.26, 2.15)	0.584	0.66 (0.22, 1.94)	0.446	0.65 (0.22, 1.93)	0.438 ^f	
Q3 [394.00, 472.00]	8 (0.79%)	0.97 (0.36, 2.60)	0.955	0.81 (0.28, 2.30)	0.690	0.79 (0.27, 2.27)	0.658 ^f	
Q4 [473.00, 1056.00]	5 (0.51%)	0.63 (0.20, 1.92)	0.412	0.53 (0.16, 1.76)	0.302	0.51 (0.15, 1.74)	0.284 ^f	
P for trend		0.508		0.372		0.349		
MAP T3 [113.22, 170.89]								
SUA								
Per SD μmol/L increase	46 (1.17%)	1.09 (0.82, 1.44)	0.567	1.02 (0.74, 1.41)	0.885	1.01 (0.69, 1.47)	0.960 ^g	0.415 ^j
HUA								
No	19 (1.00%)	Ref		Ref		Ref		0.845 ^k
Yes	27 (1.32%)	1.33 (0.73, 2.39)	0.349	1.27 (0.70, 2.31)	0.432	1.30 (0.68, 2.50)	0.427 ^h	
Quartiles of SUA								
Q1 [127.00, 325.00]	9 (0.89%)	Ref		Ref		Ref		0.826 ^l
Q2 [326.00, 393.00]	12 (1.24%)	1.40 (0.59, 3.33)	0.449	1.20 (0.49, 2.89)	0.692	1.15 (0.47, 2.84)	0.758 ⁱ	
Q3 [394.00, 472.00]	15 (1.52%)	1.72 (0.75, 3.95)	0.200	1.41 (0.59, 3.38)	0.438	1.26 (0.50, 3.18)	0.619 ^j	
Q4 [473.00, 915.00]	10 (1.02%)	1.15 (0.46, 2.84)	0.765	0.93 (0.35, 2.45)	0.876	0.85 (0.29, 2.51)	0.770 ^j	
P for trend		0.75		0.850		0.721		

MAP, mean arterial pressure; SUA, serum uric acid; HUA, hyperuricemia; Ref, reference; HR, hazard ratio; CI, confidence interval; SD, standard deviation.

Model I adjusted for age, sex, and HR.

Model II: ^aAdjusted for age, gender, HR, BMI, drinking status, Hcy, TG, LDL-C, eGFR, ALT, and antiplatelet agents. ^bAdjusted for age, sex, HR, BMI, drinking status, Hcy, TG, LDL-C, eGFR, and antiplatelet agents. ^cAdjusted for age, sex, HR, BMI, WHR, smoking and drinking status, Hcy, TG, HDL-C, LDL-C, eGFR, total bilirubin, ALT, DM, antihypertensive agents, lipid-lowering agents, and antiplatelet agents. ^dAdjusted for age, sex, HR, BMI, smoking and drinking status, Hcy, TG, HDL-C, eGFR, AST, and ALT. ^eAdjusted for age, sex, HR, BMI, smoking and drinking status, Hcy, TG, HDL-C, LDL-C, eGFR, total bilirubin, ALT, DM, antihypertensive agents, and antiplatelet agents. ^fAdjusted for age, sex, HR, BMI, smoking and drinking status, Hcy, TG, HDL-C, LDL-C, eGFR, AST, ALT, and DM. ^gAdjusted for age, sex, BMI, WHR, smoking status, Hcy, TG, HDL-C, LDL-C, eGFR, AST and ALT. ^hAdjusted for age, sex, BMI, WHR, smoking and drinking status, Hcy, TG, HDL-C, LDL-C, eGFR, AST, and ALT. ⁱAdjusted for age, HR, BMI, WHR, smoking and drinking status, Hcy, TG, HDL-C, LDL-C, eGFR, total bilirubin, ALT, DM, antiplatelet agents and the interaction terms for following variables: age, WHR, smoking and drinking status, Hcy, TG, LDL-C, eGFR, total bilirubin, and ALT. ^kAdjusted for age, sex, HR, BMI, smoking status, Hcy, TG, eGFR, ALT, antiplatelet agents and the interaction terms for following variables: age, sex, HR, BMI, smoking status, Hcy, TG, eGFR, ALT, antiplatelet agents. ^lAdjusted for age, sex, HR, BMI, WHR, smoking and drinking status, Hcy, TG, HDL-C, LDL-C, eGFR, total bilirubin, ALT, AST, antiplatelet agents and the interaction terms for following variables: age, sex, HR, BMI, WHR, smoking and drinking status, Hcy, TG, HDL-C, LDL-C, eGFR, total bilirubin, ALT, AST, antiplatelet agents.

debatable (Maloberti et al., 2020). Animal models of AIS showed that SUA might be neuroprotective (Yu et al., 1998). In humans, HUA might be an independent predictor of better outcome

after AIS (Chamorro et al., 2002). However, the primer registro mexicano de isquemia cerebral (PREMIER) study revealed that a low SUA concentration was modestly associated with a very

TABLE 7 | Hazard ratios of serum uric acid level categories for total first stroke events by antihypertensive drugs usage in different models.

Variables	Event, n (%)	Crude model		Model I		Model II		P-value for interaction
		HR (95%CI)	P-value	HR (95%CI)	P-value	HR (95%CI)	P-value	
Non-use of antihypertensive drugs								
SUA								
Per SD $\mu\text{mol/L}$ increase	38 (0.85%)	0.87 (0.62, 1.22)	0.424	0.76 (0.52, 1.12)	0.168	0.73 (0.46, 1.16)	0.179 ^a	
HUA								
No	21 (0.94%)	Ref		Ref		Ref		
Yes	17 (0.76%)	0.81 (0.42, 1.53)	0.511	0.80 (0.41, 1.53)	0.497	0.80 (0.39, 1.63)	0.533 ^b	
Quartiles of SUA								
Q1 [93.00, 325.00]	11 (0.92%)	Ref		Ref		Ref		
Q2 [326.00, 393.30]	10 (0.90%)	0.98 (0.42, 2.32)	0.967	0.84 (0.35, 2.03)	0.694	0.79 (0.31, 1.99)	0.619 ^c	
Q3 [394.00, 472.00]	10 (0.91%)	1.00 (0.42, 2.35)	0.992	0.78 (0.31, 1.95)	0.599	0.74 (0.28, 1.97)	0.545 ^c	
Q4 [473.00, 913.00]	7 (0.66%)	0.71 (0.28, 1.85)	0.488	0.53 (0.19, 1.49)	0.228	0.49 (0.15, 1.58)	0.230 ^c	
P for trend		0.510		0.229		0.237		
Use of antihypertensive drugs								
SUA								
Per SD $\mu\text{mol/L}$ increase	61 (0.83%)	1.26 (1.00, 1.58)	0.055	1.22 (0.94, 1.58)	0.128	1.11 (0.83, 1.48)	0.483 ^d	0.070 ^g
HUA								
No	19 (0.56%)	Ref		Ref		Ref		0.094 ^h
Yes	42 (1.06%)	1.93 (1.12, 3.32)	0.018	1.82 (1.05, 3.15)	0.032	1.67 (0.94, 2.99)	0.083 ^e	
Quartiles of SUA								
Q1 [38.00, 325.80]	11 (0.62%)	Ref		Ref		Ref		0.813 ⁱ
Q2 [326.00, 393.30]	13 (0.71%)	1.14 (0.51, 2.56)	0.747	1.02 (0.45, 2.31)	0.957	0.95 (0.41, 2.17)	0.898 ^f	
Q3 [394.00, 472.00]	19 (1.02%)	1.63 (0.77, 3.44)	0.198	1.36 (0.62, 2.96)	0.439	1.14 (0.51, 2.55)	0.758 ^f	
Q4 [473.00, 1056.00]	18 (0.94%)	1.51 (0.71, 3.21)	0.282	1.27 (0.57, 2.82)	0.560	0.96 (0.40, 2.30)	0.919 ^f	
P for trend		0.217		0.483		0.952		

SUA, serum uric acid; HUA, hyperuricemia; Ref, reference; HR, hazard ratio; CI, confidence interval; SD, standard deviation.

Model I adjusted for age, sex, SBP, DBP, and HR.

Model II: ^aAdjusted for age, sex, SBP, DBP, BMI, WHR, smoking, and drinking status, Hcy, TG, HDL-C, LDL-C, eGFR, AST, and ALT. ^bAdjusted for age, sex, SBP, DBP, BMI, WHR, drinking status, Hcy, TG, HDL-C, LDL-C, eGFR, AST, and ALT. ^cAdjusted for age, sex, SBP, DBP, HR, BMI, WHR, smoking and drinking status, Hcy, TG, HDL-C, LDL-C, eGFR, total bilirubin, AST, ALT, DM, lipid-lowering agents, and antiplatelet agents. ^dAdjusted for age, sex, SBP, HR, BMI, smoking status, Hcy, eGFR, and antiplatelet agents. ^eAdjusted for age, sex, SBP, DBP, HR, BMI, smoking and drinking status, Hcy, HDL-C, LDL-C, eGFR, AST, ALT, total bilirubin, and antiplatelet agents. ^fAdjusted for age, sex, SBP, DBP, HR, BMI, WHR, smoking, and drinking status, Hcy, TG, HDL-C, LDL-C, eGFR, total bilirubin, ALT, DM, antiplatelet agents and the interaction terms for following variables: age, sex, smoking, and eGFR. ^gAdjusted for age, sex, SBP, DBP, HR, BMI, smoking status, Hcy, TG, eGFR, ALT, antiplatelet agents and the interaction terms for following variables: age, sex, SBP, DBP, HR, BMI, smoking status, TG, eGFR, ALT, antiplatelet agents. ^hAdjusted for age, sex, SBP, DBP, HR, BMI, WHR, smoking and drinking status, Hcy, TG, HDL-C, LDL-C, eGFR, total bilirubin, ALT, AST, antiplatelet agents and the interaction terms for following variables: age, sex, SBP, DBP, HR, BMI, WHR, smoking and drinking status, TG, HDL-C, LDL-C, eGFR, total bilirubin, ALT, AST, antiplatelet agents.

good short-term outcome (12-month follow-up) (Chiquete et al., 2013). Wang et al. (2019) found that HUA independently predicted the poor in-hospital outcome of AIS in diabetic patients, especially in patients aged less than 75 years old.

Moreover, no evidence indicated that lowering SUA levels with drug treatment had a beneficial effect on stroke outcome. Although meta-analyses on randomized controlled trials (RCTs) suggest cardiovascular benefits with allopurinol, few high-quality RCTs have examined the allopurinol effect of urate-lowering therapy among patients with HUA or gout (Kang and Kim, 2019). Larsen et al. (2016) showed that lowering of urate by allopurinol improved cardiovascular outcomes including stroke among patients with HUA. Yen et al. (2020) found that uricosuric agents and xanthine oxidase inhibitors significantly mitigated the risks of hospitalized stroke and all-cause mortality in patients with gout. We eagerly await results from ongoing

large-scale RCTs of urate-lowering therapy on various clinical cardiovascular outcomes.

Considering that the influence of SUA on the risk of stroke events might due to the secondary association of SUA with other traditional risk factors, such as hypertension and obesity (Lehto et al., 1998; Hozawa et al., 2006; Ishizaka et al., 2007; Liang et al., 2009; Shi et al., 2017; Chaudhary et al., 2020). We did subgroup analyses in the mean arterial pressure tertiles, SBP tertiles, DBP tertiles, antihypertensive drugs usage, body mass index tertiles, and central obesity (Tables 6, 7, Supplementary Figure 3, and Supplementary Tables 5–8). Nevertheless, these above covariates could not modify the relationship between increased SUA levels and the first stroke event.

Several limitations of our study should be addressed in interpreting the results. First, we did not test the excretion or metabolite rate of SUA, which could affect the SUA levels.

Second, the levels of SUA were measured only once at baseline, and multiple determinations might be necessary to evaluate the kinetics of SUA levels. In addition, our follow-up period was not long, and fewer stroke events occurred. The relatively low incidence of stroke events reduced the strength of this finding.

CONCLUSION

To sum up, no significant evidence in the present study indicated that increased SUA levels were associated with the risk of the first stroke in Chinese adults with hypertension. Nonetheless, age played an interactive role in the relationship between HUA and the first stroke event. In the population less than 60 years old, subjects with HUA had a significantly higher risk of the first stroke than the population without HUA. In subjects older than 60 years, we did not find a significant relationship between HUA and first stroke. Definitive proof of causality and the mechanism between SUA levels and stroke outcomes requires an appropriately designed therapeutic controlled trial.

DATA AVAILABILITY STATEMENT

The original contributions presented in the study are included in the article/**Supplementary Material**, further inquiries can be directed to the corresponding author/s.

ETHICS STATEMENT

The studies involving human participants were reviewed and approved by the Ethics Committee of the Institute of Biomedicine, Anhui Medical University. The patients/participants provided their written informed consent to participate in this study.

AUTHOR CONTRIBUTIONS

FH: conception and design, data acquisition and analysis, interpretation, drafting, and final approval. LH: conception and design, data acquisition and analysis, interpretation, critical revision, and final approval. RY and FYH: data acquisition and final approval. WZ and TW: design and final approval. LZ and XH: analysis and interpretation and final approval. HB and XC: conception and design and critical revision and final approval. All authors contributed to the article and approved the submitted version.

REFERENCES

- Ames, B. N., Cathcart, R., Schwiers, E., and Hochstein, P. (1981). Uric acid provides an antioxidant defense in humans against oxidant- and radical-caused aging and cancer: a hypothesis. *Proc. Natl. Acad. Sci. U.S.A.* 78, 6858–6862. doi: 10.1073/pnas.78.11.6858
- Becker, B. F. (1993). Towards the physiological function of uric acid. *Free Radic. Biol. Med.* 14, 615–631. doi: 10.1016/0891-5849(93)90143-i

FUNDING

This work was supported by the Jiangxi Science and Technology Innovation Platform Project (20165BCD41005), the Jiangxi Provincial Natural Science Foundation (20212ACB206019), and the fund project of the Second Affiliated Hospital of Nanchang University (2016YNQN12034, 2019YNLZ12010, IIT-I-2021-002, and 2021YNFY2024).

SUPPLEMENTARY MATERIAL

The Supplementary Material for this article can be found online at: <https://www.frontiersin.org/articles/10.3389/fphys.2021.807420/full#supplementary-material>

Supplementary Figure 1 | The smooth curve of correlation between SUA levels and stroke occur probability. Smooth curve adjusted for age, sex, SBP, DBP, HR, BMI, WHR, smoking and drinking status, Hcy, TG, HDL-C, LDL-C, eGFR, ALT, total bilirubin, DM, and antiplatelet agents. This analysis was conducted using both logarithmic transformed and untransformed data. Log (relative risk, RR) can be converted to a relative risk by taking antilog. For example, a log RR of 0 implies the relative risk of 1 (no impact on the probability of death), whereas a log RR of 1 implies the relative risk of 2.71 (i.e., 2.71-fold increase in the probability of death). The piece-wise regression suggested that the relationship between SUA levels and the risk of the first stroke was linear (P -value of Log-likelihood ratio test = 0.31). eGFR, estimated glomerular filtration rate; SBP, systolic blood pressure; DBP, diastolic blood pressure; HR, heart rate, BMI, body mass index; Hcy, homocysteine; TG, total triglyceride; HDL-C, high-density lipoprotein cholesterol; LDL-C, low-density lipoprotein cholesterol; AST, aspartate aminotransferase; ALT, alanine aminotransferase.

Supplementary Figure 2 | The cumulative total first stroke risks in the study population were grouped by sex. **(A)** adjusted for age, SBP, DBP, HR, BMI, WHR, smoking and drinking status, Hcy, TG, HDL-C, LDL-C, eGFR, and ALT. **(B)** Adjusted for age, SBP, DBP, HR, BMI, Hcy, LDL-C, ALT, eGFR, and antiplatelet agents. eGFR, estimated glomerular filtration rate; SBP, systolic blood pressure; DBP, diastolic blood pressure; HR, heart rate, BMI, body mass index; Hcy, homocysteine; TG, total triglyceride; HDL-C, high-density lipoprotein cholesterol; LDL-C, low-density lipoprotein cholesterol; AST, aspartate aminotransferase; ALT, alanine aminotransferase.

Supplementary Figure 3 | The cumulative total first stroke risks in the study population grouped by mean arterial pressure. **(A)** Adjusted for age, sex, HR, BMI, drinking status, Hcy, TG, LDL-C, eGFR, and antiplatelet agents. **(B)** Adjusted for age, sex, HR, BMI, smoking and drinking status, Hcy, TG, HDL-C, LDL-C, eGFR, total bilirubin, ALT, DM, antihypertensive agents, and antiplatelet agents. **(C)** Adjusted for age, sex, BMI, WHR, smoking status, Hcy, TG, HDL-C, LDL-C, eGFR, AST, and ALT. MAP, mean arterial pressure; eGFR, estimated glomerular filtration rate; HR, heart rate, BMI, body mass index; Hcy, homocysteine; TG, total triglyceride; HDL-C, high-density lipoprotein cholesterol; LDL-C, low-density lipoprotein cholesterol; AST, aspartate aminotransferase; ALT, alanine aminotransferase.

Supplementary Figure 4 | The smooth curve of correlation between age and serum uric acid levels.

- Bos, M. J., Koudstaal, P. J., Hofman, A., Witteman, J. C., and Breteler, M. M. (2006). Uric acid is a risk factor for myocardial infarction and stroke: the Rotterdam study. *Stroke* 37, 1503–1507. doi: 10.1161/01.STR.0000221716.55088.d4
- Buonacera, A., Stancanelli, B., and Malatino, L. (2019). Stroke and hypertension: an appraisal from pathophysiology to clinical practice. *Curr. Vasc. Pharmacol.* 17, 72–84. doi: 10.2174/1570161155666171116151051
- Chamorro, A., Obach, V., Cervera, A., Revilla, M., Deulofeu, R., and Aponte, J. H. (2002). Prognostic significance of uric acid serum concentration in patients

- with acute ischemic stroke. *Stroke* 33, 1048–1052. doi: 10.1161/hs0402.105927
- Chao, T. F., Liu, C. J., Chen, S. J., Wang, K. L., Lin, Y. J., Chang, S. L., et al. (2014). Hyperuricemia and the risk of ischemic stroke in patients with atrial fibrillation—could it refine clinical risk stratification in AF? *Int. J. Cardiol.* 170, 344–349. doi: 10.1016/j.ijcard.2013.11.011
- Chaudhary, N. S., Bridges, S. L. Jr., Saag, K. G., Rahn, E. J., Curtis, J. R., Gaffo, A., et al. (2020). Severity of hypertension mediates the association of hyperuricemia with stroke in the REGARDS case cohort study. *Hypertension* 75, 246–256. doi: 10.1161/HYPERTENSIONAHA.119.13580
- Chen, Y., Cheng, J., Chen, Y., Wang, N., Xia, F., Chen, C., et al. (2020). Association between serum vitamin D and uric acid in the eastern Chinese population: a population-based cross-sectional study. *BMC Endocr. Disord.* 20:79. doi: 10.1186/s12902-020-00560-1
- Chien, K. L., Hsu, H. C., Sung, F. C., Su, T. C., Chen, M. F., and Lee, Y. T. (2005). Hyperuricemia as a risk factor on cardiovascular events in Taiwan: the Chin-Shan community cardiovascular cohort study. *Atherosclerosis* 183, 147–155. doi: 10.1016/j.atherosclerosis.2005.01.018
- Chiquete, E., Ruiz-Sandoval, J. L., Murillo-Bonilla, L. M., Arauz, A., Orozco-Valera, D. R., Ochoa-Guzmán, A., et al. (2013). Serum uric acid and outcome after acute ischemic stroke: premier study. *Cerebrovasc. Dis.* 35, 168–174. doi: 10.1159/000346603
- Corry, D. B., Eslami, P., Yamamoto, K., Nyby, M. D., Makino, H., and Tuck, M. L. (2008). Uric acid stimulates vascular smooth muscle cell proliferation and oxidative stress via the vascular renin-angiotensin system. *J. Hypertens* 26, 269–275. doi: 10.1097/HJH.0b013e3282f240bf
- Feig, D. I., Soletsky, B., and Johnson, R. J. (2008). Effect of allopurinol on blood pressure of adolescents with newly diagnosed essential hypertension: a randomized trial. *JAMA* 300, 924–932. doi: 10.1001/jama.300.8.924
- Gaffo, A. L., Jacobs, D. R. Jr., Sijtsma, F., Lewis, C. E., Mikuls, T. R., and Saag, K. G. (2013). Serum urate association with hypertension in young adults: analysis from the coronary artery risk development in young adults cohort. *Ann. Rheum. Dis.* 72, 1321–1327. doi: 10.1136/annrheumdis-2012-201916
- Gerber, Y., Tanne, D., Medalie, J. H., and Goldbourt, U. (2006). Serum uric acid and long-term mortality from stroke, coronary heart disease and all causes. *Eur. J. Cardiovasc. Prev. Rehabil.* 13, 193–198. doi: 10.1097/01.hjr.0000192745.26973.00
- Hozawa, A., Folsom, A. R., Ibrahim, H., Nieto, F. J., Rosamond, W. D., and Shahar, E. (2006). Serum uric acid and risk of ischemic stroke: the ARIC study. *Atherosclerosis* 187, 401–407. doi: 10.1016/j.atherosclerosis.2005.09.020
- Izarrary, M. C., Raman, R., Schwarzschild, M. A., Becerra, L. M., Thomas, R. G., Peterson, R. C., et al. (2009). Plasma urate and progression of mild cognitive impairment. *Neurodegener. Dis.* 6, 23–28. doi: 10.1159/000170883
- Ishizaka, N., Ishizaka, Y., Toda, E., Hashimoto, H., Nagai, R., and Yamakado, M. (2007). Higher serum uric acid is associated with increased arterial stiffness in Japanese individuals. *Atherosclerosis* 192, 131–137. doi: 10.1016/j.atherosclerosis.2006.04.016
- Jia, W., Weng, J., Zhu, D., Ji, L., Lu, J., Zhou, Z., et al. (2019). Standards of medical care for type 2 diabetes in China 2019. *Diabetes Metab. Res. Rev.* 35, e3158. doi: 10.1002/dmrr.3158
- Joint Committee for Developing Chinese guidelines on Prevention and Treatment of Dyslipidemia in Adults (2007). [Chinese guidelines on prevention and treatment of dyslipidemia in adults]. *Zhonghua Xin Xue Guan Bing Za Zhi* 35, 390–419.
- Kang, D. H., Park, S. K., Lee, I. K., and Johnson, R. J. (2005). Uric acid-induced C-reactive protein expression: implication on cell proliferation and nitric oxide production of human vascular cells. *J. Am. Soc. Nephrol.* 16, 3553–3562. doi: 10.1681/ASN.2005050572
- Kang, E. H., and Kim, S. C. (2019). Cardiovascular Safety of Urate Lowering Therapies. *Curr. Rheumatol. Rep.* 21:48. doi: 10.1007/s11926-019-0843-8
- Khalil, M. I., Salwa, M., Sultana, S., Al Mamun, M. A., Barman, N., and Haque, M. A. (2020). Role of serum uric acid in ischemic stroke: a case-control study in Bangladesh. *PLoS One* 15:e0236747. doi: 10.1371/journal.pone.0236747
- Kim, S. Y., Guevara, J. P., Kim, K. M., Choi, H. K., Heitjan, D. F., and Albert, D. A. (2009). Hyperuricemia and risk of stroke: a systematic review and meta-analysis. *Arthritis Rheum.* 61, 885–892. doi: 10.1002/art.24612
- Kuo, C. F., Yu, K. H., Luo, S. F., Ko, Y. S., Wen, M. S., Lin, Y. S., et al. (2010). Role of uric acid in the link between arterial stiffness and cardiac hypertrophy: a cross-sectional study. *Rheumatology (Oxford)* 49, 1189–1196. doi: 10.1093/rheumatology/keq095
- Lanaspa, M. A., Andres-Hernando, A., and Kuwabara, M. (2020). Uric acid and hypertension. *Hypertens Res.* 43, 832–834. doi: 10.1038/s41440-020-0481-6
- Larsen, K. S., Pottegård, A., Lindegaard, H. M., and Hallas, J. (2016). Effect of allopurinol on cardiovascular outcomes in hyperuricemic patients: a cohort study. *Am. J. Med.* 129, 299–306.e2. doi: 10.1016/j.amjmed.2015.11.003
- Lehto, S., Niskanen, L., Rönnemaa, T., and Laakso, M. (1998). Serum uric acid is a strong predictor of stroke in patients with non-insulin-dependent diabetes mellitus. *Stroke* 29, 635–639. doi: 10.1161/01.str.29.3.635
- Levey, A. S., Stevens, L. A., Schmid, C. H., Zhang, Y. L., Castro, A. F. III, Feldman, H. I., et al. (2009). A new equation to estimate glomerular filtration rate. *Ann. Intern. Med.* 150, 604–612. doi: 10.7326/0003-4819-150-9-200905050-00006
- Li, J., Muraki, I., Imano, H., Cui, R., Yamagishi, K., Umesawa, M., et al. (2020). Serum uric acid and risk of stroke and its types: the Circulatory Risk in Communities Study (CIRCS). *Hypertens Res.* 43, 313–321. doi: 10.1038/s41440-019-0385-5
- Li, M., Hou, W., Zhang, X., Hu, L., and Tang, Z. (2014). Hyperuricemia and risk of stroke: a systematic review and meta-analysis of prospective studies. *Atherosclerosis* 232, 265–270. doi: 10.1016/j.atherosclerosis.2013.11.051
- Li, M., Zhan, A., Huang, X., Hu, L., Zhou, W., Wang, T., et al. (2020). Positive association between triglyceride glucose index and arterial stiffness in hypertensive patients: the China H-type Hypertension Registry Study. *Cardiovasc. Diabetol.* 19:139. doi: 10.1186/s12933-020-01124-2
- Liang, J., Xue, Y., Zou, C., Zhang, T., Song, H., and Qi, L. (2009). Serum uric acid and prehypertension among Chinese adults. *J. Hypertens* 27, 1761–1765. doi: 10.1097/HJH.0b013e32832e0b44
- Liu, Z., Yang, H., Chen, S., Cai, J., and Huang, Z. (2019). The association between body mass index, waist circumference, waist-hip ratio and cognitive disorder in older adults. *J. Public Health (Oxf)* 41, 305–312. doi: 10.1093/pubmed/fdy121
- Maloberti, A., Giannattasio, C., Bombelli, M., Desideri, G., Cicero, A., Muiesan, M. L., et al. (2020). Hyperuricemia and risk of cardiovascular outcomes: the experience of the URRAH (Uric Acid Right for Heart Health) Project. *High. Blood Press. Cardiovasc. Prev.* 27, 121–128. doi: 10.1007/s40292-020-00368-z
- Martinon, F., Pétrilli, V., Mayor, A., Tardivel, A., and Tschopp, J. (2006). Gout-associated uric acid crystals activate the NALP3 inflammasome. *Nature* 440, 237–241. doi: 10.1038/nature04516
- Ndrepepa, G. (2018a). Elevated serum uric acid: a marker and mediator of increased stress on myocardium. *Coron. Artery Dis.* 29, 183–185. doi: 10.1097/MCA.0000000000000600
- Ndrepepa, G. (2018b). Uric acid and cardiovascular disease. *Clin. Chim. Acta* 484, 150–163. doi: 10.1016/j.cca.2018.05.046
- Pandian, J. D., Gall, S. L., Kate, M. P., Silva, G. S., Akinyemi, R. O., Ovbiagele, B. I., et al. (2018). Prevention of stroke: a global perspective. *Lancet* 392, 1269–1278. doi: 10.1016/S0140-6736(18)31269-8
- Perlstein, T. S., Gumieniak, O., Williams, G. H., Sparrow, D., Vokonas, P. S., Gaziano, M., et al. (2006). Uric acid and the development of hypertension: the normative aging study. *Hypertension* 48, 1031–1036. doi: 10.1161/01.HYP.0000248752.08807.4c
- Sautin, Y. Y., and Johnson, R. J. (2008). Uric acid: the oxidant-antioxidant paradox. *Nucleosides Nucleotides Nucleic Acids* 27, 608–619. doi: 10.1080/15257770802138558
- Shi, X., Yang, J., Wang, L., Zhao, M., Zhang, C., He, M., et al. (2017). Prospective study of serum uric acid levels and stroke in a Chinese hypertensive cohort. *Clin. Exp. Hypertens* 39, 527–531. doi: 10.1080/10641963.2017.1281938
- Shi, Y., Evans, J. E., and Rock, K. L. (2003). Molecular identification of a danger signal that alerts the immune system to dying cells. *Nature* 425, 516–521. doi: 10.1038/nature01991
- Sinha, S., Singh, S. N., and Ray, U. S. (2009). Total antioxidant status at high altitude in lowlanders and native highlanders: role of uric acid. *High. Alt. Med. Biol.* 10, 269–274. doi: 10.1089/ham.2008.1082
- Tatsumi, Y., Asayama, K., Morimoto, A., Satoh, M., Sonoda, N., Miyamatsu, N., et al. (2020). Hyperuricemia predicts the risk for developing hypertension independent of alcohol drinking status in men and women: the Saku study. *Hypertens Res.* 43, 442–449. doi: 10.1038/s41440-019-0361-0
- Toncev, G., Milicic, B., Toncev, S., and Samardzic, G. (2002). Serum uric acid levels in multiple sclerosis patients correlate with activity of disease and blood-brain

- barrier dysfunction. *Eur. J. Neurol.* 9, 221–226. doi: 10.1046/j.1468-1331.2002.00384.x
- Tu, W., Wu, J., Jian, G., Lori, J., Tang, Y., Cheng, H., et al. (2019). Asymptomatic hyperuricemia and incident stroke in elderly Chinese patients without comorbidities. *Eur. J. Clin. Nutr.* 73, 1392–1402. doi: 10.1038/s41430-019-0405-1
- Wang, P., Li, X., He, C., Zhai, Y., Sun, H., Zhang, Y., et al. (2019). Hyperuricemia and prognosis of acute ischemic stroke in diabetic patients. *Neurol. Res.* 41, 250–256. doi: 10.1080/01616412.2018.1553347
- Wang, Z., Chen, Z., Zhang, L., Wang, X., Hao, G., Zhang, Z., et al. (2018). Status of hypertension in china: results from the china hypertension survey, 2012–2015. *Circulation* 137, 2344–2356. doi: 10.1161/CIRCULATIONAHA.117.032380
- Watanabe, S., Kang, D. H., Feng, L., Nakagawa, T., Kanellis, J., Lan, H., et al. (2002). Uric acid, hominoid evolution, and the pathogenesis of salt-sensitivity. *Hypertension* 40, 355–360. doi: 10.1161/01.hyp.0000028589.66335.aa
- Yen, F. S., Hsu, C. C., Li, H. L., Wei, J. C., and Hwu, C. M. (2020). Urate-lowering therapy may mitigate the risks of hospitalized stroke and mortality in patients with gout. *PLoS One* 15:e0234909. doi: 10.1371/journal.pone.0234909
- Yu, Z. F., Bruce-Keller, A. J., Goodman, Y., and Mattson, M. P. (1998). Uric acid protects neurons against excitotoxic and metabolic insults in cell culture, and against focal ischemic brain injury in vivo. *J. Neurosci. Res.* 53, 613–625. doi: 10.1002/(SICI)1097-4547(19980901)53:5<613::AID-JNR111>3.0.CO;2-1
- Zhang, S., Liu, L., Huang, Y. Q., Lo, K., Tang, S., and Feng, Y. Q. (2020). The association between serum uric acid levels and ischemic stroke in essential hypertension patients. *Postgrad. Med.* 132, 551–558. doi: 10.1080/00325481.2020.1757924

Conflict of Interest: The authors declare that the research was conducted in the absence of any commercial or financial relationships that could be construed as a potential conflict of interest.

Publisher's Note: All claims expressed in this article are solely those of the authors and do not necessarily represent those of their affiliated organizations, or those of the publisher, the editors and the reviewers. Any product that may be evaluated in this article, or claim that may be made by its manufacturer, is not guaranteed or endorsed by the publisher.

Copyright © 2021 Hu, Hu, Yu, Han, Zhou, Wang, Zhu, Huang, Bao and Cheng. This is an open-access article distributed under the terms of the Creative Commons Attribution License (CC BY). The use, distribution or reproduction in other forums is permitted, provided the original author(s) and the copyright owner(s) are credited and that the original publication in this journal is cited, in accordance with accepted academic practice. No use, distribution or reproduction is permitted which does not comply with these terms.



OPEN ACCESS

Edited by:

Kangkang Zhi,
Shanghai Changzheng Hospital,
China

Reviewed by:

Yanmin Zhang,
Xi'an Jiaotong University, China
Patrik Andersson,
Massachusetts General Hospital
and Harvard Medical School,
United States

*Correspondence:

Kai Huang
Huangkai1@hust.edu.cn
Minglu Liang
liangml@hust.edu.cn

† These authors have contributed
equally to this work and share first
authorship

Specialty section:

This article was submitted to
Vascular Physiology,
a section of the journal
Frontiers in Physiology

Received: 06 October 2021

Accepted: 30 December 2021

Published: 03 February 2022

Citation:

Fan S, Wang C, Huang K and
Liang M (2022) Myricanol Inhibits
Platelet Derived Growth
Factor-BB-Induced Vascular Smooth
Muscle Cells Proliferation
and Migration *in vitro* and Intimal
Hyperplasia *in vivo* by Targeting
the Platelet-Derived Growth Factor
Receptor- β and NF- κ B Signaling.
Front. Physiol. 12:790345.
doi: 10.3389/fphys.2021.790345

Myricanol Inhibits Platelet Derived Growth Factor-BB-Induced Vascular Smooth Muscle Cells Proliferation and Migration *in vitro* and Intimal Hyperplasia *in vivo* by Targeting the Platelet-Derived Growth Factor Receptor- β and NF- κ B Signaling

Siyuan Fan^{1,2†}, Cheng Wang^{2,3†}, Kai Huang^{1,2,3*} and Minglu Liang^{2*}

¹ Cardiovascular Center, Liyuan Hospital, Tongji Medical College, Huazhong University of Science and Technology, Wuhan, China, ² Clinic Center of Human Gene Research, Union Hospital, Tongji Medical College, Huazhong University of Science and Technology, Wuhan, China, ³ Department of Cardiology, Union Hospital, Tongji Medical College, Huazhong University of Science and Technology, Wuhan, China

The abnormal proliferation and migration of Vascular smooth muscle cells (VSMCs) are related to many cardiovascular diseases, including atherosclerosis, restenosis after balloon angioplasty, hypertension, etc. Myricanol is a diarylheptanoid that can be separated from the bark of *Myrica rubra*. It has been reported that myricanol can anti-inflammatory, anti-cancer, anti-neurodegenerative, promote autophagic clearance of tau and prevent muscle atrophy. But its potential role in the cardiovascular field remains unknown. In this study, we investigated the effect of myricanol on the proliferation and migration of VSMCs *in vitro* and on the intimal hyperplasia *in vivo*. *In vitro* experiments, we found myricanol can inhibit the proliferation and migration of VSMCs induced by PDGF-BB. In terms of mechanism, the preincubation of myricanol can suppress the PDGF-BB induced phosphorylation of PDGFR β and its downstream such as PLC γ 1, Src, and MAPKs. In addition, NF- κ B p65 translocation was also suppressed by myricanol. *In vivo* experiments, we found myricanol can suppress the intimal hyperplasia after wire ligation of the carotid artery in mice. These results may provide a new strategy for the prevention and treatment of coronary atherosclerosis and post-stent stenosis in the future.

Keywords: myricanol, vascular smooth muscle cells, PDGF-BB, PDGFR β , intimal hyperplasia

INTRODUCTION

VSMCs are an important part of the blood vessel wall. The abnormal proliferation and migration of VSMCs are related to many diseases, including atherosclerosis, restenosis after balloon angioplasty, hypertension, etc. (Owens et al., 2004; Bennett et al., 2016). Therefore, it is necessary to inhibit abnormal proliferation and migration of VSMCs for the treatment of many diseases.

A variety of growth factors, signal molecules, and transcription factors regulates the proliferation and migration of VSMCs, in which the PDGFR β -mediated pathway plays an important role (Owens et al., 2004). Platelet-derived growth factor receptor- β (PDGFR β) is a typical receptor tyrosine kinase, whose natural ligand is platelet Derived Growth Factor-BB (PDGF-BB) (Fredriksson et al., 2004). PDGF-BB is also one of the most powerful mitogens and chemokines of VSMC and occupies an important place in a variety of vascular diseases (Ferns et al., 1991; Ross, 1993; Pompili et al., 1995; Schwartz, 1997; Heldin and Westermark, 1999). Once PDGF-BB binds PDGFR β , many pathways [such as Src, PLC γ 1 and mitogen-activated protein kinases (MAPKs)] will be activated, which promotes the proliferation and migration of cells (Andrae et al., 2008).

Myrica rubra is a traditional crop mainly grow in China and Southeast Asia, whose bark is Chinese traditional medicine used for burns and skin diseases (Kim et al., 2013). Recently, researchers have reported that several chemical constituents isolated from the bark of Myrica rubra are well recognized for their medicinal values (Shen et al., 2019), such as quercetin, dihydromyricetin, and myricetin. Myricanol is a diarylheptanoid (Yoshimura et al., 2012) that can be separated from the bark of Myrica rubra by a systematic method (Inoue, 1993). According to recent researches, myricanol has a wide variety of bioactivities such as anti-inflammatory, anti-cancer, anti-neurodegenerative, promote autophagic clearance of tau and prevent muscle atrophy (Shen et al., 2019). But its potential role in the cardiovascular field remains unknown.

Therefore, in this study, we investigated the effect of myricanol on the proliferation and migration of VSMCs *in vitro* and *in vivo*. *In vitro*, we investigated the effect of myricanol on PDGF-BB-induced proliferation and migration of VSMCs. *In vivo*, we investigated the effect of myricanol on intimal hyperplasia induced by carotid artery ligation in mice.

MATERIALS AND METHODS

Reagents

Myricanol was purchased from ChemFaces (Wuhan, China). Dulbecco's Modified Eagle's Medium (DMEM) and fetal bovine serum (FBS) were purchased from GIBCO. Recombinant human PDGF-BB was purchased from Corning Incorporated. EdU kit was purchased from Ribobio. Antibodies of the total levels and phosphorylation of PDGFR α , PDGFR β , PLC γ 1, Src, ERK1/2, JNK, p38, Rb, and p65 were purchased from Cell Signaling Technology. Anti-metalloproteinase 2 (MMP2), anti-matrix metalloproteinase 9 (MMP9), anti-Cyclin D1 (CCND1), and anti-Cyclin E1 (CCNE1) were purchased from Abcam. PCNA, E2F1, P21, P27, P53, Caspase 3, BAX, BCL2, and GAPDH were purchased from proteintech.

Cell Culture

Primary VSMCs were isolated from the thoracic aortas of SD rats weighing 150–180 g in an enzymatical way. Rat aortic arteries were removed under sterile conditions. Adventitia from the aorta was removed under a dissecting microscope. The aorta was

cut into pieces approximately 1–2 mm sections and digested with Enzyme solution (collagenase type II 3 mg/ml and elastase 1 mg/ml) for 2 h. Then cells were cultured in a flask with DMEM supplemented with 15% FBS, and passage 3–6 were used for experiments (Supplementary Figure 1).

EdU Incorporation Assay

In starvation conditions, VSMCs were treated with indicated concentrations myricanol or not for 30 min, then VSMCs were treated with PDGF-BB (30 ng/ml) for 12 h and cultured into 96-well plates (3×10^3 cells/well). After incubation with a medium containing EdU for another 2 h, the cells were fixed with 4% paraformaldehyde, and EdU Incorporation Assay was performed according to the manufacturer's instructions. Images were photographed by using Olympus cellSens Entry.

Migration Assay

For the wound healing assay, VSMCs in a 6-well plate with about 90% confluence were treated with indicated concentrations myricanol or not for 30 min in starvation conditions, then VSMCs were treated with PDGF-BB (30 ng/ml). Cell monolayers were scratched by a 200- μ l pipette tip and photos were taken under a microscope (Olympus) at 0 and 24 h.

For transwell migration assay, VSMCs were treated with indicated concentrations myricanol or not for 30 min in starvation conditions, then VSMCs were treated with PDGF-BB (30 ng/ml). Then 1×10^5 VSMCs were detached and suspended into a transwell upper surface with 200 μ l of DMEM medium with FBS free. 500 μ l of FBS-free DMEM medium with PDGF-BB (30 ng/ml) was added in the lower chamber. After 24 h incubation at 37°C, the migrated cells were fixed in 4% paraformaldehyde for 30 min, stained in 0.1% crystal violet for 15 min and photographed by microscope for six randomly assigned fields (Olympus).

Western Blot

The VSMCs were cultured into six-well plates up to 80% confluence. After being pretreated with indicated concentrations of myricanol or vehicle for 30 min, the cells were stimulated by PDGF-BB (30 ng/ml) for 5, 15, 60 min or another 24 h. Western blotting was performed following procedures described previously (Wang et al., 2019).

Nuclear and Cytoplasmic Extracts

Primary VSMCs were seeded in a round cell culture dish with a diameter of 60 mm. After the density reached 80% confluence, the cells were preadministrated with vehicle or myricanol at a concentration of 30 μ M, and PDGF-BB was administered 30 min later. After 4 h, a nuclear protein and cytoplasmic protein extraction kit (Beyotime, P0027) was used to extract the nuclear and cytosolic proteins.

Immunofluorescence Analysis

Primary VSMCs were seeded in a round cell culture dish with a diameter of 15 mm. The cells were preadministrated with vehicle or myricanol at a concentration of 30 μ M, and PDGF-BB was administered 15 min later. The cells were fixed in 4%

formaldehyde for 30 min and immunostained with p65 (CST, #8242) antibodies overnight at 4°C, then incubated with the indicated secondary antibodies for 1 h at 37°C. Nuclei were stained with DAPI for 20 min at 37°C. Photos were taken under a fluorescence microscope (Olympus).

Carotid Artery Wire Ligation Injury Model

Animal housing and procedures were approved by the Institutional Animal Care and Use Committee (IACUC) of Huazhong University of Science and Technology, and IACUC number is 2561. Surgery was performed under sterile conditions. Eight-week-old male C57BL/6 mice were anesthetized with an intraperitoneal injection of pentobarbital sodium. In ligated animals ($n = 6$), the left common carotid artery was dissected from the surrounding tissue under a microscope and ligated by using 6–0 silk suture. The right common carotid artery was dissected without ligation as a sham surgery. Then, mice were randomly divided into two groups on average. Myricanol (5 mg/kg/day) or hydration medium (PEG 400) was intraperitoneally injected into C57BL/6 mice for 14 days. Then mice were euthanized and common carotid arteries were excised. After being fixed with 4% formaldehyde and embedded in paraffin, Cross-sections of the common carotid artery were stained with hematoxylin and eosin (H&E) and elastic Masson trichrome solutions.

Statistical Analysis

SPSS v.20 was used for statistical analyses. All experiments were performed at least three times, and data are given as means \pm SEM. The two-tailed unpaired Student's *t*-test was used for comparisons of two groups and differences were considered significant at $P < 0.05$.

RESULTS

Myricanol Inhibits the Proliferation of Vascular Smooth Muscle Cells Induced by Platelet Derived Growth Factor-BB

When VSMCs are activated by various injury stimuli, they change from a resting state to a proliferative phenotype and migrate under the intima. To investigate the effect of myricanol on PDGF-BB-induced VSMCs proliferation, we performed a EdU assay. The results showed that the ability of cell proliferation was significantly improved under the stimulation of PDGF-BB and was apparently inhibited by myricanol. We found that the effect of myricanol on VSMC proliferation is dose-dependent. For example, 3 μ M of myricanol treatment showed no significant influence, whereas both 10 and 30 μ M of myricanol can significantly suppressed the proliferation of VSMCs (Figures 1A,B).

Under the action of extracellular stimulus, the expression of contractile protein in VSMC is significantly reduced, while the expression of cell cycle-related proteins increases rapidly. As shown in Figures 1C,D, the protein level of PCNA, E2F1, phosphorylated Rb, Rb, CCND1, CCNE1, p21, p27, and p53

were detected by western blot analysis. We find that CCND1, CCNE1, PCNA, E2F1, and p-Rb were significantly increased by PDGF-BB stimulation, whereas the myricanol treatment can partially or completely block the effects. Meanwhile, p53 was significantly inhibited by PDGF-BB stimulation, whereas the myricanol treatment can partially recover the effects. Different from the above results, PDGF-BB stimulation had no effect on the expression of p21 and p27, while preadministrated of myricanol increased the expression of p21.

To further confirm the effect of myricanol on cell apoptosis and necrosis, western blot and LDH assays were performed. Western blot results showed that PDGF-BB and myricanol had no effect on the protein level of caspase 3, cleaved caspase3, BAX and BCL2. LDH assay showed that PDGF-BB and myricanol had no effect on LDH release (Supplementary Figure 2). These results indicated that myricanol have no effect on cell apoptosis and necrosis.

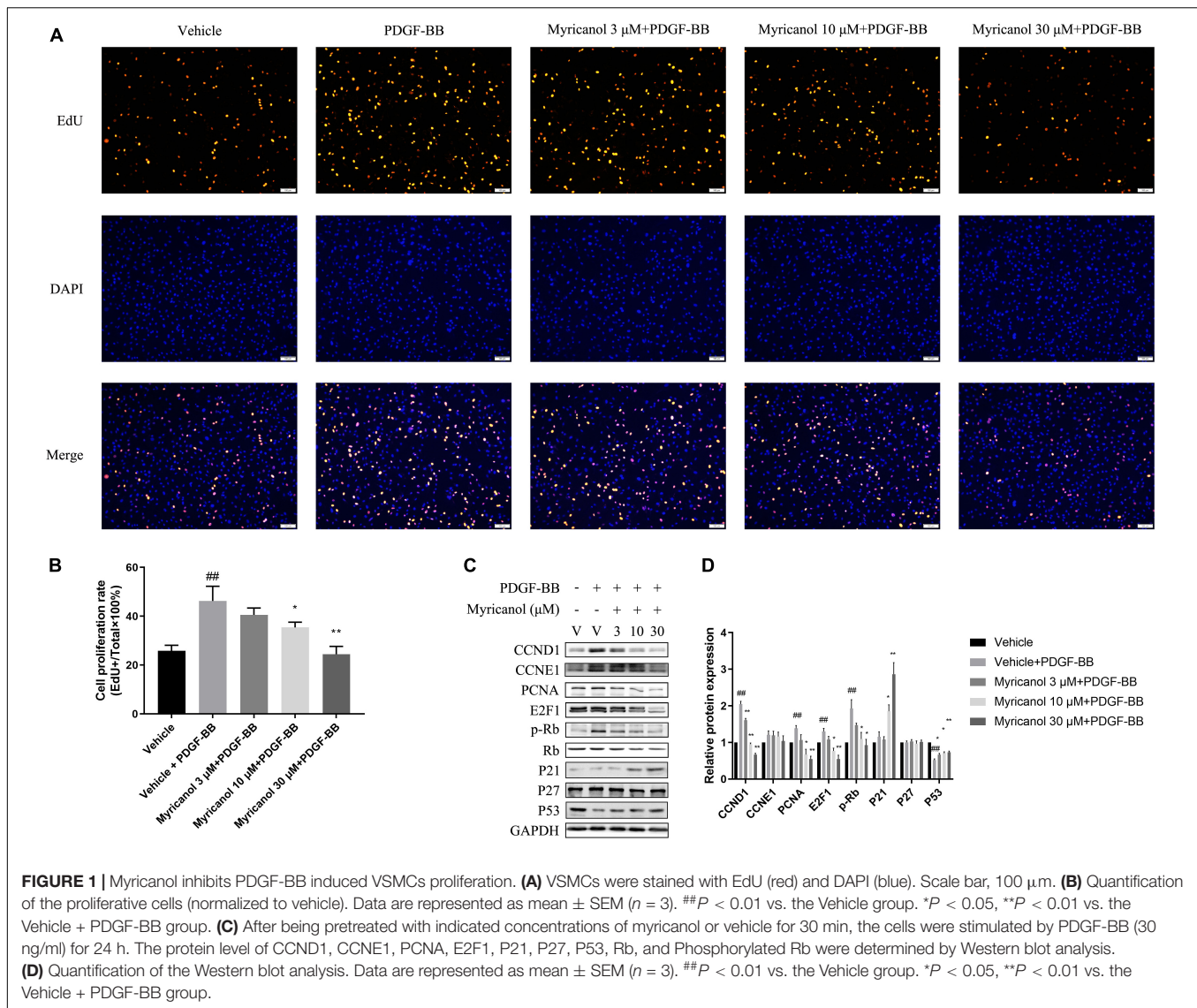
Myricanol Inhibits the Migration of Vascular Smooth Muscle Cells Induced by Platelet Derived Growth Factor-BB

To investigate whether myricanol was able to affect the migration in VSMCs, We then assessed the effect by wound healing assay and transwell migration assay (Figures 2A,C). The wound healing assay result showed that 10 and 30 μ M myricanol but not 3 μ M of myricanol could partially suppress the migration induced by PDGF-BB stimulation, and the result of the transwell migration assay seems to be similar. The migration of VSMCs was shown by the distance of the gap in the wound healing assay (Figure 2B) and the migration cell number in the transwell migration assay (Figure 2D).

In the process of intimal hyperplasia, a large number of proteoglycans and extracellular matrix remodeling related proteins (such as MMP2, MMP9) are synthesized and secreted to promote the migration of VSMCs. Therefore, the protein levels of migration-associated protein MMP2 and MMP9 were detected by western blot analysis, which increased by PDGF-BB stimulation. However, the effect on MMP2 and MMP9 seems to be different. The increasing of MMP9 protein level was significantly suppressed at 3, 10, and 30 μ M myricanol, however, increasing of MMP2 protein level can only be significantly suppressed at 30 μ M myricanol (Figures 2E,F). Further, consistent with the above results, the activity of MMP2 and MMP9 were increased by PDGF-BB stimulation, while the myricanol treatment can partially or completely block the effects as shown in Zymography assays (Supplementary Figure 3).

Myricanol Inhibits the Activation of Platelet-Derived Growth Factor Receptor Pathway and NF- κ B p65 Translocation Induced by Platelet Derived Growth Factor-BB

At present, it is known that a variety of cell pathways and their effector molecules in VSMC have undergone significant changes, and they jointly participate in the coordinated regulation of



VSMC proliferation and migration, of which PDGFR β pathway is the most important (Levitzi, 2005; Wang Y. et al., 2020). To investigate how myricanol influences the proliferation and migration of VSMC induced by PDGF-BB, we tested if myricanol could suppress the phosphorylation of PDGFR α , PDGFR β and its downstream PLC γ 1, Src and MAPK in VSMC. VSMCs were treated with vehicle or 30 μ M myricanol 30 min before exposure to PDGF-BB, and then cells were stimulated by PDGF-BB and the cytosolic products were harvested at different time point after stimulation (5 min, 15 min, 60 min). The expression of p-PDGFR α ^{Y1018}, p-PDGFR β ^{Y751}, p-PDGFR β ^{Y857}, p-PDGFR β ^{Y1021}, p-PLC γ 1, p-Src, p-JNK, p-ERK1/2, and p-p38 were increased after PDGF-BB stimulation in 5, 15, and 60 min, and pretreatment with 30 μ M myricanol repressed the phosphorylation of these proteins (except p-JNK) at the same time points after PDGF-BB stimulation (Figure 3). The specific inhibitors for PDGFR β , JNK, ERK1/2 and p38 were provided to verify the effect of myricanol. The results showed

that myricanol has weaker inhibitory effect on PDGFR α ^{Y1018}, p-PDGFR β ^{Y751}, p-PDGFR β ^{Y857}, p-PDGFR β ^{Y1021}, p-ERK1/2 and p-p38 than PDGFR β , JNK, ERK1/2 and p38 inhibitors (Supplementary Figure 4).

In addition, NF- κ B is a critical signaling in VSMC proliferation and migration (Lu et al., 2018). Our results exhibited that myricanol can inhibit the phosphorylation level of I κ B α and p65 and the nuclear translocation of p65 stimulated by PDGF-BB in VSMC (Figure 4).

Myricanol Inhibits the Neointimal Hyperplasia Induced by Carotid Artery Ligation

To assess the effect of myricanol on intimal hyperplasia after vascular injury, we used the carotid artery wire ligation model. Myricanol (5 mg/kg/day) or hydration medium (PEG 400) was intraperitoneally injected for 14 days after carotid artery ligation.

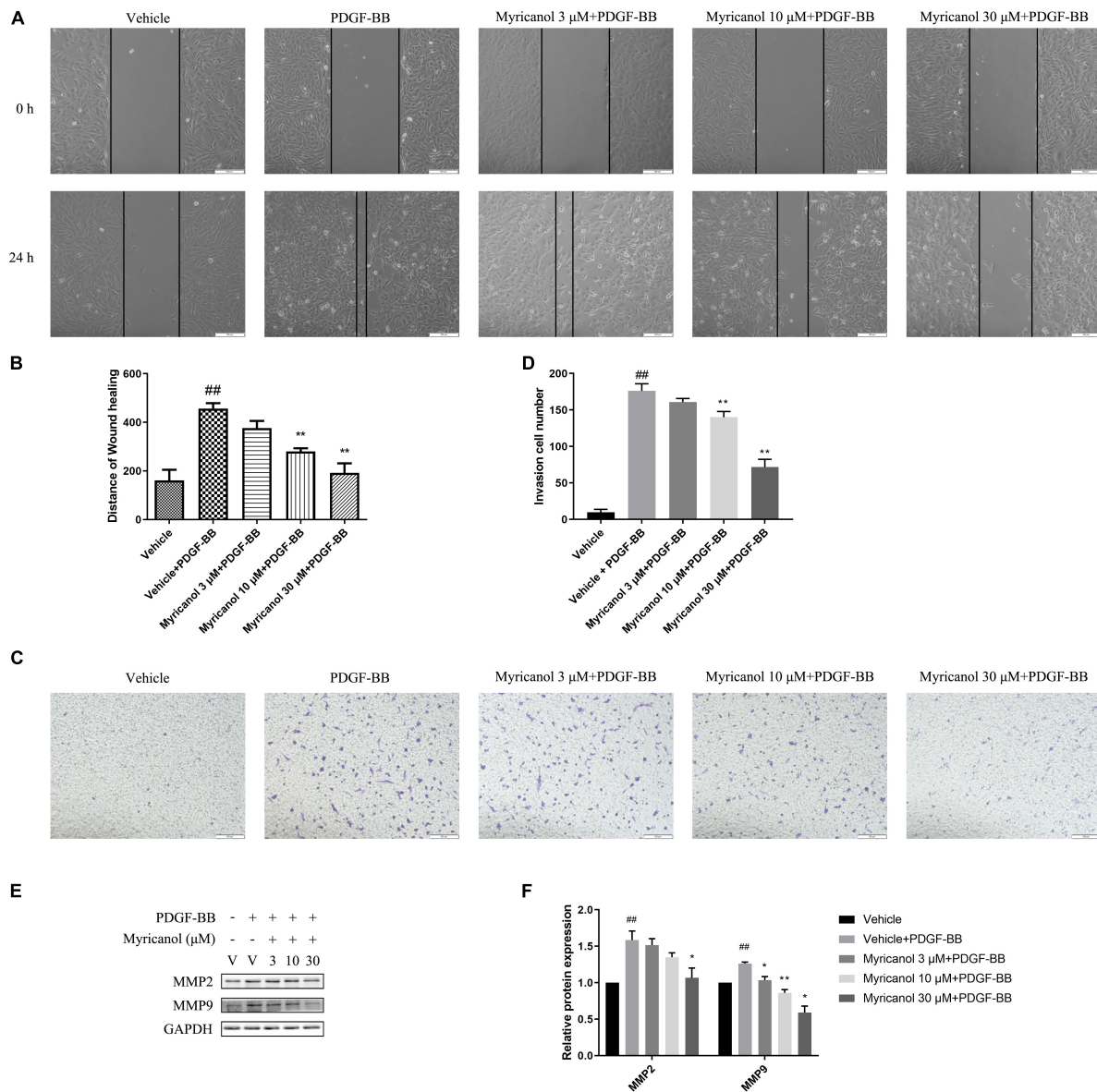


FIGURE 2 | Myricanol inhibits VSMCs migration. **(A)** In starvation conditions, cells were treated with indicated concentrations myricanol or not for 30 min, then scratched and treated with PDGF-BB (30 ng/ml) for 24 h. Scale bar, 100 μm. **(B)** Quantification of the area of wound closure (%). Data are represented as mean ± SEM ($n = 3$). ^{##} $P < 0.01$ vs. the Vehicle group. ^{**} $P < 0.01$ vs. the Vehicle + PDGF-BB group. **(C)** After treated with PDGF-BB and myricanol for 24 h, a transwell migration assay of VSMCs was performed and representative images were shown. Scale bar, 100 μm. **(D)** Quantification of migrated cells. Data are represented as mean ± SEM ($n = 3$). ^{##} $P < 0.01$ vs. the Vehicle group. ^{**} $P < 0.01$ vs. the Vehicle + PDGF-BB group. **(E)** After being pretreated with indicated concentrations of myricanol or vehicle for 30 min, the cells were stimulated by PDGF-BB (30 ng/ml) for 24 h. The protein level of MMP2 and MMP9 were determined by Western blot analysis. **(F)** Quantification of the Western blot analysis. Data are represented as mean ± SEM ($n = 3$). ^{##} $P < 0.01$ vs. the Vehicle group. ^{*} $P < 0.05$, ^{**} $P < 0.01$ vs. the Vehicle + PDGF-BB group.

Comparing with the Sham surgery group, the ligation surgery group showed that intimal hyperplasia was well developed. The sections stained with elastic Masson trichrome solutions were used to highlight the media (**Figure 5A**). Comparing with the ligation surgery group, the myricanol treated ligation surgery group showed significantly reduced intima, both the ratio of intima to media (I/M ratio) and intimal area (**Figures 5B,C**). Immunofluorescence staining showed that the myricanol-treated

ligation surgery group had significantly inhibited Ki67 expression (**Supplementary Figures 5A,B**). In addition, macrophages are known to play a role in the progression of intimal hyperplasia and other cardiovascular disorders (Zhang et al., 2021). Our results exhibited that the expression of F4/80 significantly increased in the ligation surgery group comparing with the sham surgery group, While the myricanol treatment significantly decreased F4/80 expression (**Supplementary Figures 5C,D**). These results

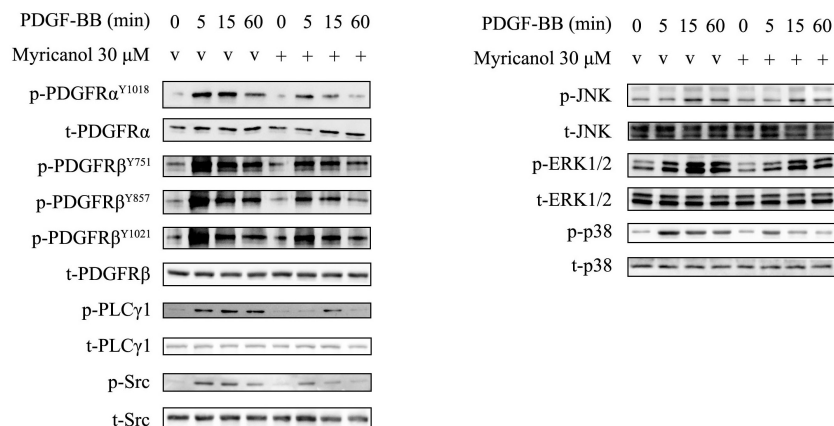
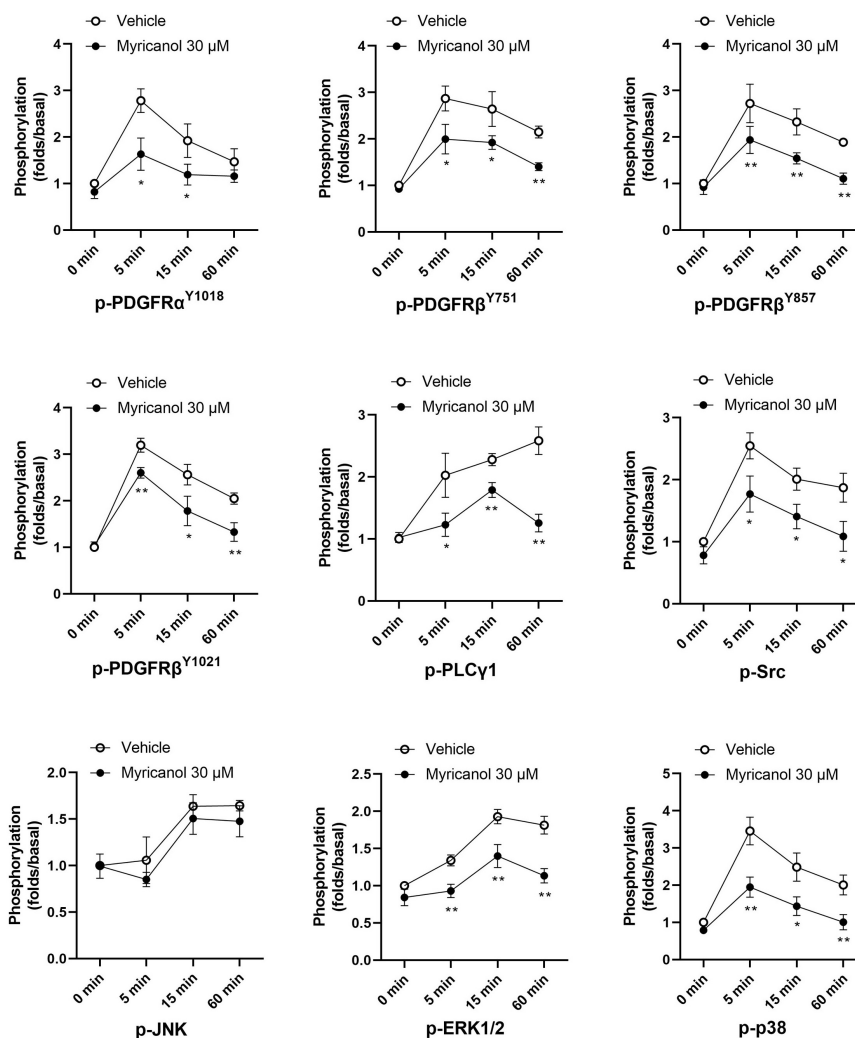
A**B**

FIGURE 3 | Effect of myricanol on the phosphorylation of PDGFR β , PLC γ 1, Src and downstream MAPKs. **(A)** The protein level of phosphorylated PDGFR α , PDGFR β , PLC γ 1 and p38 were determined by Western blot analysis. **(B)** Quantification of the Western blot analysis. Data are represented as mean \pm SEM ($n = 3$). * $P < 0.05$, ** $P < 0.01$ vs. the Vehicle + PDGF-BB group.

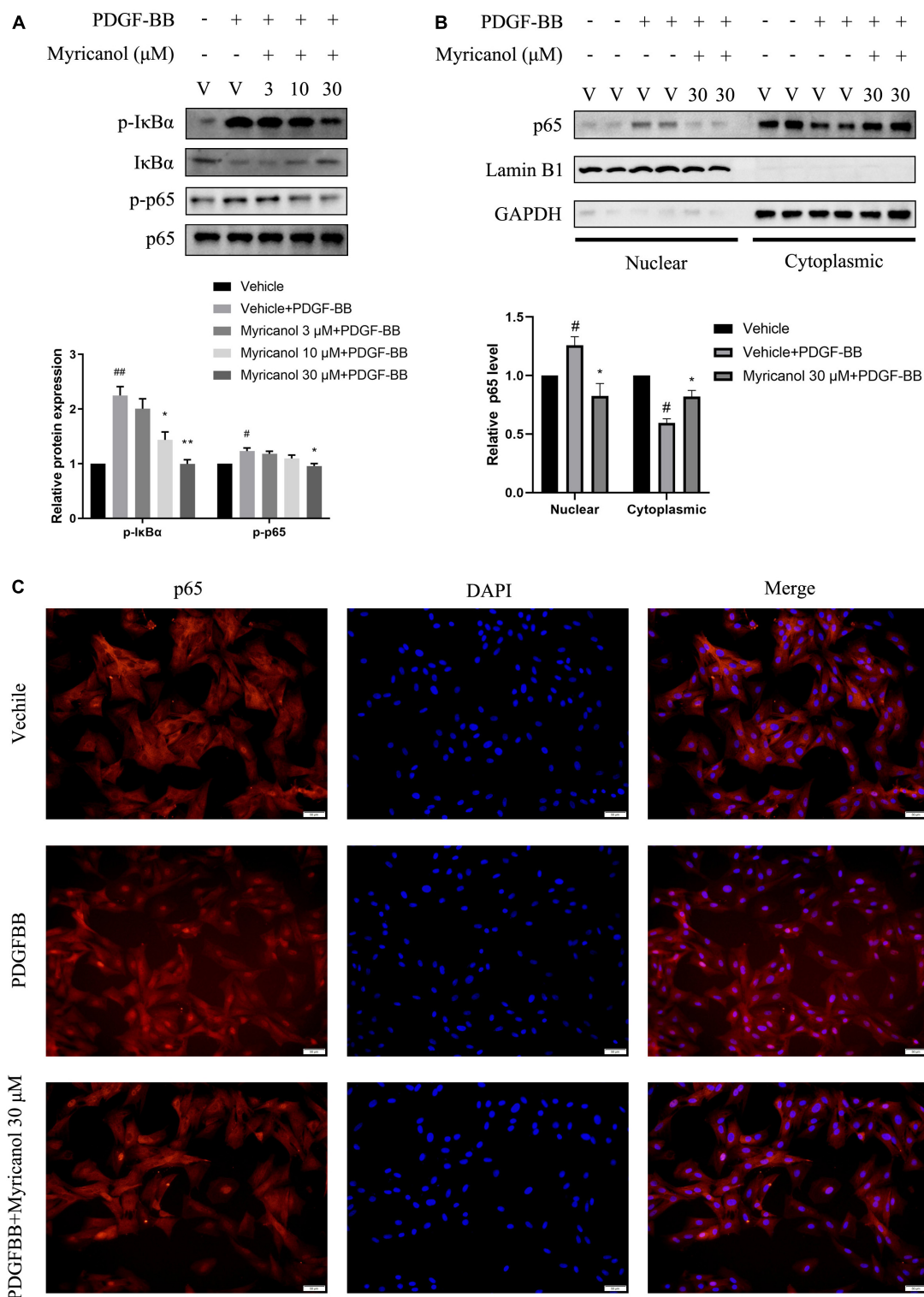


FIGURE 4 | Effects of myricanol on PDGF-BB-induced NF- κ B signaling in VSMCs. **(A)** After being pretreated with indicated concentrations of myricanol or vehicle for 30 min, the cells were stimulated by PDGF-BB (30 ng/ml) for 5 min. The protein level of p-IkBa, IkBa were determined by Western blot analysis. After being pretreated with indicated concentrations of myricanol or vehicle for 30 min, the cells were stimulated by PDGF-BB (30 ng/ml) for 30 min. The protein level of p-p65 and p65 were determined by Western blot analysis. **(B)** p65 nuclear translocation was analyzed by Western blot analysis. **(C)** p65 nuclear translocation was analyzed by immunocytochemistry. Scale bar, 50 μ m. Data are represented as mean \pm SEM ($n = 3$). $\#P < 0.05$, $\#\#P < 0.01$ vs. the Vehicle group. $*P < 0.05$, $**P < 0.01$ vs. the Vehicle + PDGF-BB group.

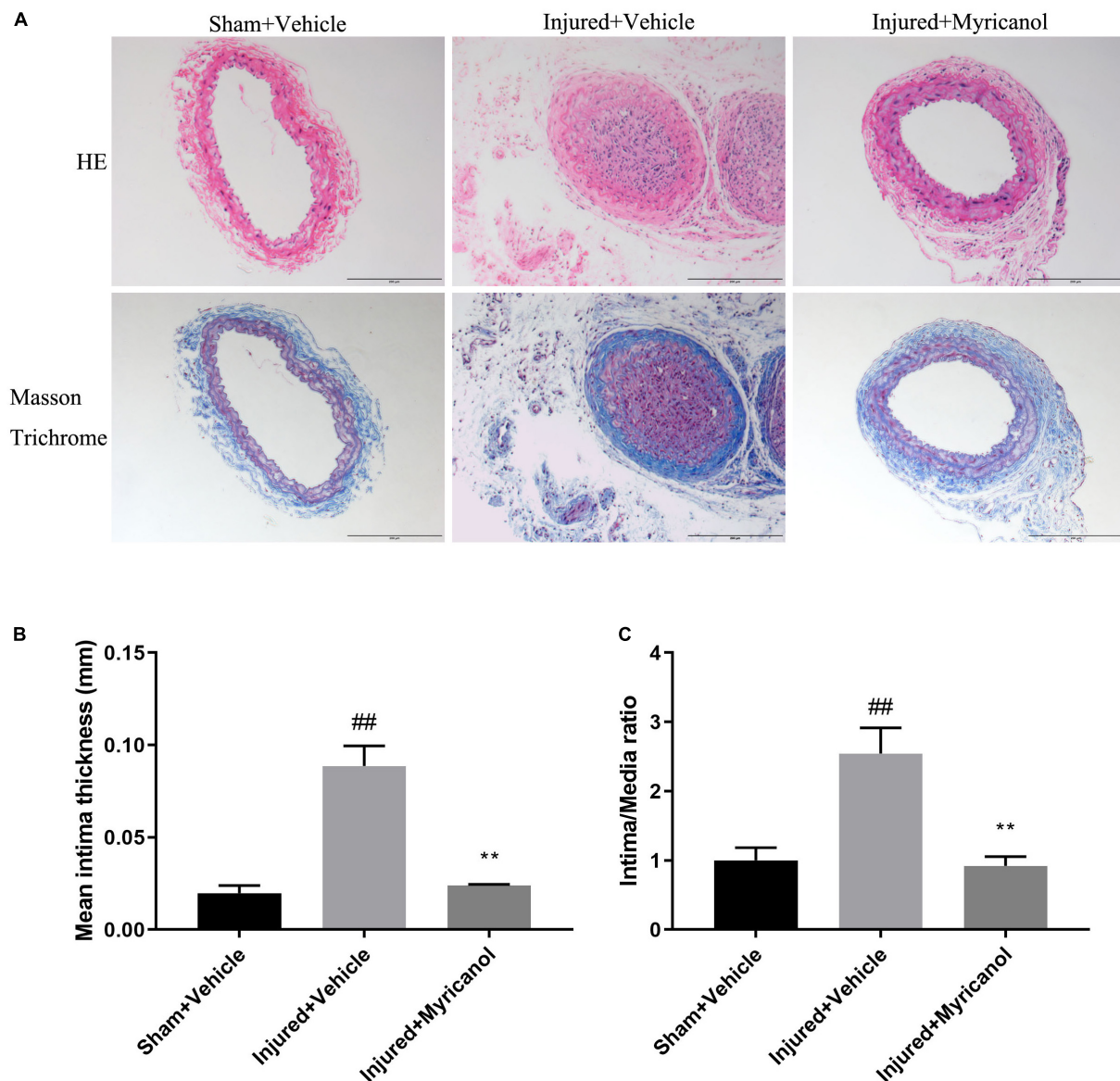


FIGURE 5 | Effect of myricanol on carotid artery ligation induced neointimal hyperplasia for 14 days. **(A)** myricanol (5 mg/kg/day) or hydration medium (PEG 400) was intraperitoneally injected for 14 days after carotid artery ligation. H&E-stained and elastic Masson trichrome-stained sections of all groups were shown. Scale bar, 200 μ m. **(B)** Quantification of the mean intimal thickness. Data are represented as mean \pm SEM ($n = 3$). ^{##} $P < 0.01$ vs. the Sham + Vehicle group. ^{**} $P < 0.01$ vs. the Injured + Vehicle group. **(C)** Quantification of the ratio of intima to media (I/M ratio). Data are represented as mean \pm SEM ($n = 3$). ^{##} $P < 0.01$ vs. the Sham + Vehicle group. ^{**} $P < 0.01$ vs. the Injured + Vehicle group.

indicate that myricanol significantly diminishes the neointimal hyperplasia induced by carotid artery ligation.

DISCUSSION

Intimal hyperplasia is a common physiological feature of cardiovascular diseases such as atherosclerosis and restenosis after angioplasty, and it is closely related to vascular remodeling. Preventing intimal hyperplasia and postoperative restenosis has always been an important research topic worldwide. Our study

for the first time investigated the effect of myricanol on the proliferation and migration of VSMCs *in vitro* and on the intimal hyperplasia *in vivo*, which suggested the therapeutic potential of myricanol in cardiovascular disease.

PDGF-BB had been proved that it can significantly improve the proliferation and migration of VSMCs *in vitro*, playing an important role in the development of many cardiovascular diseases such as atherosclerosis and restenosis (Zhan et al., 2003). Therefore, we studied whether it will be affected by myricanol that the proliferation and migration of VSMCs induced by PDGF-BB.

Firstly the EDU assay showed that myricanol could inhibit the proliferation of VSMCs, and wound healing assay and transwell migration assay showed that myricanol could inhibit the migration of VSMCs. Then, Western blot assay was used to measure the protein levels of cell proliferation and migration marker genes. Compared to the vehicle + PDGF-BB group, the PDGF-BB + Myricanol (10 and 30 μ M) treated group showed significantly lower protein levels of PCNA, E2F1, Phosphorylated Rb, and MMP9. In the early G1 phases cell cycle, the activated cyclin-dependent kinase complexes (CDKCs) are formed by the binding of CCND and CDK4/6. Then CDKCs phosphorylate Rb protein to release E2F, which leads to the transcription of E2F target genes and promotes the G1/S transition (Duronio and Xiong, 2013). We found that myricanol can reduce the protein level of CCND1 and the downstream Rb Phosphorylation, which may lead to the repression of VSMC proliferation. It is reported that the cell proliferation induced by the MAPK pathway is closely bound up with CCND1. MAPKs such as ERK1/2 and JNK can activate c-JUN, which binds to the CCND1 promoter and functions in activating transcription of CCND1 (Wee and Wang, 2017). Inhibition of ERK1/2 by curcumin and PD98059, and JNKs by SP600125 could reduce the induction of CCND1 (Qin et al., 2014; Wang H. et al., 2020). MAPKs such as ERK1/2 and p38 also play important roles in the regulation of MMP9 expression. Completely inhibiting of either p38 or ERK1/2 alone or both of them can totally downregulate MMP9 expression (Cho et al., 2000). All these results suggest that the MAPK pathway may be related to the repression of proliferation and migration induced by myricanol. Therefore, we investigated the effect of myricanol on the MAPK pathway and the upstream PDGFR β pathway.

The signal of PDGF-BB is transmitted by PDGFR β . Once PDGFR β is bound to PDGF-BB, it will experience autophosphorylation and activate downstream signal pathways such as Src, PLC, and MAPK, which promote PDGF-BB induced proliferation and migration of VSMC (Zhan et al., 2003; Andrae et al., 2008). Mitogen-activated protein kinases (MAPKs) play an important role in the proliferation and migration of VSMCs induced by PDGF-BB (Andrae et al., 2008), which is known as one of the most famous pathways regulating many cell functions such as proliferation, gene expression, differentiation, and mitosis (Johnson and Lapadat, 2002). Our results showed that myricanol could suppress the proliferation and migration of VSMC by inhibiting the phosphorylation of PDGFR β and its downstream PLC γ 1, Src, and MAPKs including ERK1/2 and p38. These results are consistent with our previous speculation. In addition, we also tested the effect of myricanol on NF- κ B signal pathway stimulated by PDGF-BB, and the results showed that myricanol can also inhibit the phosphorylated level of p65 and the nuclear translocation of p65.

Many tyrosine kinase inhibitors can suppress the intimal hyperplasia after arterial injury by inhibiting the phosphorylation of PDGFR β (Fishbein et al., 2000; Yu et al., 2001; Cheema et al., 2006; Masuda et al., 2011; Ishii et al., 2013). And p38, as a class of MAPKs, also plays an important role in vascular remodeling caused by balloon injury in rats (Zhan et al., 2003). These clues suggest that myricanol may have the potential to

treat vascular proliferative diseases such as restenosis. Therefore, we assessed the effect of myricanol on intimal hyperplasia after carotid artery wire ligation and found that 14-day treatment of myricanol can significantly diminish the intimal hyperplasia. In addition, inflammatory cytokines produced by activated macrophages are the direct promoters of neointimal formation (Zhang et al., 2021). And our results showed that myricanol can also inhibit the macrophage infiltration after carotid artery wire ligation. So myricanol inhibits the proliferation and migration of smooth muscle cells and the infiltration of macrophages, thereby reducing intimal hyperplasia.

CONCLUSION

In summary, our study illustrates the effect of myricanol on the proliferation and migration of VSMCs both *in vitro* and *in vivo* experiments. On the one hand, myricanol can inhibit the proliferation and migration of VSMC by suppressing many signaling pathways, including PDGFR β and NF- κ B signaling. On the other hand, Myricanol can suppress the intimal hyperplasia after wire ligation of the carotid artery in mice. These results may provide a new strategy for cardiovascular diseases caused by the abnormal proliferation of VSMC.

DATA AVAILABILITY STATEMENT

The raw data supporting the conclusions of this article will be made available by the authors, without undue reservation.

ETHICS STATEMENT

The animal study was reviewed and approved by the Local Animal Care and Use Committee of Huazhong University of Science and Technology.

AUTHOR CONTRIBUTIONS

ML and KH conceived, designed the experiments, prepared, and revised the manuscript. SF and CW performed the experiments and prepared the manuscript. All authors gave final approval.

FUNDING

This study was supported by the National Natural Science Foundation of China (Grant Nos. 91949201 and 81830014), and the Natural Science Foundation of Hubei Province (2020CFB429).

SUPPLEMENTARY MATERIAL

The Supplementary Material for this article can be found online at: <https://www.frontiersin.org/articles/10.3389/fphys.2021.790345/full#supplementary-material>

REFERENCES

- Andrae, J., Gallini, R., and Betsholtz, C. (2008). Role of platelet-derived growth factors in physiology and medicine. *Genes Dev.* 22, 1276–1312. doi: 10.1101/gad.1653708
- Bennett, M. R., Sinha, S., and Owens, G. K. (2016). Vascular smooth muscle cells in atherosclerosis. *Circ. Res.* 118, 692–702. doi: 10.1161/circresaha.115.306361
- Cheema, A. N., Hong, T., Nili, N., Segev, A., Moffat, J. G., Lipson, K. E., et al. (2006). Adventitial microvessel formation after coronary stenting and the effects of SU11218, a tyrosine kinase inhibitor. *J. Am. Coll. Cardiol.* 47, 1067–1075. doi: 10.1016/j.jacc.2005.08.076
- Cho, A., Graves, J., and Reidy, M. A. (2000). Mitogen-activated protein kinases mediate matrix metalloproteinase-9 expression in vascular smooth muscle cells. *Arterioscler. Thromb. Vasc. Biol.* 20, 2527–2532. doi: 10.1161/01.atv.20.12.2527
- Duronio, R. J., and Xiong, Y. (2013). Signaling pathways that control cell proliferation. *Cold Spring Harb. Perspect. Biol.* 5:a008904. doi: 10.1101/cshperspect.a008904
- Ferns, G. A., Raines, E. W., Sprugel, K. H., Motani, A. S., Reidy, M. A., and Ross, R. (1991). Inhibition of neointimal smooth muscle accumulation after angioplasty by an antibody to PDGF. *Science* 253, 1129–1132. doi: 10.1126/science.1653454
- Fishbein, I., Waltenberger, J., Banai, S., Rabinovich, L., Chorny, M., Levitzki, A., et al. (2000). Local delivery of platelet-derived growth factor receptor-specific tyrophostin inhibits neointimal formation in rats. *Arterioscler. Thromb. Vasc. Biol.* 20, 667–676. doi: 10.1161/01.atv.20.3.667
- Fredriksson, L., Li, H., and Eriksson, U. (2004). The PDGF family: four gene products form five dimeric isoforms. *Cytokine Growth Factor Rev.* 15, 197–204. doi: 10.1016/j.cytogfr.2004.03.007
- Heldin, C. H., and Westermark, B. (1999). Mechanism of action and in vivo role of platelet-derived growth factor. *Physiol. Rev.* 79, 1283–1316. doi: 10.1152/physrev.1999.79.4.1283
- Inoue, T. (1993). Constituents of *Acer nikoense* and *Myrica rubra*. On diarylheptanoids. *Yakugaku Zasshi* 113, 181–197. doi: 10.1248/yakushi1947.113.3_181
- Ishii, S., Okamoto, Y., Katsumata, H., Egawa, S., Yamanaka, D., Fukushima, M., et al. (2013). Sunitinib, a small-molecule receptor tyrosine kinase inhibitor, suppresses neointimal hyperplasia in balloon-injured rat carotid artery. *J. Cardiovasc. Pharmacol. Ther.* 18, 359–366. doi: 10.1177/1074248412472258
- Johnson, G. L., and Lapadat, R. (2002). Mitogen-activated protein kinase pathways mediated by ERK, JNK, and p38 protein kinases. *Science* 298, 1911–1912. doi: 10.1126/science.1072682
- Kim, H. H., Kim, D. H., Kim, M. H., Oh, M. H., Kim, S. R., Park, K. J., et al. (2013). Flavonoid constituents in the leaves of *Myrica rubra* sieb. et zucc. with anti-inflammatory activity. *Arch. Pharm. Res.* 36, 1533–1540. doi: 10.1007/s12272-013-0147-x
- Levitzki, A. (2005). PDGF receptor kinase inhibitors for the treatment of restenosis. *Cardiovasc. Res.* 65, 581–586. doi: 10.1016/j.cardiores.2004.08.008
- Lu, Q. B., Wan, M. Y., Wang, P. Y., Zhang, C. X., Xu, D. Y., Liao, X., et al. (2018). Chicoric acid prevents PDGF-BB-induced VSMC dedifferentiation, proliferation and migration by suppressing ROS/NFkappaB/mTOR/P70S6K signaling cascade. *Redox Biol.* 14, 656–668. doi: 10.1016/j.redox.2017.11.012
- Masuda, S., Nakano, K., Funakoshi, K., Zhao, G., Meng, W., Kimura, S., et al. (2011). Imatinib mesylate-incorporated nanoparticle-eluting stent attenuates in-stent neointimal formation in porcine coronary arteries. *J. Atheroscler. Thromb.* 18, 1043–1053. doi: 10.5551/jat.8730
- Owens, G. K., Kumar, M. S., and Wamhoff, B. R. (2004). Molecular regulation of vascular smooth muscle cell differentiation in development and disease. *Physiol. Rev.* 84, 767–801. doi: 10.1152/physrev.00041.2003
- Pompili, V. J., Gordon, D., San, H., Yang, Z., Muller, D. W., Nabel, G. J., et al. (1995). Expression and function of a recombinant PDGF B gene in porcine arteries. *Arterioscler. Thromb. Vasc. Biol.* 15, 2254–2264. doi: 10.1161/01.atv.15.12.2254
- Qin, L., Yang, Y. B., Yang, Y. X., Gong, Y. Z., Li, X. L., Li, G. Y., et al. (2014). Inhibition of smooth muscle cell proliferation by ezetimibe via the cyclin D1-MAPK pathway. *J. Pharmacol. Sci.* 125, 283–291. doi: 10.1254/jphs.13239fp
- Ross, R. (1993). The pathogenesis of atherosclerosis: a perspective for the 1990s. *Nature* 362, 801–809. doi: 10.1038/362801a0
- Schwartz, S. M. (1997). Smooth muscle migration in atherosclerosis and restenosis. *J. Clin. Invest.* 11(Suppl.), S87–S89.
- Shen, S., Liao, Q., Liu, J., Pan, R., Lee, S. M., and Lin, L. (2019). Myricanol rescues dexamethasone-induced muscle dysfunction via a sirtuin 1-dependent mechanism. *J. Cachexia Sarcopenia Muscle* 10, 429–444. doi: 10.1002/jcsm.12393
- Wang, C., Xu, W., An, J., Liang, M., Li, Y., Zhang, F., et al. (2019). Poly(ADP-ribose) polymerase 1 accelerates vascular calcification by upregulating Runx2. *Nat. Commun.* 10:1203. doi: 10.1038/s41467-019-09174-1
- Wang, H., Xiao, S., Tang, Y., Han, K., Zhang, Z., Jin, Y., et al. (2020). Activation of MAPK and Cyclin D1/CDK4 in malignant transformation of human embryonic lung fibroblasts induced by silica and benzo[a]pyrene. *Asian Pac. J. Cancer Prev.* 21, 295–300. doi: 10.31557/apjcp.2020.21.2.295
- Wang, Y., Hao, Y., Zhao, Y., Huang, Y., Lai, D., Du, T., et al. (2020). TRIM28 and TRIM27 are required for expressions of PDGFRbeta and contractile phenotypic genes by vascular smooth muscle cells. *FASEB J.* 34, 6271–6283. doi: 10.1096/fj.201902828RR
- Wee, P., and Wang, Z. (2017). Epidermal growth factor receptor cell proliferation signaling pathways. *Cancers (Basel)* 9:52. doi: 10.3390/cancers9050052
- Yoshimura, M., Yamakami, S., Amakura, Y., and Yoshida, T. (2012). Diarylheptanoid sulfates and related compounds from *Myrica rubra* bark. *J. Nat. Prod.* 75, 1798–1802. doi: 10.1021/np300212c
- Yu, J. C., Lokker, N. A., Hollenbach, S., Apatira, M., Li, J., Betz, A., et al. (2001). Efficacy of the novel selective platelet-derived growth factor receptor antagonist CT52923 on cellular proliferation, migration, and suppression of neointima following vascular injury. *J. Pharmacol. Exp. Ther.* 298, 1172–1178.
- Zhan, Y., Kim, S., Izumi, Y., Izumiya, Y., Nakao, T., Miyazaki, H., et al. (2003). Role of JNK, p38, and ERK in platelet-derived growth factor-induced vascular proliferation, migration, and gene expression. *Arterioscler. Thromb. Vasc. Biol.* 23, 795–801. doi: 10.1161/01.Atv.0000066132.32063.F2
- Zhang, Y., Fu, Y., Zhang, C., Jia, L., Yao, N., Lin, Y., et al. (2021). MED1 deficiency in macrophages accelerates intimal hyperplasia via ROS generation and inflammation. *Oxid. Med. Cell. Longev.* 2021:3010577. doi: 10.1155/2021/3010577

Conflict of Interest: The authors declare that the research was conducted in the absence of any commercial or financial relationships that could be construed as a potential conflict of interest.

Publisher's Note: All claims expressed in this article are solely those of the authors and do not necessarily represent those of their affiliated organizations, or those of the publisher, the editors and the reviewers. Any product that may be evaluated in this article, or claim that may be made by its manufacturer, is not guaranteed or endorsed by the publisher.

Copyright © 2022 Fan, Wang, Huang and Liang. This is an open-access article distributed under the terms of the Creative Commons Attribution License (CC BY). The use, distribution or reproduction in other forums is permitted, provided the original author(s) and the copyright owner(s) are credited and that the original publication in this journal is cited, in accordance with accepted academic practice. No use, distribution or reproduction is permitted which does not comply with these terms.



The Integration of Metabolomic and Proteomic Analyses Revealed Alterations in Inflammatory-Related Protein Metabolites in Endothelial Progenitor Cells Subjected to Oscillatory Shear Stress

OPEN ACCESS

Edited by:

Xiaojing Liu,
Sichuan University, China

Reviewed by:

Xuebin Qin,
Tulane University School of Medicine,
United States
Ye Zeng,
Sichuan University, China

*Correspondence:

Xiaodong Cui
xiaodongcui@wfmcc.edu.cn
Min Cheng
mincheng@wfmcc.edu.cn

[†]These authors have contributed
equally to this work and share first
authorship

Specialty section:

This article was submitted to
Metabolic Physiology,
a section of the journal
Frontiers in Physiology

Received: 30 November 2021

Accepted: 17 January 2022

Published: 16 February 2022

Citation:

Yu J, Fu J, Zhang X, Cui X and
Cheng M (2022) The Integration
of Metabolomic and Proteomic
Analyses Revealed Alterations
in Inflammatory-Related Protein
Metabolites in Endothelial Progenitor
Cells Subjected to Oscillatory Shear
Stress. *Front. Physiol.* 13:825966.
doi: 10.3389/fphys.2022.825966

Jie Yu[†], Jie Fu[†], Xiaoyun Zhang, Xiaodong Cui* and Min Cheng*

School of Basic Medicine Sciences, Weifang Medical University, Weifang, China

Background: Endothelial progenitor cells (EPCs) play essential roles in vascular repair. Our previous study suggests OSS would lead EPCs transdifferentiation into the mesenchymal cell that aggravates pathological vascular remodeling. The primary purpose of this study was to apply OSS *in vitro* in EPCs and then explore proteins, metabolites, and the protein-metabolite network of EPCs.

Methods: Endothelial progenitor cells were kept in static or treated with OSS. For OSS treatment, the Flexcell STR-4000 parallel plate flow system was used to simulate OSS for 12 h. Subsequently, an untargeted metabolomic LC/MS analysis and a TMT-labeled quantitative proteomic analysis were performed.

Results: A total of 4,699 differentially expressed proteins (DEPs) were identified, among which 73 differentially expressed proteins were potentially meaningful ($P < 0.05$), with 66 upregulated and 7 downregulated expressions. There were 5,664 differential metabolites (DEMs), of which 401 DEMs with biologically potential marker significance ($VIP > 1$, $P < 0.05$), of which 137 were upregulated and 264 were downregulated. The Pearson correlation analysis of DEPs and DEMs was performed, and the combined DEPs–DEMs pathway analyses of the KGLM database show 39 pathways. Among the DEPs, including the Phosphoserine phosphatase (PSPH), Prostaglandin E synthase 3 (PTGES3), Glutamate–cysteine ligase regulatory subunit (GCLM), Transaldolase (TALDO1), Isocitrate dehydrogenase 1 (IDH1) and Glutathione S-transferase omega-1 (GSTO1), which are significantly enriched in the citric acid cycle (TCA cycle) and fatty acid metabolic pathways, promoting glycolysis and upregulation of fatty acid synthesis. Moreover, we screened the 6 DEPs with the highest correlation with DEMs for predicting the onset of early AS and performed qPCR to validate them.

Conclusion: The comprehensive analysis reveals the following main changes in EPCs after the OSS treatment: dysregulation of glutamate and glycine metabolism and their transport/catabolic related proteins. Disorders of fatty acid and glycerophospholipid metabolism accompanied by alterations in the corresponding metabolic enzymes. Elevated expression of glucose metabolism.

Keywords: oscillatory shear stress, endothelial progenitor cells, atherosclerosis, inflammation, metabolomics, proteomics, cardiovascular disease (CVD)

INTRODUCTION

The occurrence and mortality of cardiovascular disease (CVD) are always high, endangering public health and safety. Atherosclerosis (AS) is the main cause of coronary heart disease, cerebral infarction and peripheral vascular disease (Roy et al., 2021). Chronic progressive inflammatory, metabolic diseases caused by the accumulation of lipids from the intima leads to the formation of plaques, which are prone to form in the opening, bifurcation, and bending of an artery. This formation is closely related to the anatomy and hemodynamic characteristics of these portions of vessels (Cheng et al., 2006), which indicates shear stress (SS) plays an essential role in the development of these diseases.

Shear stress is divided into high shear stress (HSS) and low shear stress (LSS), even oscillatory shear stress (OSS). According to previous findings, with the blood flow pattern shifts toward turbulence, OSS (± 4 dynes/cm², 1 Hz) at a bifurcation or bend in a blood vessel can cause endothelial dysfunction, and leads to increased monocyte adhesion, proliferation, and apoptosis, resulting in pro-inflammatory endothelial/endothelial progenitor-mesenchymal transition (Gao et al., 2020; Theofilis et al., 2021; Zhao et al., 2021). However, the mechanism of OSS on atherosclerosis has not yet been fully elucidated (Warboys et al., 2011).

Endothelial progenitor cells (EPCs) are precursors of vascular ECs and can be isolated from bone marrow cord, blood or peripheral blood, from pulmonary artery endothelium or placenta, or from induced pluripotent stem cells. Their main biomarkers are CD34, CD133, and vascular endothelial growth factor (VEGF) receptor 2. There are two type EPCs, namely early EPCs and late-stage EPCs. Early EPCs have the hematopoietic origin and promote angiogenesis through

paracrine mechanisms but are unable to produce mature endothelial cells. Late-stage EPCs have the ability to generate mature endothelial cells and then promote angiogenesis *in vitro* and *in vivo* (Peyter et al., 2021). With mobilization by tissue ischemia, cytokine stimulation, or HMG-CoA reductase inhibitors, EPCs can migrate and adhere to endothelial injury and ischemic sites, where they repair and maintain the integrity of vascular endothelial tissue (Tsfamariam, 2016; Kutikhin et al., 2018; Morrone et al., 2021). However, with the presence of cardiovascular risk factors, the number and function of EPCs decreases proportionally (Hur et al., 2004).

It is generally accepted that the shear stress system can simulate the force to vascular endothelial cells (VECs) generated by fluid flow in the vascular lumen. In this study, we treated EPCs with Flexcell STR-4000 parallel plate flow system and then proteomic and metabolomic analyses were performed. A quantitative proteomic analysis based on tandem mass labels (TMTs) was combined with a metabolomic analysis based on untargeted LC-MS to study changes in EPCs in response to OSS (± 4 dyne/cm², 1 Hz). Quantitative reverse transcription (qRT)-polymerase chain reaction (PCR) was performed to validate the proteomic and metabolomic analyses results. Our study could provide novel data for understanding the development of AS.

MATERIALS AND METHODS

Cell Culture and Experimental Groups

Endothelial progenitor cells were extracted from human umbilical venous blood and cultured *in vitro*. Briefly, mononuclear cell were gotten from human peripheral blood by density gradient centrifugation and cultured with EGM-2 MV (Lonza, Sweden) complete medium (Bei et al., 2017). Generations 5–7 of EPCs grown in the logarithmic phase were used. EPCs were randomly divided into two groups: static group (static), in which EPCs were kept in static for 12 h, and OSS group, in which OSS of ± 4 dynes/cm² at 1 Hz was applied on EPCs for 12 h. The OSS is applied by the Flexcell STR-4000 parallel plate flow system through a computer-controlled mechanical loading system (Streamer). The EPCs were seeded on glass slides coated with Fibronectin (Fn, Sigma, United States) at a concentration of 0.5 μ g/cm². The glass slides with EPCs were carefully placed in the Streamer, and OSS was applied. This study was approved by the Ethics

Abbreviations: CVD, cardiovascular disease; AS, atherosclerosis; SS, shear stress; HSS, high shear stress; LSS, low shear stress; OSS, oscillatory shear stress; EPCs, endothelial progenitor cells; VECs, vascular endothelial cells; ECs, endothelial cells; DEPs, differentially expressed proteins; DEMs, differentially expressed metabolites; UA, uric acid; AA, amino acid; BCAAs, branched chain amino acids; Met, methionine; Hcy, homocysteine; Gly, Glycine; Gln, glutamine; GSH, glutathione; Ser, serine; NO, nitric oxide; Hcy, homocysteine; LPS, lipopolysaccharide; IL-1, interleukin-1; VSMCs, vascular smooth muscle cells; NOX, nitrogen oxide; ROS, reactive oxygen species; PCA, principal component analysis; RPT, response permutation testing; PLS-DA, partial least squares–discriminant analysis; OPLS-DA, orthogonal partial least squares–discriminant analysis; VIP, variable importance of projection; SDS-PAGE, SDS- polyacrylamide gel electrophoresis; qPCR, Real-time polymerase chain reaction; PSPH, phosphoserine phosphatase; PTGES3, prostaglandin E synthase; GCLM, glutamate–cysteine ligase regulatory subunit; TALDO1, transaldolase; IDH1, isocitrate dehydrogenase cytoplasmic; GSTO1, glutathione S-transferase omega-1.

Committees Review Board at Weifang Medical University, Weifang, China.

Sample Preparation

After treatment, the glass slides with EPCs were removed from the Flexcell STR-4000 system, placed in a sterile four-well plate, washed once with $1 \times$ PBS, and then, the PBS was removed as cleanly as possible. Metabolomic samples (two groups with 16 samples) were prepared as follows: To quench cell growth, liquid nitrogen was applied to the bottom of the outer walls of the four-well plate containing the cell slides for 10 s. Methanol and distilled aqueous solution were prepared at a ratio of 4:1 by volume. Then, a total 1 mL of this methanol-water solution was added twice. The cells were scraped from the slides with a disposable cell scraper and transferred to a clean and sterile 1.5 ml centrifuge tube. The cells were stored at -80°C . Proteomic samples (two groups with six samples) were prepared as follows: at least 1×10^7 EPCs were used in each group of samples. The cells were digested with 0.25% trypsin. The cell suspension was prepared with EGM-2MV complete medium, centrifuged at 1,000 rpm for 5 min at room temperature. EPCs suspended with $1 \times$ PBS, and then centrifuged at 1,000 rpm for 5 min at room temperature. This process was repeated 3 times. The cells were stored at -80°C , and transported in dry ice to Shanghai Ouyi Biotechnology Co., Ltd., for testing.

Untargeted Metabolomic LC/MS Analysis

For the metabolic experiment, a liquid mass spectrometry system (Thermo Fisher Scientific) consisting of a Dionex U3000 UHPLC ultrahigh-performance liquid phase tandem QE plus a high-resolution mass spectrometer was used for LC-MS/MS analysis. Chromatographic separation was performed using an ACQUITY UHPLC T3 column (100×2.1 mm; $1.8 \mu\text{m}$, Waters). Mobile phase A was composed of 0.1% formic acid in the water, and mobile phase B was composed of acetonitrile containing 0.1% formic acid. The loading volume in positive and negative ESI mode was $2 \mu\text{l}$. The elution gradient settings were as follows: 5% B (0–2 min), 5–25% B (2–4 min), 25–50% B (4–8 min), 50–80% B (8–10 min), 80–100% B (14–15 min), 100% to 5% B (15–15.1 min), and 5% B (15.1–16 min); the flow rate was 0.35 mL/min. The mass spectrometry conditions were a spray voltage (V) of 3800/–3000; a capillary temperature ($^{\circ}\text{C}$) of 320/320; an auxiliary (Aux) gas heater temperature ($^{\circ}\text{C}$) of 350/350; a sheath gas flow rate (Arb) of 35/35; an aux gas flow rate (Arb) of 8/8; an S-lens RF level of 50/50; a mass range (m/z) of 100–1000/100–1000; a mass range (m/z) of 70000/70000; MS/MS resolution of 17500/17500; an NCE and stepped NCE of 10, 20, and 40 and of 10, 20, and 40, respectively. UNIFI 1.8.1. the software was used for raw data acquisition, and raw data were processed with the metabolomics processing software Progenesis Q.I. v2.3 (Non-linear Dynamics, Newcastle, United Kingdom). Then, the specific names and biological functions of differentially expressed proteins and metabolites were identified through

the UniProt¹, KEGG², and KGLM³ databases, and enrichment analyses were performed.

Tandem Mass Labels-Labeled Quantitative Proteomic Analysis

For the proteomic analysis, chromatographic separation was performed with high-pH separation liquid chromatography, and Q Exactive and EASY-nLC 1200 systems were used for the LC-MS/MS analysis and data analysis. Reversed-phase chromatography separation was performed with an Agilent 1100 HPLC system as follows: An Agilent Zorbax Extend-C18 narrow bore column (2.1×150 mm, $5 \mu\text{m}$) was used, and the detection wavelengths were UV 210 nm and 280 nm. Mobile phase A consisted of ACN- H_2O (2:98, v/v), and mobile phase B consisted of ACN- H_2O (90:10, v/v). The gradient elution conditions were 98% A (0–8 min); 98–95% A (8–8.01 min); 95–75% A (8.01–48 min); 75–60% A (48–60 min); 60–10% A (60–60.01 min); 10% A (60.01–70 min); 10–98% A (70–70.01 min); and 98% A (70.01–75 min). The flow rate was 0.300 mL/min. The chromatography conditions were as follows: a sample was loaded onto an Acclaim PepMap 100, which is a $100 \mu\text{m} \times 2$ cm precolumn (RP-C18, Thermo Fisher Scientific), at a 300 nL/min flow rate, and then, the sample was separated on an Acclaim PepMap RSLC analytical column ($75 \mu\text{m} \times 15$ cm, RP-C18, Thermo Fisher Scientific). Mobile phase A was composed of H_2O -FA (99.9:0.1, v/v); mobile phase B was composed of ACN: H_2O : FA (80:19.9:0.1, v/v/v). The gradient elution conditions were 5–30% B (0–40 min); 30–50% B (40–54 min); 50–100% B (54–55 min); and 100% B (55–60 min). The conditions for mass spectrometry were as follows: The MS mass resolution was 70,000; the automatic gain control value was $1\text{e}6$; the maximum injection time was 50 ms; the m/z range consisted of a charge-to-mass ratio of 300-to-1600; the collision energy was 32; the MS/MS resolution was 17,500; the automatic gain control was $2\text{e}5$, the maximum ion injection time was 80 ms, and the dynamic rejection time was 30 s. Protein-metabolite interaction networks provide visible interactions between functionally relevant differentially expressed proteins (DEPs) and differentially expressed metabolites (DEMs). This experiment uses the Pearson correlation calculation method to calculate DEPs-DEMs correlations, allowing proteomics and metabolomics data to be integrated to obtain common pathways and interactions between DEPs and DEMs.

Real-Time Fluorescence Quantitative PCR

Total RNA was extracted by fully lysing cells on ice with TRIzol reagent (Thermo-Invitrogen Ambion, United States). Then, total RNA was reverse transcribed to cDNA using Evo M-MLV RT Premix for qPCR (AG, China) reverse transcription kit according to the instructions. The qPCR was performed

¹<https://www.uniprot.org/>

²<https://www.kegg.jp/>

³<https://www.kegg.jp/kegg/xml/>

TABLE 1 | The primer sequences in qPCR.

Gene name		Primer sequences
GSTO1	Forward	AGCTAGAGGAGGTTCTGACTAA,
	Reverse	TTTAAC TTCATTGCTTCCAGCC;
IDH1	Forward	GATGGCAAGACAGTAGAAGCAGAGG
	Reverse	ATGGAAGCAATGGGATTGGTGGAC
TALDO1	Forward	TCAGCAAGGACCGAATCTTAT
	Reverse	TCAGCAAGGACCGAATCTTAT
GCLM	Forward	GGGCACAGGTAAAACCAATAG
	Reverse	TTTTCACAATGACCGAATACCG
PSPH	Forward	GGAAGCTTTTCTACTCAGCAGA
	Reverse	CACAGATTTTGGCTAGCTCATC
PTGES3	Forward	GTTGTCTCGGAGGAAGTGATAA
	Reverse	GTTTGTTAACCTTGCCATGA
GAPDH	Forward	GTCATCAATGGAAATCCCATCA
	Reverse	CCAGTGGA CTCCACGACGTAC

according to the instructions of SYBR Green Premix Pro Taq HS qPCR Kit (AG, China), and the reaction conditions of QuanStudio fluorescent quantitative PCR instrument (Thermo Fisher Scientific, United States). The reaction conditions were set to 95°C, 5 s, 60°C, 30 s for 40 cycles. The amplification efficiencies of GSTO1, IDH1, TALDO1, GCLM, PSPH, and PTGES3 were

calculated statistically according to Equation $2^{-\Delta\Delta CT}$, using GAPDH as an internal reference. The primer sequences for these genes are listed in **Table 1**:

RESULTS

Protein Identification and Classification After Oscillatory Shear Stress Stimulation

To compare the protein profiles at static and OSS group, TMT 6-plex labels were used for each sample. And then the relative abundance of DEPs were determined. The result showed that protein expression was significant differences between the OSS ($n = 3$) and static ($n = 3$) group. A principal component analysis (PCA) showed that the overall difference in the protein profile between the groups was obvious, and the protein analysis for each group was reproducible (**Figure 1A**). SDS-polyacrylamide gel electrophoresis (SDS-PAGE) revealed that the protein bands were evenly distributed (**Figure 1B**). The hierarchical clustering dendrogram showing the sample Euclidean distance based on credible expression quantitative data also indicated that the protein characteristics between the static and OSS groups were different (**Figure 1C**).

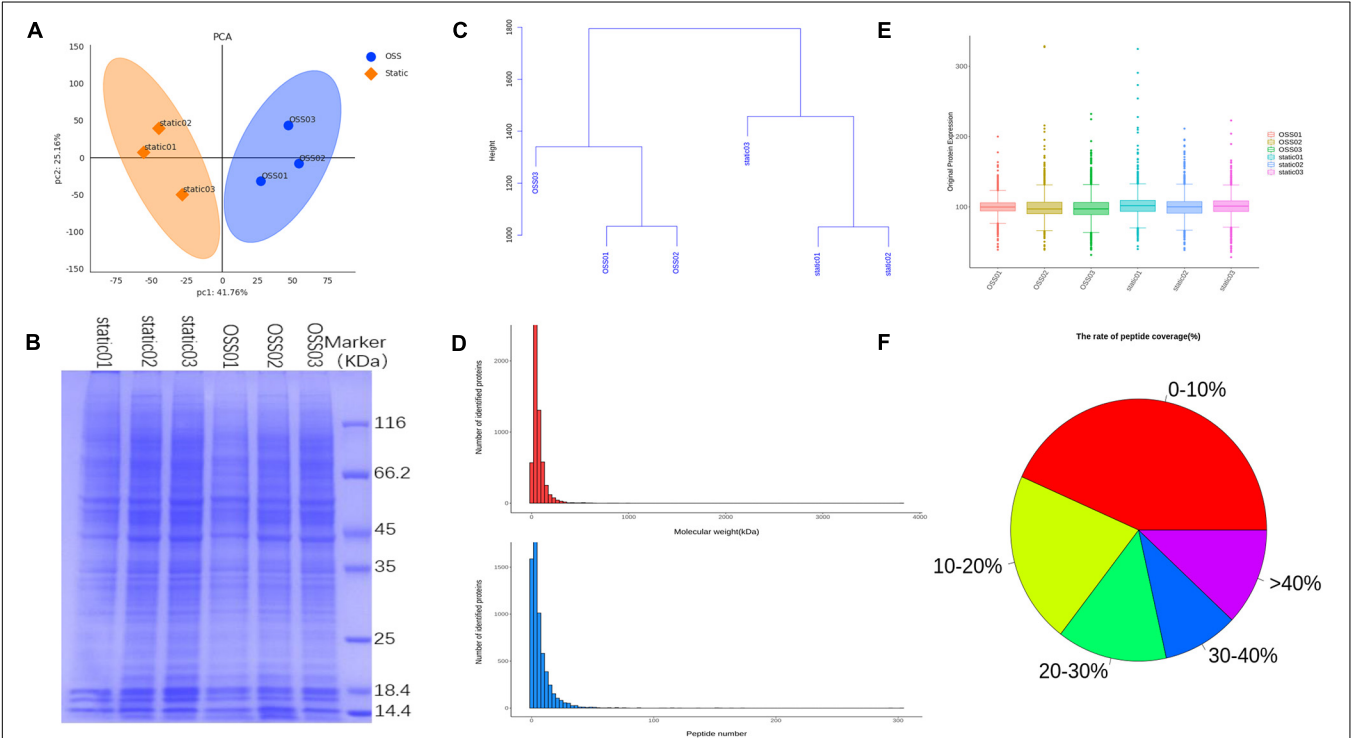
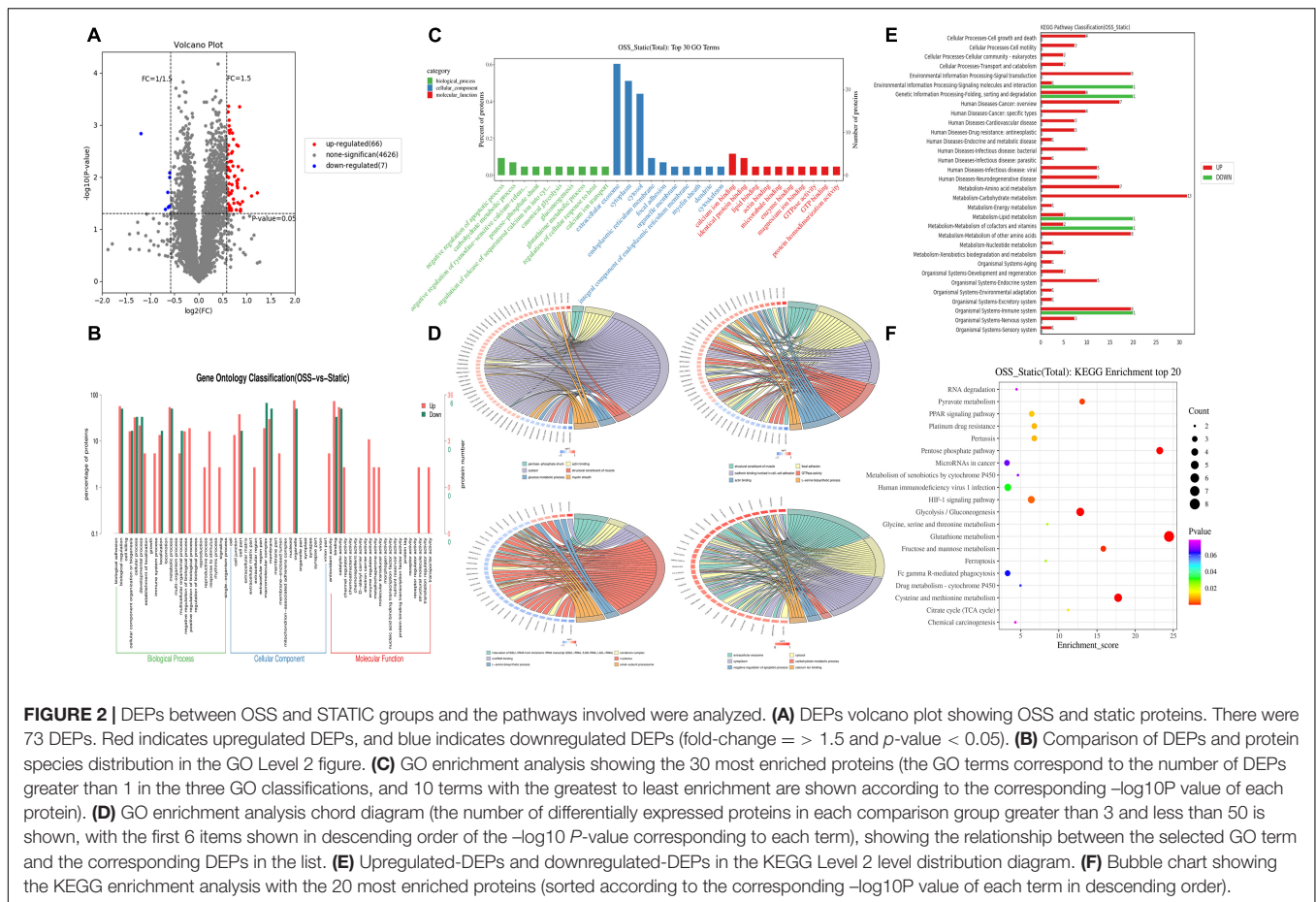


FIGURE 1 | Diagram showing the analysis of 6 samples in the OSS ($n = 3$) and static ($n = 3$) groups using a Flexcell STR-4000 parallel plate flow system. **(A)** Principal component analysis (PCA) showing the credible protein expression in the OSS and static groups. **(B)** SDS- polyacrylamide gel electrophoresis (SDS-PAGE) electropherogram showing the OSS and static proteins. **(C)** Hierarchical clustering dendrogram showing the Euclidean distances of the OSS and static samples. **(D)** The number of proteins corresponding to different molecular weights of OSS and static group bands and the distribution of the number of peptides corresponding to each qualitatively assessed protein. **(E)** Box plots show credible protein expression in the OSS and static groups. **(F)** Comparison of each peptide in OSS and static groups against background databases and the coverage index map showing the peptides relative to complete protein sequences.



The distribution of the proteins with different molecular masses and the peptide number of each qualitative protein in the raw data was uniform and consistent (Figure 1D). The box-plot showed small fluctuations in the credible protein expression levels obtained through an analysis of the static and OSS group (Figure 1E). Database search software was used to compare each peptide with the background database. The coverage index of the peptide relative to the complete protein sequence was obtained (Figure 1F).

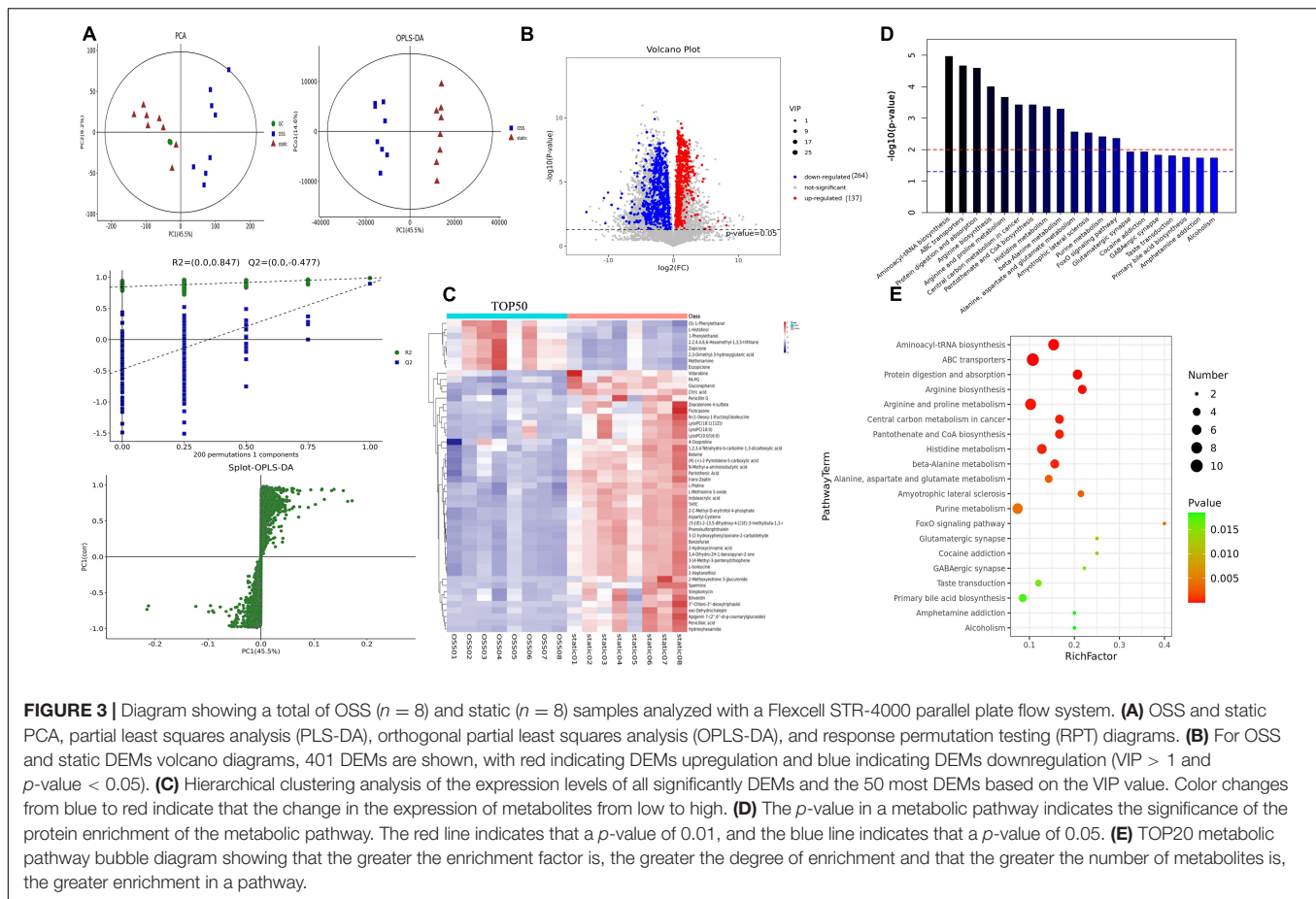
The Metabolic Pathways of Differentially Expressed Proteins Involve 13 Biological Functions Associated With the Development of Inflammation

In the proteomic dynamics experiment, 4,699 DEPs were found between the static and OSS groups. A total of 73 differentially expressed proteins were identified on the basis of a fold change ≥ 1.5 and a P value < 0.05 as criteria. We found that the expression of 66 of these DEPs was upregulated and 7 of these DEPs was downregulated (Figure 2A). According to GO and KEGG analyses (Figures 2B,F), these proteins were mainly enriched in 13 functional categories. These DEPs were mainly involved in muscles, carbohydrate metabolism, myelin, local adhesion, protein binding, GTPase activity, amino

acid metabolism, RNAs, and small subunits. Basal protrusions, exosome release, carbohydrate metabolism, negative regulation of apoptosis, and calcium ion binding were also enriched with these differentially expressed proteins (Figures 2B–D). Among these categories, glycometabolism, amino acid metabolism, fatty acid metabolic, energy metabolism, and hypoxia-inducible factor-1 signaling (Figures 2E,F) were enriched with the most differentially expressed proteins between static and OSS group. Notably, all these pathways are closely associated with the development of inflammation. These pathways might enhance metabolic effects after OSS treatment in EPCs, contributing to the development of AS.

Differential Metabolites Reflect Changes in L-Glutamate, Beta-D-Glucose, Spermine, Ornithine, Choline, and Indicate More Inflammation-Related Metabolic Markers

PCA and supervised partial least square analysis (PLS-DA) model showed that the metabolic profiles of for EPCs treated with OSS or kept in static were significantly different. This study was based on 200 response permutation tests (RPTs). With a fixed X matrix, $R^2 = (0.0, 0.847)$, $Q^2 = (0.0, 0.477)$, we found the rightmost R^2 and Q^2 points at the highest positions, and the Q^2



line was significantly lower than the R^2 line and was effectively separated. This outcome indicated that the interpretation and prediction of the model verification parameters were effective and that the model was successfully established. In addition, an orthogonal partial least squares–discriminant analysis (OPLS-DA) eliminated noise that was not related to the classification, improved the analytical power and effectiveness of the OSS and static metabolite models, and maximized the difference between the OSS and static groups (Figure 3A).

Variables with a variable importance of projection ($VIP > 1$ and $P < 0.05$) were selected as potential biomarkers, and 401 DEMs were identified, of which the level of 137 metabolites was increased, and that of 264 metabolites was decreased. And 111 DEMs were found in the KEGG database associated with specific terms and related biological functions. These DEMs, including L-glutamate, beta-D-glucose, spermine, ornithine, choline, and Betaine, all showed reduced expression after OSS treatment (Figure 3B).

Next, the Top 50 DEMs were identified with the most potential of inflammation-related metabolic markers, and a heatmap analysis was performed (Figure 3C); each colored cell on the heatmap corresponds to the concentration value in the data table. Through KEGG enrichment analysis, it was found that the metabolic pathways were mainly enriched in the following biological functions: aminoacyl biosynthesis, amino

acid metabolism, protein transport, and absorption, coenzyme metabolism, the FoxO signaling pathway, central carbon metabolism of cancer, metabolism, and muscles (Figures 3D,E).

Differentially Expressed Proteins-Differential Metabolites Correlation Analysis Was Performed and Six Differentially Expressed Proteins Were Screened and Verified

To better understand the changes in OSS on the biological functions of EPCs, the obtained proteomics and metabolomics data were integrated. The Pearson correlation calculation method was used to evaluate the correlation between DEPs and DEMs, and a correlation heatmap was drawn showing the 20 most highly correlated DEPs and DEMs (TOP 20); there were 170 pairs with $P < 0.05$, 55 pairs with $P < 0.01$ and 3 pairs with $P < 0.001$ (Figure 4A). Moreover, according to the TOP20 results of the correlation analysis between the DEPs and DEMs, the relationship pairs with a $P \leq 0.05$ were selected to draw the network diagram. The red line represents a positive correlation. The green line represents a negative correlation, and the thickness of the line represents the value of the correlation coefficient (Figure 4B). Figure 4C lists the specific names of the TOP20 DEPs and the corresponding IDs in UniProt. DEPs with the

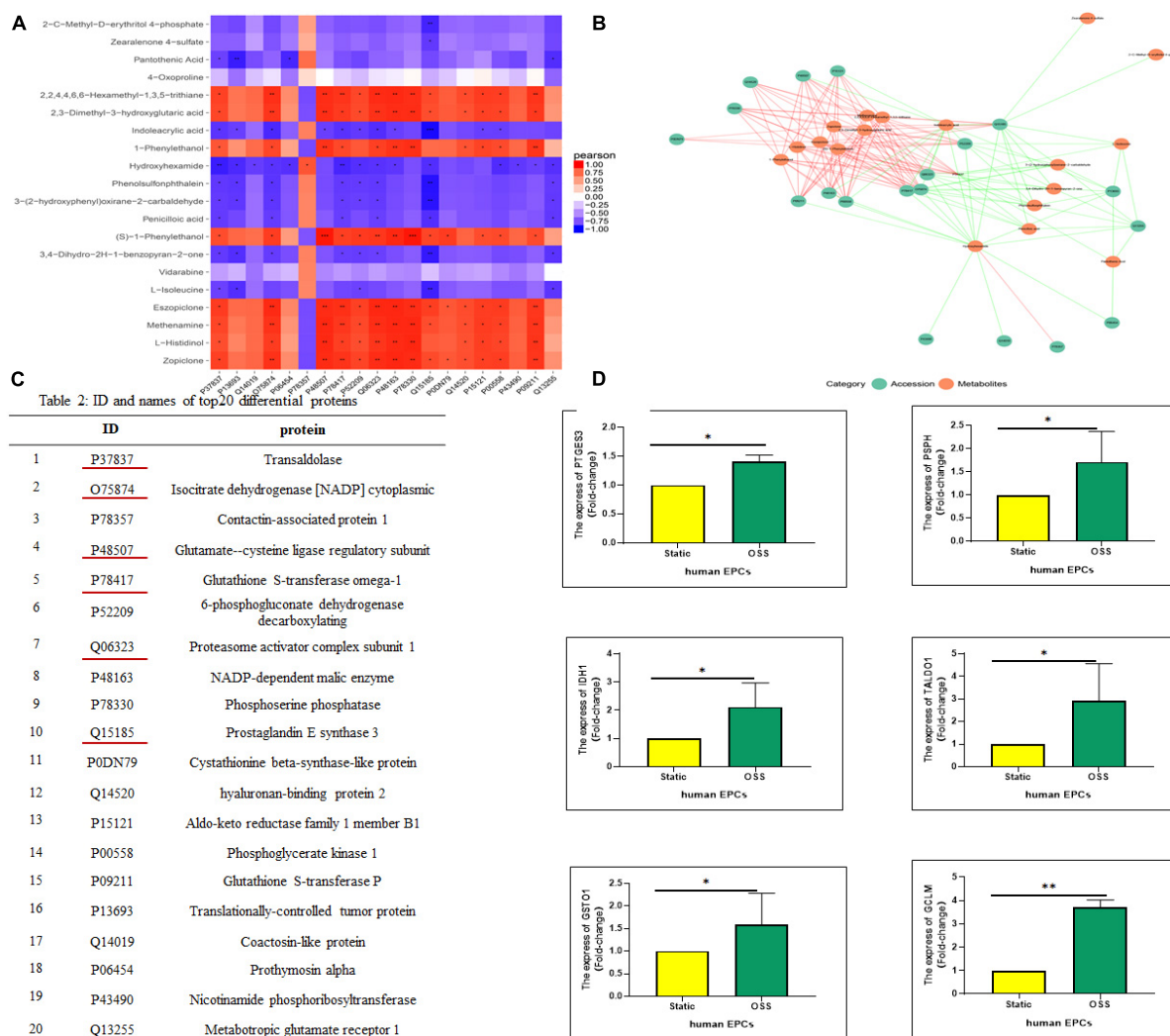


FIGURE 4 | Correlation analysis between DEPs and DEMs. **(A)** A correlation heatmap showing the TOP20 results of the correlation analysis between DEPs and DEMs, orange-red indicates a positive correlation, blue indicates a negative correlation, *** p -value < 0.001 , ** p -value < 0.01 , and * p -value < 0.05 . **(B)** The correlation between the DEPs and DEMs response intensity data based on a Pearson correlation analysis, with a p value ≤ 0.05 selected to draw a network diagram. Red represents a positive correlation, and the green represents a negative correlation. **(C)** IDs and protein names of the TOP20 DEPs in the UniProt database. **(D)** Real-time polymerase chain reaction (qPCR) shows PSPH, PTGES3, GCLM, TALDO1, IDH1, and GSTO1 expression was significantly elevated after OSS, $n = 3$, * p -value < 0.05 , ** p -value < 0.01 compared with Static by Mann-Whitney U test.

most prominent correlation were verified by qPCR (**Figure 4D**). The expression of PSPH, PTGES3, GCLM, TALDO1, IDH1, and GSTO1 increased significantly, which is highly consistent with proteomic analysis.

The Combined Differentially Expressed Proteins-Differential Metabolites Pathway Significantly Focuses the Glycolytic, Citric Acid Cycle, and Fatty Acid Metabolic Pathways

The enrichment analysis showed that the identified DEPs and DEMs were significantly enriched in specific pathways. A total

of 39 metabolic pathways were enriched with differentially expressed molecules, as shown in **Figure 5A** ($P < 0.05$).

Among them, GO and KEGG analysis of DEPs and DEMs with high enrichment scores yielded a total of 9 metabolic pathways. Combined pathway analysis of the proteins we tracked by DEPs and DEMs showed that these proteins were involved in 6 subnetworks: (1) GCLM, IDH1, and GSTO1 all regulate glutathione (GSH) metabolism, three of which are downregulated including L-glutamate, spermine and spermidine metabolites, while GSTO1 is involved in three metabolic pathways: drug metabolism-cytochrome P450, drug metabolism-other enzymes and metabolism of xenobiotics by cytochrome P450 (**Figure 5B**); (2) GCLM is involved in the metabolism of cysteine and methionine, of which two metabolite

expressions are downregulated including sulfate, methionine sulfoxide (**Figure 5C**); (3) IDH1 is involved in the TCA cycle to decrease citric acid expression (**Figure 5D**); (4) PSPH is mainly involved in the metabolism of Glycine, serine and threonine, of which the expression of three metabolites is downregulated including choline, creatine, and Betaine (**Figure 5E**); (5) TALDO1 is involved in the pentose phosphate pathway to bring down Beta-D-glucose (**Figure 5F**); and (6) PTGES3 regulates the arachidonic acid metabolic pathway (**Figure 5G**).

DISCUSSION

Cardiovascular disease remains one of the leading causes of human mortality (Zhao et al., 2019). Although research on AS, the main type of CVD, has been pervasive, the specific mechanism of AS is still unknown. AS is a chronic progressive inflammatory disease, and metabolic changes play an important role in the pathophysiology of AS. Moreover, the development of AS might be related with OSS. Previous studies have shown that many basic processes in EPCs by affecting the expression and modification of thousands of genes, proteins and metabolites. Therefore, new theories based on systems biology are needed to fully clarify the interaction between mechanical force and EPCs.

A previous study found that monocytes in the body stimulated by inflammation-inducing factors increased carbohydrate metabolism. Glycolysis was found to play a decisive role in promoting inflammation (leading to the progression of AS) (Groh et al., 2018). We found that TALDO1 was highly expressed under OSS intervention, which promoted glucose metabolism and thus contributed to the development of AS. In addition, the two rate-limiting intermediates in the TCA cycle are core eukaryotic energy metabolites that accumulate in the body, further stimulating the development of AS (Liang et al., 2021). And we have demonstrated that the expression of IDH1, a key enzyme of the TCA cycle, is increased after OSS intervention. Some studies have suggested that increased IDH1 and TCA circulating activity in pro-inflammatory cells (Koenis et al., 2018). Also the increased expression of IDH1 and TCA circulating activity could demonstrate inflammatory expression. Studies have shown that changes in amino acid metabolism are closely related to the occurrence of AS. For example, in patients with cardiovascular disease, some branched-chain amino acids (BCAAs) are considered to be early biomarkers of cellular immune activation (Gulasova et al., 2020; Zaric et al., 2020). The differential gene PSPH can directly regulate Glycine (Gly), serine (Ser), and threonine metabolism. And Gly can remodel ECs, reduce the aggregation of macrophages, induce the apoptosis of macrophages, and ameliorate atherosclerosis (Wang et al., 1999).

We found that high GCLM expression after OSS promoted cysteine and methionine metabolism, resulting in increased serum concentrations of Hcy. Moreover, GSH metabolism further contributes to fatty acid metabolism. It is generally believed that the disruption of fatty acid metabolism is a crucial link in the development of AS. Studies have shown that an increase in the concentration of phenylalanine indicates

inflammation and impaired immune activation (Gulasova et al., 2020). A study has shown that amino acid metabolism is disordered in AS. A particularly in-depth study into the role of amino acids in stabilizing inflammation revealed that glutamine, which can synthesize GSH, is vital for macrophage-induced IL-1 production in response to LPS stimulation. Glutamine also plays a potential role by feeding the arginine synthesis pathway, facilitating an increase in the microbial capacity of NO macrophages (Wallace and Keast, 1992). At the same time, a study has shown that Glycine plays an obvious role in many biological functions. For example, Glycine can reduce oxidative stress markers and Glycine supplementation can lead to anti-inflammatory effects. Studies have shown that the risk of coronary heart disease is negatively correlated with Glycine concentration in serum (Zaric et al., 2020). In addition, supplementation with the antioxidant GSH can exert an antioxidant effect to protect the vascular endothelium and reduce inflammation (Ruiz-Ramirez et al., 2014). Also, specific metabolites play a crucial role in the AS process. For example, studies have shown that different levels of the metabolite Betaine may inhibit the formation of atherosclerotic plaques by exerting anti-inflammatory effects, thereby inhibiting the occurrence and development of AS (Lv et al., 2009; Wang et al., 2011).

After OSS intervention in EPCs, PSPH expression was upregulated, regulating cysteine and methionine metabolism, eventually leading to a significant decrease in Betaine. A study showed that after cells were subjected to OSS, the betaine level decreased significantly and that 5-hydroxytryptophan, a potential biomarker of DEM with reduced concentrations after experiencing OSS intervention, was incorporated into apolipoprotein A-I, impairing cholesterol efflux activity and high-density lipoprotein biogenesis (Zamanian-Daryoush et al., 2020), promoting the occurrence and development of AS. β -Alanine and L-histidine are known to be involved in the synthesis of carnosine, which can delay inflammation and fight AS (Caruso et al., 2019). However, the expression of both beta-alanine and L-histidine was decreased in the OSS context, and therefore, they can be used as potential biomarkers for the diagnosis of AS to be further studied in depth. Moreover, biliverdin has been proven to be key to regulating cell proliferation, apoptosis and antioxidant defense (Ayer et al., 2016). Data have shown that the biliverdin level was reduced, which promoted the progression of AS. It was found that PTGES3 was highly expressed after OSS action and that PTGES3 could directly regulate arachidonic acid metabolism. Arachidonic acid is known to promote vasoconstriction and platelet agglutination and chemotaxis of neutrophils, further promoting the development of inflammation and AS.

Also, the enrichment of DEPs and DEMs in purine metabolism was more obvious after OSS stimulation. Purine metabolism in the body increases the serum Uric acid (UA) level. A study has shown that UA reduces the availability of nitric oxide (NO) and forms peroxynitrite, which can cause DNA damage and lipid peroxidation, leading to endothelial cell dysfunction and death. Therefore, the blood solubility of UA is positively correlated with the occurrence of AS and is a biomarker of cardiovascular disease risk (Yu and Cheng, 2020).

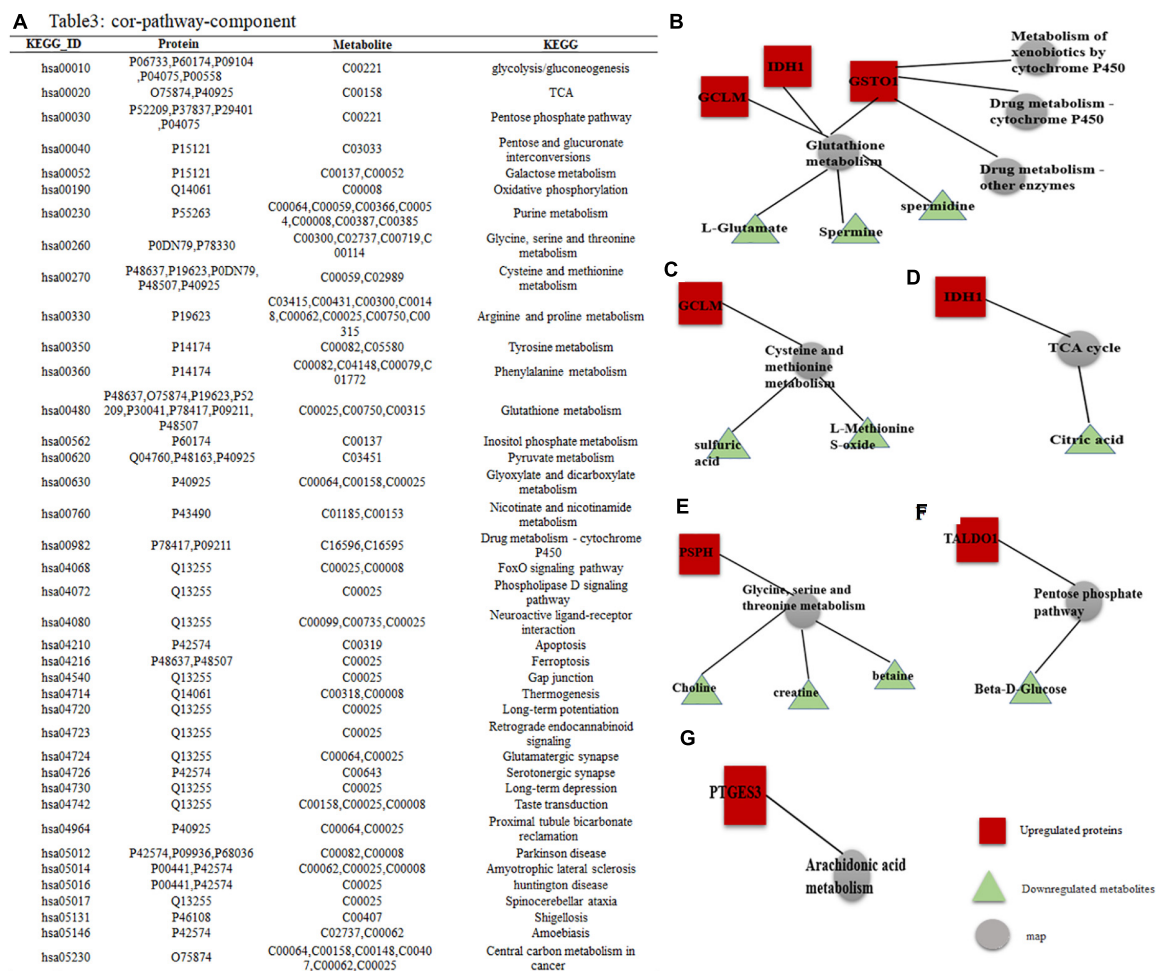


FIGURE 5 | DEPs-DEMs combined pathway analysis. **(A)** Specific KEGG IDs were found to be enriched in 39 metabolic pathways; the specific names of the DEPs and DEMs are shown. **(B–G)** Interaction network of DEPs-DEMs, red indicates upregulated proteins or metabolites, green indicates downregulated proteins or metabolites, and gray represents metabolic pathways.

Moreover, we found that the expression of UA in EPCs was reduced after OSS, and it is possible that the synthesized UA was released into the blood, promoting the development of AS. When attacked by inflammatory factors, the death rates of monocytes, vascular smooth muscle cells (VSMCs) and ECs increase, which further stimulates the occurrence and development of AS (Ackers-Johnson et al., 2015; Paone et al., 2019). For example, a study has shown that the reduced apoptosis of macrophages and increased endocytosis in blood vessel walls was realized by knocking down the lncRNA MAARS, which attenuated the progression of AS (Simion et al., 2020); yam glycosides have also been shown to inhibit oxidative stress, inflammation and apoptosis to reduce postmenopausal AS (Yang et al., 2019). Furthermore, another form of cell death, ferroptosis, is prevalent in AS. Ferroptosis is a newly discovered type of programmed cell death in which the metabolism of lipid oxides in cells and the accumulation of lipid reactive oxygen species leads to redox imbalance in cells (Dolma et al., 2003), and GCLM can promote ferroptosis (Meier et al., 2021). A study has shown

that ferroptosis occurs at the beginning and developmental stages of AS. Inhibiting ferroptosis can alleviate AS by reducing lipid peroxidation and endothelial dysfunction of AECs (Bai et al., 2020). Therefore, various mechanisms have been used to inhibit the apoptosis of three central cells of AS, macrophages, ECs, and VSMCs, or to enhance the ability of EPCs and ECs to inhibit the occurrence and development of AS.

After validation, we found that the combination of differential genes PSPH, PTGES3, GCLM, TALDO1, IDH1, and GSTO1 has the ability to act as an early biomarker for the development of AS. Meanwhile, the possibility of delaying the progression of AS by modulating certain metabolic pathways with high enrichment fractions and/or pathway-related metabolites is an element that requires further analysis. For example, directly regulating the purine pathway *in vivo*, controlling the production of UA, and regulating the NOX pathway slows the aging of EPCs and enhances their vascular repair capabilities. Therefore, the *in vitro* expansion and anti-inflammatory ability of EPCs are essential in the treatment of AS. In addition, by increasing the activity

of PSPH in the body, the rate of serine production is increased, which regulates the antioxidant capacity and anti-inflammatory capacity of EPCs, thereby delaying the development of AS. Alternatively, the biological functions of EPCs can be adjusted by directly administering relevant small molecules *in vivo* to enhance their proliferation, migration, and adhesion capabilities to fight inflammation and repair vascular damage. For example, direct administration of an appropriate dose of arginine can enhance cell function, delay the development of AS, and reduce the occurrence rate of AS (Cooke et al., 1992). However, this is all fundamental theory, and further in-depth research is needed on how to formulate the therapeutic dosages, the optimal route of administration, and the application to the clinic.

Our study reveals a comprehensive exploration into the mechanism of action of EPCs under the stimulation of OSS through molecular reactions, providing a theoretical basis for the occurrence and development of cardiovascular diseases, related mechanisms, and potential countermeasures. This study only provides a foundation for further study. However, it does not reveal a comprehensive exploration in determining the regulatory mechanism(s) of the pathways enriched with a combination of differentially expressed proteins and differentially expressed metabolites needed for further research.

CONCLUSION

A combination of protein analysis, metabolic analysis, and protein metabolism analysis was performed on static EPCs and EPCs after OSS intervention. It is speculated that the inflammatory pathways involve multiple modalities (sugar

metabolism, energy metabolism, amino acid metabolism and cell death), potential mechanisms (the aminoacyl biosynthesis pathway, ABC transporters, etc.), and potential treatment methods. This study provides a theoretical basis and essential data for future research.

DATA AVAILABILITY STATEMENT

The raw data supporting the conclusions of this article will be made available by the authors, without undue reservation.

ETHICS STATEMENT

The Ethics Committee of Weifang Medical University approved the use of human cord blood for this study.

AUTHOR CONTRIBUTIONS

XC and MC concept and design. XZ, JY, and JF proteomic and metabolomic analyses and interpretations, statistical analyses, and manuscript drafting. All authors reviewed and edited the manuscript draft and approved the final manuscript.

FUNDING

This work was supported by the National Natural Science Foundation of China (grant 81870237) and Shandong Provincial Natural Science Foundation (grant ZR2020MH020).

REFERENCES

- Ackers-Johnson, M., Talasila, A., Sage, A. P., Long, X., Bot, I., Morrell, N. W., et al. (2015). Myocardin regulates vascular smooth muscle cell inflammatory activation and disease. *Arterioscler Thromb. Vasc. Biol.* 35, 817–828. doi: 10.1161/ATVBAHA.114.305218
- Ayer, A., Zarjou, A., Agarwal, A., and Stocker, R. (2016). Heme oxygenases in cardiovascular health and disease. *Physiol. Rev.* 96, 1449–1508. doi: 10.1152/physrev.00003.2016
- Bai, T., Li, M., Liu, Y., Qiao, Z., and Wang, Z. (2020). Inhibition of ferroptosis alleviates atherosclerosis through attenuating lipid peroxidation and endothelial dysfunction in mouse aortic endothelial cell. *Free Radic. Biol. Med.* 160, 92–102. doi: 10.1016/j.freeradbiomed.2020.07.026
- Bei, Y., Das, S., Rodosthenous, R. S., Holvoet, P., Vanhaverbeke, M., Monteiro, M. C., et al. (2017). Extracellular vesicles in cardiovascular theranostics. *Theranostics* 7, 4168–4182. doi: 10.7150/thno.21274
- Caruso, G., Fresta, C. G., Fidilio, A., O'Donnell, F., Musso, N., Lazzarino, G., et al. (2019). Carnosine decreases PMA-induced oxidative stress and inflammation in murine macrophages. *Antioxidants (Basel)* 8:281. doi: 10.3390/antiox8080281
- Cheng, C., Tempel, D., van Haperen, R., van der Baan, A., Grosveld, F., Daemen, M. J., et al. (2006). Atherosclerotic lesion size and vulnerability are determined by patterns of fluid shear stress. *Circulation* 113, 2744–2753. doi: 10.1161/CIRCULATIONAHA.105.590018
- Cooke, J. P., Singer, A. H., Tsao, P., Zera, P., Rowan, R. A., and Billingham, M. E. (1992). Antiatherogenic effects of L-arginine in the hypercholesterolemic rabbit. *J. Clin. Invest.* 90, 1168–1172. doi: 10.1172/JCI115937
- Dolma, S., Lessnick, S. L., Hahn, W. C., and Stockwell, B. R. (2003). Identification of genotype-selective antitumor agents using synthetic lethal chemical screening in engineered human tumor cells. *Cancer Cell* 3, 285–296. doi: 10.1016/s1535-6108(03)00050-3
- Gao, Y., Cui, X., Wang, M., Zhang, Y., He, Y., Li, L., et al. (2020). Oscillatory shear stress induces the transition of EPCs into mesenchymal cells through ROS/PKCzeta/p53 pathway. *Life Sci.* 253:117728. doi: 10.1016/j.lfs.2020.117728
- Groh, L., Keating, S. T., Joosten, L. A. B., Netea, M. G., and Riksen, N. P. (2018). Monocyte and macrophage immunometabolism in atherosclerosis. *Semin. Immunopathol.* 40, 203–214. doi: 10.1007/s00281-017-0656-7
- Gulasova, Z., Guerreiro, S. G., Link, R., Soares, R., and Tomeckova, V. (2020). Tackling endothelium remodeling in cardiovascular disease. *J. Cell. Biochem.* 121, 938–945. doi: 10.1002/jcb.29379
- Hur, J., Yoon, C. H., Kim, H. S., Choi, J. H., Kang, H. J., Hwang, K. K., et al. (2004). Characterization of two types of endothelial progenitor cells and their different contributions to neovascularogenesis. *Arterioscler Thromb. Vasc. Biol.* 24, 288–293. doi: 10.1161/01.ATV.0000114236.77009.06
- Koenis, D. S., Medzikovic, L., van Loenen, P. B., van Weeghel, M., Huvneers, S., Vos, M., et al. (2018). Nuclear receptor Nur77 limits the macrophage inflammatory response through transcriptional reprogramming of mitochondrial metabolism. *Cell Rep.* 24, 2127–2140. doi: 10.1016/j.celrep.2018.07.065
- Kutikhin, A. G., Sinitsky, M. Y., Yuzhalin, A. E., and Velikanova, E. A. (2018). Shear stress: an essential driver of endothelial progenitor cells. *J. Mol. Cell. Cardiol.* 118, 46–69. doi: 10.1016/j.yjmcc.2018.03.007
- Liang, Y., Chen, Y., Li, L., Zhang, S., Xiao, J., and Wei, D. (2021). Krebs cycle rewired: driver of atherosclerosis progression? *Curr. Med. Chem.* doi: 10.2174/0929867328666210806105246
- Lv, S., Fan, R., Du, Y., Hou, M., Tang, Z., Ling, W., et al. (2009). Betaine supplementation attenuates atherosclerotic lesion in apolipoprotein

- E-deficient mice. *Eur. J. Nutr.* 48, 205–212. doi: 10.1007/s00394-009-0003-4
- Meier, J. K., Schnetz, M., Beck, S., Schmid, T., Dominguez, M., Kalinovic, S., et al. (2021). Iron-bound lipocalin-2 protects renal cell carcinoma from ferroptosis. *Metabolites* 11:329. doi: 10.3390/metabo11050329
- Morrone, D., Picoi, M. E. L., Felice, F., De Martino, A., Scatena, C., Spontoni, P., et al. (2021). Endothelial progenitor cells: an appraisal of relevant data from bench to bedside. *Int. J. Mol. Sci.* 22:12874. doi: 10.3390/ijms222312874
- Paone, S., Baxter, A. A., Hulett, M. D., and Poon, I. K. H. (2019). Endothelial cell apoptosis and the role of endothelial cell-derived extracellular vesicles in the progression of atherosclerosis. *Cell. Mol. Life Sci.* 76, 1093–1106. doi: 10.1007/s00018-018-2983-9
- Peyter, A. C., Armengaud, J. B., Guillot, E., and Yzydorczyk, C. (2021). Endothelial progenitor cells dysfunctions and cardiometabolic disorders: from mechanisms to therapeutic approaches. *Int. J. Mol. Sci.* 22:6667. doi: 10.3390/ijms22136667
- Roy, P., Orecchioni, M., and Ley, K. (2021). How the immune system shapes atherosclerosis: roles of innate and adaptive immunity. *Nat. Rev. Immunol.* doi: 10.1038/s41577-021-00584-1
- Ruiz-Ramirez, A., Ortiz-Balderas, E., Cardozo-Saldana, G., Diaz-Diaz, E., and El-Hafidi, M. (2014). Glycine restores glutathione and protects against oxidative stress in vascular tissue from sucrose-fed rats. *Clin. Sci. (Lond.)* 126, 19–29. doi: 10.1042/CS20130164
- Simion, V., Zhou, H., Haemmig, S., Pierce, J. B., Mendes, S., Tesmenitsky, Y., et al. (2020). A macrophage-specific lncRNA regulates apoptosis and atherosclerosis by tethering HuR in the nucleus. *Nat. Commun.* 11:6135. doi: 10.1038/s41467-020-19664-2
- Tesfamariam, B. (2016). Endothelial repair and regeneration following intimal injury. *J. Cardiovasc. Transl. Res.* 9, 91–101. doi: 10.1007/s12265-016-9677-1
- Theofilis, P., Sagris, M., Oikonomou, E., Antonopoulos, A. S., Siasos, G., Tsioufis, C., et al. (2021). Inflammatory mechanisms contributing to endothelial dysfunction. *Biomedicines* 9:781. doi: 10.3390/biomedicines9070781
- Wallace, C., and Keast, D. (1992). Glutamine and macrophage function. *Metabolism* 41, 1016–1020. doi: 10.1016/0026-0495(92)90130-3
- Wang, B. Y., Ho, H. K., Lin, P. S., Schwarzscher, S. P., Pollman, M. J., Gibbons, G. H., et al. (1999). Regression of atherosclerosis: role of nitric oxide and apoptosis. *Circulation* 99, 1236–1241. doi: 10.1161/01.cir.99.9.1236
- Wang, Z., Klipfell, E., Bennett, B. J., Koeth, R., Levison, B. S., Dugar, B., et al. (2011). Gut flora metabolism of phosphatidylcholine promotes cardiovascular disease. *Nature* 472, 57–63. doi: 10.1038/nature09922
- Warboys, C. M., Amini, N., de Luca, A., and Evans, P. C. (2011). The role of blood flow in determining the sites of atherosclerotic plaques. *F1000 Med. Rep.* 3:5. doi: 10.3410/M3-5
- Yang, Q., Wang, C., Jin, Y., Ma, X., Xie, T., Wang, J., et al. (2019). Disocin prevents postmenopausal atherosclerosis in ovariectomized LDLR^{-/-} mice through a PGC-1 α /ER α pathway leading to promotion of autophagy and inhibition of oxidative stress, inflammation and apoptosis. *Pharmacol. Res.* 148:104414. doi: 10.1016/j.phrs.2019.104414
- Yu, W., and Cheng, J. D. (2020). Uric acid and cardiovascular disease: an update from molecular mechanism to clinical perspective. *Front. Pharmacol.* 11:582680. doi: 10.3389/fphar.2020.582680
- Zamanian-Daryoush, M., Gogonea, V., DiDonato, A. J., Buffa, J. A., Choucair, I., Levison, B. S., et al. (2020). Site-specific 5-hydroxytryptophan incorporation into apolipoprotein A-I impairs cholesterol efflux activity and high-density lipoprotein biogenesis. *J. Biol. Chem.* 295, 4836–4848. doi: 10.1074/jbc.RA119.012092
- Zaric, B. L., Radovanovic, J. N., Gluvic, Z., Stewart, A. J., Essack, M., Motwalli, O., et al. (2020). Atherosclerosis linked to aberrant amino acid metabolism and immunosuppressive amino acid catabolizing enzymes. *Front. Immunol.* 11:551758. doi: 10.3389/fimmu.2020.551758
- Zhao, D., Liu, J., Wang, M., Zhang, X., and Zhou, M. (2019). Epidemiology of cardiovascular disease in China: current features and implications. *Nat. Rev. Cardiol.* 16, 203–212. doi: 10.1038/s41569-018-0119-4
- Zhao, P., Yao, Q., Zhang, P. J., The, E., Zhai, Y., Ao, L., et al. (2021). Single-cell RNA-seq reveals a critical role of novel pro-inflammatory EndMT in mediating adverse remodeling in coronary artery-on-a-chip. *Sci. Adv.* 7:eabg1694. doi: 10.1126/sciadv.abg1694

Conflict of Interest: The authors declare that the research was conducted in the absence of any commercial or financial relationships that could be construed as a potential conflict of interest.

Publisher's Note: All claims expressed in this article are solely those of the authors and do not necessarily represent those of their affiliated organizations, or those of the publisher, the editors and the reviewers. Any product that may be evaluated in this article, or claim that may be made by its manufacturer, is not guaranteed or endorsed by the publisher.

Copyright © 2022 Yu, Fu, Zhang, Cui and Cheng. This is an open-access article distributed under the terms of the Creative Commons Attribution License (CC BY). The use, distribution or reproduction in other forums is permitted, provided the original author(s) and the copyright owner(s) are credited and that the original publication in this journal is cited, in accordance with accepted academic practice. No use, distribution or reproduction is permitted which does not comply with these terms.



Mechanotransduction Regulates the Interplays Between Alveolar Epithelial and Vascular Endothelial Cells in Lung

Chuyang Lin[†], Xiaolan Zheng[†], Sha Lin[†], Yue Zhang^{*}, Jinlin Wu^{*} and Yifei Li^{*}

Key Laboratory of Birth Defects and Related Diseases of Women and Children of MOE, Department of Pediatrics, West China Second University Hospital, Sichuan University, Chengdu, China

OPEN ACCESS

Edited by:

Xiaojing Liu,
Sichuan University, China

Reviewed by:

Linhong Deng,
Institute of Biomedical Engineering
and Health Sciences, China
Xupe Huang,
Florida Atlantic University,
United States

*Correspondence:

Yue Zhang
857612594@qq.com
Jinlin Wu
373053785@qq.com
Yifei Li
liyfwcsh@scu.edu.cn

[†]These authors have contributed
equally to this work

Specialty section:

This article was submitted to
Vascular Physiology,
a section of the journal
Frontiers in Physiology

Received: 19 November 2021

Accepted: 28 January 2022

Published: 18 February 2022

Citation:

Lin C, Zheng X, Lin S, Zhang Y,
Wu J and Li Y (2022)
Mechanotransduction Regulates
the Interplays Between Alveolar
Epithelial and Vascular Endothelial
Cells in Lung.
Front. Physiol. 13:818394.
doi: 10.3389/fphys.2022.818394

Mechanical stress plays a critical role among development, functional maturation, and pathogenesis of pulmonary tissues, especially for the alveolar epithelial cells and vascular endothelial cells located in the microenvironment established with vascular network and bronchial-alveolar network. Alveolar epithelial cells are mainly loaded by cyclic strain and air pressure tension. While vascular endothelial cells are exposed to shear stress and cyclic strain. Currently, the emerging evidences demonstrated that non-physiological mechanical forces would lead to several pulmonary diseases, including pulmonary hypertension, fibrosis, and ventilation induced lung injury. Furthermore, a series of intracellular signaling had been identified to be involved in mechanotransduction and participated in regulating the physiological homeostasis and pathophysiological process. Besides, the communications between alveolar epithelium and vascular endothelium under non-physiological stress contribute to the remodeling of the pulmonary micro-environment in collaboration, including hypoxia induced injuries, endothelial permeability impairment, extracellular matrix stiffness elevation, metabolic alternation, and inflammation activation. In this review, we aim to summarize the current understandings of mechanotransduction on the relation between mechanical forces acting on the lung and biological response in mechanical overloading related diseases. We also would like to emphasize the interplays between alveolar epithelium and vascular endothelium, providing new insights into pulmonary diseases pathogenesis, and potential targets for therapy.

Keywords: mechanotransduction, alveolar epithelial cells, vascular endothelial cells, pulmonary diseases, interplays

INTRODUCTION

As an area of gas exchange, the lung has extensive vascular and bronchial-alveolar networks and displays tension properties after birth. Accordingly, mechanical stimulation contributes significantly to maintaining the normal development of pulmonary tissue as well as its functional homeostasis. The adaptation to mechanical stress is differentially regulated among various parts of the human body, with surrounding microenvironments providing different physical stimuli that activate sensory transduction signaling pathways in a tissue-specific manner. The transformation of external mechanical forces into intracellular signaling is called mechanotransduction. There are two

common types of mechanosensors—biophysical and biochemical—located on the cell membrane. Biophysical sensors help connect the extracellular matrix (ECM) with the actin cytoskeleton and reshape actin proteins and the nuclear membrane, ultimately leading to altered chromosomal structure and patterns of gene expression. Meanwhile, chemical sensors primarily influence the modification of downstream molecules, converting external biophysical signals into intracellular biochemical ones. A stable mechanical environment is required for development, especially during tissue specialization. Notably, the pulmonary microenvironment is consisted with airway structure and vascular vessels. The alveolar epithelium and vascular endothelium are supposed to subject different injuries under various pathological mechanical conditions. However, the stimulation from either epithelial or endothelial cells would remodel the gas exchange environment in consequence and affects each other *via* their communications. Thus, there are several interplays between alveolar epithelial and endothelial cells in mechanotransduction manner. Moreover, mesenchymal transition could both be identified in epithelial (EMT) and endothelial (EndMT) cells. So that, we would like to summarize the physiobiological changes under pathological mechanical stress for lung epithelial and endothelial cells, and also try to demonstrate how they influence each other.

MECHANICAL STRESS IS CRITICAL DURING PULMONARY DEVELOPMENT AND FUNCTIONAL HOMEOSTASIS

The lung is composed of epithelial cells such as the type I and type II alveolar cells (AT1 and AT2 cells), endothelial cells of the arteries, veins, and capillaries, stromal cells, and multiple immune cell types such as the monocytes and macrophages (Travaglini et al., 2020). Different cell types in the lungs vary in their ability to withstand mechanical forces during respiration and pulmonary blood flow. The alveolar unit is the basic functional unit in the lung for gas exchange and is mostly composed of AT1, AT2, and capillary endothelial cells, as well as monocytes and macrophages (Spieth et al., 2014).

During early pregnancy, the pulmonary luminal volume in the fetus is significantly low. The pulmonary pressure gradient of the lung fluid increases the elasticity of the fetal lung tissues and stimulates the lung epithelial cells to actively secrete chloride ions. These chloride ions are transported into the stroma and the lung cavity by blood. The chloride ions move along a concentration gradient toward the lumen through the chloride channels to form the lung fluid, which prevents the amniotic fluid from entering the airways; the lung fluid also removes mucus and other cell debris from the airway cavity (Cotten, 2017). In the animal models, lung fluid secretion increases when the pressure in the lumen drops below that of the amniotic fluid. Reduced amniotic fluid volume increases the gradient between intraluminal pressure and amniotic fluid pressure. This increases the lung fluid outflow and reduces the expansion pressure in the lumen and the concentrations of various growth and maturation factors (Najrana et al., 2017, 2021). The growth

factors are released when the lung tissues stretch in response to the fetal breathing movements, and stimulate the proliferation and differentiation of the epithelial cells and the production of surfactants. Early mammalian airways exhibit spontaneous transient airway obstructions due to airway peristalsis. Peristaltic contractions and airway occlusions induce rhythmic stretching and relaxation of the growing buds by directing the fluid waves to the apex of the lung. Therefore, the airway peristalsis and obstruction generate pressure and extension of the developing lung tip (Jesudason, 2009).

Alveolar development begins before birth and continues until adolescence. Postnatal periodic stretching is a key determinant of lung size and is essential for septum extension. During the respiratory cycle, the lung matrix experiences cyclic stretching because of the periodic tension that is applied on the developing lung tissue. Based on *in vitro* experimental results, 5–12% cyclic stretching is considered as physiological stress, whereas $\geq 20\%$ cyclic stretching is considered as pathological stress (Young et al., 2015). The synthesis and remodeling of the lung matrix is required for primary and compensatory lung growth. Lung elastase activity is dependent on the tensile strength. In the mice, elastase activity increases by two-fold during the alveolar stage of postnatal lung morphogenesis (Young et al., 2015). This demonstrates the effects of postnatal respiratory movement on alveolar development. Furthermore, periodic alveolar tension is mediated by the release of growth factors *via* multiple intracellular signal transduction pathways.

Endothelial cells, fibroblasts, and smooth muscle cells are continuously stimulated in the pulmonary arteries by mechanical forces such as shear stress and pulsatile blood pressure. Both shear stress and pulsatile blood pressure are altered under conditions of pulmonary hypertension (PH). In response to blood pressure, pulmonary arterial endothelial cells (PAECs) align longitudinally to form the inner tunica of the blood vessels, whereas the pulmonary arterial smooth muscle cells (PASMCs) align circumferentially to form the median layer. The composition of the ECM also contributes to arterial stiffness and modulates the mechanical forces acting on the vessel wall. ECM is secreted by the PASMCs and pulmonary artery adventitial fibroblasts (PAAF). ECM interacts with the cells through the stretch-activated channels (SAC) and receptors such as the integrins. Therefore, ECM plays a key role in the stiffness-dependent activation of vascular endothelial cells.

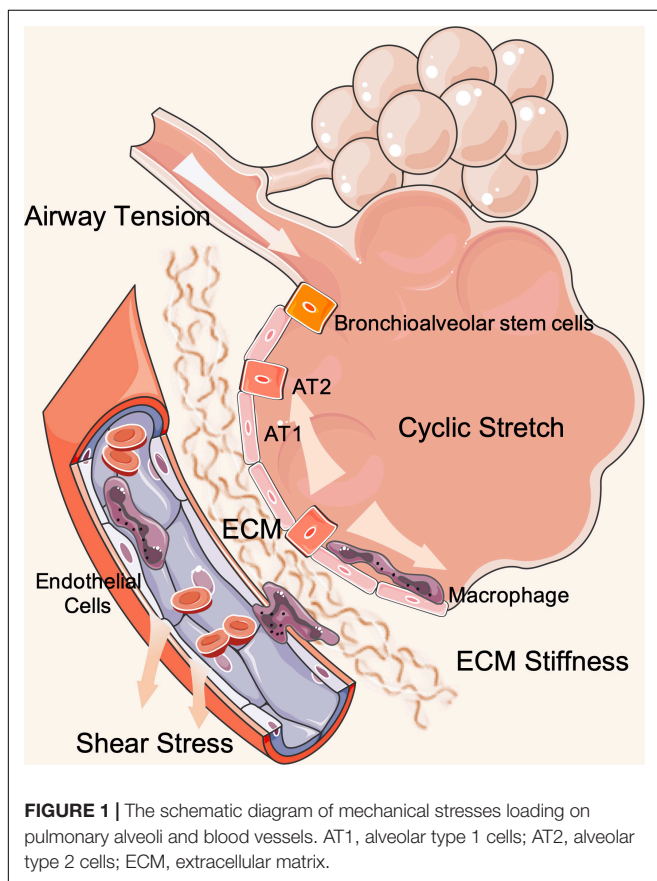
In general, the fetal lung is subjected to gradient lung fluid pressure and airway peristalsis. After birth, cyclic stretching stimulates lung development as a result of breathing movements and shear stress induced by blood flow, which act on the PAECs and the alveolar epithelium.

MECHANOTRANSDUCTION IN ALVEOLAR EPITHELIAL CELLS AND VASCULAR ENDOTHELIAL CELLS

Physical strain is characterized by the relative change in length in response to applied force. Alveolar epithelial cells are subjected to mechanical strain during breathing, whereas

vascular endothelial cells are primarily affected by shear stress, strain, and hydrostatic pressure. Distinct types of cells in the lungs experience diverse mechanical forces based on their location. For example, the apical surface of the epithelium experiences shear stress from the fluid layer in the airways and the alveoli, whereas the basolateral surface of the epithelium experiences stretch or strain due to expansion of the basement membrane. Therefore, two different types of physical forces act on the same cell type (alveolar epithelial cells) and regulate distinct biological functions *via* signal transduction pathways (Garcia et al., 2006). Furthermore, contraction of the actin cytoskeleton induces tension that is transmitted throughout the cell including the nucleus. The pulmonary cells also interact with the surrounding environment through adhesion receptors such as the integrins, which function as a link between the cytoskeleton and the ECM. The cytoskeleton is an interconnected biopolymer network within the plasma membrane that exerts a centripetal force on the surrounding matrix.

Several studies have investigated the mechanisms that regulate cellular structure, function, proliferation, differentiation, secretion, movement, and metabolism in response to mechanical stimulation by physical forces (Liao et al., 2020; Liu et al., 2021). Aberrant mechanical stretching can result in cellular barrier dysfunction, metabolic dysfunction, cytotoxicity, and inflammation (Figure 1).



Mechanical Forces Regulate the Homeostasis of Alveolar Cells

AT1 and AT2 are two different types of alveolar epithelial cells. AT1 cells do not show any proliferative capacity and are mainly involved in gas exchange, whereas, the AT2 cells can differentiate into AT1 cells and are the major source of pulmonary surface-active material. AT1 cells account for more than 95% of the alveolar surface area and respond to periodic stretches through genomic changes to modulate paracellular permeability.

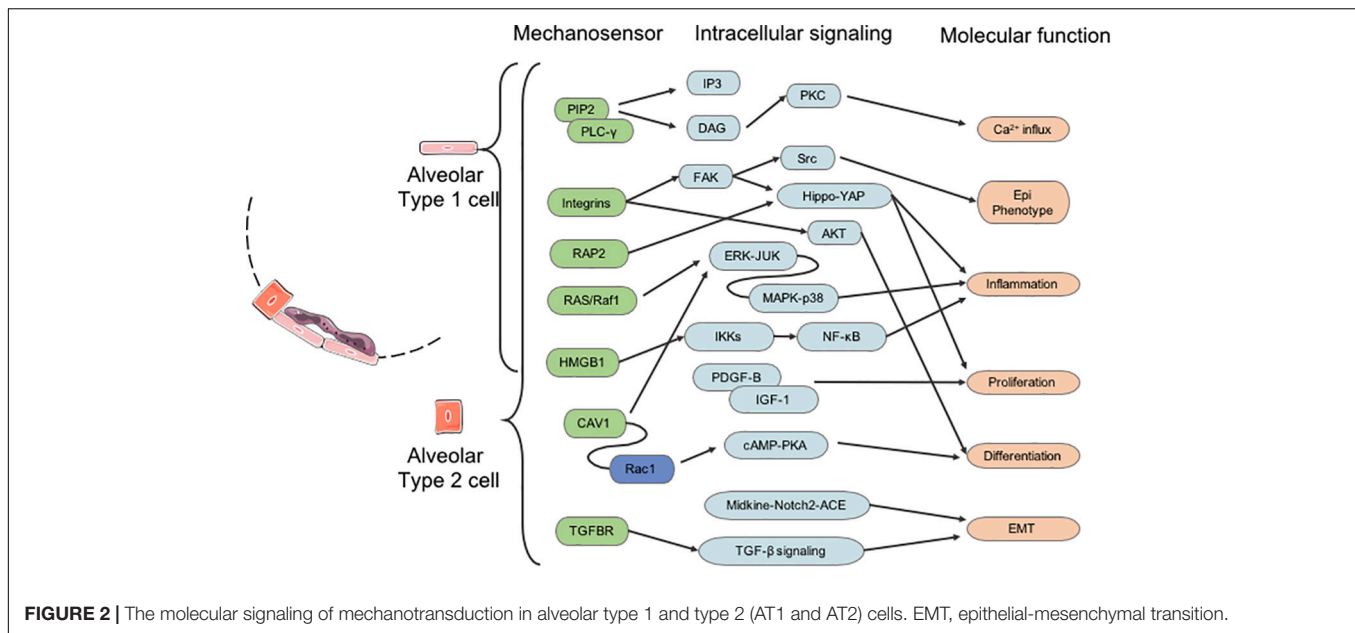
Mechanical stretching promotes proliferation (Han et al., 2005), secretion and metabolism of surface-active substances, cellular damage or death (Arold et al., 2009), and migration (Desai et al., 2008) of AT2 cells. The proliferation of alveolar epithelial cells is essential for maintaining the integrity of the epithelium, especially during the process of repair after lung injury. Mechanical forces induce mitotic activity and growth factor synthesis and secretion by the alveolar epithelial cells (Noskovičová et al., 2015). AT2 cells subjected to periodic mechanical stress in FlexCell units display increased DNA synthesis after exposure to conditioned medium from lung fibroblasts compared to those cultured under static conditions. Mechanical strain also activates the expression of platelet-derived growth factor receptor beta (PDGFRB) in the lungs during development. Synthesis and secretion of pulmonary surfactants is the major biological function of the AT2 cells. Cyclic stretch stimulates the release of surfactant phospholipids from the AT2 cells by rapidly increasing the intracellular calcium ion concentrations.

Integrins, growth factor receptors, G-protein-coupled receptors, mechanoresponsive ion channels (e.g., Ca^{2+}), and cytoskeletal strain responses are the main mediators of signal transduction pathways in response to changes in the extrinsic biochemical environment (Duscher et al., 2014). Furthermore, mechanical forces also transduce signals through several mechanosensitive focal adhesion proteins. The integrins transmit extracellular signals and induce intracellular cytoskeletal modifications (Figure 2).

Ion Channels

During fetal development, physiological stretching drives lung growth and maturation. The α -subunit of the alveolar epithelial sodium channel (ENaC) facilitates the clearance of lung fluid during the perinatal period. Mustafa et al. (2014) demonstrated that mechanical stretching induced the expression of ENaC *via* p38-mitogen-activated protein kinase (MAPK) and c-Jun N-terminal kinase (JNK).

Stretching also induces Ca^{2+} influx by activating the ion channels. TRPV4 and Piezo1 serve as the main ion channels that mediate the influx of Ca^{2+} ions in the alveolar epithelial cells. Liang et al. (2019) demonstrated that Piezo1 expression was significantly increased in the AT2 cells of patients with acute respiratory distress syndrome (ARDS); moreover, Piezo1 induced Bcl-2 dependent apoptosis *via* Ca^{2+} influx, but these effects were attenuated by inhibiting Piezo1. Mechanical stretching also induces the protein tyrosine kinases (PTK) to activate phospholipase C- γ (PLC- γ) through tyrosine phosphorylation



(Liu et al., 2014). Active PLC- γ hydrolyzes phosphatidylinositol 4,5-bisphosphate (PIP2) into 1,4,5-trisphosphate (IP3) and diacylglycerol (DAG). IP3 mobilizes Ca^{2+} from the intracellular storage sites such as the endoplasmic reticulum (ER), whereas, DAG activates protein kinase C (PKC) in the presence of intracellular Ca^{2+} (Hsiao et al., 2016; Lu et al., 2021).

Integrins-FAK-MAPK-NF- κ B

Activated integrins regulate several intracellular signaling molecules and pathways by recruiting focal adhesion proteins and the focal adhesion kinase (FAK). Besides, integrins function as a bridge between the F-actin cytoskeleton and the ECM and transduce signals generated through changes in mechanical stress. The integrin-Talin-F-actin-Nestin-SUN-nuclear lamina signaling axis modulates the nuclear envelope and induces transcriptional changes in response to the extracellular mechanical stress (Sun et al., 2016). Mechanical forces promote TRE-mediated gene expression *via* activation of RAS, ERK1/2, and JNK signaling pathways by reinforcing integrin-ECM binding (Parsons et al., 2010; Cho et al., 2017). Furthermore, p38-MAPK and several transcription factors downstream of various intrinsic signaling pathways are also activated, subsequently leading to the activation of NF- κ B (Liu et al., 2016). Integrin family members also activate I κ B kinases (IKKs), which induce the release of NF- κ B from the cytoplasm to the nucleus in response to signals for maintaining lung development and alveolarization. MAPKs and NF- κ B promote the transcription of several early response genes, which subsequently induce the transcription of inflammation-related genes *via* the cyclooxygenase (COX)-2/prostaglandin E2/Interleukin (IL)-8 signaling pathway (Dong et al., 2015).

Rho GTPase-YAP/TAZ

Rho-associated protein kinase (ROCK), myocardin-related transcription factor-A (MRTF-A), yes-associated protein 1

(YAP), and transcriptional coactivator with PDZ-binding motif (TAZ) are key players in the response of the alveolar epithelial cells to mechanical stimulation (Deng et al., 2020). Rho guanosine triphosphatase (GTPase) are a family of small G-proteins of the Ras superfamily such as Rac, Rho, and CDC42 are small GTP-binding signaling proteins that regulate cytoskeletal dynamics by mediating actin polymerization and myosin II-mediated contraction through FAK (Jiang et al., 2012; Maurer and Lammerding, 2019). RAP2a is a novel Rap GTPase that responds to mechanical stretch, but its actual function in the pulmonary system has not been established (Meng et al., 2018). Rho-mediated actin polymerization induces MRTF-A nuclear translocation, activation of α -smooth muscle actin (α -SMA) gene expression, and type I collagen synthesis (Ni et al., 2013).

Metabolic Status

Mechanical stress induces oxidative damage and ER stress in the alveolar epithelial cells, which release injury-related molecules with damage-associated molecular patterns (DAMPs) that trigger tissue repair and fibrotic response (Lionetti et al., 2005; Tanaka et al., 2017; Valentine et al., 2018). DAMPs and high mobility group box 1 (HMGB1) released by the injured tissues promote tissue repair and angiogenesis by inducing the migration and proliferation of stem cells (Yang et al., 2020). When regeneration is not successful, HMGB1 induces fibrosis by stimulating fibroblast activation and endothelial cell proliferation. Patel et al. (2020) demonstrated that hypoxia induced the activation of host macrophages *via* HMGB1, but these effects were attenuated by the dietary antioxidants.

Mechanical Forces Regulate Functions of Vascular Endothelial Cells

The mechanical forces associated with cyclical stretching and shear stress play a key role in regulating vascular function

and homeostasis of pulmonary circulation. The pulmonary microvascular endothelium is exposed to continuous or periodic stretching during spontaneous breathing and blood flow. Shear stress, stiffness, and cyclic stretch modulate the function and metabolic status of the endothelial cells. The lung microvasculature is subjected to mechanical forces including shear stress and cyclic stretch, which vary with the cardiac and breathing cycles. Endothelial cells are continuously subjected to shear stress that range from 10 to 50 dyne/cm² in the large arteries, 5 to 20 dyne/cm² in the microvasculature, and 10-fold lower in the veins compared to the arteries (Paszowski and Dardik, 2003). Physiological circulatory stretching increases the expression of the tight junction-associated protein, occludin, which strengthens the endothelial barrier and upregulates the expression of integrins in the endothelial cells. This further enhances cell adhesion in the EC monolayer and increases the resistance to hemodynamic forces or excessive vasodilation (Figure 3).

Ca²⁺ Signaling

In the pulmonary vascular endothelial cells, Ca²⁺ permeable non-selective cationic stretch-activated ion channels (SACs) share similar electrophysiological properties such as linear I–V relationship of the evoked currents with a reverse potential about 0 mV and unitary conductance around 30 pS (Ducret et al., 2010). Transient receptor potential (TRP) channels represent a superfamily of non-selective cationic channels that play a significant role in the endothelial cells. TRPV channels such as TRPV1 and TRPV4 are expressed in the PAECs (Barbeau et al., 2021). TRPV1-activated signaling pathways in the PAECs provide counterbalancing effects at the site of the blood vessel. Furthermore, TRPV4 is widely expressed in every layer of the pulmonary artery (PA) and participates in maintaining the normal biological functions of the vessels. In the PAECs, TRPV4 plays a key role in vasodilation *via* nitric oxide (NO) signaling and endothelium-derived hyperpolarizing factor (EDHF) (Sukumaran et al., 2013). Furthermore, TRPV4 interacts with the endothelial nitric oxide synthase (eNOS) in the PAECs and induces the release of NO by activating unitary Ca²⁺ influx that stimulates the guanylyl cyclase–protein kinase G pathway (Ottolini et al., 2020). Furthermore, mitochondrial impairment in PH causes accumulation of reactive oxygen species (ROS), which induce TRPV4 mediated Ca²⁺ influx. TRPC1 is expressed in the PSMCs and PAECs of rats, mice, and humans (Malczyk et al., 2013). TRPC1 is overexpressed in the PH models. In the pulmonary endothelial cells, TRPC4 regulates microvascular permeability, agonist-dependent vasorelaxation, and gene transcription (Firth et al., 2007). TRPP1 and TRPP2 are both expressed in the vascular smooth muscles and ECs of the cerebral and mesenteric arteries, and regulate blood vessel functions and myogenic tone. However, the roles of TRPP channels in the pulmonary vasculature are not known and require further investigations.

In mammals, two Piezo proteins, namely, Piezo1 and Piezo2 have been reported. Deletion of the Piezo1 gene in mice causes aberrant vascular development resulting in early embryonic death around day 10 (Li et al., 2014). Endothelial Piezo1 channels

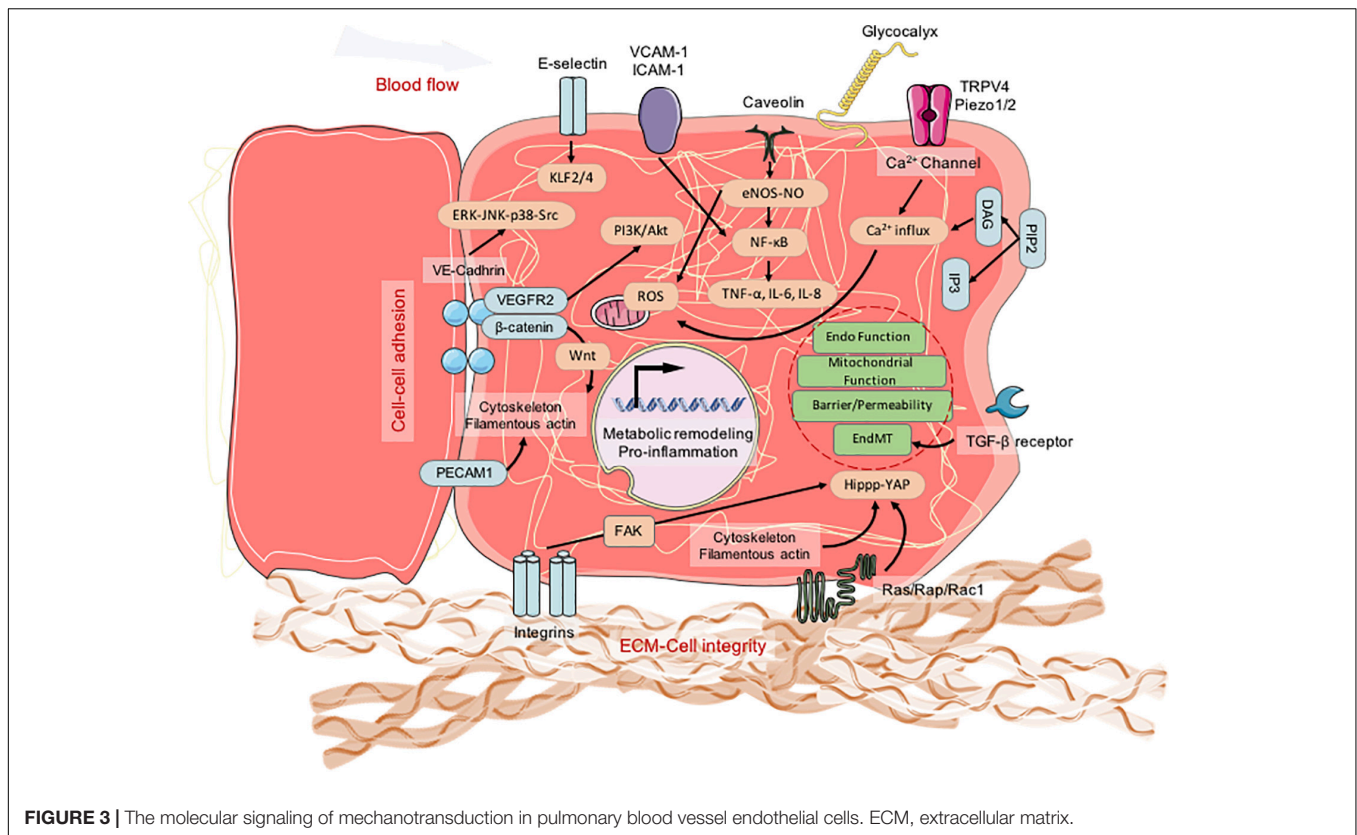
are necessary for flow-induced vasodilatation through eNOS activation and release of NO (Wang et al., 2016). Besides, NO production is also induced by ATP release through the pannexin channels, which activates the P2Y2 receptors and eNOS (Wang et al., 2016). By contrast, in the mesenteric vessels, Piezo1 induces flow-sensitive cationic ion influx in the ECs of the mesenteric vessels and depolarizes the membrane. This depolarization spreads to the adjacent PSMCs and activates the voltage gated Ca²⁺ channels, thereby inducing vasoconstriction (Rode et al., 2017). Kang et al. (2019) reported that genetic deletion or pharmacological inhibition of Piezo1 reduced the endothelial sprouting and lumen formation when induced by shear stress and the proangiogenic mediator, sphingosine 1-phosphate. Yoda1 enhanced sprouting angiogenesis by activating Piezo1. Physical stimuli triggered Piezo1-mediated Ca²⁺ influx and activated matrix metalloproteinase (MMP)-2 and membrane type 1 MMP, both of which synergistically facilitated sprouting angiogenesis (Kang et al., 2019). Piezo2 is also present in the human PAECs, but its function is currently unknown (Lambert et al., 2018).

Krüppel-Like Factor 2 and Krüppel-Like Factor 4

The Krüppel-like factor (KLF) family of transcription factors regulate integral EC functions, including growth, inflammation, migration, proliferation, cell differentiation, plasticity, and apoptosis (Chang et al., 2017). KLF2 and KLF4 are master transcription factors that regulate vasodilatory, anti-inflammatory, and antithrombotic properties of the quiescent endothelial cells (Denis et al., 2019). KLF2 and KLF4 are upregulated by disturbed flow, and subsequently suppressed PFKFB3 and PFK1, two critical proteins involved in glycolysis (Doddaballapur et al., 2015). Decreased expression of KLF2 or KLF4 induces the production of inflammatory cytokines in the endothelial cells. Stable blood flow reduces glycolysis in a KLF2-dependent manner, and increases mitochondrial biogenesis through PPARγ/PGC1 signaling (Pollak et al., 2018). Furthermore, unidirectional flow promotes the degradation of HIF-1α, which inhibits pyruvate dehydrogenase kinase 1 (PDK1) and increases mitochondrial complex I activity. Slegtenhorst et al. (2018) reported the endothelial atheroprotection role of KLF2 and its inducer, Simvastatin.

Integrins-Cytoskeleton-Lamin A

Cells respond to external forces through integrin-mediated remodeling of the ECM (Sun et al., 2016). Stretch-induced activation promotes interactions between integrins and focal adhesion proteins, thereby converting the mechanical signal into biochemical cascades. In the endothelial cells, integrins α2 and β1 stimulated the p38-MAPK signaling pathway (Bix et al., 2004). Focal adhesion integrates the actin cytoskeleton with the ECM interface and helps maintain the endothelial cell barrier integrity. Increased focal adhesion triggers the activation of small GTPase and Rho kinase signaling pathways. High magnitude cyclic stretching (18%) stimulates the formation of focal adhesion complexes that included paxillin, ERK1/2, MAPK, NF-κB, RhoA, and GEF-H1. Moreover, focal adhesion is redistributed under shear stress (15 dyn/cm²). In vascular endothelial cells, VE-cadherin acts as a link between the cytoskeleton and the adherens



junctions (Fang et al., 2019). VE-cadherin regulates the cellular orientation of endothelial cells in response to shear stress through PECAM-1, VEGFR2, and PI3K signaling (Tzima et al., 2005). Endothelial cells also sense and transmit the mechanical force-induced signals *via* gap junction-mediated propagation of Ca^{2+} signaling. Connexin-32 responds to mechanical stimulation by generating intracellular Ca^{2+} waves through N-cadherin (Ko et al., 2001). Hence, the interaction between gap and adherens junctions is critical for establishing cell-cell communications. The cytoskeleton plays a critical role in transducing mechanical stress-related signals. Deguchi et al. (2005) demonstrated that the force should be balanced between the basal actomyosin stress fibers and focal adhesion complexes in the endothelial cells. Depolymerization of F-actin, ROCK inhibitor, and PKA activation results in actin disassembly, attenuation of actomyosin assembly, and stress fiber formation. Cytoskeletal changes result in the activation of RhoA and Rac GTPases, which promote cellular reorientation and transcription responses by altering lamin A; knock-down of lamin A abolishes the changes of histone deacetylases (HDAC), thereby demonstrating the role of lamin A in regulating the chromatin state (Nayebosadri and Ji, 2013).

Rho GTPase-YAP/TAZ

Endothelial barrier regulation is dependent on the cytoskeletal rearrangements (Vogel and Malik, 2012). The small Rho GTPases, RhoA, and Rac1, are central regulators of vascular permeability through cytoskeletal reorganization (Asano-Matsuda et al., 2021). RhoA and Rac1 exert opposing functional

effects. RhoA activation promotes endothelial contraction and induces barrier disruption, whereas Rac1 stabilizes the endothelial junctions and increases barrier integrity. Ke et al. (2019) demonstrated a key role for RhoA GTPase in high cyclic stretch-induced endothelial cell barrier dysfunction. Besides, Rap1 GTPase is also involved in the regulation of cytoskeleton and cell junctions. Rap1-mediated signaling induced lung vascular EC barrier restoration; inhibition of Rap1 activity enhanced ventilator-induced lung injury (VILI) at both low- and high-volume ventilation conditions (Ke et al., 2019). The Hippo/YAP signaling pathway is also involved in mechanotransduction. YAP and TAZ are activated by stiff ECM and serve as a central regulatory hub for cellular proliferation and survival in multiple organs during tissue growth and development (Dupont et al., 2011). Furthermore, ECM stiffening promotes vascular cell growth and migration *via* YAP/TAZ-dependent glutaminolysis and anaplerosis, thereby linking mechanical stimulation to vascular metabolic dysregulation (Bertero et al., 2016). Therefore, YAP/TAZ pathway is a potential metabolic drug target in PH therapy. Greater stiffnesses (around 50 kPa) increases the proliferation and migration of endothelial cells through the YAP/TAZ signaling pathway (Bertero et al., 2016), TGF- β , Toll-like receptors, and NF- κ B (Thenappan et al., 2018). NF- κ B functions as a nuclear effector that integrates signals from multiple signaling pathways. Membrane receptors such as Toll-like receptors (Davidovich et al., 2013; Liu et al., 2013) stimulate the expression of MCP-1, a potent chemoattractant for monocytes, and increase the expression

of IL-6 and COX-2. The activation of NF- κ B is mediated by the integrins through the PI3K-PLC-PKC signaling cascade (Mussbacher et al., 2019).

Metabolic Status

Mitochondria anchor to the cytoskeleton and function as mechanotransducers by releasing ROS in response to the cytoskeletal strain (Ali et al., 2004). Besides, ROS play a key role in the activation of NF- κ B and VCAM-1. In the ECs, mitochondria-derived H₂O₂ diffuses into the cytosol in response to shear stress and initiates oxidative signaling that upregulates hemeoxygenase(HO)-1 and maintains the atheroprotective EC status (Han et al., 2009). NADPH oxidases (NOXs), mitochondria, and xanthine oxidases are the main sources of superoxide in response to mechanical stress (Ichimura et al., 2003; McNally et al., 2003). Stretch-induced ROS production in the endothelium upregulates the expression of cell adhesion molecules and chemokines in collaboration with several ROS-generating enzymes such as NADPH oxidases and eNOS. In the pulmonary endothelial cells, NO levels are increased through PI3K, AKT, and eNOS. Moreover, xanthine oxidoreductase (XOR) is activated by the p38 and ERK1/2-MAPK signaling pathways. ROS signaling is regulated by cyclic stretch in an amplitude-dependent manner and plays a critical role in various EC responses to cyclic stretch. Long-term cyclic stretching (5–12%) caused magnitude-dependent downregulation of Nox4, Cu/Zn superoxidase dismutase (SOD), MnSOD, catalase, and ROS (Goettsch et al., 2009). Cyclic stretching regulates survival and angiogenesis of endothelial cells *via* NOX-induced ROS.

Yamamoto et al. (2020) used real-time imaging technology to demonstrate the novel role of endothelial mitochondria in transducing shear stress signals by triggering ATP generation and release, and purinoceptor-mediated Ca²⁺ signaling. Glycolysis is a crucial metabolic pathway that converts glucose first to pyruvate and then to lactate. Endothelial cells are highly glycolytic (Wu and Birukov, 2019). Furthermore, the glycolytic index (lactate/glucose ratio) in cultured human umbilical vein endothelial cells (HUVECs) is around 1.74, which suggests that the endothelial cells metabolize glucose entirely into lactate (Kim et al., 2017). Thus, only a small fraction of the glycolytic intermediate pyruvate is metabolized by the mitochondrial OXPHOS. Endothelial cells, in contrary to other cell types, are as glycolytic as the tumor cells (De Bock et al., 2013a), and use very little oxygen to generate ATP (De Bock et al., 2013b). Therefore, glycolysis plays a critical role in nucleic acid synthesis and survival, whereas electron transport chain-dependent mitochondrial metabolism is required for cell proliferation, angiogenesis, and redox balance.

PATHOLOGICAL MECHANICAL STRESS INDUCES PULMONARY DISEASES

Ventilation Induced Lung Injuries and Acute Respiratory Distress Syndrome

Exposure to non-physiological stretch disrupts the normal mechanical stress response mechanisms and triggers aberrant

repair mechanisms during lung injury. Mechanical ventilation induces or exacerbates ventilation-induced lung injury (VILI). Dagenais et al. (2018) showed that scratching the AEC monolayer generates a TRPV4-dependent Ca²⁺ wave, which spreads from the margin of the scratch to the distant cells and induces abnormal activity of the epithelial sodium channel, ENaC; moreover, TRPV4 agonist, GSK1016790A, abolishes the Ca²⁺ wave and other downstream signaling events (Dagenais et al., 2018). Diem et al. (2020) demonstrated that small plasma membrane invaginations called caveolae in the AT1 cells play a key mechanotransductive role in the AT1 cells by responding to mechanical stress at the plasma membrane; these caveolae are absent in AT2 cells. Ventilation-induced stretch stimulates Ca²⁺ entry *via* caveolae-resident Piezo1-activated pannexin-1 hemichannels and results in ATP release from the AT1 cells. The released ATP triggers Ca²⁺ influx in the neighboring AT2 cells and induces inflammation by recruiting the monocytes. Liang et al. (2019) reported increased expression of Piezo1 in the AT2 cells mediates Ca²⁺ influx and triggers Bcl-2 dependent apoptosis during ARDS, but these effects are abrogated by inhibiting Piezo1. Since the vascular endothelial cells are subjected to cyclic stretch during alveolar movement, they are prone to damage during VILI. Zhang et al. (2021) reported higher Piezo1 expression in the pulmonary endothelial cells in response to high tidal volume mechanical ventilation and cyclic stretching. Enhanced expression of RhoA/ROCK1 in the endothelial cells subjected to cyclic stretch or Yoda1 treatment is significantly abrogated by Piezo1 deficiency or inhibition of Piezo1. Furthermore, inhibition of RhoA/ROCK1 signaling does not affect Piezo1 expression, but the inhibition of Piezo1 by GSMTx4 alleviates VILI-induced pathological changes (Zhang et al., 2021).

Inflammation is one of the major causes of lung injury. High tidal volume mechanical ventilation induces significant changes in microvascular permeability, neutrophil infiltration, levels of malondialdehyde, macrophage inflammatory protein-2 (MIP)-2, and NF- κ B, and the activation status of the NF- κ B repressing factor (NKRF). Yehya et al. (2019) showed that the human epidermal growth factor receptor 3 (HER3) ligand neuregulin-1 (NRG1) enhances VILI by activating HER2 and induces increased permeability and upregulation of claudin-7. HER2 activates the IL-6 receptor and the IL-6 inflammatory loop, which contributes to lung injuries. Ning et al. (2012) shows that mechanical stretch induces early apoptosis and IL-8 secretion in the AT2 cells. Furthermore, mechanical stretch upregulates ER stress and increases the expression levels of monocyte chemoattractant protein (MCP)-1/C-C motif chemokine ligand 2 (CCL2) and MIP-1 β /CCL4 pro-inflammatory chemokines in the AT2 cells, thereby enabling monocyte recruitment (Valentine et al., 2018). Furthermore, EC-derived microparticles (EMPs) are released during significant lung inflammation and injury. Zhang et al. (2014) demonstrated that during mechanical ventilation-induced VILI, NLRP3 inflammasomes released by the endothelial or epithelial cells mediated the recruitment of pulmonary macrophages and induced autophagy in the lung epithelial cells. In the *in vivo* experiments, mechanical ventilation induces lung leukocyte recruitment as well as accumulation of cells and

cytokines in the alveolar space. Cyclic stretch-induced endothelial cells activated gVPLA2, which enhances the expression levels of intercellular adhesion molecule 1 (ICAM-1) and promotes the adhesion of polymorphonuclear neutrophils to the EC, thereby inducing EC injury (Meliton et al., 2013).

Ding et al. (2012) showed that mechanical stretch significantly enhances MAP2K6 activity and HMGB1 protein expression in alveolar epithelial cells. Wolfson et al. (2014) reported increased HMGB1 expression in the human lung micro-vessel endothelial cells exposed to excessive mechanical stress *via* STAT3 and Rho GTPase signaling. Gao et al. (2014) demonstrated that pathological cyclic stretching significantly increases lung cell apoptosis by repressing Rac and increasing Rho expression levels.

Pathological elevation of lung vascular pressure or regional or generalized overdistension of pulmonary microvascular and capillary beds caused by mechanical ventilation at high tidal volumes are two commonly encountered clinical scenarios in lung diseases. Elevated mechanical strain on the lungs increases the production of ROS in both endothelial and alveolar epithelial cells and causes VILI (Poljsak et al., 2013). Cyclic stretching in AT1 cells increases the ROS levels, which enhances monolayer permeability *via* activation of NF- κ B and ERK (Davidovich et al., 2013). These data suggest that antioxidants may prevent or alleviate VILI. Song et al. (2016) shows that rat AT2 cell monolayers generates increased levels of ROS, including NO and superoxide under mechanical ventilation stress. Tanaka et al. (2017) demonstrated that non-physiological cyclic stretch increased oxidative stress by up regulating NOX and DUOX2. Mitochondria-targeted antioxidant MitoTempo significantly reduces oxidative stress and prevents the dissociation of Claudin-4 and Claudin-7 from ZO-1, thereby alleviating VILI (Song et al., 2016). Ge et al. (2019) demonstrates that hydrogen sulfide (H₂S) significantly alleviates VILI by inhibiting inflammation and oxidative stress through PERK/eIF2 α /ATF4/GADD34 and NF- κ B/MAPK pathways. ROS accumulation triggers FasL/Fas extrinsic death pathway in the AT2 cells of newborn rats under prolonged mechanical ventilation (Kroon et al., 2013). miR-135a protects the endothelial cells from pathological mechanical stretching by binding to PHLP2 and activating the PI3K/AKT pathway (Yan et al., 2018).

Pulmonary Fibrosis

Pulmonary fibrosis is caused by abnormal tissue repair process driven by the alveolar epithelium, including aberrant fibroblast and myofibroblast proliferation and excessive deposition of ECM. AT2 cells play a key role in regeneration and repair after lung injury because they can differentiate into AT1 cells, the main epithelial cell type at the alveolar-capillary barrier for gas exchange. Hence, impaired renewal capacity of AT2 cells promotes fibrogenesis and the production of profibrotic factors (Selman and Pardo, 2020).

Yes-associated protein 1 plays a key regulatory role in the mechanical tension-induced alveolar regeneration in response to lung injury by activating the CDC42/F-actin/MAPK/YAP signaling cascade (Liu et al., 2016). Activation of YAP suppresses inflammation through I κ B α -NF- κ B signaling and accelerates alveolar epithelial regeneration and regression of fibrotic lesions.

Furthermore, MAPK-mediated activation of YAP promotes alveolar regeneration in response to the mechanical tone of the lung (Liu et al., 2016). YAP also contributes to pulmonary fibrosis by promoting abnormal cell proliferation, migration, and polarity of epithelial cells *via* mTOR/PI3K/AKT signaling (LaCanna et al., 2019). The profibrotic effects of YAP are exerted through its interaction with nuclear transcriptional factors and the activation of genes involved in ECM regulation, such as PAI-1, connective tissue growth factor (CTGF), TGF- β 1, COL1A1 and COL1A2 in idiopathic pulmonary fibrosis epithelial cells; YAP also promotes fibroblast growth on stiffness matrix (Giménez et al., 2017; Lee et al., 2020). In pulmonary fibrosis, MRTF-A interacts with the serum response factor (SRF) in the nuclear matrix and promotes transcription of COL1A2 and TGF- β 1, which increases the stiffness of ECM (Luchsinger et al., 2011).

Mechanical stretch activates TGF- β 1 pathway in the AT2 cells, which alters the homeostatic pulmonary microenvironment leading to aberrant wound healing and tissue fibrosis (Kuhn et al., 2019). In an *ex vivo* model, mechanical tissue stretching induces the activation of TGF- β 1 signaling *via* the Rho/ROCK signaling pathway and interactions with α v integrins (Froese et al., 2016). Wu et al. (2020) suggested that increased mechanical tension dysregulates the functions of the AT2 cells and decreases alveolar renewal capacity; tissue stretching during spontaneous breathing results in aberrant activation of the TGF- β 1 signaling loop and fibrosis progression (Wu et al., 2020). Furthermore, loss of CDC42 in the AT2 cells promotes periphery-to-center progressive lung fibrosis (Wu et al., 2020). CDC42 maintains the proliferative potential of AT2 cells. Non-physiological mechanical tension activates the TGF- β 1 signaling loop in the AT2 cells that drives periphery-to-center progressive lung fibrosis. Besides, *Tgfb1* shRNA treatment significantly reduces the expression of *Tgfb1* in the AT2 cells and the expression levels of type I collagen in the stromal cells. This demonstrates the key function of TGF- β 1 in the AT2 cells and fibrosis progression. Moreover, the production of free TGF- β ligands is significantly reduced in the *Cdc42*-null AT2 cells (Wu et al., 2020).

Clinically, ARDS patients who receive mechanical ventilation are prone to lung fibrosis *via* EMT through the Midkine-Notch2-ACE signaling pathway (Zhang et al., 2015). Furthermore, miR-19b overexpression promoted EMT in response to mechanical stretch by down-regulating PTEN (Mao et al., 2017). These studies suggested that EMT played a significant role in lung fibrosis due to mechanical stress. Non-physiological mechanical stretch stimulated excessive ATP release from the lung alveolar cells; ATP induced the release of IL-1 β *via* activation of the NLRP3 inflammasome through P2 \times 7R receptor binding and facilitated the progression of lung fibrosis (Gicquel et al., 2017). Increased pulmonary vascular pressure induced ROS accumulation due to mitochondrial dysfunction. Moreover, reduced caveolin-1 (CAV1) prevents pulmonary endothelial ROS production with cessation of flow (Milovanova et al., 2008). Mechanical stretching inhibits ERK signaling pathway by inducing the trafficking of CAV1 from the cell membrane to the cytoplasm.

EMT is a mechanism for epithelial remodeling and repair, wherein epithelial cells lose their epithelial characteristics

and acquire mesenchymal properties (Rout-Pitt et al., 2018). Therefore, dysregulated EMT promotes pulmonary fibrosis (Hewlett et al., 2018). Mao et al. (2017) shows that miR-19b participates in the EMT process in response to mechanical stretch by activating AKT through inhibition of PTEN. Restoration of PTEN expression or inhibition of AKT phosphorylation suppresses mechanical stretch induced EMT phenotype. Impaired lung mechanics after mechanical ventilation is associated with increased hydroxyproline content of the lung tissues, and increased expression levels of TGF- β , β -catenin, and mesenchymal markers, α -SMA and Vimentin.

Vascular endothelial cells also contribute to pulmonary fibrosis *via* inflammation, metabolic alterations, and endothelial to mesenchymal transition (EndMT). EndMT is dependent on mechanical forces such as shear stress and stiffness. TGF- β -induced EndMT occurs preferentially on stiffer substrates and is inhibited by blocking the β -catenin/Wnt signaling pathway (Zhong et al., 2018). TGF- β -induced EndMT is accompanied by inhibition of fatty acid oxidation, which is required for *de novo* nucleotide synthesis and endothelial cell proliferation (Schoors et al., 2015). Inhibition of fatty acid oxidation reduces intracellular levels of acetyl-CoA, which is required for maintaining the endothelial phenotype of EV cells (Xiong et al., 2018). NLRP3 inflammasome activation contributes to mechanical stretch induced EndMT and pulmonary fibrosis (Lv et al., 2018). Increasing stiffness of lung parenchyma promotes the expression of PF-related factors such as TGF- β and HIF-1 α in the endothelial cells (Phan et al., 2021).

Pulmonary Hypertension

Shear stress, stiffness, and cyclic stretch influence the functional and metabolic states of the endothelial cells. The lung microvasculature is subjected to mechanical forces due to the cardiac output including shear stress and cyclic stretch, which vary according to the cardiac and breathing cycle. Endothelial cells are continuously subjected to shear stress that can range from 10 to 50 dyne/cm² in the large arteries, 5 to 20 dyne/cm² in the microvasculature, and 10-fold lower in the veins compared to the arteries (Paszowski and Dardik, 2003). The calculated pressure on the PAECs in the PAH patients is 20.5 ± 4.0 dyne/cm² compared to 4.3 ± 2.8 dyne/cm² in the healthy individuals. The mechanical stress on the endothelial cells persists during disease progression. Clinically, pulmonary arterial hypertension (PAH) involves elevated mean pulmonary arterial pressure, pulmonary artery wedge pressure, and pulmonary vascular resistance (Kovacs et al., 2018). The prevalence of PAH among the pulmonary fibrosis patients is dependent on the severity of pulmonary fibrosis. In the early stages or when initially diagnosed, PAH affects < 10% of patients, but as the disease progresses, the incidence of PAH increases to 32% (Lettieri et al., 2006). Thus, PAH promotes the progression of lung fibrosis by exposing the capillary endothelial cells to higher mechanical stress.

Lhomme et al. (2019) demonstrated that endothelial Piezo1 promotes intrapulmonary vascular relaxation by regulating endothelial Ca²⁺ mobilization and NO production. The inhibition of Piezo1 attenuates the increased expression of NO

and Ca²⁺ mobilization. Iring et al. (2019) showed that the endothelial mechanosensitive cation channel Piezo1 mediates fluid shear stress-induced release of adrenomedullin and subsequent Gs-coupled receptor-mediated formation of cAMP that induced eNOS synthase *via* PKA activation; deletion of Piezo1 or adrenomedullin impairs vasodilation and induces hypertension (Iring et al., 2019). Kang et al. (2016) demonstrated that elevated levels of endothelin-1 (ET-1) and increased proliferation of PAECs in the PAH patients is regulated by PPAR γ . YAP/TAZ signaling pathway is involved in the responses of endothelial cells to mechanical stress. For example, *in vitro* experiments showed that cells exposed to higher stiffness (50 kPa) increased glycolysis *via* YAP/TAZ/Hippo signaling pathway. Therefore, activation of YAP/TAZ increases the proliferation and migration of endothelial cells, ECM stiffness, and metabolic shift from OXPHOS to glycolysis (Wang and Valdez-Jasso, 2021; Woodcock et al., 2021). NOTCH1 is downstream of bone morphogenetic protein receptor type 2 (BMPR2), which is implicated in PAH through enhanced glycolysis and histone acetylation; BMPR2 induces mitochondrial dysfunction in the endothelial cells and is required for NOTCH1 activation (Liu et al., 2017).

Furthermore, several miRNAs regulate the apoptosis of endothelial cells and play a role in PF. MiR-371b-5p increases proliferation of pulmonary artery endothelial cells (PAECs) *via* PTEN-PI3K-AKT signaling pathway (Zhu et al., 2018). MiR-7 regulates serine and arginine-rich splicing factor 1 (SRSF1), which promotes PAEC migration and increases the stiffness of ECM (Wang and Valdez-Jasso, 2021).

THE INTERPLAY BETWEEN ALVEOLAR EPITHELIAL CELLS AND VASCULAR ENDOTHELIAL CELLS

Hypoxia Induced Endothelial Dysfunction

In the lungs, oxygen diffuses from the alveoli into blood circulation and carbon-di-oxide diffuses from the blood into the alveoli. However, gas exchange is impaired when alveolar epithelial cells are injured during pathological conditions such as VILI, ARDS and pulmonary fibrosis resulting in an hypoxic microenvironment. Furthermore, hypoxia causes injury to the vascular endothelial cells and activates HIF-1 α expression. HIF-1 α regulates critical vascular functions such as angiogenesis, metabolism, cell growth, metastasis, and apoptosis (Semenza, 2017). Increased HIF-1 α stabilization reprograms endothelial metabolism and activates vascular inflammation by promoting glycolysis and reducing the mitochondrial respiratory capacity, thereby increasing NOX4-derived ROS levels and activating the deubiquitinating enzyme, Cezanne (Wu et al., 2017).

Emerging evidence suggests that biomechanical stimuli also regulate HIF-1 α . In the vascular endothelium, disturbed blood flow significantly stabilizes HIF-1 α even under normoxic conditions. YAP/TAZ pathway is also involved in the metabolic homeostasis mechanisms of the PAECs. YAP and HIF-1 α promote glycolysis co-operatively because YAP localizes to the

nucleus and prevents HIF-1 α degradation (Zhang et al., 2018). In ARDS, insufficient oxygen levels promote HIF-1 α -dependent elevation of lactate levels due to increased glycolysis; moreover, HIF-1 α participates in the upregulation of TNF- α , IL-6, and IL-8. Pathological mechanical stress also activates HIF-1 α , which protects the endothelial barrier by regulating VEGFR2 and the vascular endothelial protein tyrosine phosphatase (VE-PTP) that dephosphorylates TIE2 and ANG2. Several lncRNAs (n335470, n406639, n333984, and n337322) also regulate pulmonary inflammation and fibrosis induced by cyclic stretch through hypoxia and NF- κ B signaling (Wang D. et al., 2021).

Long-term exposure to a hypoxic environment alters the redox balance and increases cellular inflammation *via* increased expression of MIP2, IL6, TNF- α and CXCL1, as well as elevated oxidative stress and apoptosis. Furthermore, ICAM1, vascular cell adhesion molecule 1 (VCAM1), and selectin mediate the interactions between the monocytes and endothelial cells *via* the NF- κ B-ERK signaling pathway (Wohlrab et al., 2018).

Endothelial Permeability Impairment Causes Fluid Leaking

Endothelial cell injury plays a significant role in the pathology of VILI and ARDS. Pulmonary edema is caused by impaired cytoskeleton and permeability of the endothelial cells. Zeinali et al. (2021) developed an *in vitro* three-dimensional (3D) micro-vessel model to investigate the effects of the 3D mechanical cyclic stretch of different magnitudes and vascular endothelial growth factor (VEGF) stimulation on a 3D perfusing vasculature; the results shows that physiological cyclic stretch restored the vascular barrier tightness and significantly decreases vascular permeability (Zeinali et al., 2021). Piezo1 activation and calpain-induced disruption of VE-cadherin adhesion in endothelial cells subjected to elevated lung micro-vessel pressure resulted in capillary stress failure and edema (Friedrich et al., 2019). Dopamine D1 receptor (DRD1) is downregulated in both surgical patients and mice exposed to mechanical ventilation. The administration of DRD1 agonist attenuates the mechanical stretch-induced lung endothelial barrier dysfunction by inhibiting deacetylation of α -Tubulin *via* cAMP/EPAC/HDAC6 signaling pathway (Wang Y. et al., 2021). Vascular homeostasis is regulated by normal shear stress sensing and barrier function, which are controlled by the adherens junctions (Stanicek et al., 2020). Endothelial glycocalyx plays a critical role in maintaining capillary fluidity and perfusion homogeneity in the microvasculature by interacting with focal adhesion proteins (Lohser and Slinger, 2015; Knoepp et al., 2020). This suggests a connection between mechanical sensing, NO production, and microvascular perfusion. Damage to the glycocalyx layer causes endothelial dysfunction because of actin cytoskeleton remodeling. Stanicek et al. (2020) demonstrated that lncRNA-LASSIE is associated with the platelet endothelial cell adhesion molecule-1 (PECAM-1) and the intermediate filament protein, Nestin; lncRNA-LASSIE deletion reduces the interaction between VE-cadherin and Nestin, thereby destabilizing the cytoskeleton (Stanicek et al., 2020). Hence, lncRNA-LASSIE is important for the regulation of barrier function. The pathobiology of

VILI and ARDS involves increased lung vascular permeability and alveolar flooding because the endothelial cells lose barrier integrity. MMP-2, MMP-9, RGD-dependent integrins, cell-cell adhesion proteins, ICAM-1, VCAM-1, and VE-cadherin play an integral role in maintaining endothelial barrier function (Wang et al., 2017).

Extracellular Matrix Stiffness Alters Lung Microenvironment

Substrate stiffness plays an important role in regulating tissue-specific endothelial response to shear stress. The physiological stiffness of lung tissue is around 1kPa. Endothelial cells subjected to higher shear stress exhibit cell quiescence marked by lower expression of inflammatory markers and higher NO levels, whereas, ECs subjected to low shear stress demonstrate activated pro-inflammatory state and low NO levels. Cellular traction stress should match substrate stiffness through force sensing at the focal adhesion; therefore, larger tensile stress is necessary to overcome substrate stiffness (Califano and Reinhart-King, 2010). Hemodynamic shear sensors are activated in response to low mechanical force (Fang et al., 2019). Substrate stiffness promotes EndMT and plays a significant role in chronic lung fibrosis diseases, which originate from AEC injury. Elevated ECM stiffness is an independent predictor of cardiovascular morbidity and mortality (Smulyan et al., 2016). Endothelial cells subjected to shear stress demonstrate decreased expression of α v and β 3 integrins, which promote migration and elongation *via* EndMT. ECM stiffness in cultured PAECs increases glycolysis and glutaminolysis while reducing mitochondrial oxygen consumption. Furthermore, stiff ECM promotes proliferation and collagen deposition in the PAECs (Bertero et al., 2016). Stiffness is also linked to metabolic signaling through HIF-1 α in the pulmonary microvasculature. Hypoxic metabolic modeling of endothelial cells promotes collagen deposition in a HIF-1 α -dependent manner (de Jong et al., 2016). Besides, YAP/TAZ pathway activated by high stiffness promotes fibrotic signaling pathways that increase the synthesis of ECM proteins (Totaro et al., 2018). Besides, increased levels of miR-143-3p in ECs under shear stress induces the release of TGF- β in collaboration with SRF and ECM reorganization by targeting collagen V- α 2 biosynthesis (Troidl et al., 2020). Therefore, increased ECM stiffness is observed in both epithelium or endothelium injuries, and alters transcription, metabolism, and inflammation in both alveolar epithelial cells and endothelial cells.

Metabolic Disorders and Oxidative Stress

Laminar shear stress generated by the blood flow stimulates endothelial cells and activates signal transduction pathways that play a significant role in vascular homeostasis (Hirata et al., 2021). Pathological mechanical stress alters the metabolic status of pulmonary endothelial cells. Functional lipidomics of human PEACs showed that laminar shear stress for 24 h significantly alters the levels of 198/761 (26%) species of lipids (Hirata et al., 2021). Lipid changes in pulmonary endothelial cells stimulated

the pro-inflammatory response by inducing the expression of VCAM-1. Besides, fragmented phospholipids generates by phospholipid oxidation and nitroxidative stress induces endothelial barrier dysfunction *via* pro-inflammatory cytokines (Hirata et al., 2021). Shear stress also decreases cholesterol in the plasma membrane, but these effects are secondary to the release of ATP. *In vitro* experiments demonstrates that addition of cholesterol to pulmonary cells restores mitochondrial function including ATP production. Furthermore, excessive release of ATP by the alveolar epithelial cells or the endothelial cells affects the lung micro-environment and influences the functions of both pulmonary cell types. Moreover, changes in the levels of metabolic compounds such as cholesterol within the lung micro-environment impaired the normal communication between the epithelium and endothelium (Yamamoto et al., 2020).

Metabolic hemostasis is altered during pathological shear stress. The abnormal blood flow reduces mitochondrial mass and function and upregulates glycolysis through HIF-1 α activation; this results in increased accumulation of ROS and defective synthesis of NO. Elevated levels of ROS prevent the degradation of HIF-1 α through a positive feedback mechanism and promote the activation of glycolytic genes (Kim et al., 2017; Wu et al., 2017). In mechanically ventilated septic patients, nitroxidative stress increases NO production, protein nitration, and lipid peroxidation. Besides, unidirectional flow increases oxidative phosphorylation (OXPHOS) and mitochondrial biogenesis *via* SIRT1, a key regulator of NOS activity (Wu and Birukov, 2019). Mitochondrial dysfunction increases localized oxidative stress and stimulated hypoxia. Therefore, injury to either alveolar epithelial cells or PAECs increases ROS levels and hypoxia in the microenvironment, which negatively impacts both cell types. Arachidonic acid (AA) significantly increases cellular stiffness. AA metabolites such as prostacyclins and epoxyeicosatrienoic acids are involved in vascular dilation; AA is metabolized to prostacyclin and epoxyeicosatrienoic acids by COX and cytochrome P450 epoxygenases, respectively (Merna et al., 2018). Increased vascular oxidative stress induces non-enzymatic production of isoprostanes from AA. The vasoconstrictor metabolites of AA and isoprostanes induced endothelial damage and impair vascular function. Therefore, oxidative stress alters the balance between vasodilator and vasoconstrictor metabolites of AA.

Shear stress modulates mitochondrial ATP production in vascular endothelial cells by triggering ATP release and Ca²⁺ signaling *via* purinoceptors (Yamamoto et al., 2020). However, abnormal Ca²⁺ signaling induces mitochondrial dysfunction. Lu et al. (2021) demonstrated that inhibition of TRPV4 disrupts the PAEC barrier *via* PKC dependent phosphorylation of Threonine 495 in eNOS. Uncoupling of eNOS promotes mitochondrial redistribution and impairs mitochondrial bioenergetics. Furthermore, acetylation is critical for the stability of the endothelial cytoskeleton. Acetylation of α -tubulin promotes microtubule stability (Kull and Sloboda, 2014; Szyk et al., 2014). Fatty acid-derived acetyl-CoA is a major regulator of cellular acetylation. Impaired mitochondrial function suppresses the acetylation levels in the pulmonary cells. The levels of HDAC6, which is involved in acetylation *via* the

canonical Wnt/ β -catenin pathway, are elevated in lung injury caused by disassembling the adherens junctions.

Activation of Inflammation and Monocyte/Macrophage Recruitment

Mechanical ventilation promotes acute lung injury and development of multiple organ dysfunction syndrome by increasing the levels of TNF- α , IL-1 β , IL-6, IL-10, MIP-2, and interferon- γ in the lavage fluid (Belperio et al., 2006). Stretching induces the production of TNF α , IL-8, and IL-6 by lung-resident macrophages and AT2 cells; whereas, exposure of lung endothelium to 20% cyclic stretch upregulates the levels of IL-8, VCAM-1, ICAM-1, and E-selectin, and mediates the adhesion of monocytes and macrophages (Iwaki et al., 2009).

Accumulation of monocytes and macrophages in the perivascular and adventitia space is a notable feature of remodeling in response to lung injuries (Stenmark et al., 2013). Monocytes and macrophages play a central role in local lung inflammation as a result of PH (Chen et al., 2016), and are associated with disease severity and progression (Willis et al., 2018). Dysregulation of chemokines such as CCL5, CCL2, and CXCL1, and their homologous receptors are related to the pathogenesis of PH because the infiltration of monocytes, macrophage polarization, and vascular remodeling in the lungs is regulated by these chemokines (Groth et al., 2014). Hypoxia-induced PH increases the expression levels of CX3CR1, CCR2, and their corresponding ligands, CX3CL1 and CCL2, in the mouse pulmonary vessels; moreover, CX3CR1 deficiency increases the proportion of monocytes and macrophages in the lungs and promotes M2 to M1 macrophage polarization, a classic activating proinflammatory phenotype (Amsellem et al., 2017). Increased strain and frequency of cyclic stretch promotes the secretion of pro-inflammatory factors by the lung-resident macrophages. For example, 12% stretching or elongation of the membrane increases the production of proinflammatory cytokines, such as TNF- α , IL-6, IL-8, and MMP9 *via* NF- κ B activation by the human alveolar macrophages. Furthermore, murine alveolar macrophages subjected to 20% cyclic stretch induces the release of IL-1 β and IL-18 as well as inflammasome activation through ROS-mediated caspase 1 and TLR4 signaling (Wu et al., 2013).

The dysfunction of alveolar epithelium induced inflammation responses and disturbed the blood flow leading to the downregulation of KLF2 *via* glycocalyx sensing mechanotransduction (Huang et al., 2017). Growth differentiation factor-15 (GDF-15), also known as macrophage inhibitory cytokine-1 or non-steroidal anti-inflammatory drug-activated gene has been identified as a biomarker of treatment response and prognosis in cardiovascular diseases. GDF-15 is a member of the transforming growth factor- β superfamily and participates in several pathological conditions such as inflammation, cancer, as well as cardiovascular, pulmonary, and renal diseases (Arkoumani et al., 2020). Endothelial cells are the source of GDF-15, which interacts with the proinflammatory cytokines and induces localized macrophage accumulation and fibrosis. The activation of host monocytes and macrophages *via*

NF- κ B signaling induces fibrosis and alveolar epithelium injuries through elevated stiffness of the ECM. Stiffness also increases endothelial inflammation *via* NF- κ B through a positive feedback mechanism, thereby enhancing lung fibrosis.

FUTURE ASPECTS AND CONCLUSION

In summary, mechanical stress and its related transduction pathways demonstrates a critical molecular biological function in development, functional maturation and pathogenesis. Typically, lung serves as the places for gas exchange, alveoli and blood vessels are essential for such biological process. The epithelial cells and endothelial cells would both undergo mesenchymal transition under various injuries. Besides, the two types of cell are all sensitive to mechanical stress. Cyclic stretch is the major source of mechanical stimulation on alveolar epithelial cells, while cyclic stretch and shear stress are loaded on vascular endothelial cells in general. In addition, the stiffness of the epithelium and endothelium is also essential to maintain the microenvironment for gas exchange. In this review, we summarized the kinds of mechanical stresses that are applied to alveolar epithelial cells and endothelial cells. We demonstrated pulmonary inflammation activation, metabolic alternation, ECM and cytoskeleton remodeling during non-physiological mechanical stress. However, the communications between the microenvironment, the alveolar epithelial cells and the vascular endothelial cells are rarely analyzed. Therefore, we propose a mechanistic picture in which several links are orchestrated for the interplays between epithelium and endothelium, and to emphasize the possibility of targeting the communications in dealing with lung injuries. In the future,

more efforts should be directed toward further elucidation of the regulatory mechanisms of these communications, and corresponding research and discovery of novel targets on mechanotransduction signaling as medication therapeutics. With the newly invented methods to deliver nucleotides into lung tissues, it is believed that eventually mechanical pathways under pathological circumstances may be rectified by genetic editing and gene therapy, which seems to be a promising strategy for exploring new cures for lung injury and disease.

AUTHOR CONTRIBUTIONS

JW and YL conceived of the presented idea. CL, XZ, and SL summarized the reference and drafted the manuscript. YZ organized the figures. YZ, JW, and YL supervised the project and contributed equally to the final version of the manuscript. All authors contributed to the article and approved the submitted version.

FUNDING

All phase of this study was supported by Key R&D Program of Sichuan Province of China (2020YFS0101 and 2020YFS0102), Central Government Funds of Guiding Local Scientific and Technological Development for Sichuan Province (2021ZYD0105), and Natural Science Foundation of China (81700360 and 82070324). The funders had no role in study design, data collection and analysis, decision to publish, or preparation of the manuscript.

REFERENCES

- Ali, M. H., Pearlstein, D. P., Mathieu, C. E., and Schumacker, P. T. (2004). Mitochondrial requirement for endothelial responses to cyclic strain: implications for mechanotransduction. *Am. J. Physiol. Lung Cell Mol. Physiol.* 287, L486–L496. doi: 10.1152/ajplung.00389.2003
- Amsellem, V., Abid, S., Poupel, L., Parpaleix, A., Rodero, M., Gary-Bobo, G., et al. (2017). Roles for the CX3CL1/CX3CR1 and CCL2/CCR2 Chemokine Systems in Hypoxic Pulmonary Hypertension. *Am. J. Respir. Cell Mole. Biol.* 56, 597–608. doi: 10.1165/rcmb.2016-0201OC
- Arkoumani, M., Papadopoulou-Marketou, N., Nicolaides, N. C., Kanakantzenbein, C., Tentolouris, N., and Papassotiropoulos, I. (2020). The clinical impact of growth differentiation factor-15 in heart disease: a 2019 update. *Crit. Rev. Clin. Lab. Sci.* 57, 114–125. doi: 10.1080/10408363.2019.1678565
- Arold, S. P., Bartolák-Suki, E., and Suki, B. (2009). Variable stretch pattern enhances surfactant secretion in alveolar type II cells in culture. *Am. J. Physiol. Lung Cell Mol. Physiol.* 296, L574–L581. doi: 10.1152/ajplung.90454.2008
- Asano-Matsuda, K., Ibrahim, S., Takano, T., and Matsuda, J. (2021). Role of Rho GTPase Interacting Proteins in Subcellular Compartments of Podocytes. *Int. J. Mol. Sci.* 22:7. doi: 10.3390/ijms22073656
- Barbeau, S., Gilbert, G., Cardouat, G., Baudrimont, I., Freund-Michel, V., Guibert, C., et al. (2021). Mechanosensitivity in Pulmonary Circulation: Pathophysiological Relevance of Stretch-Activated Channels in Pulmonary Hypertension. *Biomolecules* 11:9. doi: 10.3390/biom11091389
- Belperio, J. A., Keane, M. P., Lynch, J. P. III, and Strieter, R. M. (2006). The role of cytokines during the pathogenesis of ventilator-associated and ventilator-induced lung injury. *Semin Respir. Crit. Care Med.* 27, 350–364. doi: 10.1055/s-2006-948289
- Bertero, T., Oldham, W. M., Cottrill, K. A., Pisano, S., Vanderpool, R. R., Yu, Q., et al. (2016). Vascular stiffness mechanoactivates YAP/TAZ-dependent glutaminolysis to drive pulmonary hypertension. *J. Clin. Invest.* 126, 3313–3335. doi: 10.1172/jci86387
- Bix, G., Fu, J., Gonzalez, E. M., Macro, L., Barker, A., Campbell, S., et al. (2004). Endorepellin causes endothelial cell disassembly of actin cytoskeleton and focal adhesions through α 2 β 1 integrin. *J. Cell Biol.* 166, 97–109. doi: 10.1083/jcb.200401150
- Califano, J. P., and Reinhart-King, C. A. (2010). Substrate Stiffness and Cell Area Predict Cellular Traction Stresses in Single Cells and Cells in Contact. *Cell Mol. Bioeng.* 3, 68–75. doi: 10.1007/s12195-010-0102-6
- Chang, E., Nayak, L., and Jain, M. K. (2017). Krüppel-like factors in endothelial cell biology. *Curr. Opin. Hemat.* 24, 224–229. doi: 10.1097/moh.0000000000000337
- Chen, T., Yang, C., Li, M., and Tan, X. (2016). Alveolar Hypoxia-Induced Pulmonary Inflammation: from Local Initiation to Secondary Promotion by Activated Systemic Inflammation. *J. Vasc. Res.* 53, 317–329. doi: 10.1159/000452800
- Cho, S., Irianto, J., and Discher, D. E. (2017). Mechanosensing by the nucleus: From pathways to scaling relationships. *J. Cell Biol.* 216, 305–315. doi: 10.1083/jcb.201610042
- Cotten, C. M. (2017). Pulmonary hypoplasia. *Semin. Fetal. Neonatal. Med.* 22, 250–255. doi: 10.1016/j.siny.2017.06.004
- Dagenais, A., Desjardins, J., Shabbir, W., Roy, A., Filion, D., Sauvé, R., et al. (2018). Loss of barrier integrity in alveolar epithelial cells downregulates ENaC expression and activity *via* Ca(2+) and TRPV4 activation. *Pflugers Arch.* 470, 1615–1631. doi: 10.1007/s00424-018-2182-4
- Davidovich, N., DiPaolo, B. C., Lawrence, G. G., Chhour, P., Yehya, N., and Margulies, S. S. (2013). Cyclic stretch-induced oxidative stress increases

- pulmonary alveolar epithelial permeability. *Am. J. Respir. Cell Mol. Biol.* 49, 156–164. doi: 10.1165/rcmb.2012-0252OC
- De Bock, K., Georgiadou, M., and Carmeliet, P. (2013a). Role of endothelial cell metabolism in vessel sprouting. *Cell Metab.* 18, 634–647. doi: 10.1016/j.cmet.2013.08.001
- De Bock, K., Georgiadou, M., Schoors, S., Kuchnio, A., Wong, B. W., Cantelmo, A. R., et al. (2013b). Role of PFKFB3-driven glycolysis in vessel sprouting. *Cell* 154, 651–663. doi: 10.1016/j.cell.2013.06.037
- de Jong, S., Tinteaung, T., Withers, A. H., Davis, P. F., and Tan, S. T. (2016). Does hypoxia play a role in infantile hemangioma? *Arch. Dermatol. Res.* 308, 219–227. doi: 10.1007/s00403-016-1635-x
- Deguchi, S., Ohashi, T., and Sato, M. (2005). Intracellular stress transmission through actin stress fiber network in adherent vascular cells. *Mol. Cell. Biomech.* 2, 205–216.
- Deng, Z., Fear, M. W., Suk Choi, Y., Wood, F. M., Allahham, A., Mutsaers, S. E., et al. (2020). The extracellular matrix and mechanotransduction in pulmonary fibrosis. *Int. J. Biochem. Cell Biol.* 126:105802. doi: 10.1016/j.biocel.2020.105802
- Denis, J. F., Diabougba, M. R., Molica, F., Hautefort, A., Linnerz, T., Watanabe, M., et al. (2019). KLF4-Induced Connexin40 Expression Contributes to Arterial Endothelial Quiescence. *Front. Physiol.* 10:80. doi: 10.3389/fphys.2019.00080
- Desai, L. P., Chapman, K. E., and Waters, C. M. (2008). Mechanical stretch decreases migration of alveolar epithelial cells through mechanisms involving Rac1 and Tiam1. *Am. J. Physiol. Lung. Cell Mol. Physiol.* 295, L958–L965. doi: 10.1152/ajplung.90218.2008
- Diem, K., Fauler, M., Foiss, G., Hellmann, A., Winokurow, N., Schumacher, S., et al. (2020). Mechanical stretch activates piezo1 in caveolae of alveolar type I cells to trigger ATP release and paracrine stimulation of surfactant secretion from alveolar type II cells. *Faseb J.* 34, 12785–12804. doi: 10.1096/fj.202000613RRR
- Ding, N., Wang, F., Han, Y., Xiao, H., Xu, L., and She, S. (2012). Mitogen-activated protein kinase kinase 6 mediates mechanical stretch-induced high-mobility group box 1 protein expression in pulmonary alveolar epithelial cells. *J. Trauma Acute Care Surg.* 72, 162–168. doi: 10.1097/TA.0b013e318216f480
- Doddaballapur, A., Michalik, K. M., Manavski, Y., Lucas, T., Houtkooper, R. H., You, X., et al. (2015). Laminar shear stress inhibits endothelial cell metabolism via KLF2-mediated repression of PFKFB3. *Arterioscler. Thromb. Vasc. Biol.* 35, 137–145. doi: 10.1161/atvbaha.114.304277
- Dong, Z. W., Chen, J., Ruan, Y. C., Zhou, T., Chen, Y., Chen, Y., et al. (2015). CFTR-regulated MAPK/NF- κ B signaling in pulmonary inflammation in thermal inhalation injury. *Sci. Rep.* 5:15946. doi: 10.1038/srep15946
- Ducrot, T., El Arrouchi, J., Courtois, A., Quignard, J. F., Marthan, R., and Savineau, J. P. (2010). Stretch-activated channels in pulmonary arterial smooth muscle cells from normoxic and chronically hypoxic rats. *Cell Calcium.* 48, 251–259. doi: 10.1016/j.ceca.2010.09.011
- Dupont, S., Morsut, L., Aragona, M., Enzo, E., Giulitti, S., Cordenonsi, M., et al. (2011). Role of YAP/TAZ in mechanotransduction. *Nature* 474, 179–183. doi: 10.1038/nature10137
- Duscher, D., Maan, Z. N., Wong, V. W., Rennert, R. C., Janusz, M., Rodrigues, M., et al. (2014). Mechanotransduction and fibrosis. *J. Biomech.* 47, 1997–2005. doi: 10.1016/j.jbiomech.2014.03.031
- Fang, Y., Wu, D., and Birukov, K. G. (2019). Mechanosensing and Mechanoregulation of Endothelial Cell Functions. *Compr. Physiol.* 9, 873–904. doi: 10.1002/cphy.c180020
- Firth, A. L., Remillard, C. V., and Yuan, J. X. (2007). TRP channels in hypertension. *Biochim. Biophys. Acta.* 1772, 895–906. doi: 10.1016/j.bbadis.2007.02.009
- Friedrich, E. E., Hong, Z., Xiong, S., Zhong, M., Di, A., Rehman, J., et al. (2019). Endothelial cell Piezo1 mediates pressure-induced lung vascular hyperpermeability via disruption of adherens junctions. *Proc. Natl. Acad. Sci. U S A.* 116, 12980–12985. doi: 10.1073/pnas.1902165116
- Froese, A. R., Shimbori, C., Bellaye, P. S., Inman, M., Obex, S., Fatima, S., et al. (2016). Stretch-induced Activation of Transforming Growth Factor- β 1 in Pulmonary Fibrosis. *Am. J. Respir. Crit. Care Med.* 194, 84–96. doi: 10.1164/rccm.201508-1638OC
- Gao, J., Huang, T., Zhou, L. J., Ge, Y. L., Lin, S. Y., and Dai, Y. (2014). Preconditioning effects of physiological cyclic stretch on pathologically mechanical stretch-induced alveolar epithelial cell apoptosis and barrier dysfunction. *Biochem. Biophys. Res. Commun.* 448, 342–348. doi: 10.1016/j.bbrc.2014.03.063
- Garcia, C. S., Protá, L. F., Morales, M. M., Romero, P. V., Zin, W. A., and Rocco, P. R. (2006). Understanding the mechanisms of lung mechanical stress. *Braz. J. Med. Biol. Res.* 39, 697–706. doi: 10.1590/s0100-879x2006000600001
- Ge, X., Sun, J., Fei, A., Gao, C., Pan, S., and Wu, Z. (2019). Hydrogen sulfide treatment alleviated ventilator-induced lung injury through regulation of autophagy and endoplasmic reticulum stress. *Int. J. Biol. Sci.* 15, 2872–2884. doi: 10.7150/ijbs.38315
- Gicquel, T., Le Daré, B., Boichot, E., and Lagente, V. (2017). Purinergic receptors: new targets for the treatment of gout and fibrosis. *Fundam. Clin. Pharmacol.* 31, 136–146. doi: 10.1111/fcp.12256
- Giménez, A., Duch, P., Puig, M., Gabasa, M., Xaubet, A., and Alcaraz, J. (2017). Dysregulated Collagen Homeostasis by Matrix Stiffening and TGF- β 1 in Fibroblasts from Idiopathic Pulmonary Fibrosis Patients: Role of FAK/Akt. *Int. J. Mol. Sci.* 18:11. doi: 10.3390/ijms18112431
- Goettsch, C., Goettsch, W., Arsov, A., Hofbauer, L. C., Bornstein, S. R., and Morawietz, H. (2009). Long-term cyclic strain downregulates endothelial Nox4. *Antioxid. Redox Signal.* 11, 2385–2397. doi: 10.1089/ars.2009.2561
- Groth, A., Vrugt, B., Brock, M., Speich, R., Ulrich, S., and Huber, L. C. (2014). Inflammatory cytokines in pulmonary hypertension. *Respirat. Res.* 15:47. doi: 10.1186/1465-9921-15-47
- Han, B., Lodyga, M., and Liu, M. (2005). Ventilator-induced lung injury: role of protein-protein interaction in mechanosensation. *Proc. Am. Thorac. Soc.* 2, 181–187. doi: 10.1513/pats.200501-008AC
- Han, Z., Varadaraj, S., Giedt, R. J., Zweier, J. L., Szeto, H. H., and Alevriadou, B. R. (2009). Mitochondria-derived reactive oxygen species mediate heme oxygenase-1 expression in sheared endothelial cells. *J. Pharmacol. Exp. Ther.* 329, 94–101. doi: 10.1124/jpet.108.145557
- Hewlett, J. C., Kropski, J. A., and Blackwell, T. S. (2018). Idiopathic pulmonary fibrosis: Epithelial-mesenchymal interactions and emerging therapeutic targets. *Matrix Biol.* 71–72, 112–127. doi: 10.1016/j.matbio.2018.03.021
- Hirata, T., Yamamoto, K., Ikeda, K., and Arita, M. (2021). Functional lipidomics of vascular endothelial cells in response to laminar shear stress. *Faseb J.* 35:e21301. doi: 10.1096/fj.202002144R
- Hsiao, S. T., Spencer, T., Boldock, L., Prosseda, S. D., Xanthos, I., Tovar-Lopez, F. J., et al. (2016). Endothelial repair in stented arteries is accelerated by inhibition of Rho-associated protein kinase. *Cardiovasc. Res.* 112, 689–701. doi: 10.1093/cvr/cvw210
- Huang, T. T., Wu, D., Meliton, A., Oh, M. J., Krause, M., Lloyd, J. A., et al. (2017). Experimental Lung Injury Reduces Krüppel-like Factor 2 to Increase Endothelial Permeability via Regulation of RAGEF3-Rac1 Signaling. *Am. J. Respir. Crit. Care Med.* 195, 639–651. doi: 10.1164/rccm.201604-0668OC
- Ichimura, H., Parthasarathi, K., Quadri, S., Issekutz, A. C., and Bhattacharya, J. (2003). Mechano-oxidative coupling by mitochondria induces proinflammatory responses in lung venular capillaries. *J. Clin. Invest.* 111, 691–699. doi: 10.1172/jci17271
- Iring, A., Jin, Y. J., Albarrán-Juárez, J., Siragusa, M., Wang, S., Dancs, P. T., et al. (2019). Shear stress-induced endothelial adrenomedullin signaling regulates vascular tone and blood pressure. *J. Clin. Invest.* 129, 2775–2791. doi: 10.1172/jci123825
- Iwaki, M., Ito, S., Morioka, M., Iwata, S., Numaguchi, Y., Ishii, M., et al. (2009). Mechanical stretch enhances IL-8 production in pulmonary microvascular endothelial cells. *Biochem. Biophys. Res. Commun.* 389, 531–536. doi: 10.1016/j.bbrc.2009.09.020
- Jesudason, E. C. (2009). Airway smooth muscle: an architect of the lung? *Thorax* 64, 541–545. doi: 10.1136/thx.2008.107094
- Jiang, C., Huang, H., Liu, J., Wang, Y., Lu, Z., and Xu, Z. (2012). Fasudil, a Rho-kinase inhibitor, attenuates bleomycin-induced pulmonary fibrosis in mice. *Int. J. Mol. Sci.* 13, 8293–8307. doi: 10.3390/ijms13078293
- Kang, B. Y., Park, K. K., Kleinhenn, J. M., Murphy, T. C., Green, D. E., Bijli, K. M., et al. (2016). Peroxisome Proliferator-Activated Receptor γ and microRNA 98 in Hypoxia-Induced Endothelin-1 Signaling. *Am. J. Respir. Cell Mol. Biol.* 54, 136–146. doi: 10.1165/rcmb.2014-0337OC
- Kang, H., Hong, Z., Zhong, M., Klomp, J., Bayless, K. J., Mehta, D., et al. (2019). Piezo1 mediates angiogenesis through activation of MT1-MMP signaling. *Am. J. Physiol. Cell Physiol.* 316, C92–C103. doi: 10.1152/ajpcell.00346.2018
- Ke, Y., Karki, P., Zhang, C., Li, Y., Nguyen, T., Birukov, K. G., et al. (2019). Mechanosensitive Rap1 activation promotes barrier function of lung vascular

- endothelium under cyclic stretch. *Mol. Biol. Cell* 30, 959–974. doi: 10.1091/mbc.E18-07-0422
- Kim, B., Li, J., Jang, C., and Arany, Z. (2017). Glutamine fuels proliferation but not migration of endothelial cells. *Embo J.* 36, 2321–2333. doi: 10.15252/embj.201796436
- Knoepf, F., Ashley, Z., Barth, D., Baldin, J. P., Jennings, M., Kazantseva, M., et al. (2020). Shear force sensing of epithelial Na(+) channel (ENaC) relies on N-glycosylated asparagines in the palm and knuckle domains of α ENaC. *Proc. Natl. Acad. Sci. U S A.* 117, 717–726. doi: 10.1073/pnas.1911243117
- Ko, K. S., Arora, P. D., and McCulloch, C. A. (2001). Cadherins mediate intercellular mechanical signaling in fibroblasts by activation of stretch-sensitive calcium-permeable channels. *J. Biol. Chem.* 276, 35967–35977. doi: 10.1074/jbc.M104106200
- Kovacs, G., Dumitrescu, D., Barner, A., Greiner, S., Grünig, E., Hager, A., et al. (2018). Definition, clinical classification and initial diagnosis of pulmonary hypertension: Updated recommendations from the Cologne Consensus Conference 2018. *Int. J. Cardiol.* 272s, 11–19. doi: 10.1016/j.ijcard.2018.08.083
- Kroon, A. A., Delriccio, V., Tseu, I., Kavanagh, B. P., and Post, M. (2013). Mechanical ventilation-induced apoptosis in newborn rat lung is mediated via FasL/Fas pathway. *Am. J. Physiol. Lung Cell Mol. Physiol.* 305, L795–L804. doi: 10.1152/ajplung.00048.2013
- Kuhn, H., Zobel, C., Vollert, G., Gurcke, M., Jenszowski, C., Barina, C., et al. (2019). High amplitude stretching of ATII cells and fibroblasts results in profibrotic effects. *Exp. Lung Res.* 45, 167–174. doi: 10.1080/01902148.2019.1636424
- Kull, F. J., and Sloboda, R. D. (2014). A slow dance for microtubule acetylation. *Cell* 157, 1255–1256. doi: 10.1016/j.cell.2014.05.021
- LaCanna, R., Liccardo, D., Zhang, P., Tragesser, L., Wang, Y., Cao, T., et al. (2019). Yap/Taz regulate alveolar regeneration and resolution of lung inflammation. *J. Clin. Invest.* 129, 2107–2122. doi: 10.1172/jci125014
- Lambert, M., Capuano, V., Olschewski, A., Sabourin, J., Nagaraj, C., Girerd, B., et al. (2018). Ion Channels in Pulmonary Hypertension: a Therapeutic Interest? *Int. J. Mol. Sci.* 19, 10. doi: 10.3390/ijms19103162
- Lee, T. H., Yeh, C. F., Lee, Y. T., Shih, Y. C., Chen, Y. T., Hung, C. T., et al. (2020). Fibroblast-enriched endoplasmic reticulum protein TXNDC5 promotes pulmonary fibrosis by augmenting TGF β signaling through TGFBR1 stabilization. *Nat. Commun.* 11:4254. doi: 10.1038/s41467-020-18047-x
- Lettieri, C. J., Nathan, S. D., Barnett, S. D., Ahmad, S., and Shorr, A. F. (2006). Prevalence and outcomes of pulmonary arterial hypertension in advanced idiopathic pulmonary fibrosis. *Chest* 129, 746–752. doi: 10.1378/chest.129.3.746
- Lhomme, A., Gilbert, G., Pele, T., Deweirdt, J., Henrion, D., Baudrimont, I., et al. (2019). Stretch-activated Piezo1 Channel in Endothelial Cells Relaxes Mouse Intrapulmonary Arteries. *Am. J. Respir. Cell Mol. Biol.* 60, 650–658. doi: 10.1165/rcmb.2018-0197OC
- Li, J., Hou, B., Tumova, S., Muraki, K., Bruns, A., Ludlow, M. J., et al. (2014). Piezo1 integration of vascular architecture with physiological force. *Nature* 515, 279–282. doi: 10.1038/nature13701
- Liang, G. P., Xu, J., Cao, L. L., Zeng, Y. H., Chen, B. X., Yang, J., et al. (2019). Piezo1 induced apoptosis of type II pneumocytes during ARDS. *Respir. Res.* 20:118. doi: 10.1186/s12931-019-1083-1
- Liao, H., Qi, Y., Ye, Y., Yue, P., Zhang, D., and Li, Y. (2020). Mechanotransduction Pathways in the Regulation of Mitochondrial Homeostasis in Cardiomyocytes. *Front. Cell Dev. Biol.* 8:625089. doi: 10.3389/fcell.2020.625089
- Lionetti, V., Recchia, F. A., and Ranieri, V. M. (2005). Overview of ventilator-induced lung injury mechanisms. *Curr. Opin. Crit. Care* 11, 82–86. doi: 10.1097/00075198-200502000-00013
- Liu, D., Yan, Y., Chen, J. W., Yuan, P., Wang, X. J., Jiang, R., et al. (2017). Hypermethylation of BMPR2 Promoter Occurs in Patients with Heritable Pulmonary Arterial Hypertension and Inhibits BMPR2 Expression. *Am. J. Respir. Crit. Care Med.* 196, 925–928. doi: 10.1164/rccm.201611-2273LE
- Liu, W., Sun, Q., Zheng, Z. L., Gao, Y. T., Zhu, G. Y., Wei, Q., et al. (2021). Topographic Cues Guiding Cell Polarization via Distinct Cellular Mechanosensing Pathways. *Small* 5, e2104328. doi: 10.1002/smll.202104328
- Liu, Y. Y., Li, L. F., Fu, J. Y., Kao, K. C., Huang, C. C., Chien, Y., et al. (2014). Induced pluripotent stem cell therapy ameliorates hyperoxia-augmented ventilator-induced lung injury through suppressing the Src pathway. *PLoS One* 9:e109953. doi: 10.1371/journal.pone.0109953
- Liu, Y. Y., Li, L. F., Yang, C. T., Lu, K. H., Huang, C. C., Kao, K. C., et al. (2013). Suppressing NF- κ B and NKRF Pathways by Induced Pluripotent Stem Cell Therapy in Mice with Ventilator-Induced Lung Injury. *PLoS One* 8:e66760. doi: 10.1371/journal.pone.0066760
- Liu, Z., Wu, H., Jiang, K., Wang, Y., Zhang, W., Chu, Q., et al. (2016). MAPK-Mediated YAP Activation Controls Mechanical-Tension-Induced Pulmonary Alveolar Regeneration. *Cell Rep.* 16, 1810–1819. doi: 10.1016/j.celrep.2016.07.020
- Lohser, J., and Slinger, P. (2015). Lung Injury After One-Lung Ventilation: A Review of the Pathophysiologic Mechanisms Affecting the Ventilated and the Collapsed Lung. *Anesth Analg.* 121, 302–318. doi: 10.1213/ane.0000000000000808
- Lu, Q., Zemskov, E. A., Sun, X., Wang, H., Yegambaram, M., Wu, X., et al. (2021). Activation of the mechanosensitive Ca(2+) channel TRPV4 induces endothelial barrier permeability via the disruption of mitochondrial bioenergetics. *Redox Biol.* 38:101785. doi: 10.1016/j.redox.2020.101785
- Luchsinger, L. L., Patenaude, C. A., Smith, B. D., and Layne, M. D. (2011). Myocardin-related transcription factor-A complexes activate type I collagen expression in lung fibroblasts. *J. Biol. Chem.* 286, 44116–44125. doi: 10.1074/jbc.M111.276931
- Ly, Z., Wang, Y., Liu, Y. J., Mao, Y. F., Dong, W. W., Ding, Z. N., et al. (2018). NLRP3 Inflammasome Activation Contributes to Mechanical Stretch-Induced Endothelial-Mesenchymal Transition and Pulmonary Fibrosis. *Crit. Care Med.* 46, e49–e58. doi: 10.1097/ccm.0000000000002799
- Malczyk, M., Veith, C., Fuchs, B., Hofmann, K., Storch, U., Schermuly, R. T., et al. (2013). Classical transient receptor potential channel 1 in hypoxia-induced pulmonary hypertension. *Am. J. Respir. Crit. Care Med.* 188, 1451–1459. doi: 10.1164/rccm.201307-1252OC
- Mao, P., Li, J., Huang, Y., Wu, S., Pang, X., He, W., et al. (2017). MicroRNA-19b Mediates Lung Epithelial-Mesenchymal Transition via Phosphatidylinositol-3,4,5-Trisphosphate 3-Phosphatase in Response to Mechanical Stretch. *Am. J. Respir. Cell Mol. Biol.* 56, 11–19. doi: 10.1165/rcmb.2015-0377OC
- Maurer, M., and Lammerding, J. (2019). The Driving Force: Nuclear Mechanotransduction in Cellular Function, Fate, and Disease. *Annu Rev. Biomed. Eng.* 21, 443–468. doi: 10.1146/annurev-bioeng-060418-052139
- McNally, J. S., Davis, M. E., Giddens, D. P., Saha, A., Hwang, J., Dikalov, S., et al. (2003). Role of xanthine oxidoreductase and NAD(P)H oxidase in endothelial superoxide production in response to oscillatory shear stress. *Am J Physiol Heart Circ Physiol* 285, H2290–H2297. doi: 10.1152/ajpheart.00515.2003
- Meliton, A. Y., Muñoz, N. M., Meliton, L. N., Birukova, A. A., Leff, A. R., and Birukov, K. G. (2013). Mechanical induction of group V phospholipase A(2) causes lung inflammation and acute lung injury. *Am. J. Physiol. Lung Cell Mol. Physiol.* 304, L689–L700. doi: 10.1152/ajplung.00047.2013
- Meng, Z., Qiu, Y., Lin, K. C., Kumar, A., Placone, J. K., Fang, C., et al. (2018). RAP2 mediates mechanoresponses of the Hippo pathway. *Nature* 560, 655–660. doi: 10.1038/s41586-018-0444-0
- Merna, N., Wong, A. K., Barahona, V., Llanos, P., Kunar, B., Palikuqi, B., et al. (2018). Laminar shear stress modulates endothelial luminal surface stiffness in a tissue-specific manner. *Microcirculation* 25:e12455. doi: 10.1111/micc.12455
- Milovanova, T., Chatterjee, S., Hawkins, B. J., Hong, N., Sorokina, E. M., Debolt, K., et al. (2008). Caveolae are an essential component of the pathway for endothelial cell signaling associated with abrupt reduction of shear stress. *Biochim. Biophys. Acta* 1783, 1866–1875. doi: 10.1016/j.bbamer.2008.05.010
- Mussbacher, M., Salzmann, M., Brostjan, C., Hoesel, B., Schoergenhofer, C., Datler, H., et al. (2019). Cell Type-Specific Roles of NF- κ B Linking Inflammation and Thrombosis. *Front. Immunol.* 10:85. doi: 10.3389/fimmu.2019.00085
- Mustafa, S. B., Isaac, J., Seidner, S. R., Dixon, P. S., Henson, B. M., and DiGeronimo, R. J. (2014). Mechanical stretch induces lung α -epithelial Na(+) channel expression. *Exp. Lung Res.* 40, 380–391. doi: 10.3109/01902148.2014.934410
- Najrana, T., Ahsan, N., Abu-Eid, R., Uzun, A., Noble, L., Tollefson, G., et al. (2021). Proteomic analysis of a murine model of lung hypoplasia induced by oligohydramnios. *Pediatr. Pulmonol.* 56, 2740–2750. doi: 10.1002/ppul.25525
- Najrana, T., Ramos, L. M., Abu Eid, R., and Sanchez-Esteban, J. (2017). Oligohydramnios compromises lung cells size and interferes with epithelial-endothelial development. *Pediatr. Pulmonol.* 52, 746–756. doi: 10.1002/ppul.23662
- Nayebosadri, A., and Ji, J. Y. (2013). Endothelial nuclear lamina is not required for glucocorticoid receptor nuclear import but does affect receptor-mediated

- transcription activation. *Am. J. Physiol. Cell Physiol.* 305, C309–C322. doi: 10.1152/ajpcell.00293.2012
- Ni, J., Dong, Z., Han, W., Kondrikov, D., and Su, Y. (2013). The role of RhoA and cytoskeleton in myofibroblast transformation in hyperoxic lung fibrosis. *Free Radic. Biol. Med.* 61, 26–39. doi: 10.1016/j.freeradbiomed.2013.03.012
- Ning, Q. M., Sun, X. N., and Zhao, X. K. (2012). Role of mechanical stretching and lipopolysaccharide in early apoptosis and IL-8 of alveolar epithelial type II cells A549. *Asian Pac. J. Trop. Med.* 5, 638–644. doi: 10.1016/s1995-7645(12)60131-x
- Noskovičová, N., Petřek, M., Eickelberg, O., and Heinzelmann, K. (2015). Platelet-derived growth factor signaling in the lung. From lung development and disease to clinical studies. *Am. J. Respir. Cell Mol. Biol.* 52, 263–284. doi: 10.1165/rncmb.2014-0294TR
- Ottolini, M., Daneva, Z., Chen, Y. L., Cope, E. L., Kasetti, R. B., Zode, G. S., et al. (2020). Mechanisms underlying selective coupling of endothelial Ca(2+) signals with eNOS vs. IK/SK channels in systemic and pulmonary arteries. *J. Physiol.* 598, 3577–3596. doi: 10.1113/jp279570
- Parsons, J. T., Horwitz, A. R., and Schwartz, M. A. (2010). Cell adhesion: integrating cytoskeletal dynamics and cellular tension. *Nat. Rev. Mol. Cell Biol.* 11, 633–643. doi: 10.1038/nrm2957
- Paszkowiak, J. J., and Dardik, A. (2003). Arterial wall shear stress: observations from the bench to the bedside. *Vasc. Endovascular. Surg.* 37, 47–57. doi: 10.1177/153857440303700107
- Patel, V., Dial, K., Wu, J., Gauthier, A. G., Wu, W., Lin, M., et al. (2020). Dietary Antioxidants Significantly Attenuate Hyperoxia-Induced Acute Inflammatory Lung Injury by Enhancing Macrophage Function via Reducing the Accumulation of Airway HMGB1. *Int. J. Mol. Sci.* 21:3. doi: 10.3390/ijms21030977
- Phan, T. H. G., Paliogiannis, P., Nasrallah, G. K., Giordo, R., Eid, A. H., Fois, A. G., et al. (2021). Emerging cellular and molecular determinants of idiopathic pulmonary fibrosis. *Cell Mol. Life Sci.* 78, 2031–2057. doi: 10.1007/s00018-020-03693-7
- Poljsak, B., Šuput, D., and Milisav, I. (2013). Achieving the balance between ROS and antioxidants: when to use the synthetic antioxidants. *Oxid. Med. Cell Longev.* 2013:956792. doi: 10.1155/2013/956792
- Pollak, N. M., Hoffman, M., Goldberg, I. J., and Drosatos, K. (2018). Krüppel-like factors: Crippling and un-crippling metabolic pathways. *JACC Basic Transl. Sci.* 3, 132–156. doi: 10.1016/j.jacbs.2017.09.001
- Rode, B., Shi, J., Endesh, N., Drinkhill, M. J., Webster, P. J., Lotteau, S. J., et al. (2017). Piezo1 channels sense whole body physical activity to reset cardiovascular homeostasis and enhance performance. *Nat. Commun.* 8:350. doi: 10.1038/s41467-017-00429-3
- Rout-Pitt, N., Farrow, N., Parsons, D., and Donnelley, M. (2018). Epithelial mesenchymal transition (EMT): a universal process in lung diseases with implications for cystic fibrosis pathophysiology. *Respir. Res.* 19:136. doi: 10.1186/s12931-018-0834-8
- Schoors, S., Bruning, U., Missiaen, R., Queiroz, K. C., Borgers, G., Elia, I., et al. (2015). Fatty acid carbon is essential for dNTP synthesis in endothelial cells. *Nature* 520, 192–197. doi: 10.1038/nature14362
- Selman, M., and Pardo, A. (2020). The leading role of epithelial cells in the pathogenesis of idiopathic pulmonary fibrosis. *Cell Signal.* 66:109482. doi: 10.1016/j.cellsig.2019.109482
- Semenza, G. L. (2017). Hypoxia-inducible factors: coupling glucose metabolism and redox regulation with induction of the breast cancer stem cell phenotype. *Embo J.* 36, 252–259. doi: 10.15252/embj.201695204
- Slegtenhorst, B. R., Fajardo Ramirez, O. R., Zhang, Y., Dhanerawala, Z., Tullius, S. G., and García-Cardena, G. A. (2018). Mechano-Activated Cell Reporter System as a Proxy for Flow-Dependent Endothelial Atheroprotection. *SLAS Discov.* 23, 869–876. doi: 10.1177/2472555218761101
- Smulyan, H., Mookherjee, S., and Safar, M. E. (2016). The two faces of hypertension: role of aortic stiffness. *J. Am. Soc. Hypertens.* 10, 175–183. doi: 10.1016/j.jash.2015.11.012
- Song, M. J., Davidovich, N., Lawrence, G. G., and Margulies, S. S. (2016). Superoxide mediates tight junction complex dissociation in cyclically stretched lung slices. *J. Biomech.* 49, 1330–1335. doi: 10.1016/j.jbiomech.2015.10.032
- Spith, P. M., Bluth, T., Gama De Abreu, M., Bacelis, A., Goetz, A. E., and Kieffmann, R. (2014). Mechanotransduction in the lungs. *Minerva Anesthesiol.* 80, 933–941.
- Stanicek, L., Lozano-Vidal, N., Bink, D. I., Hooglugt, A., Yao, W., Wittig, I., et al. (2020). Long non-coding RNA LASSIE regulates shear stress sensing and endothelial barrier function. *Commun. Biol.* 3:265. doi: 10.1038/s42003-020-0987-0
- Stenmark, K. R., Yeager, M. E., El Kasmi, K. C., Nozik-Grayck, E., Gerasimovskaya, E. V., Li, M., et al. (2013). The adventitia: essential regulator of vascular wall structure and function. *Ann. Rev. Physiol.* 75, 23–47. doi: 10.1146/annurev-physiol-030212-183802
- Sukumaran, S. V., Singh, T. U., Parida, S., Narasimha Reddy Ch, E., Thangamalai, R., Kandasamy, K., et al. (2013). TRPV4 channel activation leads to endothelium-dependent relaxation mediated by nitric oxide and endothelium-derived hyperpolarizing factor in rat pulmonary artery. *Pharmacol. Res.* 78, 18–27. doi: 10.1016/j.phrs.2013.09.005
- Sun, Z., Guo, S. S., and Fässler, R. (2016). Integrin-mediated mechanotransduction. *J. Cell Biol.* 215, 445–456. doi: 10.1083/jcb.201609037
- Szyk, A., Deaconescu, A. M., Spector, J., Goodman, B., Valenstein, M. L., Ziolkowska, N. E., et al. (2014). Molecular basis for age-dependent microtubule acetylation by tubulin acetyltransferase. *Cell* 157, 1405–1415. doi: 10.1016/j.cell.2014.03.061
- Tanaka, T., Saito, Y., Matsuda, K., Kamio, K., Abe, S., Kubota, K., et al. (2017). Cyclic mechanical stretch-induced oxidative stress occurs via a NOX-dependent mechanism in type II alveolar epithelial cells. *Respir. Physiol. Neurobiol.* 242, 108–116. doi: 10.1016/j.resp.2017.04.007
- Thenappan, T., Chan, S. Y., and Weir, E. K. (2018). Role of extracellular matrix in the pathogenesis of pulmonary arterial hypertension. *Am. J. Physiol. Heart Circul. Physiol.* 315, H1322–H1331. doi: 10.1152/ajpheart.00136.2018
- Totaro, A., Panciera, T., and Piccolo, S. (2018). YAP/TAZ upstream signals and downstream responses. *Nat. Cell Biol.* 20, 888–899. doi: 10.1038/s41556-018-0142-z
- Travaglini, K. J., Nabhan, A. N., Penland, L., Sinha, R., Gillich, A., Sit, R. V., et al. (2020). A molecular cell atlas of the human lung from single-cell RNA sequencing. *Nature* 587, 619–625. doi: 10.1038/s41586-020-2922-4
- Troidl, K., Hammerschick, T., Albarran-Juarez, J., Jung, G., Schierling, W., Tonack, S., et al. (2020). Shear Stress-Induced miR-143-3p in Collateral Arteries Contributes to Outward Vessel Growth by Targeting Collagen V- α 2. *Arterioscler. Thromb. Vasc. Biol.* 40, e126–e137. doi: 10.1161/atvbaha.120.313316
- Tzima, E., Irani-Tehrani, M., Kiosses, W. B., Dejana, E., Schultz, D. A., Engelhardt, B., et al. (2005). A mechanosensory complex that mediates the endothelial cell response to fluid shear stress. *Nature* 437, 426–431. doi: 10.1038/nature03952
- Valentine, M. S., Link, P. A., Herbert, J. A., Kamga Gninzeke, F. J., Schneek, M. B., Shankar, K., et al. (2018). Inflammation and Monocyte Recruitment due to Aging and Mechanical Stretch in Alveolar Epithelium are Inhibited by the Molecular Chaperone 4-phenylbutyrate. *Cell Mol. Bioeng.* 11, 495–508. doi: 10.1007/s12195-018-0537-8
- Vogel, S. M., and Malik, A. B. (2012). Cytoskeletal dynamics and lung fluid balance. *Compr. Physiol.* 2, 449–478. doi: 10.1002/cphy.c100006
- Wang, A., and Valdez-Jasso, D. (2021). Cellular mechanosignaling in pulmonary arterial hypertension. *Biophys. Rev.* 13, 747–756. doi: 10.1007/s12551-021-00828-3
- Wang, D., Dai, C., Zhang, X., Gu, C., Liu, M., Liu, H., et al. (2021). Identification and Functional Analysis of Long Non-coding RNAs in Human Pulmonary Microvascular Endothelial Cells Subjected to Cyclic Stretch. *Front. Physiol.* 12:655971. doi: 10.3389/fphys.2021.655971
- Wang, S., Chennupati, R., Kaur, H., Iring, A., Wettschureck, N., and Offermanns, S. (2016). Endothelial cation channel PIEZO1 controls blood pressure by mediating flow-induced ATP release. *J. Clin. Invest.* 126, 4527–4536. doi: 10.1172/jci87343
- Wang, T., Gross, C., Desai, A. A., Zemskov, E., Wu, X., Garcia, A. N., et al. (2017). Endothelial cell signaling and ventilator-induced lung injury: molecular mechanisms, genomic analyses, and therapeutic targets. *Am. J. Physiol. Lung Cell Mol. Physiol.* 312, L452–L476. doi: 10.1152/ajplung.00231.2016
- Wang, Y., Liu, Y. J., Xu, D. F., Zhang, H., Xu, C. F., Mao, Y. F., et al. (2021). DRD1 downregulation contributes to mechanical stretch-induced lung endothelial barrier dysfunction. *Theranostics* 11, 2505–2521. doi: 10.7150/thno.46192
- Willis, G. R., Fernandez-Gonzalez, A., Reis, M., Mitsialis, S. A., and Kourembanas, S. (2018). Macrophage Immunomodulation: the Gatekeeper for Mesenchymal

- Stem Cell Derived-Exosomes in Pulmonary Arterial Hypertension? *Int. J. Mol. Sci.* 19:9. doi: 10.3390/ijms19092534
- Wohlrab, P., Soto-Gonzales, L., Benesch, T., Winter, M. P., Lang, I. M., Markstaller, K., et al. (2018). Intermittent Hypoxia Activates Duration-Dependent Protective and Injurious Mechanisms in Mouse Lung Endothelial Cells. *Front. Physiol.* 9:1754. doi: 10.3389/fphys.2018.01754
- Wolfson, R. K., Mapes, B., and Garcia, J. G. N. (2014). Excessive mechanical stress increases HMGB1 expression in human lung microvascular endothelial cells via STAT3. *Microvasc. Res.* 92, 50–55. doi: 10.1016/j.mvr.2013.12.005
- Woodcock, C. C., Hafeez, N., Handen, A., Tang, Y., Harvey, L. D., Estephan, L. E., et al. (2021). Matrix stiffening induces a pathogenic QKI-miR-7-SRSF1 signaling axis in pulmonary arterial endothelial cells. *Am. J. Physiol. Lung Cell Mol. Physiol.* 320, L726–L738. doi: 10.1152/ajplung.00407.2020
- Wu, D., and Birukov, K. (2019). Endothelial Cell Mechano-Metabolomic Coupling to Disease States in the Lung Microvasculature. *Front. Bioeng. Biotechnol.* 7:172. doi: 10.3389/fbioe.2019.00172
- Wu, D., Huang, R. T., Hamanaka, R. B., Krause, M., Oh, M. J., Kuo, C. H., et al. (2017). HIF-1 α is required for disturbed flow-induced metabolic reprogramming in human and porcine vascular endothelium. *Elife* 30:6. doi: 10.7554/eLife.25217
- Wu, H., Yu, Y., Huang, H., Hu, Y., Fu, S., Wang, Z., et al. (2020). Progressive Pulmonary Fibrosis Is Caused by Elevated Mechanical Tension on Alveolar Stem Cells. *Cell* 180, 107.e–121.e. doi: 10.1016/j.cell.2019.11.027
- Wu, J., Yan, Z., Schwartz, D. E., Yu, J., Malik, A. B., and Hu, G. (2013). Activation of NLRP3 inflammasome in alveolar macrophages contributes to mechanical stretch-induced lung inflammation and injury. *J. Immunol.* 190, 3590–3599. doi: 10.4049/jimmunol.1200860
- Xiong, J., Kawagishi, H., Yan, Y., Liu, J., Wells, Q. S., Edmunds, L. R., et al. (2018). A Metabolic Basis for Endothelial-to-Mesenchymal Transition. *Mol. Cell.* 69, 689.e–698.e. doi: 10.1016/j.molcel.2018.01.010
- Yamamoto, K., Nogimori, Y., Imamura, H., and Ando, J. (2020). Shear stress activates mitochondrial oxidative phosphorylation by reducing plasma membrane cholesterol in vascular endothelial cells. *Proc. Natl. Acad. Sci. U S A.* 117, 33660–33667. doi: 10.1073/pnas.2014029117
- Yan, X., Li, W., Yang, L., Dong, W., Chen, W., Mao, Y., et al. (2018). MiR-135a Protects Vascular Endothelial Cells Against Ventilator-Induced Lung Injury by Inhibiting PHLPP2 to Activate PI3K/Akt Pathway. *Cell Physiol. Biochem.* 48, 1245–1258. doi: 10.1159/000492010
- Yang, J., Pan, X., Wang, L., and Yu, G. (2020). Alveolar cells under mechanical stressed niche: critical contributors to pulmonary fibrosis. *Mol. Med.* 26:95. doi: 10.1186/s10020-020-00223-w
- Yehya, N., Song, M. J., Lawrence, G. G., and Margulies, S. S. (2019). HER2 Signaling Implicated in Regulating Alveolar Epithelial Permeability with Cyclic Stretch. *Int. J. Mol. Sci.* 20:4. doi: 10.3390/ijms20040948
- Young, S. M., Liu, S., Joshi, R., Batie, M. R., Kofron, M., Guo, J., et al. (2015). Localization and stretch-dependence of lung elastase activity in development and compensatory growth. *J. Appl. Physiol.* 118, 921–931. doi: 10.1152/japplphysiol.00954.2014
- Zeinali, S., Thompson, E. K., Gerhardt, H., Geiser, T., and Guenat, O. T. (2021). Remodeling of an in vitro microvessel exposed to cyclic mechanical stretch. *APL Bioeng.* 5:026102. doi: 10.1063/5.0010159
- Zhang, R., Pan, Y., Fanelli, V., Wu, S., Luo, A. A., Islam, D., et al. (2015). Mechanical Stress and the Induction of Lung Fibrosis via the Midkine Signaling Pathway. *Am. J. Respir. Crit. Care Med.* 192, 315–323. doi: 10.1164/rccm.201412-2326OC
- Zhang, X., Li, Y., Ma, Y., Yang, L., Wang, T., Meng, X., et al. (2018). Yes-associated protein (YAP) binds to HIF-1 α and sustains HIF-1 α protein stability to promote hepatocellular carcinoma cell glycolysis under hypoxic stress. *J. Exp. Clin. Cancer Res.* 37, 216. doi: 10.1186/s13046-018-0892-2
- Zhang, Y., Jiang, L., Huang, T., Lu, D., Song, Y., Wang, L., et al. (2021). Mechanosensitive cation channel Piezo1 contributes to ventilator-induced lung injury by activating RhoA/ROCK1 in rats. *Respir. Res.* 22:250. doi: 10.1186/s12931-021-01844-3
- Zhang, Y., Liu, G., Dull, R. O., Schwartz, D. E., and Hu, G. (2014). Autophagy in pulmonary macrophages mediates lung inflammatory injury via NLRP3 inflammasome activation during mechanical ventilation. *Am. J. Physiol. Lung Cell Mol. Physiol.* 307, L173–L185. doi: 10.1152/ajplung.00083.2014
- Zhong, A., Mirzaei, Z., and Simmons, C. A. (2018). The Roles of Matrix Stiffness and β -Catenin Signaling in Endothelial-to-Mesenchymal Transition of Aortic Valve Endothelial Cells. *Cardiovasc. Eng. Technol.* 9, 158–167. doi: 10.1007/s13239-018-0363-0
- Zhu, G., Zhang, W., Liu, Y., and Wang, S. (2018). miR-371b-5p inhibits endothelial cell apoptosis in monocrotaline-induced pulmonary arterial hypertension via PTEN/PI3K/Akt signaling pathways. *Mol. Med. Rep.* 18, 5489–5501. doi: 10.3892/mmr.2018.9614

Conflict of Interest: The authors declare that the research was conducted in the absence of any commercial or financial relationships that could be construed as a potential conflict of interest.

Publisher's Note: All claims expressed in this article are solely those of the authors and do not necessarily represent those of their affiliated organizations, or those of the publisher, the editors and the reviewers. Any product that may be evaluated in this article, or claim that may be made by its manufacturer, is not guaranteed or endorsed by the publisher.

Copyright © 2022 Lin, Zheng, Lin, Zhang, Wu and Li. This is an open-access article distributed under the terms of the Creative Commons Attribution License (CC BY). The use, distribution or reproduction in other forums is permitted, provided the original author(s) and the copyright owner(s) are credited and that the original publication in this journal is cited, in accordance with accepted academic practice. No use, distribution or reproduction is permitted which does not comply with these terms.



Testosterone Contributes to Vascular Dysfunction in Young Mice Fed a High Fat Diet by Promoting Nuclear Factor E2–Related Factor 2 Downregulation and Oxidative Stress

Rafael M. Costa^{1,2*}, Rhéure Alves-Lopes^{1,3}, Juliano V. Alves¹, Carolina P. Servian², Fabíola L. Mestriner¹, Fernando S. Carneiro¹, Núbia de S. Lobato² and Rita C. Tostes^{1*}

¹ Department of Pharmacology, Ribeirão Preto Medical School, University of São Paulo, Ribeirão Preto, Brazil, ² Academic Unit of Health Sciences, Federal University of Jataí, Jataí, Brazil, ³ British Heart Foundation, Glasgow Cardiovascular Research Centre, Institute of Cardiovascular and Medical Sciences, University of Glasgow, Glasgow, United Kingdom

OPEN ACCESS

Edited by:

Dongze Zhang,
University of Nebraska Medical
Center, United States

Reviewed by:

Julia Shanks,
The University of Auckland,
New Zealand
Roger Lyrio Santos,
Federal University of Espírito Santo,
Brazil

*Correspondence:

Rafael M. Costa
rafael_menezes@ufjf.edu.br
Rita C. Tostes
rtostes@usp.br

Specialty section:

This article was submitted to
Vascular Physiology,
a section of the journal
Frontiers in Physiology

Received: 16 December 2021

Accepted: 31 January 2022

Published: 08 March 2022

Citation:

Costa RM, Alves-Lopes R, Alves JV, Servian CP, Mestriner FL, Carneiro FS, Lobato NS and Tostes RC (2022) Testosterone Contributes to Vascular Dysfunction in Young Mice Fed a High Fat Diet by Promoting Nuclear Factor E2–Related Factor 2 Downregulation and Oxidative Stress. *Front. Physiol.* 13:837603. doi: 10.3389/fphys.2022.837603

Obesity, an important risk factor for cardiovascular disease, promotes vascular oxidative stress. Considering that free testosterone levels remain within the reference range, especially in obese young men and that testosterone stimulates reactive oxygen species (ROS) generation, we sought to investigate whether testosterone interferes with obesity-associated oxidative stress and vascular dysfunction in male mice. We hypothesized that testosterone favors ROS accumulation and vascular dysfunction in high fat diet (HFD)-fed obese mice. We also questioned whether testosterone downregulates the nuclear factor E2–related factor 2 (Nrf2), one of the major cellular defense mechanisms against oxidative stimuli. Male C57Bl/6J mice were submitted to orchiectomy or sham-operation. Mice received either a control diet (CD) or HFD for 18 weeks. Vascular function was assessed in thoracic aortic rings and molecular mechanisms by which testosterone contributes to vascular dysfunction were determined. HFD reduced acetylcholine-induced vasodilation and increased vascular ROS generation in sham mice. Castration prevented these effects. Treatment of castrated mice fed either the CD or HFD with testosterone propionate decreased acetylcholine vasodilation. HFD decreased Nrf2 nuclear accumulation, events linked to decreased mRNA expression and activity of Nrf2-regulated enzymes (catalase, heme oxygenase-1, peroxiredoxin, and thioredoxin). These events were prevented in HFD-fed castrated mice. Bardoxolone, a Nrf2 activator, increased nuclear accumulation of Nrf2, decreased ROS generation and improved acetylcholine vasodilation in HFD-fed sham mice. *In vitro*, testosterone increased ROS generation and decreased Nrf2 nuclear accumulation. These effects were prevented in the presence of an androgen receptor antagonist, an inhibitor of gene transcription and an inhibitor of the pro-oxidant enzyme NOX-1. These results indicate that testosterone downregulates Nrf2, leading to oxidative stress and vascular dysfunction in HFD-fed obese young mice.

Keywords: obesity, testosterone, vascular dysfunction, Nrf2, oxidative stress

HIGHLIGHTS

- Testosterone contributes to vascular dysfunction in young obese.
- Vascular dysfunction in young obese is associated with testosterone-induced oxidative stress.
- Testosterone contributes to decreased Nrf2 transcriptional factor signaling, compromising the antioxidant function in the vascular system.
- The decrease in testosterone levels during the development of obesity in young individuals attenuates oxidative stress, improving the performance of the transcription factor Nrf2 and consequent prevention of vascular dysfunction.

INTRODUCTION

Obesity is a major cause of morbidity and mortality in a large part of the world population (Andersson and Vasan, 2018; Csige et al., 2018). Numerous comorbid conditions are associated with adult obesity, including type 2 diabetes mellitus, arterial hypertension, and other cardiovascular and metabolic disorders (Krauss et al., 1998; Kahn et al., 2006; Jiang et al., 2016; Costa et al., 2018). Excessive fat accumulation is widely considered the result of interactions between environmental, genetic and epigenetic factors, which disturb the balance between the caloric intake and energy expenditure, leading to increased risk of illness (Hill, 2006). The prenatal period and the first years of an individual's life were identified as critical phases for the development of body composition (Stettler and Iotova, 2010). High birth weight is associated with an increased risk of obesity in adulthood (Yu et al., 2011; Zhao et al., 2012). Furthermore, faster weight gain in children is also associated with an increased risk of overweight and obesity later in life (Monteiro and Victora, 2005; Ong and Loos, 2006; Druet et al., 2012). Fat deposition in childhood and early adulthood also accounts for increased cardiovascular risk (Nadeau et al., 2011; Caprio et al., 2020). However, it is unclear how body mass gain during the transition from early to middle adulthood, when most body mass gain occurs, relates to subsequent health consequences.

One important factor that has been associated with both childhood and adult obesity are testosterone levels (Kelly and Jones, 2013; Mancini et al., 2021). Nevertheless, little attention has been directed toward the role of androgenic steroids on the mechanisms of cardiovascular and metabolic alterations in obesity. Although still a controversial topic, androgens are widely associated with higher risk of cardiovascular disease in men. In fact, abusive use of synthetic androgens by athletes leads to premature cardiovascular complications and the male gender itself is an independent risk factor for cardiovascular disease (Kloner et al., 2016). In addition, there is abundant epidemiological and clinical evidence linking a decline in testosterone levels with vascular dysfunction, atherosclerotic process, stroke and cardiovascular mortality (Bhasin and Herbst, 2003; Lopes et al., 2012; Alves et al., 2020). One explanation for the lack of agreement amongst these studies is that testosterone may shift target tissues susceptibility to damage by

mechanisms that depend on the concentration, duration and source (exogenous androgen, salt of testosterone), as well as the age, sex and health/disease state of the individual undergoing testosterone treatment.

Oxidative stress, a disturbance in the balance between the production of free radicals and antioxidant defenses, plays a critical role in the pathophysiology of obesity and obesity-associated complications (Betteridge, 2000). Obesity itself induces systemic oxidative stress through mechanisms that involve superoxide anion generation from NADPH oxidases, oxidative phosphorylation, and chronic inflammation. Adipose tissue dysfunction in obesity leads to increased reactive oxygen species (ROS) generation and inadequate cellular antioxidant defense (Furukawa et al., 2004; Zhou et al., 2021). In the cardiovascular system, oxidative stress occurs concomitantly with endothelial dysfunction, increased vascular contractility, growth and apoptosis of vascular smooth muscle cells (VSMC), lipid peroxidation and increased extracellular matrix protein deposition (da Costa et al., 2017; Costa et al., 2018). Testosterone and its metabolites affect the main components that control/modulate ROS generation and degradation (Tostes et al., 2016). Testosterone induces ROS generation in VSMC via NADPH oxidases, with greater production in cells from hypertensive compared with normotensive animals (Chignalia et al., 2012). Testosterone also induces mitochondria-derived ROS generation and apoptosis in VSMC, effects mediated via androgen receptor activation (Lopes et al., 2014). Testosterone stimulates the generation of superoxide anion (via xanthine oxidase) and nitric oxide, increasing peroxynitrite production and stimulating apoptosis (Puttabyatappa et al., 2013). Cyclooxygenase2-dependent ROS production is obligatory for testosterone-induced immune cells migration (Chignalia et al., 2015), which may contribute to inflammation and target organ damage. Collectively, these data indicate that in oxidative conditions, androgen signaling further increases cell damage.

Antioxidants are compounds or enzymatic systems that scavenge or neutralize free radicals (Kawagishi and Finkel, 2014). In this sense, the nuclear factor E2-related factor 2 (Nrf2) is one of the major defense mechanisms against oxidative and proteotoxic stress in cells (Cuadrado et al., 2019). Under physiological conditions, Nrf2 is usually associated with Keap-1, a repressor protein found in the cytoplasm (Horie et al., 2021). Stressors, such as free radicals, favor the translocation of Nrf2 to the cell nucleus. The accumulation of nuclear Nrf2 allows its binding to the antioxidant response element of genes that code antioxidant proteins (Nguyen et al., 2009). Growing evidence indicates that decreased or defective Nrf2 activity contributes to oxidative stress, favoring the pathophysiology of cardiovascular disorders found in obesity (da Costa et al., 2019).

While it is clear that testosterone regulates ROS generation, it is undefined whether male sex hormones contribute to the progressive vascular oxidative damage caused by obesogenic diets. In this study, we questioned whether loss of androgens in young male mice changes the tissue's hormonal landscape, yielding a vascular oxidative status that differs from that observed in adult males. Accordingly, we used castrated young male mice

to determine whether androgens confer protection or exacerbate vascular oxidative damage induced by an obesogenic diet. We hypothesized that testosterone, signaling through androgen receptors, negatively impacts Nrf2/Keap1 signaling. We also determined whether testosterone treatment changes Nrf2/Keap1 signaling. Finally, we determined *in vitro* effects of testosterone on ROS generation and Nrf2 nuclear accumulation, using endothelial cells treated with vehicle or the androgen receptor antagonist flutamide. Alternatively, the functional and molecular components were measured in the presence of vehicle or the Nrf2 activator bardoxolone.

MATERIALS AND METHODS

Animals, Orchiectomy, and Diets

All experimental protocols were performed in accordance with the recommendations of the Brazilian Guidelines for the Care and Use of animals for Scientific and Teaching Purposes and the Guidelines for the Practice of Euthanasia (CONCEA-MCT, 2013), having been approved by the Ethics Committee on Animal Use of the University of São Paulo, Ribeirão Preto, Brazil (Protocol n° 206/2016).

Four-week-old male C57Bl/6J mice were obtained and maintained in the Animal Facility of the University of São Paulo, Ribeirão Preto, Brazil on 12-h light/dark cycles under controlled temperature ($22 \pm 1^\circ\text{C}$) and humidity (50–60%) with *ad libitum* access to food and water. Mice were anesthetized (ketamine and xylazine at doses of 75 and 15 mg/kg, respectively, intraperitoneally), the efferent duct of each testicle was ligated, and the testicles were removed. Sham mice were submitted to the same surgical procedures without efferent duct ligation or testicles removal. After a 1-week acclimatization period, mice were divided into two groups: (1) mice maintained on a control diet [CD (protein 22%, carbohydrate 70%, and fat 8% of energy, PragSolucoes)], and (2) mice receiving a high-fat diet [HFD (protein 10%, carbohydrate 25%, and fat 65% of energy, PragSolucoes)]. After 18 weeks on the CD or HFD, mice were euthanized by carbon dioxide (CO_2) inhalation without removing mice from their home cage. Death was confirmed by cardiac arrest. Studies followed the ARRIVE guidelines for reporting experiments on experimental animals.

Biochemical Profile

Glucose levels were determined using a glucose analyzer (Accu-Check, Roche Diagnostics). Total cholesterol and triglyceride concentrations were determined in serum samples from mice fasted for 12 h (da Costa et al., 2018), by enzymatic colorimetric method (Dolco®). Plasma insulin concentration (ng/mL) was determined by radioimmunoassay (Insulin Kit®).

Testosterone Replacement and Plasma Measurement

Plasma testosterone levels were determined in sham, castrated and testosterone-treated mice using the IMMULITE 1000 Immunoassay System (Enzo Life Sciences®, New York, NY,

United States). After 18 weeks on the CD or HFD, testosterone-treated mice received intramuscular injections of testosterone-propionate [dissolved in peanut oil, 5 mg/kg body weight per day (Sigma Aldrich, San Luis, MO, United States)], for 15 days.

Assessment of Vascular Function

Thoracic aorta was rapidly removed, transferred to an ice-cold (4°C) Krebs Henseleit-modified solution [(in M) 130 NaCl, 14.9 NaHCO_3 , 4.7 KCl, 1.18 KH_2PO_4 , 1.17 $\text{MgSO}_4 \cdot 7\text{H}_2\text{O}$, 5.5 glucose, 1.56 $\text{CaCl}_2 \cdot 2\text{H}_2\text{O}$ and 0.026 EDTA] gassed with 5% CO_2 and 95% O_2 to maintain a pH of 7.4, and dissected into 2 mm rings. Aortic rings were mounted in a wire myograph to measure isometric tension, as previously described (da Costa et al., 2017). Vessels were allowed to equilibrate for about 30 min in Krebs Henseleit solution. After the stabilization period, endothelial function was assessed by testing the relaxant effect of acetylcholine (ACh, 10^{-6} M) on vessels contracted with phenylephrine (PE, 10^{-7} M). Aortic rings exhibiting a vasodilator response to ACh greater than 70–80% were considered endothelium-intact vessels. Cumulative concentration-response curves to ACh (10^{-10} to 10^{-4} M) were performed in aortic rings from the various experimental groups.

Relaxation responses to ACh were also determined after incubation with either the selective superoxide anion (O_2^-) scavenger tiron (10^{-4} M, 30 min) or the Nrf2 activator bardoxolone (10^{-6} M, 3 h). Each vascular preparation was tested with a single agent.

Cultured Endothelial Cells and Experimental Design

Endothelial cells were commercially purchased. An immortalized line of human umbilical vein endothelial cells, EA.hy926, (ATCC® CRL-2922™) was used. Cells were cultured in Dulbecco's Modified Eagle Medium (DMEM) supplemented with 10% fetal bovine serum (FBS) in a CO_2 incubator, at 37°C , 5% CO_2 . After confluence, cells were maintained in the presence of 2% FBS (Rodrigues et al., 2021). Cells were stimulated with testosterone for various times (10^{-7} M, 15 min to 6 h). To determine testosterone effects on NADPH oxidase activity, cells were preincubated with a NOX1 inhibitor ML171 (10^{-4} M, 1 h). To investigate genomic and non-genomic effects of testosterone, cells were incubated with the androgen receptor antagonist flutamide (10^{-5} M, 1 h) and the gene transcription inhibitor actinomycin D (10^{-5} M, 1 h), respectively, previous to exposure to testosterone.

Measurement of Reactive Oxygen Species

Dihydroethidium

Reactive Oxygen Species generation was assessed by dihydroethidium (DHE), as previously described (Costa et al., 2016). Aortas were embedded in the optimal cutting temperature (OCT™) embedding medium and stored at -80°C . Fresh-frozen specimens were cross-sectioned at 10 μm thickness and placed on slides covered with poly-(L-lysine). Tissues were loaded with the non-selective dye for ROS detection DHE (5×10^{-6} M in phosphate buffer 10^{-6} M) for 30 min at

37°C. Images were collected on a ZEISS microscope and the results are expressed as fold changes relatively to the control. Fluorescent images were analyzed by measuring the mean optical density of the fluorescence in a computer system (Image J software) and normalized by the area.

Amplex Red

Thoracic aortae were frozen, macerated and centrifuged. Fifty μL -aliquots of the supernatant were removed and hydrogen peroxide (H_2O_2) was determined fluorometrically by measuring Amplex Red (8×10^{-6} M) conversion (Molecular Probes, Invitrogen, Carlsbad, CA, United States) to the fluorescent compound resorufin, in the presence of horseradish peroxidase (4 U/mL). Resorufin fluorescence was detected in a plate fluorimeter (SynergyTM 2 Multi-Detection Microplate Reader, BioTek Instruments, Santa Clara, CA, United States) using excitation and emission wavelengths of 530 and 590 nm, respectively. The fluorescence values were normalized by the total amount of tissue proteins.

Lucigenin

Generation of O_2^- was measured by lucigenin luminescence using NADPH as the substrate. Aortae from control and obese mice were homogenized in an assay buffer (50 mM KH_2PO_4 , 1 mM EGTA, and 150 mM sucrose, pH 7.4) with a glass-to-glass homogenizer. 100 μL of sample, lucigenin (5 μM), NADPH (0.1 mM) and assay buffer were used. Luminescence was measured for 30 cycles of 18 s each, in a luminometer (Orion II Luminometer, Berthold Detection Systems, Pforzheim, Germany). Basal readings were obtained and the reaction was started by the addition of the substrate. Basal and buffer blank values were subtracted from the NADPH-derived luminescence. O_2^- was expressed as relative luminescence units (RLU)/mg protein.

Measurement of Thiobarbituric Acid Reactive Substances

Thiobarbituric acid reactive substances (TBARS) concentration was determined colorimetrically (at 540 nm) in aortas homogenates with a commercially available kit (#10009055, Cayman Chemical, United States), following the manufacturer's instructions. TBARS concentration was determined using a standard curve of malondialdehyde and the results are expressed as μM /mg protein.

NOx

Plasma nitrate concentrations were determined by subtracting the nitrite values from the NOx values (nitrite + nitrate). For the determination of NOx, the Griess reaction was used. Plasma samples were incubated with nitrate reductase, at 37°C for 12 h, in a light-free environment. The Griess reagent was added and reading was performed by spectrophotometry at 540 nm.

Thioredoxin Reductase, Superoxide Dismutase, and Catalase Activities

Thioredoxin reductase (TrxR) activity was determined in aortas using a commercially available kit (#CS0170, Sigma-Aldrich, San

Luis, MO, United States). Enzymatic activity was assessed by determining the difference between the time-dependent increase in absorbance at 412 nm in the presence of the TrxR activity inhibitor from total activity. One activity unit equaled 1 mM 5'-thionitrobenzoic acid formed/mg protein. Thoracic aortae were homogenized in 300 μL of Krebs Henseleit and centrifuged at $18,000 \times g$ for 15 min at 4°C. The supernatants were analyzed for superoxide dismutase (SOD) or catalase (CAT) activities. SOD activity was evaluated using a commercially available kit (#19160, Sigma-Aldrich, San Luis, MO, United States). The results were normalized for protein concentration, and SOD activity is expressed as % inhibition rate/mg protein. CAT activity was assayed by H_2O_2 consumption and measured in a spectrophotometer at 240 nm. One CAT unit (U) was defined as the amount of enzyme required to decompose 1 μM of H_2O_2 /min/mg protein.

Nuclear Factor E2-Related Factor 2 Activity

To determine nuclear accumulation of Nrf2, the nuclear fraction from cell or tissue lysates were separated using the Active Motif nuclear extract kit (Active Motif, Carlsbad, CA, United States) following the manufacturer's protocol. Cells or tissue were resuspended in 1X hypotonic buffer and centrifuged for 30 s at $12,800 \times g$ at 4°C. Nuclear pellets were resuspended in lysis buffer provided by the manufacturer. The suspension was incubated for 30 min on ice on a rocking platform set at $5 \times g$ and then centrifuged for 10 min at $12,800 \times g$. The supernatant was transferred to a pre-chilled microcentrifuge tube. TransAMTM Nrf2 ELISA kit (Active Motif) was used to measure nuclear accumulation of Nrf2 at a wavelength of 450 nm.

Quantitative Real-Time Reverse Transcription-Polymerase Chain Reaction

Total RNA was isolated from aortae using Trizol[®] (Invitrogen, Carlsbad, CA, United States). RNA was treated with DNase I (1 U/ μL , Promega) and used for first-strand cDNA synthesis, accordingly to the manufacturer instructions. mRNA levels were quantified in triplicate by qPCR StepOnePlusTM Life Technologies. Specific primers (TaqManTM) for RT-qPCR were as follows: mouse SOD-1 [*Mm01344233_g1*], Catalase [*Mm00437992_m1*], Heme oxygenase-1 [*Mm00516005_m1*], Peroxiredoxin-1 [*Mm01621996_s1*] and β -actin [*Mm00607939_s1*], purchased from Life Technologies. PCR cycling conditions included 10 min at 95°C, followed by 40 cycles at 95°C for 15 s, 60°C for 1 min, and 72°C for 60 s. Dissociation curve analysis confirmed that signals corresponded to unique amplicons. Specific mRNA expression levels were normalized relatively to β -actin mRNA levels using the comparative $\Delta\Delta\text{Ct}$ method.

Western Blot Analysis

Aortas were frozen in liquid nitrogen and homogenized in a lysis buffer [50 mM Tris/HCl, 150 mM NaCl, 1% Nonidet P40, 1 mM ethylenediaminetetraacetic acid (EDTA), 1

$\mu\text{g/mL}$ leupeptin, 1 $\mu\text{g/mL}$ pepstatin, 1 $\mu\text{g/mL}$ aprotinin, 1 mM sodium orthovanadate, 1 mM phenylmethylsulfonyl fluoride (PMSF), and 1 mM sodium fluoride]. The tissue extracts were centrifuged, and total protein content was quantified using the Bradford method (Bradford, 1976). Proteins (40 μg) were separated by electrophoresis on 10% polyacrylamide gel, and transferred on to nitrocellulose membranes. Non-specific binding sites were blocked with 5% bovine serum albumin (BSA) in Tris-buffered saline (TBS) containing 0.1% Tween 20 (for 1 h at 24°C). Membranes were incubated with antibodies (at the indicated dilutions) overnight at 4°C. Antibodies were used as follows: anti-keap1 (1:1,000 dilution; Abcam), anti-NOX1 (1:1,000 dilution; Cell Signaling), anti-NOX4 (1:1,000 dilution; Cell Signaling), anti- β -actin (1:1,000 dilution; Sigma), and anti-GAPDH (1:10,000 dilution; Sigma). After incubation with secondary antibodies, signals were obtained by chemiluminescence, visualized by autoradiography and quantified densitometrically.

Data and Statistical Analyses

The individual concentration–response curves were fitted into a curve by non-linear regression analysis. pD_2 (defined as the negative logarithm of the EC_{50} values) and maximal response (Emax) were compared by Two-way ANOVA with Bonferroni post-test. The results of the molecular experiments were analyzed by Mann Whitney test or Two-way ANOVA, followed by the Bonferroni post-test. Data were assessed for normality with Shapiro-Wilk test. The Prism software, version 9.0 (GraphPad Software Inc., San Diego, CA, United States) was used to analyze these parameters as well as to fit the sigmoidal curves. Data are presented as mean \pm SEM. N represents the number of mice used. p values less than 0.05 were considered significant.

RESULTS

The High Fat Diet Effects on Adiposity in Young Mice Is Not Under the Influence of Testosterone

Table 1 details the characteristics of the animal groups. At the beginning of the experimental protocol, sham and castrated mice displayed similar body weight. Both groups gained weight during the protocol development. However, the weight gain was higher in mice fed the HFD as compared to the CD-fed group. Castrated and Sham mice on the HFD showed similar body weight gain. Similarly, testosterone treatment did not modify weight gain in HFD- or CD-fed mice. Castration effectively reduced endogenous androgen levels, as evidenced by the undetectable levels of testosterone in castrated animals. Castrated mice fed the CD and treated with testosterone propionate (5 mg/kg body weight) exhibited supraphysiological levels of testosterone, whereas castrated HFD-fed mice treated with the same dose of testosterone propionate (5 mg/kg body weight) exhibited testosterone levels similar to those observed in the sham group.

No differences in serum glucose were observed between sham and castrated mice fed the CD. However, HFD increased serum glucose in sham mice. Insulin and total cholesterol plasma levels

were also increased in HFD-fed sham mice compared to CD-fed sham mice. Castration did not change increased serum glucose, insulin or total cholesterol levels induced by the HFD, but decreased triglyceride plasma levels in mice fed both the CD and HFD (**Table 1**). These results indicate that metabolic changes evoked by the HFD in young mice are not affected by either castration or supraphysiological levels of circulating testosterone.

Castration Prevents Vascular Dysfunction in High Fat Diet-Fed Mice

We then assessed the involvement of testosterone on vascular dysfunction in HFD-fed mice considering its independent association with cardiovascular complications. Castrated and sham-operated mice were fed the HFD and vascular function was evaluated. As shown in **Figure 1A**, no differences in SNP-induced vascular relaxation were observed between CD sham and HFD sham mice. In contrast, HFD reduced ACh-induced vascular relaxation in sham mice in comparison with CD-fed sham mice (**Figure 1B**). In mice fed the CD, there were no differences in ACh-induced vasodilatation between the sham and castrated groups. However, castration prevented HFD-induced vascular dysfunction (**Figure 1C**). Treatment of castrated mice maintained on the CD with testosterone propionate decreased ACh-induced vasodilation. The effects of castration on ACh vasodilation in HFD-fed mice, i.e., increased ACh vasodilation, were lost upon testosterone propionate treatment (**Figure 1D**). **Table 2** shows the maximum response and pD_2 values.

Castration Prevents Vascular Oxidative Stress in High Fat Diet-Fed Mice

We next determined whether testosterone contributes to increased vascular ROS generation in mice on the HFD. As expected and already reported, HFD decreased plasma NO $_x$ (**Figure 2A**) and increased aortic TBARS levels (**Figure 2B**). Basal levels of ROS, determined by DHE fluorescence intensity (**Figure 2C**), were significantly increased in arteries from HFD-fed sham mice. In addition, aortas from HFD sham mice exhibited increased generation of O $_2^{\cdot-}$ (**Figure 2D**) and H $_2$ O $_2$ (**Figure 2E**), determined by lucigenin chemiluminescence and amplex red, respectively. Castration prevented increased vascular ROS induced by HFD. No differences were observed in ROS generation between sham and castrated mice on the CD. Similarly to castration, tiron improved ACh-induced vascular relaxation in HFD sham mice (**Figure 2F**). No additional effects were observed with the combination of tiron and castration, i.e., tiron did not further improve ACh vasodilation in HFD castrated mice (**Figure 2G**), indicating that both tiron and castration interfere with similar pathways. **Table 3** shows the maximum response and pD_2 values.

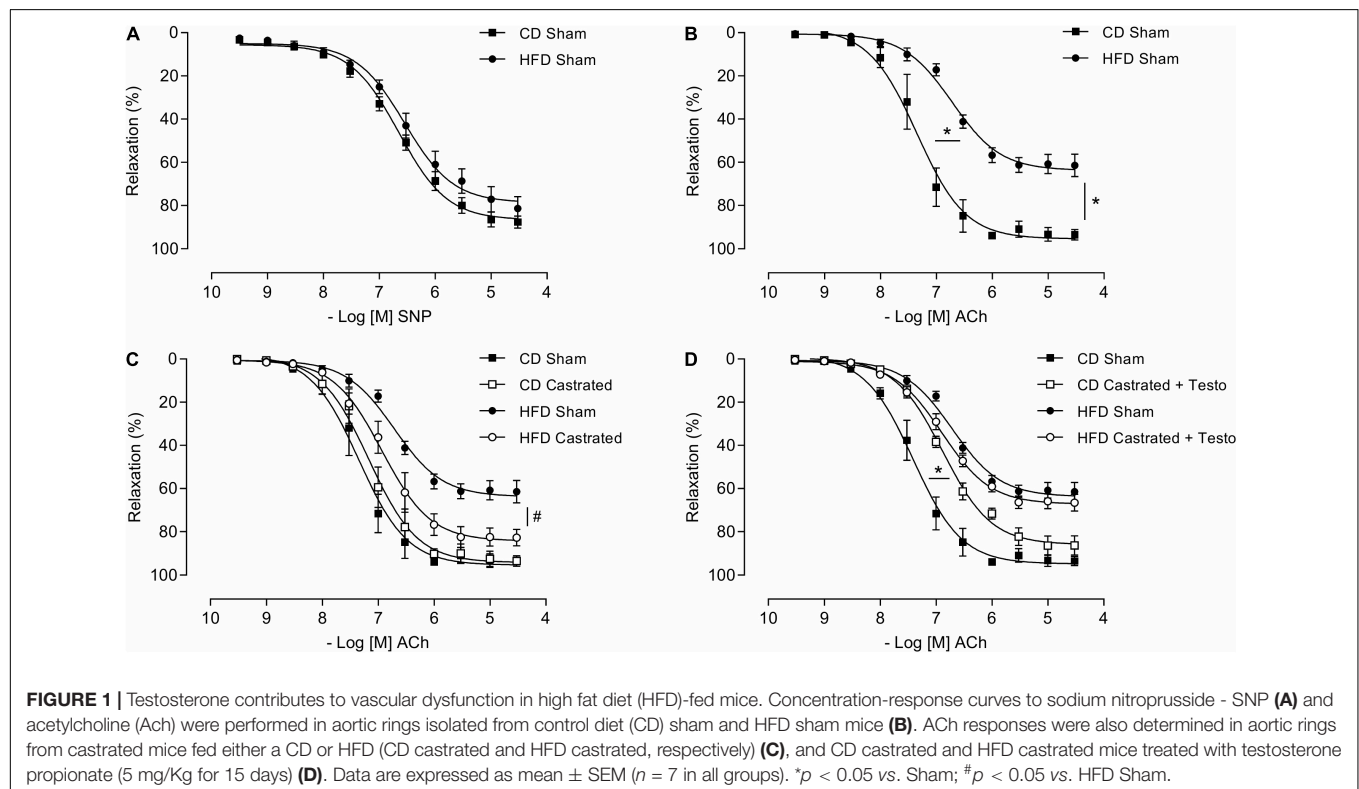
Castration Prevents Downregulation of the Antioxidant System in High Fat Diet-Fed Mice

Nuclear factor E2-related factor 2 signaling is a major regulator of cellular antioxidant systems. HFD increased vascular Keap-1 protein expression (**Figure 3A**). In addition, HFD decreased nuclear accumulation of Nrf2 (**Figure 3B**), which was associated

TABLE 1 | Body weight and biochemical profile in the experimental groups of mice.

	CD Sham	CD Castrated	HFD Sham	HFD Castrated	CD Castrated + Testo	HFD Castrated + Testo
Body weight (g)	28.1 ± 0.4	26.7 ± 0.6	43.8 ± 0.4*	41.7 ± 0.8	28.9 ± 0.5	45.1 ± 0.3
Testosterone (ng/mL)	7.7 ± 0.7	0.9 ± 0.4*	6.4 ± 0.8	0.6 ± 0.2 [#]	11.4 ± 1.1*	7.8 ± 1.2
Glucose (mg/dL)	79.8 ± 3.1	84.8 ± 2.8	184.3 ± 5.9*	141.4 ± 10.7 [#]		
Insulin (ng/mL)	3.6 ± 0.2	3.4 ± 0.3	8.2 ± 0.6*	7.4 ± 0.5		
Total Cholesterol (mg/dL)	81.6 ± 3.5	80.1 ± 3.2	121.6 ± 6.6*	129.1 ± 6.5		
Triglyceride (mg/dL)	67.1 ± 5.4	45.3 ± 6.1*	106.3 ± 10.1*	57.3 ± 8.5 [#]		

Values are expressed as mean ± SEM (n = 10–12). CD, control diet; HFD, high fat diet. Two-way ANOVA: *p < 0.05 vs. CD Sham; [#]p < 0.05 vs. HFD Sham.

**TABLE 2** | Emax and pD₂ values of sodium nitroprusside and acetylcholine-induced relaxation in thoracic aorta arteries.

	CD Sham (SNP)	HFD Sham (SNP)	CD Sham (ACh)	HFD Sham (ACh)	CD Castrated (ACh)	HFD Castrated (ACh)	CD Castrated + Testo (ACh)	HFD Castrated + Testo (ACh)
Emax	86.6 ± 1.6	79.6 ± 2.4	95.3 ± 2.7	63.7 ± 1.7*	94.1 ± 2.5	84.2 ± 2.4 [#]	85.8 ± 1.6	67.1 ± 1.3
pD ₂	6.65 ± 0.05	6.54 ± 0.08	7.34 ± 0.08	6.71 ± 0.07*	7.16 ± 0.07	6.93 ± 0.08	6.88 ± 0.05*	6.89 ± 0.05

Values are expressed as mean ± SEM (n = 7). CD, control diet; HFD, high fat diet; SNP, sodium nitroprusside; ACh, acetylcholine. Two-way ANOVA: *p < 0.05 vs. CD Sham; [#]p < 0.05 vs. HFD Sham.

with a decrease in mRNA expression of Nrf2-regulated enzymes, such as SOD-1 (Figure 3C), catalase (Figure 3D), heme oxygenase-1 (Figure 3E), peroxiredoxin (Figure 3F) as well as with decreased activity of the enzymes thioredoxin (Figure 3G), SOD (Figure 3H) and catalase (Figure 3I). These events were also prevented in castrated HFD-fed mice, indicating that Nrf2-regulated redox balance in the vasculature of obese mice is modulated by testosterone. No differences were observed in Nrf2 antioxidant system between sham and castrated mice on the CD.

Castration Prevents Vascular Dysfunction in High Fat Diet-Fed Mice by Mechanisms That Involve Nuclear Factor E2-Related Factor 2 Activation

Activation of the Nrf2 system by bardoxolone improved ACh-induced vascular relaxation in HFD-fed sham mice (Figure 4A). The effects of bardoxolone and castration on ACh vasodilation were similar in HFD-fed mice (Figure 4B),

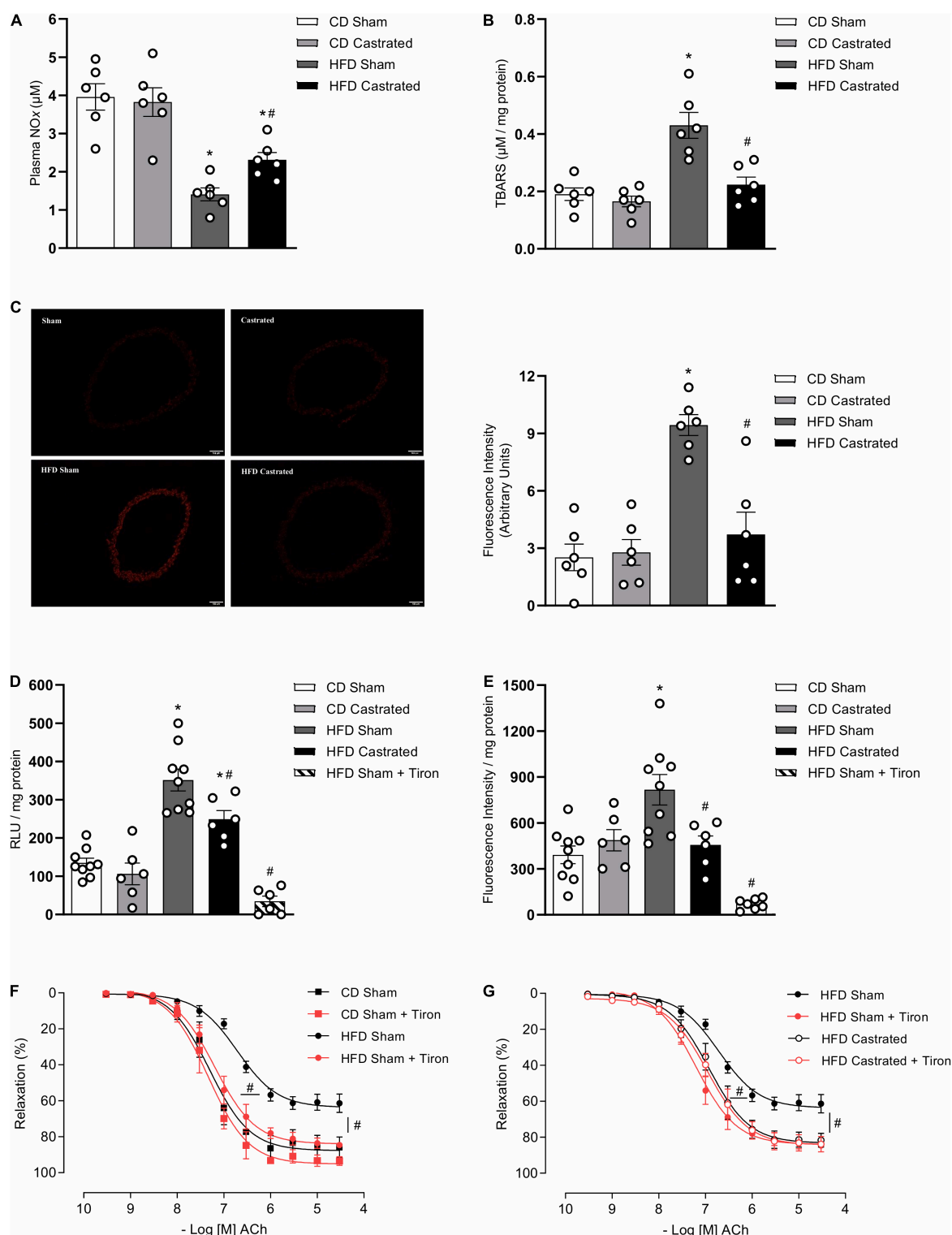
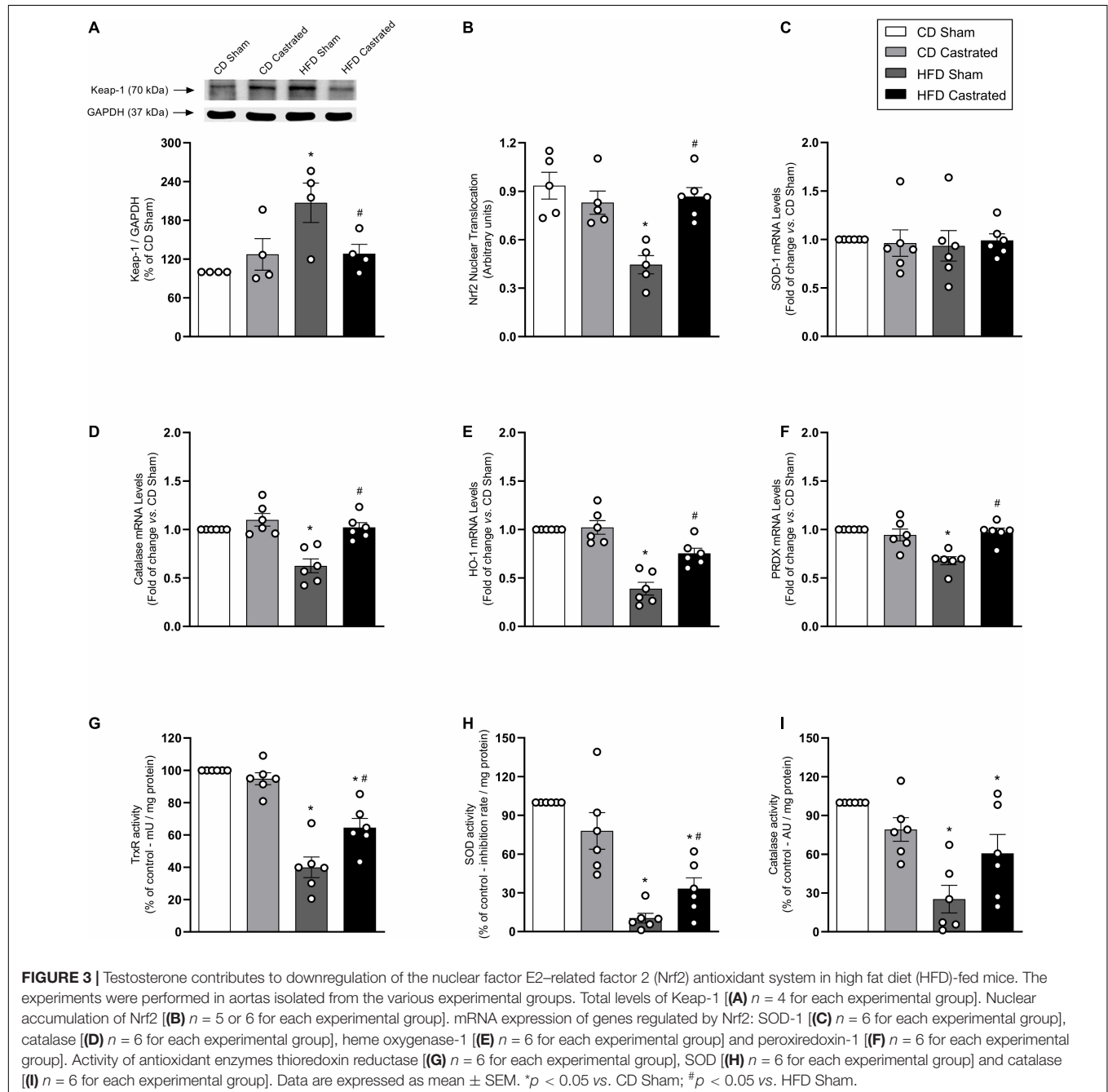


FIGURE 2 | Testosterone contributes to vascular oxidative stress in high fat diet (HFD)-fed mice. Plasma NOx [(A) $n = 6$ for each experimental group], TBARS [(B) $n = 6$ for each experimental group], reactive oxygen species generation – measured by DHE [(C) $n = 6$ for each experimental group], superoxide anion generation – measured by lucigenin [(D) $n = 6$ or 9 for each experimental group], and hydrogen peroxide levels – determined by amplex red [(E) $n = 6$ or 9 for each experimental group] were evaluated in aortas isolated from mice of the different experimental groups. Concentration-response curves to acetylcholine (ACh) were performed in aortic rings isolated from control diet (CD) sham, HFD sham, and HFD castrated mice in the presence of Tiron (10^{-4} M) [(F,G) $n = 7$ in all groups]. Data are expressed as mean \pm SEM. * $p < 0.05$ vs. CD Sham; # $p < 0.05$ vs. HFD Sham.

TABLE 3 | Emax and pD₂ values of acetylcholine-induced relaxation in thoracic aorta arteries incubated with vehicle or Tiron.

	CD Sham	CD Sham + Tiron	HFD Sham	HFD Sham + Tiron	HFD Castrated	HFD Castrated + Tiron
Emax	87.7 ± 3.1	95.1 ± 2.5	63.7 ± 1.7	83.9 ± 1.9 [#]	83.2 ± 2.3 [#]	84.2 ± 2.2
pD ₂	7.30 ± 0.10	7.33 ± 0.08	6.71 ± 0.07	7.19 ± 0.06 [#]	6.92 ± 0.08 [#]	6.95 ± 0.07

Values are expressed as mean ± SEM (n = 7). CD, control diet; HFD, high fat diet. Two-way ANOVA: [#]p < 0.05 vs. HFD Sham.



with no additional effects being observed in arteries from castrated mice incubated with bardoxolone. Bardoxolone did not change vascular reactivity in sham or castrated mice fed the CD. Bardoxolone increased nuclear accumulation of Nrf2

in vessels from HFD-fed sham mice (Figure 4C) and decreased HFD-induced vascular ROS generation (Figure 4D). Notably, no synergism was observed between the effects of bardoxolone and castration. In addition, bardoxolone improved catalase and heme

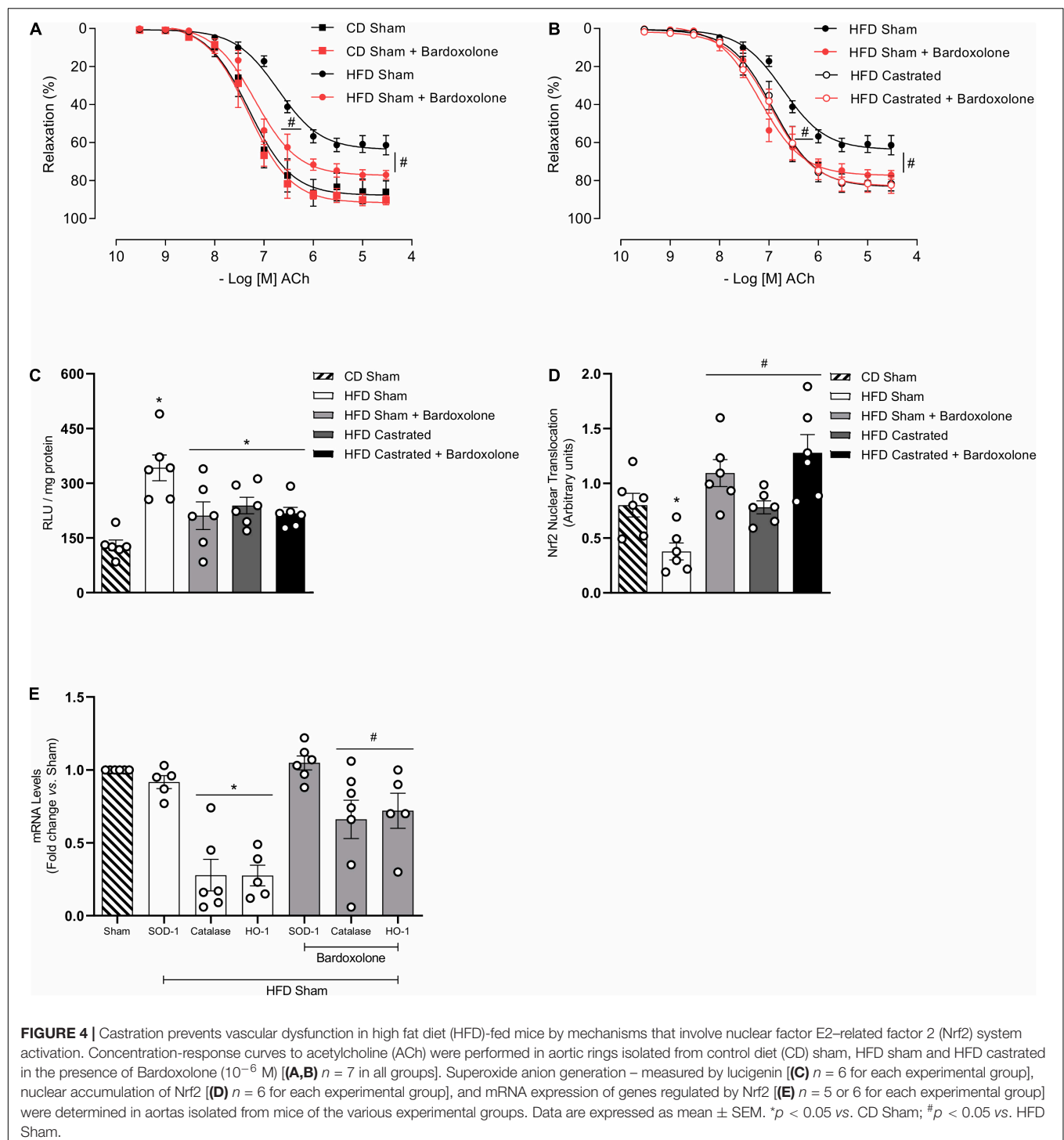


TABLE 4 | Emax and pD_2 values of acetylcholine-induced relaxation in thoracic aorta arteries incubated with vehicle or Bardoxolone.

	CD Sham	CD Sham + Bardoxolone	HFD Sham	HFD Sham + Bardoxolone	HFD Castrated	HFD Castrated + Bardoxolone
Emax	87.7 \pm 3.1	91.7 \pm 2.2	63.7 \pm 1.7	77.2 \pm 1.8 [#]	83.2 \pm 2.3 [#]	82.8 \pm 2.3
pD_2	7.30 \pm 0.10	7.31 \pm 0.06	6.71 \pm 0.07	7.18 \pm 0.07 [#]	6.92 \pm 0.08 [#]	6.94 \pm 0.06

Values are expressed as mean \pm SEM ($n = 7$). CD, control diet; HFD, high fat diet. Two-way ANOVA: [#] $p < 0.05$ vs. HFD Sham.

oxygenase-1 mRNA expression (**Figure 4E**). **Table 4** shows the maximum response and pD_2 values.

Castration Prevents Increased NADPH Oxidase Expression in High Fat Diet-Fed Mice

NADPH oxidase is the main source of free radicals in the vasculature. HFD increased NOX1 expression in aortas, which was prevented in castrated HFD-fed mice (**Figure 5A**). No difference was observed in the antioxidant system between sham and castrated mice fed the CD. In addition, no difference was observed in NOX4 (**Figure 5B**) expression among the different experimental groups.

NOX-1 Contribution to Testosterone-Induced Reactive Oxygen Species Generation and Endothelial Dysfunction

Considering that testosterone modulates endothelial cell function as well as oxidative and inflammatory processes in endothelial cells, we further determined molecular mechanisms involved in testosterone-mediated endothelial dysfunction, by using EA.hy926 cells. Testosterone induced a time-dependent ROS generation in EA.hy926 cells (**Figure 6A**), with maximum generation occurring at 2 h. In addition, testosterone increased nuclear accumulation of Nrf2 from 30 min, but this increase was reduced after 3 h of stimulation with testosterone (**Figure 6B**). Incubation of EA.hy926 cells with bardoxolone prevented ROS generation (**Figure 6C**). Testosterone-induced ROS generation at 3 and 6 h was prevented by ML171, a NOX1 inhibitor (**Figure 6D**). To investigate the possible mechanisms (genomic and non-genomic) whereby testosterone induces ROS production at 3 and 6 h, ROS generation was determined in the presence of flutamide and actinomycin D. Pre-incubation with flutamide prevented testosterone-induced ROS generation at 3 h, but not at 6 h. On the other hand, incubation with actinomycin D prevented testosterone-induced ROS generation at 6 h, but not at 3 h (**Figure 6E**). Actinomycin D prevented the decrease in Nrf2 activity induced by testosterone. Testosterone-induced decrease in Nrf2 activity was not observed in the presence of flutamide (**Figure 6F**).

DISCUSSION

The present study shows that testosterone plays a critical role in the progressive vascular oxidative damage caused by obesogenic diets in young male mice, mediating a set of changes that are very similar to those previously described in adult males. Accordingly, we demonstrated that testosterone, via androgen receptors, induces NOX1-dependent oxidative stress and negatively impacts Nrf2/Keap1 signaling, one of the main protective responses to oxidative stress.

It is extensively known that testosterone does not contribute exclusively to the development of the male reproductive system and sexual maturation. Clinical and experimental

evidence shows that testosterone also modulates cardiovascular homeostasis and produces important cardiac and vascular effects in physiopathological conditions, including obesity (Torres et al., 2007; Wang et al., 2011; Fui et al., 2014). Adult wistar rats fed a sucrose-rich diet exhibit increased vascular contractions to noradrenaline and this increase is prevented by castration (Vasudevan et al., 2006; Perez et al., 2009). In line with these observations, the present study shows that obesity in young male mice impairs vascular function, as evidenced by the decrease in acetylcholine-mediated vasodilation. Castration of these young animals also prevented obesity-associated endothelial dysfunction. The findings that testosterone replacement in castrated young obese mice impairs vasodilation, confirms that testosterone negatively influences vascular tone during obesity development in young mice.

Although the mechanisms by which obesity causes vascular dysfunction in adult are still not completely known, it is clear that this condition is associated with vascular oxidative stress, increased vasoconstriction and decreased vasodilation (Stapleton et al., 2008). Accordingly, our data clearly show that obesity induced by a high fat diet in young mice also increases free radical's generation in the vasculature, increases lipid peroxidation and reduces NO bioavailability. In addition, castration prevents oxidative stress and improves endothelial function in arteries of obese mice, indicating that testosterone is pro-oxidant and contributes to vascular dysfunction in young obesity. This is in agreement with previous studies demonstrating that, in adult experimental models, testosterone increases ROS generation in VSMC via NADPH oxidase- (Chignalia et al., 2012) and mitochondrial respiratory chain-dependent mechanisms (Lopes et al., 2014).

Free radical's levels are controlled by intracellular defense mechanisms that rely on the expression and activity of antioxidant enzymes. The Nrf2 system is essential for redox balance in the cardiovascular system. Nrf2 activation has vasoprotective effects via reduction of ROS and increased bioavailability of NO (Mann et al., 2007; Lopes et al., 2015). In adult obesity, the Nrf2 system is downregulated, since Nrf2 translocation to the nucleus is decreased in arteries of obese mice. In addition, expression of Keap-1, which negatively regulates Nrf2 degradation, maintaining Nrf2 in the cytosol, was increased in arteries from obese mice. Increased Keap-1 expression may account for the decreased vascular nuclear translocation of Nrf2. This is supported by studies showing decreased activity of Nrf2 in adipose tissue (Zamora-Mendoza et al., 2018) and renal cells of obese mice (Chin et al., 2013). In addition, mesenteric arteries of obese animals that do not express the leptin receptor exhibit decreased Nrf2 activity, which contributes to oxidative stress and increased vasoconstriction. Treatment of these animals with the Nrf2 activator L-sulforaphane reduces ROS and improves vascular function (Alves-Lopes et al., 2016). These data further support our results showing that decreased Nrf2 activity impairs vascular function and that activation of the Nrf2 system by bardoxolone prevents high fat diet-induced vascular dysfunction in young obese mice.

Castration increases Nrf2 activity and the expression and activity of antioxidant enzymes in arteries of obese mice, clearly

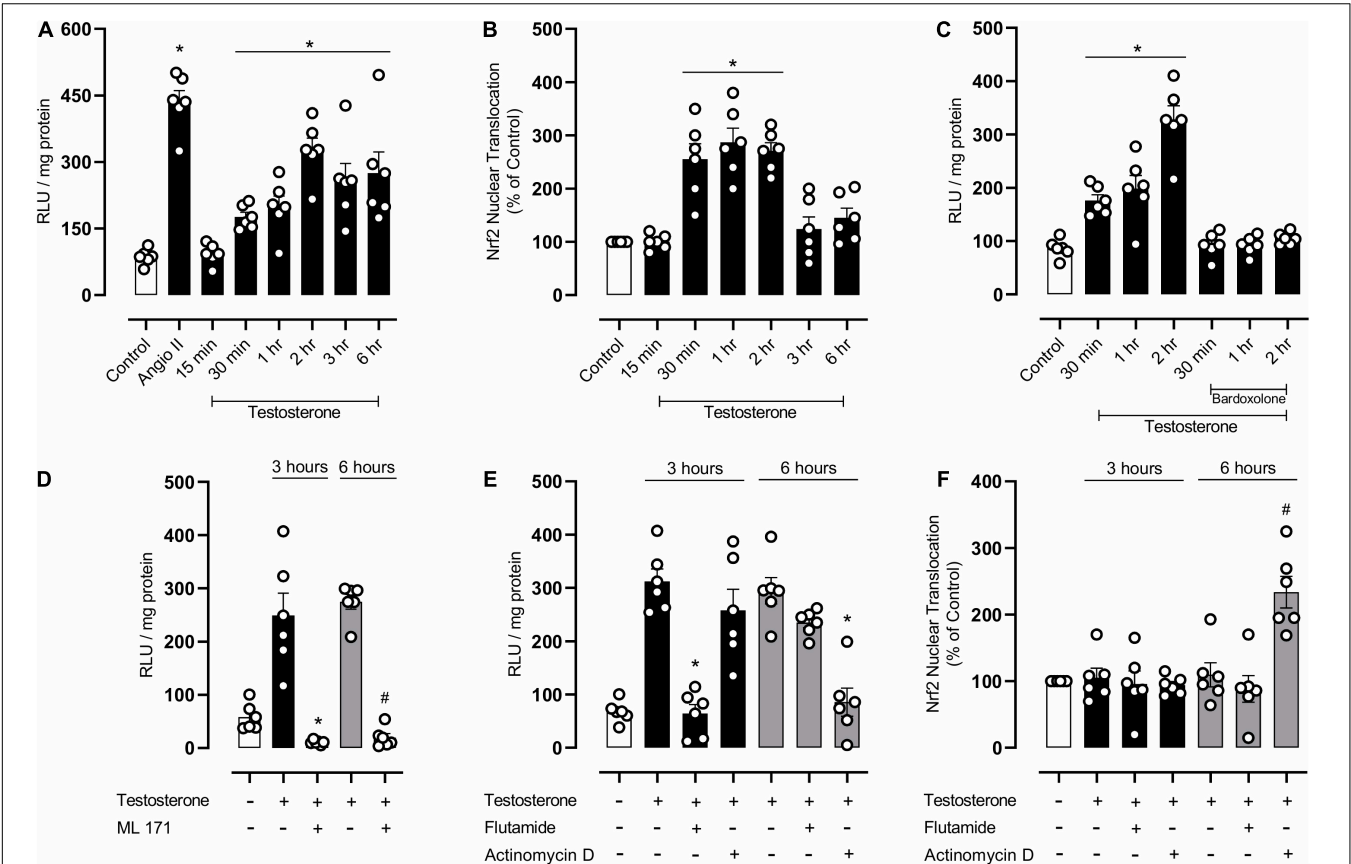
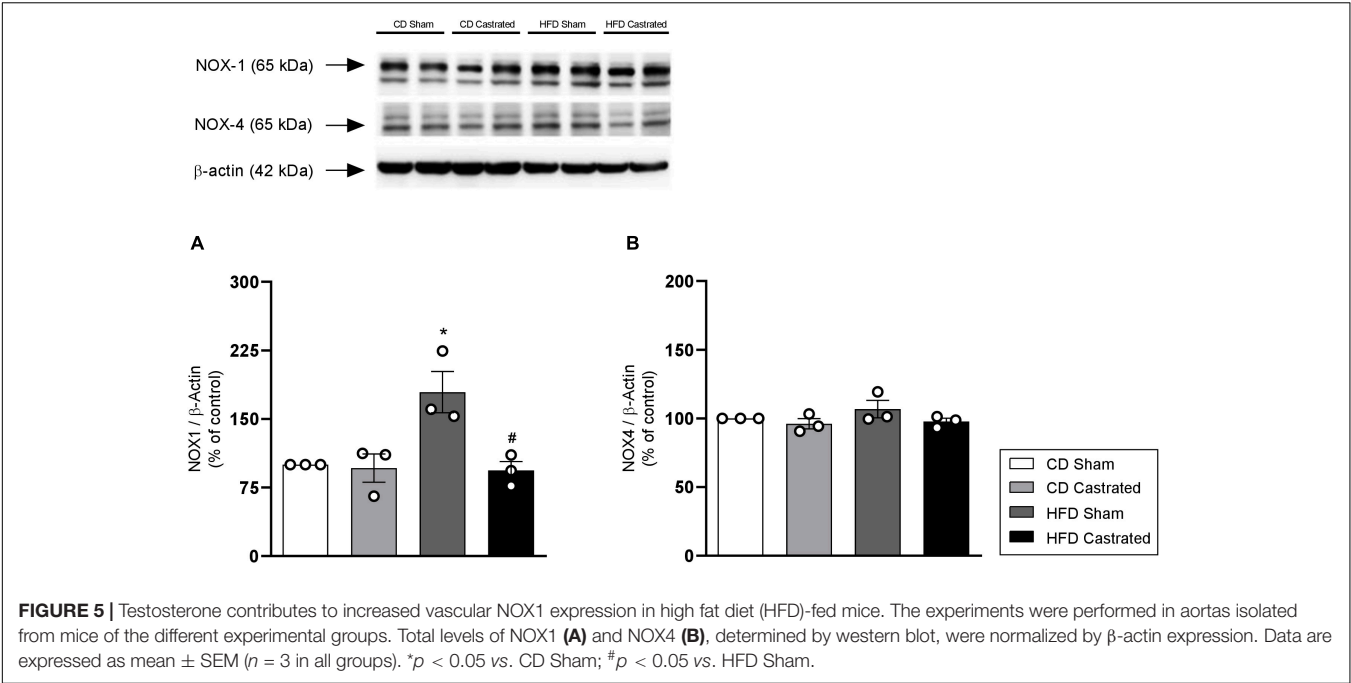


FIGURE 6 | Testosterone induces a biphasic increase in reactive oxygen species (ROS) generation by mechanisms that involves NOX1 activation and downregulation of nuclear factor E2-related factor 2 (Nrf2) activity in endothelial cells. Superoxide anion generation was measured by lucigenin [(A,C-E) $n = 6$ or 7 for each experimental group] and nuclear accumulation of Nrf2 [(B,F) $n = 6$ for each experimental group]. Data are expressed as mean \pm SEM. * $p < 0.05$ vs. Control; # $p < 0.05$ vs. Testosterone.

indicating that testosterone negatively regulates Nrf2 signaling during transition from early to middle adulthood, when most body mass gain occurs. Considering that fat deposition early in life accounts for increased cardiovascular risk in adulthood, the effects of testosterone, demonstrated in our study, may represent an important mechanism mediating this process.

A link between Nrf2 and testosterone has been previously reported in adult experimental models. Nrf2 knockout mice exhibit increased ROS generation and fluctuations in plasma testosterone levels due to Leydig cell deficiency (Chen et al., 2015). Recent data from our group showed that hyperglycemia, a condition found in diabetes mellitus, reduces Nrf2 activity, increases the activity of pro-oxidant enzymes and ROS generation, leading to vascular (pudendal arteries) dysfunction. Considering that this vascular bed is highly responsive to the actions of testosterone (Alves-Lopes et al., 2016), this reinforces the hypothesis that blood vessels are modulated by redox mechanisms sensitive to testosterone even during fat accumulation early in life.

Arteries of young obese mice exhibited increased expression of NOX1, a NAD(P)H oxidase isoform, and, interestingly, castration prevented this increase. Accordingly, it has been reported that testosterone increases the expression of NADPH oxidase subunits in VSMC, increasing ROS generation and cell migration (Chignalia et al., 2012). We sought to further explore the mechanisms activated by testosterone that culminate in endothelial dysfunction and subsequent vascular dysfunction. In cultured endothelial cells, testosterone increased ROS generation in a time-dependent manner; initially by non-genomic actions and activation of androgen receptors and later by genomic effects. Testosterone also decreased Nrf2 activity by mechanisms that rely on gene transcription. Similar to the present findings, it was reported that ROS generation induced by testosterone depends on early-activated genomic mechanisms and also on lately-activated non-genomic mechanisms (Chignalia et al., 2015).

In conclusion, the present study demonstrated that testosterone downregulates the Nrf2 antioxidant system, favoring NOX1 activity, ROS accumulation and vascular dysfunction in HFD-fed young obese mice. These findings indicate that testosterone constitutes an important mediator of the progressive vascular oxidative damage caused by obesogenic diets in young

male mice, favoring a vascular oxidative status that is similar to that observed in adult obesity.

DATA AVAILABILITY STATEMENT

The raw data supporting the conclusions of this article will be made available by the authors, without undue reservation.

ETHICS STATEMENT

The animal study was reviewed and approved by Ethics Committee on Animal Use (CEUA) of the University of São Paulo, Ribeirão Preto, Brazil (Protocol no 206/2016).

AUTHOR CONTRIBUTIONS

RC, NL, FC, and RT participated in the design of the study, provided the reagents and analytical tools, and wrote the manuscript. RC, RA-L, JA, CS, and FM performed the experiments and data analysis. All authors contributed to the article and approved the submitted version.

FUNDING

This research received funding from the São Paulo Research Foundation (FAPESP, grant no. 2013/08216-2, Center for Research in Inflammatory Diseases - CRID) and Conselho Nacional de Desenvolvimento Científico e Tecnológico (CNPq), Grant No. 433898/2018-6.

SUPPLEMENTARY MATERIAL

The Supplementary Material for this article can be found online at: <https://www.frontiersin.org/articles/10.3389/fphys.2022.837603/full#supplementary-material>

REFERENCES

- Alves, J. V., da Costa, R. M., Pereira, C. A., Fedoce, A. G., Silva, C. A. A., Carneiro, F. S., et al. (2020). Supraphysiological levels of testosterone induce vascular dysfunction via activation of the NLRP3 inflammasome. *Front. Immunol.* 11:1647. doi: 10.3389/fimmu.2020.01647
- Alves-Lopes, R., Neves, K. B., Montezano, A. C., Harvey, A., Carneiro, F. S., Touyz, R. M., et al. (2016). Internal pudendal artery dysfunction in diabetes mellitus is mediated by NOX1-Derived ROS-, Nrf2-, and Rho kinase-dependent mechanisms. *Hypertension* 68, 1056–1064. doi: 10.1161/HYPERTENSIONAHA.116.07518
- Andersson, C., and Vasan, R. S. (2018). Epidemiology of cardiovascular disease in young individuals. *Nat. Rev. Cardiol.* 15, 230–240. doi: 10.1038/nrcardio.2017.154
- Betteridge, D. J. (2000). What is oxidative stress? *Metabolism* 49, 3–8. doi: 10.1016/s0026-0495(00)80077-3
- Bhasin, S., and Herbst, K. (2003). Testosterone and atherosclerosis progression in men. *Diabet. Care* 26, 1929–1931. doi: 10.2337/diacare.26.6.1929
- Bradford, M. M. (1976). A rapid and sensitive method for the quantitation of microgram quantities of protein utilizing the principle of protein-dye binding. *Anal. Biochem.* 72, 248–254. doi: 10.1006/abio.1976.9999
- Caprio, S., Santoro, N., and Weiss, R. (2020). Childhood obesity and the associated rise in cardiometabolic complications. *Nat. Metab.* 2, 223–232. doi: 10.1038/s42255-020-0183-z
- Chen, H., Jin, S., Guo, J., Kombairaju, P., Biswal, S., and Zirkin, B. R. (2015). Knockout of the transcription factor Nrf2: effects on testosterone production by aging mouse Leydig cells. *Mol. Cell. Endocrinol.* 409, 113–120. doi: 10.1016/j.mce.2015.03.013
- Chignalia, A. Z., Oliveira, M. A., Debbas, V., Dull, R. O., Laurindo, F. R., Touyz, R. M., et al. (2015). Testosterone induces leucocyte migration by NADPH

- oxidase-driven ROS-and COX2-dependent mechanisms. *Clin. Sci.* 129, 39–48. doi: 10.1042/CS20140548
- Chignalia, A. Z., Schuldt, E. Z., Camargo, L. L., Montezano, A. C., Callera, G. E., Laurindo, F. R., et al. (2012). Testosterone induces vascular smooth muscle cell migration by NADPH oxidase and c-Src-dependent pathways. *Hypertension* 59, 1263–1271. doi: 10.1161/HYPERTENSIONAHA.111.180620
- Chin, M., Lee, C. Y. I., Chuang, J. C., Bumeister, R., Wigley, W. C., Sonis, S. T., et al. (2013). Bardoxolone methyl analogs RTA 405 and dh404 are well tolerated and exhibit efficacy in rodent models of Type 2 diabetes and obesity. *Am. J. Physiol. Renal Physiol.* 304, F1438–F1446. doi: 10.1152/ajprenal.00387.2012
- CONCEA-MCT (2013). Ministério da Ciência, Tecnologia e Inovação Conselho Nacional de Controle de Experimentação Animal. Diretriz Brasileira para o Cuidado e a Utilização de Animais para Fins Científicos e Didáticos – DBCA. Brazilian Government. Available online at: <https://pages.cnpem.br/ceua/wp-content/uploads/sites/56/2015/06/DBCA.pdf>
- Costa, R. M., Filgueira, F. P., Tostes, R. C., Carvalho, M. H. C., Akamine, E. H., and Lobato, N. S. (2016). H₂O₂ generated from mitochondrial electron transport chain in thoracic perivascular adipose tissue is crucial for modulation of vascular smooth muscle contraction. *Vasc. Pharmacol.* 84, 28–37. doi: 10.1016/j.vph.2016.05.008
- Costa, R. M., Neves, K. B., Tostes, R. C., and Lobato, N. S. (2018). Perivascular adipose tissue as a relevant fat depot for cardiovascular risk in obesity. *Front. Physiol.* 9:253. doi: 10.3389/fphys.2018.00253
- Csige, I., Ujvárosy, D., Szabó, Z., Lőrincz, I., Paragh, G., Harangi, M., et al. (2018). The impact of obesity on the cardiovascular system. *J. Diabetes Res.* 2018:3407306.
- Cuadrado, A., Rojo, A. I., Wells, G., Hayes, J. D., Cousin, S. P., Rumsey, W. L., et al. (2019). Therapeutic targeting of the NRF2 and KEAP1 partnership in chronic diseases. *Nat. Rev. Drug Discov.* 18, 295–317. doi: 10.1038/s41573-018-0008-x
- da Costa, R. M., Fais, R. S., Dechandt, C. R., Louzada-Junior, P., Alberici, L. C., Lobato, N. S., et al. (2017). Increased mitochondrial ROS generation mediates the loss of the anti-contractile effects of perivascular adipose tissue in high-fat diet obese mice. *Br. J. Pharmacol.* 174, 3527–3541. doi: 10.1111/bph.13687
- da Costa, R. M., Rodrigues, D., Pereira, C. A., Silva, J. F., Alves, J. V., Lobato, N. S., et al. (2019). Nrf2 as a potential mediator of cardiovascular risk in metabolic diseases. *Front. Pharmacol.* 10:382. doi: 10.3389/fphar.2019.00382
- da Costa, R. M., Silva, J. F. D., Alves, J. V., Dias, T. B., Rassi, D. M., Garcia, L. V., et al. (2018). Increased O-GlcNAcylation of endothelial nitric oxide synthase compromises the anti-contractile properties of perivascular adipose tissue in metabolic syndrome. *Front. Physiol.* 9:341. doi: 10.3389/fphys.2018.00341
- Druet, C., Stettler, N., Sharp, S., Simmons, R. K., Cooper, C., Smith, G. D., et al. (2012). Prediction of childhood obesity by infancy weight gain: an individual-level meta-analysis. *Paediatr. Perinat. Epidemiol.* 26, 19–26. doi: 10.1111/j.1365-3016.2011.01213.x
- Fui, M. N. T., Dupuis, P., and Grossmann, M. (2014). Lowered testosterone in male obesity: mechanisms, morbidity and management. *Asian J. Androl.* 16:223. doi: 10.4103/1008-682X.122365
- Furukawa, S., Fujita, T., Shimabukuro, M., Iwaki, M., Yamada, Y., Nakajima, Y., et al. (2004). Increased oxidative stress in obesity and its impact on metabolic syndrome. *J. Clin. Invest.* 114, 1752–1761. doi: 10.1172/JCI21625
- Hill, J. O. (2006). Understanding and addressing the epidemic of obesity: an energy balance perspective. *Endocr. Rev.* 27, 750–761. doi: 10.1210/er.2006-0032
- Horie, Y., Suzuki, T., Inoue, J., Iso, T., Wells, G., Moore, T. W., et al. (2021). Molecular basis for the disruption of Keap1–Nrf2 interaction via Hinge & Latch mechanism. *Commun. Biol.* 4:576. doi: 10.1038/s42003-021-02100-6
- Jiang, S. Z., Lu, W., Zong, X. F., Ruan, H. Y., and Liu, Y. (2016). Obesity and hypertension. *Exp. Ther. Med.* 12, 2395–2399.
- Kahn, S. E., Hull, R. L., and Utzschneider, K. M. (2006). Mechanisms linking obesity to insulin resistance and type 2 diabetes. *Nature* 444, 840–846. doi: 10.1038/nature05482
- Kawagishi, H., and Finkel, T. (2014). Unraveling the truth about antioxidants: ROS and disease: finding the right balance. *Nat. Med.* 20, 711–713. doi: 10.1038/nm.3625
- Kelly, D. M., and Jones, T. H. (2013). Testosterone: a metabolic hormone in health and disease. *J. Endocrinol.* 217, R25–R45. doi: 10.1530/JOE-12-0455
- Kloner, R. A., Carson, C., Dobs, A., Kopecky, S., and Mohler, E. R. (2016). Testosterone and cardiovascular disease. *J. Am. Coll. Cardiol.* 67, 545–557.
- Krauss, R. M., Winston, M., Fletcher, B. J., and Grundy, S. M. (1998). Obesity: impact on cardiovascular disease. *Circulation* 98, 1472–1476.
- Lopes, R. A. M., Neves, K. B., Carneiro, F. S., and Tostes, R. (2012). Testosterone and vascular function in aging. *Front. Physiol.* 3:89. doi: 10.3389/fphys.2012.00089
- Lopes, R. A. M., Neves, K. B., Pestana, C. R., Queiroz, A. L., Zanotto, C. Z., Chignalia, A. Z., et al. (2014). Testosterone induces apoptosis in vascular smooth muscle cells via extrinsic apoptotic pathway with mitochondria-generated reactive oxygen species involvement. *Am. J. Physiol. Heart Circ. Physiol.* 306, H1485–H1494. doi: 10.1152/ajpheart.00809.2013
- Lopes, R. A., Neves, K. B., Tostes, R. C., Montezano, A. C., and Touyz, R. M. (2015). Downregulation of nuclear factor erythroid 2–related factor and associated antioxidant genes contributes to redox-sensitive vascular dysfunction in hypertension. *Hypertension* 66, 1240–1250. doi: 10.1161/HYPERTENSIONAHA.115.06163
- Mancini, M., Pecori Giraldo, F., Andreassi, A., Mantellassi, G., Salvioni, M., Berra, C. C., et al. (2021). Obesity is strongly associated with low testosterone and reduced penis growth during development. *J. Clin. Endocrinol. Metab.* 106, 3151–3159. doi: 10.1210/clinem/dgab535
- Mann, G. E., Rowlands, D. J., Li, F. Y., de Winter, P., and Siow, R. C. (2007). Activation of endothelial nitric oxide synthase by dietary isoflavones: role of NO in Nrf2-mediated antioxidant gene expression. *Cardiovasc. Res.* 75, 261–274. doi: 10.1016/j.cardiores.2007.04.004
- Monteiro, P. O. A., and Victora, C. G. (2005). Rapid growth in infancy and childhood and obesity in later life—a systematic review. *Obes. Rev.* 6, 143–154. doi: 10.1111/j.1467-789X.2005.00183.x
- Nadeau, K. J., Maahs, D. M., Daniels, S. R., and Eckel, R. H. (2011). Childhood obesity and cardiovascular disease: links and prevention strategies. *Nat. Rev. Cardiol.* 8, 513–525. doi: 10.1038/nrcardio.2011.86
- Nguyen, T., Nioi, P., and Pickett, C. B. (2009). The Nrf2-antioxidant response element signaling pathway and its activation by oxidative stress. *J. Biol. Chem.* 284, 13291–13295. doi: 10.1074/jbc.R900010200
- Ong, K. K., and Loos, R. J. (2006). Rapid infancy weight gain and subsequent obesity: systematic reviews and hopeful suggestions. *Acta Paediatr.* 95, 904–908. doi: 10.1080/08035250600719754
- Perez, I., El Hafidi, M., Carvajal, K., and Baños, G. (2009). Castration modifies aortic vasoreactivity and serum fatty acids in a sucrose-fed rat model of metabolic syndrome. *Heart Vessels* 24:147. doi: 10.1007/s00380-008-1098-x
- Puttabayattappa, Y., Stallone, J. N., Ergul, A., El-Remessy, A. B., Kumar, S., Black, S., et al. (2013). Peroxynitrite mediates testosterone-induced vasodilation of microvascular resistance vessels. *J. Pharmacol. Exp. Ther.* 345, 7–14. doi: 10.1124/jpet.112.201947
- Rodrigues, D., Costa, T. J., Silva, J. F., Neto, J. T. D. O., Alves, J. V., Fedoce, A. G., et al. (2021). Aldosterone negatively regulates Nrf2 activity: an additional mechanism contributing to oxidative stress and vascular dysfunction by aldosterone. *Int. J. Mol. Sci.* 22:6154. doi: 10.3390/ijms22116154
- Stapleton, P. A., James, M. E., Goodwill, A. G., and Frisbee, J. C. (2008). Obesity and vascular dysfunction. *Pathophysiology* 15, 79–89.
- Stettler, N., and Iotova, V. (2010). Early growth patterns and long-term obesity risk. *Curr. Opin. Clin. Nutr. Metab. Care* 13, 294–299. doi: 10.1097/MCO.0b013e328337d7b9
- Torres, I. P., El Hafidi, M., Zamora-González, J., Infante, O., Chavira, R., and Baños, G. (2007). Modulation of aortic vascular reactivity by sex hormones in a male rat model of metabolic syndrome. *Life Sci.* 80, 2170–2180. doi: 10.1016/j.lfs.2007.04.006
- Tostes, R. C., Carneiro, F. S., Carvalho, M. H. C., and Reckelhoff, J. F. (2016). Reactive oxygen species: players in the cardiovascular effects of testosterone. *Am. J. Physiol. Regul. Integr. Comp. Physiol.* 310, R1–R14. doi: 10.1152/ajpregu.00392.2014

- Vasudevan, H., Nagareddy, P. R., and McNeill, J. H. (2006). Gonadectomy prevents endothelial dysfunction in fructose-fed male rats, a factor contributing to the development of hypertension. *Am. J. Physiol. Heart Circ. Physiol.* 291, H3058–H3064. doi: 10.1152/ajpheart.00598.2005
- Wang, C., Jackson, G., Jones, T. H., Matsumoto, A. M., Nehra, A., Perelman, M. A., et al. (2011). Low testosterone associated with obesity and the metabolic syndrome contributes to sexual dysfunction and cardiovascular disease risk in men with type 2 diabetes. *Diabetes Care* 34, 1669–1675. doi: 10.2337/dc10-2339
- Yu, Z. B., Han, S. P., Zhu, G. Z., Zhu, C., Wang, X. J., Cao, X. G., et al. (2011). Birth weight and subsequent risk of obesity: a systematic review and meta-analysis. *Obes. Rev.* 12, 525–542. doi: 10.1111/j.1467-789X.2011.00867.x
- Zamora-Mendoza, R., Rosas-Vargas, H., Ramos-Cervantes, M. T., Garcia-Zuniga, P., Perez-Lorenzana, H., Mendoza-Lorenzo, P., et al. (2018). Dysregulation of mitochondrial function and biogenesis modulators in adipose tissue of obese children. *Int. J. Obes.* 42, 618–624. doi: 10.1038/ijo.2017.274
- Zhao, Y., Wang, S. F., Mu, M., and Sheng, J. (2012). Birth weight and overweight/obesity in adults: a meta-analysis. *Eur. J. Pediatr.* 171, 1737–1746.
- Zhou, Y., Li, H., and Xia, N. (2021). The interplay between adipose tissue and vasculature: role of oxidative stress in obesity. *Front. Cardiovasc. Med.* 8:131. doi: 10.3389/fcvm.2021.650214
- Conflict of Interest:** The authors declare that the research was conducted in the absence of any commercial or financial relationships that could be construed as a potential conflict of interest.
- Publisher's Note:** All claims expressed in this article are solely those of the authors and do not necessarily represent those of their affiliated organizations, or those of the publisher, the editors and the reviewers. Any product that may be evaluated in this article, or claim that may be made by its manufacturer, is not guaranteed or endorsed by the publisher.
- Copyright © 2022 Costa, Alves-Lopes, Alves, Servian, Mestriner, Carneiro, Lobato and Tostes. This is an open-access article distributed under the terms of the Creative Commons Attribution License (CC BY). The use, distribution or reproduction in other forums is permitted, provided the original author(s) and the copyright owner(s) are credited and that the original publication in this journal is cited, in accordance with accepted academic practice. No use, distribution or reproduction is permitted which does not comply with these terms.

Advantages of publishing in Frontiers



OPEN ACCESS

Articles are free to read
for greatest visibility
and readership



FAST PUBLICATION

Around 90 days
from submission
to decision



HIGH QUALITY PEER-REVIEW

Rigorous, collaborative,
and constructive
peer-review



TRANSPARENT PEER-REVIEW

Editors and reviewers
acknowledged by name
on published articles

Frontiers

Avenue du Tribunal-Fédéral 34
1005 Lausanne | Switzerland

Visit us: www.frontiersin.org

Contact us: frontiersin.org/about/contact



REPRODUCIBILITY OF RESEARCH

Support open data
and methods to enhance
research reproducibility



DIGITAL PUBLISHING

Articles designed
for optimal readership
across devices



FOLLOW US

@frontiersin



IMPACT METRICS

Advanced article metrics
track visibility across
digital media



EXTENSIVE PROMOTION

Marketing
and promotion
of impactful research



LOOP RESEARCH NETWORK

Our network
increases your
article's readership